

ADA278515

UNITED STATES AIR FORCE

SUMMER RESEARCH PROGRAM -- 1993

SUMMER RESEARCH-PROGRAM FINAL REPORTS

VOLUME 15

WRIGHT LABORATORY

RESEARCH & DEVELOPMENT LABORATORIES

5800 Uplander Way

Culver City, CA 90230-6608

**Program Director, RDL
Gary Moore**

**Program Manager, AFOSR
Col. Hal Rhoades**

**Program Manager, RDL
Scott Licoscas**

**Program Administrator, RDL
Gwendolyn Smith**

**Program Administrator, RDL
Johnetta Thompson**

Submitted to:

AIR FORCE OFFICE OF SCIENTIFIC RESEARCH

Bolling Air Force Base

Washington, D.C.

December 1993

94-12289



DTIC QUALITY INSPECTED 3

94 4 21 073

**Best
Available
Copy**

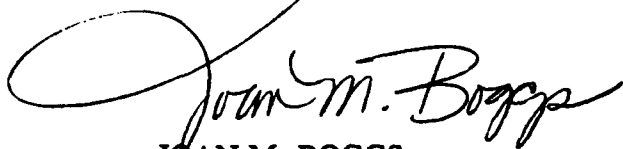
MEMORANDUM FOR DTIC (Acquisition)
(Attn: Pat Mauby)

SUBJECT: Distribution of USAF (AFOSR Summer Research Program (Air Force Laboratories) and Universal Energy Systems, Inc., and the Research Initiation Program

FROM: AFOSR/XPT

Joan M. Boggs
110 Duncan Avenue, Suite B115
Bolling AFB DC 20332-0001

1. All of the books forwarded to DTIC on the subjects above should be considered Approved for Public Release, distribution is unlimited (Distribution Statement A).
2. Thank you for processing the attached information.



JOAN M. BOGGS
Chief, Technical Information Division

HSAP + 5FRP Reports
(1992 Vol 13, 14, 16) (Vol 1, 2, 3, 4) 1991

6SRP (Vol 10 + 11) 1993
SRP

HSAP (Vol 12-16 - 1993)

14 Books

Master Index For High School Apprentices

Ackermann, Laura
7801 Wilshire NE
La Cueva High School
Albuquerque, NM 87122-0000

Laboratory: PL/LI
Vol-Page No: 13- 5

Alexanderson, Sarah
7173 FM 1628
East Central High School
San Antonio, TX 78263-0000

Laboratory: AL/HR
Vol-Page No: 12-25

Antonson, Stephan
800 Cypress St.
Rome Catholic High School
Rome, NY 13440-0000

Laboratory: RL/IR
Vol-Page No: 14-12

Arnold, Katherine
1400 Jackson-Keller
Robert E. Lee High School
San Antonio, TX 78213-0000

Laboratory: AL/OE
Vol-Page No: 12-30

Baits, Mark
248 North Main Street
Cedarville High School
Cedarville, OH 45314-0000

Laboratory: WL/FI
Vol-Page No: 15-11

Baker, Eugenia
501 Mosely Dr.
A. Crawford Mosley High School
Lynn Haven, FL 32444-0000

Laboratory: AL/EQ
Vol-Page No: 12-19

Bakert, Jonathan
Oneida St.
Sauquoit Valley Central High S
Sauquoit, NY 13456-0000

Laboratory: RL/ER
Vol-Page No: 14- 7

Banaszak, Brian
9830 W. National Rd.
Tecumseh High School
New Carlisle, OH 45344-0000

Laboratory: WL/PO
Vol-Page No: 15-44

Barber, Jason
1000 10th St.
Floresville High School
Floresville, TX 78114-0000

Laboratory: AL/CF
Vol-Page No: 12- 8

Bautista, Jennifer

Laboratory: WL/MN
Vol-Page No: 15-26

Accession For	
NTIS CRA&I	<input checked="" type="checkbox"/>
DTIC TAB	<input type="checkbox"/>
Unannounced	<input type="checkbox"/>
Justification	
By <i>lti</i>	
Distribution /	
Availability Codes	
Dist	Avail and/or Special
A-1	

HSAP Participant Data

Behm, Jessica
3301 Shroyer Rd.
Kettering Fairmont High School
Kettering, OH 45429-0000

Laboratory: WL/ML
Vol-Page No: 15-21

Berty, Sara
4524 Linden Ave.
Carroll High School
Dayton, OH 45432-0000

Laboratory: AL/OE
Vol-Page No: 12-31

Blanchard, William

Laboratory: WL/MN
Vol-Page No: 15-27

- 0

Bond, Ryan
North Jackson St.
Tullahoma High School
Tullahoma, TN 37388-0000

Laboratory: AEDC/
Vol-Page No: 16- 1

Bowlby, Andrea
Mudge Way
Bedford High School
Bedford, MA 1730-0000

Laboratory: PL/GP
Vol-Page No: 13- 1

Brecht, Jason
5400 Chambersburg Road
Wayne High Achool
Huber Heights, OH 45424-0000

Laboratory: WL/FI
Vol-Page No: 15-12

Brown, David
12200 Lomas Blvd. NE
Manzano High School
Albuquerque, NM 87112-0000

Laboratory: PL/WS
Vol-Page No: 13-19

Cabral, Aaron
800 Odelia NE
Albuquerque High School
Albuquerque, NM 87102-0000

Laboratory: PL/SX
Vol-Page No: 13-13

Camero, Lisa
2515 Navajo St.
South San Antonio High School
San Antonio, TX 78224-0000

Laboratory: AL/AO
Vol-Page No: 12- 2

Campanile, Nicholas
2660 Dayton-Xenia Rd.
Beavercreek High School
Beavercreek, OH 45434-0000

Laboratory: WL/EL
Vol-Page No: 15- 7

HSAP Participant Data

Carranza, Jason
505 S. Ludlow St.
Chaminade-Julienne High School
Dayton, OH 45402-0000

Laboratory: WL/AA
Vol-Page No: 15- 1

Carroll, Shawn
1400 Jackson Keller St.
Robert E. Lee High School
San Antonio, TX 78213-0000

Laboratory: AL/CF
Vol-Page No: 12- 9

Casares, Carmen
1215 N. St. Mary's
Providence High School
San Antonio, TX 78215-0000

Laboratory: AL/AO
Vol-Page No: 12- 3

Cayton, Sabrina
5005 Stahl Rd.
James Madison High School
San Antonio, TX 78247-0000

Laboratory: AL/AO
Vol-Page No: 12- 4

Chuang, Eleanore
2660 Dayton-Xenia Rd.
Beavercreek High School
Beavercreek, OH 45434-0000

Laboratory: AL/CF
Vol-Page No: 12-10

Ciomperlik, Kara
7173 FM 1628
East Central High School
San Antonio, TX 78263-0000

Laboratory: AL/OE
Vol-Page No: 12-32

Cook, Theresa

Laboratory: WL/MN
Vol-Page No: 15-28

- 0

Cosgrove, Kathlyn
727 E. Hildebrand
Incarnate Word High School
San Antonio, TX 78284-0000

Laboratory: AL/CF
Vol-Page No: 12- 5

Dalley, Kevin
2660 Dayton-Xenia Rd.
Beavercreek High School
Beavercreek, OH 45434-0000

Laboratory: WL/AA
Vol-Page No: 15- 2

Danelo, David
25 Burwood St.
San Antonio Christian School
San Antonio, TX 78216-0000

Laboratory: AL/HR
Vol-Page No: 12-26

HSAP Participant Data

Davis, James
1000 School Ave.
Rutherford High School
Panama City, FL 32404-0000

Laboratory: AL/EQ
Vol-Page No: 12-20

DeBrosse, Nick
3301 Shroyer Rd.
Kettering Fairmont High School
Kettering, OH 45429-0000

Laboratory: WL/PO
Vol-Page No: 15-45

Decker, Michael
2601 Oneida St.
Sauquoit Valley Central School
Sauquoit, NY 13456-0000

Laboratory: RL/ER
Vol-Page No: 14- 8

Deibler, Nancy

Laboratory: WL/MN
Vol-Page No: 15-29

- 0

Dodsworth, Christopher
4916 National Rd.
Northmont High School
Clayton, OH 45315-0000

Laboratory: WL/EL
Vol-Page No: 15- 8

Dominguez, Janette
114 E. Gerald Ave.
Harlandale High School
San Antonio, TX 78214-0000

Laboratory: AL/HR
Vol-Page No: 12-27

Ellena, Brandon
711 Anita Dr.
Tehachapi High School
Tehachapi, CA 93561-0000

Laboratory: PL/RK
Vol-Page No: 13- 9

Ethridge, Blake
7801 Wilshire Blvd.
La Cueva High School
Albuquerque, NM 87122-0000

Laboratory: PL/LI
Vol-Page No: 13- 6

Felderman, James
N. Jackson St.
Tullahoma High School
Tullahoma, TN 37388-0000

Laboratory: AEDC/
Vol-Page No: 16- 2

Feucht, Danny
5833 Student St.
West Carrollton High School
West Carrollton, OH 45418-0000

Laboratory: WL/PI
Vol-Page No: 15-13

HSAP Participant Data

Finch, David
501 Niagara Ave.
Colonel White High School
Dayton, OH 45405-0000

Laboratory: AL/OE
Vol-Page No: 12-33

Focht, Jeremy
2660 Dayton-Xenia Rd.
Beavercreek High School
Beavercreek, OH 45434-0000

Laboratory: WL/ML
Vol-Page No: 15-22

Foley, Jennifer
2660 Dayton-Xenia Rd.
Beavercreek High School
Beavercreek, OH 45434-0000

Laboratory: WL/EL
Vol-Page No: 15- 9

Foth, Angela
501 Mosley Dr.
A. Crawford Mosley High School
Lynn Haven, FL 32444-0000

Laboratory: AL/EQ
Vol-Page No: 12-21

Fowler, Brendon
Chenango Ave.
Clinton Senior High School
Clinton, NY 13323-0000

Laboratory: RL/C3
Vol-Page No: 14- 2

Garcia, Stephanie
650 Ingram
Oliver Wendell Holmes
San Antonio, TX 78238-0000

Laboratory: AL/AO
Vol-Page No: 12- 6

Garcia, Alejandro
2515 Navajo St.
South San Antonio High School
San Antonio, TX 78224-0000

Laboratory: AL/CF
Vol-Page No: 12-11

Garcia, Andrea
6701 Fortuna Rd. NW
West Mesa High School
Albuquerque, NM 87121-0000

Laboratory: PL/SX
Vol-Page No: 13-14

Gavornik, Jeffrey
5110 Walzem Rd.
Roosevelt High School
San Antonio, TX 78239-0000

Laboratory: AL/CF
Vol-Page No: 12-12

Giles, Mark
1204 Harrison Ave.
Bay High School
Panama City, FL 32401-0000

Laboratory: AL/EQ
Vol-Page No: 12-22

HSAP Participant Data

Ginger, David
500 E. Franklin St.
Centerville High School
Centerville, OH 45459-0000

Laboratory: WL/ML
Vol-Page No: 15-23

Gonzalez, Christopher
1400 Jackson-Keller
Robert E. Lee High School
San Antonio, TX 78234-0000

Laboratory: AL/OE
Vol-Page No: 12-34

Gooden, Christie

Laboratory: WL/MN
Vol-Page No: 15-30

-

- 0

Grabowski, Holly
Shawsheen Rd.
Andover High School
Andover, MA 1810-0000

Laboratory: RL/ER
Vol-Page No: 14- 9

Gurecki, David
800 Cypress St.
Rome Catholic High School
Rome, NY 13440-0000

Laboratory: RL/C3
Vol-Page No: 14- 1

Hanna, Melissa
1312 Utica St.
Oriskany Central High School
Oriskany, NY 13424-0000

Laboratory: RL/IR
Vol-Page No: 14-13

Harrison, Deanna

Laboratory: WL/MN
Vol-Page No: 15-31

- 0

Hartsock, David
3491 Upper Bellbrook Rd.
Bellbrook High School
Bellbrook, OH 45305-0000

Laboratory: WL/PO
Vol-Page No: 15-46

Hayduk, Eric
800 Cypress St.
Rome Catholic High School
Rome, NY 13440-0000

Laboratory: RL/OC
Vol-Page No: 14-16

Hemmer, Laura

Laboratory: WL/MN
Vol-Page No: 15-32

- 0

HSAP Participant Data

Mill, Thuan
North Jackson St.
Tullahoma High School
Tullahoma, TN 37388-0000

Laboratory: AEDC/
Vol-Page No: 16- 3

Hodges, Melanie
5833 Student St.
West Carrollton High School
West Carrollton, OH 45418-0000

Laboratory: WL/PO
Vol-Page No: 15-47

Jeffcoat, Mark

Laboratory: WL/MM
Vol-Page No: 15-33

- 0

Jost, Tiffany
Lincoln Rd.
Lincoln-Sudbury Regional High
Sudbury, MA 1776-0000

Laboratory: PL/GP
Vol-Page No: 13- 2

Kitty, Alexandra
3900 W. Peterson
Our Lady of Good Counsel High
Chicago, IL 60659-3199

Laboratory: PL/RK
Vol-Page No: 13-10

Kozlowski, Peter
500 E. Franklin St.
Centerville High School
Centerville, OH 45459-0000

Laboratory: WL/ML
Vol-Page No: 15-24

Kress, Barry

Laboratory: WL/MM
Vol-Page No: 15-34

- 0

Kulesa, Joel
940 David Rd.
Archbishop Alter High School
Kettering, OH 45429-0000

Laboratory: WL/EL
Vol-Page No: 15-10

Lormand, Bradley
PO Drawer CC
Rosamond High School
Rosamond, CA 93560-0000

Laboratory: PL/RK
Vol-Page No: 13-11

Maloof, Adam
251 Waltham St.
Lexington High School
Lexington, MA 2173-0000

Laboratory: RL/ER
Vol-Page No: 14-10

HSAP Participant Data

Marlow, Chris
925 Dinah Shore Blvd.
Franklin County High School
Winchester, TN 37398-0000

Laboratory: ARDC/
Vol-Page No: 16- 4

Martin, Amy
3301 Shroyer Rd.
Kettering Fairmont High School
Kettering, OH 45429-0000

Laboratory: WL/FI
Vol-Page No: 15-15

Matthews, Suzanne
5323 Montgomery NE
Del Norte High School
Albuquerque, NM 87109-0000

Laboratory: PL/SX
Vol-Page No: 13-15

McEuen, Eric
800 Odalia Rd. NE
Albuquerque High School
Albuquerque, NM 87102-0000

Laboratory: PL/VT
Vol-Page No: 13-17

McGovern, Scott
3491 Upper Bellbrook Rd.
Bellbrook High School
Bellbrook, OH 45305-0000

Laboratory: WL/AA
Vol-Page No: 15- 3

McPherson, Sandra
Jefferson & Grove St.
Bishop Brossart High School
Alexandria, KY 41001-0000

Laboratory: WL/ML
Vol-Page No: 15-25

Mange, Sean
Route 294
Adirondack High School
Boonnville, NY 13309-0000

Laboratory: RL/C3
Vol-Page No: 14- 3

Merrill, Benjamin
3491 Upper Bellbrook Rd.
Bellbrook High School
Bellbrook, OH 45305-0000

Laboratory: WL/FI
Vol-Page No: 15-16

Middleton, Charles
4524 Linden Ave.
Carroll High School
Dayton, OH 45432-0000

Laboratory: WL/FI
Vol-Page No: 15-17

Miksch, Virginia
727 E. Hildebrand
Incarnate Word High School
San Antonio, TX 78284-0000

Laboratory: AL/CF
Vol-Page No: 12-13

HSAP Participant Data

Moore II, Elliot

Laboratory: WL/MN
Vol-Page No: 15-35

, - 0

Morris, Rebecca
727 E. Hildebrand
Incarnate Word High School
San Antonio, TX 78284-0000

Laboratory: AL/HR
Vol-Page No: 12-28

Morton, Gilbert
2001 McArthur Dr.
Coffee County Central High Sch
Manchester, TN 37355-0000

Laboratory: AEDC/
Vol-Page No: 16- 5

Neitzel, Laura
N. St. Mary's
Providence High School
San Antonio, TX 78215-0000

Laboratory: AL/OE
Vol-Page No: 12-35

Nguyen, Quynhtrang
5833 Student St.
West Carrollton High School
West Carrollton, OH 45418-0000

Laboratory: AL/CF
Vol-Page No: 12-14

Nielsen, Eric
500 Turin Rd.
Rome Free Academy
Rome, NY 13440-0000

Laboratory: RL/C3
Vol-Page No: 14- 4

Northcutt, Chris
925 Dinah Shore Blvd.
Franklin County High School
Winchester, TN 37398-0000

Laboratory: AEDC/
Vol-Page No: 16- 6

Olson, Amanda
1000 School Ave.
Rutherford High School
Panama City, FL 32404-0000

Laboratory: AL/EQ
Vol-Page No: 12-23

Ondrusek, Kimberly
7173 FM 1628
East Central High School
San Antonio, TX 78263-0000

Laboratory: AL/HR
Vol-Page No: 12-29

Ortiz, Benjamin
6701 Fortuna Rd. NW
West Mesa High School
Albuquerque, NM 87105-0000

Laboratory: PL/LI
Vol-Page No: 13- 7

HSAP Participant Data

Page, Melissa
501 Mosley Dr.
A. Crawford Mosley
Lynn Haven, FL 32444-5609

Laboratory: WL/FI
Vol-Page No: 15-18

Panara, Michael
500 Turin St.
Roma Free Academy
Roma, NY 13440-0000

Laboratory: RL/C3
Vol-Page No: 14- 5

Penn, Alexander

Laboratory: WL/MN
Vol-Page No: 15-36

-

- 0

Perry, Kyle

Laboratory: WL/MN
Vol-Page No: 15-37

Crestview High School

- 0

Pletcher, Mary

Laboratory: WL/MN
Vol-Page No: 15-38

- 0

Pletl, Anne
Burrstone Rd.
Notre Dame
Utica, NY 13502-0000

Laboratory: RL/C3
Vol-Page No: 14- 6

Prevost, Daniel
3301 Shroyer Rd.
Kettering Fairmont High School
Kettering, OH 45429-0000

Laboratory: WL/PO
Vol-Page No: 15-48

Price, Kristy
North Jackson St.
Tullahoma High School
Tullahoma, TN 37388-0000

Laboratory: AEDC/
Vol-Page No: 16- 7

Protz, Christopher
501 Mosley Dr.
A. Crawford Mosley High School
Lynn Haven, FL 32444-5609

Laboratory: AL/EQ
Vol-Page No: 12-24

Rader, Thomas
1505 Candelaria NW
Valley High School
Albuquerque, NM 87107-0000

Laboratory: PL/WS
Vol-Page No: 13-20

HSAP Participant Data

Ray, Kristopher
401 Eagle Blvd.
Shelbyville Central High School
Shelbyville, TN 37160-0000

Laboratory: AEDC/
Vol-Page No: 16- 8

Reed, Tracy
711 Anita Dr.
Tehachapi High School
Tehachapi, CA 93561-0000

Laboratory: PL/RK
Vol-Page No: 13-12

Riddle, Cheryl
Highway 55
Moore County High School
Lynchburg, TN 37352-0000

Laboratory: AEDC/
Vol-Page No: 16- 9

Rodriguez, Luis
5400 Chambersburg Rd.
Wayne High School
Huber Heights, OH 45424-0000

Laboratory: AL/CF
Vol-Page No: 12-15

Rosenbaum, David

Laboratory: WL/MN
Vol-Page No: 15-39

- 0

Salinas, Carol
727 E. Hildebrand
Incarnate Word High School
San Antonio, TX 78212-0000

Laboratory: AL/CF
Vol-Page No: 12-16

Schanding, Sarah
7173 FM 1628
East Central High School
San Antonio, TX 78162-0000

Laboratory: AL/CF
Vol-Page No: 12-17

Schatz, William
500 Turin St.
Rome Free Academy
Rome, NY 13440-0000

Laboratory: RL/IR
Vol-Page No: 14-14

Schindler, David
Drawer 1300
Los Lunas High School
Los Lunas, NM 87031-0000

Laboratory: PL/LI
Vol-Page No: 13- 8

Senus, Joe
500 Turin St.
Rome Free Academy
Rome, NY 13440-0000

Laboratory: RL/IR
Vol-Page No: 14-15

HSAP Participant Data

Servaites, Jonathan
500 E. Franklin St.
Centerville High School
Centerville, OH 45459-0000

Laboratory: WL/PO
Vol-Page No: 15-49

Shao, Min
869 Massachusetts Ave.
Arlington High School
Arlington, MA 2174-0000

Laboratory: PL/GP
Vol-Page No: 13- 3

Simon, Ryan
701 E. Home Rd.
Springfield North High School
Springfield, OH 45503-0000

Laboratory: AL/OE
Vol-Page No: 12-36

Smith, Adam
Phillips Academy
Andover, MA 1810-0000

Laboratory: PL/GP
Vol-Page No: 13- 4

Solscheid, Jill
500 E. Franklin St.
Centerville High School
Centerville, OH 45459-0000

Laboratory: AL/OE
Vol-Page No: 12-37

Spry, David
555 N. Hyatt St
Tippecanoe High School
Tipp City, OH 45371-0000

Laboratory: WL/PO
Vol-Page No: 15-50

Starr, Jennifer
221 E. Trotwood Blvd.
Trotwood Madison Sr. High Scho
Trotwood, OH 45426-0000

Laboratory: WL/AA
Vol-Page No: 15- 4

Strickland, Jefferey
501 Mosley Dr.
A. Crawford Mosley High School
Lynn Haven, FL 32444-0000

Laboratory: WL/PI
Vol-Page No: 15-19

Tecumseh, Tony
5323 Montgomery NE
Del Norte High School
Albuquerque, NM 87110-0000

Laboratory: PL/VT
Vol-Page No: 13-18

Terry, Nathan
75 Chenango Ave.
Clinton High School
Clinton, NY 13323-0000

Laboratory: RL/ER
Vol-Page No: 14-11

HSAP Participant Data

Thomson, Randy

Laboratory: WL/MN

Vol-Page No: 15-40

, - 0

Triana, Zayda

Laboratory: AL/AO

727 E. Hildebrand

Vol-Page No: 12- 7

Incarnate Word High School

San Antonio, TX 78212-2598

Trossbach, Christina

Laboratory: WL/MN

Vol-Page No: 15-41

, - 0

Tseng, Miranda

Laboratory: WL/FI

3301 Shroyer Rd.

Vol-Page No: 15-20

Kettering Fairmont High School

Kettering, OH 45429-0000

Tutin, Darcie

Laboratory: WL/MN

Vol-Page No: 15-42

, - 0

Vaill, Christopher

Laboratory: RL/OC

Route 31

Vol-Page No: 14-17

Vernon-Verona-Sherrill Central

Verona, NY 13478-0000

Ward, Jon

Laboratory: WL/MN

Vol-Page No: 15-43

, - 0

Waterman, Sara

Laboratory: AEDC/

North Jackson St.

Vol-Page No: 16-10

Tullahoma High School

Tullahoma, TN 37388-0000

Weidner, Suzanne

Laboratory: AL/OE

7173 FM 1628

Vol-Page No: 12-38

East Central High School

San Antonio, TX 78263-0000

West, Johnny

Laboratory: WL/AA

2026 Stapleton Court

Vol-Page No: 15- 5

Belmont High School

Dayton, OH 45404-0000

HSAP Participant Data

Wick, Matthew
6400 Wyoming Blvd.
Albuquerque Academy
Albuquerque, NM 87109-0000

Laboratory: PL/WS
Vol-Page No: 13-21

Williams, Scott
3511 Dayton-Xenia Rd.
Beavercreek High School
Beavercreek, OH 45434-0000

Laboratory: WL/AA
Vol-Page No: 15- 6

Wright, Rudy
6701 Fortuna Rd. NW
West Mesa High School
Albuquerque, NM 87121-0000

Laboratory: PL/SX
Vol-Page No: 13-16

Young, Matthew
5005 Stahl Rd.
James Madison High School
San Antonio, TX 78247-0000

Laboratory: AL/OE
Vol-Page No: 12-39

Zimmerman, Amy
4524 Linden Ave.
Carroll High School
Dayton, OH 45432-0000

Laboratory: AL/CF
Vol-Page No: 12-18

PROGRAMMING IN ADA

Jason P. Carranza

AAAF3

Wright-Patterson Air Force Base

Final Report for:

AFOSR Summer Research Program

Wright Laboratory

Sponsored by:

Air Force Office of Scientific Research

August 1993

1-1

PROGRAMMING IN ADA

Jason P. Carranza
WL/AAAF3
Wright-Patterson Air Force Base

ABSTRACT

During the summer of 1993, I participated in the Air Force Office of Scientific Research (AFOSR) High School Apprenticeship Program as an apprentice of Charles B. Hicks at Wright-Patterson Air Force Base. During this time, my main goal was to learn the computer language "Ada". The first half of my summer was spent learning and reading about "Ada". In order to improve my programming skills, I wrote numerous programs and sections of source code. By the second half of the summer I was able to write full programs, packages, and associated testdrivers with little outside help. It was during this time that I finished my project which dealt with improving and completing a project initially started by a former AFOSR student. Using the many advantages of "Ada", I completed the project successfully within the allotted time.

PROGRAMMING IN ADA

Jason P. Carranza

INTRODUCTION

With a small amount of actual experience with computers, I was at first hesitant when starting the High School Apprenticeship Program. I had only minor experience with computer games and programming and had never experienced the wide variety of computer systems and software development environments available at WL/AAAF3. During the program, I gained invaluable knowledge with a VAX-VMS computer system and a SUN workstation. With the use of these two computers I was able to experience the advantages and disadvantages of different Ada compilers and development environments. The Vi editor, which is available on most UNIX workstations, was much more difficult to use due to the utilization of two modes: the command mode, and the insert mode. Even though the Vi editor was much harder to understand, once a person becomes familiar with the Vi environment, it is a quick, effective, and versatile tool. The Language Sensitive Editor (LSE) on the VAX-VMS was much easier to use and understand because it did not have the confusing modes that the Vi editor had. In addition, the LSE was more user-friendly. However, the LSE was not as versatile as the Vi editor and was more limiting in what it could do.

DISCUSSION

My first few weeks were spent learning how to use the VAX-VMS system, then learn "Ada" from the Ada-Tutor on the VAX-VMS system. Before coming to this job, I already had one year of programming in Turbo Pascal from high school. Because of this important experience, I was able to learn "Ada" quickly. After first relearning about enumerated types, arrays, records,

recursion, strings,...,etc., I learned about linked lists and packages.

During this relearning stage, I realized how similar "Ada" was to Turbo Pascal. Many of the variable declarations as well as the procedure declarations were basically the same, except for functions which were only slightly different. Recursion declarations was one of the "Ada" structures that I had a great deal of problems with. In the Ada Programmer's Handbook by Dean W. Gonzalez, it defines recursion as "the use of a particular entity to define itself". To sum it up, recursion is when code calls itself. For example, a procedure might call itself when incorrect input is given as an error checking device. Instead of writing a large number of lines over, the procedure calls itself and starts over again. The only drawback with recursion is that it uses a great amount of memory. However, with the use of recursion, the source code of a procedure is shorter, but is generally harder to understand.

Functions in Turbo Pascal are slightly different than functions in "Ada". In Turbo Pascal, input/output (I/O) statements such as, `writeln("Hello")`, cannot be written in the function body. Also in Turbo Pascal, the function name is the variable that is being returned. Ada allows I/O statements to be in the function body. In "Ada", the programmer has to define a separate variable to be returned, instead of using the function name as the variable.

Linked lists are a very important part of "Ada". Instead of using arrays, which use a great amount of memory, linked lists are used. When arrays are declared, a certain amount of memory is set aside for that one array. In a linked list, no memory is initially set aside. When memory is needed, a linked list will use that one memory space. During the program, if the link is no longer needed, it can easily be given back to the computer for

other uses. In an array, the space set aside is not given back to the computer until the program is terminated.

There are two types of linked lists: single linked lists, and double linked lists. Pointers are the basis of both single linked lists and double linked lists. Pointers are defined as a variable that holds an address of another variable. Pointers organize the linked list into a chain of links by keeping track of where all the addresses of the information or storage/memory spaces are. Pointers are initially set to point to null or nothing. When information needs to be added, the pointer points to an address where information can be stored. When the storage space is no longer needed, it can be given back to the computer for other purposes.

SINGLE LINKED LIST



Figure 1

In a single linked list, there are two pointers used: the head, and tail (refer to Figure 1). The head points to the first address while tail points to the last address in a list. What points to the addresses in the middle of the linked list? The answer is simple. At each address is stored an internal pointer (.next). When a new link is added, this internal pointer (.next) points toward the new address and continues to point to that address until told otherwise. The internal pointer (.next) in the new address points toward the address that the old pointer used to point towards. During this whole time, the tail points toward the last piece of information. If a new link is

added after the tail, then the tail is moved to point towards that new last piece of information. To sum everything up, everything between head and tail points in one direction and is linked like a chain with head at the beginning and tail at the end. If one link of a chain is added, the link before and after the new link has to be connected to the new link.

DOUBLE LINKED LIST

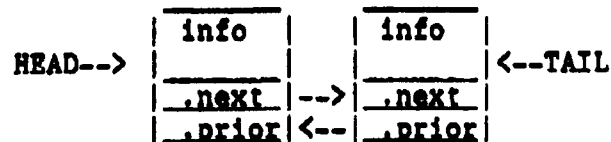


Figure 2

A double linked list is essentially the same as a single linked list except that there are two internal pointers (.next, .prior) in an address (refer to Figure 2). Instead of each link pointing towards the next link, one pointer points toward the link or address ahead of it (.next), and the other pointer points towards the link or address behind it (.prior).

After exploring linked lists, I spent two weeks struggling to learn strings, mainly the disadvantages of strings in "Ada". Strings are very limiting in "Ada". Characters and integers each have a package designed to be used specifically for characters and integers, while strings do not have such a package. I had to write a package designed to do exactly this called, STRFNS. This package allowed me to compare, search, translate, and assign strings to other strings.

After my uphill battle with strings, I worked with a text package called, TEXT. Using variables defined as type text was much easier than using

many different variables for one string. The type text consisted of a record of a string and an integer. The string held the value of the input, while the integer would store the length of the string. Instead of using many different variables, I could use one variable that held all the information I needed. I wrote a package for type text similar to that of strings, except that this package went a little further. The TEXT package was programmed to compare variables of type text, translate strings into type text, get input of type text, and give output of type text. It took me two days to write the text package, compared to two weeks for the string package.

Through my experience with the assorted packages I programmed, I had the chance to finally comprehend packages. Until this summer, I had only used packages, but had never written or really understood one. Packages are a valuable advantage of "Ada". There are two parts to a package: the package specification, and the package body. The package specification contains the variable declarations for the package body and also contains all the function and procedure names the programmer may use. It does not, however, contain the source code of the functions and procedures, only the names and comments. The package body contains the functions and procedures along with the source code. When using a package, the user only sees the package specification, not the package body. Another advantage of packages is that a programmer can save a great deal of time because the programmer does not have to continue writing the same source code over for each program. He calls the package name in the program, and all the functions and procedures in that package specification is at the use of the programmer.

Results

After working with most of the different source code structures of "Ada",

I started my final project. The point of this project was to prove how far I had advanced in programming with "Ada". I was given the source code of a multi-package program which ran a menu for a VAX-VMS system. The code was poorly written, and wasn't versatile enough because it could only run on one specific VAX-VMS system. Originally, the program was about 1200 lines. After deleting a large amount of code, adding several procedures, and adding in error checking structures, the program was 1000 lines.

CONCLUSION

When looking back over the whole summer, I know I learned a great deal. During this summer, I realized that I want to work with computers. The experience I gained with computers and computer programming in "Ada" will help me at any college that I attend and also will help me in future jobs dealing with computers.

Computer Performance in Function Decomposition

Kevin M. Dalley

**Final Report for:
High School Apprenticeship Program
Air Force Office of Scientific Research**

**System Concepts Group
Avionics Directorate
Wright Laboratory**

August 16, 1993

**Computer Performance
in Function
Decomposition**

Kevin M. Dalley

Abstract

The growth rate of run times of function decomposition with a tabular and non-tabular setting using a fixed number of cares was studied. To start with, six random recursive functions were chosen having an input range from 8 to 14 variables with the output of this function being a binary string. Portions of this binary string were then "masked" in two forms, one tabular and the other non-tabular. This masking is done by taking a fixed number of cares from the binary string and leaving the placement of the others in a don't care format where the polarity is not known. Then a computer program attempts to decompose the function into sub-functions and the run time is recorded. After the results were gathered, The non-tabular setting had better performance in low number of cares experiments, while the tabular stayed constant no matter what number of cares were used.

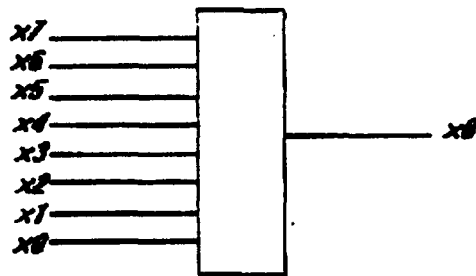
**Computer Performance
in Function
Decomposition**

Kevin M. Dalley

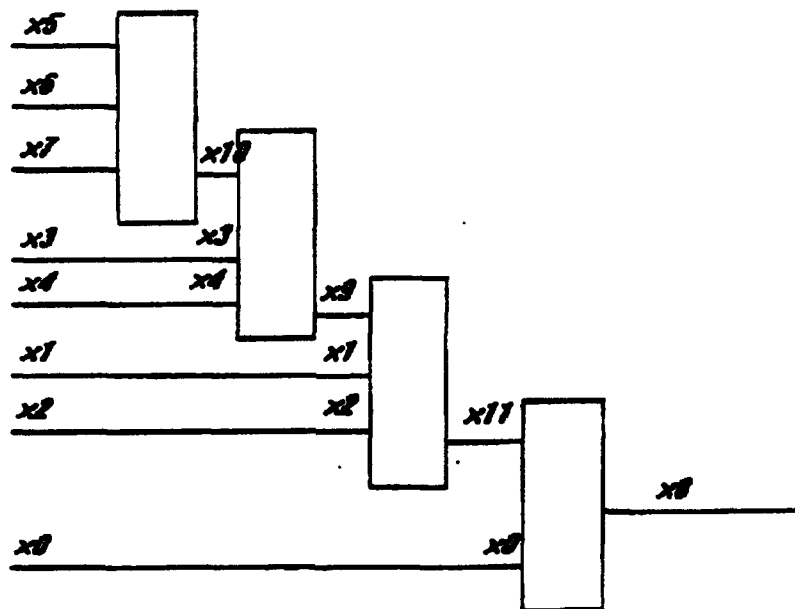
Introduction

In recent computer testing, programmers and researchers are trying to develop a type of "pattern sensitive" program that can detect order, structure or regularity [1] in a natural environment. The problem is to make a program robust enough in order to detect all of the many patterns that appear. A way to show "pattern-ness" is through Decomposed Function Cardinality (DFC). The DFC can be found for any problem containing a sense of order or structure to it. The researchers of Pattern Theory at Wright Labs have developed FLASH (Function Learning and Synthesis Hotbed) along with a technical report [2], a program planned to be a robust pattern finding algorithm that will create a function, take the binary output from that function and sample the elements (take a given portion of "cares" and leave the others "masked"), reconstruct the original function from the sampled data, and find the DFC of the function.

This program was the key tool to the studies and experiments practiced here. This is a physical example of an undecomposed Benchmark Function (#19). (The Benchmark Functions are a standardized group of 30 different 8 variable functions used by AART for groups of partition and other decomposition plan testing.)



This is an example of the same Benchmark Function (#19) decomposed.



Discussion of Problem

The primary objective of the program that my work evolved around was set to determine the "tabular" versus "non-tabular" growth rates for a fixed number of "cares" using randomly generated functions, then taking a sampling of those for decomposition and finally recording the time that it took to decompose the sampled binary string. This data gathered from the run time of these would be set into graphs and charts to see which version would have better performance.

Methodology

The two approaches, tabular and non-tabular, are two different ways of recording the binary string. The tabular approach is where the string listed in a long string of cares and don't cares. The cares are represented as 1's or 0's and the don't cares are represented as X's. The number of variables directly determines the number of elements in the binary string in an exponential form. Therefore, if using 8 variables, then there would be 256 elements of that created binary string consequently, using 14 variables would create a binary string of 16384 elements in length. Depending on the size of the string, the number of sampled cares went from 64 cares to 100% cares. Therefore, the tests run on an 8 variable function would work with 64 cares, 128 cares, and 256 cares which is 100% cares, seeing as there are 256 elements.

Example of tabular 64 "cares" 8 variable random function.

```
XX0X1XXX0XX1XX0XX1XX01X0XXX1XXX0XX1XX01XXX1XXX0XXX1XXXXXX
XXX0XX1XXX0XXX0XXX1XXX0XX0XX0XX0XXX1XXX1XXXXXX1XX0XX1XXX0XXX
XXX1XXXXXXX1XXX1XXXXXXX1XX1XX1XX0XX0XXX11XXX1XXX1XX1XXXXX
XX1XXXX1XXX0XXXX1XXX0XX0XXX1XX0XX0X1XXX0XX1XXX1XXX0XXX
X0XX1XXX1XX0XX1X
```

The non-tabular approach is different only by the way that it stores the binary string. The placement of each care is recorded along with the polarity of that care, and the don't cares are not recorded in the new file. The following example is a portion of an example of a non-tabular 64 care 8 variable random function.

Example of non-tabular 64 "cares" 8 variable random function

```
3 1
4 0
6 0
11 1
17 1
25 0
33 0
43 1
50 0
56 0
57 1
58 0
65 1
70 0
71 1
77 0
79 1
83 1
85 0
90 0
93 1
96 0
```

If the previous example was not a "portion" the data set would continue on until there were 64 entries (cares).

The reason that these two procedures were chosen is for the fact that when you have a 14 variable function, the decomposition program will have to look through 16384 different cares and don't cares in a tabular approach regardless of the number of cares chosen, while the non-tabular approach only has to look through the number of cares given. For example, a 14 variable function is running on both tabular and non-tabular with 128 cares; the decomp plan (the pre-determined form that FLASH tries to find the DFC of a function) will have to scan through 16384 elements in the tabular before decomposition, whereas the non-tabular will only have 128 elements. Because of this, the hypothesis was that the non-tabular would perform better than the tabular. With this in mind, all the test runs were executed from 8 to 14 variables and from 64 cares to all cares. This data is what is the bulk of my report.

Being that a computer can not spontaneously generate a random number, a seed must be given to the computer as a basis for the randomness. With this seed, the computer does many redundant math processes so as to make the final output a number highly unrelated to the original seed. When the computer creates the random function, it automatically uses the seed of 0 in it's computations; therefore, if two functions were made the same way, then the output should be verbatim. When the random samples are taken from the random function's binary string, FLASH prompts the user for a seed. For a basis of comparison, the seed was chosen to be 1 and stayed that way throughout all experiments. Likewise, if those two same functions were sampled the same way, the new binary strings would be verbatim. The actual values of 0 and 1 have no significance in themselves, but

just the fact that they are constant throughout all experiments is enough to eliminate the varying degree in the experiments.

Some of the data gathered from the standard FLASH run times from decomposition had surprising results. Because of this, some excursions were chosen to see how these differences related to the standard testing. These excursions varied with select experiments from 12 to 14 variables and from 128 cares to 512 cares. The first excursion that was done was a constant 0. In these tests, instead of having a random function create a random binary string, the binary string had a constant 0. From this, samples were taken and then decomposed. The second and third excursions were done using the same random binary strings, but this time, changing the decomp plan. The decomp plan is the way that FLASH sets up the partitions and the direction that it scans the binary string for the decomposition. The two excursions were Mostly Row and Mostly Column. In Mostly Row, it scans mostly the rows in the decomposition, and in Mostly Column, it scans mostly columns.

Results

Tables 1 and 2 show the run time growth in tabular and non-tabular FLASH runs using the standard procedures with random functions. The horizontal axis of the two charts represents the number of variable inputs. The vertical axis represents the number of cares. The blank portions in tables 1 and 2 are the impossible experiments, where the number of cares exceeds the elements in the binary string. Tables 5 through 10 are charts of the excursions done. Tables 3 and 4 are portions of table 1 and 2 used for comparison with the excursion tables. Likewise in these charts, the horizontal axis is number of variables, and the vertical bar is number of cares.

Run Times for tabular and non-tabular FLASH runs

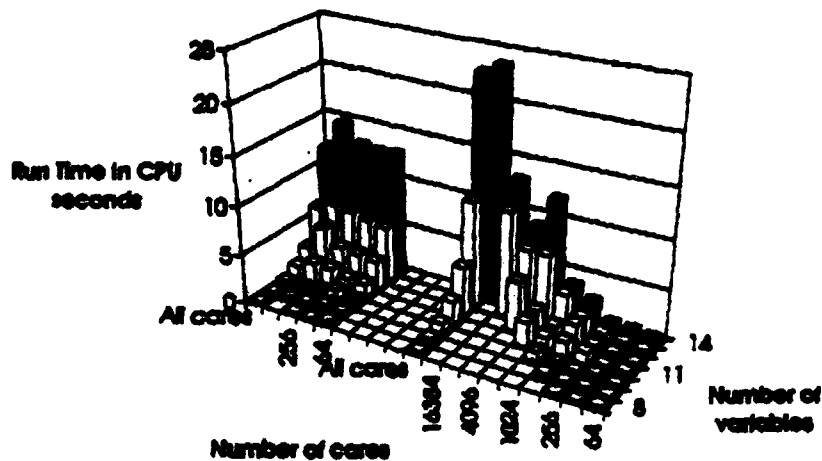
# of cases	# of variable inputs						
	8	9	10	11	12	13	14
512	0.129	0.312	0.59	1.383	2.586	6.164	11.749
256	0.132	0.367	0.657	2.066	3.508	6.874	14.55
128	0.14	0.558	1.211	1.559	3.289	6.116	12.577
64	0.293	0.367	0.774	1.476	3.015	5.859	12.703

Table 1: Tabular approach

# of cases	# of variable inputs						
	8	9	10	11	12	13	14
All cases	0.23	0.547	1.109	2.469	5.101	10.992	22.589
16384							23.615
8192						10.89	13.108
4096					5.168	7.484	8.874
2048				2.488	2.731	7.414	12.008
1024			1.148	1.527	1.645	3.898	3.797
512		0.55	0.586	1.609	2.402	2.133	2.718
256	0.25	0.332	0.332	1.21	0.836	0.997	0.965
128	0.133	0.426	0.613	0.442	0.66	0.715	0.753
64	0.246	0.192	0.183	0.383	0.214	0.441	0.535

Table 2: Non-Tabular approach

Run Time for tabular and non-tabular FLASH runs



Run Time data for decomposition plan excursions

Tabular

# of cases		# of variables		
		12	13	14
	512		6.874	
	256	3.508	6.597	12.78
	128		6.116	

Table 3: Tabular Random

Non-Tabular

# of cases		# of variables		
		12	13	14
	512		2.133	
	256	0.836	0.997	0.965
	128		0.716	

Table 4: Non-Tabular Random

# of cases		# of variables		
		12	13	14
	512		5.659	
	256	2.734	5.706	11.91
	128		5.665	

Table 5: Tabular Constant

# of cases		# of variables		
		12	13	14
	512		1.051	
	256	0.57	0.613	0.821
	128		0.571	

Table 6: Non-Tabular Constant

# of cases		# of variables		
		12	13	14
	512		5.374	
	256	2.527	5.347	17.448
	128		5.367	

Table 7: Tabular Most Row

# of cases		# of variables		
		12	13	14
	512		0.684	
	256	0.325	0.334	0.871
	128		0.184	

Table 8: Non-Tabular Most Row

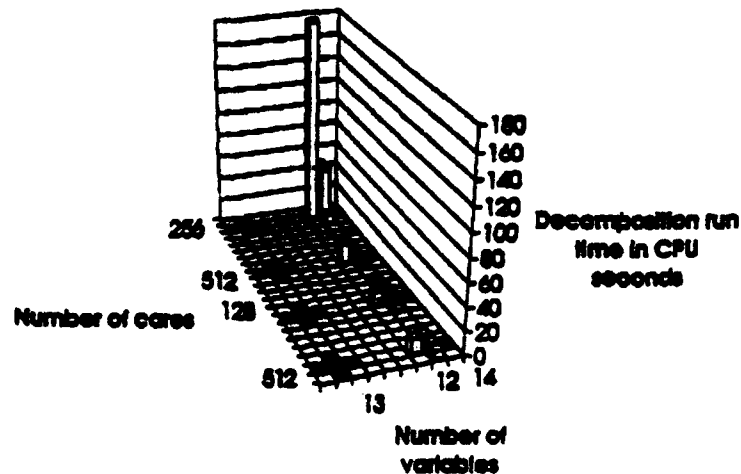
# of cases		# of variables		
		12	13	14
	512		7.973	
	256	2.898	45.606	179.247
	128		45.536	

Table 9: Tabular
Most Column

# of cases		# of variables		
		12	13	14
	512		1.582	
	256	0.836	0.664	1.199
	128		0.485	

Table 10 Non-Tabular
Most Column

Run Time data for decomposition plan excursions



The results for the tabular run times in standard testing showed that the testing is not very sensitive to the given number of cares in each experiment, but there is an exponential growth in incrementation from variable to variable. The non-tabular standard test runs, however, show great sensitivity to the number of cares chosen and the number of variables used. Only on all cares does the growth appear to be exponential. With small amounts of cares, the growth is minimal, and with larger amounts of cares, the growth is increased.

In the Constant excursions, the run time was better for non-tabular vs. tabular, and all the Constant excursions had faster run times than the standard random counter parts. The Most Row tabular excursion correlated well with the Constant tabular excursion, but the Most Row non-tabular excursion ran faster than the Constant non-tabular excursion. There were some definite differences with the Most Column tabular excursion, seeing as the 14 variable test was ten times slower than the Most Row tabular excursion, and the 13 variable 128 and 256 care experiments were about nine times slower than the Most Row tabular excursion. However, the Most Column non-tabular excursion did not differ highly from the other excursions. In decomposition, if the function has a good DFC, then it will decompose. A problem encountered, was that with random functions having a good DFC will spend time in those sub-functions and decompose them. This adds run time to those functions with better DFC's, but not to those of which with bad DFC's.

Conclusion

The results of the standard experiments show that the performance of the non-tabular is greater than that of tabular in small care sampling, but gets worse than that of tabular when the number of cares closes toward all cares. The run time for a non-tabular approach is not very sensitive to the type of decomposition or the type of binary string.

The tabular is not very sensitive to the type of binary string, but does not work well with a Mostly Column decomp plan. After working with FLASH, a bug was found in the program that caused the computer to spend tremendous amounts of time resolving a small bit of code in the program.

References

[1] Dr. Timothy D. Ross, Michael J. Noviskey, Timothy N. Taylor, and David A. Gadd. *Pattern Theory: an Engineering Paradigm for Algorithm Design*. Final Technical Report WL-TR-91-1069, Wright Laboratory, USAF, WL/AART, WPAFB, OH 45433-6543, August 1991

[2] Dr. Timothy D. Ross. *Function Decomposition Strategy for the Function Learning and Synthesis Hotbed*. Technical Memorandum, Wright Laboratory, USAF, WL/AART, WPAFB, OH 45433-6543, August 1992.

Appendix A

The decomposition plan used for standard FLASH runs is the following:

Decomp Plan:

Selection Plan:

0 = use shared variables

12 = method

2 = first part type

1 = stopping condition

1 = stopping condition parameter

Evaluation Plan:

1 = no of partition tests

1 = measure challenger by

1 = measure champ by

4 = threshold in n

1 = champ_multiplier

1 = Random No generator seed (>0)

1 = dp_for_best_part_children_is_same

Appendix B

The decomposition plan used for Mostly Row FLASH runs is the following:

Decomp Plan:

Selection Plan:

- 0 = use shared variables**
- 11 = method**
- 0 = first part type**
- 1 = stopping condition**
- 1 = stopping condition parameter**

Evaluation Plan:

- 1 = no of partition tests**
- 1 = measure challenger by**
- 1 = measure champ by**
- 4 = threshold in n**
- 1 = champ_multiplier**
- 1 = Random No generator seed (>0)**
- 1 = dp_for_best_part_children_is_same**

Appendix C

The decomposition plan used for Mostly Column FLASH runs is the following:

Decomp Plan:

Selection Plan:

0 = use shared variables

12 = method

0 = first part type

1 = stopping condition

1 = stopping condition parameter

Evaluation Plan:

1 = no of partition tests

1 = measure challenger by

1 = measure champ by

4 = threshold in n

1 = champ_multiplier

1 = Random No generator seed (>0)

1 = dp_for_best_part_children_is_same

Appendix D

Actual partitions for each decomp plan used.

	Standard	Mostly Column	Mostly Row
Number 8	10001111	10000000	01111111
of 9	000001111	100000000	011111111
Variables 10	1000011111	1000000000	0111111111
11	00000011111	10000000000	01111111111
12	100000111111	100000000000	011111111111
13	0000000111111	1000000000000	0111111111111
14	10000001111111	10000000000000	01111111111111

**FINAL REVIEW OF SOFTWARE PACKAGES USED IN VARIOUS
COMMUNICATION APPLICATIONS**

Scott McGovern

Junior

**Bellbrook High School
3491 Upper Bellbrook Road
Bellbrook, Ohio 45305**

**Final Report for:
AFOSR Summer Research Program, Wright Laboratory,
Electronic Warfare Division**

**Sponsored by: Air Force Office of Scientific Research
Research & Development Laboratories, Culver City, CA**

August 1993

FINAL REVIEW OF SOFTWARE PACKAGES USED IN VARIOUS COMMUNICATION APPLICATIONS

**Scott McGovern
Junior
Bellbrook High School**

Abstract

Contained within this report are evaluations of software packages used in the day-to-day operation in electronic warfare and communications. Harvard Graphics, Mathcad, DADiSP, Graph Tool, Microsoft Visual Basic and Excel were evaluated. A brief explanation of each program will be followed by the application for which it was used.

FINAL REVIEW OF SOFTWARE PACKAGES USED IN VARIOUS COMMUNICATION APPLICATIONS

Scott McGovern

Introduction

Today's engineer is almost dependent on his computer. Most of the work he does in the day is done on his computer. He can create a waveform, plot it, and analyze it without getting up from his chair. This can be accredited to the growing power of the computer. Everyday advancements are being made, making life easier for computer users. To take advantage of these advancements people have to buy the software. Most of these advanced software packages are very expensive. For a new program, a person might be looking at a \$25,000 price tag, or even more. Though this software isn't for the everyday user but for business, the price is still high. Another setback with the growth of technology is the learning time. Many of these new programs are very complex. These software packages can sit on the shelf for months due to the lack of time to learn how to use the program. These problems are overshadowed by the amazement of the advances in the computer world. Hopefully as computers advance even further, these problems will be fixed.

GraphTool

GraphTool is designed to plot information on different types of graphs and charts. GraphTool has the ability to graph in two or three dimensions. It lets the user plot area charts, bar charts, xy plots, column charts, pie charts, scatter plots, and vector plots in two dimensions. It is able to plot carpet plots, earth plots, scatter plots, shadow-contour plots, surface plots, and vector plots in three dimensions. The program is easy to use and self-explanatory. The different menus guide the user through the program with little to no difficulty. With the exception of some three dimensional plots, GraphTool is quick to plot the information provided by the user and edits the plot as soon as the generating equation is edited.

As a project on GraphTool, I used the Gauss Function

$$f(xy) = e^{-\pi \left[\frac{x-x_0}{b} \right]^2} + e^{-\pi \left[\frac{y-y_0}{b} \right]^2}$$

to create three different graphs. The purpose of this application is to measure the intensity of light, for instance, when shone at a figure. At the tip of the figure the light is the most intense. As the light goes around the object it becomes weaker. Figures 1, 2, and 3 show this theory. Changing the variables in the equation changes the size and the shape of the figure as shown.

For the first graph I made $x_0 = 0$, $y_0 = 0$, and $b = 1$. This produced what is seen in Figure1. For the second plot, Figure2, I edited the equation, making $x_0 = 1$, $y_0 = 1$, and $b = 1$. This centered the figure at 1,1 instead of 0, as it was before. Finally, I edited the equation once more, this time making $x_0 = 0$, $y_0 = 0$ and $b = 2$. As seen in Figure3, the figure expanded, becoming wider, while staying centered at 0.

Figure 1

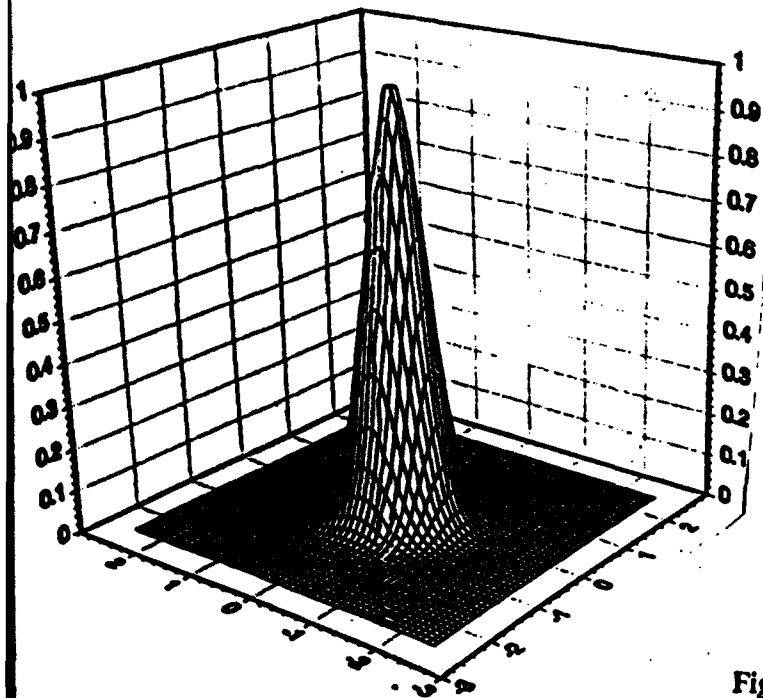


Figure 2

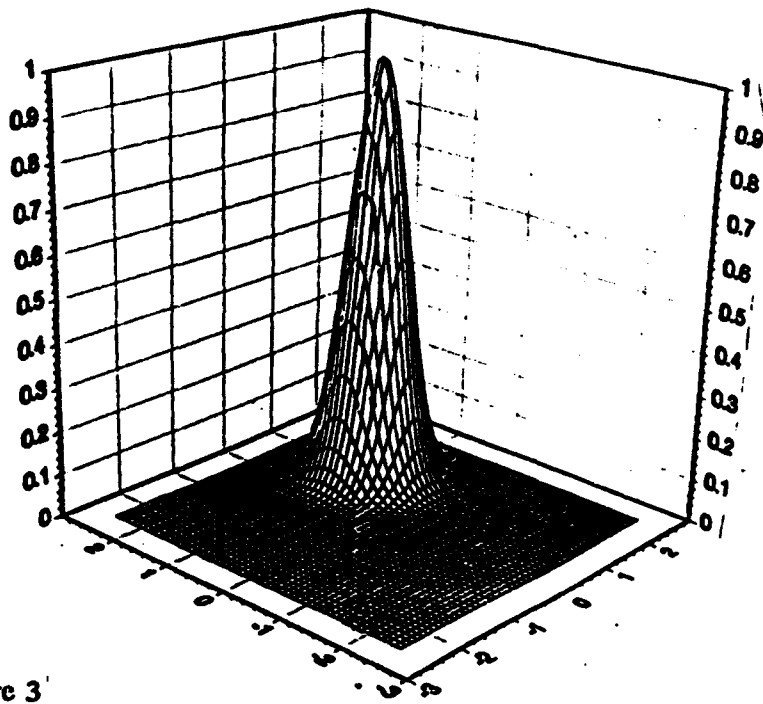
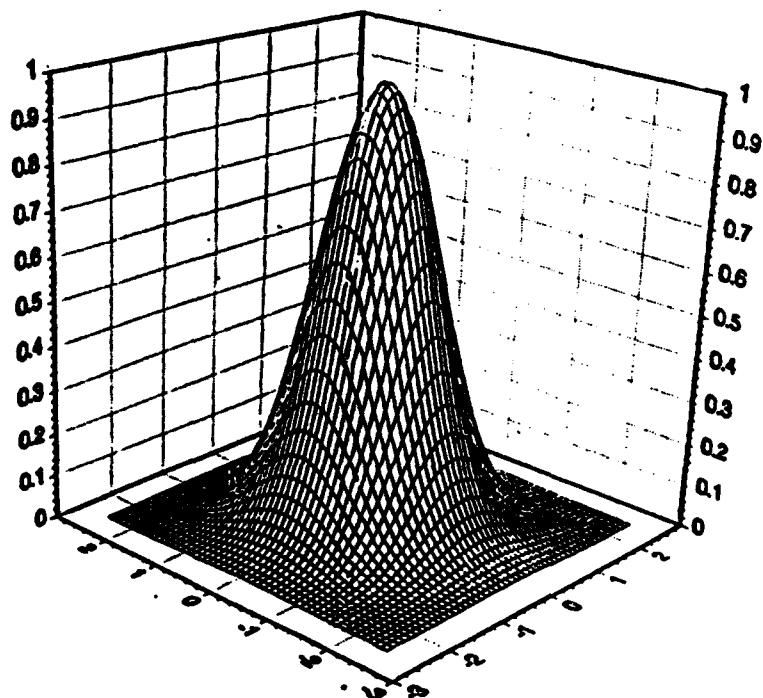


Figure 3



Mathcad,v3.0

Mathcad is a very useful program. It allows the user to work with numbers, formulas, text, and graphs. It too is very easy to use. To the left of the writing surface is a list of the different functions performed by Mathcad. The user only has to click the button for the function he or she wants and Mathcad will carry out that function. Everything on the screen appears as it would if written by hand. Text can be added as a reference without affecting the processing of the formulas. Mathcad allows the user to graph the results of an equation or series of equations. Mathcad automatically generates the scale that applies to the plot.

Mathcad allows the user to import information from other sources. I imported information from a SunSparc program put on disk and converted to what Mathcad could read. I was doing this because the information was originally graphed on the Sun but when it was printed out, the Sun included the window containing the graph. To get rid of the window we tried importing the information to Mathcad and then graphing it. After getting the information plotted on a graph, we printed it, finding that the graph wasn't big enough. It showed the information perfectly, but was too small in size for a presentation. Even after expanding the graph to the size of the screen it still wasn't big enough.

I also used Mathcad to write a program that generates shift register PN codes. By specifying the tap settings in the top row of matrix A in the program, maximum length codes are generated. These codes are the longest possible random codes that can be generated with those taps. Picking the tap settings that will give you the maximum length code takes a while because of the many possibilities. In the program I used I followed a list of polynomials. The program shown is from the polynomial, x^5+x^2+1 , where the fifth and second blocks are tapped. Also in this program, I have graphed the result of the evaluation of the periodic auto correlation as it would be seen in the frequency domain on a spectrum analyzer. I also used the polynomials, $x^5+x^4+x^3+x^2+1$ and $x^5+x^4+x^2+x+1$. The graphs for these were similar to the first polynomial, but the code they generated was different.

Harvard Graphics,v3.0

Harvard Graphics is a chart making program. It isn't as powerful as GraphTool, but it is used more for graphs used in presentations or reports. Harvard Graphics lets the user choose to create pie charts, xy charts, and organizational charts. It took no time to learn how to use this program. Creating charts with this program took little time. Harvard Graphics lets the user change the information on a chart very easily, making it very user friendly.

This program generates shift register PN codes. Maximum size codes result from setting the correct taps in the first row of matrix A.

$Nr := 5$ the number of stages in the shift register

$N := 2^{Nr}$

$v := \begin{bmatrix} 1 \\ 1 \\ 1 \\ 1 \\ 1 \end{bmatrix}$ initial starting condition for the shift register

$m := \begin{bmatrix} 0 \\ 0 \\ 0 \\ 0 \\ 1 \end{bmatrix}$ output control vector for shift register

$A := \begin{bmatrix} 0 & 1 & 0 & 0 & 1 \\ 1 & 0 & 0 & 0 & 0 \\ 0 & 1 & 0 & 0 & 0 \\ 0 & 0 & 1 & 0 & 0 \\ 0 & 0 & 0 & 1 & 0 \end{bmatrix}$ shift register matrix for the MLcode
This is a (5,2) MLcode

$c_0 := v^{<0>} \cdot m$ initial output of shift register

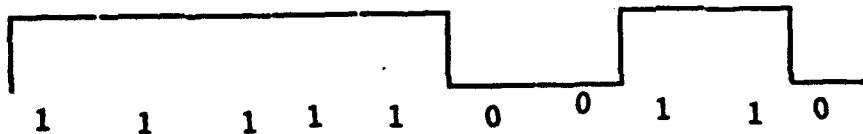
$j := 1..N-2$ $i := 0..Nr-1$

$v_{i,j} := \text{mod} \left[\left[A \cdot v^{<j-1>} \right]_i, 2 \right]$

$c_j := v^{<j>} \cdot m$

compute the periodic auto-correlation function

The column to the right is the PN code generated by this program. The reason that the code only contains 1's and 0's is because it is a digital code. Below is what the first ten numbers in the sequence look like in the waveform.



$k := 0..N-2$

$j := 0..N-2$

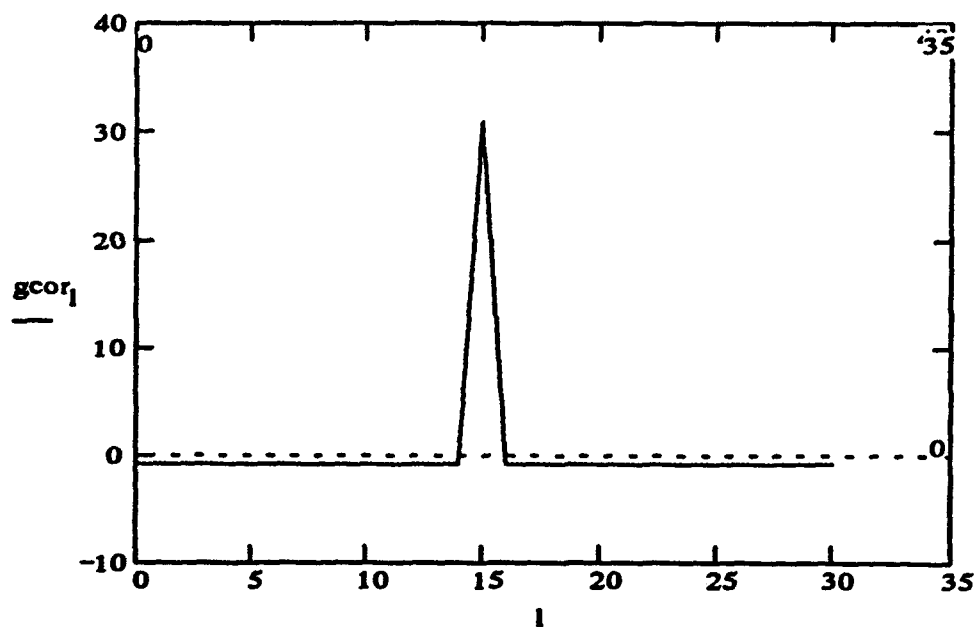
$c_j := \text{if}[c_j=0, -1, c_j]$

$vc_{j,k} := c_{\text{mod}[(j+k), N-1]}$

$rcor_k := vc^{<k>} \cdot c$

$l := 0..N-2$

$gcor_l := rcor_{\text{mod}\left[\left[l + \frac{N}{2}\right], N-1\right]}$



c =

1
1
1
1
1
1
0
0
1
1
0
1
0
0
0
0
1
0
1
1
0
1
1
1
0
0
0

Harvard Graphics not only creates charts but also allows the user just to draw. I laid out the floor plan of a lab that my mentor will soon be moving into by just choosing "Draw" from the main menu. The grid on Harvard Graphics made it easy to scale the size of the room. Moving the figures which represented the different desks, lab tables, bookcases, etc., was tough with the grid and the "click to" on. The "click to" make the boxes go to the closest place on the grid. After turning the grid and "click to" off, it was easier to put the figures exactly where I wanted them instead of just having them close to that spot. Harvard Graphics allowed me to label each piece with the text box. After writing the name of the piece of furniture, I placed the label on it and used the group function from the choice bar to the left of the screen. By doing this, I connected the name to the piece of furniture so that when I moved the furniture, the name would go with it. I also used Harvard Graphics to make a model of a communication system. As with the floorplan, I used the "Draw" mode.

DADiSP,v2.01

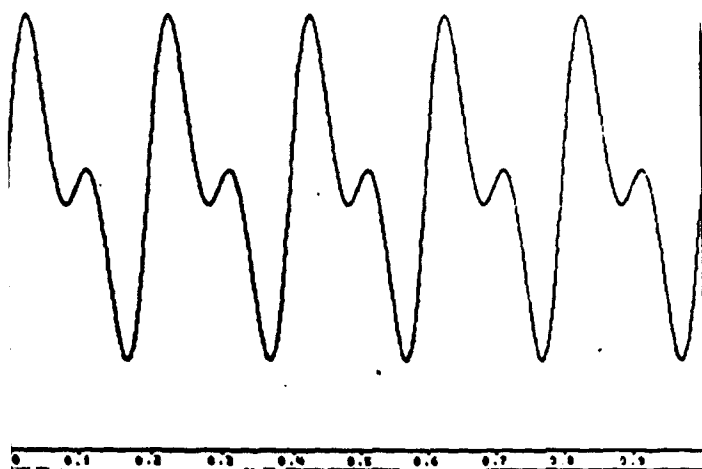
DADiSP is a program that generates waveforms. DADiSP stands for Data Analysis and Digital Signal Processing. It is set up like a spreadsheet, but instead of boxes, it allows the user to put information in windows. The user can refer to these windows when entering information just as in spreadsheets. Each window is assigned its own number. In referring to the windows the user can use "w2", this tells the program that you want the information in window 2 to be a factor in the window you are currently working in.

I used DADiSP for an AM modulation and an FM modulation. I began the AM modulation by creating a signal by adding two sine waves together, shown in W1. Alone, this signal could be disrupted by noise, other signals, etc. To make sure this doesn't happen the signal is modulated or moved down the spectrum where disruption is less likely. To do this the original signal must be multiplied by a pure sine wave, called the carrier (W2). The result of this is seen in W3, as we would see it in the time domain. It can also be seen in W5, the spectrum of the new signal. In W4 there is only one band or spike because it is the spectrum of the pure sine wave. Now that the original signal has been added to the carrier the four other spikes appear, called sidebands. Notice that there are two on each side. This is because when the signal was modulated it was placed on both sides of the carrier. The reason there are two sidebands on each side is because the original signal was made up of two sine waves. If the carrier was to be stripped off, the result would be the spectrum of the original signal.

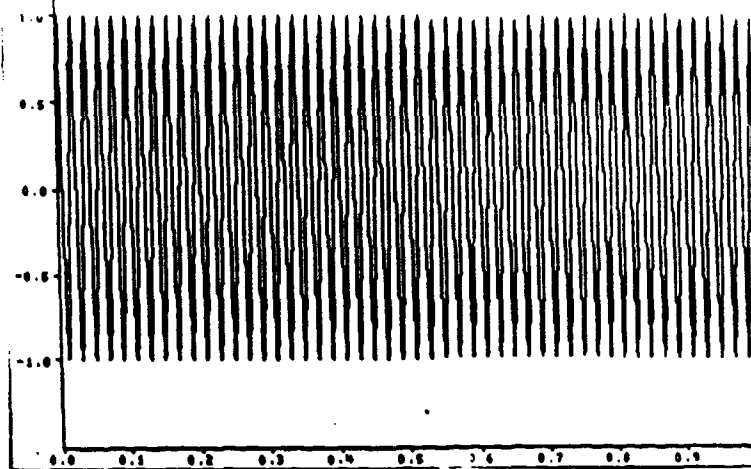
In the FM modulation I started with a sine wave. Like AM modulation, you are trying to move this signal, but instead of changing the amplitude, you are changing the frequency. The sine

AM modulation

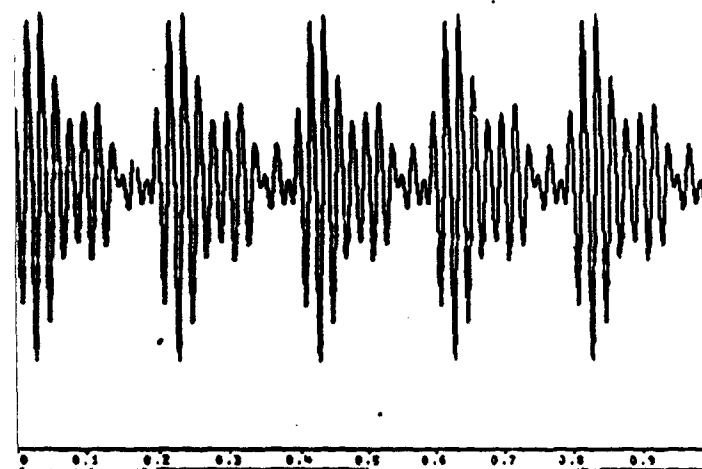
Y: 1000 * (1000.0 - 0.67 * t) * cos(1000.0 * t - 0.5)



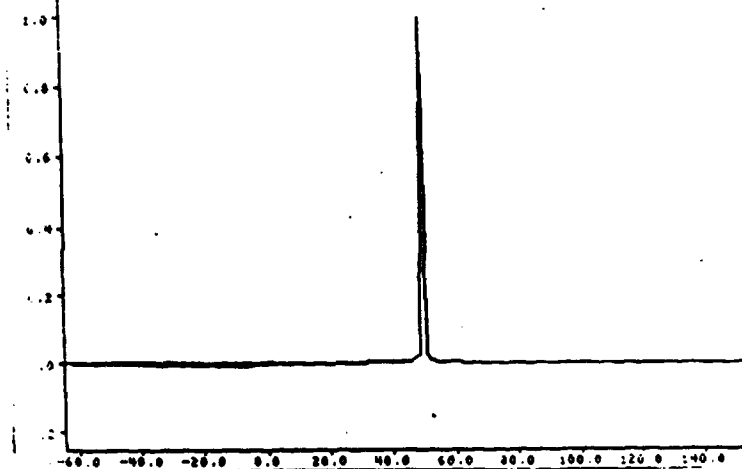
M: 5000 * cos(1000.0 * t - 0.5)



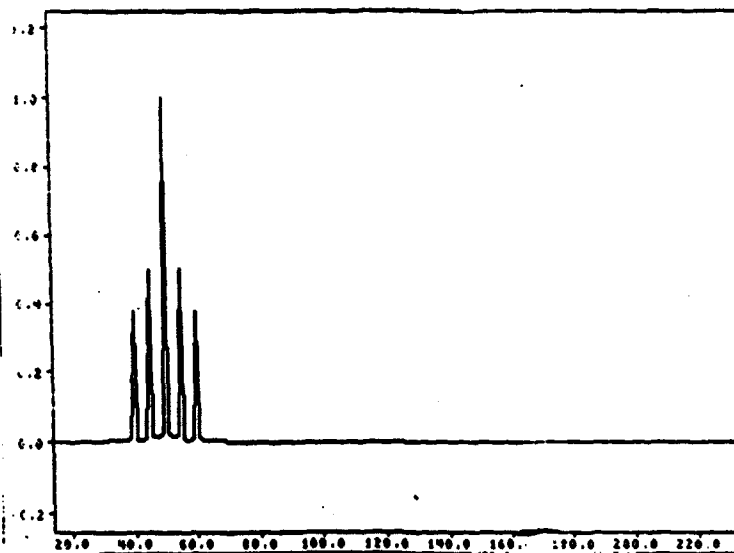
Y: 1000 * cos(1000.0 * t - 0.5)



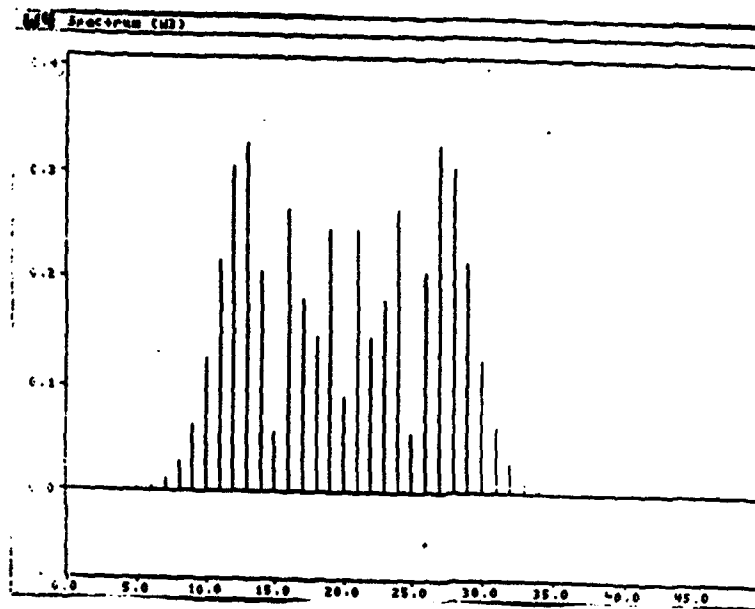
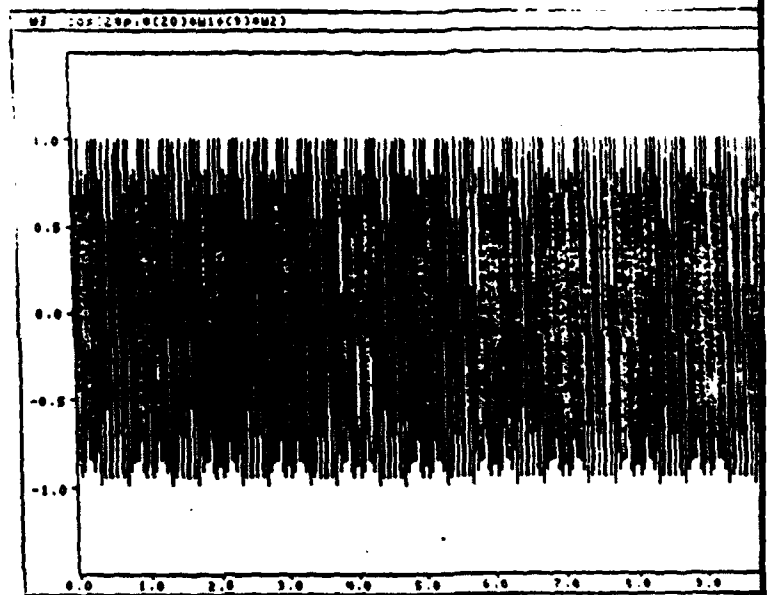
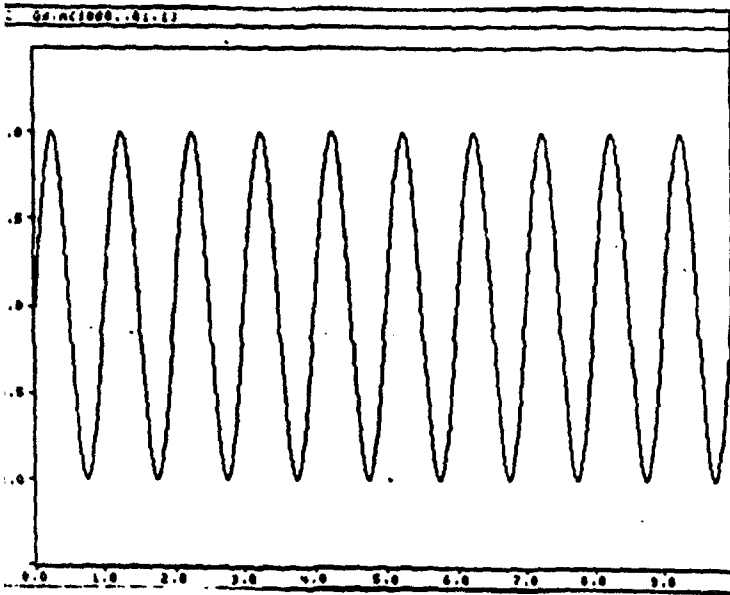
M: Spectrum (u2)



Y: Spectrum (u2)



FM modulation



wave in W2 was used to change the frequency of another higher frequency or sinusoidal function to give what is seen in W3. It can be seen that the frequency has been changed greatly. In W3 it can also be seen that the signal fluctuates, going from a lower frequency to a high frequency. W4 shows how the spectrum of the new signal and the original sine wave are totally unrelated.

Microsoft Visual Basic

Visual Basic is designed to run in front of other programs and give them commands. It is based on writing code in the Basic language. This is one of those programs that had been waiting for someone to use so they set me on it. I was to learn all I could about the program and tell everyone how the program worked. I slowly made progress by looking through the user's guide, then the language guide, and finally the online help menus. I created some of the little projects from the user's guide, such as a setup that during run time would reply "You clicked me," in a text box after hitting the command button that was labeled "Click Me!". As a way to get more familiar with the program, I made an investment calculator. I set up four text boxes for the initial amount, percent interest, duration in years, and total amount respectively. During run time, the user would enter the numbers of his choice, click the command button labeled "Calculate Total Interest," and the total would appear in the last box labeled "Total Interest." Another way to become familiar with the program was to create a blackjack game. I helped some, but my lack of knowledge of the Basic language made it hard for me to write some of the programs. After becoming familiar with the program I wrote a couple of little hints to make using the program easier for people just beginning to use the program. In the write-up it should be noted that I used the programmer's guide for the definitions of the things I was not familiar working with. These are mostly the last couple of definitions under the "ToolBox" heading.

Microsoft Excel.v3.0

Microsoft Excel is a very useful spreadsheet. It is easy to use with extensive online help. The only difficulty I had with this program was picking the correct paste function for my calculations. I used Excel to set up a spreadsheet to solve for signal-to-noise ratio for a radar system given the range, power, antenna gain, radar cross section, temperature, frequency bandwidth, and noise factor. Using the following equation,

$$\frac{Signal}{Noise} = \frac{PtGAeo}{(4\pi R^2)KT_nBFn}$$

I substituted in those values mentioned above. Each of the variables in this equation is defined on the next page. The Antenna Aperature (Ae) was calculated within the program, as was the wavelength.

Visual Basic

Saving and Recalling Projects

When you start Visual Basic, it automatically opens a new project. To open a previously saved project, the user must choose the "Open Project" command from the File menu. Then the user must select the "Project Window" command from the Window menu. The user must then highlight the name of the project in that window and then click the "View Form" command button.

After finishing work on a project, the user must go to the File menu and select either the "Save Project" or the "Save Project As..." command. Both of these will save the project as shown, but the "Save Project As..." command enables the user to change the name of the project being saved.

Visual Basic does not save individual files to be recalled. These files must be saved as a project. The "Save File" command in the File menu only saves the current form in the project. This form cannot be called up by itself. It must be opened as part of a project.

Tool Box

The Tool Box provides fifteen applications to the user. The Tool Box allows the user to create the different applications on the form. Through the use of basic programming, any of these applications can interact with another. The following is a brief explanation of each of the applications:

1. **Picture Box** - contains a graphical image (bitmap or icon) through the use of simple code. The code isn't directly placed in the box itself, usually contained in the command button. Text can also be printed out onto the picture box through the same method.
2. **Label** - control box in which a caption is placed to show the purpose or procedure of another box. Has no code written in it, but code refers to the name of the label to recognize the box it labels.
3. **Text Box** - enables user to write or print out text to a box. As with the picture box, code isn't written in but instead the box is referred to in the code of a command button.
4. **Frame** - used to group option buttons or other controls. Carries out no special function.
5. **Command Button** - control that carries out a command or action. In run mode this button is usually clicked to start procedure. Most of the written code in the program is written in this control box.
6. **Check Box** - control used to represent an option (on/off, true/false) that the user can set or clear by clicking during the run mode. An "X" appears when the box is selected.
7. **Option Button** - Control similar to a Check Box, but it is used as part of a group. Only one button can be selected at a time during the run mode.
8. **List Box** - provides a list of choices to the user during the run mode.

9. Combo Box - similar to the list box, but the user can enter or select items from the list provided during the run mode.
10. Horizontal scroll bar - control that appears as a scroll along a horizontal axis. It is not attached to a window, but can be used as an alternative way of getting input and displaying output during the run mode.
11. Vertical scroll bar - same characteristics as the horizontal scroll bar but is instead on the vertical axis.
12. Timer - control that responds to the passage of time: specifically, a period which the programmer specifies. A form may have multiple timers, each set at a different interval. Only control not seen during the run mode.
13. Drive list box - control that displays a list of all valid drives in the user's system. A drive list box finds and switches between valid disk drives at run time.
14. Directory list box - control that displays a hierarchical list of directories. Enables the user to select directories and paths at run time.
15. File list box - control that displays a list of filenames selected according to their attributes. Finds and specifies files to be opened, saved, or otherwise manipulated at run time.

Division with Visual Basic

Visual Basic uses two forms of division, real and integer. When writing code for these operations the user must know the difference between the two. The symbol for real division is /, whereas the symbol for integer division is \.

*Note - Program automatically converts values to real or integer, whichever the user chooses.

Ex.

x is an integer	x = 3	
y is an integer	y = 11	11/3 = 4
z is an integer	z = y/x = 11/3	but
		11\3 = 3

The Immediate Window

The Immediate Window appears in the break mode during run time. When the break mode is selected from the Run menu the immediate window appears on the screen. It is most useful when trying to debug your program. Typing "Debug.Print [item in program] ;" will print out the error in the immediate window so you can fix it. This process works best when your variable is known to change, like putting the statement in a loop that repeatedly alters the statement.

Another way to debug the program is to type a "?" at the beginning of the line and then put in the variable.

? x		? card(1)
82	or as in the blackjack program	3
? y		? suit(1)
23		1

If, for instance, you wanted to know what the value for the second card was, all you would have to do is scroll up the list and change the 1 to a 2, instead of retyping the line.

Properties

Below the list of menus on the Visual Basic screen is the properties bar. The first box that appears on the bar contains a list of different properties that can be used. Clicking the down arrow button next to the box, allows the user to view the different choices for the application. It should be noted that not all of the applications have the same properties available to them. Listed below are brief explanations of some of the most commonly used properties:

1. Caption - The caption property is used with forms, click boxes, command buttons, frames, labels, menus, and option buttons. Use this property to label a form or control descriptively.
2. CtlName - This property is used with all applications. By default, the CtlName is automatically set. For instance, when you create a frame, the CtlName will be "Frame1." The user must change this name into one that will describe the function of the application because this will be the name referred to in the written code.
- * 3. Alignment - Used with labels. Aligns text within the label.
Left Justify = 0 (default)
Right Justify = 1
Center = 2
- * 4. Autosize - Used with labels and picture boxes. Automatically resizes control to fit its contents.
True = 1 Automatically resizes
False = 2 (default) Keeps size constant
- * 5. Autoredraw - Used with forms and picture boxes.
True = (-1) Enables automatic repainting of a form on a picture box. Graphics and print output are written to the screen and images are stored in the memory.
False = (0) (default) Disables automatic repainting and writes only to the screen.
6. Back Color / Fore Color - Used with forms, check boxes, combo boxes, command buttons (Back Color only), directory list boxes, drive list boxes, file list boxes, frames, labels, list boxes, option buttons, picture boxes, and text boxes. Back Color sets or returns the background color of an object. Fore Color sets or returns the foreground color used to display text and graphics in an object.

There are two ways to get the color you want in the object you want it in. The first and easiest is to click the desired property and then just go down to the color pallet and click the color of your choice. The other way is to type the hexadecimal code for that color in the box to the right of the property box.

*Note - For all of those marked above, there are subgroupings within each property. To be able to choose from those groupings you can go to the box to the right of the property box and click the down arrow key. This will show all of the choices for each property.

Problem: Determine the signal-to-noise ratio out of the IF filter for targets having cross sections of 25m^2 and 50m^2 at ranges of 50, 100, and 200 km. Use single hit detection.

Solutions

**Signal-to-Noise Computation
Radar Cross Section 25**

Range (m)	5.00E+04	1.00E+05	2.00E+05
Power (w)	50000.00	50000.00	50000.00
(dB)	46.99	46.99	46.99
Antenna Gain	1000.00	1000.00	1000.00
(dB)	30.00	30.00	30.00
Frequency (GHz)	2000.00	2000.00	2000.00
Wavelength (m)	0.15	0.15	0.15
Antenna Aperature (sqm)	1.79	1.79	1.79
Radar Cross Section (sqm)	25.00	25.00	25.00
Temperature (Centigrade)	17.00	17.00	17.00
(Kelvin)	290.00	290.00	290.00
Frequency Bandwidth (MHz)	2.00	2.00	2.00
Noise Factor	1.21	1.21	1.21
Solve for Signal-to-Noise (dB)	23.71	11.66	-0.38

**Signal-to-Noise Computation
Radar Cross Section 50**

Range (m)	5.00E+04	1.00E+05	2.00E+05
Power (w)	50000.00	50000.00	50000.00
(dB)	46.99	46.99	46.99
Antenna Gain	1000.00	1000.00	1000.00
(dB)	30.00	30.00	30.00
Frequency (GHz)	2000.00	2000.00	2000.00
Wavelength (m)	0.15	0.15	0.15
Antenna Aperature (sqm)	1.79	1.79	1.79
Radar Cross Section (sqm)	50.00	50.00	50.00
Temperature (Centigrade)	17.00	17.00	17.00
(Kelvin)	290.00	290.00	290.00
Frequency Bandwidth (MHz)	2.00	2.00	2.00
Noise Factor	1.21	1.21	1.21
Solve for Signal-to-Noise (dB)	26.72	14.67	2.63

Variables Defined

Pt = Power Transmitted

G = Antenna Gain

Ae = Antenna Aperature

σ = Radar Cross Section

K = Boltzman's constant ($1.38\text{E}-23$)

T_a = Temperature (Kelvin)

B = Frequency bandwidth

F_n = Noise Factor

To convert the final answer into decibels (dB) I took the log of the result of the equation and then multiplied by 10. After getting the spreadsheet set up, I solved an actual problem.

Conclusion

Each of the programs that I evaluated can perform multiple functions, making them very useful in the office. Not all applications are as limited as the ones that I used. I worked with the basics mostly. I really didn't get too in depth with any one program, though some projects were more in depth than others. Working with programs wasn't all I did during my tour. Sure, most of the time I was on a computer, but there were times I wasn't. During my tour, I also briefly used a digital spectrum analyzer and oscilloscope to observe different types of signals. I did little things like this throughout my tour, while doing most of my work on the computer. I would do little things to help out, such as install different programs. While here I installed the DOS6 upgrade and WordPerfect for Windows which most of this report is done on. This report goes over my work with the different programs, but there is no way to sum up all the things I've learned during my tour. I came into this program with the feeling that I wanted to be an engineer, and after experiencing it firsthand, I know I want to become an engineer. I'm not totally positive, but I think I will try and major in electrical engineering. As for the communications end, I'll make that decision in the future after seeing more of my options.

References

Microsoft Visual Basic Programmer's Guide, 1991, Microsoft Corporation

THE CHANCE OF A LIFETIME

**Jennifer A. Starr
student
Trotwood Madison Sr. High**

Final Report for: AFOSR Summer Research Program

Wright Laboratory

Sponsored by: Air Force Office of Scientific Research

Boiling Air Force Base, Washington, D.C.

July 1993

CHANCE OF A LIFETIME

Jennifer A. Starr
student
Trotwood Madison Sr. High

ABSTRACT

This report will explain the knowledge obtained, while working at Wright Patterson Air Force Base. It will cover computer operation, hypermedia ,and various computer applications In addition, this report will discuss my experience with Internet. Examples of the work done in the past eight weeks will be shown.

A CHANCE OF A LIFETIME

Jennifer Starr

INTRODUCTION

"Opportunity is often difficult to recognize; we usually expect it to beckon us with beepers and billboards." This is a quote by William Arthur Ward which I can relate to. I was given the opportunity to learn, in eight weeks, about computer engineering. This was a great opportunity, because I was exposed to an area of interest to me. During the summer, I learned about computer hardware and software. In addition, I learned how to program in Ada. Overall, this job enabled me to gain a better understanding of computers and programming. It gave me an chance to learn about computers though hands on experience.

DISCUSSION

Before coming to Wright Patterson Air Force Base, I knew nothing about programming and very little about computers. Over the course of time, I learned a great deal.

Programming is defined as the logical decomposition of a problem into a set of procedures for execution on some computer structure in order to generate a solution to the initial problem. The computer is given logical instructions in the correct order using a programming language. It took me a while to understand and practice this.

Ada is a high-level programming language. In other words, it is a notation that is intended to be natural and convenient for writing and reading computer programs. Ada is a blend of mathematical notation with English words and phrases that are used with precise meanings. In

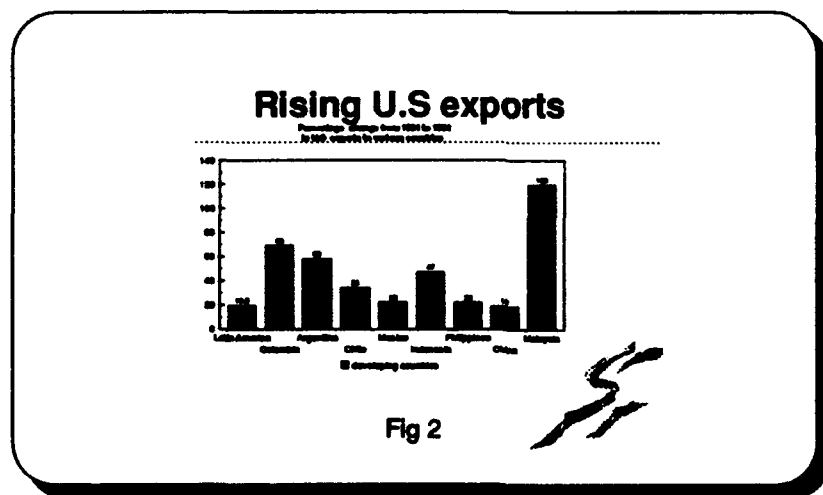
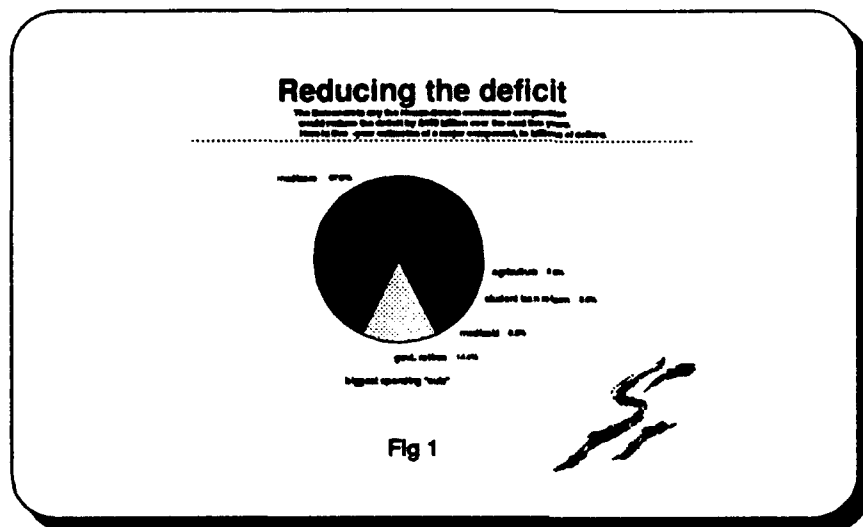
this respect it is similar to other high-level languages such as Fortran and Pascal. However, it is different from low-level machine languages and assembly languages, which require programs to be written in terms of the instruction sets and registers. Ada has three units: packages, procedures, and tasks. An Ada package contains a specification and a body. Generally, the specification identifies what procedures and functions are in the package. The body contains the actual code for the procedures and functions identified in the specification. My knowledge about programming has expanded more than ever. It shocked and pleased me the first time a program was written by myself without the help of my mentor. It made me feel good to know that I was beginning to comprehend programming.

Unlike programming, the computer was easier to understand. Several terms were discussed in the process of learning about the computer. The difference between single and multi-user systems was learned. A single-user system, allows one user to access the computer at the same time. On the other hand, a multi-user system is such that multiple users can access the computer simultaneously. The operating system is another term that was learned. The operating system is a set of functions that translate user requests to operations that can be performed by the computer. For example, the PC operating system is DOS and the VAX operating system is VMS. The appendix following the report has some sample programs that I wrote after learning how to program.

Another part of training was dedicated to learning to use word processing software. The word processor used was Ami Pro. In fact, Ami Pro was used to create this report. Ami Pro has a spelling checker which allows the author to correct misspelled words. In addition, it also has a

grammar checker which assists in identifying grammatical errors and supply suggestions on corrections. It also has a diverse variety of styles in which the text can be written. Ami Pro also has graphical capabilities which allows the user to create pie, line, and bar graphs. Figures 2 & 3 contain examples of pie and bar graphs.

During the summer, I was also exposed to a technology known as hypermedia. Hypermedia is



a way of combining textual, audio, video, and graphical information for presentation. A popcorn popper manual was used as an example of hypermedia.

The creation of a hypermedia popcorn popper manual was done in several steps. The first step was to enter the text and graphics into the computer, using a text editor and scanner. The manual was then "marked up" according to a predefined mark up language. For example, the manual was separated by the main headings and subheadings by using ".c1." and ".c2." respectively. Afterwards, a document description file which contains summary about the documents that make up the library, was created. It is mandatory that a document exists for each description. If a document is removed the document description must also be removed. Next, the document loader was executed. The document loader is the application that loads documents into the "document project." The "Document Project" is a database that stores documents, figures, tables, movies, and audio. The next step was to import the document description and the document. This enables them to be located anywhere on the hard disk. After that, the document project was put into the index. Lastly, the reference system was updated by adding the document to the library menu.

Finally, this summer I learned about a computer network called Internet. Internet is the world's largest computer network. On this network numerous computers can connect and communicate with each other. All the networks, using the IP protocol, cooperate to form a seamless network for their collective users, this includes federal, regional, campus, and some foreign networks. All these networks put together are only part of what makes up the Internet because now other non-IP networks are connected. There is no single authority figure for the Internet as a whole. Everyone pays for their part of the Internet. It was interesting how a message can be sent around the world on this network and then receive a reply from anyone that is connected to the network.

Several years after the Internet was implemented, a tool called Archie was developed to help users search for information. Archie is a system which allows searching of file indexes to locate publicly available information. The appendix contains an example of the use of Archie.

CONCLUSION

A great deal of new knowledge was obtained while working at Wright Patterson. I still plan to learn how to program graphics in the future. I enjoyed spending my summer at Wright Laboratory. It was an experience I'll never forget. The most important thing I learned while working here is that when opportunities like this come knocking at the door, let them in and appreciate them because if you don't they'll pass you by.

Appendix

JS>r average
enter the number for a---> 30.0
another number for a --->45.0
another number for a --->48.0
another number for a --->-999.0
The average is --> 41.000

JS>r square
enter a_number -->
34.0
1156.000
1.15600E+03

JS>r square
enter a_number -->
6.0
36.000
3.60000E+01

JS>r velocity
enter a number for d-->200.0
enter a number for t-->4.0
velocity is ---> 50.000

> prog ada

ost cac.washington.edu (140.142.100.1)
ast updated 06:57 6 Jul 1993

Location: /local/emacs-18.57/lisp
FILE -rw-rw-r-- 19512 bytes 00:00 9 Apr 1988 ada.el

ost cac.washington.edu (140.142.100.1)
ast updated 06:57 6 Jul 1993

Location: /local/emacs-18.57/lisp
FILE -rw-rw-r-- 16382 bytes 01:00 9 Jan 1991 ada.elc

ost cac.washington.edu (140.142.100.1)
ast updated 06:57 6 Jul 1993

Location: /local/emacs.pmax4.0/lisp
FILE -rw-r--r-- 19512 bytes 00:00 9 Apr 1988 ada.el

ost cac.washington.edu (140.142.100.1)
ast updated 06:57 6 Jul 1993

Location: /local/emacs.pmax4.0/lisp
FILE -rw-r--r-- 16382 bytes 00:00 11 Apr 1988 ada.elc

ost cac.washington.edu (140.142.100.1)
ast updated 06:57 6 Jul 1993

Location: /local/emacs.sun386/lisp
FILE -rw-rw-r-- 19512 bytes 00:00 9 Apr 1988 ada.el

ost cac.washington.edu (140.142.100.1)
ast updated 06:57 6 Jul 1993

Location: /local/epoch-next/lisp
FILE -rw-r--r-- 19512 bytes 00:00 16 Oct 1990 ada.el

ost cac.washington.edu (140.142.100.1)
ast updated 06:57 6 Jul 1993

Location: /local/epoch-pmax/lisp
FILE -rw-r--r-- 19512 bytes 00:00 16 Oct 1990 ada.el

**COMPARISON OF THE FIGURES OF MERIT FOR THE BASELINE NON-EXHAUSTIVE SEARCH METHODS
VERSUS THE NUMBER OF PARTITIONS**

A STUDY IN PATTERN THEORY

Johnny R. West, Jr.

Student

Belmont High School

2323 Mapleview Ave.

Dayton, Ohio 45420

Final Report for:

High School Apprenticeship Program

Wright Laboratory / AART-2

Sponsored by:

Air Force Office of Scientific Research

Wright-Patterson Air Force Base, Dayton, Ohio

August 1993

**COMPARISON OF THE FIGURES OF MERIT FOR THE BASELINE NON-EXHAUSTIVE SEARCH METHODS
VERSUS THE NUMBER OF PARTITIONS**

A STUDY IN PATTERN THEORY

**Johnny R. West, Jr.
Student
Belmont High School
Dayton, Oh.**

ABSTRACT

The recent advancements in machine learning theory, computational complexity, and logic minimization has lead to a new study in the world of computer science referred to as Pattern Theory. This is the study of how computers recognize patterns and, more importantly, the study of "pattern-ness." Through years of extensive research and experimentation, a robust Occam based pattern recognition and learning has been developed. However, this program is not as fast as it needs to be, nor is it as convenient as it needs to be for application to "real world" problems. Currently, these problems are being researched.

PATTERN THEORY MEMO- August 5, 1993

Johnny R. West, Jr.

High School Apprenticeship Program of Research and Development Lab and the Air Force Office of Scientific Research for WL/AART-2

*COMPARISON OF THE FIGURES OF MERIT FOR THE BASELINE
NON-EXHAUSTIVE SEARCH METHODS VERSUS
THE NUMBER OF PARTITIONS*

1.0 BACKGROUND

The Pattern Theory Paradigm is the result of a recent convergence of ideas from logic minimization, computational complexity, and machine learning theory¹. It is a promising, new approach to robust pattern finding. One of the keys to this robustness is the ability to decompose, or break up, a function into smaller parts for use. The basic test for doing this is called Ashenhurst-Curtis Decomposition. In the late 1950's, R. L. Ashenhurst published the basic test for determining whether or not a binary function decomposes. In particular, the test tells us whether or not F and Φ exists so that a binary function f can be represented by a composition of F and Φ . In other words, is there a truth to the representation:

$$f(x_1, x_2, x_3, x_4) = F(\Phi(x_1, x_2), x_3, x_4)$$

This test became the basis for considerable new work in logic minimization. We refer to the partition of f 's inputs (or variables) into inputs for Φ and inputs for F as simply a "partition" or a "variable partition."

The result of doing a partition test on any one partition never changes. However, the question of how to arrive at "good" partitions, or a partition search strategy, is not as easy to find. By "good" we mean partitions that decompose to optimal. The partition space, or simply the number of partitions, is equivalent to x^y partitions, where x is the number of groups in which each input may be placed, and y is the number of variables, or inputs. The variable x is dependent on whether or not "shared" variables are being used. The set of groups $\{\Phi, F\}$ is called a "disjoint" set because the input must be in either group Φ or in group F . This gives x a value of 2. However, the set of groups $\{\Phi, F, \Phi \text{ and } F\}$ represents "shared" variables, since any input can be in both Φ and in group F . This would give x a value of 3. So, for a function with eight inputs the partition space is 2^8 , 256, or there are 256 disjoint partitions to search through. The methods used to find a good partition were exhaustive, meaning they performed the decomposition test on every partition throughout the hierarchy. This test is impractical because of the large amounts of time and memory needed to run the test thoroughly.

In order to compensate for these problems, new search strategies have been devised. These strategies, or decomposition plans, selectively perform decomposition tests. They are performed to find

¹ Timothy D. Ross, Michael J. Noviskey, Timothy N. Taylor, and David A. Gadd. Pattern Theory: An Engineering Paradigm for Algorithm Design. Final Technical Report WL-TR-91-1060, Wright Laboratory, USAF, WL/AART, WPAFB, OH 45433-6543, August 1991.

the optimal partitions, the partitions that give the best decomposition, with ease. This saves time and memory.

In order to use any strategy, a measurement of the "wellness" of a partition must be evaluated. There are many ways of arriving at these figures of merit, but which way is the best? Which way will be the fastest and the most accurate? How much speed is given up for a more accurate measure? What truly is the most accurate measure?

The purposes of this study were to: (1) supply information to help determine whether the sum of child cardinalities (SOCC) or the sum of grandchild cardinalities (SOGCC) is a better figure of merit (FOM) for selecting partitions during the decomposition process and; (2) for each FOM, determine the best strategy for getting the partition to be evaluated. This will help to determine the fastest and most efficient way to find partitions with the minimum decomposed function cardinality (DFC).

2.0 DEFINITIONS

The Algorithms:

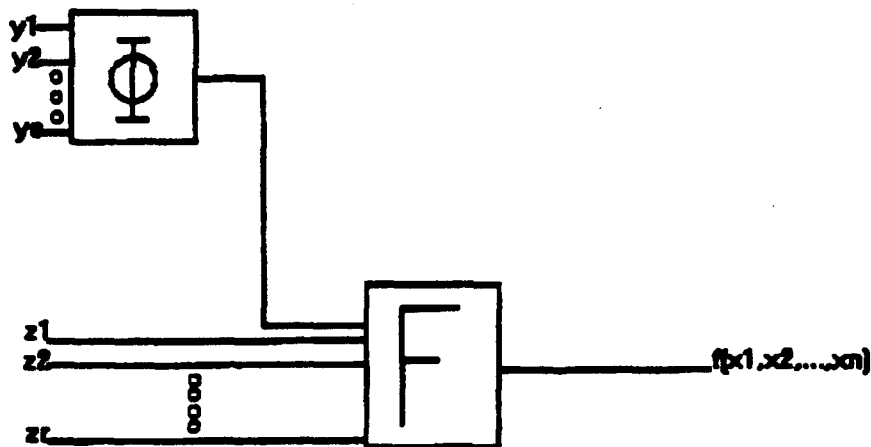
The Increasing Row to Column Ratio Algorithm means that the partitions were chosen for evaluation in sequential order, starting with one row x seven columns and ending with seven rows x one column and choosing all partitions with i row variables before choosing any partitions with $i+1$ row variables.

The Decreasing Row to Column Ratio Algorithm means that the partitions were chosen for evaluation in sequential order opposite IRC, starting with seven rows x one column and ending with one row and seven columns.

The Random Algorithm means that the partitions were not selected sequentially. They were selected randomly with replacement. With replacement means that after a partition was selected, it could be selected again. In example, if you have three red balls and two blue balls in a bag and randomly take one out, then you toss whatever ball you have aside and draw another, that would be random *without* replacement. As you kept drawing, you would eventually get all the balls out of the bag. However, in random *with* replacement, you would have replaced the ball and, you could after five tries, withdraw the same ball five times.

Cardinality:

Cardinality is the number of elements in a set. For functions (a set of ordered pairs) it is the possible values raised to the power of the number of inputs. For example, for the function pictured on the next page:



the sub-function Φ has a cardinality of 2^3 , or 8, while sub-function F has a cardinality of 2^4 , or 16, if and only if the inputs to the function are all disjoint and are all represented in the drawing (i.e. $s=r=3$).

The Sum of Child Cardinality of a function is the sum of the cardinalities of the sub-functions of a function after first-level decomposition. In the above function, the sum would be 24.

The Sum of Grandchild Cardinality of a function is the sum of the cardinalities of the sub-functions of sub-functions of a function (second-level decomposition). This is not pictured in the above function.

A Figure of Merit is a way of determining the value of a partition, e.g. SOCC and SOGCC.

Decomposed Function Cardinality is the figure of merit acquired when a function is decomposed.

Decomposition:

Ashenhurst-Curtis Decomposition is a way of breaking down a function into smaller parts. The function pictured above can be written as $f(y_1, y_2, y_3, z_1, z_2, x)$. This equation is too large in the sense of digital circuit design. It has a cardinality of 2^6 or 64. In other words, it takes 64 bits of memory to store this function. If it is decomposed, it becomes $f(F(\Phi(y_1, y_2, y_3), z_1, z_2, x))$. While it is more difficult for the human mind to comprehend, it has a small cardinality of $2^3 + 2^4 = 8 + 16 = 24$. By decomposing the function, 40 bits of memory has been saved. This is just one example of what function decomposition is capable of. There are many other applications.

3.0 PROCEDURE

3.1 Partition Selection Experiments

First, the partition selection algorithms were examined.

3.1.1 Order of Partition Selection

In these experiments, we were concerned with the order in which the partitions were evaluated. Specifically, we were concerned with the results of examining the partitions in a particular order based on the numbers of row and column variables in a partition.

We used FLASH, the *Function Learning And Synthesis Hotbed* (a program developed under the Wright Lab Pattern Theory Project) to generate the data using the Increasing Row to Column Ratio (IRC) algorithm for the SOCC and SOGCC for the set of 30 functions referred to as the Benchmark Set of Functions. However, we used only 27 out of the first 30 Benchmark Functions in this study. The three excluded functions did not decompose and therefore would supply no information to the study. These functions were binary with eight inputs, so the number of partitions that we evaluated 256 partitions for each function.

We acquired the best FOM for SOCC and SOGCC for each partition by using the data supplied by FLASH. The FOM for partition n is the FOM for the $n+1^{\text{th}}$ partition looked at. For example, the FOM for partition five simply means that at the sixth partition looked at by the decomposition plan, the FOM was X , keeping in mind that partition one actually occurs before any partitions are looked at. The best FOM is acquired by looking at the figures of merit in order and determining if it is lower than the previous best. If it is better than the "old best" it becomes the "new best." If, however, it is not better than the old best, the IRC data for the 5^{th} partition looked at becomes the value of the old best. In pseudo-code:

```
begin
  x = 0
  best = 999
  repeat
    x = x + 1;
    get basic_data for partition x;
    if basic_data < best
      then
        best := basic_data;
        IRC_data_for_xth_partition_looked_at := best;
  until x = number_of_possible_values_for_each_input number_of_inputs
end.
```

For example, if the original, or basic, FOM data for the first five partitions are:

PARTITION NUMBER	FOM
1	256
2	48
3	124
4	28
5	256

the IRC data, or "best FOM so far" data, for each partition would be:

PARTITION NUMBER	FOM
1	256
2	48
3	48
4	28
5	28

Since this process is tedious and slow (considering 256 partitions on 27 functions and two figures of merit), we developed a simple yet efficient Microsoft QBASIC program to do this process. We then graphed this data using Microsoft Excel and saved the charts for future use.

We then created the Decreasing Row to Column Ratio (DRC) Algorithm data. To do this, we reversed the original FOM data and evaluated it similarly to the IRC data. Using the original FOM data:

PARTITION NUMBER	FOM
1	256
2	48
3	124
4	28
5	256

we then reversed the original data to:

PARTITION NUMBER	FOM
1	256
2	28
3	124
4	48
5	256

then evaluated the data as seen if the partitions were looked at in reverse order as the DRC data:

PARTITION NUMBER	FOM
1	256
2	28
3	28
4	28
5	28

giving us the necessary DRC data. We again developed a short Microsoft QBASIC program to do the necessary data manipulation. We then plotted this data with Microsoft Excel and stored this for future use. Keep in mind that all the above data is purely fictitious and is here only in the hopes that it will help the reader understand the procedures involved.

3.1.2 Random Selection

The data for the Random (RAND) Algorithm was not as easy to generate. The objective here was to synthesize what would happen if we went through the partitions in a purely random order, as opposed to IRC and DRC. We could have done many random samplings and averaged it. However, we wanted a more direct and accurate approach. This approach called for some experimental basis, as noted in the procedure that follows. First, we generated experimental data in the form of histograms with FLASH. A histogram might have looked similar to:

POM	Number of Occurrences
16	6
8	1
4	1
2	1
1	3

We generated histograms such as these for each of the 27 Benchmark Functions being evaluated in both the SOCC and SOGCC formats. Again, the above histogram is purely fictitious and is only here for the benefit of the reader. To this point, the data worked with was purely experimental, meaning we generated it using FLASH. The data plotted, however, is theoretical data, based on experimentally generate histograms, as obtained using the procedure that follows.

James F. Frenzel, a professor in the Department of Electrical Engineering from the University of Idaho, supplied the following theory to obtain the data needed:

Assuming n partitions are being looked at, the probability that a certain figure of merit is the best figure of merit is equal to the n^{th} power of the figure of merit's occurrences plus the number of occurrences of better figures of merit divided by the total number of partitions minus the probability that any better figure of merit is the best figure of merit. The expected best (theoretical) figure of merit would then be the sum of each probability multiplied by its respective figure of merit.

We derived the following formulas from this theory and the table (keep in mind that the variable n represents the number of the partition being looked at in all cases):

FOM	Number of Occurrences
16	6
8	1
4	1
2	5
1	3

$$\text{probability}(16 \text{ is best FOM}) = (6/16)^n - 0$$

$$\text{probability}(8 \text{ is best FOM}) = (7/16)^n - (6/16)^n$$

$$\text{probability}(4 \text{ is best FOM}) = (8/16)^n - (7/16)^n$$

$$\text{probability}(2 \text{ is best FOM}) = (13/16)^n - (8/16)^n$$

$$\text{probability}(1 \text{ is best FOM}) = (16/16)^n - (13/16)^n$$

$$\begin{aligned} \text{expected best}(\text{partition } n) = & \text{probability}(16 \text{ is best FOM}) * 16 + \text{probability}(8 \text{ is best FOM}) * 8 + \\ & \text{probability}(4 \text{ is best FOM}) * 4 + \text{probability}(2 \text{ is best FOM}) * 2 + \\ & \text{probability}(1 \text{ is best FOM}) * 1 \end{aligned}$$

An explanation:

In the 3rd equation, probability is the function, 4 is the figure of merit read from the chart, 8 is the sum of the occurrences to that point (6 + 1 + 1), 16 is the total number of occurrences (6 + 1 + 1 + 5 + 3), n is the number of partitions being looked at (in the case of this study 1,256) and, 7 is the number of occurrences of figures of merit better than the current figure of merit (6 + 1).

So, the theoretical figure of merit of the fifth partition ($n = 5$) of this function, assuming this function is represented correctly by the above histogram, would be:

$$\text{probability}(16 \text{ is best FOM}) = .0074157715 - 0 = .0074157715$$

$$\text{probability}(8 \text{ is best FOM}) = .0160284042 - .0074157715 = .0086126292$$

$$\text{probability}(4 \text{ is best FOM}) = .03125 - .0160284042 = .0152215958$$

$$\text{probability}(2 \text{ is best FOM}) = .354092598 - .03125 = .322842598$$

$$\text{probability}(1 \text{ is best FOM}) = 1 - .354092598 = .645907402$$

$$\text{expected best}(\text{partition } 5) = 1.540032359$$

By writing this theory into a Microsoft QBASIC program and supplying it with the proper histograms, we were able to generate all the RAND data points. Then we graphed the data with Microsoft Excel and stored for future use. Please note that these RAND data points are strictly theoretical. We obtained none of the RAND data points by using FLASH.

To make the trends in the data more comparable between functions of different DFCs, we normalized all the data by using Axtell's normalization technique, which is the following:

For each partition in each function:

$$\text{normalized(FOM)} = ((256 - \text{FOM}) / (256 - \text{Lowest FOM of Function}))$$

This brings everything into the same scale. Now all the numbers become a decimal representation of less than or equal to one where negative is indicative of increase on the cardinality of a decomposition, one is 100% decomposition, zero is 0% decomposition. The lowest FOM of the function is the lowest known FOM (or minimum DFC) over the entire function. This normalization technique allows us to make decisions based on the graph of the data. As a rule, by the time we reach the last partition, we reach the lowest FOM. We label these new values as percentage of optimal, optimal being the best FOM that this particular function can have.

3.2 Figure of Merit Experiments

The next logical step was to study the figures of merit themselves. In order to determine which partitions were the best, a good FOM had to be established. To compare them, several tests were run.

3.2.1 Percent of Optimal

In this experiment, for each function we compared the FOM values of each partition with what we knew to be as "true", or best known optimal. This gave us a good idea of which partitions were the best to look at.

In order for this experiment to work, a set of optimals had to be established. We compiled a list of true optimals from all the decomposition methods we had including, but not limited to: Child

Cardinality, Grandchild Cardinality, A.F.D. (Ada Function Decomposer), and manually. Then, we extracted the partition data from FLASH's output files. Using Axtell's normalization technique, we scaled the data and plotted it with Microsoft Excel for comparison. This was done for the first 27 functions in the Benchmark Set. The data pointed to certain partitions being optimal more frequently than others. In order to better study this phenomenon, another test was devised.

3.2.2 Optimality Counts

The best way to see which partitions occurred most frequently was to actually count the number of times that each partition was optimal in all functions. This way, any trends could be noted and studied further. To extrapolate the optimal partitions from each function, a Microsoft QBASIC program was developed. This program gave us a listing of exactly which partitions were optimal in each function. To count the number of times they occurred throughout all the functions, another Microsoft QBASIC program was developed. What we found is that while certain blocks of partitions are never optimal over the 27 functions, certain partitions that occur near (within three partitions of) or, in some cases, directly after a major event in the way a partition is evaluated, tend to have a very high frequency of optimality. This means that certain events may cause, or at least are indicative of optimal partitions. This would give us a way to "predict" the optimality of a partition, or at least know where a good starting point for our search is. However, this is only theory and we have no evidence to back it up at this time. A major cause of this phenomenon may be our choice of functions for the Benchmark Set. These tests were run for data generated by both the SOCC and the SOGCC algorithms. To better visualize the results, the data was plotted using Microsoft Excel.

3.2.3 Partition Matching

The next step was to determine the correlation of the optimal partitions from child cardinality and the optimal partitions from grandchild cardinality. Using the data files of optimal partitions from the last experiment, a Microsoft QBASIC program was developed to determine the correlation between these two sets. Specifically, it found all of the matches to the child cardinality optimal set in the grandchild

cardinality optimal set, and found all of the matches to the grandchild cardinality optimal set in the child optimal set. An explanation of the printout:

3.2.4 Least Sets of Optimals

In an attempt to further study the optimal partition sets of a function, several attempts were made to determine the least set, or smallest set, of optimal partitions that would represent every function. Non Polynomial, or NP functions are classified as functions where the time it takes to find a solution increases faster than polynomial as function(number of input variables). This problem, however, is classified as "NP hard", which means that a fast solution to this problem is probably impossible. The problem of set coverage is classified as NP hard. After many failed attempts to get a perfect set of optimal partitions, a "fairly perfect", or "near perfect", set was compiled.

The first attempt at this problem was a basic "search and destroy" algorithm. It searched through an array of all the optimal partitions for the 27 functions, and tried to account for the functions with the partition that occurred most frequently by searching from the first function to the last function, skipping over any already accounted for function. It keeps processing like that until all of the functions have been accounted for. Unfortunately, certain degree of randomness occurs in this algorithm. Enough so, if the program is redesigned to start at the last function and end with the first function, the answer set is different. This was not entirely unacceptable, but did not provide the absolute best set, either.

While examining the data, we discovered that the optimal partitions of a certain functions were subsets of other functions. These subsets were the basis for the next experiment. A pseudo-code representation of the program is on the next page.

```

program bad_attempt;

begin
  read in FN X Partition array;
  done = false
  while not done do
    begin
      find largest valid function;
      repeat
        search other valid functions for subsets;
        if subset_found = true then eliminate subset
          else goto next function;
      until out_of_functions = true;
      invalidate largest valid function;
      mark it as a base function;
      if no_valid_functions_left = true then
        done = true;
      end;
      determine number of occurrences of partitions in base functions;
      select optimal set;
      write optimal set;
    end.
  end.

```

As the name of the program might indicate, the experiment was unsuccessful. The program gave us a set of four optimal partitions. This, however, was not the answer we were trying to reach. The program selected the best set from the subsets. Whereas all the subsets were represented, not all of the functions were represented. Keep in mind that { 2, 3 } is a subset of the major set { 2, 3, 5, 8 }, but if 5 occurs the most in the major sets, the subset, in this case, will not be represented.

The idea then came to try to "cross-reference" the original data and the new data. The theory was that by first eliminating what it could by subset, then determining the best set from the remaining unrepresented subsets, a better optimal set could be compiled. However, the resulting set was no better than the original. The problem is to be studied further later.

4.9 CONCLUSIONS

The initial results of this study indicate that the IRC algorithm is definitely the best of the three baseline non-exhaustive search methods. However, it is not clear which of the figures of merit (SOCC and SOGCC) should be used to determine the fitness of a partition. At first glance, it seems that grandchild cardinality is a safe assumption as the best. However, 70.6% of the time the partitions that are optimal child cardinality are optimal for grandchild cardinality. This would prove to make child cardinality dominant considering that grandchild cardinality takes a much longer time to process than it takes to use child cardinality. This is only speculation and at this time there is no evidence to back it up.

These results may be anecdotal --biased by the figures of merit, or functions in the Benchmark Set. Additional experimental and theoretical work is necessary before the results presented here can be considered conclusive.

Scott Williams's report not available at time of publication.

Interpolation in Load-Pull Measurement System's Power Device Characterization

Nicholas T. Campanile
Beavercreek High School
University of Cincinnati
Cincinnati, OH

Lois Kehias
Wright Laboratory
Wright Patterson AFB, OH

Final Report for:
Summer Research Program
Wright Laboratory

Sponsored by:
Air Force Office of Summer Research
Wright Patterson Air Force Base, Dayton, OH

August 1993

INTERPOLATION IN LOAD-PULL MEASUREMENT SYSTEM'S
POWER DEVICE CHARACTERIZATION

Nicholas T. Campanile
Beavercreek High School

WL/ELM

Abstract

The primary summer focus was on the analysis of a load amplifier and the measurement of impedance's at various tuner states. Taking actual measurements is a time consuming and inefficient process for the professional world. Therefore, it is necessary to consider that an amount of values is accurate without actually measuring them but by effectively gathering data by interpolation. EEsof's commercial package Anacat allows for such a program to be written while storing the newly created data in recallable files.

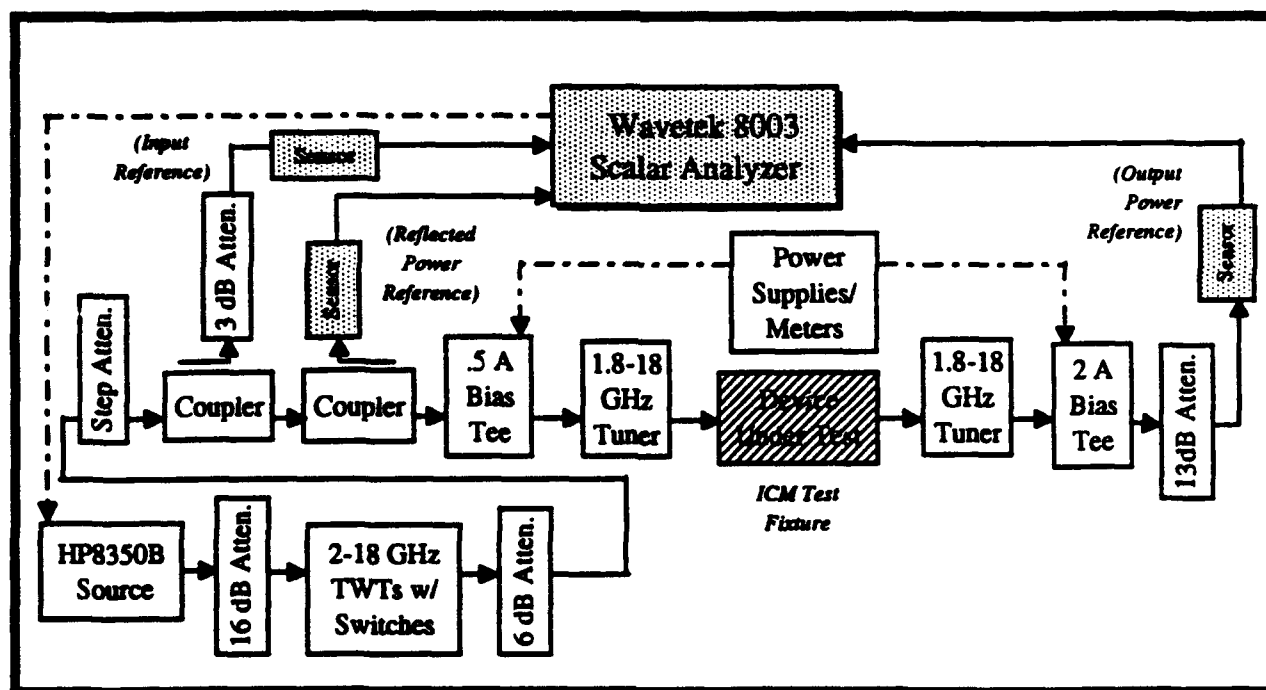
INTERPOLATION IN LOAD-PULL MEASUREMENT SYSTEM'S

POWER DEVICE CHARACTERIZATION

Nicholas T. Campanile

INTRODUCTION:

Accurate power device characterization is critical in achieving high yields and design success with few design/fabrication iterations. However, in the early history of microwave transistor power amplifiers, the amplifier had to be disassembled so that the experimentally determined source and load reflection coefficients could be measured. Load pull measurements alleviated this problem by allowing for impedance measurements which did not require amplifier disassembly. Below is a load pull system setup:

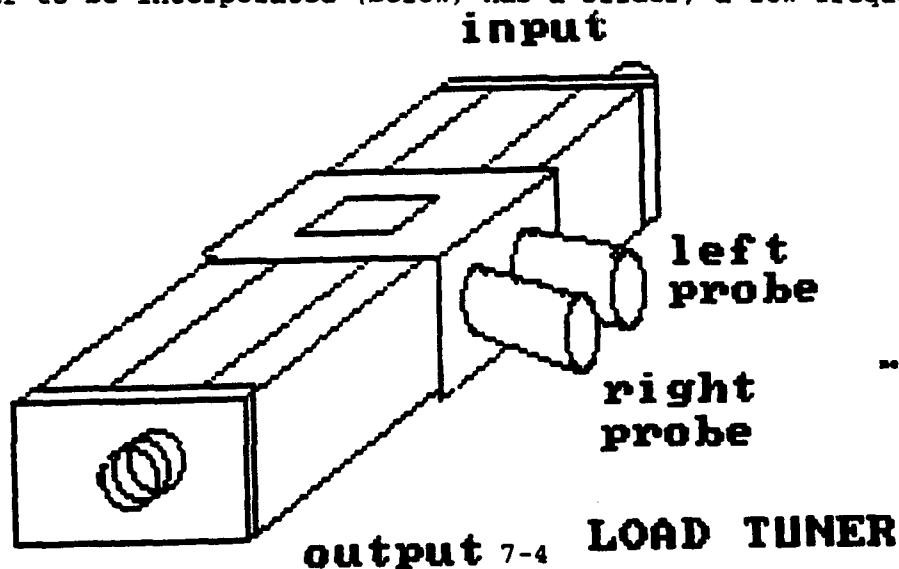


**BLOCK DIAGRAM OF SCALAR POWER SET-UP FOR LOAD-PULL MEASUREMENTS
(FOR POWER DEVICE LARGE-SIGNAL CHARACTERIZATION)**

Large signal device modeling and load/source pull measurements are two approaches presently being used to meet power amplifier performance goals. This task focused on software and system development of a passive source/load pull measurement system which is used to perform microwave scalar power measurements on in-house (Solid State Electronics Directorate, Wright Laboratory) developed novel, high-power density, heterojunction bipolar transistors (HBT's).

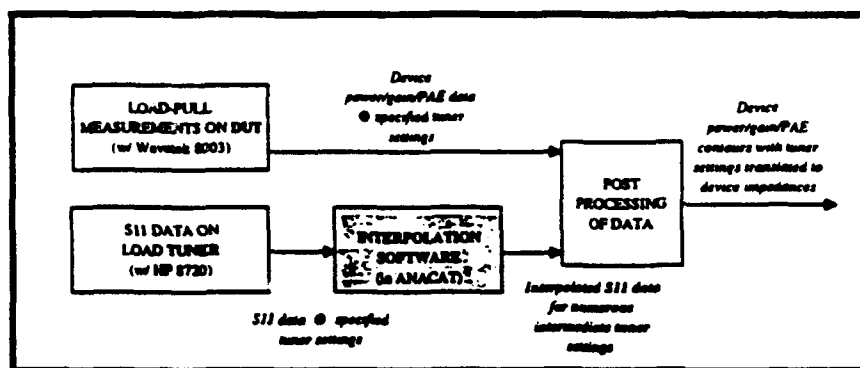
Discussion of Problem:

Load pull measurements provide power transistor input and output impedance match information under large signal conditions. Output power, gain, and power-added-efficiency contours can be mapped under various impedance match conditions. These contours are then used in designing input and output matching circuits for power amplifiers. Measurements of the S-parameters were taken for approximately 720 manually set impedance states. This accomplishment still left thousands of states uncalculated. To save time, the implementation of an interpolation program became a necessity. The tuner to be interpolated (below) has a slider, a low frequency (left) probe,

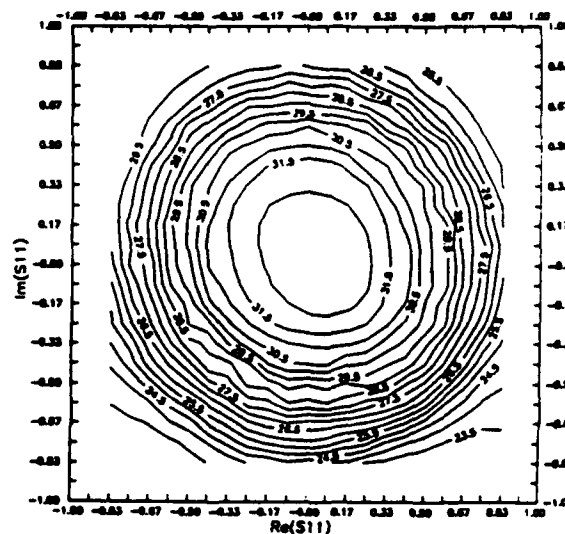


measured states were
every 10th slider pos
every 3rd probe pos

and a high frequency (right) probe. Since measurements were to be taken mainly at 10 gigahertz (GHz), the ideal interpolation program must interpolate for slider and right probe positions. EEsos's Anacat, which uses a scripting language similar to BASIC, was used to develop the programs necessary for interpolation. Below is a chart of how Anacat, the network analyzer, and the load pull measurement system interact to eventually give a contour plot (right).



POWER DEVICE CHARACTERIZATION FLOW CHART



EXAMPLE OF POWER CONTOUR PLOT
(3-D representation of output power @ various output impedance match conditions)

Methodology:

Upon my arrival at Wright Laboratory, the idea of a user defined interpolation program had not only been discussed but also started. Dr. James Hwang, a consultant from Lehigh University had already written two user script programs on Anacat to interact with stored impedance states. The first program was a single frequency extract program. Anacat stores data of one tuner setting (i.e. slider position, left probe position, right probe position) for a range of frequencies (usually we measured between two and eighteen gigahertz); however, the extract program recalls the measured data of one frequency through different tuner positions. Due to Anacat's

setup, though, when data is displayed the tuner range is displayed under the frequency heading. Please note this in plotted charts. This first program is the basis for all other Anacat programs written by both Dr. Hwang and me; furthermore, this first program was a good reference for me to look at while trying to understand the MLF (language) file system -- I could "look and learn" as opposed to having to read the manual. Dr. Hwang's second program actually did interpolations for unmeasured slider positions, thus setting the stage for numerous other interpolation possibilities.

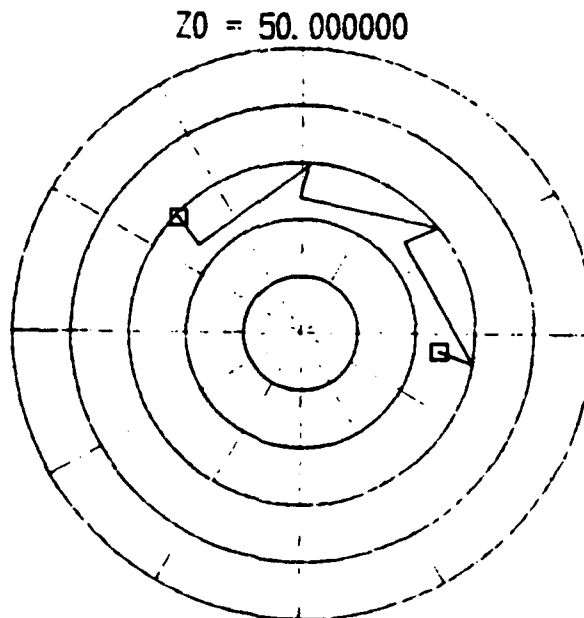
Creating left or right probe interpolator programs was not too difficult because many of the same principles used in the slider interpolation program could be implemented. The recalled files and interpolation functions had to be revised while new angle debugging situations had to be accounted for; but for the most part, no new code needed to be added.

Quite the reverse was true while I dealt with my final program. The final program was to be a user defined interpolation program allowing for the simultaneous interpolation between right probe and slider positions to support measurements between tuner positions 503309 and 993333 (sli lfp rtp). Many questions arose in designing this program. What extra variables need to be added? What limitations will the program have? What is the most efficient way to set up the program? In order to cut down on processing time, I wrote a program that would call two previously stored measurements and interpolate the positions between these measurements (i.e. 503309 & 603312 would be recalled to interpolate 523311). The problem with this program principle was that there was nothing in the interpolation subroutine to decipher differences between change in slider position and change in right probe position. The end result

was a smooth curve going from position one to position two as opposed to the jagged curve I was expecting. In order for the program to work correctly, four positions had to be considered (i.e. 503309, 503312, 603309, 603312). In this setup, three interpolations are done -- two are done to interpolate the probe position at its respective slider position and the final interpolation combines the two slider positions. Had the previous idea worked, it still would have been limited in that it couldn't jump between different tested values (the slider must stay in range of ten multiples and the probe must stay in range of three multiples). The final version had no measurement restrictions; however, processing time practically quadrupled due to the added code. See appendix I for a flowchart of program setup.

Results:

The final output of interpolated data from 723310 to 723311 appears like this:

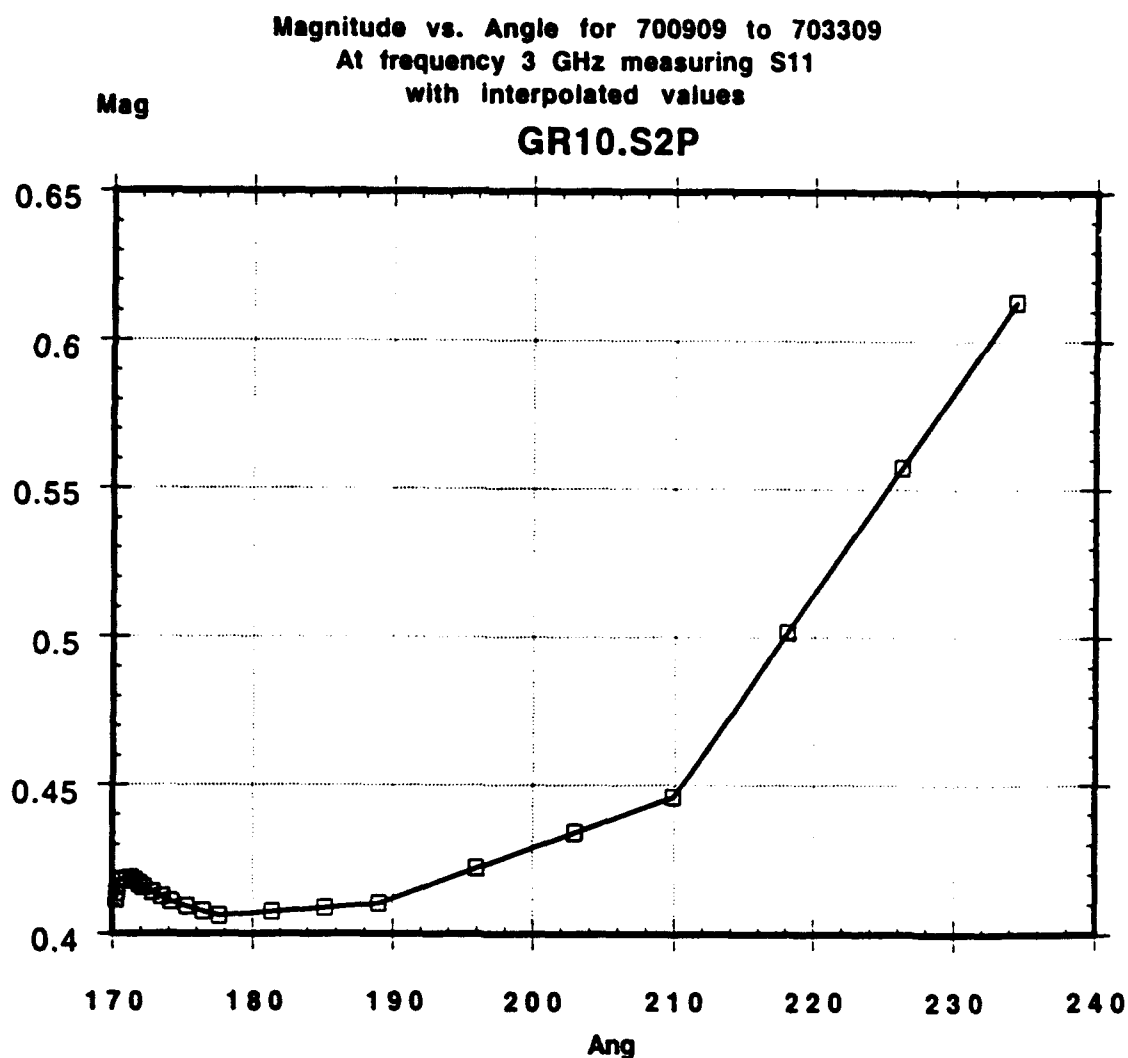


Freq(GHz): 723310. to 783311.

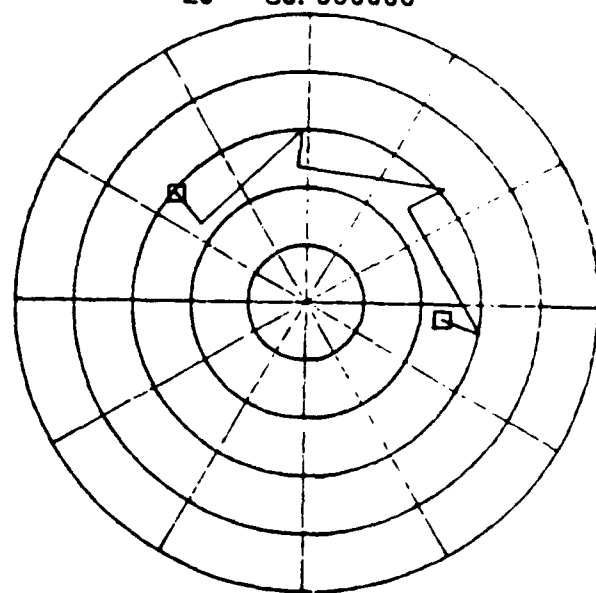
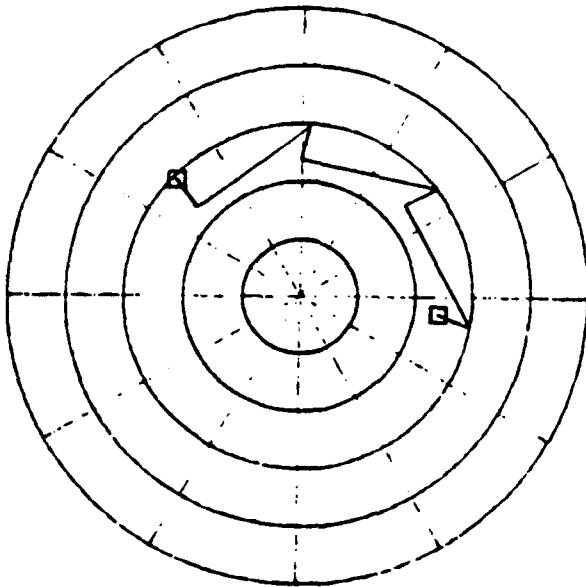
Note the straight lines are just connectors between the jagged interpolated

measurements. Had my original double interpolation routine been used instead, there would have been a smooth curve going from one box to the other-- not representing the actual impedances.

After finishing a program it is important to verify that it works. I verified the single interpolation program by graphing the gathered magnitude and angle calculations for interpolated and measured states. The interpolated data appears at one third intervals of the measured data as expected.



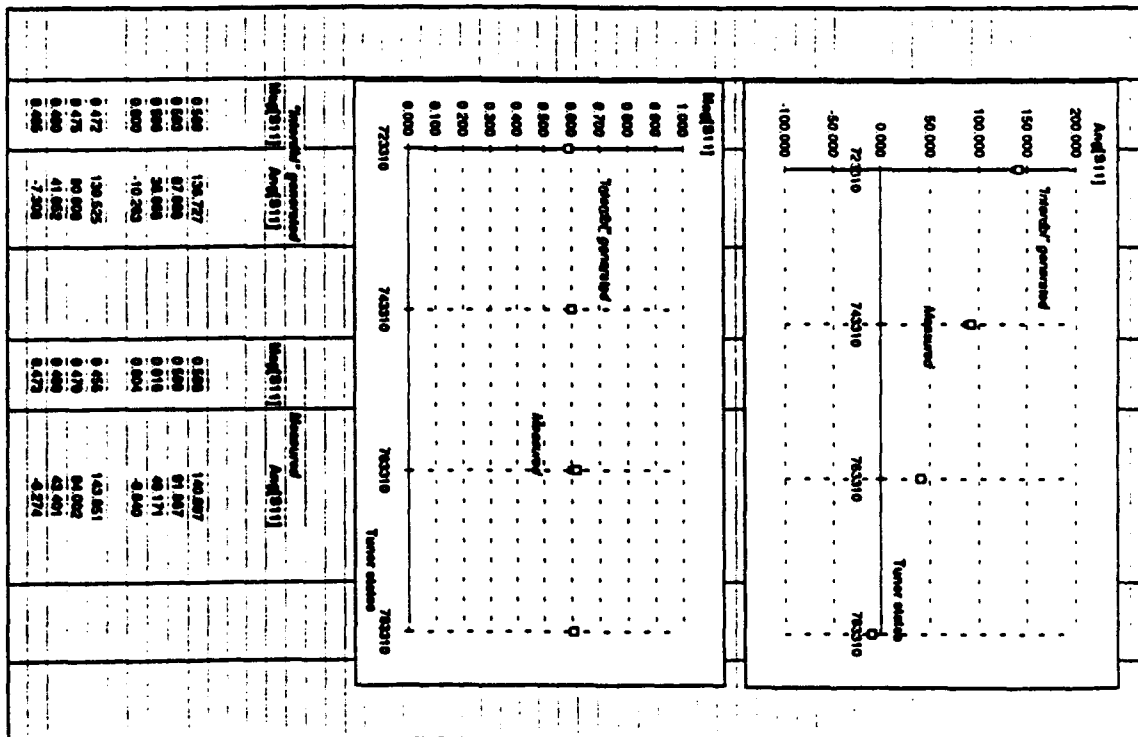
To verify the double interpolation program, I took actual measurements through Anacat from an HP 8720 network analyzer to compare to the interpolated data at $Z_0 = 50.000000$



Freq(GHz): 723310. to 783311.

Freq(GHz): 723310. to 783311.

the same position. The following chart illustrates the measurement / interpolation comparison.



Conclusions:

By using Anacat and the scripting program I wrote, one can quickly and accurately illustrate path and direction of impedance states as the slider and right probe change positions.

To illustrate how vital a method it is to interpolate impedances rather than measuring all of them, it is necessary to consider what had happened before I worked with the Anacat program. For use as foundation measurements, my mentor along with Dr. Hwang measured data from the network analyzer at 720 different positions. This task took three straight ten hour days. After my program was finished, I was able to define it to calculate about 3000 positions in one sitting. This took an estimated four to six hours, for which I never once had to be at the computer!

References:

Michael G. Adlerstein and Mark P. Zaitlin; "Power Contours For Microwave

HBTs"; Ratheon Research Division; Lexington, MA; copyright 1993.

Ken Kotzebu; "Load Pull Methods and Applications"; Hewlett - Packard Co.;

Santa Rosa, CA.

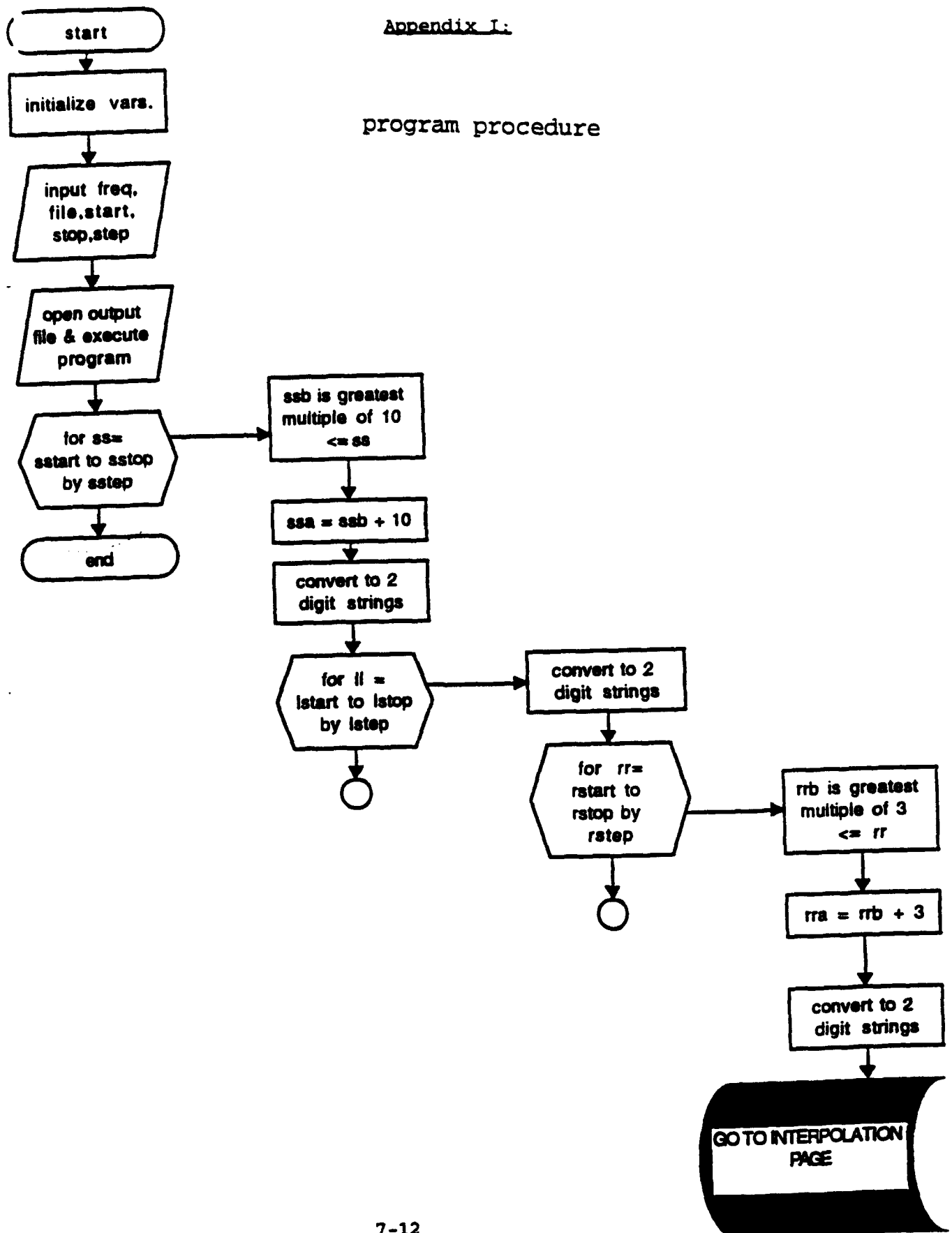
M.P. Mack et. al.; "Microwave Operation of High Power InGaP/GaAs

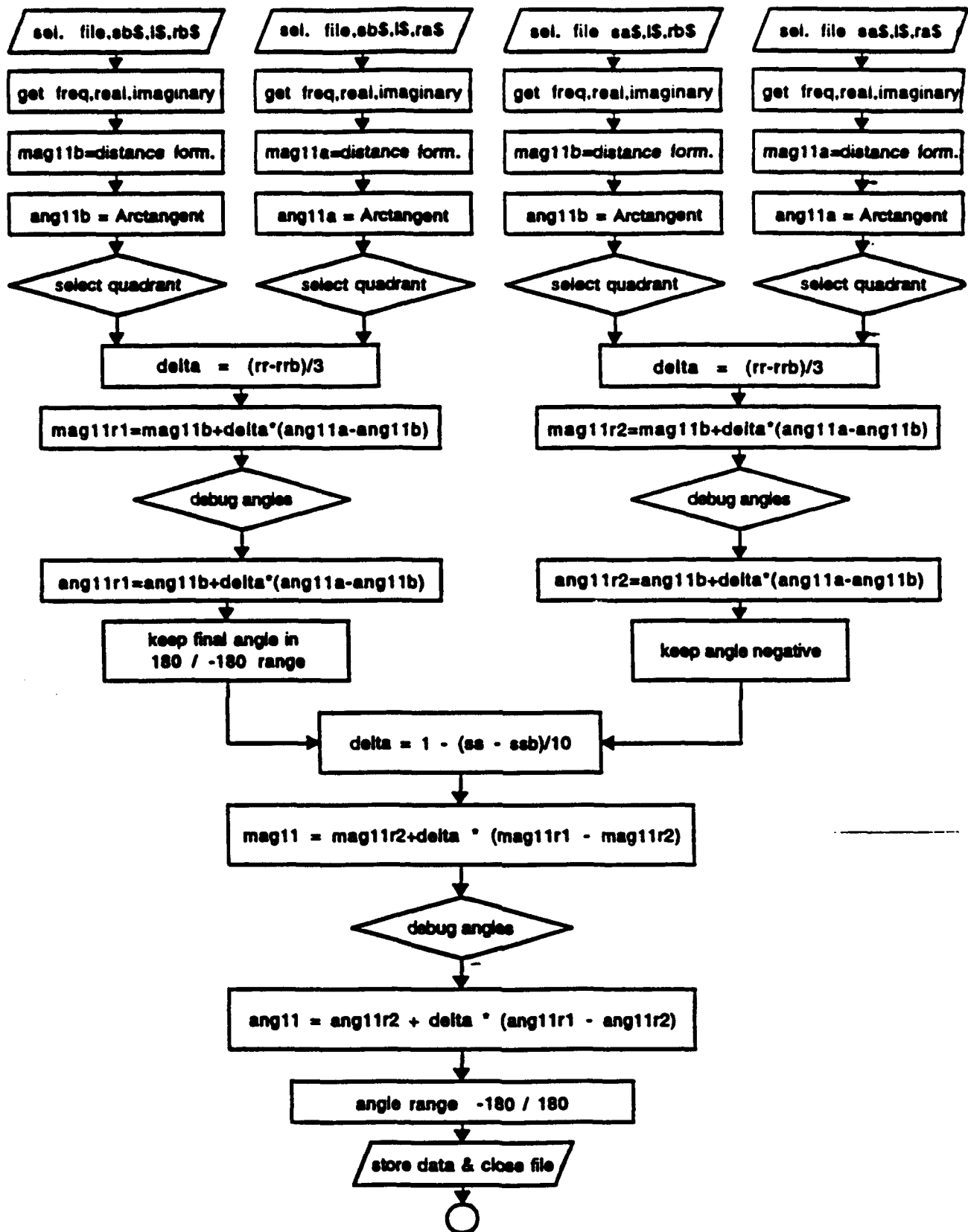
Heterojunction Bipolar Transistors"; Electronics Letters; copyright

1993; vol. 29, No. 12.

Appendix I:

program procedure





Appendix II:

!TO EXTRACT SINGLE FREQUENCY DATA FROM S-PARAMETER FILES AND
!MERGE THE SINGLE FREQUENCY DATA INTO AN MDF FILE ?.S2P
!FREQUENCY DATA IN THE FILE WILL BE REPLACED BY TUNER POSITION SSSLRR
!LEFT TUNER SLUG POSITIONS MUST HAVE BEEN MEASURED
!rt pribe & SLIDER POSITIONS THAT HAVE NOT BEEN MEASURED WILL BE INTERPOLATED
!HOWEVER, FINAL SLIDER POSITION MUST BE LESS THAN 100
!WHEN PROMPTED YOU MAY GIVE THE SAME INITIAL AND FINAL POSITIONS TO EXTRACT
!SINGLE POSITION DATA. IN THIS CASE GIVE ANY INCREMENTAL VALUE EXCEPT ZERO
!MARCH 5, 1993, JAMES C.M. HWANG, LEHIGH UNIVERSITY, (215) 758-5104
!July 1993, revised by Nick Campanile to DO THE DOUBLE INTERPOLATION

! DATA SPECEFICATIONS AND INTIALIZE VARIABLES

INTEGER SSA, SSB !nearest integers above or below SS
integer RRA, RRB !nearest integers above or below RR
REAL DELTA !difference between SS and SSB
REAL FF !frequency in GHz
REAL SS !current tuner slider position
REAL LL !current left slug position
REAL RR !current right slug position
REAL RE11, IM11, MAG11, ANG11 !real & imaginary value,magnitude,angle for S11
REAL RE12, IM12, MAG12, ANG12
REAL RE21, IM21, MAG21, ANG21
REAL RE22, IM22, MAG22, ANG22
REAL RE11A, RE11B, IM11A, IM11B !s-parameters of nearest slider positions
REAL RE12A, RE12B, IM12A, IM12B !above and below for interpolation purpose
REAL RE21A, RE21B, IM21A, IM21B
REAL RE22A, RE22B, IM22A, IM22B
REAL MAG11A, MAG11B, ANG11A, ANG11B
REAL MAG12A, MAG12B, ANG12A, ANG12B
REAL MAG21A, MAG21B, ANG21A, ANG21B
REAL MAG22A, MAG22B, ANG22A, ANG22B
REAL MAG11R1,MAG11R2,ANG11R1,ANG11R2 !intermediate interpolation values

DIM DS !data base file name without SS.DAT
DIM FS !frequency in GHz
DIM SS, SSTART\$, SSTOP\$, SSTEP\$
!current, initial, final and incremental slider positions
DIM SAS, SBS !string representations of SSA and SSB
DIM LS, LSTART\$, LSTOP\$, LSTEP\$
!current, initial, final and incremental left slug positions
DIM RS, RSTART\$, RSTOP\$, RSTEP\$
!current, initial, final and incremental right slug positions
DIM RAS, RBS !string representations of RRA and RRB
DIM FIS !MDF file name to save the extracted data

USERIN "enter frequency __GHz", FS !input data values
USERIN "enter data file name __SS.DAT", DS
USERIN "enter initial slider position", SSTART\$!"50"<=SSTART\$<="100"
USERIN "enter final slider position", SSTOP\$
USERIN "enter slider increment", SSTEP\$!must be greater then 0
USERIN "enter initial left slug position", LSTART\$!"09"<=LSTART\$<="33"
USERIN "enter final left slug position", LSTOP\$
USERIN "enter left slug increment", LSTEP\$!must be greater then 0
USERIN "enter initial right slug position", RSTART\$!"09"<=RSTART\$<="33"
USERIN "enter final right slug position", RSTOP\$
USERIN "enter right slug increment", RSTEP\$!must be greater then 0

USERIN "save under file name __.S2P", FIS !save file
FIS = FIS & ".S2P"
IF EXIST(FIS) THEN
IF USERYN("overwrite existing file? ") THEN
OPEN 1, "OUTPUT", FIS !store in exterior file
CLOSE 1

```

END IF
END IF

IF NOT USERYN("O.K. to execute? ") THEN GOTO DONE      !execute program

FOR SS = VAL(SSTART$) TO VAL(SSTOPS) STEP VAL(SSTEPS) !open slider loop
SS = LJUST$(STR$(SS), 2)                               !store SS as a string
SSB = 10*INT(SS/10)  !initialize SSB as the greatest multiple of 10 <= SS
IF SSB < 50 THEN SSB = 50
SBS = LJUST$(STR$(SSB), 2)                             !store SSB as string
SSA = SSB + 10     !initialize SSA as the smallest multiple of 10 > SS
IF SSA > 99 THEN SSA = 10
SAS = LJUST$(STR$(SSA), 2)                             !use only the first 2 digits of position

FOR LL = VAL(LSTART$) TO VAL(LSTOPS) STEP VAL(LSTEPS) !open left probe loop
L$ = STR$(INT(LL))                                     !store LL as a string
IF LEN(L$) < 2 THEN L$ = "0" & L$                     !concatinate "0" before a single digit #

FOR RR = VAL(RSTART$) TO VAL(RSTOPS) STEP VAL(RSTEPS) !open right probe loop
R$ = STR$(INT(RR))                                     !store RR as a string
IF LEN(R$) < 2 THEN R$ = "0" & R$                     !concatinate "0" before a single digit #
RRB=3*(INT(RR/3))   !initialize RRB as the greatest multiple of 3 <= RR
IF RRB<9 THEN RRB=9
RBS=STR$(RRB)                                             !store RRB as a string
IF LEN(RBS) < 2 THEN RBS= "0" & RBS                   !concatinate "0" before a single digit #
RRA = RRB + 3      !initialize RRA as the smallest multiple of 3 > RR
RAS = STR$(RRA)    !store RRA as a string
IF LEN(RAS) < 2 THEN RAS= "0" & RAS                   !concatinate "0" before a single digit #
IF RAS = "36" THEN RAS = "33"                         !keep largest number within range limit

FF = VAL(F$) * 1e9                                     !convert gigahertz to hertz
!DISP DS & SBS, L$, RBS
!BREAK
MSEL DS & SBS, L$, RBS                                !magnitude/angle procedure for pt BB
FGETS11 FF, RE11B, IM11B                               !recall stored measurement values
FGETS12 FF, RE12B, IM12B
FGETS21 FF, RE21B, IM21B
FGETS22 FF, RE22B, IM22B
MAG11B = SQR(RE11B*RE11B+IM11B*IM11B)                  !distance formula to find magnitude
ANG11B = 57.29577951*ATN(IM11B/RE11B)                  !arctangent to find angle
IF RE11B < 0 THEN                                       !quadrant selector routine
  IF IM11B < 0 THEN
    ANG11B = ANG11B - 180
  ELSE
    ANG11B = ANG11B + 180
  END IF
END IF
MAG12B = SQR(RE12B*RE12B+IM12B*IM12B)
ANG12B = 57.29577951*ATN(IM12B/RE12B)
MAG21B = SQR(RE21B*RE21B+IM21B*IM21B)
ANG21B = 57.29577951*ATN(IM21B/RE21B)
MAG22B = SQR(RE22B*RE22B+IM22B*IM22B)
ANG22B = 57.29577951*ATN(IM22B/RE22B)
! DISP DS & SBS, L$, RAS
! BREAK
MSEL DS & SBS, L$, RAS                                !magnitude/angle procedure for pt. BA
FGETS11 FF, RE11A, IM11A                               !recall stored measurement values
FGETS12 FF, RE12A, IM12A
FGETS21 FF, RE21A, IM21A
FGETS22 FF, RE22A, IM22A
MAG11A = SQR(RE11A*RE11A+IM11A*IM11A)                  !distance formula to find magnitude
ANG11A = 57.29577951*ATN(IM11A/RE11A)                  !arctangent to find angle
IF RE11A < 0 THEN                                       !quadrant selector routine
  IF IM11A < 0 THEN
    ANG11A = ANG11A - 180
  ELSE

```



```

    ANG11A = ANG11A + 180
  END IF
END IF

MAG12A = SQR(RE12A*RE12A+IM12A*IM12A)
ANG12A = 57.29577951*ATN(IM12A/RE12A)
MAG21A = SQR(RE21A*RE21A+IM21A*IM21A)
ANG21A = 57.29577951*ATN(IM21A/RE21A)
MAG22A = SQR(RE22A*RE22A+IM22A*IM22A)
ANG22A = 57.29577951*ATN(IM22A/RE22A)

DELTA = (RR-RRB)/3                                !first probe interpolation
MAG11R1 = MAG11B+DELTA*(MAG11A-MAG11B)            !magnitude interpolation
IF ANG11A < ANG11B THEN
  IF ANG11A < 0 AND ABS(ANG11A-ANG11B)>180 THEN ANG11A=ANG11A+360
END IF
ANG11R1 = ANG11B+DELTA*(ANG11A-ANG11B)            !angle interpolation
IF ANG11R1 > 180 THEN ANG11R1 = ANG11R1 - 360      !keep angle positive
MAG12 = MAG12B+DELTA*(MAG12A-MAG12B)
ANG12 = ANG12B+DELTA*(ANG12A-ANG12B)
MAG21 = MAG21B+DELTA*(MAG21A-MAG21B)
ANG21 = ANG21B+DELTA*(ANG21A-ANG21B)
MAG22 = MAG22B+DELTA*(MAG22A-MAG22B)
ANG22 = ANG22B+DELTA*(ANG22A-ANG22B)

!DISP DS & SAS, LS, RBS
!BREAK
MSEL DS & SAS, LS, RBS                            !magnitude/angle procedure for pt AB
FGETS11 FF, RE11B, IM11B                          !recall stored measurement values
FGETS12 FF, RE12B, IM12B
FGETS21 FF, RE21B, IM21B
FGETS22 FF, RE22B, IM22B
MAG11B = SQR(RE11B*RE11B+IM11B*IM11B)             !distance formula to find magnitude
ANG11B = 57.29577951*ATN(IM11B/RE11B)             !arctangent to find angle
IF RE11B < 0 THEN                                  !quadrant selector routine
  IF IM11B < 0 THEN
    ANG11B = ANG11B - 180
  ELSE
    ANG11B = ANG11B + 180
  END IF
END IF
MAG12B = SQR(RE12B*RE12B+IM12B*IM12B)
ANG12B = 57.29577951*ATN(IM12B/RE12B)
MAG21B = SQR(RE21B*RE21B+IM21B*IM21B)
ANG21B = 57.29577951*ATN(IM21B/RE21B)
MAG22B = SQR(RE22B*RE22B+IM22B*IM22B)
ANG22B = 57.29577951*ATN(IM22B/RE22B)
! DISP DS & SAS, LS, RAS
! BREAK
MSEL DS & SAS, LS, RAS                            !magnitude/angle procedure for pt. AA
FGETS11 FF, RE11A, IM11A                          !recall stored measurement values
FGETS12 FF, RE12A, IM12A
FGETS21 FF, RE21A, IM21A
FGETS22 FF, RE22A, IM22A
MAG11A = SQR(RE11A*RE11A+IM11A*IM11A)             !distance formula to find magnitude
ANG11A = 57.29577951*ATN(IM11A/RE11A)             !arctangent to find angle
IF RE11A < 0 THEN                                  !quadrant selector routine
  IF IM11A < 0 THEN
    ANG11A = ANG11A - 180
  ELSE
    ANG11A = ANG11A + 180
  END IF
END IF

MAG12A = SQR(RE12A*RE12A+IM12A*IM12A)
ANG12A = 57.29577951*ATN(IM12A/RE12A)

```

A:\INTERDBL.MLF

```

MAG21A = SQRT(RE21A*RE21A+IM21A*IM21A)
ANG21A = 57.29577951*ATN(IM21A/RE21A)
MAG22A = SQRT(RE22A*RE22A+IM22A*IM22A)
ANG22A = 57.29577951*ATN(IM22A/RE22A)

DELTA = (RR-RRB)/3                                !second probe interpolation
MAG11R2 = MAG11B+DELTA*(MAG11A-MAG11B)             !magnitude interpolation
IF ANG11A < ANG11B THEN
    IF ANG11A < 0 AND ABS(ANG11A-ANG11B)>180 THEN ANG11A=ANG11A+360
END IF
ANG11R2 = ANG11B+DELTA*(ANG11A-ANG11B)             !angle interpolation
IF ANG11R2 > 0 THEN ANG11R2 = ANG11R2 - 360         !keep angles negative
MAG12 = MAG12B+DELTA*(MAG12A-MAG12B)
ANG12 = ANG12B+DELTA*(ANG12A-ANG12B)
MAG21 = MAG21B+DELTA*(MAG21A-MAG21B)
ANG21 = ANG21B+DELTA*(ANG21A-ANG21B)
MAG22 = MAG22B+DELTA*(MAG22A-MAG22B)
ANG22 = ANG22B+DELTA*(ANG22A-ANG22B)

DELTA = 1-(SS-SSB)/10                             !combine interpolation
MAG11 = MAG11R2+DELTA*(MAG11R1-MAG11R2)           !interpolate magnitude
IF ANG11R2 >= ANG11R1 THEN
    ANG11 = ANG11R2+DELTA*(ANG11R1-ANG11R2)       !interpolate angles
ELSE
    ANG11 = ANG11R2+DELTA*(ANG11R1+360-ANG11R2)
END IF
IF ANG11 > 180 THEN ANG11 = ANG11 - 360           !keep angle range bet. -180 & 180
MAG12 = MAG12B+DELTA*(MAG12A-MAG12B)
ANG12 = ANG12B+DELTA*(ANG12A-ANG12B)
MAG21 = MAG21B+DELTA*(MAG21A-MAG21B)
ANG21 = ANG21B+DELTA*(ANG21A-ANG21B)
MAG22 = MAG22B+DELTA*(MAG22A-MAG22B)
ANG22 = ANG22B+DELTA*(ANG22A-ANG22B)

OPEN 1, "APPEND", FIS                             !re-open file in append mode
WRITE 1, SS & LS & RS\                             !store data
    & " " & STR$(MAG11) & " " & STR$(ANG11)\
    & " " & STR$(MAG12) & " " & STR$(ANG12)\
    & " " & STR$(MAG21) & " " & STR$(ANG21)\
    & " " & STR$(MAG22) & " " & STR$(ANG22)
CLOSE 1

NEXT RR                                             !close right probe loop
NEXT LL                                             !close left probe loop
NEXT SS                                             !close slider loop
DONE:                                              !end program
END

```

CALIBRATION OF A REACTIVE ION ETCHING SYSTEM

**Chris Dodsworth
WL/ELR**

**Final Report for:
High School Apprenticeship Program
Wright Laboratories**

**Sponsored by:
Air Force Office of Scientific Research
Wright-Patterson Air Force Base
Dayton, Ohio**

August 1993

Calibration of a Reactive Ion Etching System

Chris Dodsworth
WL/ELR
Wright-Patterson AFB

Abstract

A calibration of the mass flow controllers in our Reactive Ion Etching system in the cleanroom was performed. The correct flow rates for five different gases at multiple settings was determined and graphed. In addition, the maximum flow rates for the gases was also determined and compared to the previous values. This new data will be helpful to researchers because it will enable them to perform reproducible etches.

I studied circuit design for the remainder of the time. I created and attempted to build a traffic light controller using combinatorial logic. Although the model I built did not work, an analysis of the circuit design showed that the design was correct. I came to the conclusion that some of the circuit components used were bad.

CALIBRATION OF A REACTIVE ION ETCHING SYSTEM

Chris Dodsworth

I. Introduction

During the term of my 1993 summer research program, I focused my efforts on two major projects. The first of these was the calibration of the mass flow controllers in our Wafr Batch Series 70 Dual Chamber Reactive Ion Etching (RIE) machine. The mass flow controllers regulate the flow of gas into the chamber. This is a critical measurement, as a small variation in gas concentration or pressure could lead to a non-reproducible etch. To insure that the RIE users would obtain the correct amount of gas flow, a series of graphs were created which correlate the percentage setting on the machine to the actual flow rate in standard cubic centimeters per minute (sccm). The second major focus of my summer research term was understanding basic electronic devices, such as capacitors and transistors, and then utilizing that knowledge to build some basic circuits. This project was not as task-specific as the other; rather, it was designed to provide me with a basic understanding of electronics in preparation for college.

II. RIE Calibration

The Wafr Batch Series Dual Chamber 70 Reactive Ion Etching machine is used to etch through various layers on a wafer and is a key tool in the fabrication of heterojunction bipolar transistors (HBTs). The wafer is placed in an aluminum chamber which is evacuated to .001 torr. Gases then flow into the chamber through miniature holes evenly distributed at the top of the chamber. An RF generator creates a plasma in the chamber by breaking up the gas molecules and exciting the electrons in the resulting ions. These ions are pulled down toward the wafer by a DC bias created by the potential of the plasma relative to the bottom electrode. They can perform either a physical or a chemical etch, or some combination of the two. A physical etch refers to the process of removing layers on the wafer by physically bombarding them with ions; in a chemical etch, the ions react with the layer they are etching to produce a new volatile etch product which is drawn out of the

chamber by the vacuum pump. While a chemical etch can be performed in either the RIE or a simple dish filled with the gas's corresponding acid, a physical etch can only be accomplished inside the RIE. The advantage to a physical etch is shown in figure 1. While a chemical etch is usually isotropic, etching in all directions, a physical etch will provide a very anisotropic etch, creating very straight structures with vertical sidewalls and little undercut. The amount of anisotropic etching one gets from a plasma is dependent on several factors, such as the type of gas used, the DC bias, and the gas pressure. The higher the DC bias, the more anisotropic the etch will be. However, increasing the DC bias too much results in damage to the wafer caused by the impact of the high energy ions. The gas pressure also contributes to the nature of the etch. The higher the pressure, the more isotropic the etch will be. This is due to the reduction in the mean free path of the ions that results from the greater number of gas molecules in the chamber. The ions fail to achieve a significant downward acceleration because of the increase in the number of collisions per unit time. Because of this, they are more readily propelled along other planes, thus etching the structure from all directions. It now becomes apparent why the calibration of the mass flow controllers is so critical; an error in gas flow can result in an altogether different etch. A mass flow controller (*figure 2*) works by sensing a temperature change caused by the flow of gas. A power supply provides a constant power input to the heater, located at the midpoint of the sensor tube. When there is no gas flow, the heat reaching each temperature sensor is equal. When gas flows through the tube, the upstream sensor is cooled while the downstream sensor is heated, producing a temperature difference. This difference is directly proportional to the gas mass flow according to the equation

$$\Delta T = A * P * C_p * m \quad (1)$$

ΔT = change in temperature ($^{\circ}\text{K}$)

C_p = specific heat of gas at constant pressure ($\text{kJ} / \text{kg}^{\circ}\text{K}$)

P = heater power (kJ/sec)

m = mass flow (kg/sec)

A = constant of proportionality ($\text{S}^2 \cdot \text{k}^2 / \text{kJ}^2$)

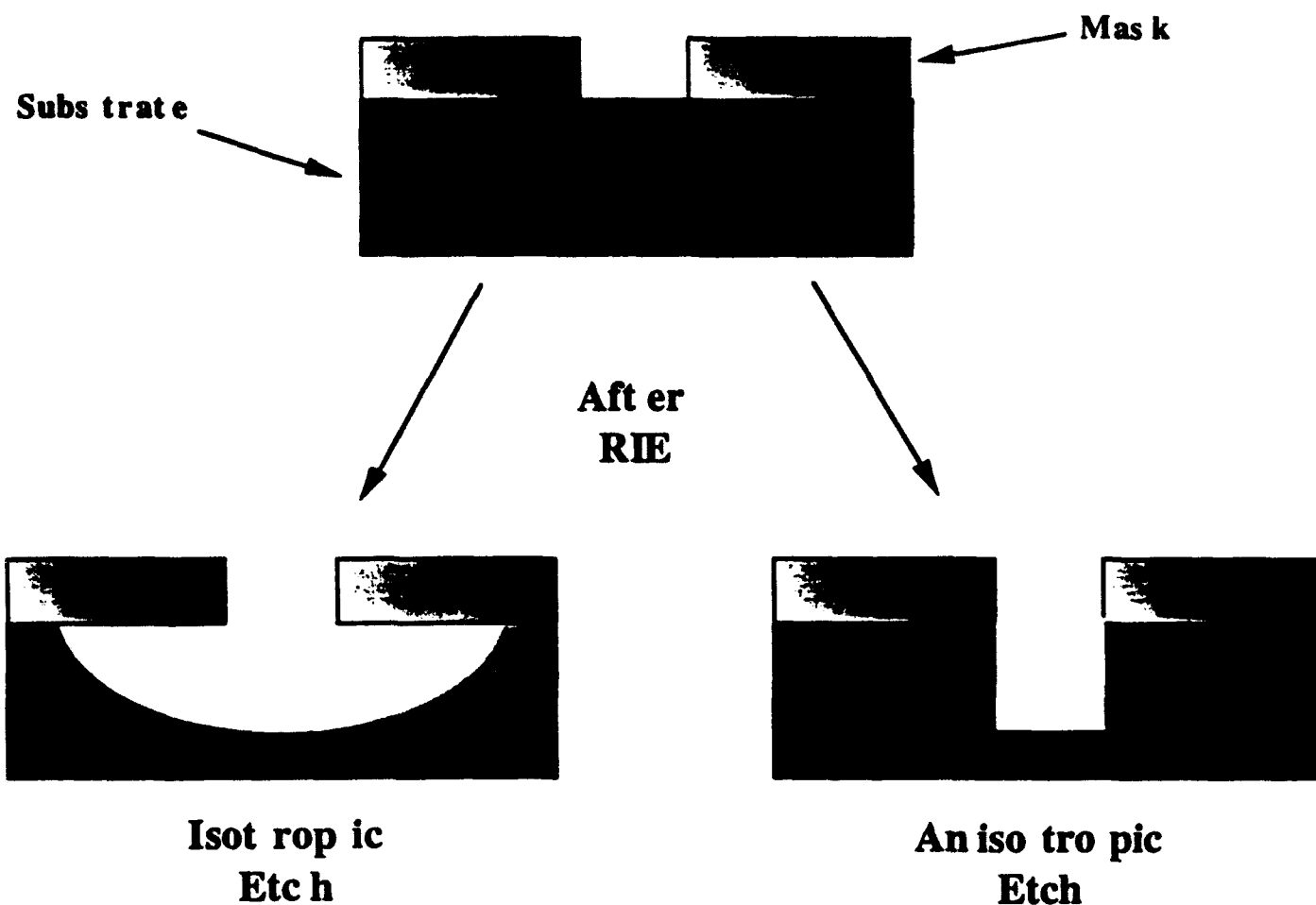


figure 1. Examples of different types of etches. A physical etch produces a very anisotropic structure, while a chemical etch will produce a more isotropic one.

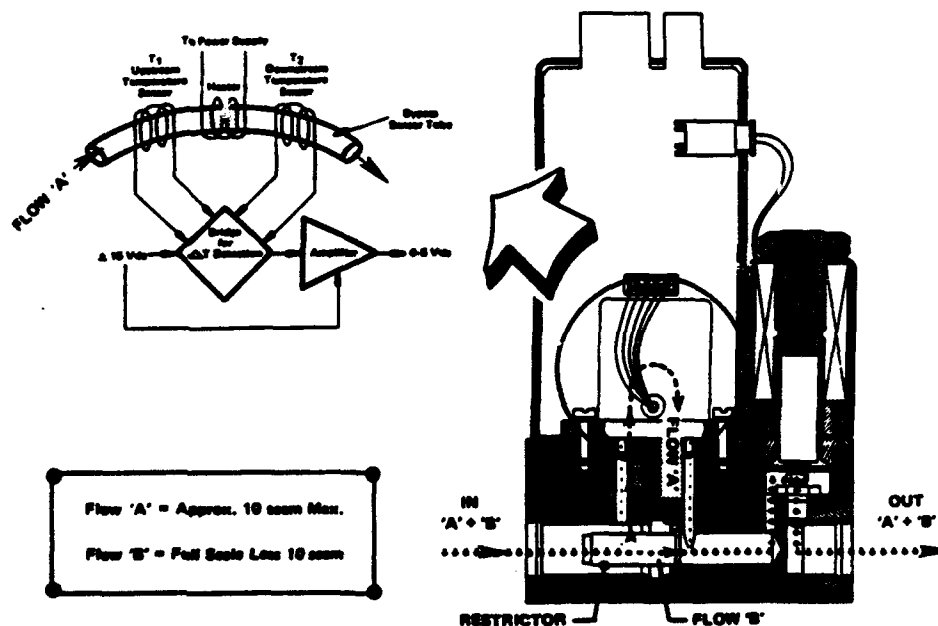


figure 2. Schematic of a mass flow controller.

III. Testing Methodology

The RIE allows the user to key in a percentage of the maximum flow rate for each gas. The mass flow controller then uses a flow restrictor to allow that percentage of gas to flow. In order to ascertain if the mass flow controllers were indeed working correctly, the flow rate was determined mathematically and then compared to what the value should be. The RIE chamber was first pumped down to .002 torr. One gas was turned on at a certain flow percentage, and the resulting pressure was noted. The vacuum was then turned off, and the gas was allowed to flow for a set amount of time. The resulting change in pressure was recorded. Since the volume and the temperature of the chamber is known, it is possible to calculate the gas flow rate according to the equation

$$Q = \frac{\Delta P \cdot T \cdot V}{t} \cdot 78.9 \quad (2)$$

Q = flow rate of gas (sccm)

t = time (seconds)

ΔP = change in pressure (torr)

T = temperature ($^{\circ}\text{K}$)

V = volume (Litres)

78.9 = constant converting torr*L/sec into SCCM

The flow percentages used were 10%, 20%, 50%, 70%, 90%, and 100%. The correct flow for each of these settings was calculated by taking that percentage of the maximum flow rate achieved at 100%.

IV. Results and Discussion

The data obtained through this testing process was placed in a spreadsheet and then graphed. In general, it was found that the heavier gases strayed more from the ideal than the lighter ones (*figure 3*). This was anticipated, since the equation applies to ideal gases, and intermolecular forces of attraction are greater among the heavier molecules. In addition, it was found that the maximum flow rates for the gases were different than what they were believed to be (*figure 4*). This was very true in the cases of Helium and Oxygen. The graphs will compensate for the non-

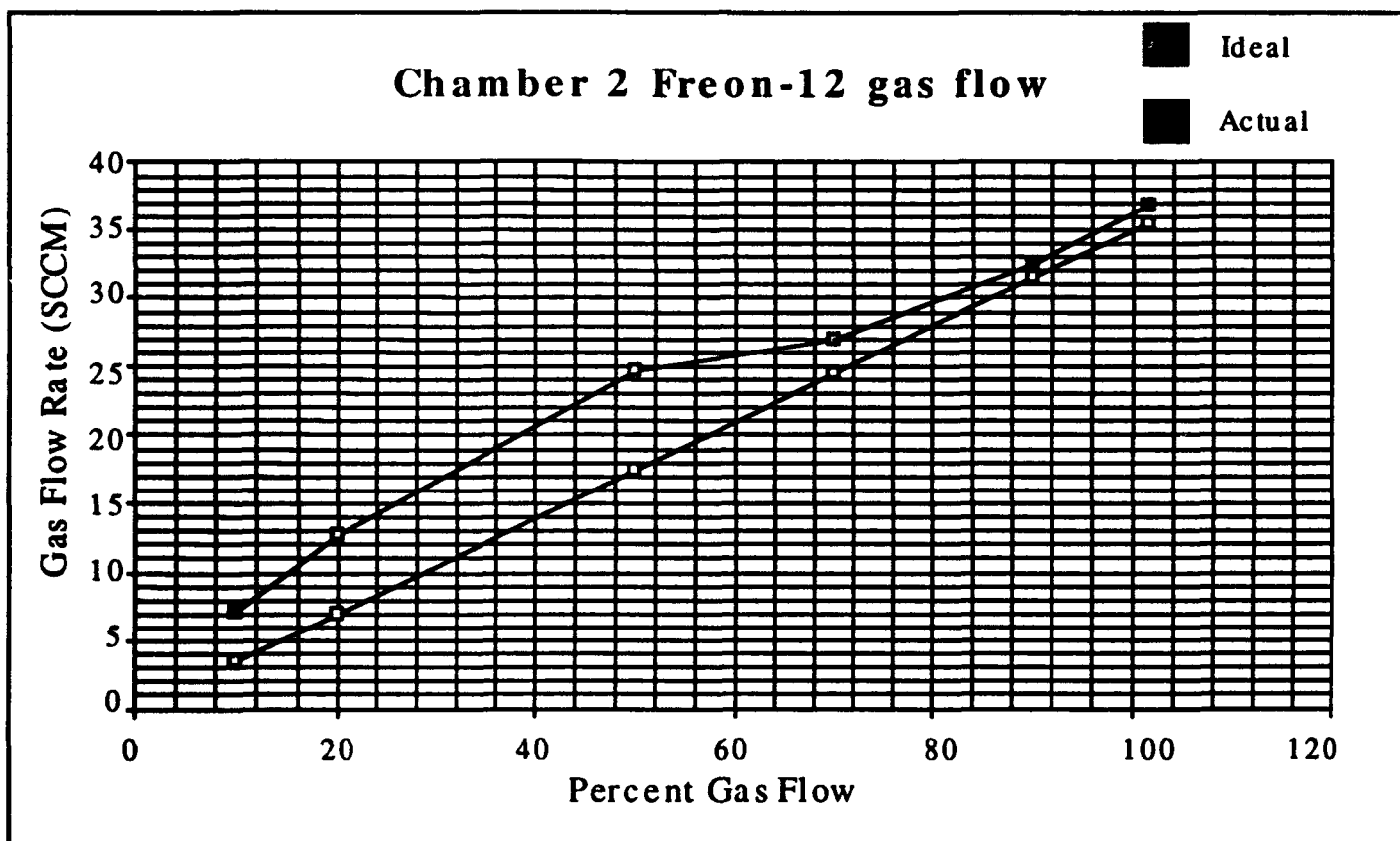
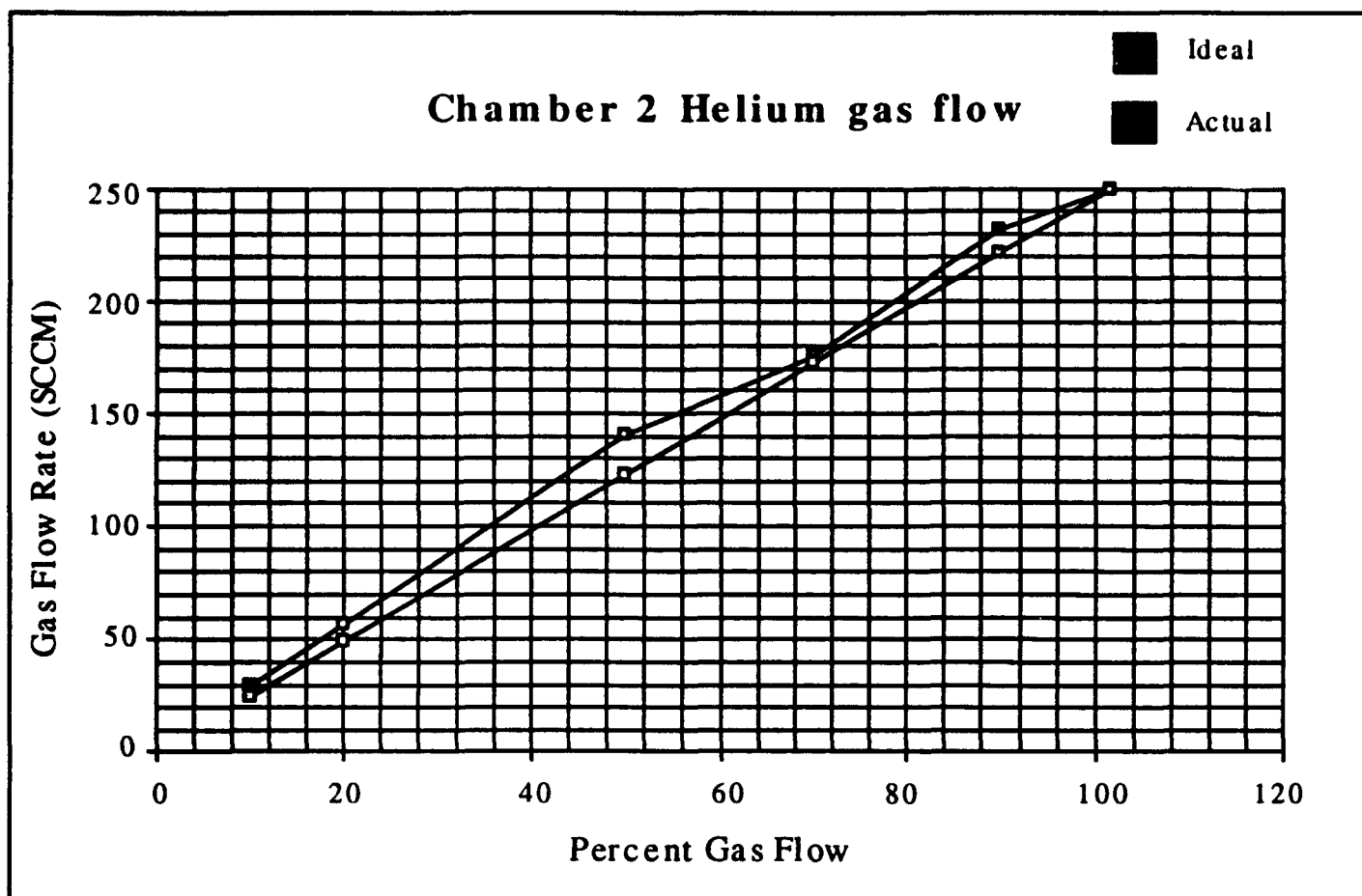


figure 3. Graphs of Helium gas and Freon gas flow. Helium, the more ideal gas, strays less from its expected flow than does Freon.

Chamber 1

<u>Gas</u>	<u>Old Max Flow Rate</u>		<u>New Max Flow Rate</u>	
Oxygen	100	SCCM	87.8	SCCM
Helium	290.8	SCCM	234.6	SCCM
Freon-14	84	SCCM	80.2	SCCM

Chamber 2

<u>Gas</u>	<u>Old Max Flow Rate</u>		<u>New Max Flow Rate</u>	
Freon-12	35	SCCM	36.1	SCCM
Oxygen	100	SCCM	131	SCCM
Helium	290.8	SCCM	246.2	SCCM
Argon	145	SCCM	99.3	SCCM

figure 4. Old and new maximum flow rates for RIE gases in both chambers.

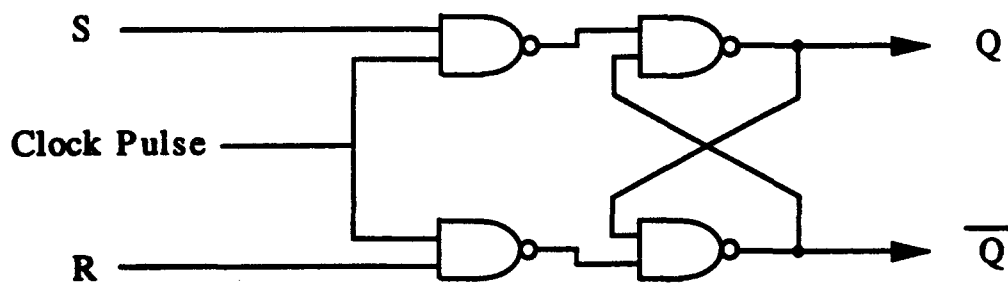


figure 5. An S/R (set/reset) flip-flop with inputs S and R, and outputs Q and not(Q). The flip-flop will change states only when there is a clock pulse, and will hold that state indefinitely.

linearity of the mass flow controllers by providing the RIE user with an accurate knowledge of the flow rate at whatever flow percentage is desired.

V. Electrical Circuit Design

After completing the calibration of the RIE, I concentrated on electrical circuit design and analysis. I spent an initial week studying basic circuit components, such as resistors, capacitors, and transistors. I then breadboarded an S/R flip-flop, shown in figure 5. This served as an introduction to the study of combinatorial logic, which combines both sequential logic, such as binary adders, and state machines, which use flip flops. Once I had a good understanding of combinatorial logic, I put it into practice with the design of a traffic light controller. The controller is designed to drive 7 lights: 3 on a side street, 3 on a main street, and a turn signal from the main street to the side street. There are two inputs: a reset switch, which sets the main street light to green and the side street to red, and a car sensor switch which tells the controller when there is a car on the side street. The state diagram (*figure 6*) is designed so that the main street light will always be green until there is a car on the side street. When a car does come, the controller will then automatically cycle through all the lights. After designing the state diagram, I created the Karnaugh maps for the input to each of the flip flops. A Karnaugh map (*figure 7*) is a tool used to simplify the logic. A 1 is placed wherever the input will be true; a 0 is placed where it will be false. Any grouping of 1s indicate a redundancy. Thus, it is possible to reduce large boolean equations to a simpler form without going through the gyrations of boolean algebra. After I derived all the equations for the flip flops and the output lights, I drew the circuit schematic. To ascertain the circuit's functionality, I wrote a pascal program that would build a truth table for a circuit, given the circuit equations. I also breadboarded the circuit. Unfortunately, the breadboarded circuit did not work. However, when we manually analyzed the circuit, it did work. Therefore, we believe that faulty components were the cause of the circuit's failure.

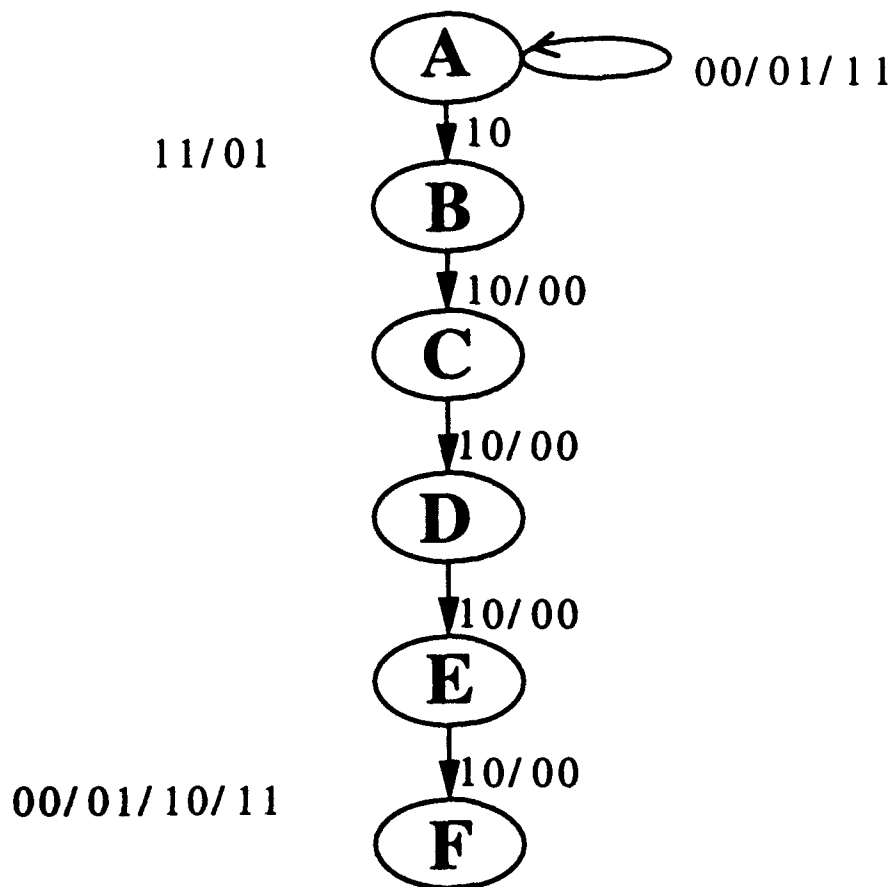


figure 6. State diagram of traffic light controller. The numbers beside the arrows show when the controller changes to a different state. The first number represents the car sensor; the second number, the reset switch.

D₃

y ₃ y ₂ y ₁	00	01	11	10
0 0 0	0	0	0	0
0 0 1	0	0	0	0
0 1 1	0	0	0	0
0 1 0	1	0	0	1
1 0 0	1	0	0	1
1 0 1	0	0	0	0

figure 7. A Karnaugh map for D₃, the D-flip-flop that puts out y₃. With the help of the map, the equation reduces to y₃ = not(R) AND not(y₁).

VI. Conclusion

This summer, I performed a calibration of the Mass Flow Controllers in the RIE system and I designed and tested a combinatorial logic circuit. The new data obtained from the MFC calibration should be of help to researchers. The tests revealed that the MFCs were not providing the proper gas flow. However, the graphs and data collected allow researchers to compensate for that by correctly correlating the gas flow with the percentage setting of gas flow on the machine. This provides an extremely effective way to insure reproducible etches. I learned how to design and create logic circuits capable of performing various tasks. I then utilized this knowledge to design a traffic light controller. While I was unable to build a working model, a hand check of the circuit diagram showed that it did work. Moreover, I gained a better understanding of the circuit design process.

STUDYING THE TRANSMISSION CURVE OF KTP

**Jennifer A. Foley
High School Apprentice
Electro-Optics Sources Branch
Wright Laboratory, Wright Patterson Air Force Base**

**Beavercreek High School
2940 Dayton-Xenia Rd.
Beavercreek, Ohio 45385**

**Final Report for:
AFOSR High School Apprenticeship Program
Wright Laboratory**

**Sponsored by:
Air Force Office of Scientific Research
Bolling Air Force Base, Washington, D.C.**

August 1993

STUDYING THE TRANSMISSION CURVE OF KTP

Jennifer A. Foley
High School Apprentice
Electro-Optics Sources Branch
Wright Laboratory, Wright Patterson Air Force Base

Abstract

The characteristics of the nonlinear crystal KTP were studied primarily using the Nicolet FT-IR. The Perkin Elmer Lambda 9 was also used, though, to measure the transmission of KTP. These instruments measure the transmission of specific wavelengths through a substance. This study lead to the testing of different techniques for using the Nicolet and the Perkin Elmer. During an experiment, certain aspects, such as the amount of time the compartment had been purged, were altered to see how the measurement was affected. By attempting different methods, it is believed that the best possible results were found for studying the crystals. Once this was done, the true transmission of a 10mm long crystal was determined. This was accomplished by subtracting out losses in transmission due to Fresnel reflection and absorption of water vapor and carbon dioxide. An equation was also developed to predict the true transmission of a KTP crystal despite its length. Data from the transmission of two other crystals, 7mm and 13mm in length, were used for predicting the transmission of a 10mm long crystal. The predicted and actual transmission curves show excellent agreement.

STUDYING THE TRANSMISSION CURVE OF KTP

Jennifer A. Foley

Introduction

The first task undertaken was to find the true transmission curve of Potassium Titanyl Phosphate, KTiOPO_4 (KTP). This was to be done by subtracting any absorption due to water vapor or carbon dioxide and any Fresnel reflection. While attempting this, it was observed that changes occurred in the transmission depending on the existing conditions in the spectrometer compartment. For example, the longer the compartment was purged, the fewer absorption peaks due to water vapor and carbon dioxide occurred. Also, the amount of transmission was highly dependent on how the crystal was located in relation to the beam. Therefore, in order to obtain the best possible measurement, setting the instruments correctly was first studied. It was noted while studying transmissions of different crystals that the amount of transmittance was dependent upon the path length of the crystal. Using a 10mm crystal as the standard, a 7mm crystal acted as a basis to predict the transmission of a 10mm crystal. The same was also done using a 13mm crystal.

Apparatus

The Nicolet Fourier Transform Infrared (FT-IR) spectrometer was used primarily for the study. Before a measurement can be taken, the beam splitter must first be aligned to maximize throughput. Then, any apparatus needed to take the measurement must be placed in the compartment. After this, a nitrogen purge is turned on to push out any elements in the atmosphere that may affect the measurement, such as carbon dioxide and water vapor. Testing was first done to find the correct amount of time needed for purging. This was accomplished by taking transmission scans of an empty compartment after it had been purged for different amounts of time. It was discovered by measuring the depth of the spike at 4.3 microns that it was reduced the most after twenty or twenty-five minutes of purging (Figure A).

Once the compartment has been purged for approximately twenty minutes a background scan is run. This accounts for any substances in the compartment. It then subtracts these from the measurement so that only the sample being tested is part of the resulting curve. (The purge may be left on even during a measurement.) After the background, the sample to be measured should be placed normal to the beam. Because the compartment has been opened to place the crystal inside, it is best to let the system purge for about ten minutes before taking the measurement. Numerous measurements, or scans, may be taken until the majority of water vapor and carbon dioxide peaks are gone. This is just an indication of how well the compartment has been purged and has no

bearing on the signature curve of the material.

The Perkin Elmer Lambda 9, another spectrometer that was used for measuring the transmission of KTP, must also be purged before a measurement is taken, but only for about five minutes. To ensure that the amount of purging is correct, a scan of the empty compartment might be made. Once everything is ready, the sample should be placed in the compartment and a measurement should be taken.

The Nicolet measures the wavelength region between 1.35 and 28.57 microns. Scans taken at the extreme ends of this region may not be accurate, though, because of the stress on the detectors. The Perkin Elmer measures a range of 0.185 to 3.2 microns.

Methodology

The transmission of a KTP crystal measuring $10 \times 10 \times 10 \text{ mm}^3$ was first measured in the Nicolet over a range of 1.35 to 28.57 microns. A measurement was then made using the Perkin Elmer in the 0.185 to 3.2 micron region. Transferring this data to SigmaPlot, a software package used for graphing data, the corresponding regions were able to be graphed to ensure the accuracy of the measurements. This graph is displayed in Figure B.

Once this had been established, two other KTP crystals of varied lengths were obtained so that they might also be tested (Figure C). Data points from these were loaded into SigmaPlot where a math transform was performed. Using the equation $R = [(n_{in} - n_{out}) / (n_{in} + n_{out})]^2$, the amount of Fresnel reflection (R) was calculated. The index of refraction for air was used as n_{in} , but because KTP is a nonlinear crystal, the index of refraction is different for each axis and for each wavelength. Values for 1.4 and 4.0 microns for the same axis were placed into the equation for n_{out} .

The values calculated for R were placed in the equation $T = (1 - R)$, where T represents the transmission of the crystal. The values obtained for T were then squared to account for the two surfaces of the crystal through which the light must pass. Transmission at 1.4 microns was calculated to be eighty-eight percent, while transmission at 4.0 microns was calculated to be eighty-six percent. Therefore, the average value of both transmissions was about eighty-seven percent. Looking at the graph that was plotted of the original transmissions and assuming that the region between 2.0 and 2.75 microns contains no absorption, it is observed that the transmission with the Fresnel losses is about eighty-three percent (Figure C). Essentially this would mean that the transmission in this wavelength region is one hundred percent when correction has been made for Fresnel losses. The assumption that there is only reflection and no absorption in this region is based on the graph that plots alpha, the absorption coefficient, versus wavelength (Figure D). The graph shows that there is very little absorption occurring between 2.0 and

2.75 microns. Therefore, any loss of transmission is due to reflection and scattering. It was decided best to use eighty-three percent because it was an amount that was actually measured, not just calculated, and because it takes into account some loss of transmission due to scattering.

The value T was then placed into the equation $T_n = Te^{-\alpha l_n}$ in which the absorption coefficient, α , was solved for using a known transmission, T_n , and length of the crystal, l_n . The absorption coefficient was then placed into the equation $T_p = Te^{-\alpha l_p}$ to find the predicted transmission of a crystal with a specific path. This predicted value corrects for any Fresnel losses. For a predicted transmission which does not correct for Fresnel losses, the same equation may be used but the value T is not placed into the equation. It must be noted that the absorption coefficient which is used for the prediction is only a constant at the wavelength at which it was calculated, but it may be used with a crystal of any length path. In this experiment, two different crystals, one 7mm long and the other 13mm long, were used as bases for predictions. The predicted transmissions were for a crystal with a 10mm path. The actual transmission of a KTP crystal with a 10mm path was then compared with the predictions (Figure E).

To find the transmission curve for a KTP crystal of 10mm in length with correction for Fresnel losses and absorption of carbon dioxide and water vapor, the compartment of the Nicolet FT-IR was first purged with nitrogen to clear the atmosphere. Once a background was taken, any absorption by carbon dioxide and water vapor were subtracted from the measurement by the computer. Assuming that no absorption occurred between 2.0 and 2.75 microns, the amount of transmission should be one hundred percent because any loss is due to Fresnel reflection. At this point, the amount of transmission should be divided by eighty-three percent to obtain a true transmission curve for the given crystal (Figure F).

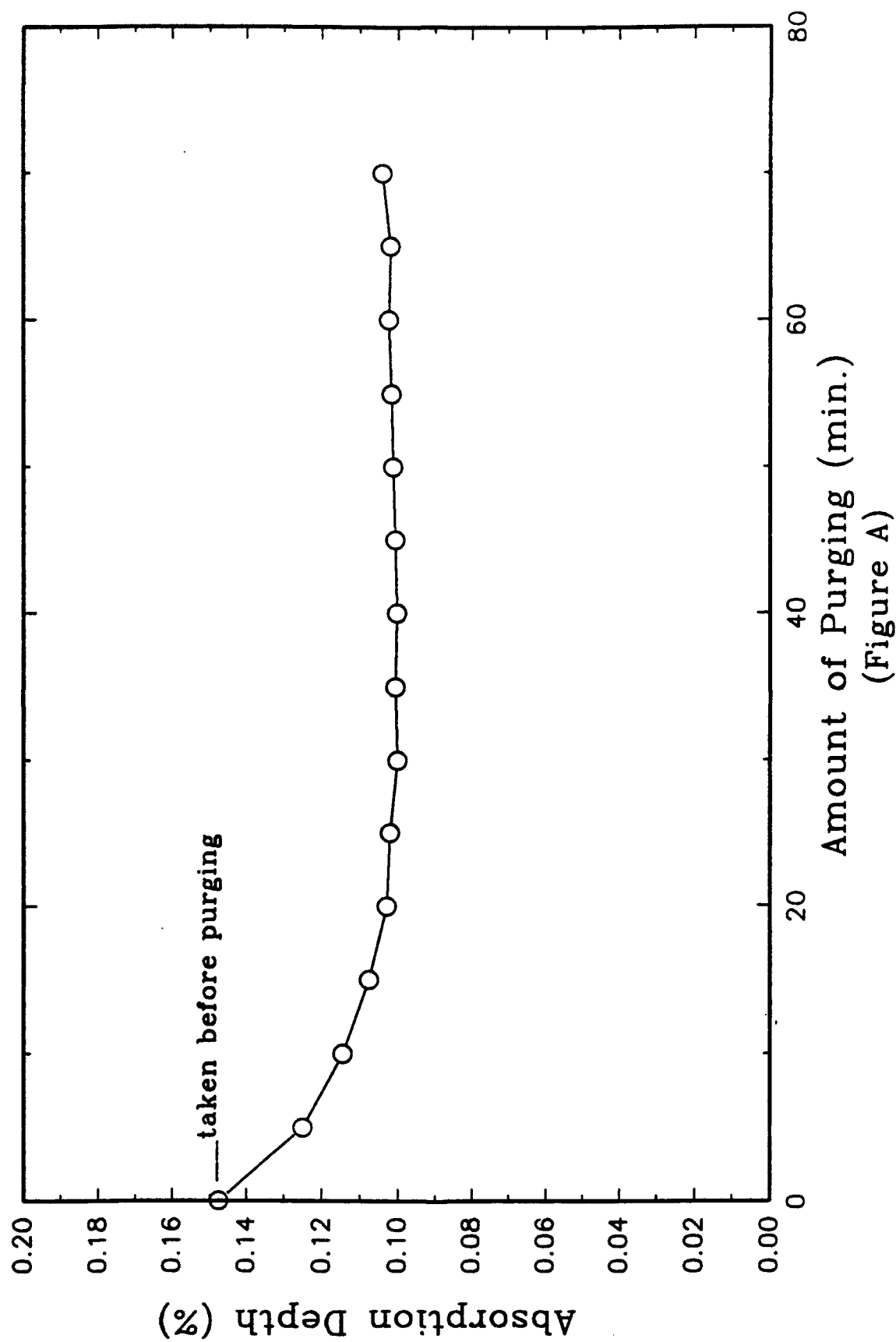
Results

Measuring transmission without absorption due to carbon dioxide and water vapor was very successful. Transmission curves were made of these substances (Figures G and H) and the signatures of neither were found in the KTP curves. The approximate amount of time necessary for purging the compartment was also found (Figure A). The corresponding absorption coefficients for any given wavelength were very similar between the 7mm, the 10mm, and the 13mm crystal (Figure D). This verifies that α is a constant for each wavelength and is not dependent on the length of the crystal. The value T , used to correct for Fresnel reflection, was also accurate due to its similarity to the calculated value. The predictions for a 10mm crystal based on the 7mm and the 13mm crystal were highly accurate (Figure E).

Conclusion

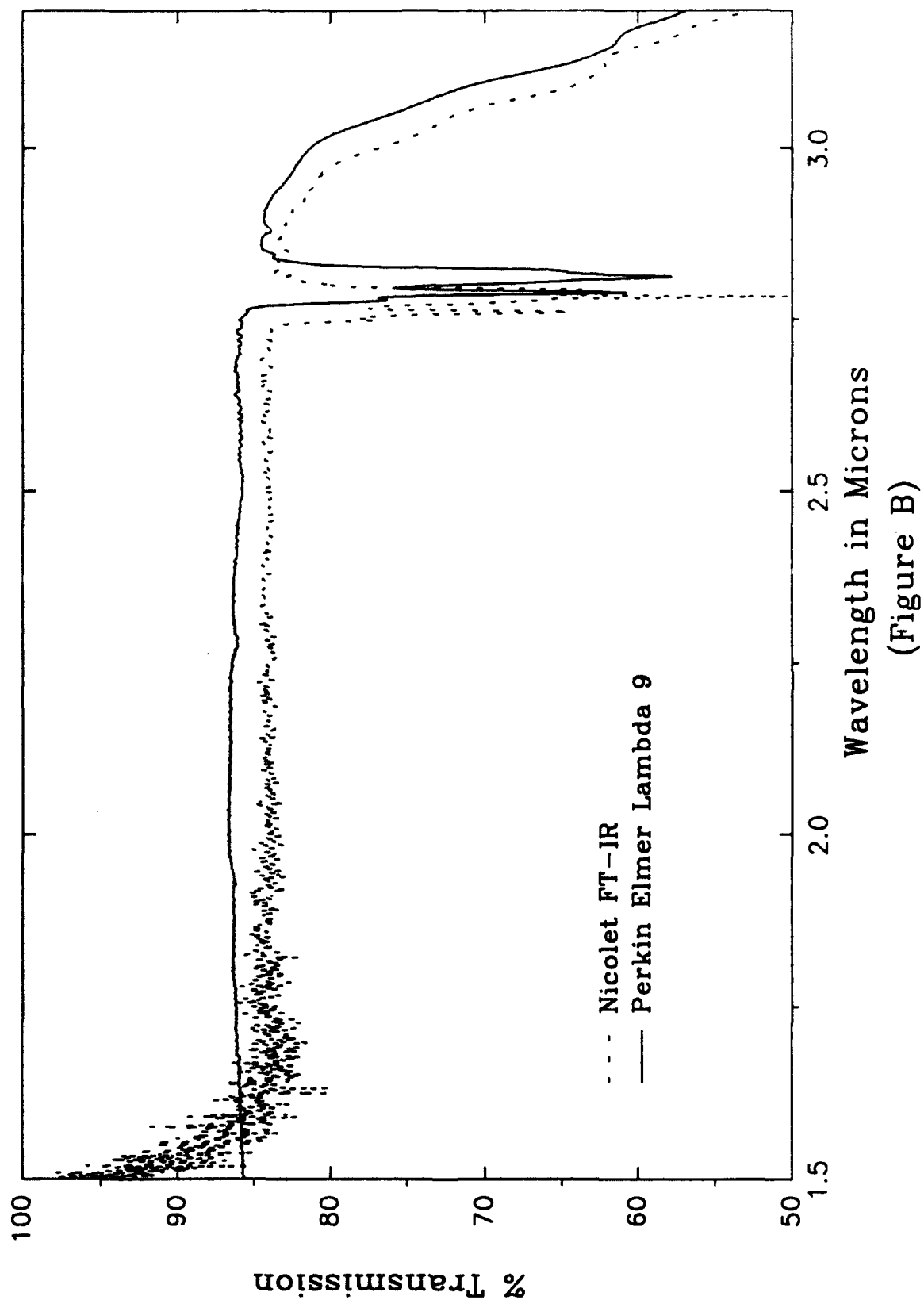
The results of this experiment are important because the equations used, primarily $T_p = Te^{-\alpha l}$ and $R = [(n_{in} - n_{out}) / (n_{in} + n_{out})]^2$, can be used to calculate the absorption coefficient for a specific wavelength, to calculate the amount of Fresnel reflection, or to predict the transmission of a crystal with a different length than the one that was measured. These equations can be applied to any material and to any wavelength. Attention was focused on KTP and the 2.0 to 5.0 micron region because of their importance for midinfrared lasers, one of the primary research interests of the Air Force. Knowing the true transmission will aid in discovering if other elements are affecting the transmission of a substance. By being able to predict transmission, it will be easier to decide what size crystal of the material is needed to achieve the desired transmission without actually having to measure many different crystals.

Purging of the Atmosphere Depth of Spike at Approximately 4.3 Microns

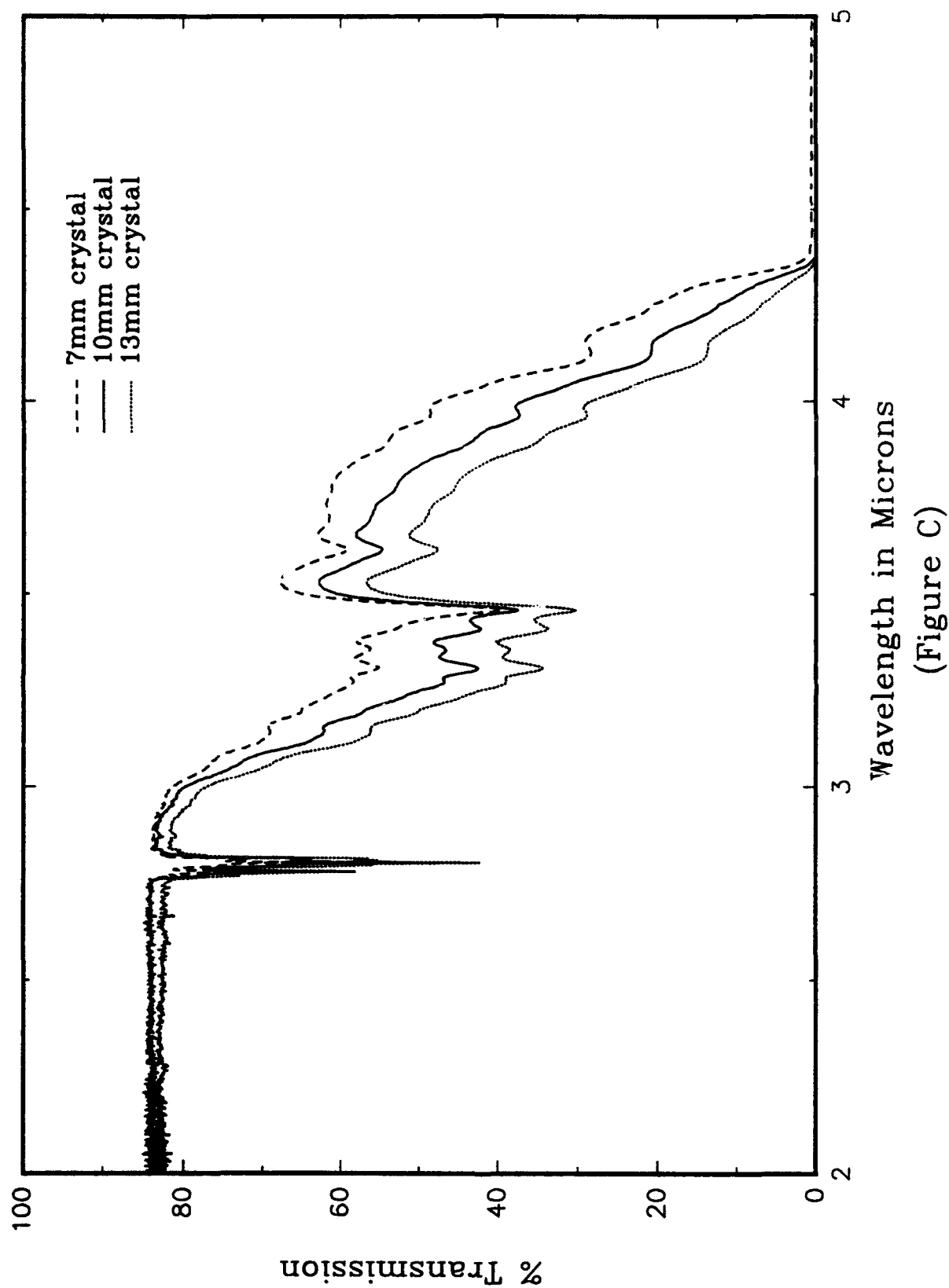


Comparison of KTP

(using the Perkin Elmer Lambda 9 and the Nicolet FT-IR)



Transmission of KTP Crystals



KTP Crystal

Absorption Coefficient (Alpha) vs. Wavelength

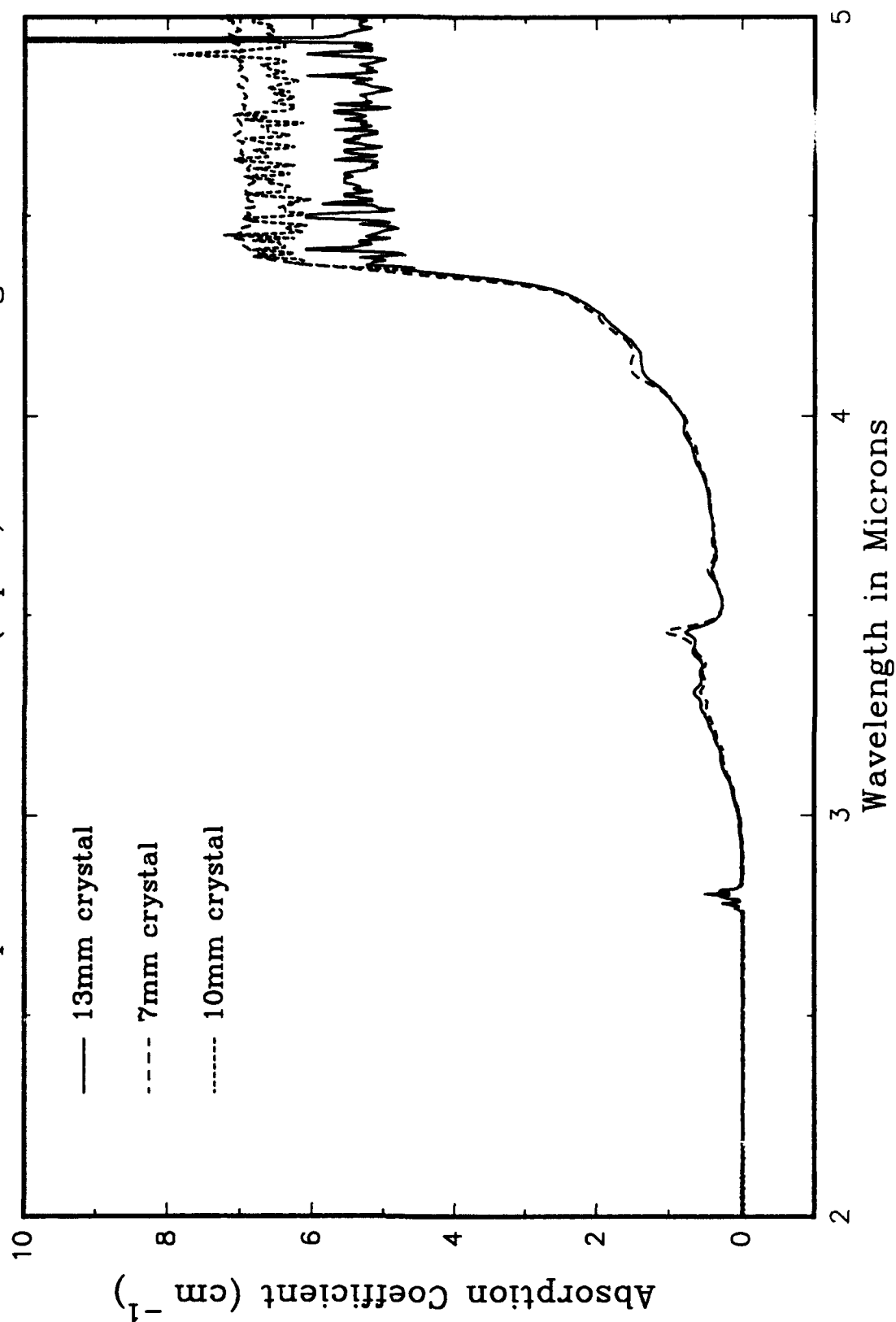


(Figure D)

Predictions vs. an Actual Transmission of a 10mm Long KTP Crystal

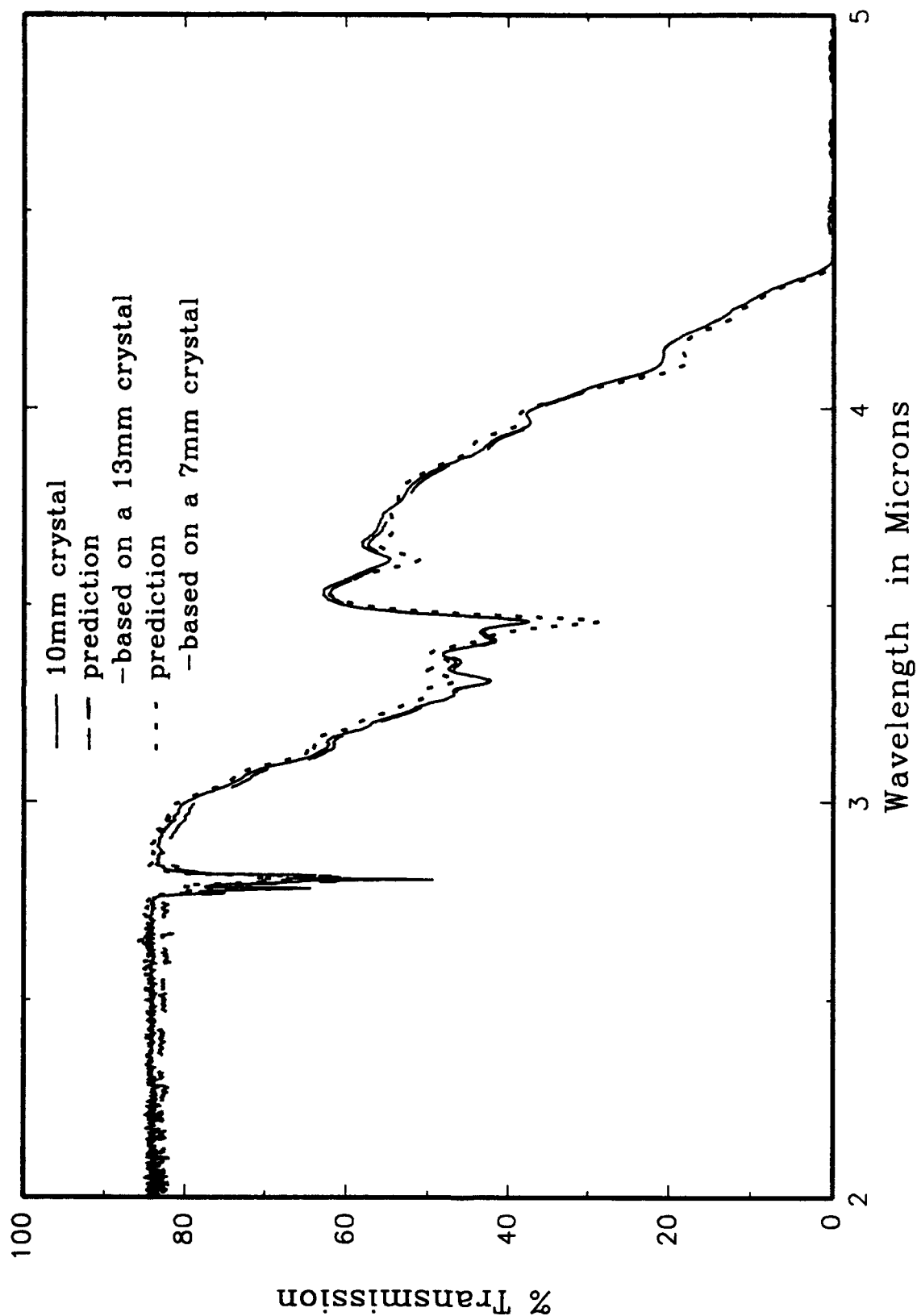


(Figure E)

Transmission of a 10mm KTP Crystal
With and Without Fresnel Reflection

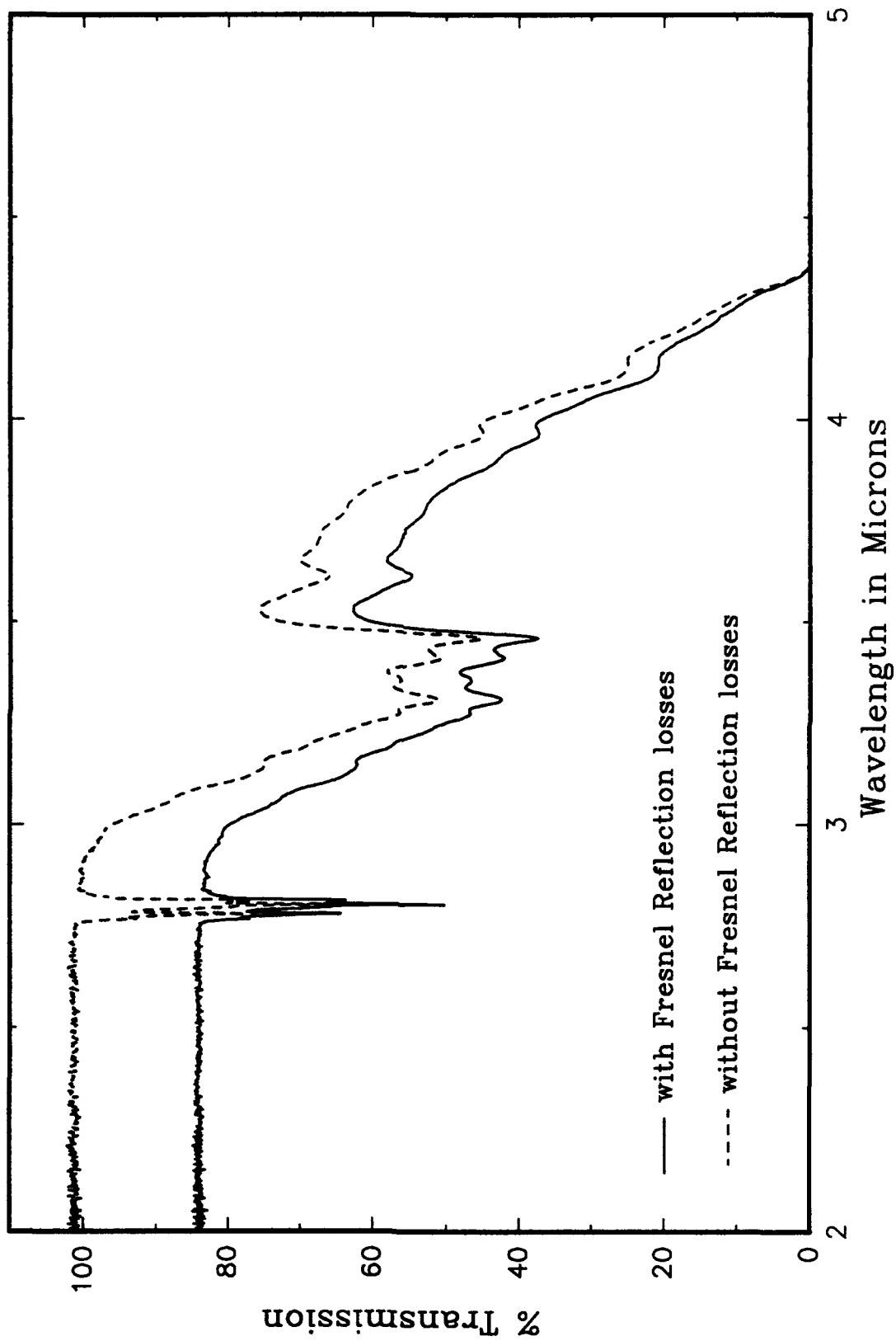


(Figure F)

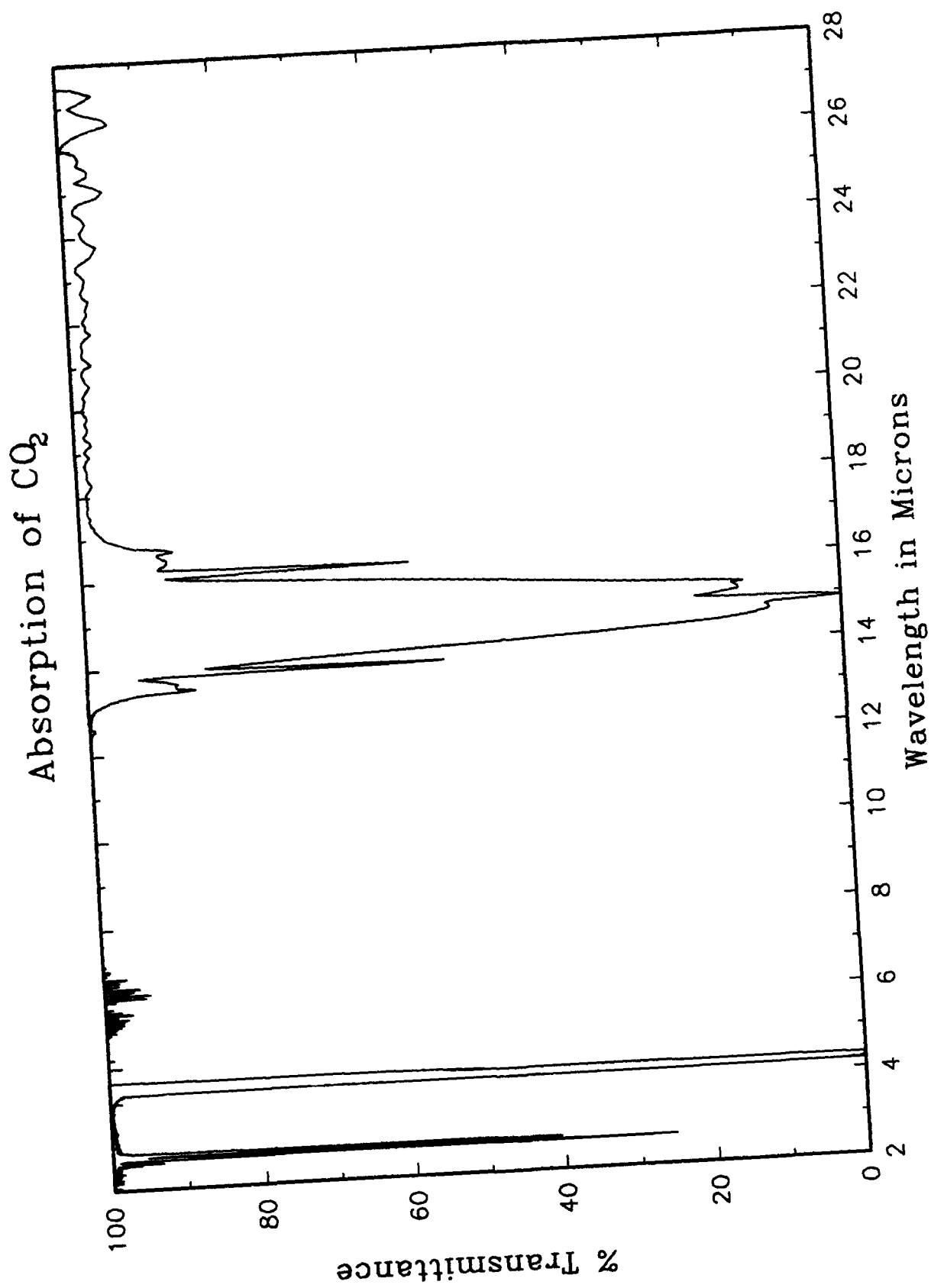
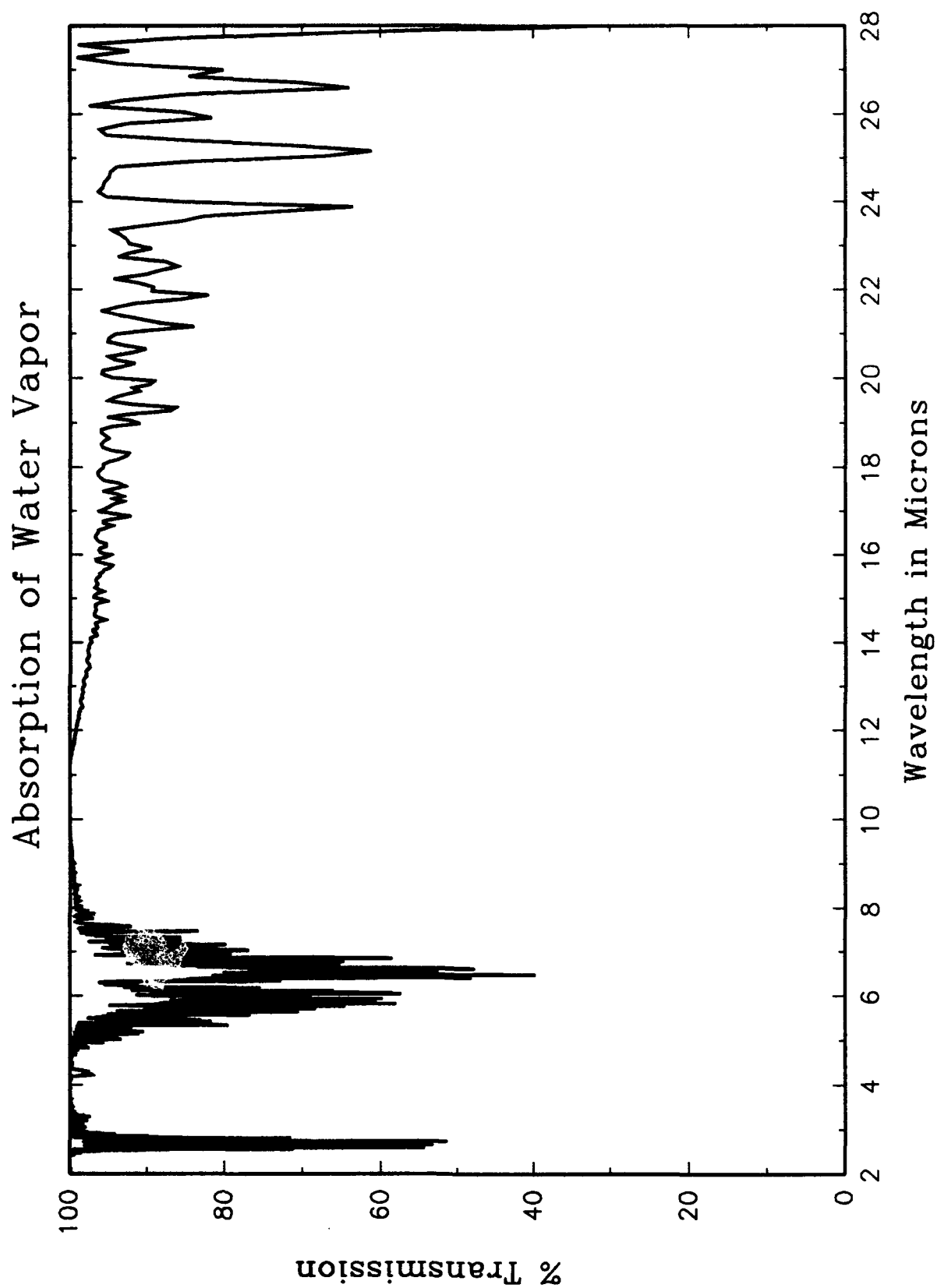


(Figure G)



Ion Implantation Simulation in Three Dimensions

**Joel Kulesa
Archbishop Alter High School
Bradley University
Peoria, Ill**

**Dr. Charles Cerny
Wright Laboratory
Wright Patterson AFB, OH**

**Final Report for:
Summer Research Program
Wright Laboratory**

**Sponsored by:
Air Force Office of Summer Research
Wright Patterson Air Force Base, Dayton, OH**

August, 1993

Ion Implantation Simulation in Three Dimensions

Joel Kulesa

Archbishop Alter High School

Bradley University

Peoria, Ill

Dr. Charles Cerny

Wright Laboratory

Wright Patterson AFB, OH

Abstract

A program that simulates Ion Implantation was developed so that an aging BASIC program could be replaced. This program would not only duplicate the former program but would improve upon the existing program through better simulation and improved graphics plotting routines. The result was a package written in portable C on the Sun workstation that could be easily expanded in the future. In-house simulation routines such as these prove how computer simulations make electronic designs much cheaper and less labor intensive.

Introduction

In 1945 the first totally electronic computer was born. Called the ENIAC, it represented the latest technology at the time. This particular system filled an entire large room and required countless technicians to keep it running. Not too long after the ENIAC was built, a new technology was pioneered that would change the face of computers and electronics forever. That revolution known as the Integrated Circuit made electronic devices more efficient, compact, and reliable. Bulky electron tubes would then be replaced with small black IC packages that could perform the job of several thousand tubes.

A similar technological revolution is happening now, only this particular revolution replaces IC laden circuit boards with Very Large Scale Integration chips. VLSI chips replace complex multi-chip circuit boards and assemblies with one highly compact electronic module. This module has the full capabilities of the original circuit plus additional speed, increased reliability, and substantial heat reductions.

VLSI technology works on the simple premise that when you pack circuitry closer together, electrons have less distance to travel, which means that they can reach their destination faster. Faster electron interactions give the overall circuit a speed boost. However, speed is not the only benefit to implementing VLSI circuits. Any time electrons move through a conductor heat is generated. Since VLSI packs the circuitry closer together and the electrons have to pass through less wiring, thus less heat is generated. This can be even taken one step further. Since heat is essentially "wasted" energy, the less heat that is produced by a circuit, the less energy that is needed to power that

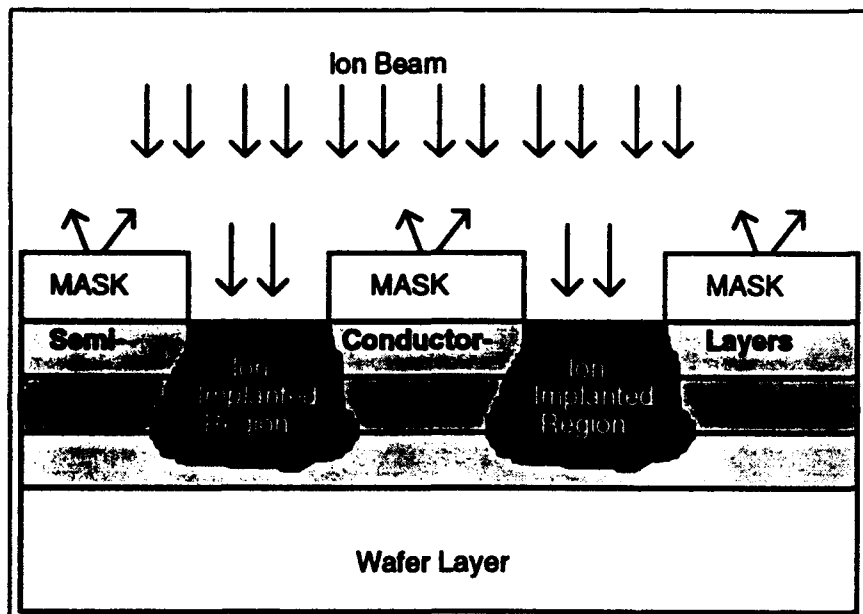
circuit -- and less power means lower operating costs and smaller power supplies. VLSI has the ability to vastly improve upon almost every aspect of electronic circuit design. However, this new technology has not been fully developed therefore there are several difficulties to overcome.

Problems

A major concern among VLSI designers is just how far can this circuit down sizing can go. When designers attempt to push the size envelope a bit more, sometimes the result is not so advanced. Chips would either overheat, act unreliably, or just self-destruct. To better understand why this is happening, a basic understanding of how VLSI circuits are built is necessary.

VLSI circuits are built up from a one to three inch round disc known as a wafer. The wafer can be compared to the foundation of a building with the only difference being that millions of "buildings" will fit on any particular wafer and that they will rarely be taller than 10 microns. Different layers of semiconducting materials are laid down on the wafer in sequence. These layers will eventually be patterned into electronic circuits but before that can happen, the electrical properties of the materials must be modified. A technique known as ion implantation is one common way to modify the conductive properties of these substances. Ion implantation involves the acceleration of charged particles known as ions onto selected areas of the wafer. The trick is to make sure only the right parts get hit by the ion beam. This selective application of ions is achieved through the use of a mask. A mask is a layer of an inert substance that blocks

specific portions of a wafer from a selected process -- in this case the mask blocks the ion flow. The problem is that the mask doesn't guarantee that ions only reach regions directly beneath their edges. Why is that? When the ions pass the edges of the mask on their route through the semiconductor materials, they scatter laterally a certain amount. This scattering limits the density of the device since the closer one packs circuits onto a chip the closer the diffusion regions



will get. If they get too close, short circuits result and the device becomes worthless.

To prevent this from happening there are two methods to

determine just how dense circuits can get. One is trial and error; the other is computer simulation. The trial and error method is nice because it produces physically measurable results which work (or do not) in real life. Unfortunately this method is both time consuming and expensive. The material cost alone can run \$10,000 per test using the trial and error method. On the other hand, the computer simulation method can produce similar results but it does so on a much quicker time scale. Furthermore the cost of simulation is much lower since there is a one time charge for the software (either purchased or developed in-house) which can be used countless times. It doesn't take a genius to

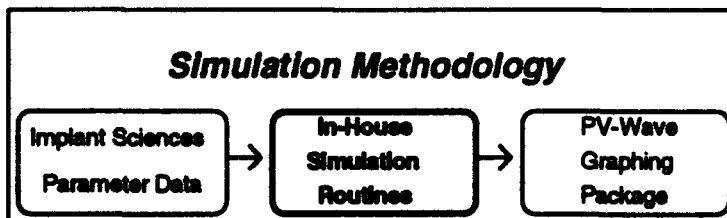
figure out that the computer simulation models offer significant advantages over the experimentation method.

Methodology

Unfortunately at this moment there is very little simulation software on the market for this technology. Previously, a package from Implant Sciences Inc (IS), was used but it was not able to plot multiple device layers at one time, plus it couldn't calculate a three dimensional model. It was decided to write a custom package that would extend the abilities of the IS program.

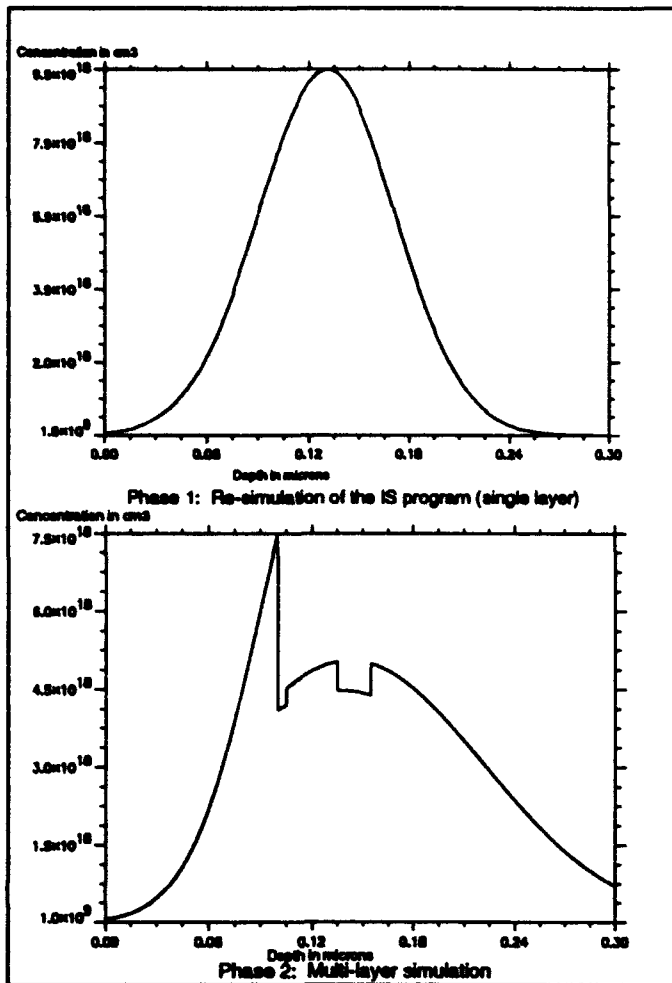
The completion of the software package was divided into several simpler steps to guarantee accuracy and to make programming easier. The first step was to take parameters that were calculated by the IS program and use them to re-simulate the single-layer, single-dimension plot that the IS program could already do. Once the simulations matched, the next step was to let the program simultaneously calculate multiple substances. Again these results were verified to be accurate. The final step was to use an error function to show the ion distribution in the lateral or y-direction.

One important goal of this project was to eliminate the in-house duplication of commercially available software. This goal was met through our use of the IS software parameters and through the use of a



powerful workstation based scientific graphing package called PV-Wave.

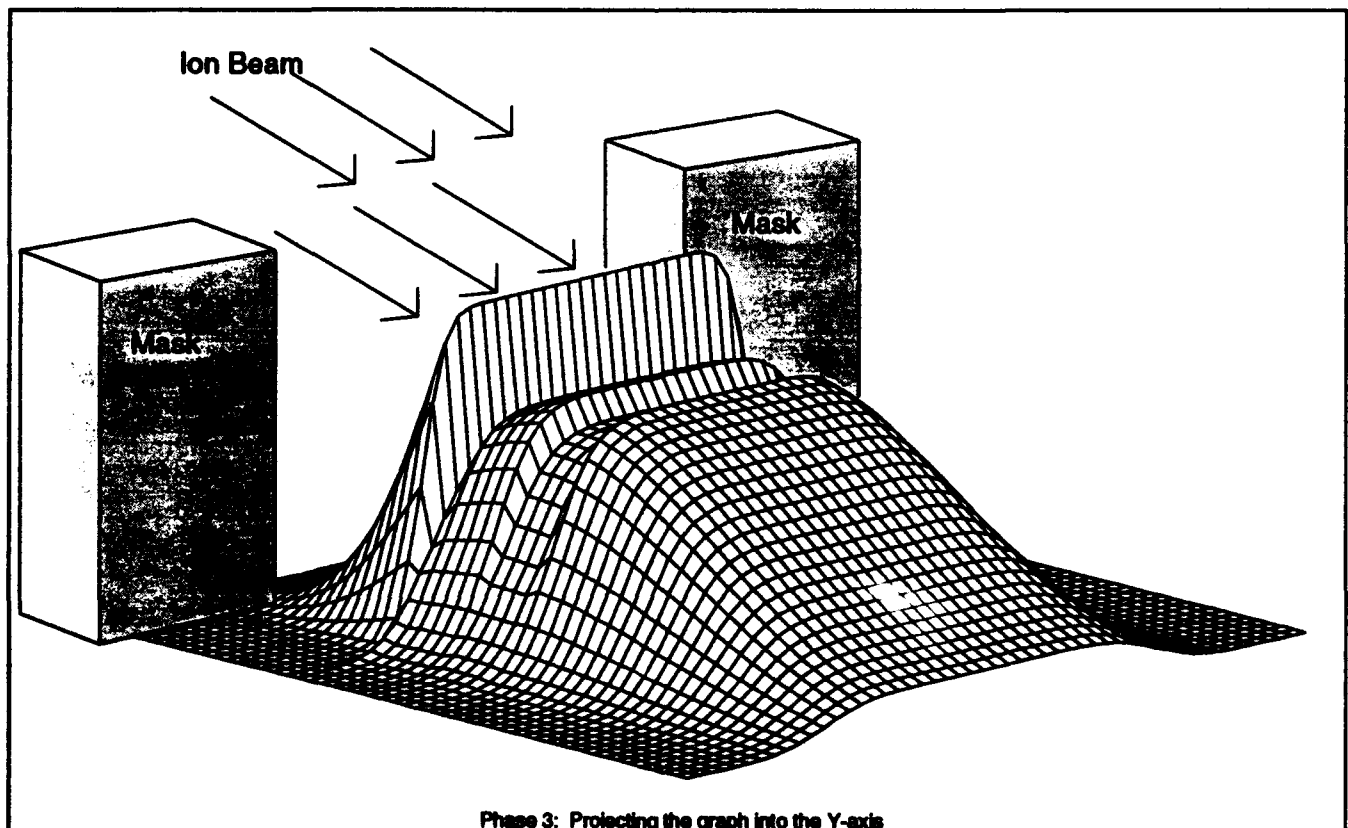
Instead of writing custom X-Windows graphics routines, PV-Wave took the output from the simulation



and displayed it in a clear and concise manner. PV-Wave allowed the three dimensional plots to be viewed from any angle or axis thus allowing easy visualization of whether a design would function or not.

Results and Conclusions

Due to the improved graphing and calculation routines, this program vastly outpaced the IS's aged software package.



Simulation routines such as this one, shows how powerful (and cost effective) modern computers can be when used to verify a design or theory before actually implementation. Several of the graphs in this document are actual output plots of the ion implantation simulator which were used to evaluate designs. Due to the brief nature of the Summer Internship, complete results and conclusions are not possible but one thing was quite apparent: ion implantation simulation is the one of the quickest ways to verify the validity of new designs that are so critical in the continuing nature of today's electronic revolution.

COMPUTER AIDED DESIGN
OF ACES-II FLIGHT ESCAPE MODULE

Mark D. Baits
High School Apprentice

Cedarville High School
248 North Main Street
Cedarville, Ohio 45314

Final Report for:
High School Apprenticeship Program
Wright Laboratory

Sponsored by:
Air Force Office of Scientific Research
Wright-Patterson Air Force Base, Dayton, OH

August 1993

COMPUTER AIDED DESIGN
OF ACES-II FLIGHT ESCAPE MODULE

Mark D. Baits
High School Apprentice
Cedarville High School

Abstract

The computer aided design (CAD) of the Advanced Dynamic Anthropomorphic Manikin (ADAM) test dummy was generated for use in Computational Fluid Dynamics (CFD) testing. The CAD drawing of the ACES-II ejection seat was provided by the United States Navy. The ACES-II ejection seat is the current model incorporated in the F-15 and F-16 cockpits. A CAD drawing of the ADAM was needed to perform Computational Fluid Dynamics (CFD) of both the seat and a test dummy during the crew escape sequences. The CAD drawing of the ADAM was made to fulfill the first requirement of the CFD generation.

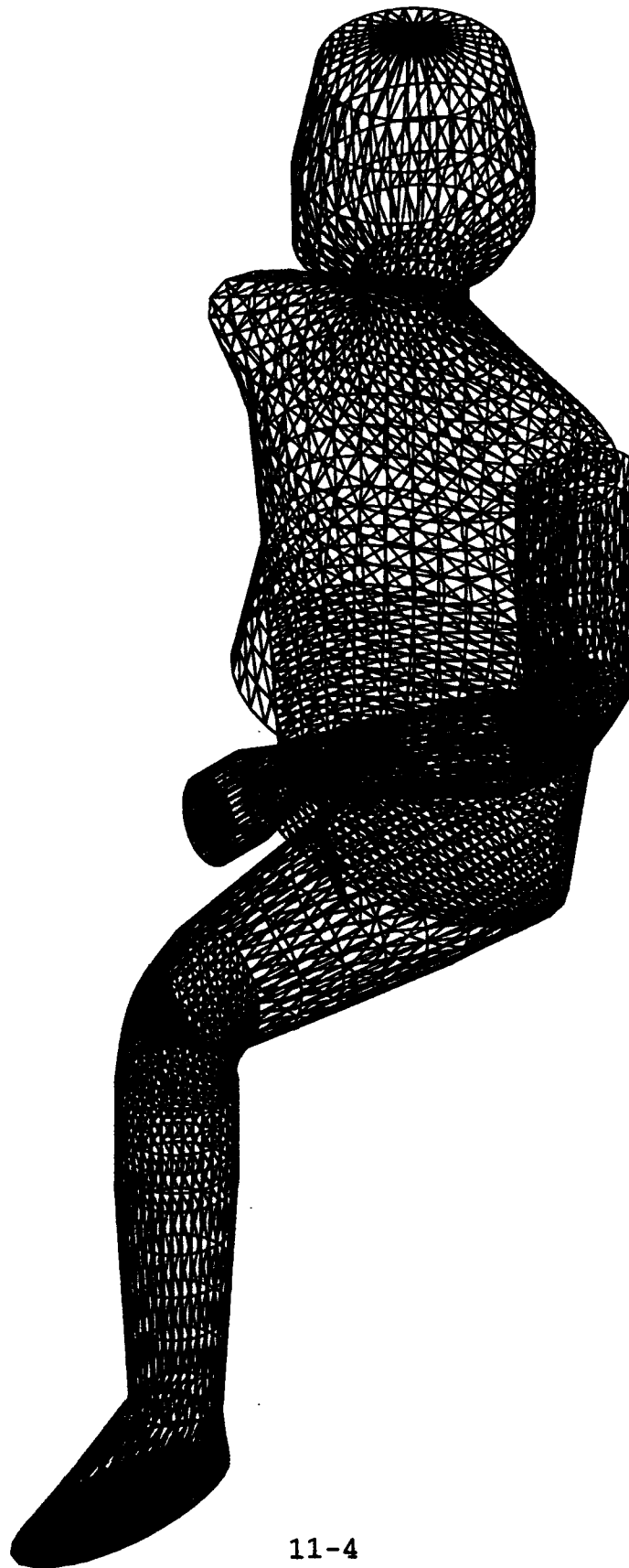
COMPUTER AIDED DESIGN
OF ACES-II FLIGHT ESCAPE MODULE

Mark D. Baits

Table of Figures

Computer Aided Design of Advanced Dynamic Anthropomorphic Manikin (ADAM)	Page 11-4
---	-----------

Figure 1 - CAD Drawing of ADAM



COMPUTER AIDED DESIGN
OF ACES-II FLIGHT ESCAPE MODULE

Mark D. Baits

Introduction

The purpose of this project was to create a Computer Aided Drawing (CAD) of the ACES-II flight ejection seat with a pilot. This drawing was needed to perform Computational Fluid Dynamic (CFD) analysis of this seat during an ejection sequence. The CFD data gathered would later be used to study many different ejections. An analysis of the different ejections would be used to modify the seat and extend the flight envelope in which a pilot may safely eject. The ACES-II flight ejection seat was chosen for study because it is the seat currently incorporated in the F-15 and F-16 fighter jets. The current envelope for safe ejection in the ACES-II seat extends to speeds slightly faster than Mach 1. At speeds greater than this, the pilot's head and helmet act as a wing and produce lift. Current state of the art technology uses CFD testing to produce the data necessary to evaluate the flight characteristics the pilot and seat combination may encounter during an ejection sequence. CFD testing was to be used as opposed to wind-tunnel testing due to the greater speed at which the data could be produced.

Methodology

The ACES-II seat was chosen for CAD modeling due to its current use in the F-15 and F-16 fighter jets. Therefore, there is a large compilation of accident data available for use concerning this seat. The seat also provides a suitable test base for which to incorporate advanced technology using CFD analysis. The CAD data for the seat was provided by the Naval Air Warfare Center, Aircraft Division, Warminster, Pennsylvania. The CAD data was in Initial Graphics Exchange Specification (IGES) format. A translator was used to convert the IGES code into Cadkey code for our computer systems. A suitable CAD drawing of a pilot was needed to incorporate with the ACES-II seat. After discussion with systems engineers, it was decided that a versatile test dummy was needed so that the CAD drawing could be incorporated with other ejection seats and used to produce additional data. The CAD drawing of the manikin and the other seats would later be united to run Three-Dimensional Computational Fluid Dynamics at various

angles of attack. Then the test data would be used to experiment with different seat designs and extend the flight ejection envelope.

Data was found for a test dummy at Armstrong Laboratories that was in a format not recognizable by our computer systems. Another test dummy, the Advanced Dynamic Anthropomorphic Manikin (ADAM), also provided by Armstrong Laboratories, was chosen to utilize with the ACES-II seat. It was chosen because of the multi-purpose utilities that could be employed with the CAD drawing of this dummy. Some of these include: (1) CFD analysis with the ACES-II seat, (2) extensive aerodynamic study and animation, (3) simulation of different flight gear, helmets and oxygen masks, and (4) combination with a number of other seats to produce data. Finally, the ADAM was chosen due to its size. The dummy's size represents the size of ninety-five percent of the pilots in the United States Air Force. Thus it was of a scale feasible for CFD data that represents the actual flight ejection sequence as accurately as possible.

The existing CAD data of the ADAM also was not available in a format recognizable by our computer systems. No translator was available; therefore, the manikin had to be measured using vernier calipers and the data collected was used to put together a CAD drawing. The original drawing had to be discarded because of its block construction. The connected cylinders and blocks that comprised the model did not accurately represent the individual limbs of a human. Such a construction would produce questionable aerodynamic data, because a block acts differently than a smooth surfaced torso or head. Conversation with section engineers revealed that a model closer to real life was needed. After brainstorming, it was decided that the second drawing should be made of polygon meshes with an enlarged head representing the helmet. Further refinements included smoothing the elbow and knee joints to represent an actual human body as closely as possible, thus providing accurate aerodynamic data during CFD generation. The hands were made of spheres, because a closed fist resembles a sphere more so than a block. The model was rendered as a polygon mesh, representing the skin surface of the pilot, as opposed to a block figure composed of boxes and cylinders. These polygons allow for later renderings of the manikin as a solid. A solid rendering of the ADAM would provide additional data that would include mass and inertial properties.

At first, Computer Aided Design of the manikin was performed on an IBM compatible personal computer using Cadkey version 3.53. Cadkey was chosen due to its availability and its capability of rendering solids out of wire-frame models. Due to the size of the part file, the drawing could not be finished on the personal computer system. The ADAM had to be completed on a UNIX-based Silicon Graphics Indigo2 (SGI) Extreme. Therefore, knowledge about operating the UNIX system had to be acquired before any further modeling could continue. This SGI computer system allowed for the size of the file and also produced renderings at a much greater speed. Cadkey version 5.04 on the SGI also includes Stereo Lithography Applications. Such applications allow for quick manufacturing of the part composed of plastic resins for further analysis. The CAD data is sent to a stereo lithograph machine that generates a plastic part of the CAD drawing.

Data from different ejection seat technologies can later be acquired and used to modify the current seat. Current Russian escape seat (K36 series) technology incorporates a flow diverter directly in front of the pilot to alleviate increased air pressure and lift on the head. A ventilated helmet is also used by the Russians to minimize pressure in the event of air pushing up on the helmet. Existing technology and further refinements can be compiled to develop a new seat for the F-15 and F-16.

Results

The CAD drawing of the test dummy was correctly drawn and scaled to fit the ACES-II ejection seat for CFD testing (Figure 1). Figure 1 is a polygon rendering of the ADAM as it appeared on the personal computer. The other leg and arm are not shown due to the limits placed on the personal computer system to store and manipulate that additional amount of data. The finished rendering completed on the SGI could not be printed because of the lack of file transportability. The SGI file differs in that the dummy is fully drawn, seated at a thirty degree angle of declination and has spheres for hands, as opposed to blocks. Additionally, the helmet is shaded as an ellipsoid, as opposed to the stacked block construction that is shown in Figure 1.

HIGH SCHOOL APPRENTICESHIP PROGRAM FINAL REPORT

**1993 WL/FIVEC EXPERIENCES
REVIEWED**

**BY: JASON BRECHT
AUGUST 6, 1993
DISCRETE BASE PAGE NUMBER 12**

Many times in my life I have been offered opportunities which enrich both my intelligence and my problem solving skills. This summer, another one of these opportunities presented itself. I applied for and was accepted into the HSAP (High School Apprenticeship Program) at Wright Patterson Air Force Base. Although I did not realize it at the time, my stay on the military base would not only enhance my intelligence, which is one concrete aspect of my knowledge, but would also provide me with a much more practical and well-rounded education. The knowledge which I will take with me from this job will make me a better person, not only in the immediate future, but for the rest of my life.

My official job title was "Data Collection Analyst." I feel it was fortunate that the job description did not directly apply. My first day on the job I met George Kurylowich, my supervisor, and Dave Brown, a man with whom I would be working with very closely for the next two months. Dave introduced me around the office, and almost immediately I felt comfortable. The other office employees all welcomed me and treated me as if I had been there for years. I was now an official member of the Environmental Control Branch of the Flight Dynamics Directorate (FIVEC). I was then taken to see the test site.

At the test site I learned of microencapsulated phase change material (micro PCM) and how it was supposed to revolutionize the future of avionics. The micro PCM capsules tested were approximately 10 to 30 micrometers in diameter. The theory behind micro PCM technology is that when the PCMs are encapsulated and suspended in a carrier fluid, they increased the heat capacity of that fluid by up to 400%. The combination of the PCMs and the carrier fluid is then classified as a slurry. In a future where more complex avionics are born from more advanced technology, a coolant fluid would be needed in order to cool increased avionics heat loads which result from increased energy densities on the boards. As heat is applied to the micro PCMs, the phase change material melts and absorbs heat. The latent heat of melting increases the effective heat capacity of the fluid near the melting temperature of the phase change material. PCMs seemed like the ideal solution to high energy avionics cooling. The PCM slurry was tested in a loop which consisted of two main components, a water coolant loop and an avionics coolant loop. The avionics coolant loop was to flow through a simulated avionics board, a board similar to those planned in the next generation of fighter aircraft, in order to apply heat to the slurry. The slurry then would flow through the hot side of a heat exchanger. The chilled water loop would flow from a water chiller, through the cool side of the heat exchanger (in order to transfer heat from the fluid), and back into the chiller. The result was a very compact yet effective test loop which provided much information about the advantages and disadvantages of the micro PCM slurry. Through temperature, pressure, and flow measurements that were taken from different locations in the test loop, conclusions could be drawn about the feasibility and practicality of the slurry. My job was to write a computer program which would arrange all of the information compiled from the computer test rig data acquisition system into a well-organized and comprehensive format. The task took several days. I also wrote a program which would pull information from the data spreadsheets and place it into a table to be used for graphing the information.

Chet Brewster, the head administrator of the TAVLAB (Thermal and Vibrations Lab), the area where the test loop was located, tasked me with a project after my computer programs were complete. I was to enter all of the ozone depleting chemicals from the lab's MSDSs (Material Safety Data Sheets) into a database so that any file could be called up by its chemical name, trade name, or file number. There were over 100 MSDS forms which consisted of approximately 300 chemicals. It was my first attempt at working with a database software program, and this project took me quite a bit longer than my first two tasks. The manual labor of copying all of the chemicals to notebook

paper took me two days, and the database itself took me one week to complete. The database gave me an opportunity and a purpose to work with computers in a new advanced way which I never had before. But working with a database was only one of the many things I learned to do on a computer.

I learned how to manipulate files and information to make them more user friendly. Before my experience on base, I had no idea that a computer had more than one drive to select from. I worked with several different computer software packages, including Microsoft Excel, Microsoft Word, Harvard Graphics, and PC Shell, all interfaced through MS DOS Windows. At one point, I used a HP Scanner to scan fifth generation copies into Paintbrush, a drawing program, so that I could enhance them and make them appear like their originals. I now feel comfortable on a computer where as before I felt just plain lost. True, I was spoiled by working on a 486, but the knowledge I will carry with me from this job will be practical for many years to come.

Perhaps the most informative time I spent in the lab was acquired when Dave left Mike Browning, a technician, and I to run the test loop for a week while he was out of the office. Both Mike and I received a very practical education that week. We even developed our own scientific law which states: "Everything that can go wrong will go wrong immediately after the lead engineer leaves town." During that week, our heat exchanger clogged and we lost approximately 2,000 dollars worth of PCM slurry. But by pooling our problem solving skills we cleaned out the heat exchanger, leveled off the system, and had the loop running again in no time. Our test results never quite came out the same again because the concentration of the PCMs in the carrier fluid had been reduced. I was disappointed that this had happened until I learned that discovering problems with experimental interactions is just as important to research and development as making sure the product works perfectly. As Carl "The Man Who Knows Everything" Williams, another technician in the lab, so elegantly put it, "If nothing goes wrong with an experiment then you probably haven't learned anything."

Over the course of the past two months, I didn't just learn about developing technology and advanced computer systems. The most important lesson I learned was how to work with and get along with all of my co-workers in a professional work-place. All of my colleagues were wonderful and deserve my deepest gratitude for the kindness and acceptance they have shown me. The lessons that I will carry with me from this experience will not soon be forgotten.

My summer job was supposed to be about scientific knowledge and research, and it was. But it was also so much more. This program provided me not only with the opportunity to enhance my scientific knowledge, but also provided me with an environment where I could grow as a person. This program accomplished its goals and many things far beyond them. I can only hope that the other HSAF students had as good of an experience as I have. I feel that there are a few events in each person's life which shapes his future and creates a lasting impact on that person. This summer job has been one of those experiences for me. I wish your company continued success in the future and that you provide many others with the opportunity you have provided me.

FROM 80 CENT THERMOCOUPLES TO MULTIMILLION
DOLLAR AIRCRAFT

DANIEL E. FEUCHT, high school apprentice under

Joe. Pokorski

West Carrollton High School

5833 Student Street

West Carrollton, Ohio 45418

Final Report for:

High School Apprenticeship Program

Wright Laboratory/Flight Dynamics Directorate

Structures Test Branch

Sponsored by:

Research and Development Laboratories

Culver City, Ca.

August 1993

FROM 80 CENT THERMOCOUPLES TO MULTIMILLION

DOLLAR AIRCRAFT

Daniel E. Feucht
High School Apprentice
West Carrollton High School

Abstract

During my summer experience with WL/FIBT I learned and experienced many new things. I also got to work with many interesting people during my time with WL/FIBT. Aircraft go through many vigorous testing environments and maneuvers in the course of one lifetime. At FIBT they test the fatigue of the aircraft while performing these maneuvers while at the same time applying loads to them. During my time here I participated in many tests including: the "Lightly Loaded Splice Subcomponent," "Elevated Temperature Aluminum Testing," burst tests, and F-15 and fuel tank fatigue testing. Most of my time was spent designing a Pressure Dump Manifold for tests to be run in the future. This was designed to release all pressure to the test specimen if something was to go wrong. The making of this manifold helped me to develop my understanding of the Design-Cad 3d system better.

FROM 80 CENT THERMOCOUPLES TO MULTIMILLION

DOLLAR AIRCRAFT

Daniel E. Feucht

Fuel Tank Test Methods

The purpose of this project is to develop effective methods for sealing integral fuel tanks on aircraft today and in the future. This project is directed toward utilization of the test facility in support for a McDonnell Aircraft Company program, a General Dynamics IRAD for quick seal damage repair methods, and a PRAM program with a spray sealant evaluation for carrier aircraft wings.

During this summer I helped to prepare a specimen to be tested. I worked on a generic fuselage tank setup shown in figure 2.1. The first thing we had to do was put on thermocouples so that heat could be watched carefully. It took us a couple of days to hook up all the thermocouple wires, and after we hooked up the wires the tank was then put in a testing structure where it would be heated and tested for leaks and to see if the sealing method worked. This tank was not being tested yet at the time of our departure.

Lightly Loaded Splice Subcomponent (LLSS)

The McDonnell Douglas Corporation has made up a Titanium Matrix Composite (TMC) which replicates a typical X-30 fuselage portion. The Wright Labs are involved in the testing of this section to evaluate the fabrication and performance aspects of the thin and stiffened structures as in the X-30 and its program. This splice represents the splice of two 80 inch radius portions of fuselage at the ring of the frame.

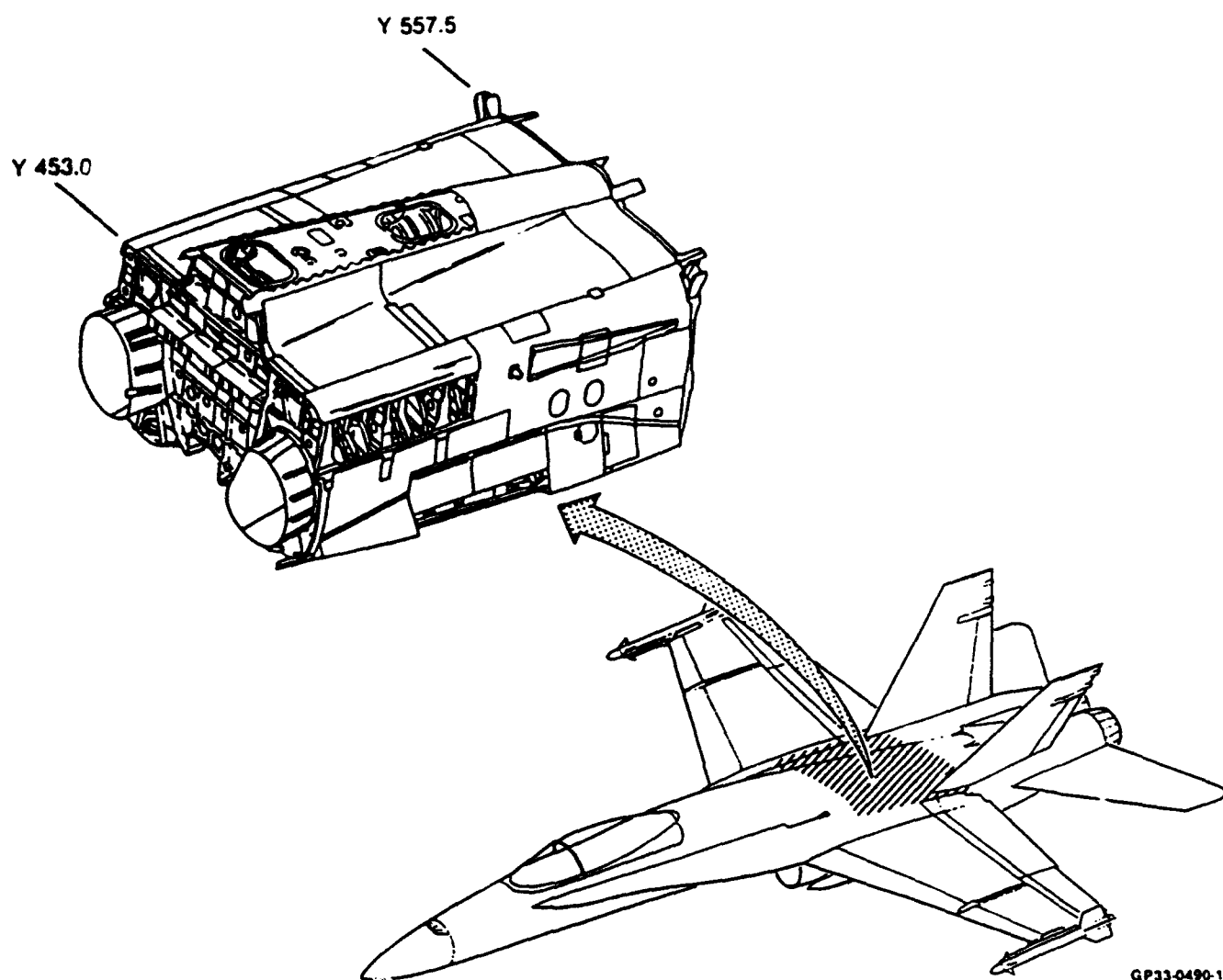


FIGURE 2-1
GENERIC INTEGRAL TANK CONFIGURATION DEFINITION

During the summer I did not work on this part of the testing but I did get to watch a test be run on this splice, where they were going to fail the splice section with compression. This test was unsuccessful because the section could not be broken with the instruments attached to it at that time. When the plate would not break they stopped the test and waited to hear from the Douglas Corporation for further instructions.

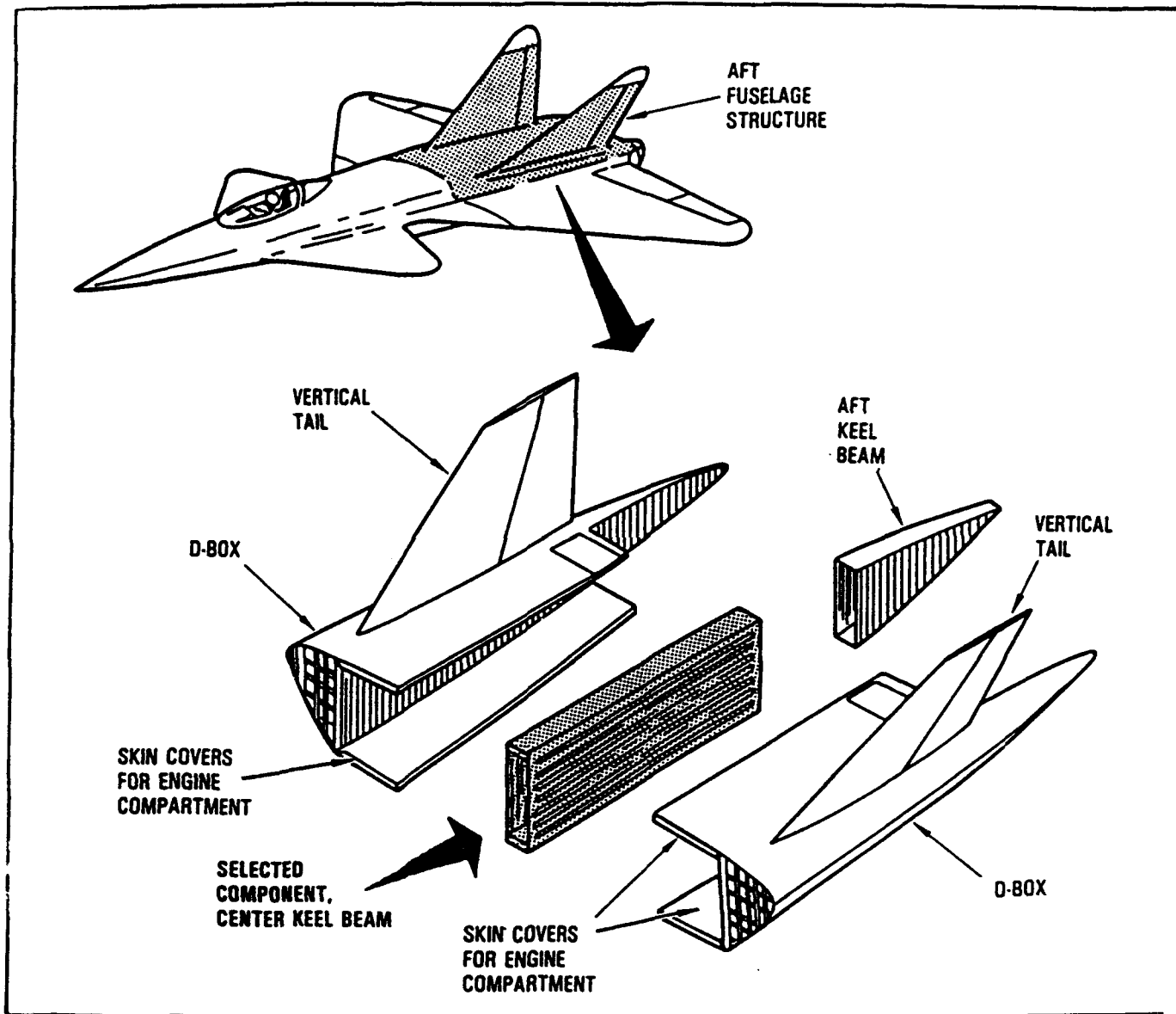
F-15 Wing and Wing Carry-Thru Structure Fatigue Test

The current USAF F-15 fleet usage is four times greater than expected. This severity has caused questions of the ability of the F-15 structure to meet the original design life of 8000 flight hours. A new fatigue test using flight loads representative of actual fleet usage is currently in progress at the Structures Test Branch. The test spectrum is comprised of thirteen flight conditions varying from a positive 9.92 Gs to a negative 1.89 Gs. The test calls for 24000 flight hours to be applied.

During my time at the lab this summer I never worked on the F-15 fatigue tests but I did watch them put 1100 flight hours on the aircraft. During my last week at WL they were stripping the aircraft for inspection at a later date.

Elevated Temperature Aluminum Program (ETAP)

The ETAP test component is an aft fuselage center keel beam. The object of the test is to verify by full scale testing that the keel beam meets the structural criteria used for its design. Additional objectives are to verify analysis, determine the failure modes, and assess the validity of the structural criteria for future ETAP designs. Static tests, durability, and damage tolerance will be accomplished while exposing the beam shear webs to an elevated temperature area. A picture on page 13-6 shows where the keel beam is located as compared to the rest of the aircraft.



Conclusion

During my time at Wright Labs I experienced many new and interesting things which will stay with me for my entire life. I feel that these things will help me to be a better person and will make my future a lot more knowledgeable. I was involved in alot of projects that were fun and yet educational and I believe that this experience gives a lesson of the hard work involved in the field of engineering. This lesson is what I think makes the HSAP program a program to remember.

Richard Leon's report not available at time of publication

**MAPPING COMPUTER
NETWORKS**

**Amy Martin
High School Apprentice
Computer Resources Team**

**Kettering Fairmont High School
3301 Shroyer Road
Kettering, Ohio 45429**

**Final Report for:
Summer Research Program
Wright Laboratory**

**Sponsored by:
Air Force Office of Scientific Research
Bolling Air Force Base, Washington, D.C.**

August 1993

MAPPING COMPUTER NETWORKS

**Amy Martin
High School Apprentice
Computer Resources Team
Kettering Fairmont High School**

Abstract

The mapping of the computer networks in building 450 and 24C was done. Previous maps were scanned in on Paintbrush, cleaned up, and corrected, or hand-drawn sketches were made into graphs. Harvard Graphics was used to type in a report for a Technical Management Review. Familiarity was also gained with WordMarc word processing, the aircraft inventory data system, BTS Disspla, the UNIX and PRIME systems, and Silicon Graphics.

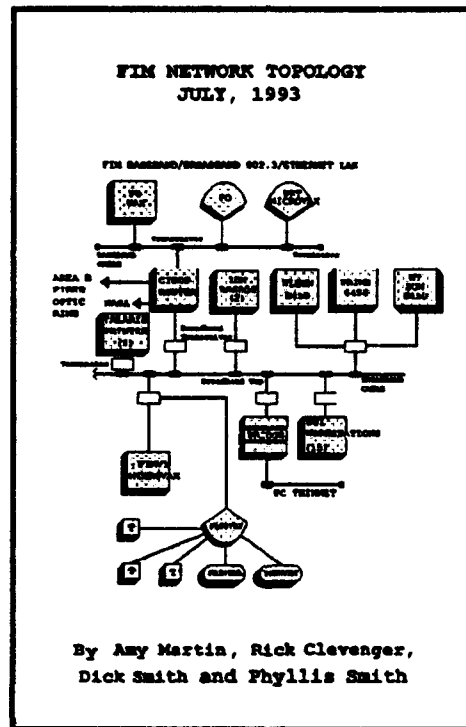
MAPPING COMPUTER NETWORKS

Amy Martin

As a high school apprentice I became familiar with many computers, computer languages, and computer programs. This knowledge may be helpful in college and the career world. I also became familiar with how the computer networking in buildings 450 and 24C work by mapping them.

The largest project I worked on while with the Computer Resources Team in Flight Dynamics was a network report. The network report first explains how the system works through explanations and definitions of the different elements in the network. Then the network is shown with graphs. These graphs show how the computer systems are

connected. Broadband and Baseband Ethernet, ThickNet, and ThinNet connect the systems. Some graphs show where PC network taps are placed in rooms

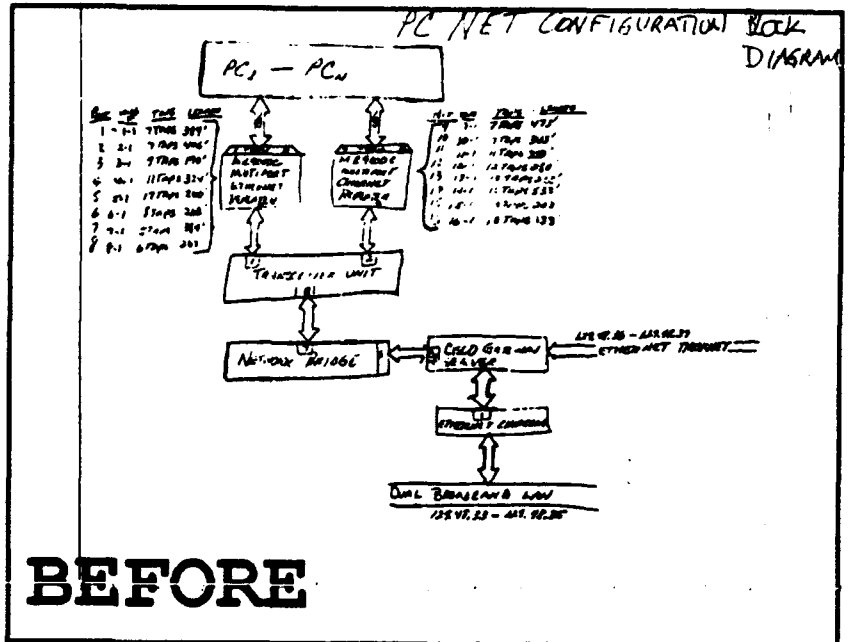


throughout both buildings. With these taps a computer can be connected to the network. By being hooked up to the network the user will actually work off of

server. In building 450, A Wing there are two servers which contain the Windows program. By working off of the network the user doesn't have to fill their C drive with programs but instead receives programs from a server.

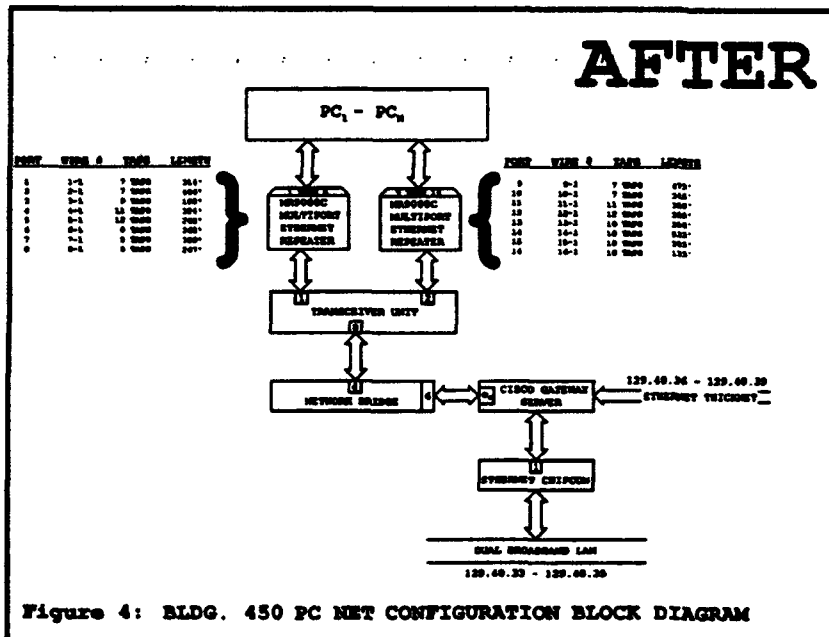
I was either given a previous graph or a hand-drawn graph of some part of the network. I then took the graph and scanned it into Paintbrush. During scanning lines become crooked and various extra dots appear on the graph. Then by looking at the original graph I cleaned up the drawing (see Before/After examples). This is often difficult. Sometimes what had become a large black dot after being scanned in had to be

turned into a drawing of a computer terminal. After the graph was cleaned up my mentor sketched in the changes to the network and I updated the graphs. The graphs included maps of the Building 450 Ethernet and Asynchronous Local Area Network, Building 24C FIM Local Area Network, Building 24C FIM PC ThinNet and



Terminal Service, Building 450 PC Net Configuration, Building 450 Dual Broadband Network, Building 450 "A" Wing basement, first floor, and second floor PC network tap locations and ICU locations, Building 450 "E" Wing first floor PC network tap locations and ICU location, Building 450 Broadband ICU Room Number and Serial Number, and Building 24 C tap locations on the Mezzanine, First Floor, and Second Floor. The written explanations and graphs were compiled into a report for which a graph of the Network Topology was used as a title page.

I also did various other jobs as an apprentice. On Harvard Graphics I laid out the text for the Computational Aeromechanics Technical Management Review. This report included the status, progress made in the past year, projected accomplishments, objective, approach, schedule, funding profile, and issues of the



Computer Resources Team. I also gained experience with UNIX and PRIME systems. On the PRIME system I worked with WordMarc word processing to type in a Statement of Work for the Aeromechanics Division, and I

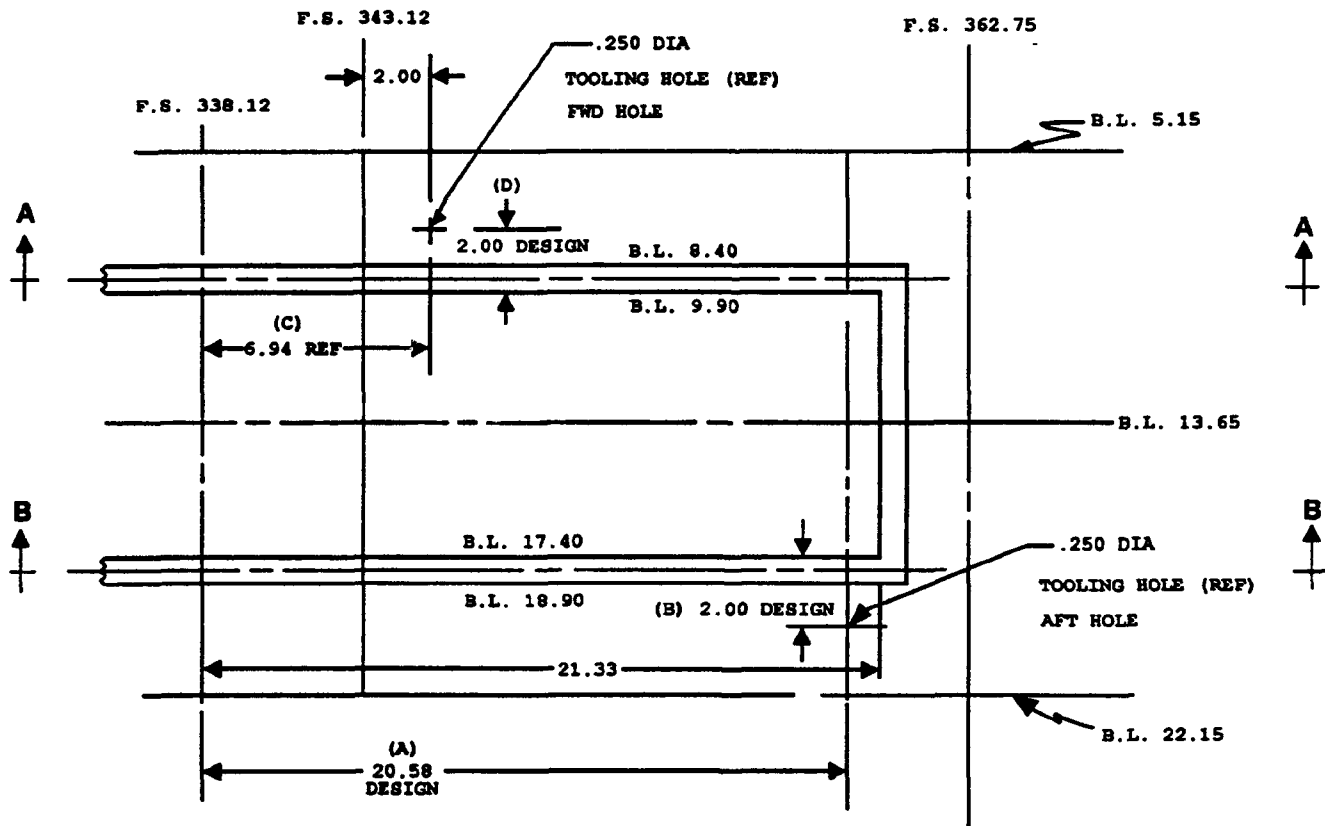
worked with the aircraft inventory data system. The aircraft inventory data system is a record of planes from the United States, Great Britain, Russia, and other foreign countries, spacecraft, and civilian aircraft. With this program my job was to input and correct data (see Aircraft Information example). These records include statistics about the planes found in an aircraft magazine. However, much of the information was not available and simply had to be listed as unknown. The end product was printed out and compiled in a binder.

I also plotted several graphs for John Fehl on

BTS Disspla. These graphs dealt with testing he had done on the T-38 Speed Brake. First I worked on the PRIME system plotting graphs and printing them (see T-38 Speed Brake graph). Then I was given a drawing to form on Paintbrush (see Speed Brake - Sketch From Drawing 2-16500, below). This drawing was revised several times until Mr. Fehl was satisfied with the results.

Overall I improved my knowledge of computers and I learned what having a full time job is like.

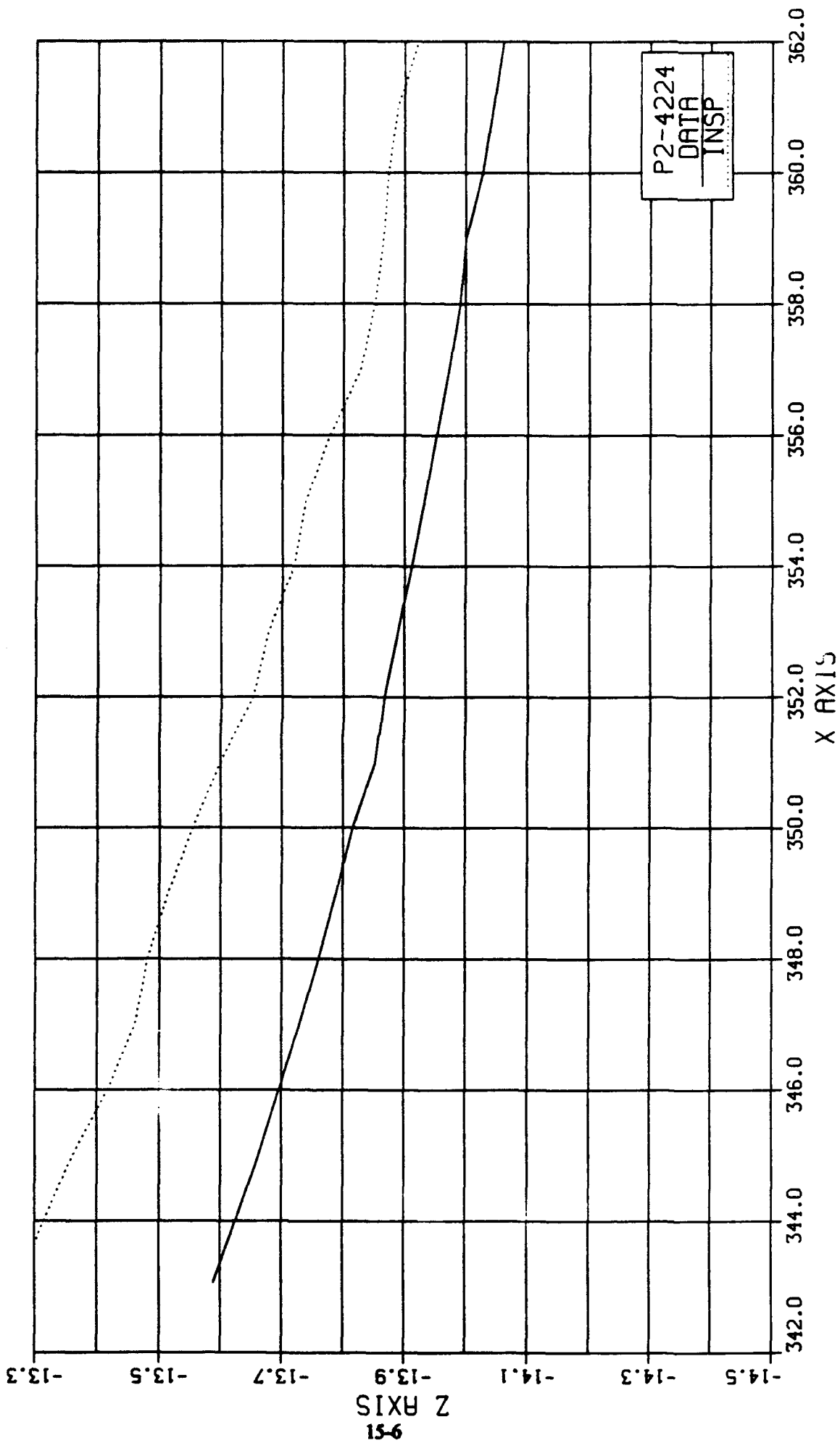
15-5



Speed Brake - Sketch From Drawing 2-16500

T-38 SPEED BRAKE

NUMBER 2,-4 B.L. 22.45



A I R C R A F T I N F O R M A T I O N

1 SYSTEM NAME -	C-141
2 TYPE -	Cargo Aircraft
3 PRIMARY MISSION -	Air-drop/troop carrier
4 NICKNAME -	Starlifter
5 DOD SERVICE -	USAF
6 MANUFACTURER -	Lockheed-Georgia Co.
7 STATUS -	Operational
8 FIRST FLIGHT -	'B' Model Delivered December 1979
9 CREW -	3-8
10 OVERALL LENGTH -	168.3 ft
11 WING SPAN -	159.9 ft
12 WING AREA -	3228 sq ft
13 MAX HEIGHT	39.3 ft
14 TAKE OFF GROSS WEIGHT (LBS) -	344900 lbs
15 ECM -	70000 lb. payload (A) / 94508 lb. payload (B)
16 OFFENSIVE RADAR TYPE -	N/
17 DEFFENSIVE AVIONICS -	N/A
18 WT. ARMAMENT / FUEL -	Unknown
19 MAX SPEED -	566 mph
20 RANGE (SPECIFY NM OR M) -	1970 mi. (A) / 2550 n. mi. (B)
21 SERVICE CEILING (FT) -	Unknown
22 POWER PLANT -	4 X PGE TF39-1C (A) / TF-33-P-7 (B)
23 POWER PLANT TYPE -	Turbofan
24 POWER PLANT MFG. -	General Electric (A) / Pratt & Whitney (B)
25 ENGINE DIMENSIONS -	Unknown
26 ENGINE THRUST (LBS) -	21000 lb. (B)
27 RADAR WARNING RECEIVER -	Unknown
28 ARMAMENT -	N/A
29 GUN TYPE -	N/A
30 GUN ROUNDS -	N/A
31 COST PER AIR CRAFT -	Unknown
32 WING LOADING -
33 . . .TAKEOFF (LB/FT2) -	Unknown
34 . . .COMBAT (LB/FT2) -	Unknown
35 THRUST-TO-WEIGHT RATIO -
36 . . .TAKEOFF -	Unknown
37 . . .COMBAT -	Unknown
38 SUSTAINED TURNING RATE -
39 . . .(MACH 0.9	Unknown
40 INSTANTANEOUS TURNING RATE -
41 . . .(MACH 0.9 & 15000 FT)	Unknown
42 RATE OF CLIMB -	Unknown
43 . . .(SEA LEVEL TO 36000 FT)	Unknown

ELECTRONIC DOCUMENTATION AND DESIGN

Benjamin J. Merrill

**Bellbrook High School
3491 Upper Bellbrook Rd.
Bellbrook, OH 45305**

**Final Report for:
High School Apprentice Program
Wright Laboratories
Flight Control Division**

**Sponsored by:
Research and Development Laboratories
Culver City, California**

August 1993

ELECTRONIC DOCUMENTATION

AND DESIGN

**Benjamin J. Merrill
Bellbrook High School**

Abstract

My apprenticeship was hosted by the Flight Dynamics Control Integration and Assessment Branch of Wright Laboratories. I was involved with a few of the many different kinds of work that go on here. My main focus was on the documentation of electronic devices and the components that make up these devices. I also did some designing of digital circuits and the initial testing of these circuits. Overall, I feel I've learned a great deal about what it's like working in an office environment, and have a good feel for what I can expect in the fields of engineering and science.

ELECTRONIC DOCUMENTATION AND DESIGN

Benjamin J. Merrill

Introduction

My summer apprenticeship at Wright Laboratories took place in the Control Integration and Assessment Branch of the Flight Dynamics Directorate. Their focus here is on ground-based aircraft simulations for integrating and assessing aerospace technologies. Through simulation runs and post-simulation data analysis they are able to increase aircraft performance, survivability, and strike effectiveness. My mentor was Ron Ewart who is the Principal Scientist at this facility.

Discussion

My main focus for this eight weeks has been with the Simulator Network Analysis Project (SNAP). This program is working to develop a tool that will test the fidelity and effectiveness of simulations at the network level. It measures the time delays from one network node to another, correlating these measured delays as a function of network loading.

My main task in this project has been the documentation of the hardware that makes up each SNAP computer. I worked with both EASYCAD2 and TANGOSCH software packages in creating and updating drawings of the different computer boards and schematics of each one. These drawings will be used to produce, debug, and maintain the SNAP computers. I started

Title: SWEEP
File: sweep.fcd
Date: June 23 1993

TOP VIEW

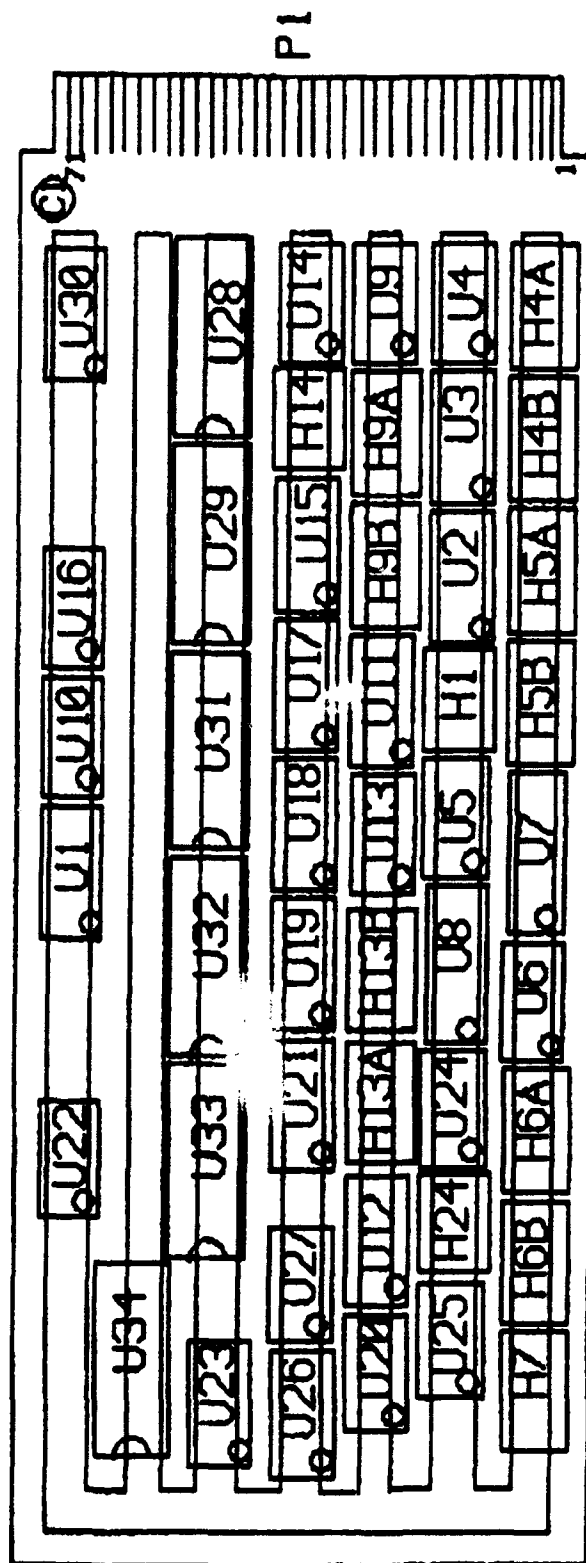


Figure 1

with drawing the computer boards to show where each microchip is located on the various boards. Figures 1 and 2 are the drawings for the sweep card. Figure 1 shows the different chips and headers on the card and Figure 2 shows the make-up of each the headers which consist of resistors or capacitors. I also did some work updating the schematics of these cards. The schematics are the actual designs that are laid out before the component is built. As each card was debugged, various changes were made and I was responsible for showing these changes on the schematics and producing a new copy.

Aside from documentation, I also did a small amount of digital design. I was involved with the initial designing steps for a high speed data switch. This switch, when completed, would allow the graphics generator to be controlled from four different drivers. The problem was to design a switch which would control which of the four separate drivers would be connected by pressing their corresponding button. There was also to be an automatic channel which would detect which driver was feeding the switch information and automatically switch to that channel. I started with a simple design using TTL microchips and built a design up step by step until the desired outcome was reached. I tested the design on a breadboard driving LEDs as the outputs. Once it was determined the logic would work, I implemented the design onto a larger programmable microchip. This reduced the number of chips in the machine from ten to one and made debugging much

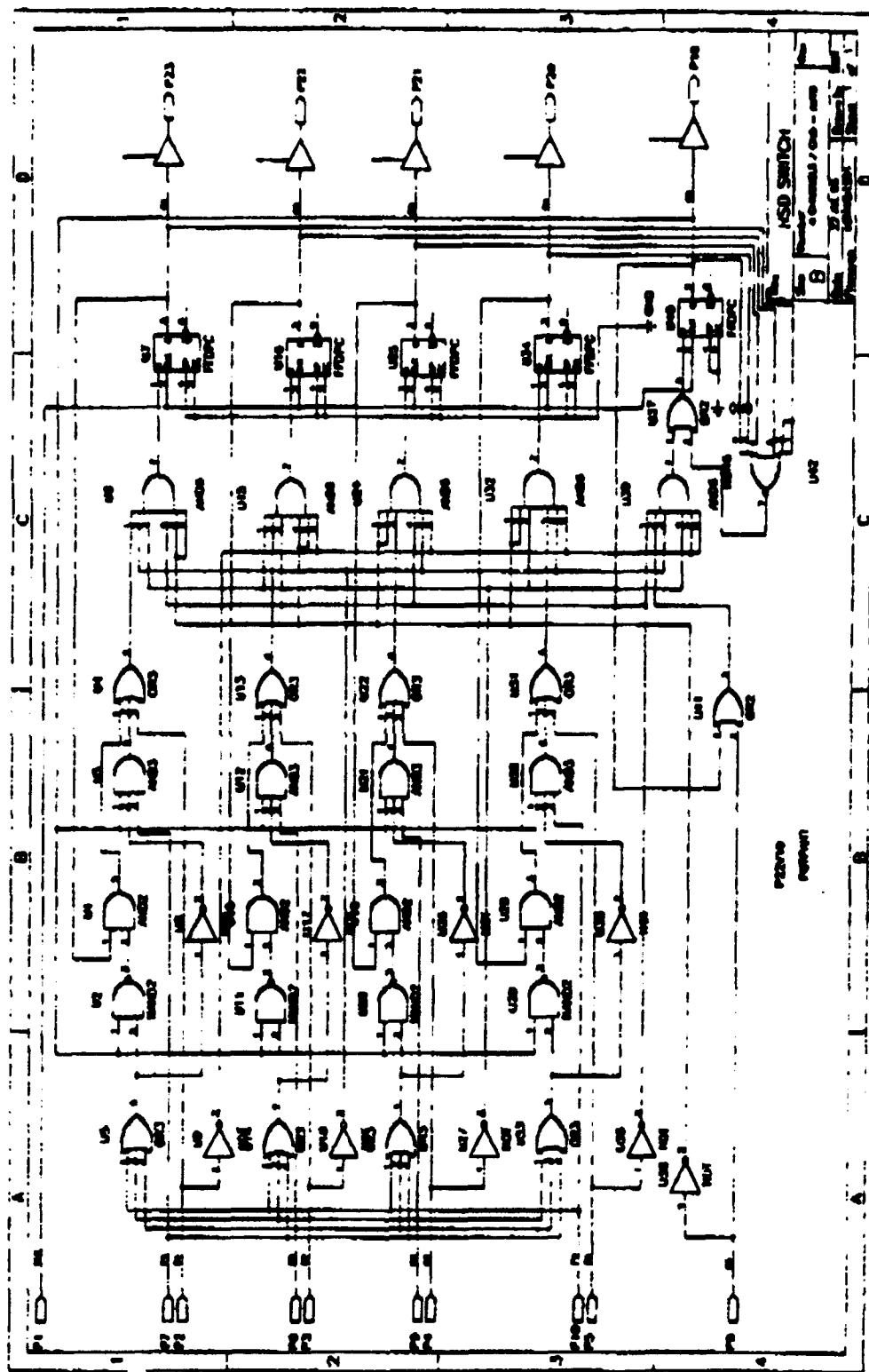


Figure 3

quicker and easier. Figure 3 shows the final schematic of the logic on the programmable chip.

Conclusion

Overall, I felt my experience with the High School Apprenticeship program was a very beneficial experience. I had a chance to learn a lot about electronics and flight simulators. More importantly I got a chance to experience many different aspects of the science and engineering field and develop a feel for which of these I like the best. I also got a feel for what a full-time job is like. Both of these will help me to determine what I have the most interest in doing later in my life and were the most beneficial parts of this program.

AN EXPERIENCE IN STRUCTURES TESTING

Charles J. Middleton
Carroll High School

Final Report for:
High School Apprenticeship Program
Wright Laboratory

Sponsored by:
Air Force Office of Scientific Research

August 1993

An Experience in Structures Testing

Charles J. Middleton

ABSTRACT

I was assigned to Wright Laboratory, Flight Dynamics Directorate, Structures Test Branch, under Amar Bhungalia, project engineer, at Wright Patterson Air Force Base. I worked with my mentor along with various other engineers and technicians on a diverse group of projects during my stay there. I assisted on the setup of the Fuel Tank Test Methods and the Elevated Temperature Aluminum Program (ETAP). I designed, edited, and redesigned a hydraulic manifold for use on the ETAP using DesignCAD-3d on a Unisys PW² Advantage computer. I helped to create a Macro program for the analysis of data for the F-16 Transparency Evaluation Test. I assisted in the design of the structural framework for the Structural Assessment Vulnerability Evaluation. I assisted in running the Leading Edge Flux Meter Calibration Test and analyzing data for it. I worked in preparing and constructing graphite composites in the Composites Lab. I was also able to view the Lightly Loaded Splice Subcomponent Fatigue Testing, the Conductive Shield Heat Exchanger Sub-Elements X-30 Nozzle Active Cooled Structure Fatigue Test, and the F-15 Wing and Wing Carry-Through Structure Fatigue Test.

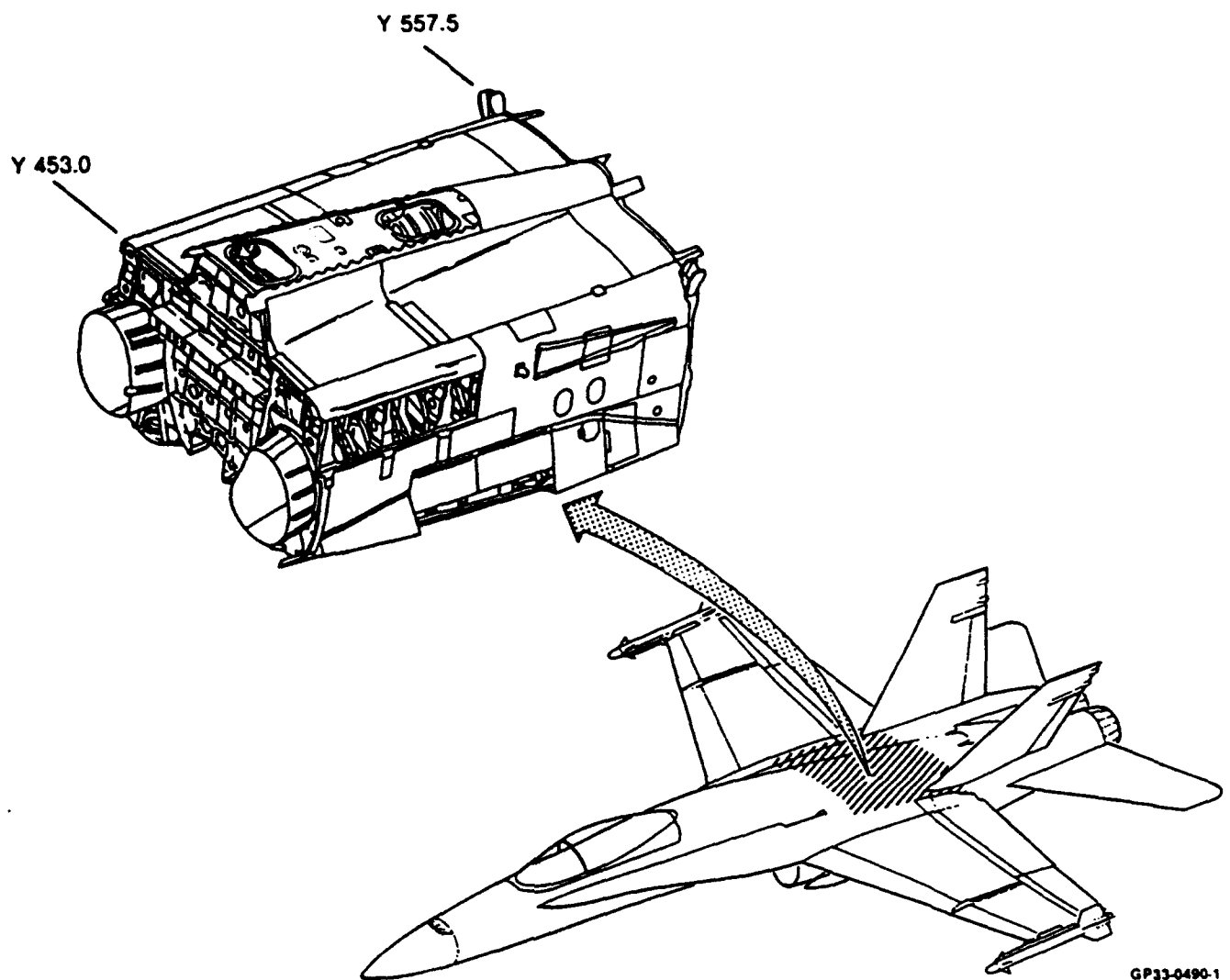
An Experience in Structures Testing

Charles J. Middleton

I was assigned to Amar Bhungalia, a project engineer, at Wright Laboratory, Flight Dynamics Directorate, Structures Test Branch, at Wright Patterson Air Force Base. I worked not only with Amar but also with many different engineers and technicians in my building. I was responsible for a variety of minor works on various projects and for the complete design of a hydraulic manifold for use as the dump system in the ETAP test.

I was involved in wiring, electronic assembly of thermocouple plugs, attachment of thermocouples, and other preparatory measures for the Fuel Tank Test Methods. The objective of this effort is to develop effective methods for certification and evaluation of the fuel tank containment integrity of current and future aircraft integral fuel tanks. The effort is currently directed toward utilization of the test facility in support of a McDonnell Aircraft Co. IRAD program, a General Dynamics IRAD for rapid damage repair methods, and a PRAM program involving spray sealant evaluation for transport aircraft wings. (See diagram page 17-4.)

I was also involved in wiring and setup for the Elevated Temperature Aluminum Program (ETAP) test. The ETAP test component is an aft fuselage center keel beam. The objective of the test program is to verify by full scale testing that the center keel beam meets the structural criteria used for its design. Additional objectives are to verify analysis, determine the critical failure modes, and assess the



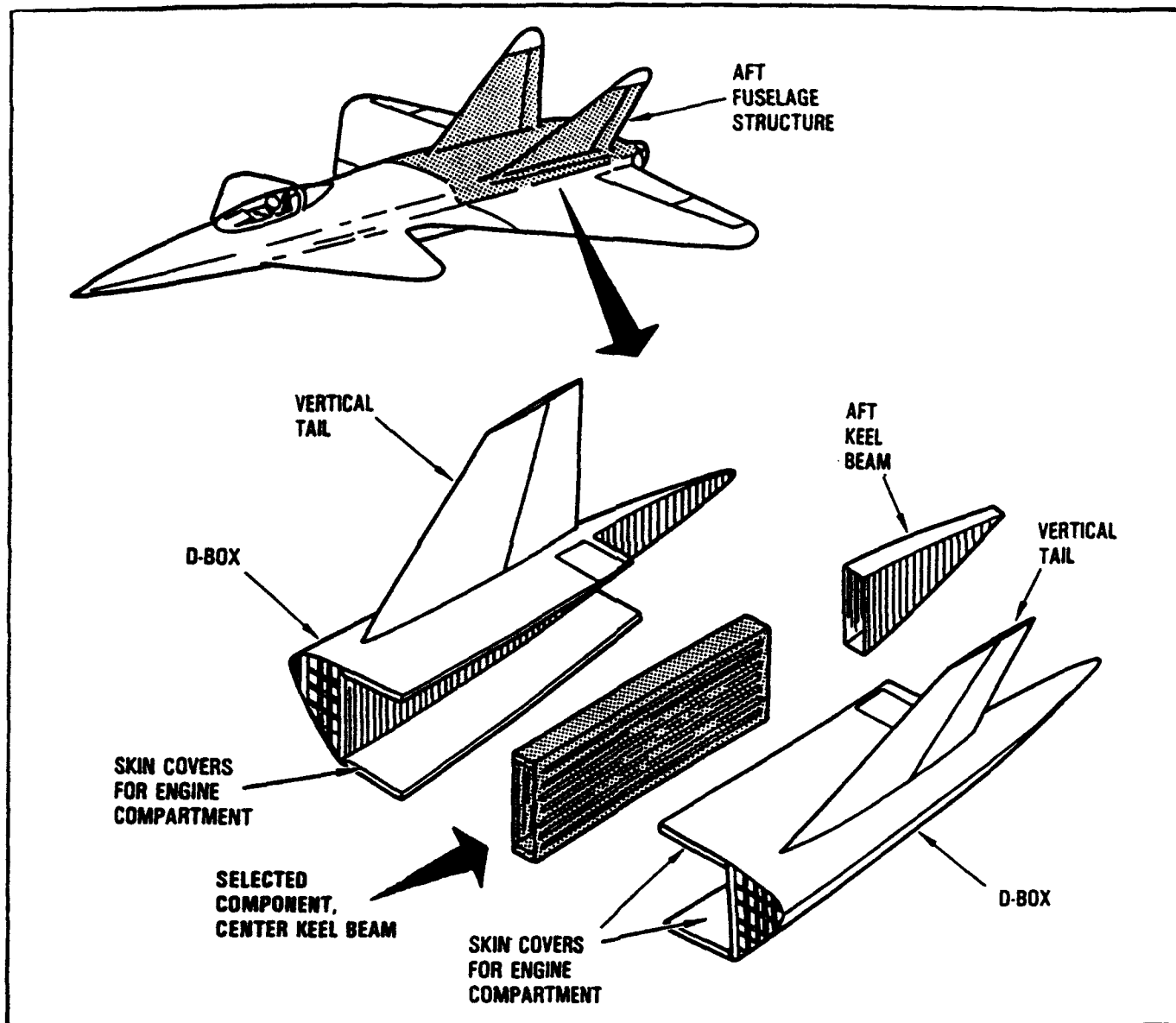
GP33-0490-1

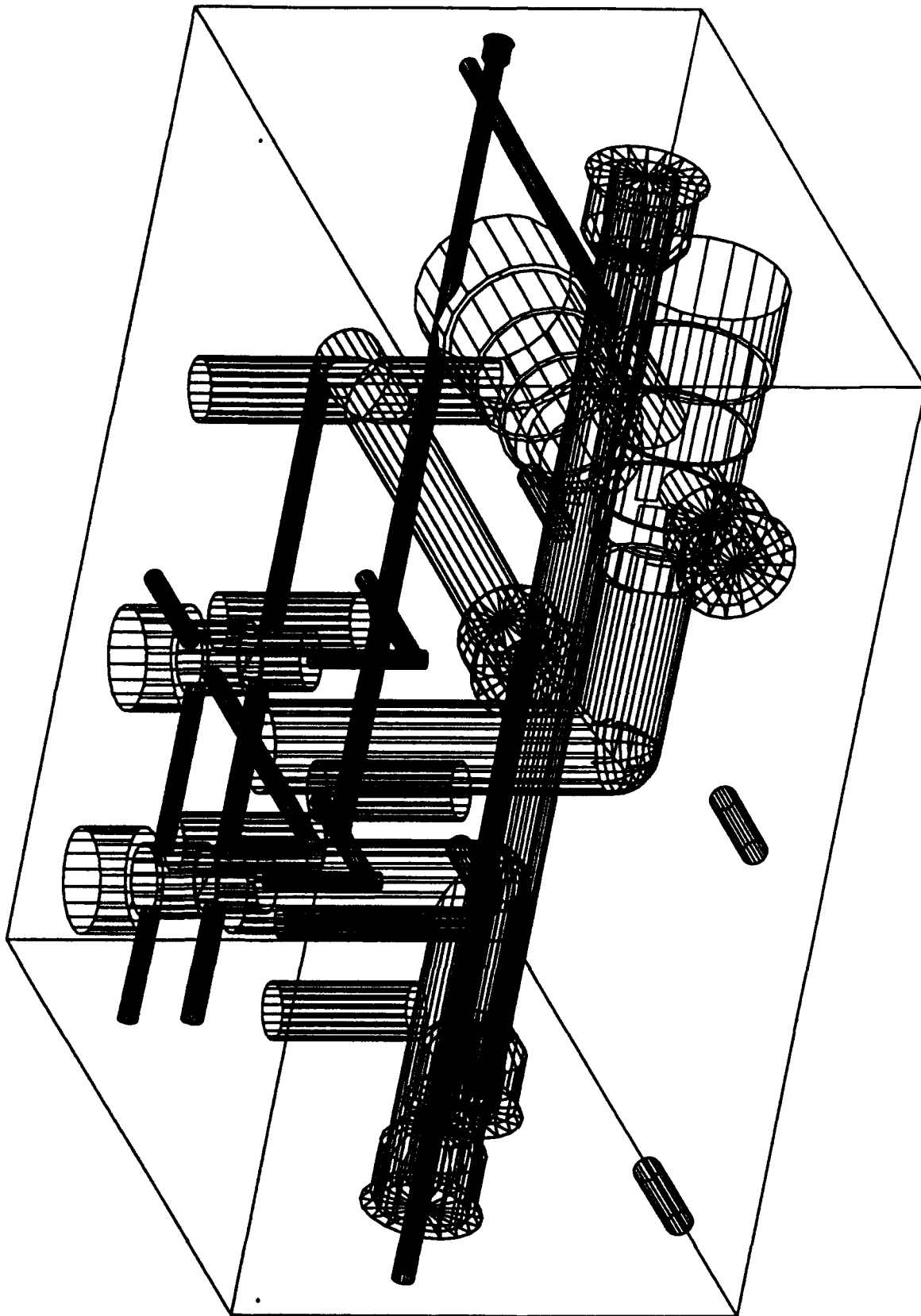
FIGURE 2-1
GENERIC INTEGRAL TANK CONFIGURATION DEFINITION

validity of the structural criteria for future elevated temperature aluminum designs. Durability, damage tolerance, and static tests will be accomplished while exposing the keel beam shear webs to an elevated temperature environment. (See diagram page 17-6.)

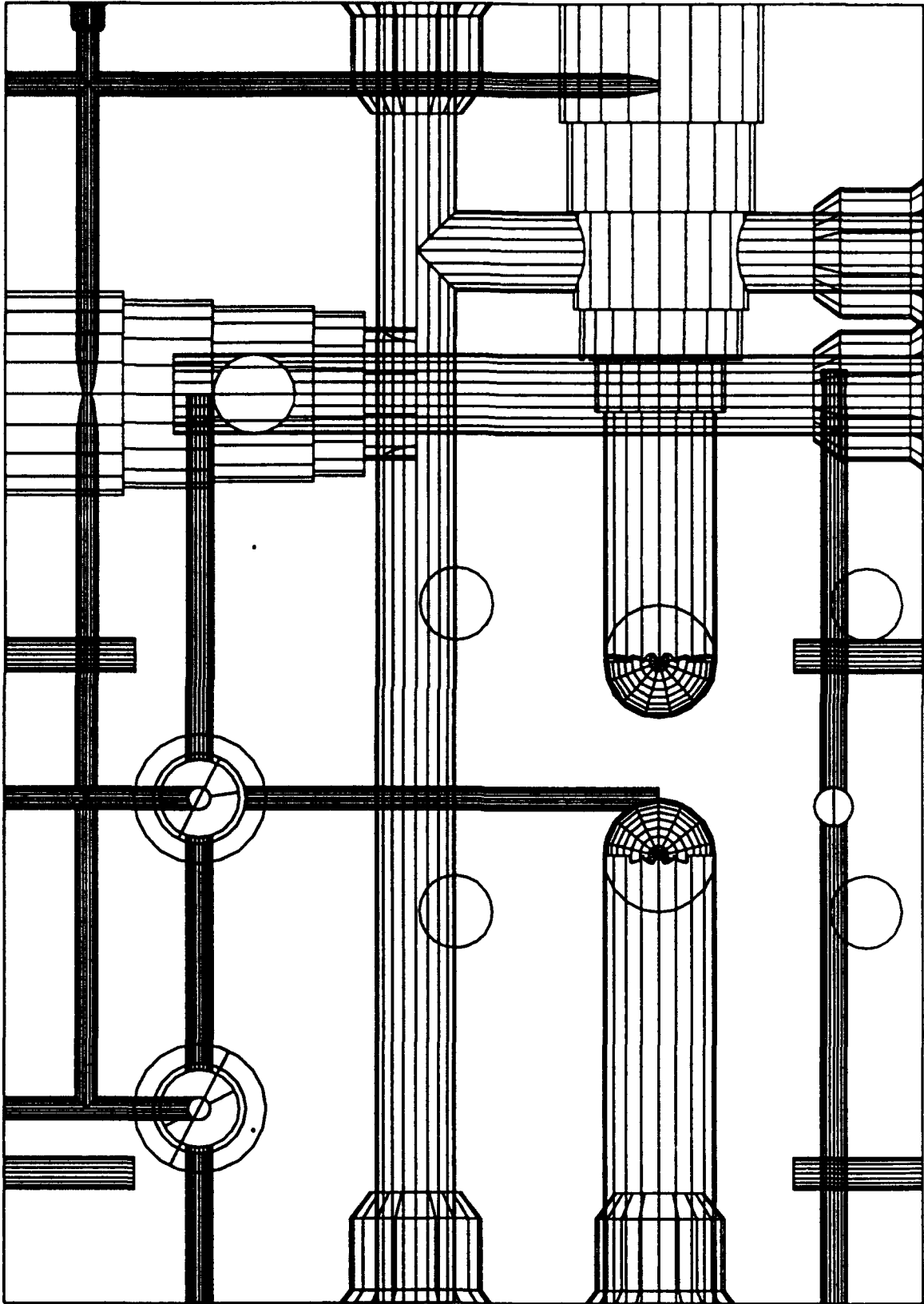
More importantly, I designed, edited, and redesigned a hydraulic manifold for use on the ETAP. I used the DesignCAD-3d program on the Unisys PW² Advantage computer. After being given an initial geometrical data and rough preliminary design and familiarizing myself with the program, I designed a three-dimensional model of the manifold, which was to be used as a hydraulic dump system. After pointing out a few problems and trying to fix them, I was permitted to redesign the entire manifold using my own ideas. The manifold is a ten inch by seven inch by five inch block of aluminum with various cavities in it for valves and fluid lines. After completing my new design, I had to make different views and cross-sections of it and then put dimensions on them before they were finally sent to the machine shop for manufacturing. The diagrams on pages 17-7 through 17-9 detail the design of this hydraulic dump system.

I also used the DesignCAD-3d to alter the design of the structural framework of the Structural Assessment Vulnerability Evaluation. This test involves firing a powerful laser at a plate of carbon composite material as it is bent under high amounts of load. It will demonstrate the internal strength of the material and its resistance to concentrated laser heating. The diagram on page 17-10 shows the setup for that test.

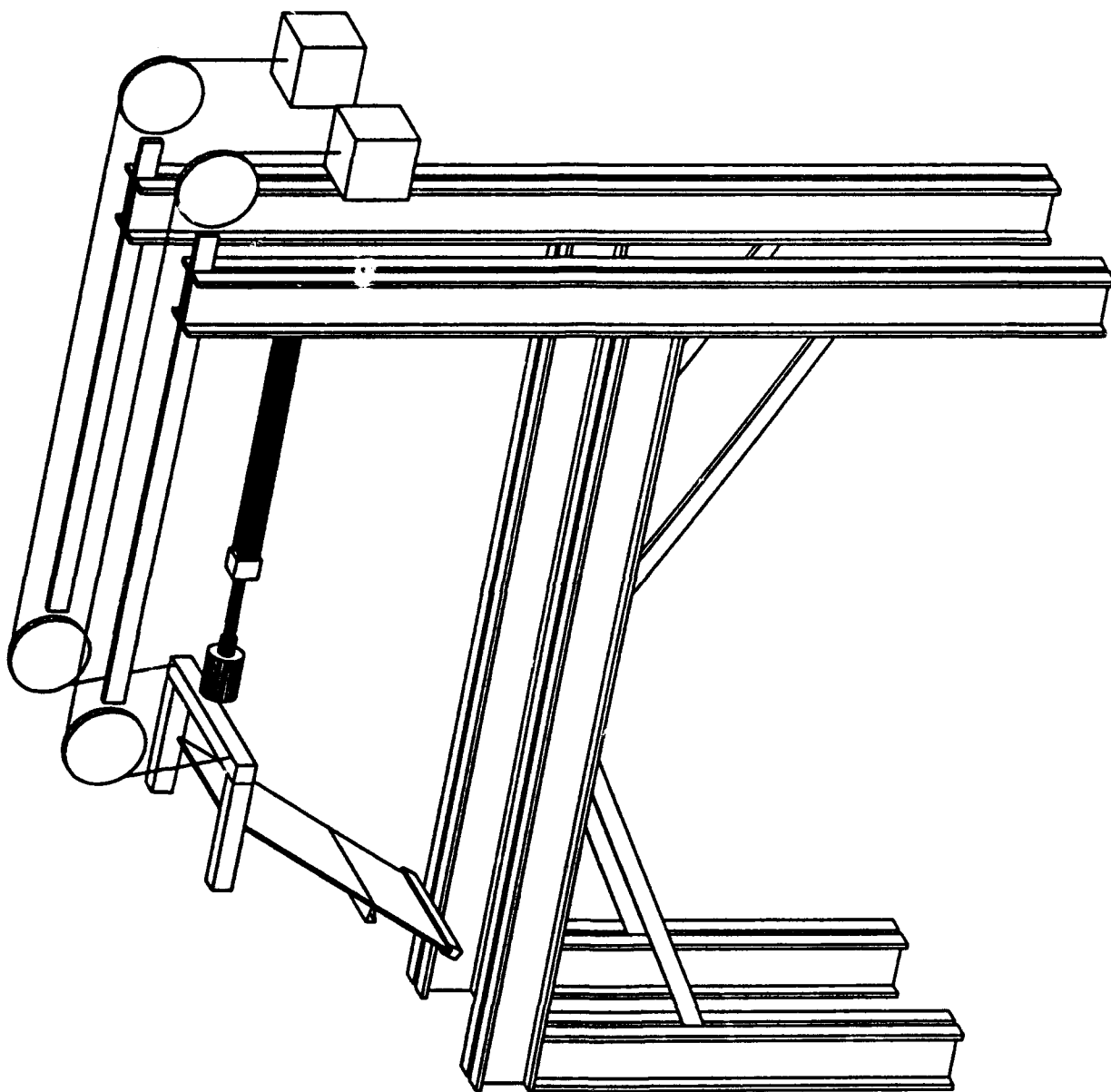




17-7







I helped to create a Macro program for the F-16 Transparency Evaluation Test. This test simulates the fatigue that a typical F-16 canopy would undergo during various missions during its lifetime. The program that I worked on was used in the analysis of data for the past four years of the test. It was also done on a Unisys computer using the programming language that was required.

I assisted in running the Leading Edge Flux Meter Calibration Test. This test involved finding the consistency of a plate of graphite composite material with respect to the aspect of high intensity heating. Quartz lamps were used to heat the specimen as high as 1500 degrees Fahrenheit, and instruments measured heat and temperature at various spots throughout the material. I also helped in the data analysis of this test, smoothing and averaging data results.

I worked briefly with the Composites Laboratory which is separate from the Structures Test Branch but is in the same building. There I was involved in preparing and constructing sheets of graphite composites. These carbon composites are meticulously assembled and sealed. Then they are "cooked" in an Autoclave at high temperature and pressure in order to make them the strong, light and durable materials that they are.

Additionally, I was able to view and discuss in detail the workings of three other tests. These tests taught me just as much through observation as my work with the others did.

I viewed the F-15 Wing and Wing Carry-Thru Structure Fatigue Test. Current USAF F-15 fleet usage is approximately four times as severe as anticipated. This severity has caused the F-15 SPD to question the

ability of the F-15 aircraft structure to meet the original design life of 8000 flight hours. A new fatigue test incorporating flight loads representative of actual fleet usage is currently in progress at the Structures Test Branch. The test spectrum is comprised of thirteen flight conditions varying from a positive 9.92 Gs to a negative 1.89 Gs. The test plan calls for 24,000 flight hours to be applied.

I saw the Lightly Loaded Splice Subcomponent Test. McDonnell Douglas Corporation has fabricated a TMC subcomponent which represents a typical X-30 fuselage section. WL/FIBT is involved in the testing of this subcomponent to evaluate the fabrication and performance aspects of thin, stiffened structures as related to the X-30 program. This article simulates the splice of two 80 inch radius sections of fuselage at a ring frame. This test as well as the "Burst Test" is being undertaken as part of the highly esteemed National Aero-Space Plane Program (NASP).

I also viewed this "burst test", or the Conductive Shield Heat Exchanger Sub-Elements X-30 Nozzle Active Cooled Structure Test. The purpose of this program is to develop, demonstrate, and validate critical technologies required to satisfy the X-30 phase 2 technical objectives for actively cooled airframe nozzle structures. This is a joint development program between airframe contractors (General Dynamics, Rockwell, and McDonnell Douglas) augmented with government participation to develop actively cooled nozzle panels. The primary objective of the sub-element demonstration is to provide "building block" data to support development of large scale nozzle cooled panels. WL/FIBT is performing a series of tests to support this program. One of

these tests is a burst test to demonstrate pressure level at which the specimen may burst.

CONCLUSIONS:

Being able to involve myself in so many high technology and important tests at a research facility of the stature of the one I was fortunate enough to find myself at has been an experience of inestimable value to me. I was able to work with so many extremely professional people in such a productive environment on a consequential group of projects. I learned much about engineering as a career and saw the kind of work that I may someday perform. I learned about what government work is like, and I must say that I had a very positive experience on the Base. I was able to talk to both military and civilian personnel concerning work with the Air Force. My knowledge of Structures Testing was vastly increased. In addition, I picked up tidbits of wisdom about life in general. I am extremely glad that I was chosen for this program and decided to accept.

ACKNOWLEDGEMENTS:

I would like to thank the following people for their guidance and instruction during my apprenticeship:

Amar Bhungalia	Jim Eichenlaub	Tim Sikora
Ray Fisher	Scott Hamilton	Larry Kretz
Larry Marcum	Doug Dolvin	Ron Dittmer
John Pappas	Fred Hussong	Joe Pokorski

THE EFFECTS OF MOISTURE ON THE
TENSILE STRENGTH OF CONCRETE

Melissa A. Page

William S. Strickland - Mentor

Final Report for:
AFOSR Summer Research Program
Wright Laboratory
WLFIVCS Tyndall AFB, FI 32403-5323

June 14 - August 6, 1993

THE EFFECTS OF MOISTURE ON THE
TENSILE STRENGTH OF CONCRETE

Melissa A. Page
Student, AFOSR Summer Research Program
Wright Laboratory
WLFIVCS, Tyndall AFB FL 32403-5323

ABSTRACT

The study measured the effect of moisture on the tensile strength of concrete. Forty-six samples were cut from the same J-Mix concrete. The samples were divided into three groups; each group was exposed to different moisture levels. Sixteen "wet" samples were tested after remaining in water for three days. Fifteen "half-dry" samples were tested after being dried in an oven until their moisture was decreased by 5%. Fifteen "dry" samples were tested after drying reduced their moisture by 10%. Ten samples from each group were tested using the Split-Hopkinson Pressure Bar. The results were recorded on an oscilloscope; the transmitted wave was used for the calculations. The remaining samples from each group were tested on the Forney Machine for quasi-static load rates. The data showed that the "dry" samples showed higher tensile strength during quasi-static tests while the "wet" samples were more resilient at higher load rates in dynamic testing.

THE EFFECTS OF MOISTURE ON THE TENSILE STRENGTH OF CONCRETE

Melissa A. Page

Introduction

While a participant in the High School Apprenticeship Program at Tyndall Air Force Base, the authoor conducted tests on the effects of moisture on the tensile strength of concrete. Previous tests had charted the effects of moisture and strain rate on the compressive strength of concrete. (Reference 1) Other tests were performed concerning the effects of moisture on direct tension. (Reference 2) But no experiments had been conducted regarding the effects of moisture on the tensile strength of concrete.

Objective

How the pressence of moisture will affect a structure has always been an important factor in construction. The knowledge of how a concrete specimen exposed to moisture will react to both high and low-load rates, when placed on a larger scale, can be very useful. The data gathered from this experiment can provide insights into how a structure exposed to different levels of moisture would hold up under the pressure of direct attack. The data can also be applied to domestic issues, such as bridges and roads.

Approach

The concrete samples used in the experiment were cut, sawed, and polished from the same J-Mix concrete. All samples were two inches in length and diameter. Forty-six samples in all were tested, thirty in dynamic tests, sixteen in quasi-static tests. Sixteen samples were tested after remaining in water for three days. For simplicity's sake, these are called the "wet" samples. The remaining thirty samples were removed from water and dried for different amounts of time in an oven until their moisture dropped by a certain percentage. Three samples from each group of fifteen were weighed every hour; the measurement was then divided by the initial weight to determine the new percentage of moisture. Fifteen samples were dried until their moisture was reduced by 5% (resulting moisture - 95%); these samples are called "half-dry." The remaining samples had their moisture decreased by 10% (resulting moisture - 90%); these samples are called "dry."

Methodology

The Forney Machine was used to perform the quasi-static tests. Six wet samples, five half-dry samples, and five dry samples were divided between splitting tensile tests and direct compression tests in the following manner:

	Splitting Tensile	Direct Compression
Wet	4	2
Half-dry	3	2
Dry	3	2

For the spitting tensile tests, the samples went through other preparations. Each sample was marked on its top surface across its diameter. On either side of the sample two aluminum rods were attached using adhesive spray. (Figure 1 and 1a) These rods were placed on either side of the line in order to evenly distribute the load during tests.

The prepared sample was then placed in the Forney Machine so that the pressure was first impressed to the aforementioned aluminum rods. (Figure 2) Pressure was applied until the sample failed, or reached its maximum load. The maximum load was then converted into the load rate (pounds/minute). The load was then divided by the static modulus to find the strain rate (1/s). The strain rate was then converted into pounds per square inch (psi). The individual psi measurements for each group were then averaged together. The resulting number, the tensile static strength (f'_ts), was used later on for other calculations.

Direct compression tests were run mainly because the information gathered is often valued by other researchers. These tests to find the compressive strength did offer additional data to compare the samples with. (Figure 3)

The Split-Hopkinson Pressure Bar (SHPB) was used for the dynamic tests. It consists of a gas gun, a striker, an incident bar, and a transmitter bar. (Figure 4 and 4a) A release of built-up gas pressure from the gas gun causes the striker to hit the incident bar, generating a stress wave. This wave travels through the incident bar,

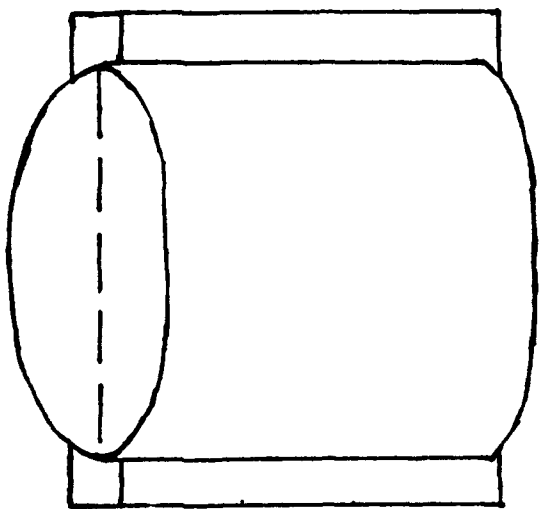


Fig. 1
Side view of prepared sample.

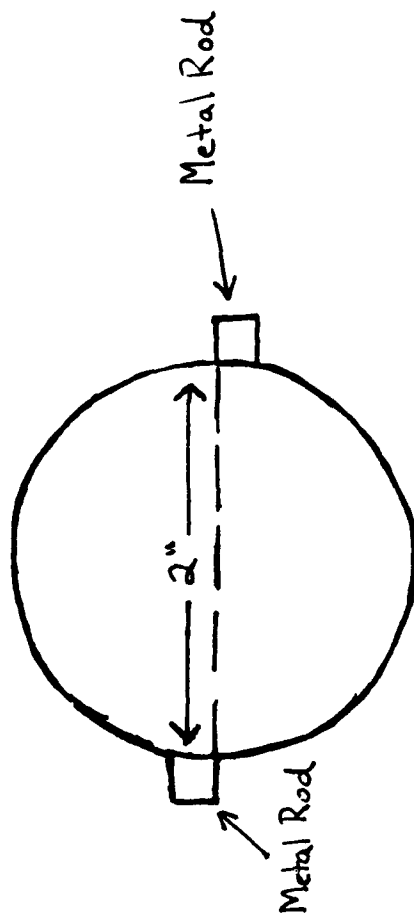


Fig. 1a
Top view of prepared sample.

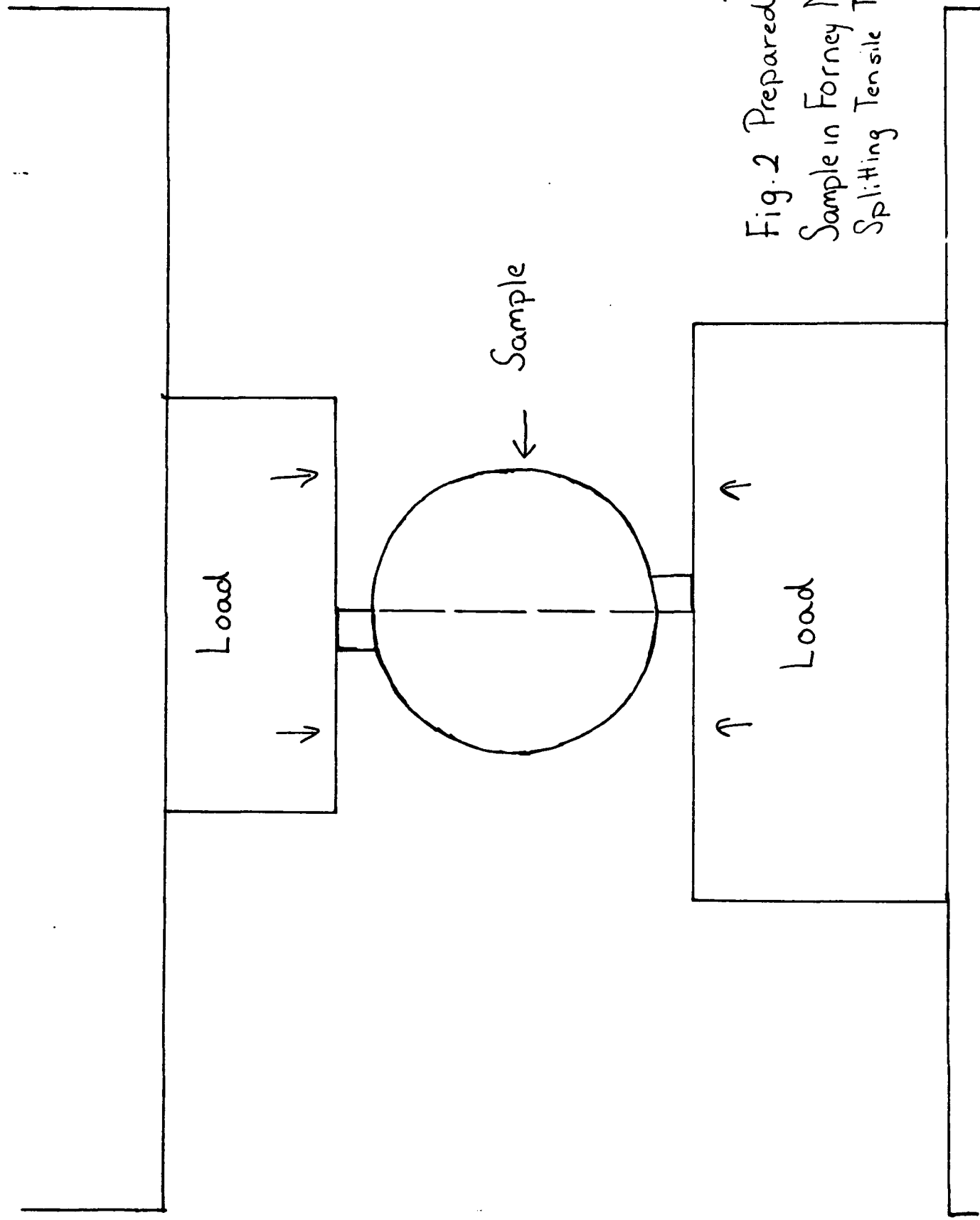


Fig. 2 Prepared
Sample in Forney Machine
Splitting Tensile Test

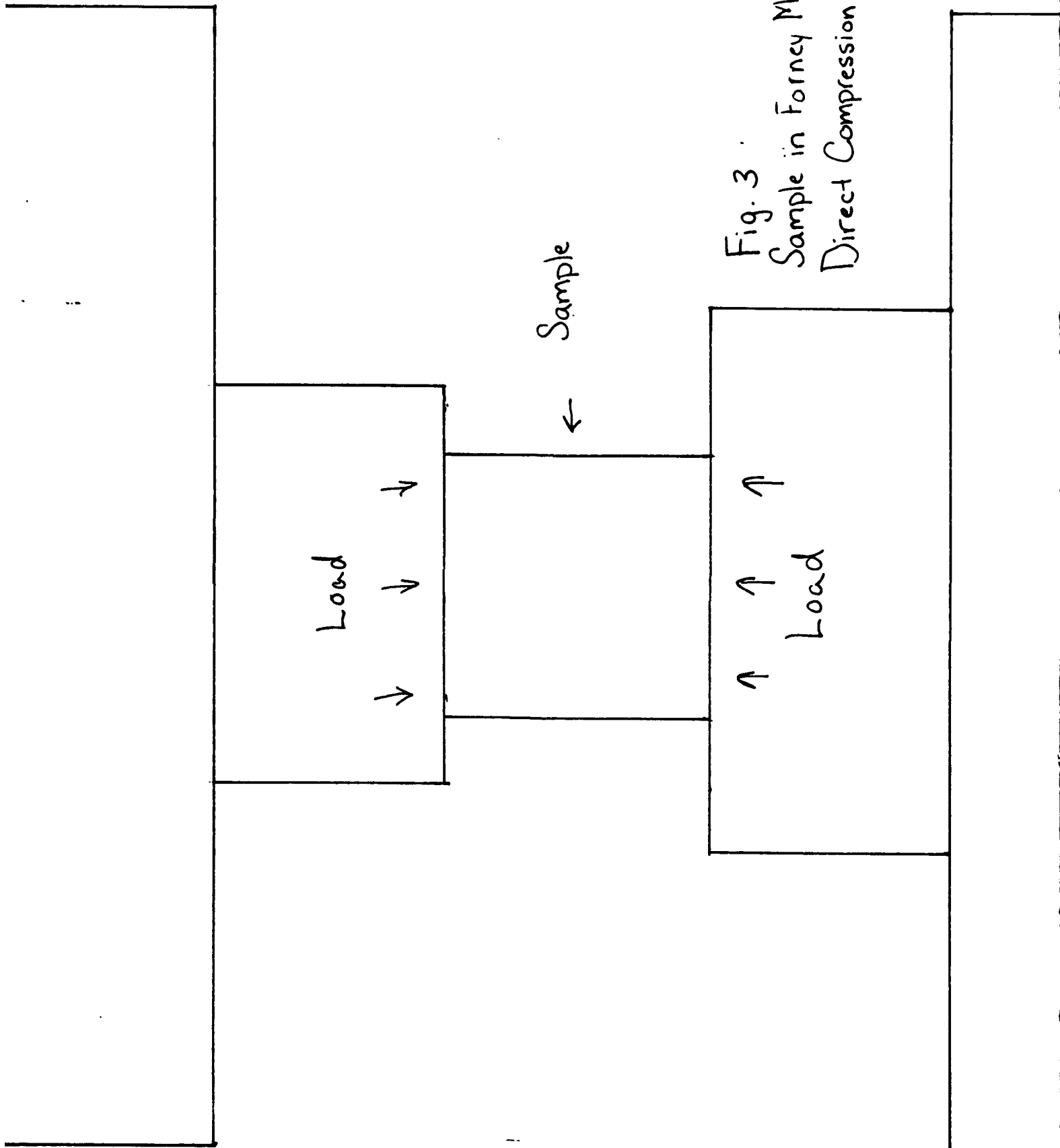


Fig. 3
Sample in Forney Machine
Direct Compression Test

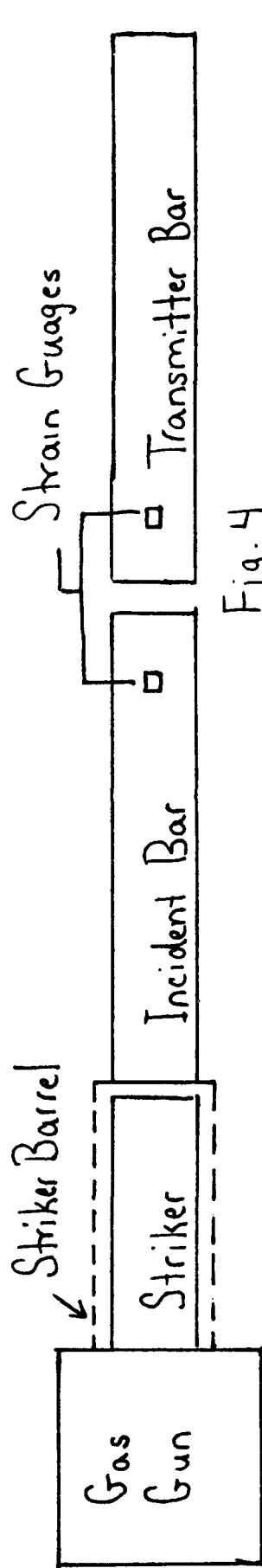


Fig. 4

Split-Hopkinson Pressure Bar (SHPB)

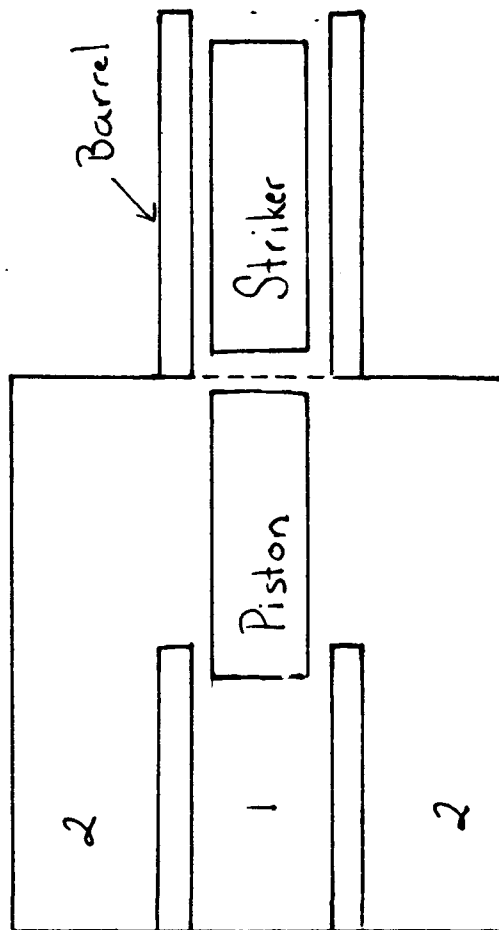


Fig. 4a Gas gun.

the sample, and the transmitter bar. Data is collected from strain gauges placed equidistance from the sample. The data is registered on an oscilloscope, and measurements are taken. (Reference 3)

The SHPB was used primarily because of its ability to achieve high as well as low-loading rates. The striker can also be changed. For the tests, the fifty-inch striker was used for the low range rates (8, 9, and 15 psi), while the twenty-six-inch striker was used for higher rates (50, 125 psi).

Ten samples were tested from each group in the SHPB. Every group underwent the tests under the same conditions; the only difference was their moisture content. This assured a certain uniformity in the data. Each sample was prepared in the same way as the splitting tensile tests on the Forney were, and then placed between the incident bar and the transmitter bar. (Figure 5) The oscilloscope was set to trigger at 300 microseconds (uS), and the gas gun was set to the pressure at which the test would be conducted (e.g. 15 psi). The gas gun was then fired. (At a high pressure, a protective box was placed over the sample.) The reading from the oscilloscope was stored, and the sample fragments put into bags and labeled.

After the signal from the SHPB was stored on a disk, the oscilloscope was switched to Memory Channel Q3, which displays the part of the stress wave transmitted through the sample. The transmitted wave was then used to determine the stress rate. (Figure 6)

$$\text{Stress Rate} = \Delta = \text{Peak Voltage} \times 2058$$

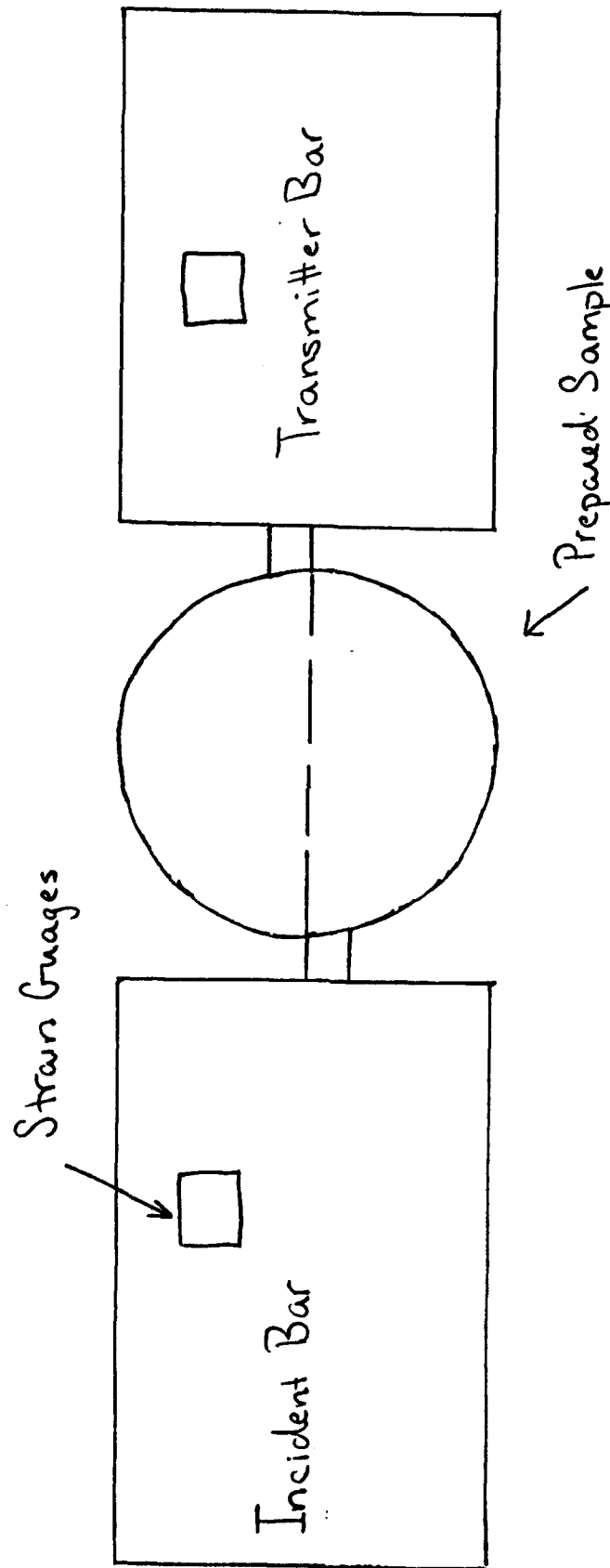


Fig. 5
Prepared Sample in Split-Hopkinson Pressure Bar

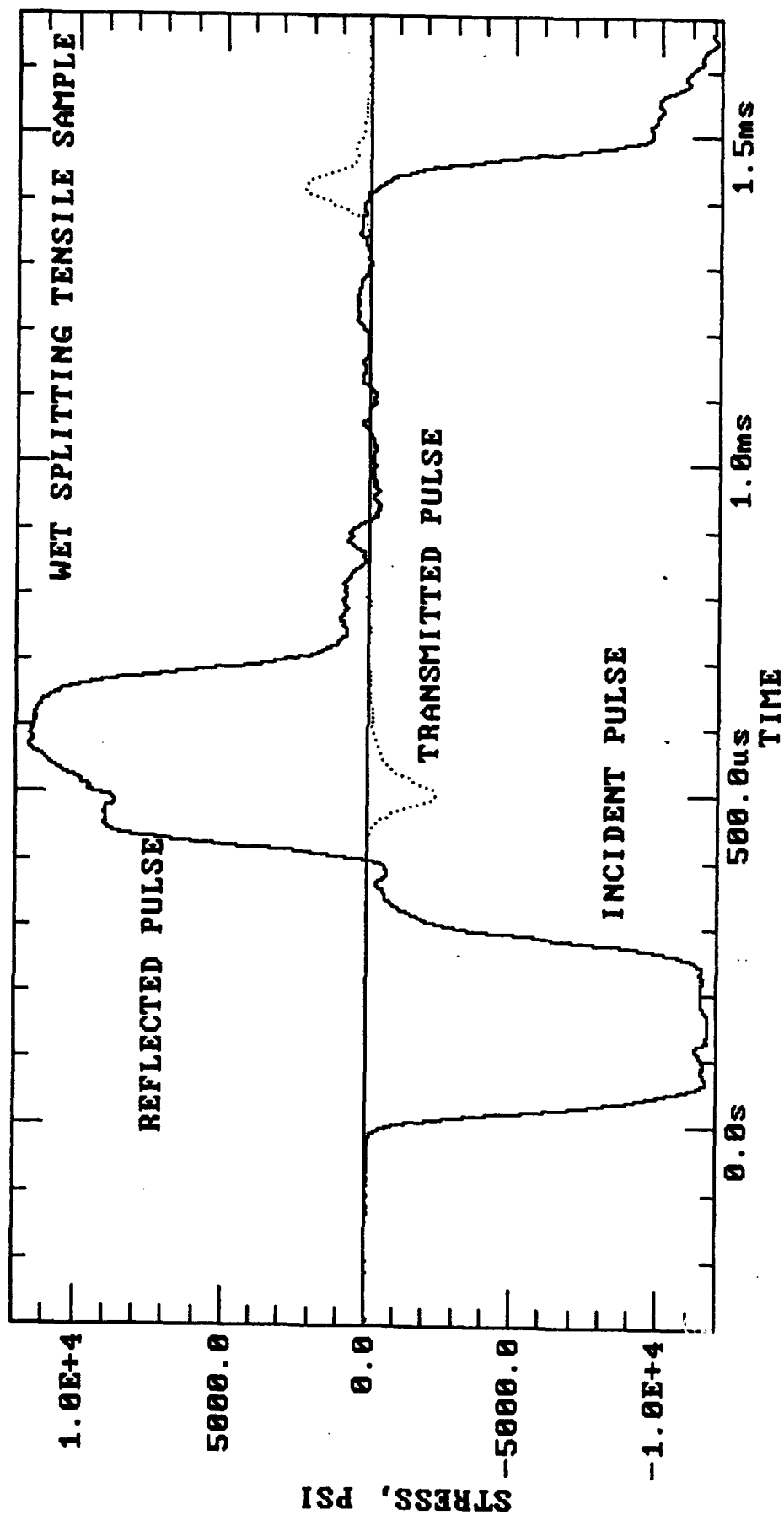


Fig. 6 Example of oscilloscope readout.

This number was then divided by two to determine the dynamic tensile stress.

$$\text{Dynamic Tensile Stress} = f'_{td} = \sigma / 2$$

The dynamic tensile strength was then divided by the static tensile strength (f'_{ts}) found earlier on the Forney Machine. This set of numbers became the y-axis on the data charts.

$$f'_{td}/f'_{ts} = \text{Dynamic Tensile Strength/Static Tensile Strength}$$

Other measurements were made using the Q3 Memory Channel. The load rate was determined by first finding the slope of the line. The two points chosen to be the slope were then subtracted from one another, leaving a voltage reading and a time reading. The load rate was then calculated in the following manner:

$$\text{Load Rate} = \text{Voltage Reading} \times 2058 / 2(\text{Time Reading})$$

Other calculations were made to find the strain rate.

Data

Table 1 presents the numerical results from the SHPB and Forney Machine tests. Chart 1 presents the same data in graphical form.

STRAIN RATE EFFECTS ON CONCRETE STRENGTH

WET/DRY SPLIT TEN TESTS, J-MIX

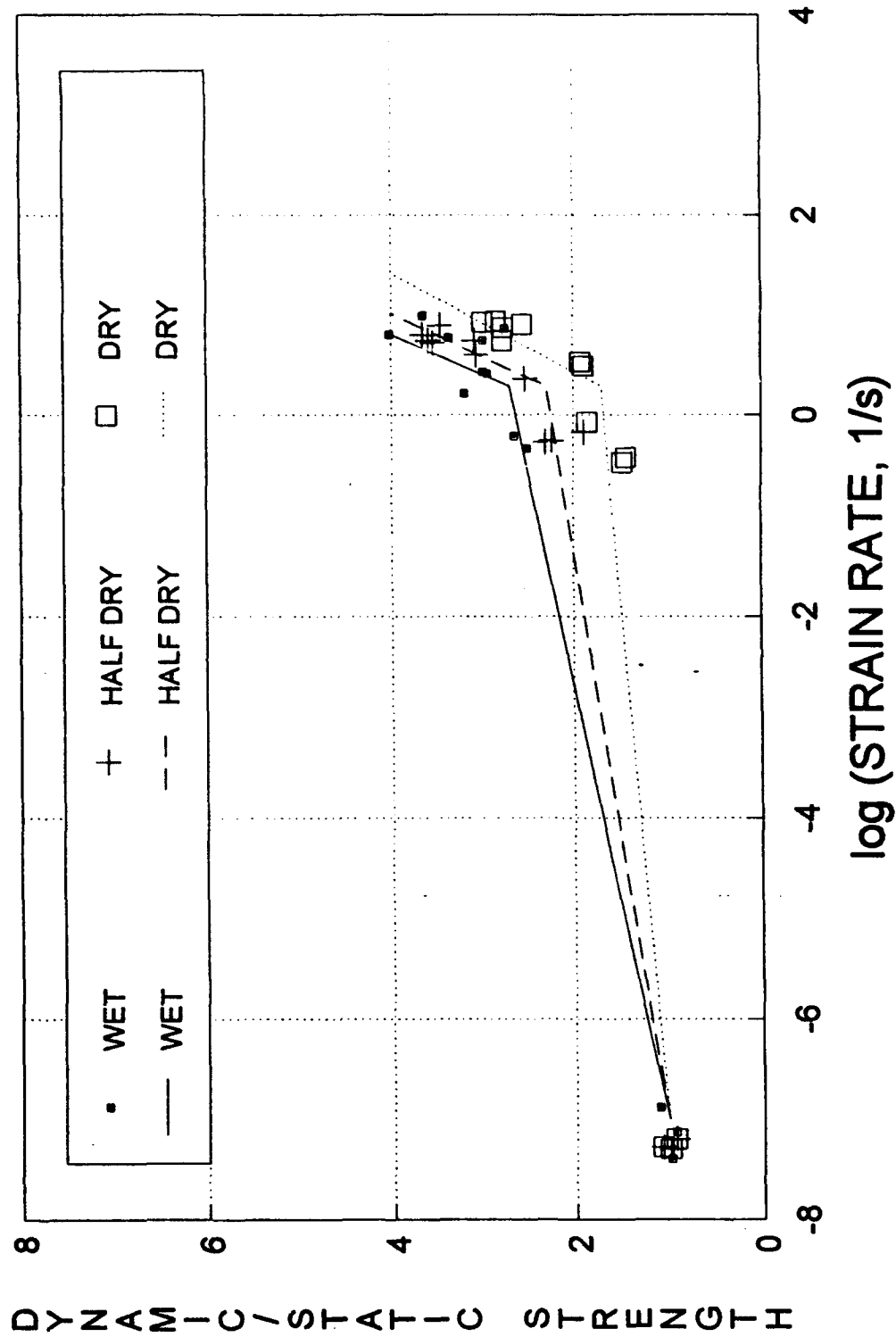


Chart 1 Graph of test results

Table 1 Numerical results from tests

X Data	WET	HALF DRY	DRY	WET
-7.13	0.93			
-7.4	0.98			
-6.68	1.1			
1	3.65			
0.87	2.74			
0.78	3.36			
0.75	2.98			
0.44	2.98			
0.42	2.94			
0.81	4.02			
-0.33	2.51			
-0.21	2.65			
0.22	3.2			
-0.17		1.89		
-0.25		2.24		
-0.27		2.31		
0.75		3.59		
0.37		2.53		
0.61		3.06		
0.75		3.06		
0.81		3.65		
0.73		3.54		
0.9		3.46		
-7.3		0.99		
-7.2		0.93		
-7.28		1.07		
-7.3			0.99	
-7.2			0.93	
-7.28			1.07	
-0.07			1.85	
-0.42			1.43	
-0.47			1.47	
0.75			2.77	
0.5			1.89	
0.54			1.92	
0.93			2.99	
0.88			2.76	
0.91			2.55	
0.94			2.84	
-7				1
0.3				2.7
0.812				4
-7				
0.3				
1.02				
-7				
0.3				
1.415				

Table 1 (Concluded)

X Data	HALF DRY	DRY
-7.13		
-7.4		
-6.66		
1		
0.87		
0.78		
0.75		
0.44		
0.42		
0.81		
-0.33		
-0.21		
0.22		
-0.17		
-0.25		
-0.27		
0.75		
0.37		
0.81		
0.75		
0.81		
0.73		
0.9		
-7.3		
-7.2		
-7.28		
-7.3		
-7.2		
-7.28		
-0.07		
-0.42		
-0.47		
0.75		
0.5		
0.54		
0.93		
0.88		
0.91		
0.94		
-7		
0.3		
0.812		
-7	1	
0.3	2.3	
1.02	4	
-7		1
0.3		1.7
1.415		4

Conclusions

When the SHPB and Forney Machine test results were plotted, the graph showed that the dry samples had a higher strength in static tests, and the wet samples were stronger during dynamic tests. (Chart 1 and Table 1) It also appeared that more aggregate broke during the dry and half-dry tests than during the wet tests. The direct compression tests conducted on the Forney Machine showed that the dry samples had a greater compressive strength than did the wet and half-dry samples.

Based on the data, the following conclusions on the effects of moisture on the tensile strength of concrete can be made:

1. High moisture levels generate a high strain rate sensitivity in dynamic testing.
2. Low moisture levels yield a higher compressive strength.

REFERENCES

1. Ross, C.A., Tedesco, J.W., and Kuennen, S.T., "Effects of Strain Rate on Concrete Strength," accepted for publication in ACI Materials Journal.
2. Reinhardt, H.W., Rossi, P., and Mierran, J.G.M., "Joint Investigation of Concrete at High Rates of Loading," Materials and Structures 23, 1990, pp 213-216.
3. Ross, C.A., "Split-Hopkinson Pressure Bar Test," HQ Air Force Engineering and Services Center, Tyndall AFB, FL, 1989.

MODIFICATION OF M18 FOR EMAA EXTINGUISHING PURPOSES

**Jefferey R. Strickland
High School Research Student**

**Final Report for:
Summer Research Program
Wright Laboratory**

**Sponsored by:
Air Force Office of Scientific Research
Wright Laboratory, Panama City, FL**

August 1993

MODIFICATION OF M18 FOR EMAA EXTINGUISHING PURPOSES

Jefferey R. Strickland

High School Research Student

Abstract

A new class of fires suppressants, known as Encapsulated Micron Aerosol Agents (EMAA), having superior volumetric efficiency, low initial and life cycle costs, low toxicity, no known global atmospheric environmental impacts, and with the potential for a wide variety of applications, is being developed through a joint program between the private sector and the U. S. Air Force. Through the modification of the M18 smoke grenade an evaluation of a portable method for the delivery of EMAA can be accomplished. This innovative application is one of the many possible with this promising new agent.

MODIFICATION OF M18 FOR EMAA EXTINGUISHING PURPOSES

Jefferey R. Strickland

INTRODUCTION

The search for replacements and alternatives for the halon family of chemical fire suppressants has coincided with the development of novel materials and techniques that provide new options for fire protection. One class of materials that has good potential for filling several roles formerly performed by halons is aerosols. The U.S. Air Force has entered into a Cooperative Research and Development Agreement with Spectrex, Inc. to further the development of aerosol technology for a number of fire suppression applications. Encapsulated Micron Aerosol Agents (EMAA) is the title given by the U.S. Air Force to this research program. By implementing old technology such as the M18 smoke grenade unique and applicable apparatuses for safety enhanced and portable use are available.

METHODOLOGY

Aerosol science or particle mechanics draws from several scientific disciplines to formulate the science that underlies its principle areas of research. Aerosol refers to a system of liquid or solid particles suspended in a gaseous medium. Several common aerosols are fumes, smoke, mists, fog, and haze. Based on the state of the suspended substance, liquid or

solid, dispersion and condensation aerosols are differentiated. Dispersion aerosols are formed by the atomization of solids and liquids while condensation aerosols are formed through the condensation of superheated vapors or chemical reaction in the gaseous state. EMAA is a dispersion aerosol that is delivered to the protected space through the combustion of the solid tablet. Prior to EMAA, dispersion aerosols have been created through crushing, grinding, blasting, or drilling of solid matter. The dynamics of aerosols are important considerations for two reasons. First, the ability of the particles to the particle size and the residence time of the fire suppressant. Second, the aerosol, if it is to replace gases in certain applications, must be able to flow around obstacles.

EMAA is initially a solid material that can originate in a variety of forms: solid, powder, or gel. The active component, an oxidizer, and a reducer are combined with a filler. These components are ground into a fine powder and mixed with an epoxy resin binder. Upon ignition of the material, the combustion products are ejected as a dispersion aerosol, with the solid particles floating in the air and the gaseous combustion products.

Successful fire suppression requires that one or more of the four factors that tend to propagate a fire be interrupted. These factors together with their suppression mechanisms are listed on the following table.

Table 1 Factors governing fire propagation

Factor	Suppression Mechanism	Method
Fuel	Removal	Vapor seal
Oxygen	Exclusion	Smothering
Heat	Absorbance	Cooling
Chain reaction	Inhibition	Stop Reaction

EMAA aerosols are hypothesized to function through several mechanisms to suppress fire, the most prominent of which is chemical inhibition of the chain reaction. Other mechanisms such as heat absorption are also possible while oxygen exclusion is not a path for aerosol fire suppression.

APPARATUS

The M18 Smoke Hand Grenade is the apparatus one of the innovative applications used in EMMA fire extinguishing. This grenade will emit red smoke for 50 to 90 seconds. Safety clips are not required with these grenades.

The grenade body, composed of thin sheet metal, is filled with red smoke composition. The filler is topped with a starter mixture.

The Hand Grenade Fuze, M201A1 is a pyrotechnic delay-igniting fuze. The body contains a primer, first-fire mixture, pyrotechnic delay column, and ignition mixture. Assembled to the body are a striker, striker spring, safety lever, and safety pin with pull ring. The split end of the

safety pin has a angular spread.

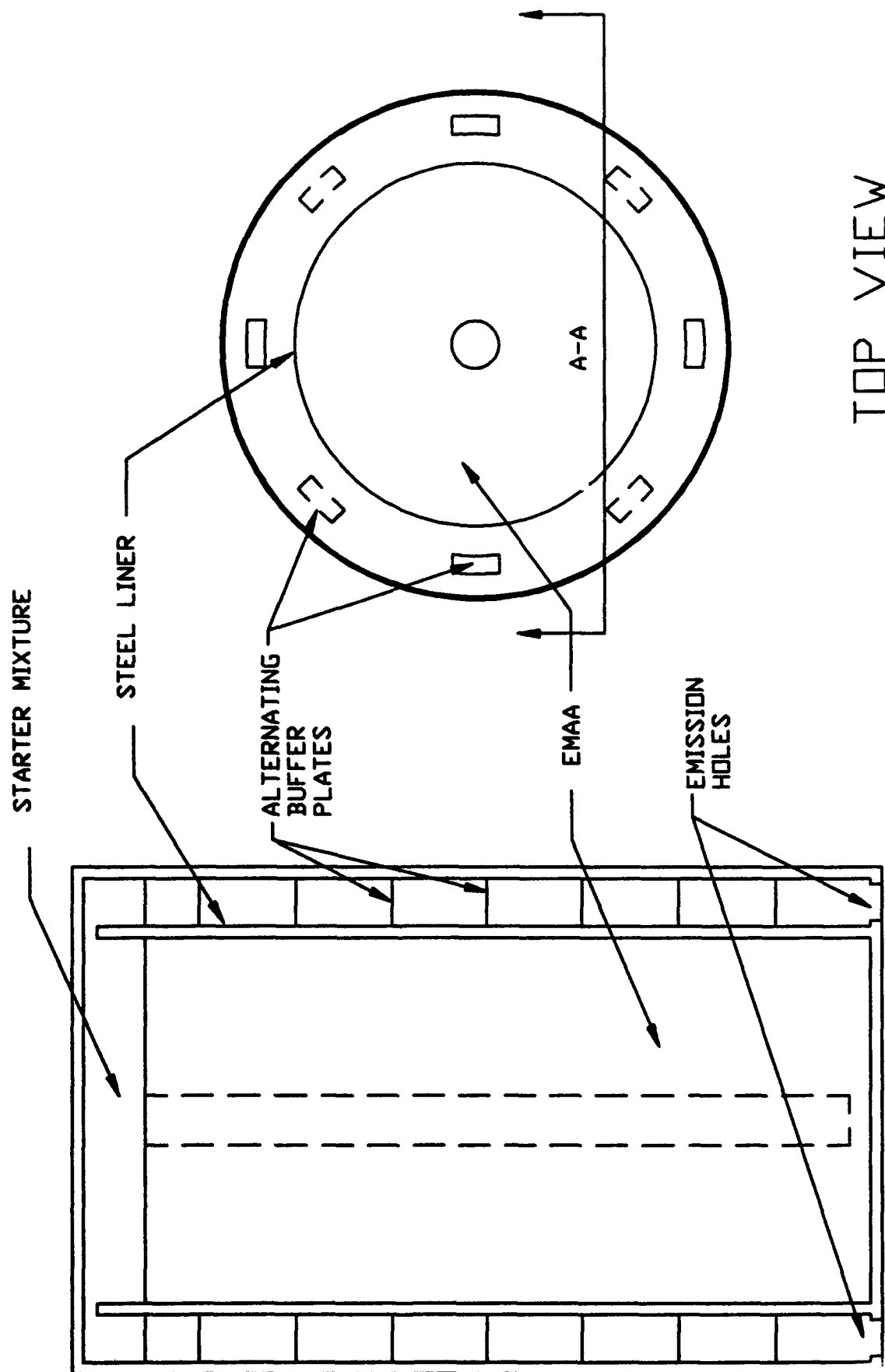
Removal of the M201A1 Fuze safety pin permits release of the safety lever. When the safety lever is released, it is forced away from the grenade body by a striker acting under the force of a striker spring. The striker rotates on its own axis and strikes the percussion primer. The primer initiates the first-fire mixture. The fuze delay element, ignition mixture, and grenade starter mixture and filler are initiated in turn by the preceding component. The pressure sensitive tape is blown off the emission holes and the colored smoke emits from these holes.

With these specified modifications the M18 can be implemented as portable and safe addition to fire fighting equipment. See (Figure 1).

1. Replace smoke composition, filler, with Encapsulate Micron Aerosol Agent (EMAA). This replacement allows for affective fire suppression.
2. Expand canister to compensate for specified dimension of EMAA 16 x 7.4 cm. To extinguish 20 cubic meters of fire one kilogram or 630 cubic centimeters of EMAA is required.
3. Replace current starter mixture with a mixture capable of, at minimum, a 2000 K combustion temperature to compensate for EMAA ignition temperature.

4. Employ alternating buffers for control of EMAA fire emissions. If fire emissions are not controlled it is possible to reignite extinguished material. This is a simple but necessary advancement for safety as well as mechanical improvement.

MODIFIED M18



TOP VIEW

SECTION A-A

EXPERIENCE IN THE METHODOLOGY SECTION AT
AT WRIGHT-PATTERSON AIR FORCE BASE

Miranda H. T. Tseng
High School Apprentice
Methodology Section

Wright-Patterson Air Force Base
WL/FIVS
1901 Tenth Street
WPAFB, Ohio 45433-7605

Final Report for:
Air Force Office of Scientific Research
Summer Research Program

Sponsored by:
Air Force Office of Scientific Research
Wright-Patterson Air Force Base, Dayton, Ohio

EXPERIENCE IN THE METHODOLOGY SECTION AT
WRIGHT-PATTERSON AIR FORCE BASE

Miranda H.T. Tseng
High School Apprentice
Methodology Section
Wright-Patterson Air Force Base

Abstract

In the Survivability Enhancement Branch of the Vehicle Subsystem Division, information was obtained about the survivability and vulnerability of composites through basic research and testing conducted in a gunnery range. Different types of data were collected from the tested composite panel and from associated reports. Accumulated results were put into a data base that contained raw data from previous tests. This data base was then updated and completed. The findings were in turn reduced and analyzed for further use. Plans for future tests to support methodology development were also made. These plans included the determination of data that will be needed to support the thesis of these developmental tests. Besides research settings, a general work atmosphere was observed and the ability to fit into the office environment was gained.

EXPERIENCE IN THE METHODOLOGY SECTION
AT WRIGHT-PATTERSON AIR FORCE BASE

Miranda H. T. Tseng

The vulnerability of aircraft and other military vehicles is important in the survival rate of its operators. The extent of this vulnerability is tested by the Survivability Enhancement Branch of the Vehicle Subsystems Division. This department of the Flight Dynamics Directorate specifically tests composite panels from military vehicles by simulating possible threatening engagements with enemy projectiles. The damage is then evaluated and possible improvements are tried. Throughout this cycle, military armorment is gradually improved.

Tests are run at one of four ranges at Wright-Patterson Air Force Base in Dayton, Ohio. At the range, a gas or black powder gun is set up to fire either missile warhead fragment simulators or armor-piercing incendiary rounds. At the front of the muzzle of the gun, the panel being tested is set up with sensors at the front or back of the it. Possible sensors used are break papers, electromagnetic coils, light screens, and wire triggers. These sensors time the projectile so that impact and residual velocities along with other variables may be calculated. Cameras triggered to open their shutters before the projectile is shot are set up to capture the firing of the round. The cameras can also record any fireballs that ignite when the projectile hits the composite panel. If a fireball starts and is caught on film, it is then classified into five possible categories that describe its incendiary ignition.

Besides fireballs and projectile timing, other data are collected or calculated. Before testing, the impact and residual weights of the panel and projectile are recorded. Details from the panel such as lay-up and material type are also documented. Furthermore, various facts from the test set-up, including obliquity angle and projectile size, are noted. After the panel has been damaged, data are taken off the panel and a C-scan taken off it. From the panel itself, maximum deep delamination is collected along

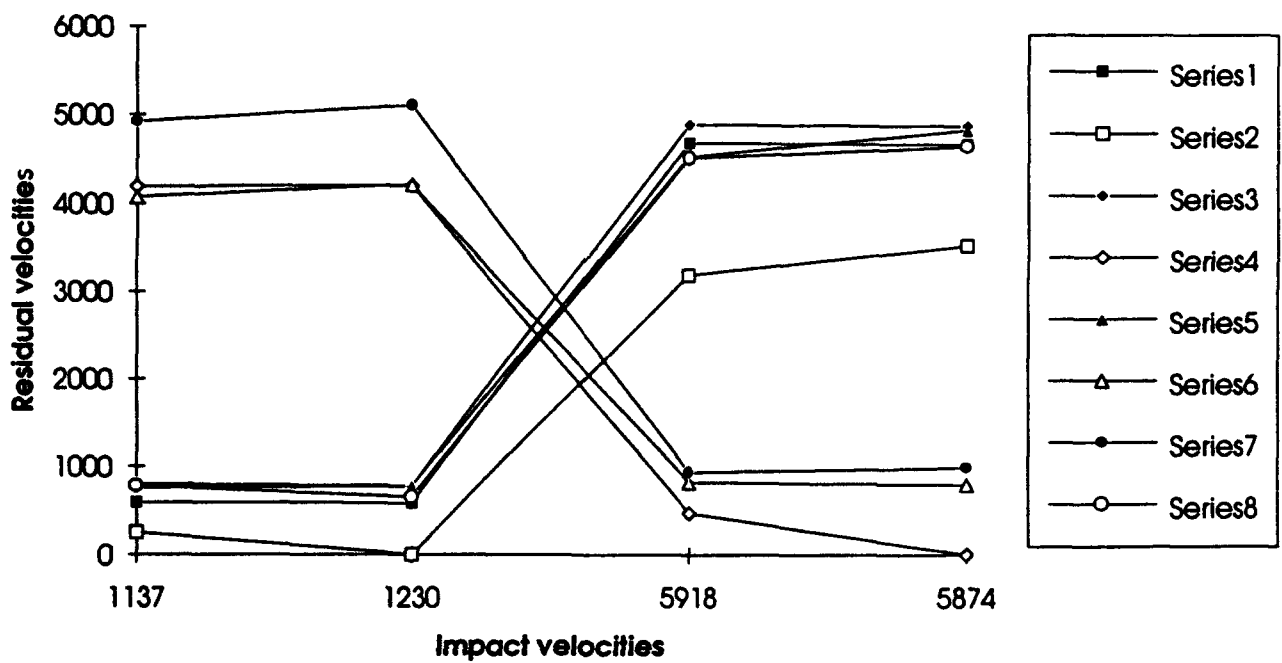
with the distance of the damage along the x- and y-axis. The same information is taken off of the perforation in the panel. From the C-scan, total area is determined in addition to the three things mentioned above. Another type of data is taken from the witness panel, which is set further down the range. It is used to record the amount of yaw the projectile gains. These data are used to determine what the target will do to the projectile. It is also used to predict information relative to a second panel. Plans for a future test to verify these predictions are being made.

After the data are collected, they are either analyzed or used in collaboration with other tests. The purpose of evaluating data is to find relationships between the different variables using graphs. Variables are especially noted when the display of the results show multiple graphs to be identical. This information is used in future tests to see if the same relationships are repeated. If it is, a theory is usually developed. The data are also used for predicting algorithms. When patterns in the data are observed, the data are then used to derive equations to predict the terminal ballistics of the projectile. In turn, the data is then used in vulnerability models to predict the levels of vulnerability of military vehicles.

As the armorment of military vehicles advances, future testing of it must be planned. The planning involves making up a test plan that includes the configuration of the range. Arrangements must also be made for the collection and organization of data. This process involves establishing the type of data needed along with the method in which the data will be collected. Planning also entails signing up for the range and making sure that people are available to work at the test site. These arrangements take variable amounts of time but often become quite tedious and time- consuming.

This apprenticeship gave insight to the testing process from the beginning to the end. A key tool used in the testing process was the personal computer. Wright-Patterson Air Force Base offered many opportunities to learn various computer programs. Throughout the summer, the student mastered programs such as "Excel" and "Harvard Graphics". Proficiency in such programs will help open future opportunities.

Residual Velocities vs Impact Velocities



Experience in the computer system "Silicon Graphics" was also gained. Simple experimentation allowed further knowledge in basic computer use. Knowledge in non-electronic tools was also acquired. Understanding planimeters and calipers will be useful when electronic devices such as calculators and computers are not available. Since comprehension of non-electronic tools is rare, this learning experience was most worthwhile. In addition general observation of the work atmosphere provided experience in fitting into an office environment. Sitting at a desk for a long time was a new experience. A work attitude was also developed since the behavior called for in an office is quite different from the behavior required in school. It was also necessary to learn how to deal with people in person and on the phone. These skills will be a great benefit in any office or job.

This summer job sponsored by Research and Development Laboratories provided many benefits for students interested in jobs heavily based on math and science. By spending time in an engineer's environment, a student can learn a great deal about what an engineer actually does. He or she sees not only the finished product the engineer produces but also all the hard work that goes into generating the result. Advantageous as this job is, a few improvements could be made. The first suggestion is to find a way to standardize the jobs since the work the students do varies greatly. Some have jobs that confine them to desks and computers in a closed room all day while others have hands-on, active positions. Blending the two types of work would give a more realistic demonstration of a permanent job since work generally does not consist of only desk work or laboratory work, but is a combination of both. Patterning the jobs would also give mentors ideas on what the students can do. Since the position is only for a summer, the time should be spent wisely. However much time is wasted when the mentor must discover the interests and talents of the student. If a survey of interest is given along with the application, the mentor may have a better idea of the student's capabilities and be able to create a work plan for the summer.

As this position is reaching an end, the testing procedure begins to repeat its cycle. It will not reiterate merely through a scientist's procedure but through a student's unique learning experience. As stated

before, the high school apprenticeship program sponsored by Research and Development Laboratories was very beneficial. It allowed a student to continue their learning process through the summer. The apprentice not only learned skills useful in college but abilities that can be used throughout the future. This job provided a good transition from the educational environment to the working world.

COLOR NEUTRAL RUGATE FILTERS

Jessica M. Behm

**Final Report for:
AFOSR Summer Research Program
Wright Laboratory**

**Sponsored by:
Air Force Office of Scientific Research
Wright Patterson Air Force Base, Dayton, Oh.**

August 1993

COLOR NEUTRAL RUGATE FILTERS

Jessica M. Behm

ABSTRACT

The description of a transmissive rugate filter designed to reflect a portion of the visible spectrum and yet not appear to have a dominant color. The filter design criteria were chosen so that the filter rejects portions of the visible spectrum from 0.38 to 0.78 microns. Observing a scene through this type of optical filter one perceives it to be color neutral, although it is somewhat darker. The design constraints require a solar light source. The eye bounds the wavelength range over which perceived coloration is affected. For this work the spectral characteristics of both the incident light and the standard human eye determine the spectral tailoring of the reflection bands. Rugate filter design and fabrication technology permits a very wide variety in the number, location, bandwidth, and peak height of all reflection bands. The result is a color neutral rugate filter having reflection bands tailored to provide the human user with maximum color discrimination capability.

COLOR NEUTRAL RUGATE FILTERS

JESSICA M. BEHM

INTRODUCTION

There exists a wealth of research in the field of color science such as documented by textbooks devoted to the topic.^{1,2} A methodology has been developed to calculate the color qualities of a transmissive filter illuminated by a variety of standard sources as viewed by the human eye. This paper presents results obtained from applying this methodology to rugate filter designs. The spectral performance of rugate filters can be tailored by altering the refractive index profile of the filter. The goal is to design color neutral rugate filters through refractive index profile tailoring. It shall proceed from a rugate filter having a single reflection band located in the visible portion of the spectrum. All subsequent rugate filter designs shall maintain the same coating and optical thickness. In addition, the changes to the spectral location and bandwidth of the original reflection band shall be minimized. The following calculations assume that light has a normal angle of incidence for all the rugate filter designs presented.

SINGLE-BAND RUGATE FILTER

This paper shall start with a rugate coating having a simple sine wave refractive index profile deposited onto a glass substrate with a refractive index of 1.52 (Fig. 1a). The five parameters that define this sine wave refractive index profile are:

- n_a (average refractive index) = 2.0
- n_{pv} (peak-to-valley refractive index excursion) = 0.15
- $n_a P$ (period of the sine wave in optical thickness) = 0.22 μm
- q (phase at the substrate in radians) = 0
- N (number of sine wave cycles) = 100.5

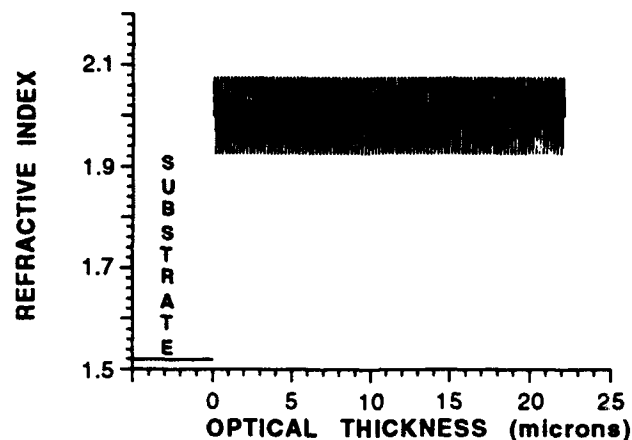


Fig. 1a. Sine wave refractive index profile.

This optical coating has an optical thickness of 22.11 μm which produces a single reflection band in the visible spectrum. The reflection band located at 0.44 μm and has a full width at half maximum (FWHM) bandwidth of approximately 17 nm (Fig. 1b). Note that the spectral performance of this rugate filter is shown over the visible wavelength range, defined to be from 0.38 to 0.78 μm .

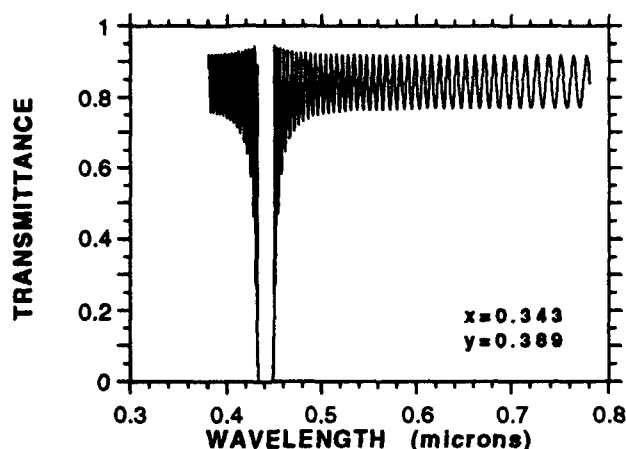


Fig. 1b. Transmittance spectrum having a single reflection band

THE STANDARD SOURCE AND OBSERVER

The Commission International de l'Éclairage (CIE) or International Commission on Illumination recommends standards for describing the source of illumination. Solar light shall be used for the illuminant. Although there are others, one CIE standard source is recommended for general use. This is standard source D₆₅ which simulates average natural daylight (Fig. 2). Therefore, this shall be the only source of illumination modeled in this paper.

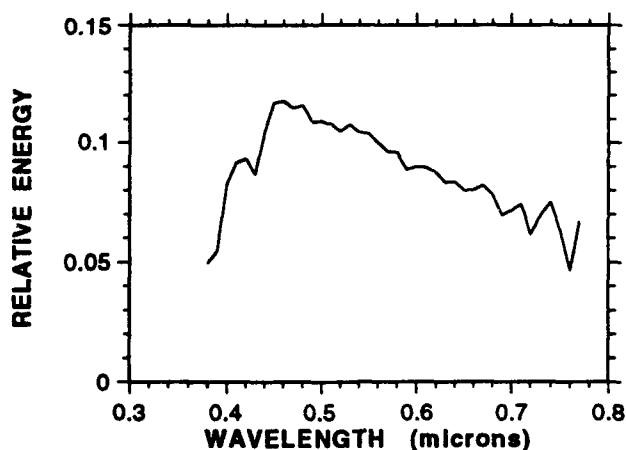


Fig. 2. CIE standard source D₆₅ which simulates average natural daylight

A standard observer having color vision which represents the average human with normal color vision has also been identified by the CIE. It is the intent to use the recommended CIE standard observer rather than attempt to discuss how one arrives at such a standard. However, a simple understanding of the CIE standard observer is useful. The intensities of three narrow bands of red, green and blue light are combined and adjusted to match an adjacent test color. This results in three values (tristimulus values) describing the test color. However, one of the three narrow bands of light may be combined with the test color rather than the other two remaining bands to achieve the match. For this case, the narrow band of light that is combined with the test color has a negative value. However, all negative tristimulus values disappear by performing a mathematical transformation. The resulting positive values are

identified as the CIE color matching functions \bar{x} , \bar{y} , and \bar{z} (Fig. 3). Note that \bar{z} has a non zero value over the 0.38 to 0.55 μm range in wavelength.

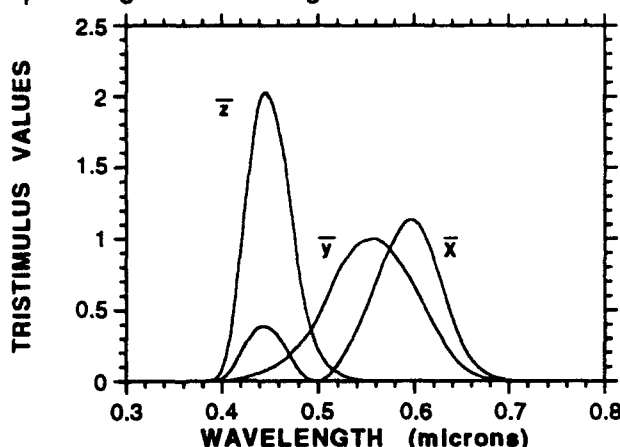


Fig. 3. CIE color matching functions \bar{x} (—), \bar{y} (—), and \bar{z} (—)

A spectrum of color is plotted from the ratio of the three CIE color matching functions to their sum as a function of wavelength. The three resulting values are commonly referred to as chromaticity coordinates x , y , and z and sum to unity. Therefore, it is sufficient to work with any two of the three chromaticity coordinates. Accepted practice results in a plot of the x versus y chromaticity coordinate and are termed a chromaticity diagram (Fig. 4). The spectrum of color as a function of wavelength bounds the chromaticity diagram by the well known horseshoe-shape curve. All real colors are contained within this closed horseshoe-shape curve.

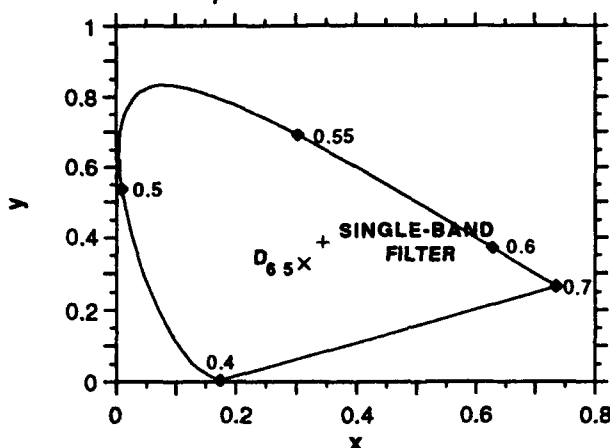


Fig. 4. 1931 chromaticity diagram. Wavelengths in microns are identified along the horseshoe-shaped spectrum. Standard source D_{65} is located at (x) and the filter of Fig. 1 is located at (+).

CIE standard source D_{65} has coordinates of $x = 0.313$ and $y = 0.329$ ($z = 0.358$) on the CIE 1931 chromaticity diagram. The location of this point is denoted by the (x) in Fig. 4. This point on the chromaticity diagram is assumed to be where one perceives no coloration, i.e., the color is neutral. Therefore, an optical filter having chromaticity coordinates matching those of CIE standard source D_{65} is defined to be color neutral.

The method of calculating the chromaticity coordinates (rounded to the nearest thousandth's place) for the optical filters modeled in this paper account for the illuminant, filters, and observer which are the CIE standard source D_{65} , rugate filters, and CIE standard observer respectively. Billmeyer and Saltzman present a clear description and schematic of the methodology for this calculation.² However, simply stated the products of the illuminant, rugate filter, and three CIE color matching functions are divided by their sum from 0.38 to 0.78 μm . The resulting three values are the chromaticity coordinates

for a standard observer viewing light transmitted through the filter. The single reflection band rugate filter described in Fig. 1 has chromaticity coordinates of $x = 0.343$ and $y = 0.389$ ($z = 0.268$) which is located by the cross symbol (+) in Fig. 4. The total throughput of this single band rugate filter is 0.79 over the 0.38 to 0.78 μm wavelength range.

An additional measure of rugate filter performance viewed by the human eye is determined by daytime (photopic) and nighttime (scotopic) vision. A spectral shift in performance to shorter wavelengths occurs between the CIE standard photopic and scotopic observer (Fig. 5). The numeric values for photopic and scotopic vision are the total intensity of light viewed through a rugate filter by the human eye relative to the intensity viewed by the human eye with the rugate filter. The photopic and scotopic values for the single band of Fig. 1 are 0.83 and 0.77 respectively.

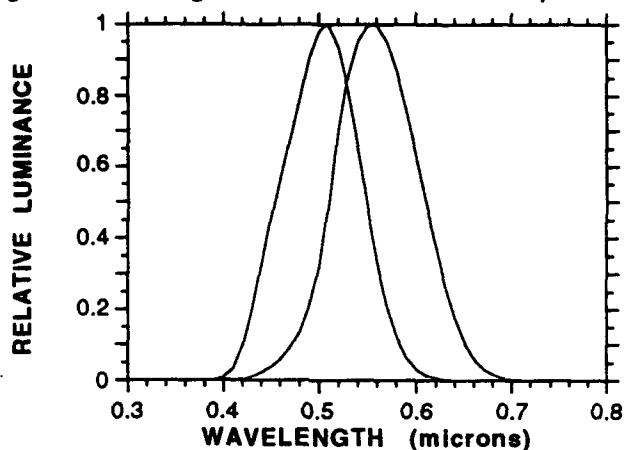


Fig. 5. Luminous efficiency of the eye for photopic (—) and scotopic (--) vision.

THE COLOR NEUTRAL RUGATE FILTER

In order to produce a color neutral rugate filter a second sine wave can be tailored and superimposed to the original sine wave refractive index profile described in Fig. 1a. This second sine wave is defined by $n_{pv} = 0.212$, $n_{ap} = 0.284 \mu\text{m}$, $q = 1.2761... \pi$, and $N = 77.852$ cycles. The optical thickness of the resulting rugate coating is still 22.11 μm (Fig. 6a).

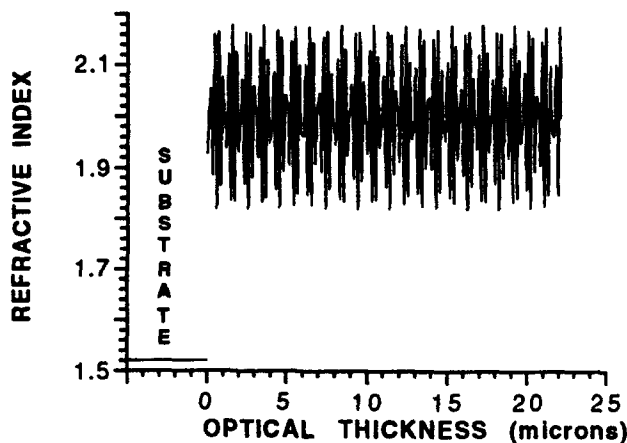


Fig. 6a. Refractive index profile resulting from the superposition of two sine waves.

The presence of this second sine wave yields an additional reflection band having a FWHM bandwidth of approximately 32 nm located at 0.568 μm (Fig. 6b). Note that this reflection band is located in the wavelength region where z is effectively zero. This tailored two band rugate filter has chromaticity coordinates of $x = 0.313$ and $y = 0.329$ ($z = 0.358$). The photopic and scotopic values for this filter are 0.54 and 0.69 respectively. While the total throughput of this filter from 0.38 to 0.78 μm is 0.70.

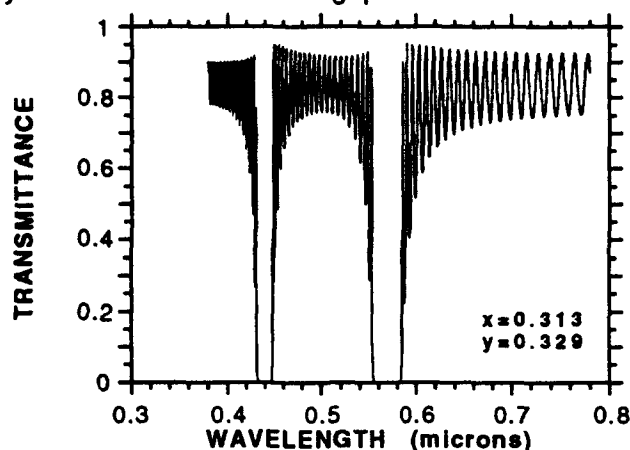


Fig. 6b. Transmittance spectrum of a color neutral rugate filter ($x = 0.313$, $y = 0.329$, and $z = 0.358$) having two reflection bands.

Overall performance of this rugate filter can be improved with the inclusion of refractive index matching at the substrate/coating and coating/air interfaces and refractive index profile apodization. The original refractive index sine wave described in Fig 1 is superimposed with a sine wave defined by $n_{pv} = 0.16$, $n_{aP} = 0.2835 \mu\text{m}$, $q = 1.75 \pi$, and $N = 77.989$ cycles (Fig. 7a).

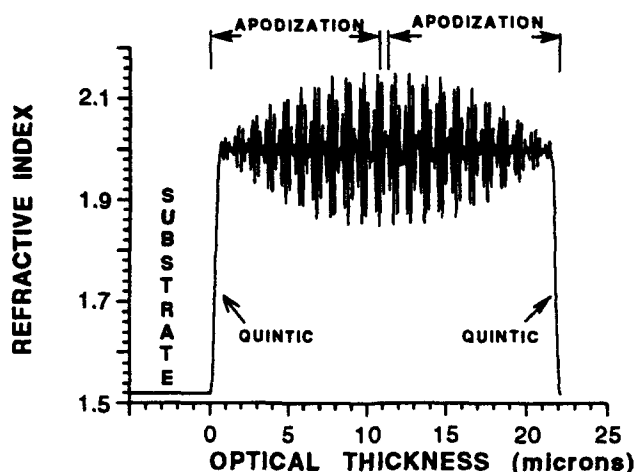


Fig. 7a. Refractive index profile resulting from the superposition of two sine waves which are apodized and index matched at the substrate and air interfaces.

The chromaticity coordinates for this color neutral rugate filter are $x = 0.313$ and $y = 0.329$ ($z = 0.358$). Thereby, resulting in a two band color neutral rugate filter having enhanced throughput (Fig. 7b). The FWHM bandwidth of the reflection band at 0.567 μm is approximately 27 nm. The photopic and scotopic values for this filter are 0.71 and 0.82 with a total throughput of 0.82 over the 0.38 to 0.78 μm wavelength region. Note that this filter has performance values that compare well with the original single band filter except for the photopic vision which suffers from the presence of the reflection band at 0.567 μm .

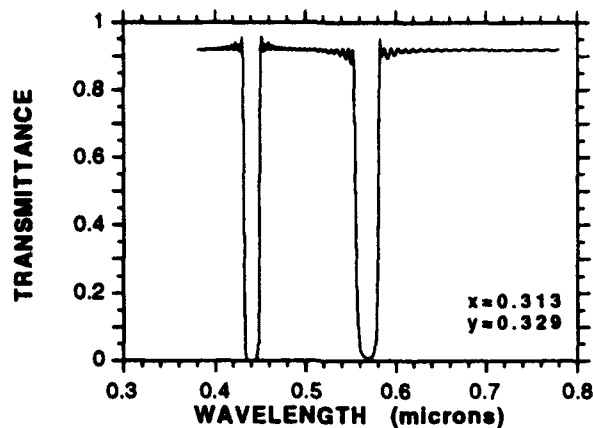


Fig. 7b. Transmittance spectrum of a color neutral rugate filter ($x = 0.313$, $y = 0.329$, and $z = 0.358$) having two reflection bands with enhanced throughput.

There are other designs that can yield results similar to the previous filter design. For example, a sine wave having $n_{pv} = 0.28$, $n_a P = 0.284 \mu\text{m}$, $q = 1.23... \pi$, and $N = 8.5$ cycles can be superpositioned with the original sine wave refractive index profile of Fig. 1a. This filter design also includes refractive index matching and refractive index profile apodization (Fig. 8a). Note from Fig. 8a that this second sine wave starts at the air/coating interface and continues only a short distance into the coating.

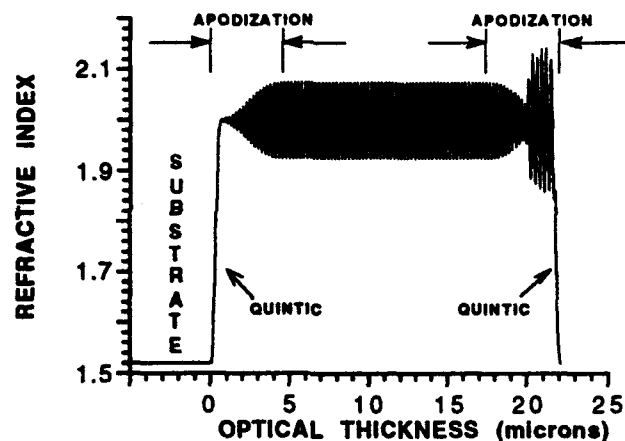


Fig. 8a. Refractive index profile resulting from the superposition of two sine waves (one extending only from $19.7 \mu\text{m}$ to the air interface) which are apodized and index matched at the substrate and air interfaces.

This second sine wave produces a shallow broad reflection band at $0.568 \mu\text{m}$. This band has a transmittance minimum of 0.53 and a FWHM bandwidth of approximately 75 nm (Fig. 8b). However, this filter design transmits light at the wavelengths used in changing chromaticity coordinates. The chromaticity coordinates for this filter are $x = 0.313$ and $y = 0.329$ ($z = 0.358$). The photopic and scotopic values for this filter are 0.71 and 0.78 with a total throughput of 0.82 over the 0.38 to 0.78 μm wavelength range. These three performance values agree with those of the two band filter described in Fig. 7 except for scotopic vision which decreased by 0.04 (i.e., from 0.82 to 0.78).

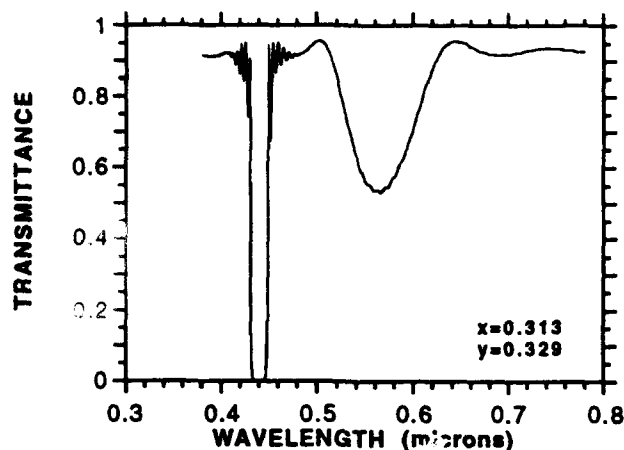


Fig. 8b. Transmittance spectrum of a color neutral rugate filter ($x = 0.313$, $y = 0.329$, and $z = 0.358$) having one deep narrow and one shallow broad reflection band with enhanced throughput.

CONCLUSION

This paper demonstrates that color neutral rugate filters can be designed by refractive index profile tailoring. It assumes a rugate filter having a single reflection band is located at $0.44 \mu\text{m}$, however, this band could of easily have been located anywhere in the visible. This would result in a different starting point on the chromaticity diagram (i.e., different x and y values). Additional refractive index sine waves and profile tailoring the chromaticity coordinates of the resulting filter can be reasonably controlled. More than one rugate filter design can be used for changing the chromaticity coordinates to obtain the location of choice on the chromaticity diagram. This paper assumes that the chromaticity coordinates of CIE standard source D₆₅ is the optimum location in obtaining a color neutral rugate filter. However, this may not be the ultimate desired location. This could be especially true when accounting for the spectral shift to shorter wavelengths exhibited by rugate filters that encounter light having non normal angles of incidence.

REFERENCES

1. G. Wyszecki and W. S. Stiles, Color science concepts and methods, quantitative data and formulas, John Wiley and Sons, New York, 1957.
2. F. W. Billmeyer and M. Saltzman, Principles of color technology, pages 45 and 46, John Wiley and Sons, New York, 1981.

**A STUDY OF METHODS OF DEVELOPING A
CARBON-CARBON STRUCTURAL FOAM**

**Jeremy D. Focht
Beavercreek High School Graduate**

**Final Report for:
AFOSR Summer Research Program
Wright Laboratories
Nonmetallic Structural Materials Branch
Wright Patterson Air Force Base
Beavercreek, Ohio 45432**

**Sponsored by:
Air Force Office of Scientific Research**

August 1993

A STUDY OF METHODS OF DEVELOPING A CARBON-CARBON STRUCTURAL FOAM

Jeremy D. Focht
Beavercreek High School Graduate

Abstract

The formation of a carbon-carbon foam that would possess all the characteristics of a solid composite material was desired in this experiment. A carbon mesophase pitch was used to form the actual carbon-carbon material itself. In order to create the kind of foam desired, two methods were attempted. The first was the mixing of the pitch with a nitrogen-releasing blowing agent. The second was the saturating of the pitch with highly pressurized toluene. Experimental results show that the use of the blowing agent creates foams with cells too big to retain any practical portion of the strength of the composite material itself. Pressurizing the pitch with toluene showed much better results with cell sizes within acceptable limits. However, the foams created by this method were shown to contain closed cell structures, which indicates incomplete penetration of the pitch and consequently, incomplete foaming in certain parts of the sample.

A STUDY OF METHODS OF DEVELOPING A CARBON-CARBON STRUCTURAL FOAM

Jeremy D. Focht

Introduction

In the past ten years, much research has been done in the field of composite materials. This has been because of their much superior strength and much lighter weight than metals and other materials. Recently, carbon-carbon has been researched for use in the aerospace field because of its extremely light weight, superior tensile strength, and its almost nonexistent expansion when exposed to heat. The strength of carbon-carbon composites comes from the alignment of carbon molecules in long strands. The belief is that when a carbon-carbon sample is foamed, the carbon strands will still retain their alignment through the ligaments of the foam created. By retaining this alignment, the strength of the material will be preserved as long as the cell size of the foam remains consistent throughout the sample. The cells cannot be larger than 30 microns to 1 mm in diameter if the strength of the material is to be preserved (the theoretical size varies, depending upon the source consulted). By using a carbon-carbon composite foam instead of a solid composite, weight could be saved without sacrificing the strength of the material which holds much interest with the aerospace field. Also by using a foam, much of the volume taken up by the structure is actually empty space, which will save on the amount of material used to create the composite. Since the materials to create carbon-carbon are still not cheap, this would lead to the saving of money in manufacturing.

Methodology

The first method used to create carbon-carbon foams is the mixing of the carbon-carbon medium with a blowing agent. The foam is created by heating the medium to its softening point. At this point, the blowing agent releases gas through a chemical decomposition reaction and creates multitudes of spherical cells evenly spread out throughout the medium of roughly the same size. By adjusting the ratio of the amount of blowing agent to the amount of medium, the size of the cells can theoretically be controlled. This method relies heavily on the complete mixing of the two media, as well as the even distribution of the blowing agent throughout the entire medium. It also requires a blowing agent

that releases a gas at or slightly below the medium's softening point. Also since this is a carbon-carbon material being foamed, the gas released should not be oxygen. Oxygen gas would immediately oxygen stabilize the medium and make it rigid upon the first exposure to O₂ gas, preventing further expansion in the foam cell structure. Another variable in the formation of the foam using a blowing agent is the duration at the medium's softening temperature. If not enough time is spent at the medium softening point, the blowing agent will not release enough gas to foam the medium to the desired porosity. If too much time is spent at the softening point, large cell structures will be formed that cause the medium to be brittle and weak instead of displaying the desired composite strength.

Another method used in developing a carbon-carbon foam is that of saturating the medium with a highly pressurized liquid. The foam is created by first saturating the medium with this liquid at a high pressure. Then the medium is heated to its softening point, expanding the liquid trapped inside the solid and creating a uniform foam cell structure. The size of the foam cells can be controlled by adjusting the pressure at which the medium is saturated. Again, the duration at the softening point should affect the degree of porosity and size of the foam cells.

Experimental Setup and Procedure

The medium used for methods of producing foam is AR 760 Mesophase Pitch (obtained from Mitsubishi). In the first method, the blowing agent used was EXPANDEX 175™. It releases nitrogen gas at anywhere from 225 °C to 250 °C. The pitch's softening point was 240 °C. The pitch was heated to a liquid state and the blowing agent was added in a 2.5 grams of pitch to 1 gram of blowing agent ratio. The mixture was very thoroughly mixed and then allowed to cool. Samples were then created of approximately 2.5 grams each. Each sample was placed in a programmable ashing furnace and heated in the presence of nitrogen to 240 °C at varying rates of heating from 5 °C per minute to 25 °C per minute. All samples were allowed to cool by letting the heat escape by opening the furnace to the outside environment.

The second method was carried out by placing an approximately 2.5 gram sample of the pure pitch (without blowing agent) in a glass beaker submerged in 80 mL of toluene. This glass beaker was then transferred to a pressure furnace and nitrogen was then pumped into the furnace until the desired pressure was reached. The furnace was kept at room

temperature and at a constant pressure for 24 to 72 hours (depending on the test). The samples were pressurized from 600 psi to 1600 psi (again depending on the test). The sample was then removed from the toluene, weighed (after letting the excess toluene evaporate), and placed in an aluminum foil container to be heated in a programmable ashing furnace. It was heated in the presence of nitrogen gas to prevent oxygen stabilization. The sample was then heated at variable rates (from 5 °C per minute to 50 °C per minute) to 240 °C or 250 °C.

Results

The first method of mixing the pitch with a blowing agent produced foams with a wide range of cell sizes. The cells were far too large to be useful in any sort of structural use (2 mm to 1 cm in diameter). The cell size could be controlled somewhat by the heating rate, but the gas was released too much all at once, no matter how quickly it was heated. The different sizes of cells in the foam were believed to be caused by the blowing agent's concentration being more in one area than the other. This ratio was determined to be impractical. Other ratios of blowing agent to pitch might yield better foams, but the tests are not yet completed. Instead, another method was pursued because of the difficulty of cooling it quickly enough to release only part of the gas in the blowing agent.

The second method yielded much better results. The foams created had cells that were much more uniform in size. The foam cell size was within the practical limits for structural use listed earlier in this paper. It was found that the heating rate of the saturated pitch had little to no effect on the foams. The length of the pressurization also had little effect, as long as it was pressurized for 24 hours (any less was not within the scope of this experiment). The samples pressurized for 72 hours did not show any more weight gain than those pressurized at the same pressure for only 24 hours. However, the pressure at which the pitch was saturated proved to be a control for the size of the cells formed. The greater the pressure, the larger the cells. While the foams made up until now have many of the characteristics desired, they contained some closed cells, which may indicate incomplete saturation of the toluene throughout the pitch. The pitch might be heated to its softening point and then pressurized while it is cooling to saturate it evenly throughout. But all in all, this method seems much more conducive to the manufacture of carbon-carbon foams.

Related Project

The discussion of the foams has been of the size of cells and not the strength or structure. One pursuit at the Wright Laboratories is to understand what structures in foams are strong and what are not. They examine this by plotting the X and Y coordinates of a cross-section of foam, cutting away a thin layer of foam (30 to 40 microns at most), and plotting the next cross-section of foam. In this way, they can place these cross sections on top of one another using a CAD (Computer Aided Design) program and view the ligament structure of the foam at a microscopic level.

One of the problems run across was that the plotting instrument exported only X and Y coordinates. In order to view them on top of one another, a Z coordinate must be assigned to each set of X and Y coordinates. Each layer consists of up to a dozen different shapes and each shape consists of hundreds of X and Y pairs. While the adding of a Z coordinate to each pair could be done by manipulating the file with different word processing and spreadsheet programs, the process took hours to accomplish for just one layer. Once this was accomplished, the data had to be inserted with some code so that the CAD program that they used to view the data could plot them in a three-dimensional layout. In addition, they also wanted to thicken each cross section in order that they could be viewed more clearly. However, this was another process that would take a considerable amount of time.

This was given to me as a process to automate using a computer program. By using THINK Pascal™ as a programming tool. I wrote a computer program to take the X and Y coordinate files from the plotter program and convert them into code that the CAD program could understand. I also enabled each set of data created to give the user an option for the thickness of each layer displayed. This computer program could then process a dozen layers in less than one hour, saving days of human labor. It also will enable them to see the layers more clearly using the thickening option installed with every set of data given to the CAD program.

This took a considerable amount of time to program at the laboratories, and it was my main pursuit while I was there. Hopefully, it will be useful to the research done on many different types of foams at Wright Laboratories.

**AN INTRODUCTION TO BASIC ORGANIC
LABORATORY TECHNIQUES**

**David Ginger
High School Summer Apprentice**

**Final Report for: AFOSR Summer Research Program
Wright Labs, Materials, Polymer Branch**

**Sponsored by:
Air Force Office of Scientific Research**

AN INTRODUCTION TO BASIC ORGANIC LABORATORY TECHNIQUES

David Ginger
High School Summer Apprentice

Abstract

Basic techniques of organic chemistry were studied and applied. Such techniques included vacuum and fractional distillation, purification and recrystallization, thin layer chromatography, column chromatography, and the collection of infrared spectrum. In addition, several reactions were carried out under the direction of M. H. Dotrong.

AN INTRODUCTION TO BASIC ORGANIC LABORATORY TECHNIQUES

David Ginger

Introduction

During the course of the eight week high school summer apprenticeship, basic laboratory techniques of organic chemistry were studied and applied in a variety of situations. Such techniques included vacuum and fractional distillation, purification and recrystallization, thin layer chromatography, column chromatography, and the collection of infrared spectra. The general procedures used are outlined below, sometimes with information regarding specific instances of their application. In addition, several reactions were carried out under the direction of M. H. Dotrong. These too are reported below, along with relevant information regarding the compounds synthesized.

Thin Layer Chromatography (TLC)

Thin layer chromatography (or TLC) is generally used as a quick test to check the purity or identity of a product. It relies on the differential migration of compounds along an adsorbent test strip as they are carried by an eluting solvent. This differential migration is caused by differences in the attractive forces the compounds experience towards the adsorbent layer and the solvent. Compounds which are attracted more to the adsorbent layer, will migrate more slowly than those which are attracted less. Likewise, those which are attracted more towards the eluting solvent will migrate up the TLC test strip faster than those which are not attracted strongly to it. Thus, the selection of the adsorbent layer and the eluting solvent can be important factors in determining the success of the TLC separation. TLC test strips consist of a thin layer of adsorbent (commonly silica gel) backed by a layer of plastic, are commercially available, and are often treated with an ultraviolet dye to make the separated spots more visible. This means that it is probably

more convenient to vary the eluting solvent to enhance a separation rather than to vary the adsorbent layer.

General Procedure: One half of a TLC test strip is marked with a light, horizontal pencil line approximately one centimeter from the bottom of the strip. The compounds to be analyzed are dissolved in a solvent and a small amount of each mixture is placed on the pencil line with a capillary tube, and each spot is then labeled with pencil. The spots should be kept as small as possible in order to enhance resolution. Thus, when creating the spots, it is advantageous to dissolve the compounds in a rapidly evaporating solvent, to keep them from spreading. The TLC strip is then placed in a chamber containing the eluting solvent. The level of the solvent in the chamber should reach just below the line of spots on the test strip. The chamber may be packed with filter paper in order to ensure that the air in the chamber is saturated with solvent. This prevents rapid evaporation of the solvent from the edges of the test strip which could result in uneven solvent migration and a poor separation. The strip should be removed from the chamber before the solvent reaches its top. If the adsorbent layer has been treated with a UV dye, the finished test strip may then be analyzed under a UV light source to make the spots more visible.

Column Chromatography

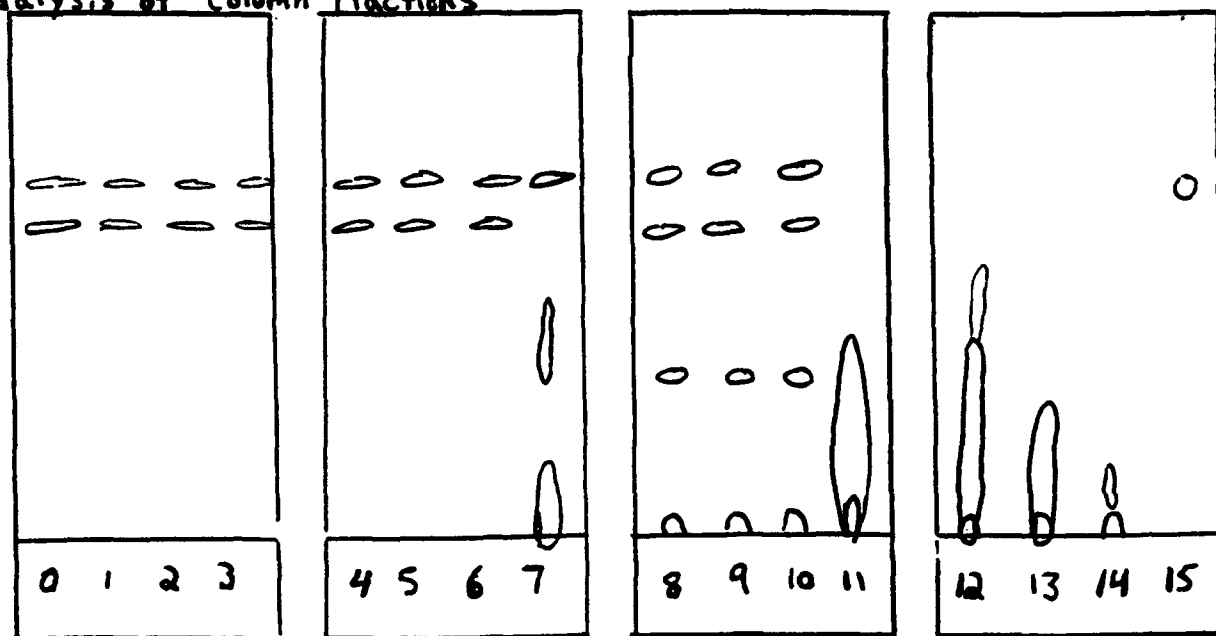
Column chromatography relies on the same principles as thin layer chromatography to achieve a separation, however, in column chromatography, the solvent flows down through a large adsorbent layer rather than up a thin one. Column chromatography is used more for the isolation of a product than for the analysis of one because it is much more time consuming than TLC.

Specific Procedure: Under the direction of M.H. Dotrong, a chromatography column with stopcock was first packed with a small wad of glass wool. The silica gel that was to be packed into the column was then stirred in the solvent (hexanes and acetone, 1:1) to remove air pockets which could disrupt an even flow rate through the column. Two pieces

of filter paper were placed over the glass wool and the silica gel/solvent mixture was poured into the column and allowed to settle. Another piece of filter paper, followed by a layer of sand, was then placed on top of the settled silica gel to form an even surface and the solvent was allowed to run out past the top of the sand. The mixture to be separated was then dripped onto the sand so as not to disturb the even surface. After the mixture layer had dropped below the top of the sand, more solvent was continuously added to elute the compounds. Fractions were collected at 15ml intervals and TLC was used to check the contents of each fraction (see figure 1 below). Like fractions were combined.

Results: Based on the TLC's results, the separation was not wholly successful. Fractions 0-6 included a mixture of starting products, fractions 7-10 included all four compounds, fractions 11-14 contained the desired product and what was likely the product of a side reaction, and fraction 15 contained contamination from the rubber stopper that was used to keep the column from drying out over night.

Figure 1
TLC Analysis of Column Fractions



Recrystallization

Recrystallizations are commonly used to purify a solid product. In a recrystallization, the goal is to completely dissolve the product in a boiling solvent, and then to reform the crystals by allowing the solvent to cool. Colored impurities may be removed by boiling with activated charcoal, and insoluble impurities are removed by hot filtration. It is obviously advantageous to use a solvent in which the impurities are insoluble even at high temperatures, and in which the product is much more soluble at high temperatures than at low temperatures.

General Procedure: The compound to be purified is refluxed in an amount of solvent sufficient to dissolve it completely. If colored impurities are present, a small amount of activated charcoal may be added after the compound has completely dissolved, but not while the solvent is boiling. Note that some product, as well as the colored impurity, will adsorb to the carbon. Hence, charcoaling should only be used when necessary. While the solution is still hot, it should be filtered through folded filter paper. The solution should be allowed to cool to room temperature or below, then filtered again to recover the recrystallized solid, and washed with cold solvent to remove any impurities clinging to the surface of the crystals.

Fractional Distillation Under Vacuum

Fractional distillation separates two or more substances on the basis of boiling point differences. The fractioning column typically contains protrusions along its interior surface, which create a series of levels at which the solution is boiling, thus enabling a more precise separation. Carrying out the distillation under vacuum allows one to boil compounds that would normally oxidize or decompose at temperatures below their boiling points at atmospheric pressure, and also allows the distillation of compounds whose boiling points are so high as to prevent distillation at atmospheric pressure.

General Procedure: The solution is heated by a heating mantle, and stirred with a

magnetic stir bar in a round bottomed flask. The fractioning column is attached to the neck of the flask and a thermometer is inserted in the proper inlet in the column. A multi-flask "cow" adapter is connected to the condenser end of the fractioning column, and appropriate sized round bottomed flasks are connected to the adapter. The water in and out lines, as well as the vacuum line, are then connected to the appropriate nozzles on the column. From the nozzle on the column, the vacuum line is then connected to a 'T' valve, from which one line is connected to a manometer and another line is connected to a trap immersed in liquid nitrogen to prevent solvent vapors from damaging the vacuum pump. A line is then connected from the trap to the vacuum pump itself. The 'T' valve should be turned so as to connect only the manometer and vacuum pump. The vacuum pump should then be activated and the pressure allowed to stabilize. Once the pressure has stabilized, and it has been determined that no significant leaks are present in pump/trap and manometer branches, the 'T' valve may be opened to include the distillation glassware assembly into the vacuum circuit. By this stage, a failure of the pressure to reduce to adequate levels can be traced directly to the glassware setup. Usually, rotating the glass-glass joints to spread the vacuum grease evenly will solve this problem. Once the pressure has equilibrated, the power may be applied to the heating mantle by means of a variable transformer. The "cow" adapter is then rotated so as to collect each fraction in a separate flask.

Results: 3-dodecylthiophene was distilled in the above manner, yielding three fractions. One at 40-41°C (.1mm), the second at 50-52°C (.1mm), and the third at 130-135°C (.1mm). From its known boiling point, the third fraction was determined to be the product.

Infrared Spectroscopy

Infrared spectroscopy provides information regarding the functional groups of an organic molecule. Additionally, by comparison with known spectra, it can be used to confirm the identity of a compound. The characteristic spectra of an organic compound is caused by its absorbance of infrared radiation at energies corresponding to those at which

the bonds in its component functional groups rotate, bend and stretch. The spectrum of each compound is so unique that two samples with identical spectra must, in fact, be the same compound. Two common means for preparing samples for scanning are the KBr pellet method, and the liquid film method. The KBr method is used with solid samples, and the liquid film method is used with either liquid samples, or samples in a solution.

General Procedure, KBr Pellet Method: A small amount of the sample and a larger amount of spectral grade KBr powder are placed in a shaker vial. The vial is then mechanically shaken with a glass bead inside it until a homogeneous mixture is obtained. A small portion of this mixture is transferred to a small hollow cylinder. Steel heads fitted to the interior diameter of the cylinder are positioned on either side of the sample and the sample is distributed evenly between them so as to form a thin disk. The cylinder assembly is then placed into a press at 20,000+ psi for around 30 seconds. The high pressure causes the mixture to fuse into a transparent glassy disk. After the background scan is taken, the sample is placed into the scanning chamber and, after the chamber has been purged with nitrogen to eliminate carbon dioxide which might cause a signal, the spectrum is collected. Afterwards the cylinder and heads should be cleaned.

General Procedure, Liquid Film Method: An amount of the liquid sample just sufficient to completely cover the surface is placed on an KBr plate. A second KBr plate is placed on top of the first, and the two are mounted into a carriage assembly. After a background scan is taken, the assembly is placed into the scanning chamber and, after the chamber has been purged with nitrogen, the spectrum is collected. The plates should be cleaned with methylene chloride or another anhydrous solvent, as KBr is hygroscopic and any absorbed water will interfere with future spectra. Likewise the plates should be stored in a moisture free environment.

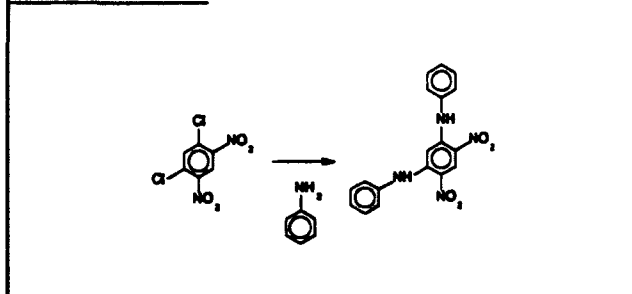
Results: Example spectra are included as relevant information following the reactions discussed below.

Reactions:

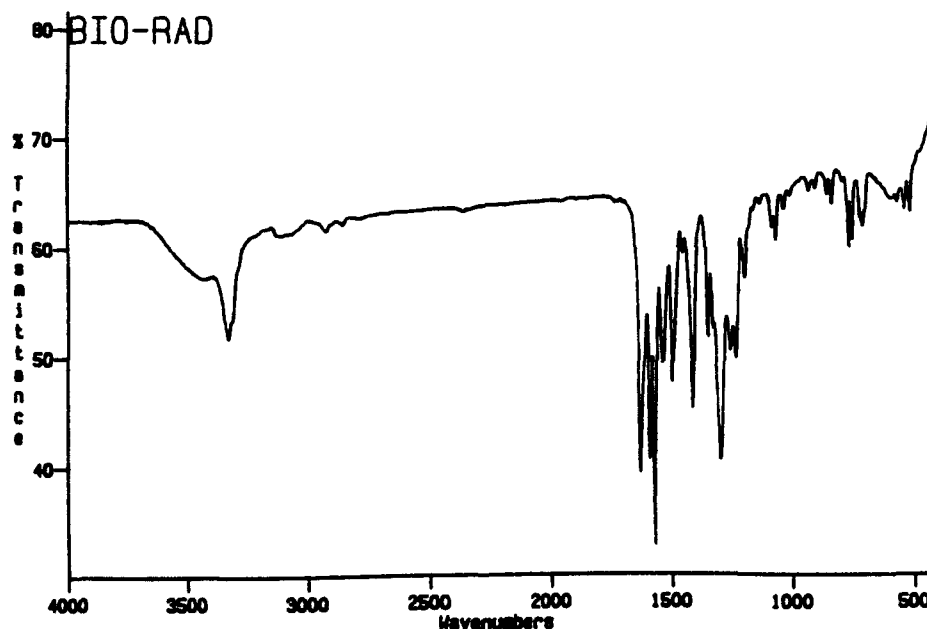
1,5-Diannilino-2,4-dinitrobenzene

Under the direction of M.H. Dotrong, 50g of 1,3-dichloro-4,6-dinitrobenzene and 106ml of fresh distilled aniline were mixed with a magnetic stir bar in a 250ml flask and heated to 140°C in an oil bath for 4 hours. The resulting dark orange mass was mixed with 150ml of ethanol to form a slurry and then dissolved in approximately 700ml of hot ethyl acetate and mixed with an equal volume of hot methanol to precipitate the product. The infrared spectrum may be found below.

Synthesis of 1,5-diannilino-2,4-dinitrobenzene



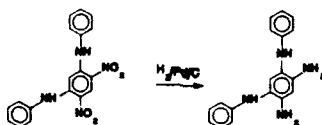
IR Spectrum of 1,5-diannilino-2,4-dinitrobenzene



1,3- Diammino-4,6-diannilobenzene

Under the direction of M. H. Dotrong, 50g of 1,5-diannilo-2,4-dinitrobenzene, 2.5g of palladium on carbon, and 650ml of degassed THF were shaken in a Parr bottle for 20 hours under hydrogen at 55psi. The product was then precipitated with the addition of 1000ml of hexanes. The solid was collected, dried under nitrogen and recrystallized from benzene. The melting point was not determined because the compound decomposes before melting.

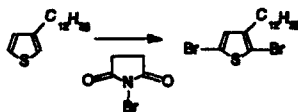
Synthesis of 1,3-diammino-4,6-diannilobenzene



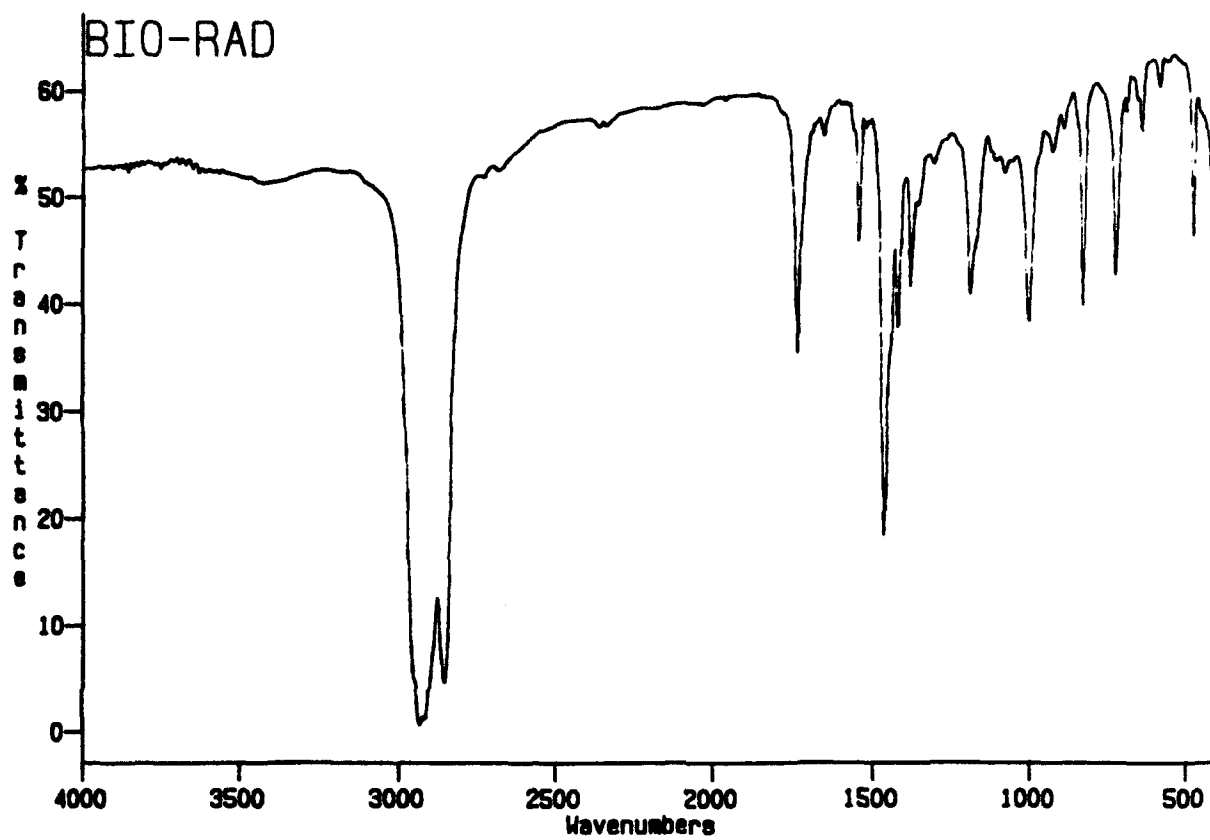
2,5-Dibromo-3-dodecylthiophene

Under the direction of M.H. Dotrong, 30.20g of 3-dodecylthiophene were stirred in 200ml of DMF at room temperature. A solution of 42.72g of NBS in 250ml of DMF were dropped slowly into the mixture in the absence of light. The mixture was then stirred for 3 hours at 40°C. After checking the clear, yellow product with the GC to determine if the starting material had completely reacted, the mixture was poured onto ice. It was then extracted with approximately 1000ml of diethyl ether, washed with water, dried over sodium sulfate and distilled twice at 170-173°C at .1mm pressure. The infrared spectrum may be found below.

Synthesis of 2,5-dibromo-3-dodecylthiophene



IR Spectrum of 2,5-dibromo-3-dodecylthiophene



**ELECTRICAL ANALYSIS OF $\text{YBa}_2\text{Cu}_3\text{O}_{7-x}$ SUPERCONDUCTING
THIN FILMS AND BULK SAMPLES**

Peter G. Kozlowski

**Centerville High School
500 East Franklin Street
Centerville, Ohio**

**Final Report for :
AFOSR Summer Research Program
Materials Directorate
Wright Laboratory
Wright Patterson Air Force Base, Ohio**

**Sponsored by :
Air Force Office of Scientific Research
Boiling Air Force Base, Washington, D.C.**

August 1993

ELECTRICAL ANALYSIS OF $\text{YBa}_2\text{Cu}_3\text{O}_{7-x}$ SUPERCONDUCTING THIN FILMS AND BULK SAMPLES

Peter G. Kozlowski
Centerville High School

Abstract

High temperature superconducting thin films and bulk samples of the Y-Ba-Cu-O system were studied in order to characterize their electrical properties. The preparation of high critical temperature $\text{YBa}_2\text{Cu}_3\text{O}_{7-x}$ films on single crystalline SrTiO_3 and Al_2O_3 was done by laser ablation. In all cases, c-axis oriented films with critical temperature of about 90 K were obtained. On patterned films we obtained a critical current density of 10^6 A/cm^2 . Bulk samples, having a much larger cross-sectional area, exhibit lower critical current densities, approximately 10^3 A/cm^2 . Both thin films and bulk samples were measured by a four point technique and were tested through a range of temperature from 77 K (liquid nitrogen) to 300 K (room temperature).

ELECTRICAL ANALYSIS OF $\text{YBa}_2\text{Cu}_3\text{O}_{7-x}$ SUPERCONDUCTING THIN FILMS AND BULK SAMPLES

Peter G. Kozlowski

INTRODUCTION

The electrical resistance of high temperature superconducting materials falls to zero when they are cooled to temperatures below critical which are still above the temperature of liquid nitrogen (77 K). This makes the superconductive transport properties of high critical temperature superconductors an important aspect for future applications. The electrical properties of these materials in both bulk and thin film form were measured by using a four-point technique capable of measuring very low values of resistance. The properties which were measured include the normal state resistivity as a function of temperature, the temperature at which the transition to superconductive properties occurs (critical temperature), and the maximum current (critical current) which can be carried by the material in the superconducting state before the material begins to show resistance.

METHODOLOGY

Superconducting thin films were grown on SrTiO_3 substrates by using an ArF excimer laser operating at a wavelength of 193 nanometers, pulse duration of 15 nanoseconds, and a repetition rate of 20 Hertz. The focussed laser beam was rastered across a rotating, stoichiometric $\text{YBa}_2\text{Cu}_3\text{O}_{7-x}$ target with an energy density at the target of approximately 1.5 J/cm^2 . The surface of the target was cleaned, prior to film growth, by ablating the target in situ for 5 minutes with excimer radiation. The target to substrate distance was 6 centimeters [1].

The single crystal SrTiO_3 substrates were cleaned by rinsing in trichloroethylene, acetone, and methanol, after which they were subjected to a 30 minute ultraviolet-ozone treatment. After being loaded into the growth chamber, the substrates were heated to approximately 850°C in O_2 (100 mTorr) for 30 minutes. Film growth was carried out at approximately 750°C in O_2 (100 mTorr) and required 30 minutes [2]. The deposition rate was typically 0.4 nm/s , and the resultant film thickness ranged from 0.6 to $0.9 \text{ }\mu\text{m}$, as measured with a stylus profilometer. Immediately after deposition, the growth chamber was backfilled with O_2 to a final pressure of 1 atmosphere. The resulting films were superconducting as grown and were wet-chemically patterned into a 4-probe structure which allows measurements of resistivity (ρ) and critical current densities (J_c). Then, four gold wires were attached to the sample with silver paint and it was annealed for 1 hour

at 400°C. The transport properties were then measured by this 4-point technique with the current leads and voltage leads being attached to the thin film as shown in Figure 1.

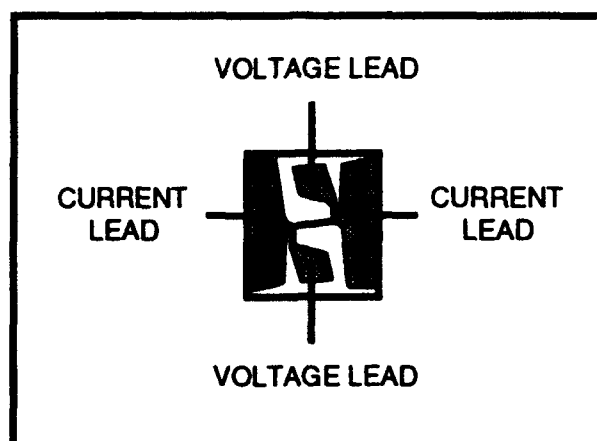


Figure 1. Schematic layout of a thin film prepared for transport measurements.

Bulk samples made of yttrium barium copper oxide were first prepared in a tube furnace under flowing oxygen. This procedure varies according to how long the sample is treated and at what temperature. The particular samples that we measured were made of 1-2-3 ($\text{YBa}_2\text{Cu}_3\text{O}_{7-x}$) + 5 weight percent of $\text{Y}_2\text{BaCuO}_{7-x}$ (2-1-1), and silver. The pelletized sample underwent a melt-process procedure consisting of many steps at different parameters. First, the sample was heated to 1055°C and remained at this temperature for approximately 30 minutes. Second, the temperature was lowered to 1015°C and remained there for 20 minutes. Then at the rate of 2°C/hr, temperature was rapidly lowered to 960°C. Finally, at a rate of 240°C/hr the temperature was ramped to room temperature. Annealing of sample took place for two days at 450°C under flowing oxygen. The pellet was then cut into a rectangular small bar using a diamond saw. On average, a bulk sample has the dimensions of approximately 5 mm (length) by 2 mm (width) by 1 mm (thickness). The four leads attached to the bulk sample may have different configurations as shown in Figure 2.

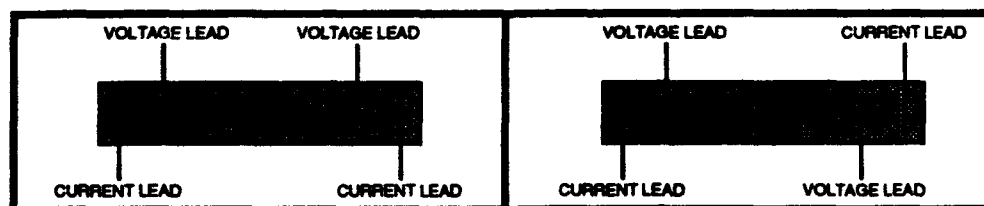


Figure 2. Schematic layout of bulk sample prepared for transport measurements.

The transport measurements were carried out by using the four probe technique on both the bulk samples and thin films. In both cases, a voltmeter showed the readings between the two voltage leads and a current source of 10 mA was applied across the superconductor with an ammeter which took readings through the current leads. A thin film connected in this way is shown in Figure 3.

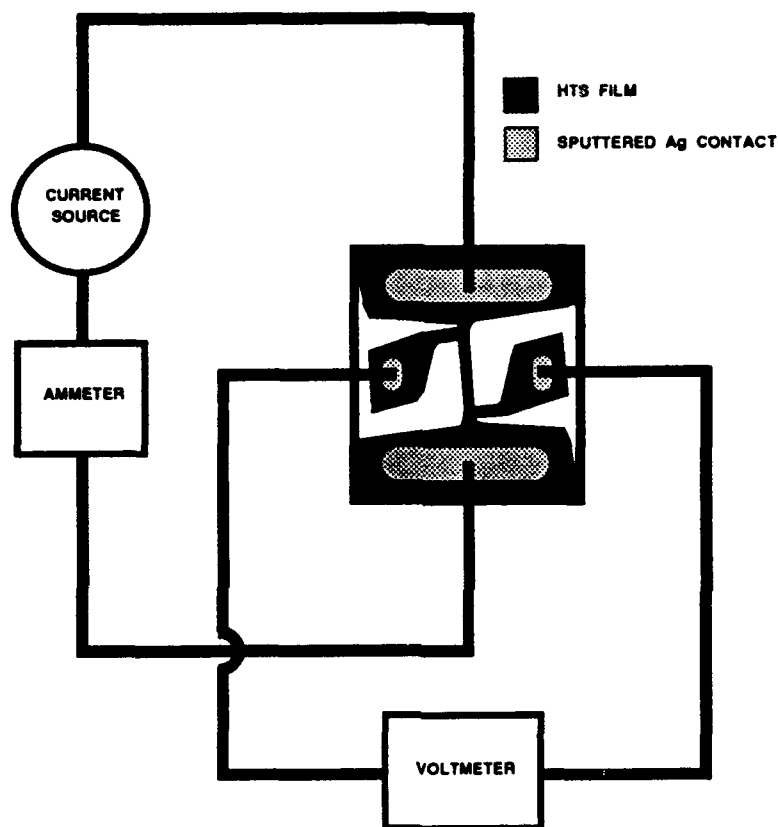


Figure 3. Four-probe technique for transport measurements.

This four wire measurement technique is capable of measuring very low values of resistance [3]. All experiments are completely automated with computer control to set the sample temperature, set the sample current, and collect all current and voltage readings. The properties which are measured include the normal state resistivity, the critical temperature, and the critical current density.

RESULTS

The normal state resistivity were measured as a function of temperature from room temperature down to the temperature at which the transition to superconductive behavior occurs

(the critical temperature). High-quality $\text{YBa}_2\text{Cu}_3\text{O}_{7-x}$ thin films grown in-house by pulsed laser ablation with transition widths of about 1 K have been measured. The resistivity curve (Figure 4) of one of the measured samples shows a critical temperature of 90 K.

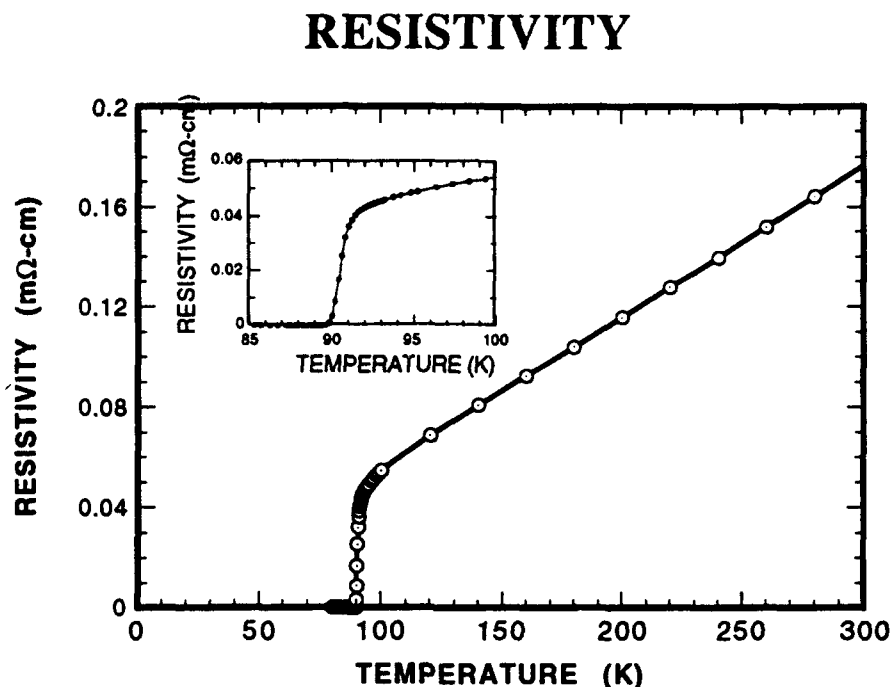


Figure 4. Resistivity versus temperature dependence.

To calculate the resistivity of a thin film or bulk sample, the formula :

$$\text{Resistivity} = \frac{R \cdot A}{l}$$

was used where R is the resistance of the sample in $\text{m}\Omega$, A is the cross-sectional area, and l is the distance between the voltage leads [4]. Again, the resistivity curve is used for indicating the critical temperature of the sample.

The voltage as a function of current was measured at different temperatures to determine the maximum current (the critical current) which can be carried by the material in the superconductivity state before the material begins to show resistance. High quality thin films grown in-house have critical current densities of $5 \cdot 10^6 \text{ A/cm}^2$ at 77 K (Figure 5) shows a typical voltage versus current graph of a sample. Keeping the temperature constant at 20 K, 40 K, 60 K, 70 K, 77 K, 85 K, and

89.5 K, the current value is increased and voltage is measured. In superconducting state, the material has no voltage and thus explains the primary superconducting principle that the material's resistance also equals zero. According to Ohm's Law, $V=IR$ and thus $R=V/I$. When different current values are run through the sample at and below its critical temperature, the voltage is zero. And so, mathematically, when voltage equals zero in the equation $R=V/I$ ($I>0$), any value of current will give a resistance of zero [5]. At temperatures above the critical temperature, the voltage becomes greater than zero and thus the material has resistance.

CRITICAL CURRENT DENSITY (J_c)

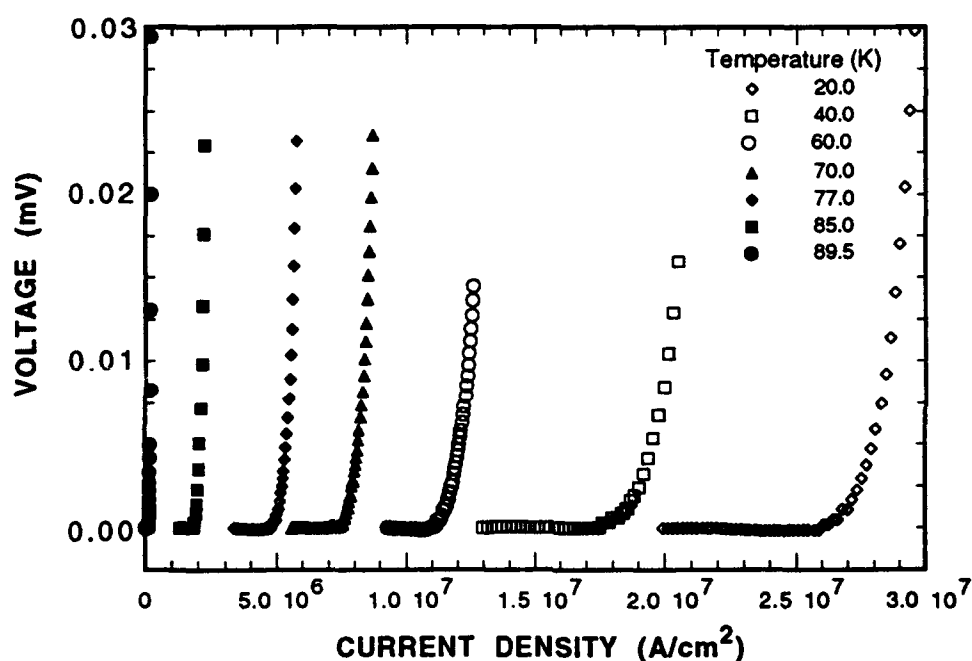


Figure 5. Voltage versus current density.

The critical current density of a sample is calculated as follows :

$$\text{Critical Current Density} = \frac{I_c}{A}$$

where I_c is the critical current and A is the cross-sectional area of the sample.

Two other methods were used to determine the quality of the films. One is x-ray diffraction which is used to determine the crystallographic orientation of the films. No phases other than the $\text{YBa}_2\text{Cu}_3\text{O}_{7-x}$ were observed in any of the films. The x-ray data for the films with high critical current densities show strong peaks of reflections indicating a preferential orientation of the c-axis

perpendicular to the surface of the film. Another method used was scanning electron microscopy which was used to examine the film surface microstructure. Films with high critical current densities have relatively smooth and continuous surfaces with no visible granular features. They also contain surface features which appear to be inclusions about 1 μ m in diameter. Further investigations of these surface features and methods of avoiding their formation are in progress.

CONCLUSION

The expanding field of superconductivity has accomplished numerous successes since the first high temperature ceramic superconductor was discovered and developed by Miller. Currently, more and more pressure is placed upon the study of the properties of superconductors in order to learn how they differ and compare to ones made earlier and to be able to apply them to technological uses which will certainly benefit society in the years to come. The WL/MLPO laboratory has expanded into one of the leaders in the field of superconductivity and has by far had some of the best results in its research.

In conclusion, the thin film and bulk sample superconductors produced here at Wright-Patterson Air Force Base have excellent transport properties with an enormous potential for future applications.

REFERENCES

- [1] D.W. Chung, I. Maartense, T.L. Peterson, P.M. Hemenger, J. Appl. Phys. **68**, 3772 (1990).
- [2] I. Bransky, J. Bransky, I. Maartense, T.L. Peterson, J. Appl. Phys. **66**, 5510 (1989).
- [3] H. Adrian, C. Tome-Rosa, G. Jacob, A Walkenhorst, M. Maul, M. Paulson, M. Schmitt, P. Przyslupski, G. Adrian, M. Huth, T. Becherer, Supercond. Sci. Technol. **4**, 166 (1991).
- [4] G. Adrian, W. Wilkens, H. Adrian, M. Maul, Supercon. Sci. Technol. **4**, 169 (1991).
- [5] G. Deutscher, K.A. Muller, Phys. Rev. Lett. **59**, 1745 (1987).

**A STUDY OF THE MINIMUM DEVIATION METHOD
FOR REFRACTIVE INDEX MEASUREMENTS**

**Sandra R. McPherson
High School Apprentice
Bishop Brossart High School**

**Final Report for:
Summer Research Program
Wright Laboratory, Materials Directorate (WL/MLPO)**

**Sponsored by:
Air Force Office of Scientific Research
Bolling Air Force Base, Washington, D.C.**

August 1993

A STUDY OF THE MINIMUM DEVIATION METHOD FOR REFRACTIVE INDEX MEASUREMENTS

Sandra R. McPherson
High School Apprentice
Bishop Brossart High School

Abstract

The index of refraction, which is a measure of how light travels through a substance, is a basic characterization done by scientists after a new material is created. We discuss three types of crystalline material and how to measure each one's refractive index. A spectrometer is used to record the data and we discuss how the data is taken and analyzed. Indices at several wavelengths need to be done because of dispersion. Five runs are done on each prism and a standard deviation (STD) is calculated on the computer. Quartz was used as a practice sample until our STD was below 10^{-3} . When that was accomplished new materials from Crystal Associates, RTA and KTP:Na were measured. The data taken proved to be accurate enough for us and the index measurements were sent to Crystal Associates to be used.

A STUDY OF THE MINIMUM DEVIATION METHOD FOR REFRACTIVE INDEX MEASUREMENTS

Sandra R. McPherson

Introduction

Index of refraction is one of the basic characterizations for all types of materials. In fact, as new materials are developed, one of the first characterizations performed is the index of refraction. The index defines how fast light travels through the material and the 'bend' (refraction) the light incurs upon passing from a material of one index to a second material with a different index. The Materials Directorate here at Wright-Patterson Air Force Base is in the business of creating new materials to meet the Air Force's needs. In the Electronic and Optical Materials Branch, Nonlinear Optics group, new crystalline materials are developed on a daily basis and knowing the index is very important. In the lab is an experiment that allows us to measure the index on a prism-shaped sample of the material to be tested.

Discussion

To discuss the orientation of the material, we first point out that there are three different types of crystalline material we can study: isotropic, bi-axial and uniaxial¹. Isotropic materials are the simplest type of crystalline materials. In every direction inside the crystal, the index is the same. One prism is cut in any orientation and the index is measured with unpolarized light. (If we think of light as a bunch of arrows, all in different directions, coming out of the light source as follows, this is unpolarized light, as seen in FIGURE 1.)

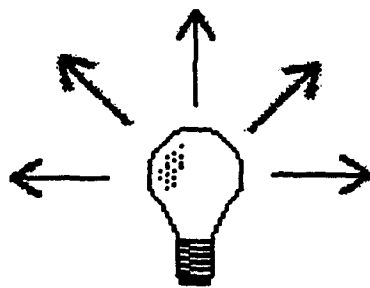


FIGURE 1
Light source representing unpolarized light

Uniaxial materials have two indices of refraction. To measure both the indices, we have a prism of the material made like this with axes as seen in FIGURE 2.

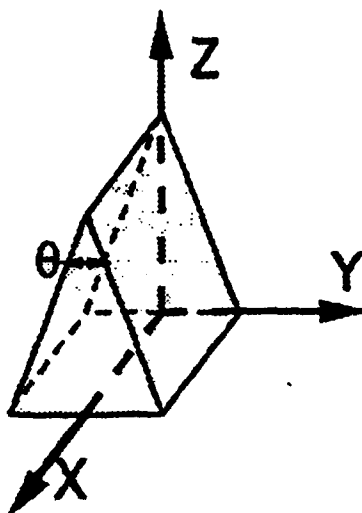


FIGURE 2
3D drawing showing prism axes

In this way, if we can use light polarized in the vertical direction, we can get one index and if we use light polarized horizontally, we can get the second index. (From the definition of unpolarized light, if we now take that same light source and place a polarized sheet in front of it, the arrows come out all pointing in one direction as FIGURE 3 depicts.)

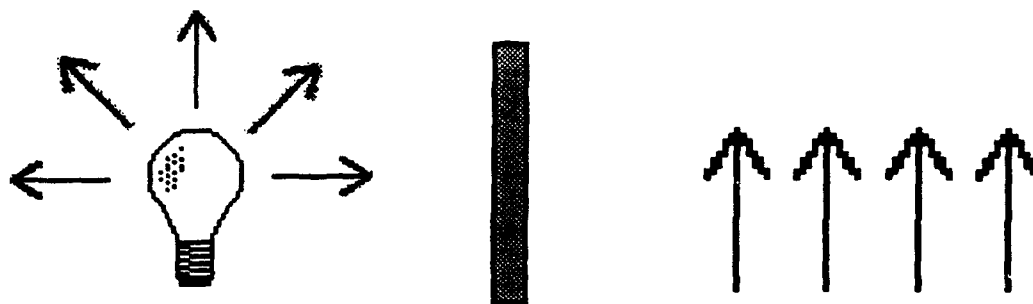


FIGURE 3

Light source and polarizer showing polarized light (in this case vertical)

The third type of crystalline material is called bi-axial. This material has three indices of refraction. We use basically the same procedure for recording index on this material, however since there are three indices, we require two prisms of the material cut as shown in FIGURE 4.

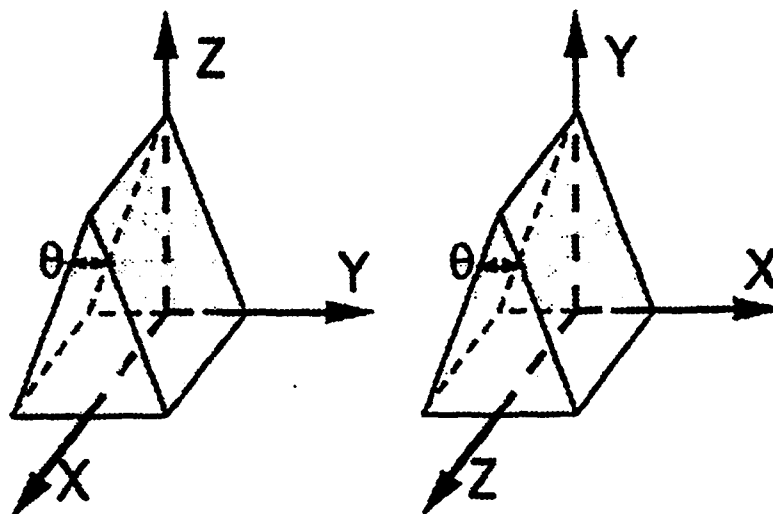


FIGURE 4

3D drawing showing prism axes for bi-axial materials

Once again, using polarized light gives us all three indices. As is evident, one of the axis will be repeated, however it will give us a check on the other measured values so it is worthwhile doing.

Having determined the type of material and how the samples should be cut, we can then determine the index of refraction. The following derivation proves how we calculate the index from experimental data²:

Theta (θ) is the angle the input beam makes with the perpendicular to the prism face and phi (ϕ) is the prism angle. The incident light is refracted inside the prism (shown here as a horizontal line) and then again upon exiting the prism. If we draw a line that cuts the prism angle and is perpendicular to the refracted beam inside the prism, the angle that line makes with the prism face is called alpha (α). Using the fact that the sum of the three angles of a triangle equals 180° , we can solve for α as follows in FIGURE 5.

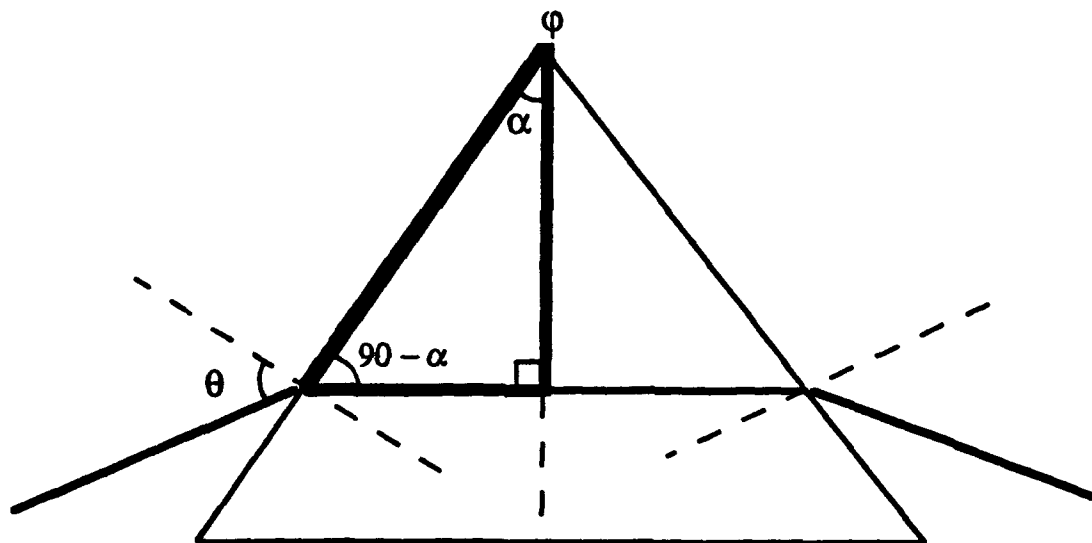


FIGURE 5
Derivation for α

By symmetry

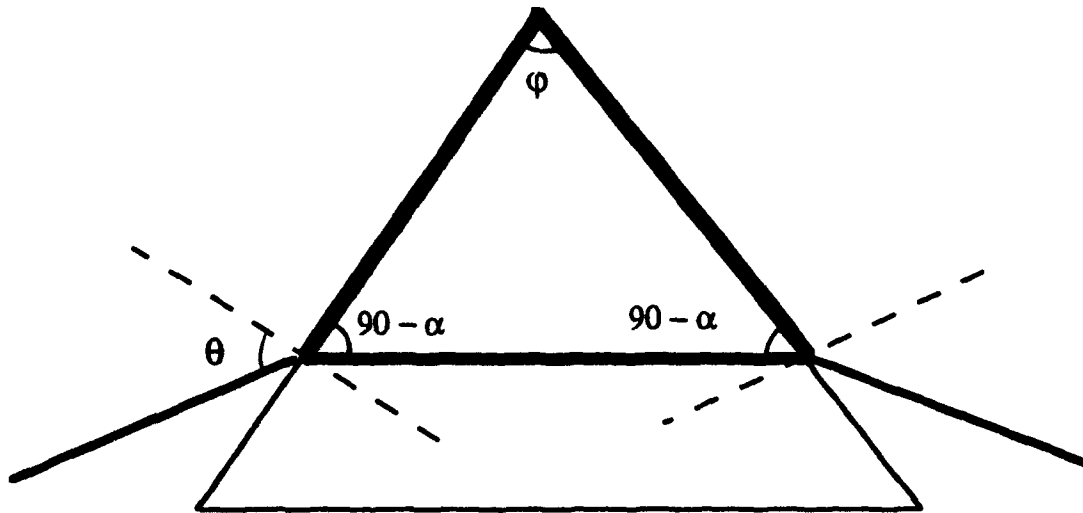


FIGURE 6
Derivation for α continued

Again, using the fact that the sum of the three angles of a triangle is 180° , we can write

$$(90^\circ - \alpha) + (90^\circ - \alpha) + \phi = 180^\circ$$

Solving for α

$$\alpha = \phi/2$$

Now, if we look at a close-up of the prism face at the input ray (FIGURE 7), we want to solve for the angle between the rays before and after refraction. We use the fact that opposite angles made by two intersecting lines are equal, and the fact that if we have a right angle (90°) and we know the value of part of it as x° , the other section is $90^\circ - x^\circ$ (same procedure is used for 180°).

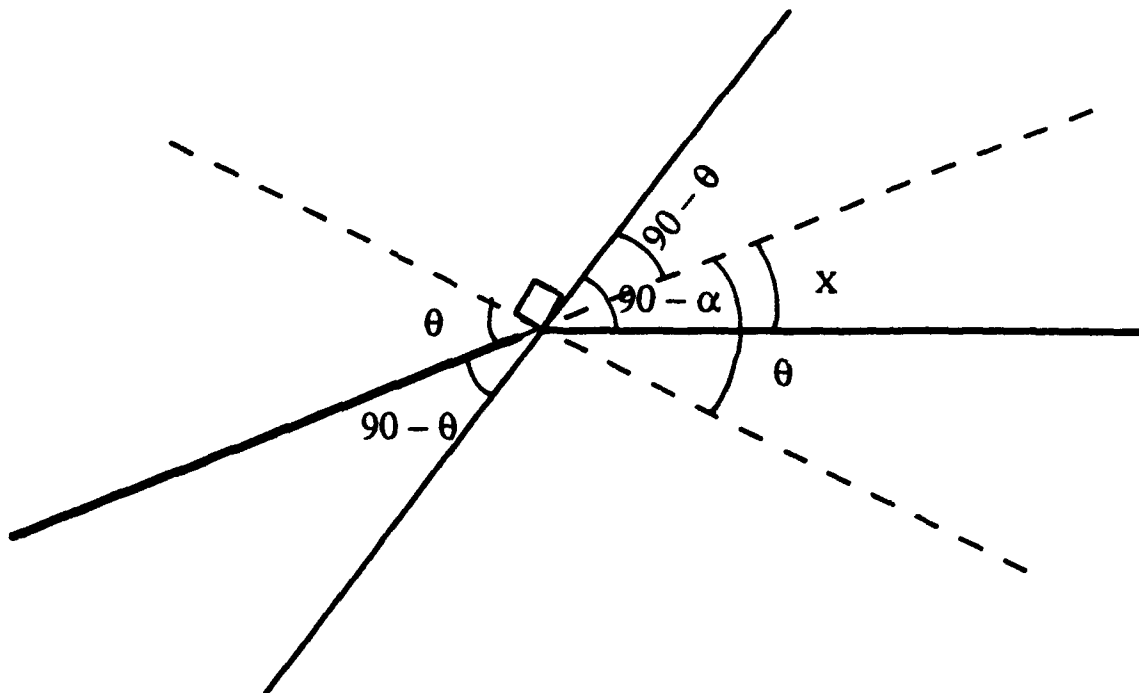


FIGURE 7
Derivation for x

$$(90^\circ - \alpha) - (90^\circ - \theta) = x$$

Solving for x

$$x = \theta - \alpha$$

Next, we sum the angles of the following triangle to solve for θ using FIGURE 8.

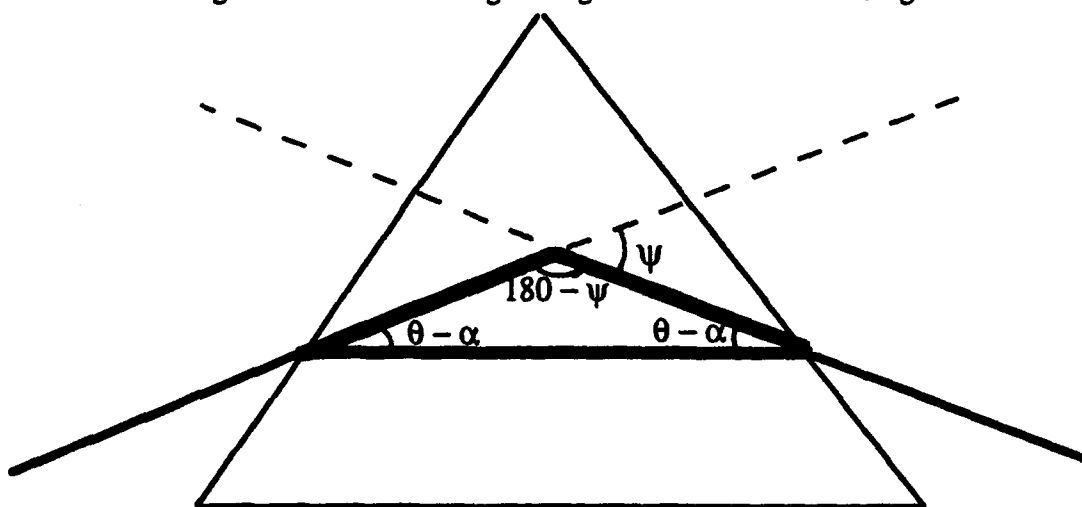


FIGURE 8
Derivation for θ

$$(\theta - \alpha) + (\theta - \alpha) + (180^\circ - \psi) = 180^\circ$$

Solving for θ

$$\theta = \frac{\varphi + \psi}{2}$$

Finally, we have the information we need to solve for the index using a Physics equation called Snell's Law². Snell's Law relates the angles inside and outside any boundary with different indices on each side:

$$n_1 \sin(\theta_1) = n_2 \sin(\theta_2)$$

Where the subscripts mean on each side of the boundary. In this case, '1' means air and '2' means prism. Therefore, knowing the index of air to be 1.0, θ_1 in this case is θ , n_2 is n and θ_2 is α and we can write

$$\sin\left[\frac{1}{2}(\psi + \varphi)\right] = n \sin\left(\frac{1}{2}\varphi\right)$$

or

$$n = \frac{\sin\left[\frac{1}{2}(\psi + \varphi)\right]}{\sin\left(\frac{1}{2}\varphi\right)}$$

This is the formula that will be used by the *Mathematica* program to calculate the index from the recorded data.

Methodology

We measure the index of refraction by minimum deviation method with a Gaertner L124 spectrometer. An Oriel Hg-Xe high intensity white light is used as a source of light and it is directed through a Digikrom 240 monochromator to separate the colors using a diffraction grating. A polarizer is placed at the output of the monochromator. All wavelengths in the visible spectrum can be used, and near

infrared (NIR) measurements are possible with an Electrophysics handheld electroviewer which converts NIR radiation to a visible image. A specific wavelength enters the collimator which spreads out the input light so it is larger than the sample. The sample, cut into the shape of a prism so that light can pass through it and be refracted, is sitting on a table that swivels at the base to allow it to move and has an adjustable height. The light is incident of one face of the prism and is refracted out the other face.

On the other side of the prism table is a telescope used to focus the light coming out of the prism. At the end of the telescope is an eyepiece that we look through to see the light. The prism table is then slowly twisted toward the inside until the light reverses its direction. This is the called minimum deviation and is shown in FIGURE 9.

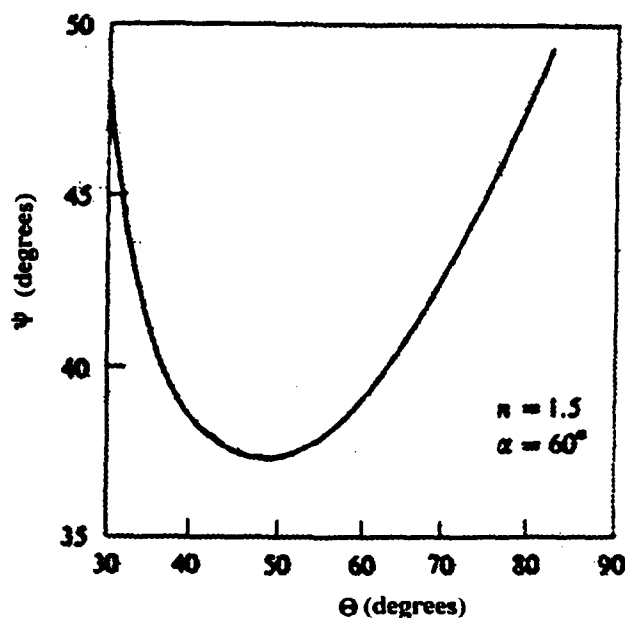


FIGURE 9
Minimum deviation angle versus input angle
for a prism of index 1.5 and angle of 60°

FIGURE 9 depicts deviation (in our case ϕ) versus incident angle (α). The angle will go no smaller once it has reached the bottom of the plot. This is the point where the light has reached it furthest inside position, as it was described earlier.

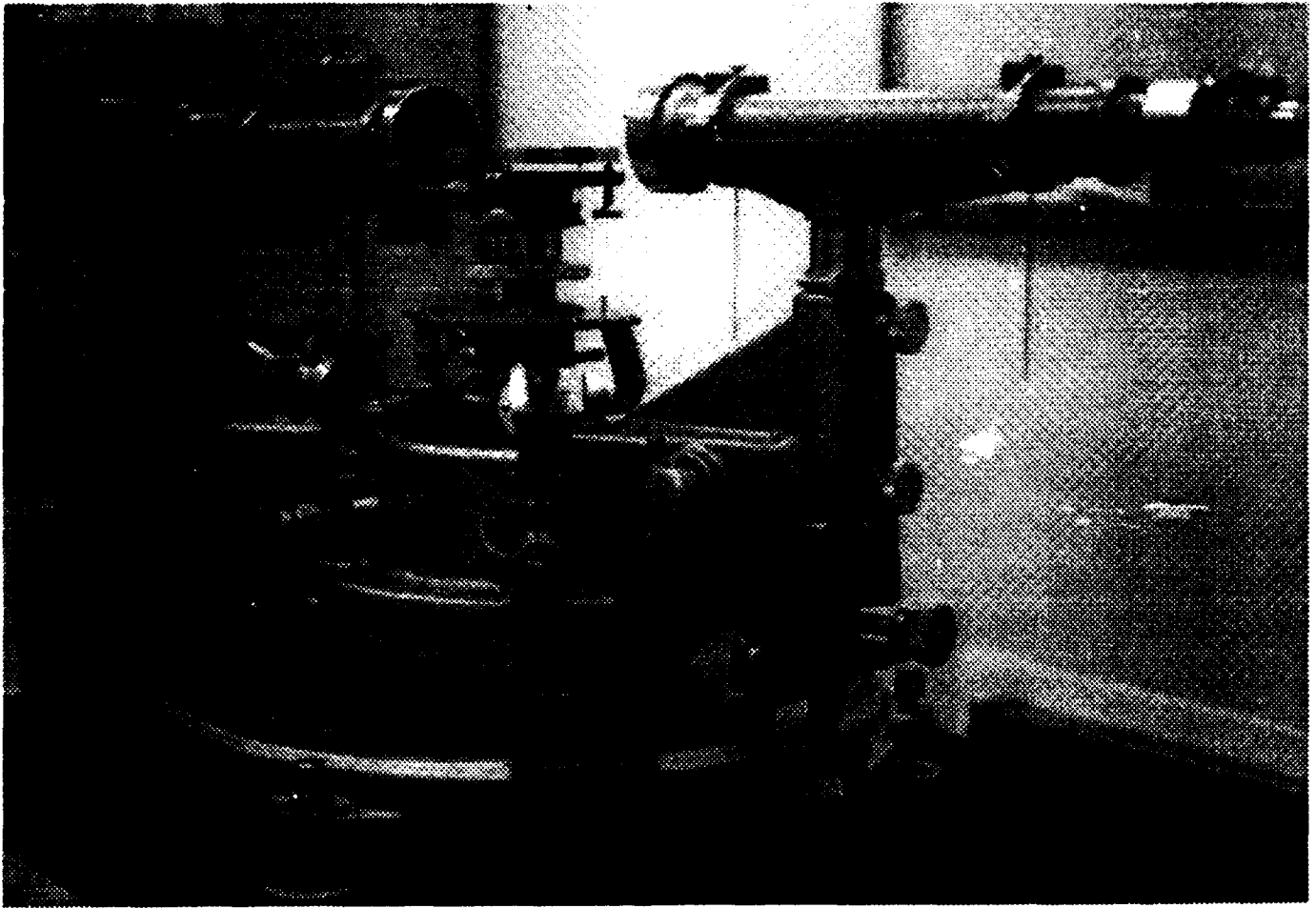


FIGURE 10
Gaertner L124 spectrometer

FIGURE 10 is the spectrometer used in this study to measure index using minimum deviation. To the right is the telescope with the eyepiece. The flat platform in the middle is the moveable prism table. To the right of the prism table is the collimator. The black box on the far left is the monochromator. Two of the

microscopes used to measure the angle as described below are seen, one below the collimator, and the other to the left of the telescope.

To record data, the prism table is left at the point where the light is at its furthest position to the inside and the telescope is locked into place. It is important that the table be left at the point of minimum deviation, or the measurements will be incorrect. Also, the telescope is attached to a divided circle that angle measurements are taken from, so it is imperative that the telescope does not move. A fine adjust helps to center the beam on the crosshairs located inside the eyepiece. (These are merely a constant spot to place the beam for measuring.) Four microscopes are situated 90° apart around the bottom of the prism table so the graduated circle can be read down to half second arc. These numbers, which are in degrees, minutes and seconds, are used to determine the angle of the beam as it comes out.

For each wavelength, both the right and left side of the prism must be measured. This is explained in FIGURE 11.

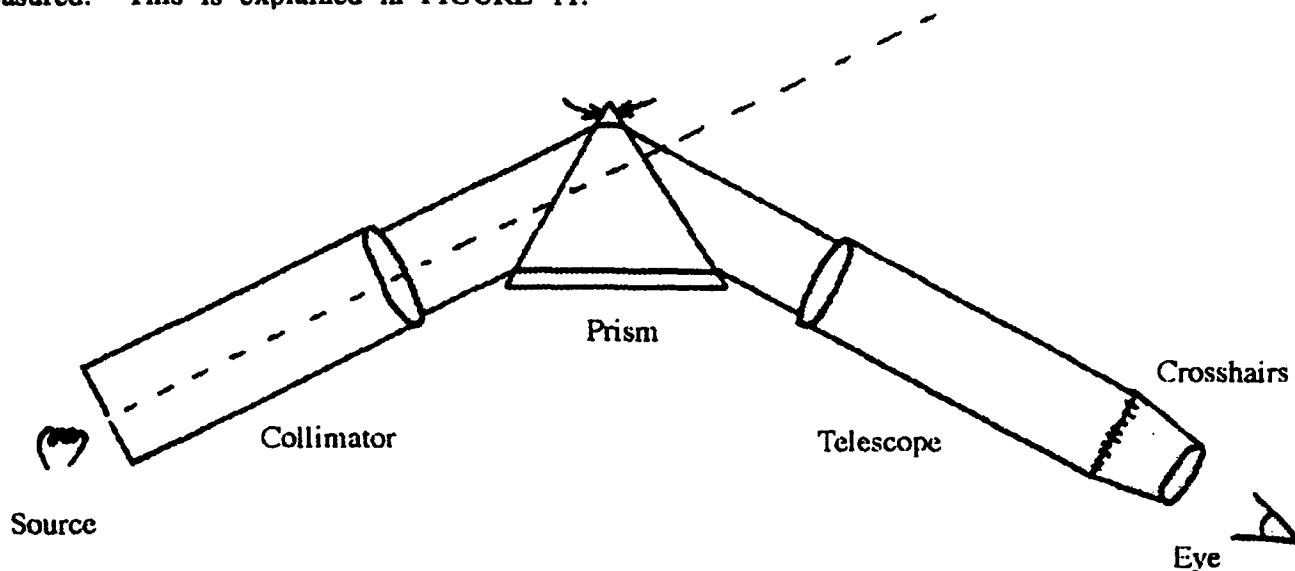


FIGURE 11
Schematic of spectrometer

When the light enters the left prism face, it is refracted. However, we want to measure the light's straight path through the prism, which you can't see (shown by dashed line in FIGURES 11 and 12). We accomplish this by measuring the light as it is refracted on the left and then the right sides. The left is subtracted from the right. Since it is known that the straight line is 180° , then we can subtract the difference between the left and right from 180 to get ψ .

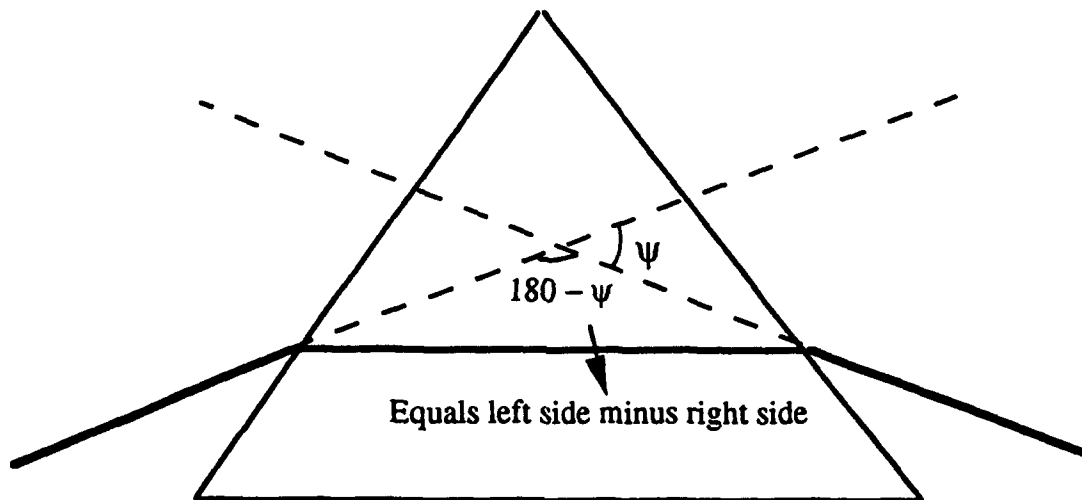


FIGURE 12
Diagram showing how ψ is found

The wavelength is changed after both sides are measured and minimum deviation is found again. Each wavelength bends more at different wavelength, meaning the index varies with wavelength. This is known as dispersion⁴ and is the reason for the "rainbow" formed when white light goes through a prism.

This process is repeated over a wavelength range, called a run, that varied between prisms. The standard number of runs was 5 for each axis.

All numbers recorded were entered into a program written by my mentor for the Software package *Mathematica* version 2.2. designed to calculate the index. All 5 runs on each sample are compared and a standard of deviation (STD) is calculated. (STD is how our index numbers varied between runs.) How small the STD is determines the accuracy of the final index number. No number is accepted unless its STD is smaller than 10^{-3} .

Results

Before actually beginning on new materials, samples of known indices were studied so as to ensure we could repeat the measurements while the STD remained smaller than 10^{-3} . We began with Quartz and only did the visible spectrum of 430-670 nm (where 1 nm = 10^{-9} m) in increments of 20 nm, 700-1000 nm in steps of 50 nm and 1064 nm in steps of 20 nm. This material was known to be an isotropic material so unpolarized light was used and only one index was measured. The results are shown in FIGURE 13.

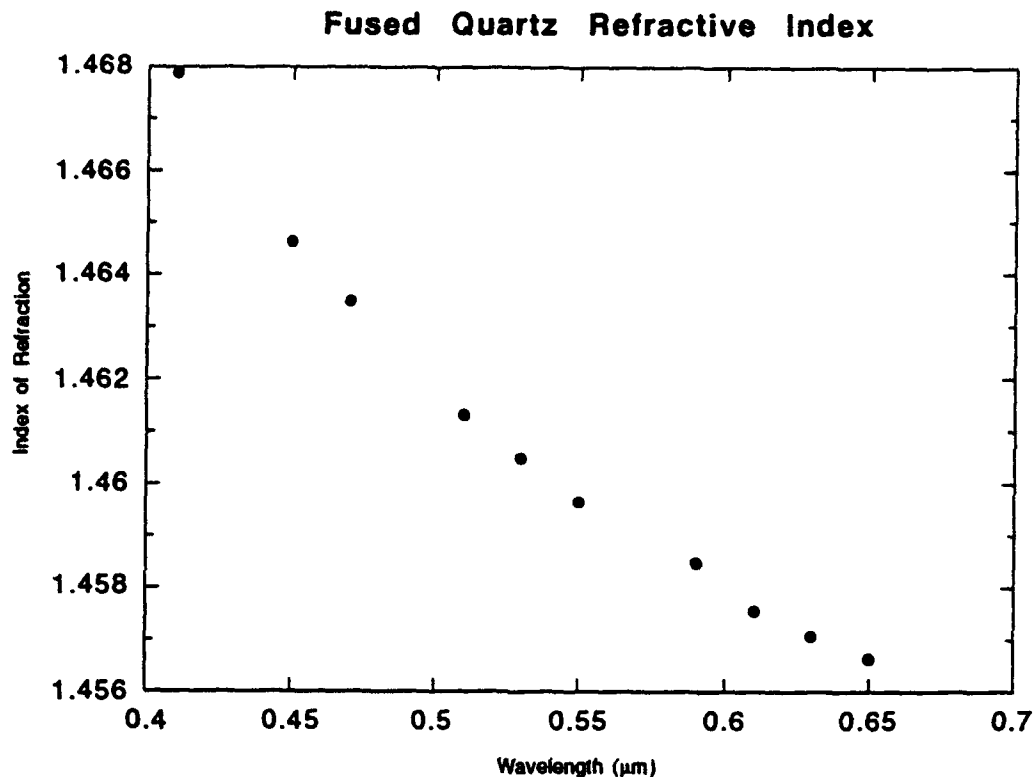


FIGURE 13
Refractive index data for quartz

Then, we moved on to a new material, RTA. This sample was sent to Wright Labs from Crystal Associates, in Waldwick, New Jersey, to be measured. Crystal Associates determined this material to be bi-axial so two prisms of different orientation were sent to be measured. This meant that polarized light needed to be used on both of the prisms. Each prism was measured first doing 5 runs on vertically polarized light, and then 5 on the horizontally polarized light. However, on one of the prisms only 3 runs on the horizontal polarization were done because it was determined that this was one of the axes that were equal. We recorded measurements for both the visible and NIR

range of 430-670 nm in increments of 20 nm, 700-1000 nm in steps of 50 nm and 1064 nm. The results, as sent to Crystal Associates, are seen in FIGURE 14.

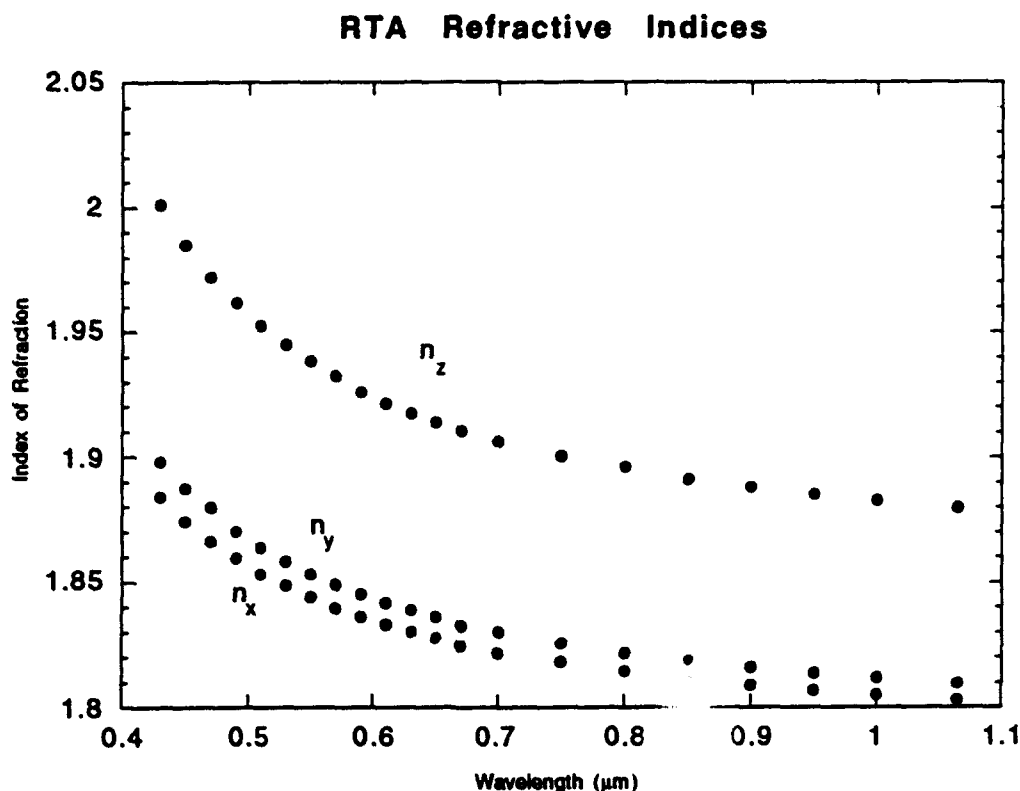


FIGURE 14
Refractive index data for RTA

A second new material, KTP:Na was begun, also from Crystal Associates. Like the RTA, this material is also bi-axial. The same series of wavelengths used for RTA were recorded. As time had run out on this study, not all five runs for each polarization were completed. For the first prism 4 runs were completed for the horizontally polarized light and 3 were done for vertical. Only 4 runs were completed on the second prism for vertically polarized light and none on horizontal because

there was not enough time. Measurements will be resumed later on by someone else at Wright Laboratory. The measurements taken are shown FIGURE 15.

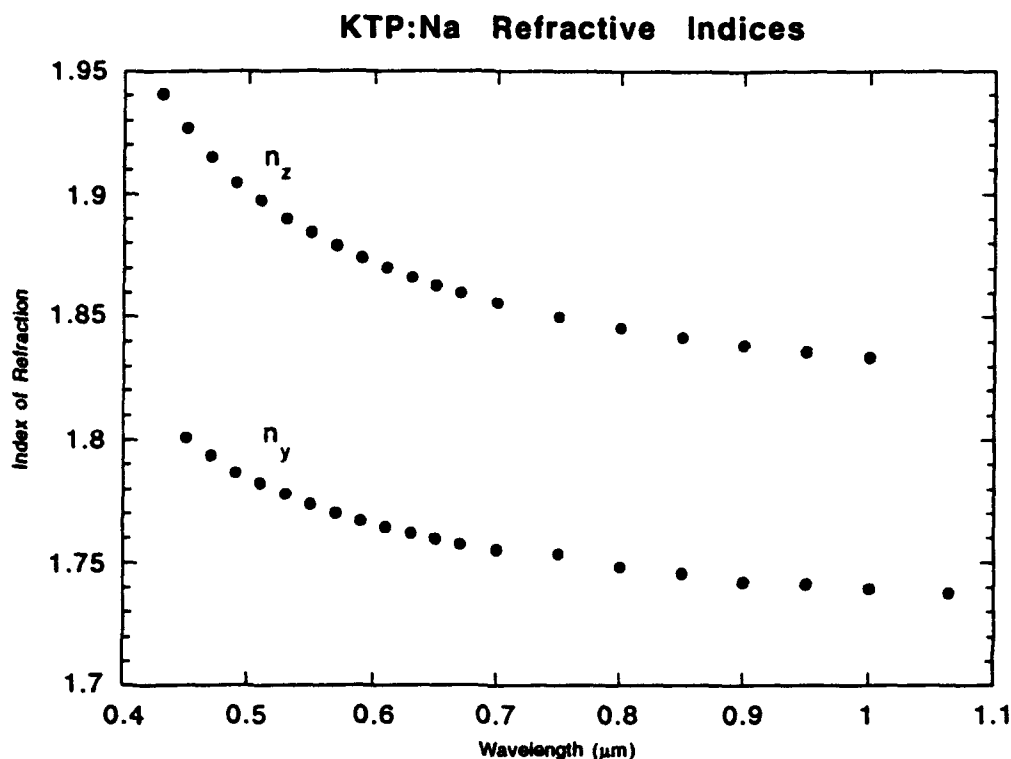


FIGURE 15
Refractive index data for KTP:Na

Conclusion

The index of refraction measurements recorded by us in this study proved to be accurate enough for use by the scientists who developed the new materials. The final numbers and the plots for RTA and KTP:Na shown in this study were sent to Crystal Associates. There they will be used to help in the characterization of those materials.

References

1. Saleh, Bahaa E. A., and Malvin Carl Teich, *Fundamentals of Photonics*, John Wiley and Sons, New York. 1991. p.211.
2. Halliday, David and Robert Resnick, *Fundamentals of Physics*, Second Edition, John Wiley and Sons, New York. 1986. p.748.
3. Klein, Miles V. and Thomas E. Furtak, *Optics*, Second Edition, John Wiley and Sons, New York. 1986. p. 97.
4. Sears, Francis W., Mark W. Zemansky and Hugh D Young, *University Physics*, Sixth Edition, Addison-Wesley Publishing Company, Reading. 1982. p. 725.

**ORGANIZATION AND EVALUATION OF FRAGMENT SHATTER TEST
DATA RESULTS USING THE MICROSOFT EXCEL SPREADSHEET**

**Jennifer R. Bautista
High School Apprentice
Warheads Branch**

**Wright Laboratory Armament Directorate
WL/MNMW
Eglin AFB, FL 32542-5434**

**Final Report For:
High School Apprenticeship Program
Wright Laboratory Armament Directorate**

**Sponsored By:
Air Force Office of Scientific Research
Bolling Air Force Base, Washington D.C.**

August 1993

ORGANIZATION AND EVALUATION OF FRAGMENT SHATTER TEST DATA RESULTS USING THE MICROSOFT EXCEL SPREADSHEET

**Jennifer R. Bautista
High School Apprentice
Computational Mechanics Section, Warheads Branch
Wright Laboratory Armament Directorate
Eglin Air Force Base, Florida**

Abstract

During my second summer in the HSAP program, I organized and evaluated fragment shatter test data for over 800 experiments done by NSWC. In order to organize the data, make xy plots, and evaluate discrepancies in the information, I utilized the Microsoft EXCEL spreadsheet. The information was sorted according to specific criteria and put into small groups of similar information, so that engineers in my section will be able to pinpoint particular data points. Once the organization was complete, xy plots of impact velocity versus residual mass and residual velocity were charted, and test shots which appeared to be questionable were identified.

ORGANIZATION AND EVALUATION OF FRAGMENT SHATTER TEST DATA RESULTS USING THE MICROSOFT EXCEL SPREADSHEET

Jennifer R. Bautista

INTRODUCTION

My project for the summer was based on the fragment shatter test, performed by the Naval Surface Warfare Center (NSWC), Applied Research Associates (ARA), and the Denver Research Institute (DRI). The fragment shatter test involves cubical, metal fragments which are fired at a metal plate at different velocities, angles, and orientations, shown in Figure 1. One purpose of the fragment shatter test is to develop penetration equations for use in vulnerability assessment. With information about these penetrations, predictions can be made about lethality and survivability of certain targets. Currently my mentor, Mr. Michael E. Nixon, is exploring the use of hydrocodes to model these tests. The Computational Mechanics Section works closely with hydrocodes, which are complex computer codes that simulate warhead formation, penetration, and response. If accurate, they can eliminate some range tests and facilitate design of new models.

METHODOLOGY

The original fragment shatter test database consisted of approximately 800 test shots, with information pertaining to projectile material, shape, mass, and Brinell hardness; plate material and thickness; angle of obliquity; impact angle; impact velocity; residual velocity and residual mass; number of behind-armor fragments from the projectile and mass of those fragments; number of behind-armor fragments from the plate and the mass of those fragments; and whether or not the main projectile fractured in the test (see Figure 2). I eliminated some of these categories, rearranged the other columns, and revised some column titles for clarity. Subsequently I grouped the data into small groups of test shots which were specifically related to each other according to

particular criteria: projectile mass and material, plate thickness and material, and impact velocity. The result was a series of small, specialized groups of data, shown in Figure 3.

The next step was charting a series of xy plots of residual mass and velocity. The Microsoft EXCEL spreadsheet program provides users with various capabilities for creating clear and concise charts. We chose to plot our data series using an xy line plot. For each group of data, two charts were created: residual mass and velocity. The percentage of remaining mass or velocity was plotted versus the striking velocity of the projectile; thus, for each specific group of data, there is a visual representation of how much of the projectile remains and how fast it is going. Figure 4 shows an example of each.

For the larger groups of information, we noticed a few discrepancies in some of the xy plots: for example, in a group of data where the projectiles travel from 4000 to 8000 fps and pierce the plate, most retain around 60 or 70% of their original mass. We found some data points which indicated that a test shot in this series retained 98% of its original mass, which of course is questionable when viewed in the light of the other tests. An example of these questionable points is shown in Figure 5. There is every possibility that this data could be bonafide information, but for accurate development of penetration equations, the information must be correct. We will consult NSWC, ARA, and DRI to review these questionable points in order to clarify our information.

The final step was placing the information in a format that will be easy to use in the future. I formatted the data and charts so that the engineers in my section will have an easy-to-use reference for prospective use.

RESULTS

The organization and evaluation were completed, and the final product will be used in the future for development of penetration equations. The questionable data points have also been singled out and their authenticity will be checked. Not only have I produced a product that will be used in the future by the engineers of the Computational Mechanics Section, but I have gained valuable knowledge of the fragment shatter test, its applications in vulnerability assessment, and

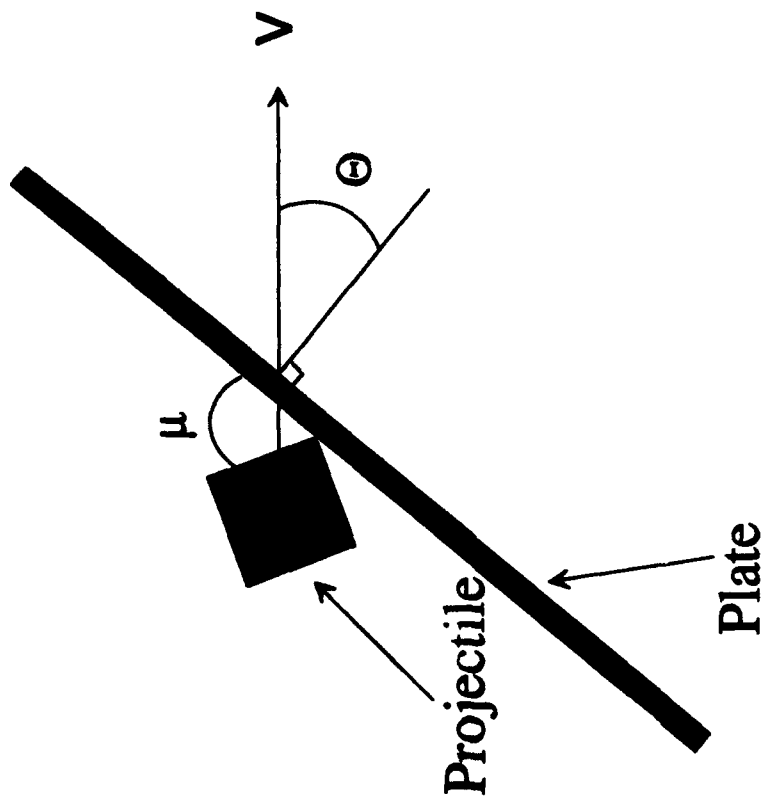
as a result of my other "mini-projects" during the summer, a working knowledge of Silicon Graphics Iris Indigo workstations, the UNIX operating system, personal computers, the Microsoft Windows environment. The result of this summer is not merely what I have produced for the Wright Laboratory Armament Directorate, but the many things I have learned about the technical fields and the working world.

ACKNOWLEDGMENTS

First, I would like to thank the Lord for providing this opportunity to me.

Of course, I owe many thanks to my mentor, Mr. Michael Nixon. His guidance has been invaluable throughout my two summers here, and I look forward to another wonderful summer. I would like to thank my fellow apprentice and "partner in crime" Elliot Moore II for two wonderful years of companionship, help, humor, guidance. I must thank the Sverdrup contractors who work in our section, Ms. Pam Cortner, Mr. Randy Anderson, and Mr. Bizhan Aref, for helping me correct some of my problems. I would like to acknowledge the other members of our section, Dr. Bill Cook, Dr. Harbans Sidhu, Mr. Ed Bradley, Mr. John Collins, and our section chief, Maj. Howard Gans, for their help and support during the summer. I could not have asked for a more receptive or helpful environment in which to work and learn, and I owe everyone my thanks.

BEFORE IMPACT



AFTER IMPACT

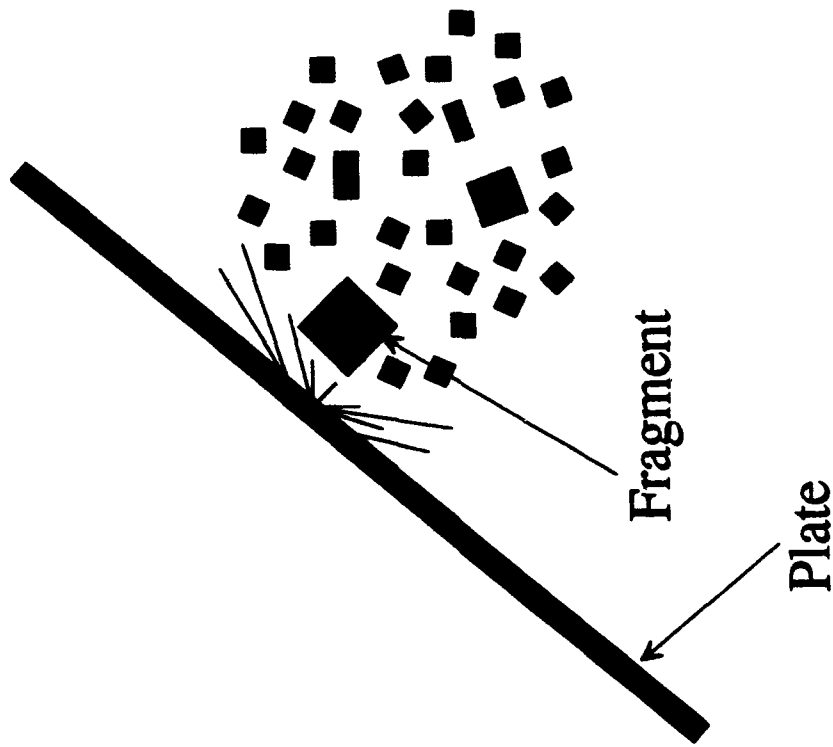


Figure 1: Parameter Identification for the Breakup Study

NSWC/ARA/DRI FRAGMENT SHATTER TEST RESULTS

Shot No.	Projectile		Plate		Thick (in)	Obliq	Impact Vel. (ft/sec)	Impact Angle deg	Fracture (Y/n)	Vr (ft/sec)	Mfcl (gms)	Nc	Mfct (gms)	Ns	Mfst (gms)
	Matl.	Bhn	Shape	Mass (gms)	Matl.	Bhn									
1-1	1018 ST	235	Cube	31	2024 AL	120	0	3440	6.0	N	31.0	0	0.0	1	0.9
1-2	1018 ST	235	Cube	31	2024 AL	120	0	4088	6.0	N	31.0	0	0.0	1	0.7
1-3	1018 ST	235	Cube	31	2024 AL	120	0	4632	5.0	Y	28.0	3	2.6	1	0.7
1-4	1018 ST	235	Cube	31	2024 AL	120	0	5276	9.0	Y	23.3	3	7.5	3	1.0
1-5	1018 ST	235	Cube	31	2024 AL	120	0	6900	5.0	Y	7.5	4	21.5	0	0.0
1-6	1018 ST	235	Cube	31	2024 AL	120	0	7800	10.0	Y	9.0	5	19.6	0	0.0
1-7	1018 ST	235	Cube	31	2024 AL	120	0	6183	8.0	Y	17.0	3	13.0	0	0.0
1-8	1018 ST	235	Cube	31	2024 AL	120	0	7656	6.3	Y	10.1	5	15.8	3	32.6
2-1	1018 ST	235	Cube	31	2024 AL	120	0	3901	4.0	Y	22.0	2	8.3	1	1.2
2-2	1018 ST	235	Cube	31	2024 AL	120	0	2902	3.0	N	31.0	0	0.0	2	1.3
2-3	1018 ST	235	Cube	31	2024 AL	120	0	3827	2.0	Y	26.0	1	4.9	2	0.8
2-4	1018 ST	235	Cube	31	2024 AL	120	0	8049	7.8	Y	7.5	6	14.9	X	X
3-1	1018 ST	235	Cube	31	2024 AL	120	0	3097	2.0	N	31.0	0	0.0	2	1.7
3-2	1018 ST	235	Cube	31	2024 AL	120	0	3810	4.0	Y	19.1	2	12.2	3	1.6
3-3	1018 ST	235	Cube	31	2024 AL	120	0	4982	2.0	Y	7.9	4	18.2	1	0.3
3-4	1018 ST	235	Cube	31	2024 AL	120	0	5875	11.0	Y	16.8	4	11.6	1	1.3
3-5	1018 ST	235	Cube	31	2024 AL	120	0	2683	4.0	N	31.1	0	0.0	2	2.6
3-6	1018 ST	235	Cube	31	2024 AL	120	0	7123	4.0	Y	6.0	7	18.0	0	0.0
3-7	1018 ST	235	Cube	31	2024 AL	120	0	7728	20.0	Y	15.8	4	9.9	0	0.0
4-1	1018 ST	235	Cube	31	2024 AL	120	0	3223	5.0	N	31.0	0	0.0	2	3.8
4-2	1018 ST	235	Cube	31	2024 AL	120	0	4128	4.0	Y	10.6	3	19.4	8	3.7
4-3	1018 ST	235	Cube	31	2024 AL	120	0	4805	3.0	Y	8.4	4	20.4	5	2.4
4-4	1018 ST	235	Cube	31	2024 AL	120	0	8310	12.6	Y	3.5	7	10.4	X	X
4-5	1018 ST	235	Cube	31	2024 AL	120	0	5862	12.1	Y	7.5	6	18.4	X	X
4-6	1018 ST	235	Cube	31	2024 AL	120	0	4225	3.5	Y	7.9	3	21.7	1	0.3
4-7	1018 ST	235	Cube	31	2024 AL	120	0	5454	24.0	Y	21.7	3	6.9	2	1.9

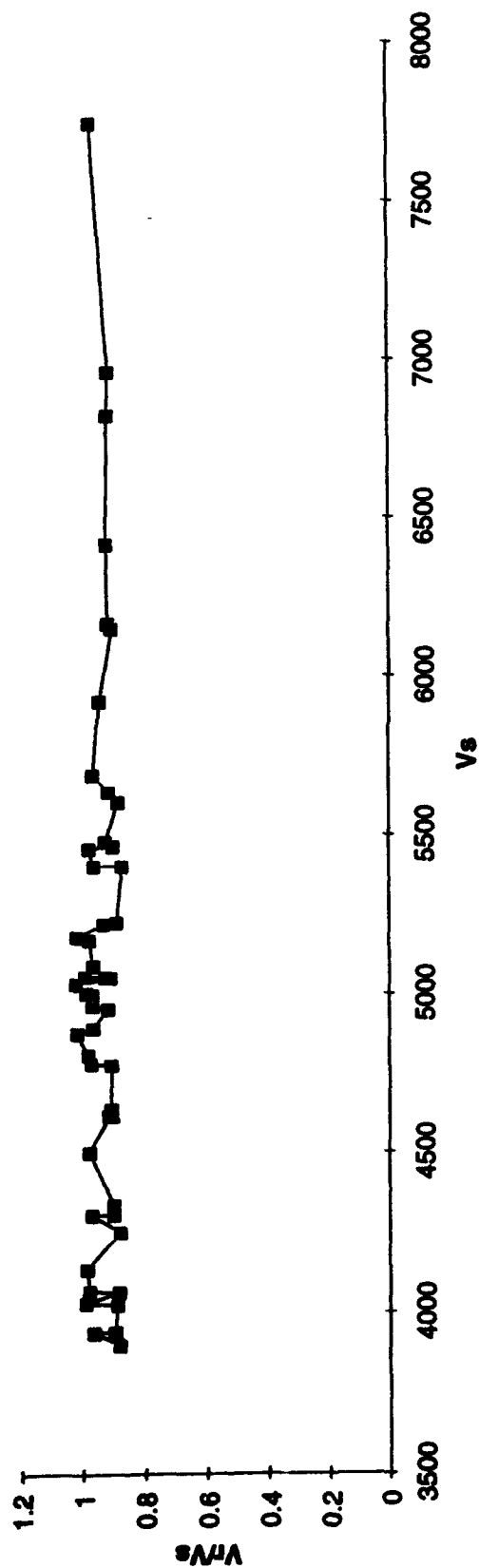
Figure 2: Original Data in Unorganized Format

NSWC/ARA/DRI Fragment Shatter Test Data: 4140 Steel Against 2024 Aluminum

Projectile Matl.	Plate Matl.	Mass Thickness	Impact vel. (ft/sec)	Obliq	Impact angle deg.	Vr (ft/sec)	Residual		Mass of		Fracture (Y/N)		
							mass (grms)	# Proj frags	proj. frags (grms)	# Target frags		target frags (grms)	
4140 ST	2024 AL	60	0.080	3820	0	5.1	X	59.9	0	0.0	2	1.1	N
4140 ST	2024 AL	60	0.080	3899	0	3.0	3435	50.7	2	8.0	5	2.9	Y
4140 ST	2024 AL	60	0.080	3938	0	5.0	3790	58.1	3	2.7	4	5.2	N
4140 ST	2024 AL	60	0.080	3940	0	3.0	3531	52.8					Y
4140 ST	2024 AL	60	0.080	3976	0	10.7	X	55.1	2	9.1	1	4.5	Y
4140 ST	2024 AL	60	0.080	4025	0	2.0	3574	48.0					N
4140 ST	2024 AL	60	0.080	4030	0	5.0	3982	35.3	3	23.6	5	3.2	Y
4140 ST	2024 AL	60	0.080	4063	0	4.0	3580	41.6	6	16.4	5	3.1	Y
4140 ST	2024 AL	60	0.080	4066	0	3.0	3981	50.5	2	9.2	6	2.9	Y
4140 ST	2024 AL	60	0.080	4134	0	8.0	4082	46.6	3	11.0	2	3.7	Y
4140 ST	2024 AL	60	0.080	4230	0	9.5	X	48.3	2	10.5	1	4.1	Y
4140 ST	2024 AL	60	0.080	4252	0	3.0	3730	35.1	7	23.3	6	2.8	Y
4140 ST	2024 AL	60	0.080	4257	0	36.9	X	59.4	0	0.0	0	0.0	N
4140 ST	2024 AL	60	0.080	4303	0	9.0	4172	45.9	5	12.6	2	4.1	Y
4140 ST	2024 AL	60	0.080	4305	0	4.0	3870	36.4	4	20.8	4	2.8	Y
4140 ST	2024 AL	60	0.080	4335	0	4.0	3889	40.2	3	17.8	4	2.5	Y
4140 ST	2024 AL	60	0.080	4394	0	7.1	X	45.1	1	6.3	11	5.5	Y
4140 ST	2024 AL	60	0.080	4459	0	7.2	X	44.3	2	13.6	5	4.3	Y
4140 ST	2024 AL	60	0.080	4495	0	3.9	X	49.5	1	9.9	0	0.0	Y

Figure 3: Organized Fragment Shatter Test Data

4140 Steel (60) Against 2024 Aluminum (0.080): Residual Velocity



4140 Steel (60) Against 2024 Aluminum (0.080): Residual Mass

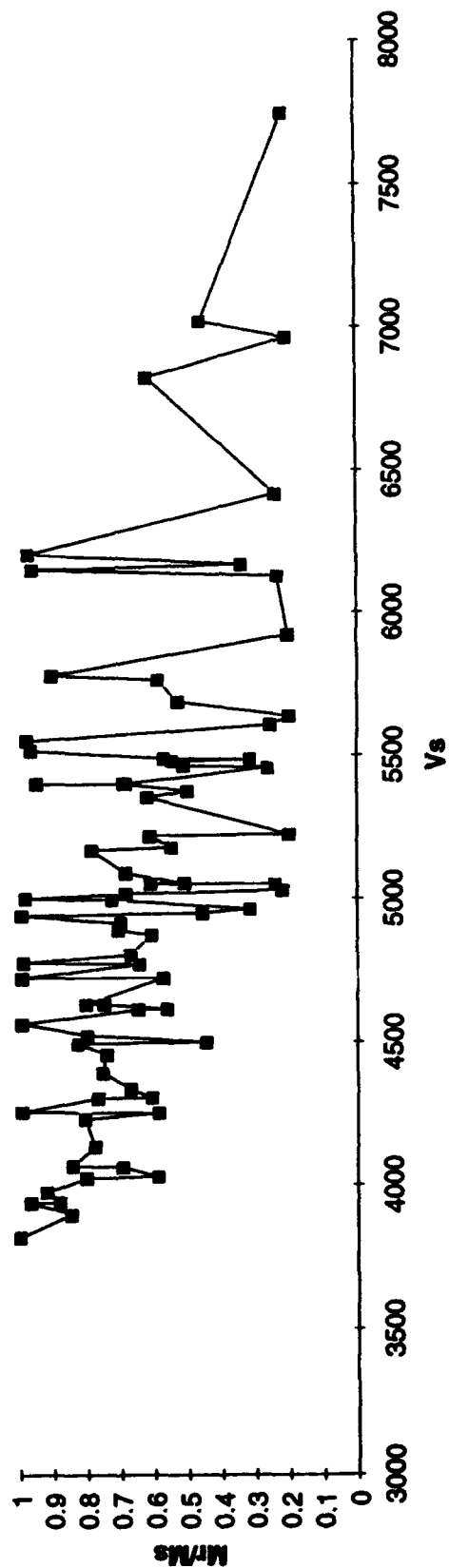


Figure 4: XY Plots of Residual Mass and Velocity

4140 Steel (60) Against 2024 Aluminum (0.080): Residual Mass

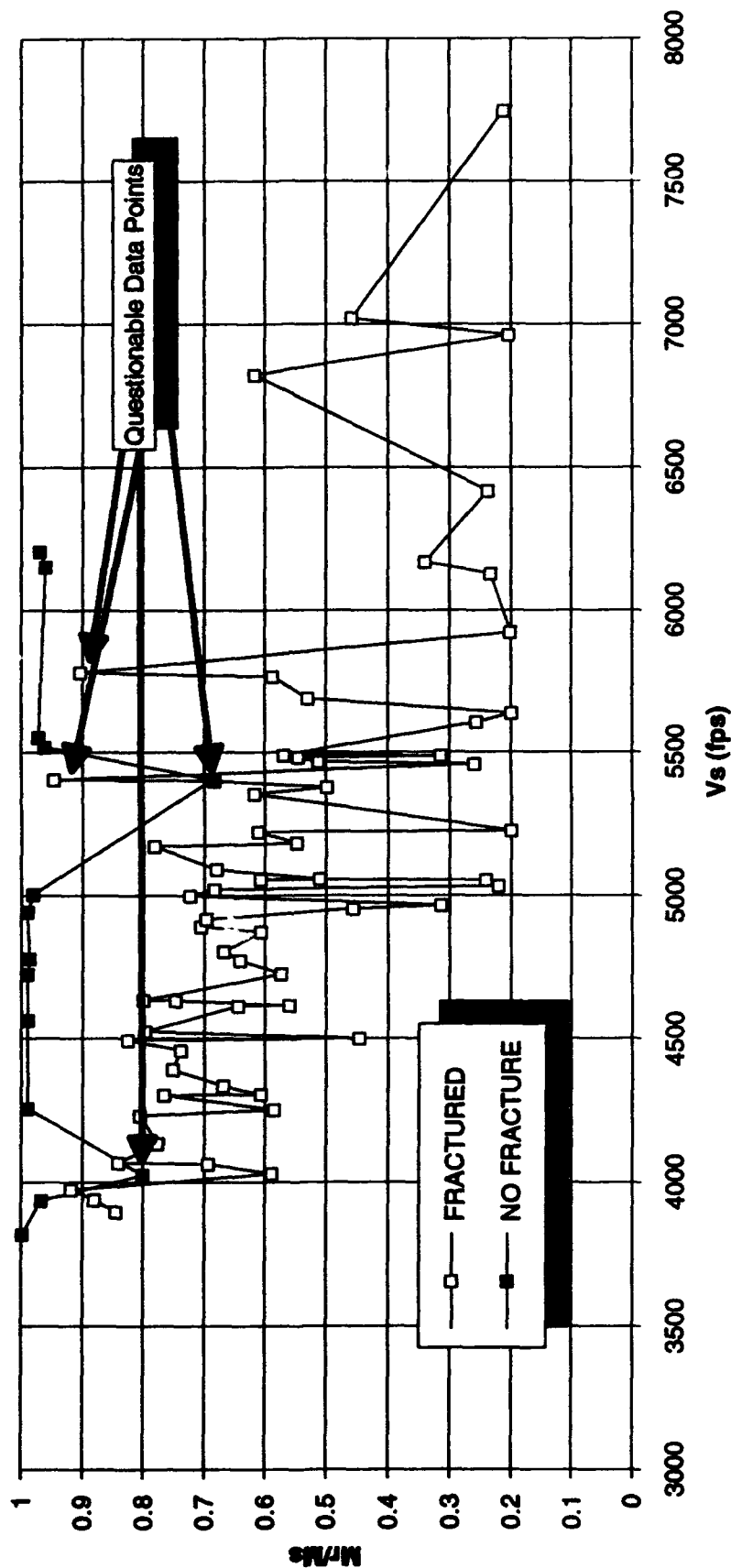


Figure 5: Example of Questionable Data Points

William Blanchard's report not available at time of publication.

**FROM MINDS TO MISSILES:
THE DESIGN, DEVELOPMENT, AND TESTING OF
AERODYNAMIC MODELS**

**Theresa J. Cook
High School Apprentice
Aerodynamics Branch**

**Wright Laboratory Armament Directorate
WL/MNAA
Eglin Air Force Base, FL 32542**

**Final Report for:
High School Apprenticeship Program
Wright Laboratory Armament Directorate**

**Sponsored by:
Air Force Office of Scientific Research
Bolling Air Force Base, Washington D.C.**

August 1993

FROM MINDS TO MISSILES:
THE DESIGN, DEVELOPMENT, AND TESTING OF
AERODYNAMIC MODELS

Theresa J. Cook
High School Apprentice
Aerodynamics Branch
Wright Laboratory Armament Directorate

Abstract

The aerodynamic qualities of weapon airframes and munitions can be examined through the use of scale models and analysis of free-flight test data. The different stages of aerodynamic modeling were studied in three different programs: the GBU-28, a precision guided bomb, HAVE DASH II, an air-to-air missile, and the PGU31-B, an armor-piercing munition. The GBU-28 was studied with the Projectile Design Analysis System, while the properties of the HAVE DASH II and the PGU31-B were investigated in the Aeroballistic Research Facility and the Ballistic Experimentation Facility. The data obtained from the finished tests was determined to be accurate, while the work done on ongoing testing has yet to be evaluated. All the results obtained will be used to provide control data for the programs.

FROM MINDS TO MISSILES: THE DESIGN, DEVELOPMENT, AND TESTING OF AERODYNAMIC MODELS

Theresa J. Cook

Introduction

For several years, scientists and engineers have utilized the opportunities provided through the analysis of free-flight test data to investigate the aerodynamic properties of missiles, munitions, and other projectiles. By measuring the aerodynamics and calculating the aerodynamic coefficients of these models, scientists can get an idea of how the full-scale missile will fly and can input this data into their fire and flight control programs. Free-flight analysis has a decided advantage over tests conducted in wind tunnels because of the absence of the effects caused by the sting on which the models are mounted. Free-flight analysis can provide more accurate drag measurements and other aerodynamic terms than a wind tunnel, but is less efficient in measuring pressure on the body and can not accurately test at high angles of attack. However, free-flight analysis gives a more comprehensive view of the missile's trajectory because the model's actual flight path can be followed. By the use of two orthogonal camera stations, the engineer can determine the model's spatial position as well as its angular orientation. The spatial position and angular orientation of the model provide six pieces of information, which are also known as the Six Degrees of Freedom (6DOF). By entering the Six Degrees of Freedom into equations of motion, the aerodynamic terms of the projectile can be determined. These equations, convolutions of Newton's second law, $F=ma$, are derived to fit the terms specified by the engineer and are taken to a certain degree dependent upon the accuracy desired.

The engineer's tasks during the aeroballistic free-flight testing are usually done in three phases. The first of these is to analyze the projectile's design to ensure its feasibility. This part of the process was studied with the GBU-28 using PRODAS. The second step in the aerodynamic testing procedure is to actually shoot the models in the range and collect the data from these shots. This was practiced with the HAVE DASH II program in the Aeroballistic Research Facility (ARF) and the Ballistic Experimentation Facility (BEF). The third and final phase of the process is for the engineer to examine the data collected from the tests and report on the results. The PGU-31/B was used for this part of the procedure.

GBU-28

The GBU-28, or "Bunker Buster," was a precision guided bomb developed and used by the United States Air Force during the Persian Gulf War. When the war started, the Air Force realized it did not have the type of bomb needed to effectively travel through one hundred feet of dirt and rock and then through twenty feet of reinforced concrete, or to get into the Iraqi command bunkers. In seventeen days, the engineers at Wright Laboratories and Eglin Air Force Base designed and produced the GBU-28. It was then shipped to Saudi Arabia, where it was used to hit the main Iraqi command bunker on the last day of the war. In that somewhat rushed situation, the engineers did not have much time to investigate the aerodynamics and flight pattern of the GBU-28's configuration. Now the Air Force is interested in how and why the GBU-28 flies, so tests have been planned with scale models to be analyzed in the free-flight range. The data from these tests will be used to corroborate earlier wind tunnel results and add to the bomb's aerodynamic database.

Before the models are actually made, however, the design is run through a

preliminary program, the PROjectile Design Analysis System (PRODAS). This is a comprehensive program for ballistic analysis written in the FORTRAN language by Arrow Tech. It is capable of projectile modeling, calculating physical properties, conducting aerodynamic, stability, and trajectory analyses, and estimating interior and exterior ballistics. To start, the projectile is modeled on the computer in elements. Each element must be defined by its left diameter, right diameter, length, length in reference to the whole body, density (the material of which that particular element is made), element code, radius, and color if desired. The element code specifies what part of the body the element is, such as boattail, fin, ogive, flare, or body. PRODAS then takes these elements and creates a composite model that is similar to the original aerodynamically, using a database of projectile parts and pieces that have known terms and coefficients.

The GBU-28 is a fairly complex configuration, with several changes in the diameter throughout the length of the body and three distinct fin groups (Fig. 1). A problem was encountered when the fins were modeled. The aft wing, composed of two fin groups, had a small protrusion at the front that could not be drawn correctly by PRODAS. This piece was determined to be inconsequential and omitted from the model, but the remaining fin proved still too complex for PRODAS to handle. The composite model created by the program was imprecise and the results of the tests run on that model were unfavorable. The aft wings of the PRODAS model were then changed to a shape that was easier for the program to correctly emulate, but that had the same area as the prototype fins and were expected to have similar properties (Fig 2.). The model produced by PRODAS after these changes had been made was much more accurate and the results of these tests more favorable. The GBU-28 tests from PRODAS affirmed the results obtained from earlier tests in that the model is stable and has the aerodynamic terms that were expected of it. To proceed with the program, fifteen models have been made and

will be tested in the ARF. The PRODAS analyses showed the configuration to be stable and ready for testing in the ARF.

HAVE DASH II

The HAVE DASH II is an air-to-air missile designed by the Aerovehicles Branch of the Wright Laboratories Armament Directorate. It is a conformal carriage weapon airframe, meaning that it is specially designed to fit snugly up against the body of aircraft. Conventional weapons pylons present several problems. The configuration of the pylon creates large amounts of drag that the aircraft must overcome. Pylons also produce a distinctive radar signature, making the aircraft more easily detected and placing the pilot in greater danger. A conformal carriage weapon airframe reduces both of these effects. The HAVE DASH II is made of composite materials engineered to lower drag and has been shaped to produce the lowest amount of drag possible. The fins on the HAVE DASH II also fold to allow the missile to be carried internally and to be stored with greater ease. The missile has one flat side which rotates to the bottom when launched. The combination of this flat surface and specially designed fins provides enough lift to allow the HAVE DASH II to use the bank-to-turn method, the same method as used in conventional aircraft.

Over the past several months, the HAVE DASH II configuration has been tested in the ARF and the BEF. These are both facilities where free-flight analyses are conducted. The ARF is the inside range, consisting of a concrete tunnel approximately six hundred feet long lined with the orthogonal camera stations used to photograph the models as they fly down the range. The BEF is the outdoor range, where the models are shot prior to being shot inside to ensure their reliability. Some of the subsonic shots are also conducted outside at the BEF. The HAVE DASH II program has involved several shots in both the

ARF and the BEF. Eight models were shot in the ARF using the High Performance Gun, a powder gun with a three inch diameter barrel. The velocities of these shot ranged from Mach 0.98 to Mach 1.91. The data from these shots is currently being reduced. The physical properties of the models - mass, distance of the center of gravity from the nose, length, height, width, moments of inertia about the X, Y, and Z axes, and speed - as well as the atmospheric conditions of the range at the time of the shot were entered in a database in a format that could easily be used for the Aeroballistic Research Facility Data Analysis System (ARFDAS) data reduction program. Engineers use ARFDAS to extract the aerodynamic information from the experimentally measured trajectories. In essence, the engineer uses ARFDAS to develop a theoretical trajectory that matches the experimentally measured trajectory. The terms used to develop the theoretical trajectory then provide the aerodynamic results.

Some preparatory shots for subsonic tests at the BEF were conducted using the medium chamber, single barrel, compressed air gun. In order to attain the desired velocities, a pressure curve was needed to ascertain the correct air pressure to charge the gun up to. This curve was generated using the following formula:

$$V_p = E_f \sqrt{\frac{2P_c V_c (1 - K^{(1-\gamma)})}{(\gamma - 1)M_p}}$$

where

$$K \equiv \frac{A_b L_b + V_b}{V_c}$$

and

V_p = Muzzle velocity of the projectile

P_c = Chamber pressure

γ	= Ratio of gas specific heats
M_p	= Projectile mass
A_b	= Launch tube cross sectional area
L_b	= Launch tube length
E_f	= Efficiency factor.

All variables except for P_c , chamber pressure, were held constant. Some unit conversions were necessary to acquire the proper output. By altering the amount of pressure (psi) entered in the equation, the curve was generated and graphically displayed through the use of Axum. Two curves were calculated, one at one hundred percent efficiency and one at eighty five percent efficiency (Fig. 3). The eighty-five percent efficiency curve was then used in the planning of the shot and proved to be accurate.

PGU-31/B

The PGU-31/B is an armor-piercing penetrator mounted in a forty millimeter round ammunition. The Special Operations Forces, sponsors of this program, were interested in the penetrator's aerodynamic qualities and testing has been conducted in the ARF. A problem arose, however, when the project engineers tried to find a way to measure the models' roll rate. Normally, a small pin is mounted on the back of the model. This spin pin is then read off the film and its position in space is calculated by using the two orthogonal views taken of the model as it flies downrange. By observing the change in the position of the spin pin from one station to the next, the roll rate of the projectile is measured. Without a spin pin, it is nearly impossible to determine the roll rates off the film. Spin pins could not be installed on the PGU-31/B models because they were already mounted in the ammunition and were too small for the pins to be added correctly.

The solution to this problem was found to be quite simple, although somewhat archaic. Three plywood boxes were constructed and placed in the range. One was positioned immediately out of the blast chamber, one at approximately sixty meters downrange, and one at one hundred and fifty meters from the gun. Each of these boxes had three pieces of photographic paper (because of its strength) that were eight inches apart stretched across the opening. As the PGU-31/B flew through the paper, the fins cut it, leaving a clear view of the model's angular orientation at the time it passed through the paper. When the shots were finished, the paper was taken down and the angles of each model as it flew through each piece of paper were measured manually with a plumb line and a protractor. The eight inch spacing between each sheet of paper was calculated to ensure the model would not rotate over ninety degrees in that space, which would have made the angles confusing to measure and would have resulted in incorrect roll data. After the raw angular data had been extracted from the roll sheets, the actual roll rates were calculated for each shot. This data was entered in a spreadsheet and plotted separately for each of the sixteen shots (Fig. 4). These plots were sized so that they could be visually compared quantitatively with experimental plots from ARFDAS. The data was determined to be accurate and the data reduction for the PGU-31/B program is nearly completed.

Conclusions

The three projects worked on this summer: the GBU-28, the HAVE DASH II, and the PGU-31/B demonstrated the various processes involved in the testing and evaluation of aerodynamic models. The PRODAS tests done for the GBU-28 program confirmed initial estimates and prepared the program for further work. The results gained from this

work also helped to validate the PRODAS program. The HAVE DASH II is an ongoing project, and work is continuing with the configuration. Although the actual testing is finished, the data that is received must be organized and analyzed. The PGU-31/B tests are coming to a close now that the roll rates have been determined and the data is evaluated. The High School Apprenticeship Program is an invaluable experience for students to learn what the "real world" of engineering is like and should be encouraged and promoted extensively. I have had a great time for the past two years and look forward to coming back again.

you're not model scale .330
3007 LENGTH . 9.137 IN

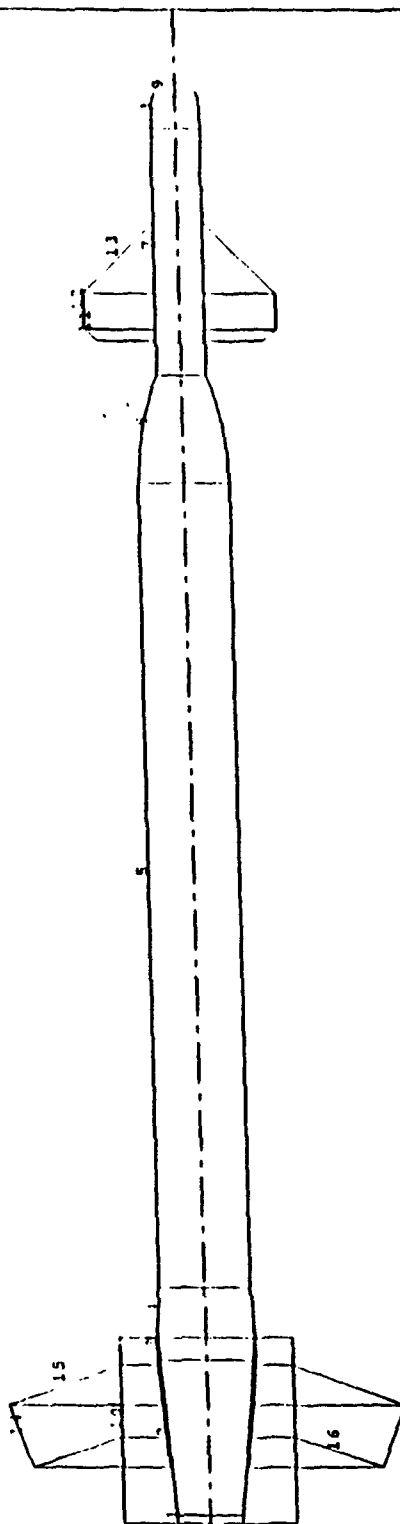


Fig. 1 PRODAS Model of the GBU-28 with Complex Fins

PRODAS VERSION 5.5

FILENAME: GBU28

gbu28 arf model

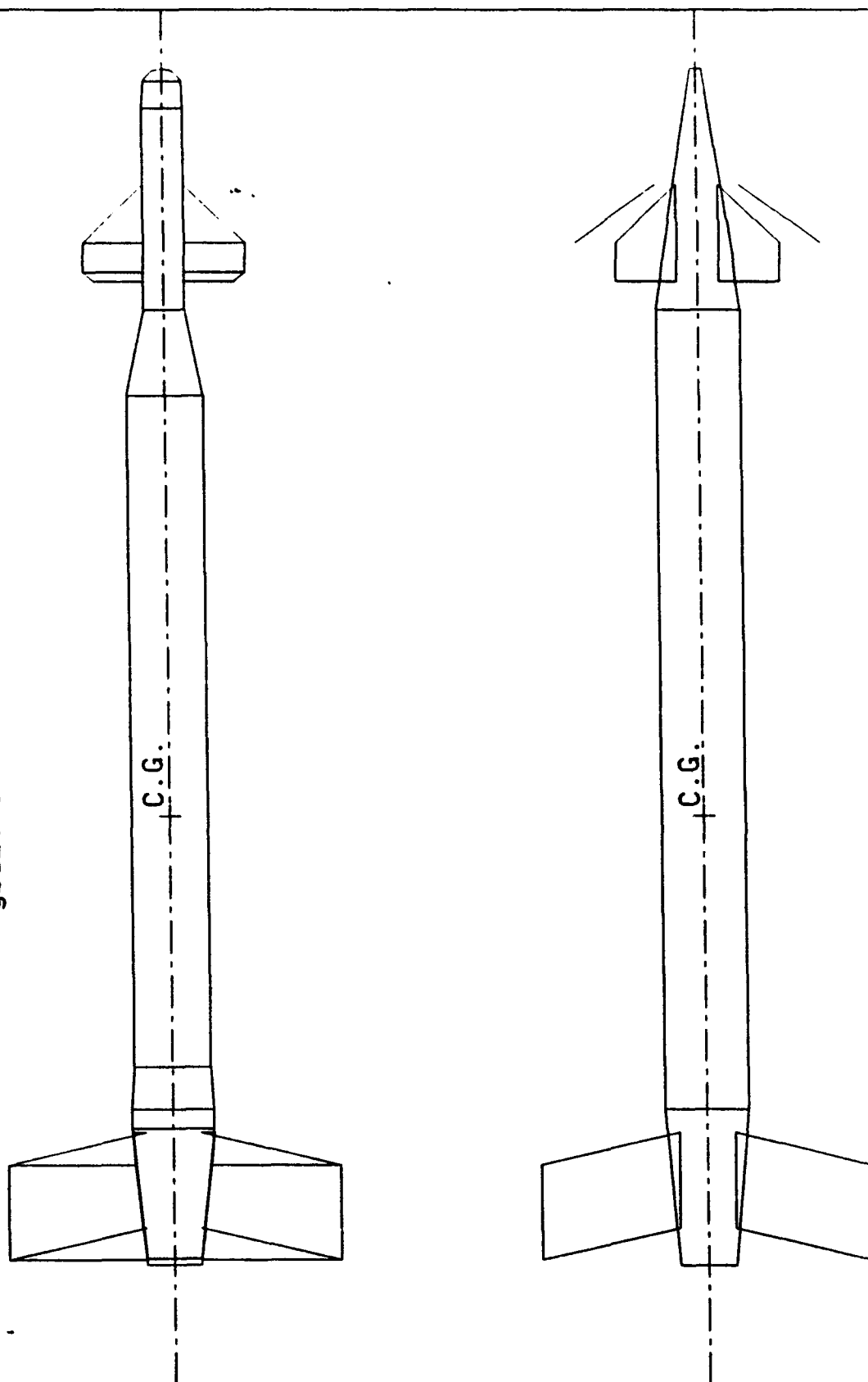


Fig. 2 PRODAS Model of the GBU-28 with Simplified Fins

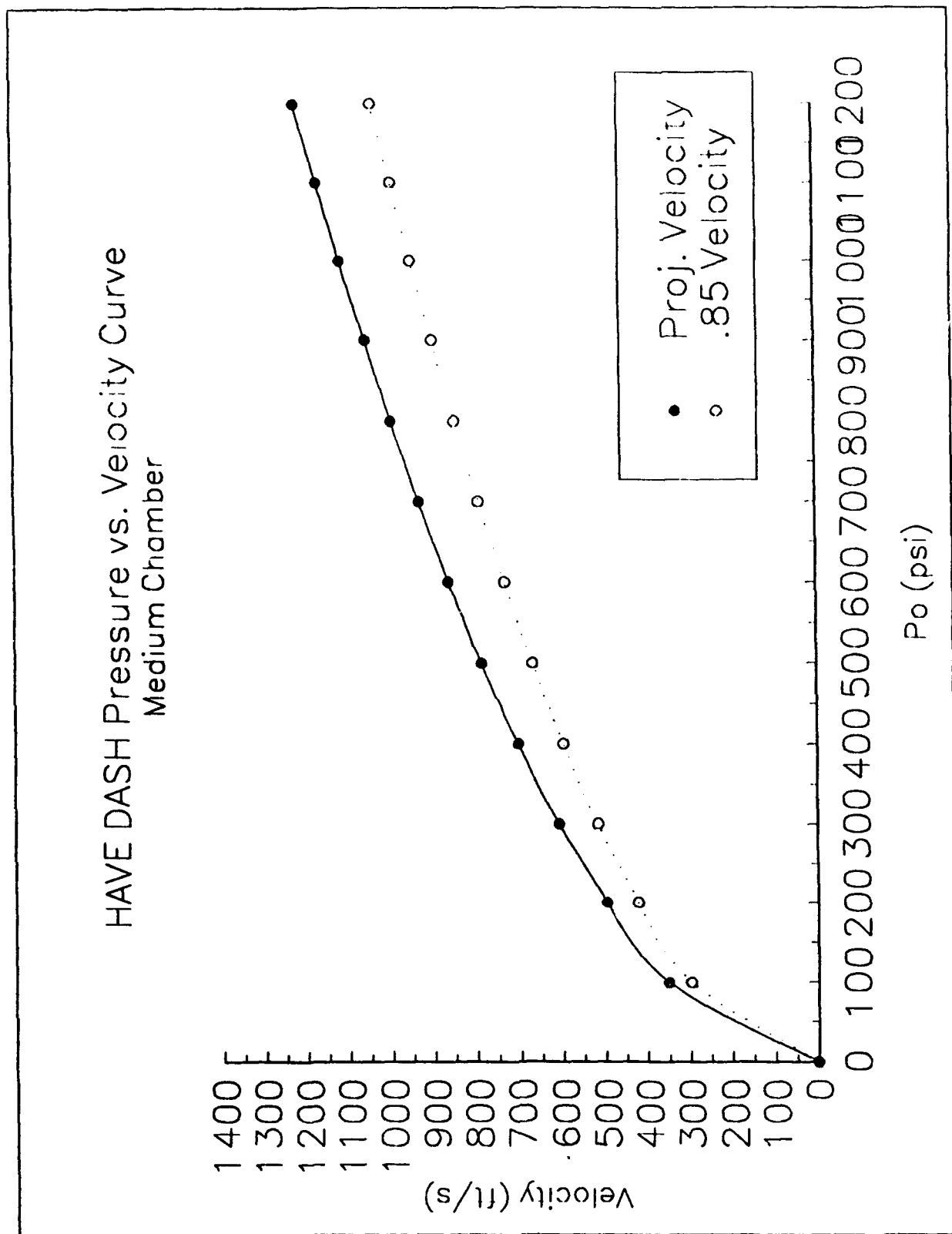


Fig. 3 Pressure Curve for HAVE DASH II Shots at the BEF

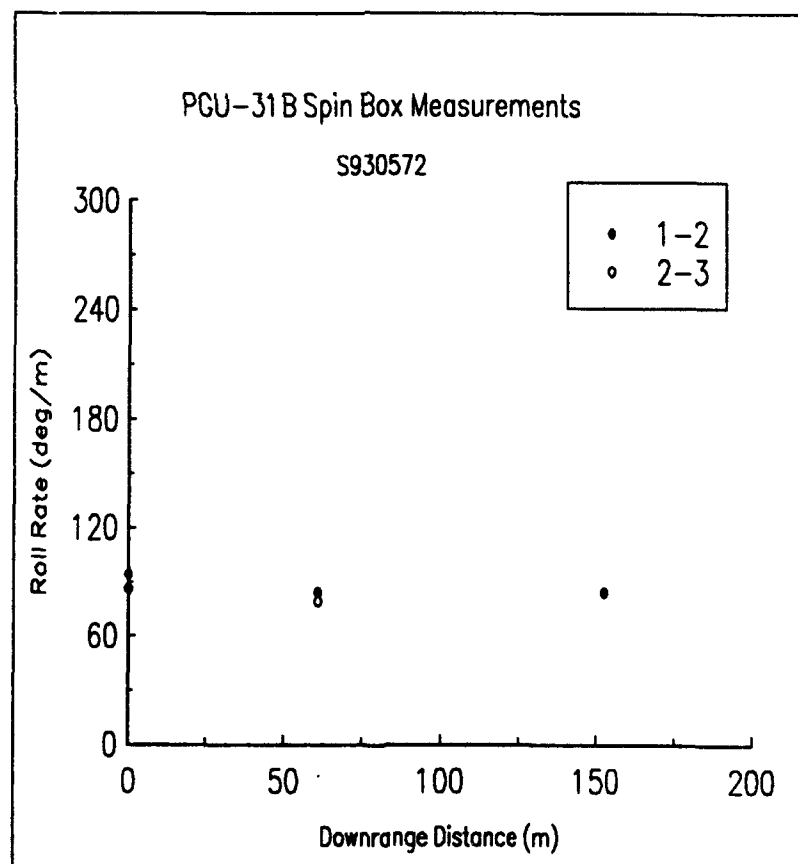
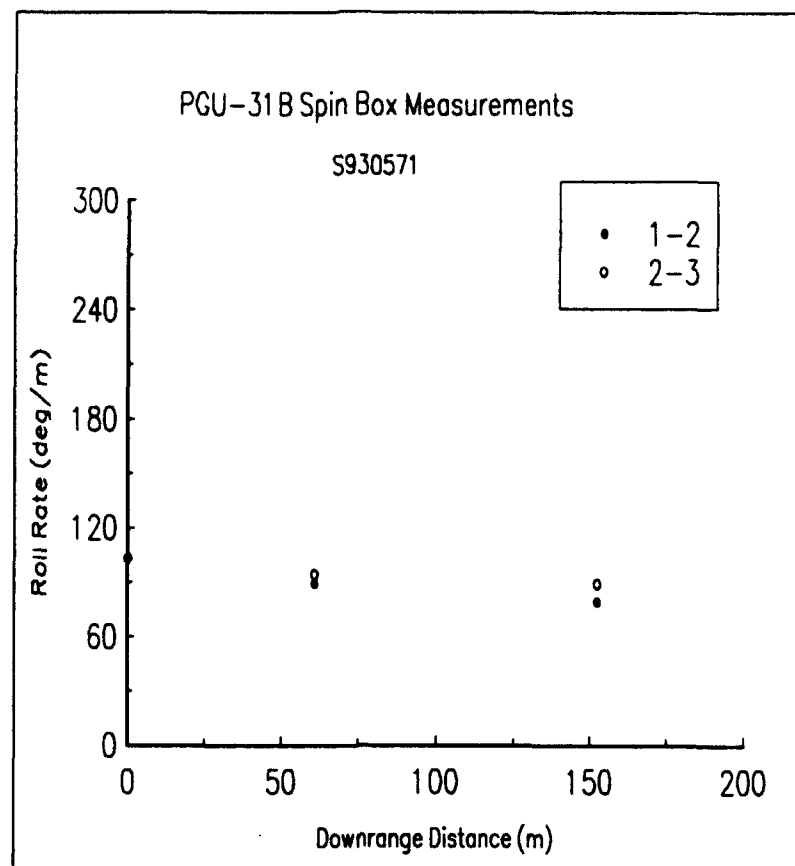


Fig. 4 Spin Rate Plots for PGU31-B

**CHARACTERIZATION OF SOILS FROM RANGE 22
TO DETERMINE CONTAMINATION**

**Nancy H. Deibler
High School Apprentice
Environics Branch**

**Wright Laboratory Armament Directorate
WL/MNOE
Eglin AFB, Florida 32542-5434**

**Final Report for:
High School Apprenticeship Program
Wright Laboratory Armament Directorate**

**Sponsored by:
Air Force Office of Scientific Research
Bolling Air Force Base, Washington D.C.**

August 1993

CHARACTERIZATION OF SOILS FROM RANGE 22 TO DETERMINE CONTAMINATION

Nancy Deibler

ABSTRACT

Metal contamination in soil is a hazard to the environment. Since munitions testing using a large range of metals have taken place at Range 22 since the early 1940's, there is a possibility of metal contamination in the soils on Range 22. If the level of metal contamination in the soils at Range 22 is known then modification of testing to prevent any further contamination and/or the precise treatment of the soils can be executed to decontaminate the soil. Metal contamination in the soils at Range 22 was investigated. A total of 16 soil samples was taken in selective areas at Range 22. The soil samples were characterized in the chemical laboratory. The soil samples' pH and metal content were determined using instruments in the laboratory. The element of metal, amount of each metal, and the pH of each soil sample was found and compared to controls of similar soil texture for their contamination level. The results show that there is possible iron and aluminum contamination in some soils at Range 22. Further testing, such as, contour analysis and core soil testing will make it possible for conclusions to be drawn on metal contamination of soils at Range 22.

CONTENTS

INTRODUCTION	4
BACKGROUND	4
PROCEDURES	4
RESULTS	7
CONCLUSION	10
MISCELLANEOUS	11
ACKNOWLEDGMENTS	11
BIBLIOGRAPHY	13

INTRODUCTION

The characterization of the soils at Range 22 has not been accomplished. The purpose of my summer project was to accomplish this survey. Range 22 is the range located on the main base site. My project's results started a record of the metal content of the soils from Range 22. With these results and the results of further testing, the impact on the environment from the munitions testing will be known. With this information, efforts can be made to decrease human impact and decontaminating the range.

BACKGROUND

A broad range of metals has been used in testing at Range 22. Aluminum, brass, steel, tantalum, lead, and copper are some of the most commonly used metals. Many different metals were tested at the range during World War II. Almost any metal that has been used in weapons has been used at Range 22. A wide range of tests has taken place at Range 22. A wind tunnel, air guns, powder guns, light gas guns, nets to clear mines, B52 tests, fuse testing, and explosive sensitivity tests are some of the tests that have been conducted at Range 22. Since Range 22 has been exposed to so many different types of tests involving weapon systems and materials that may cause metal contamination, the chance of contamination is high.

"Life is vital to soil and soil is vital to life."(Louis M. Thompson and Frederick R. Troeh). Soil is essential for plant life in a natural environment. From the soil, plant roots get mechanical support, essential elements, water, and oxygen. Plants provide oxygen for animals and oxygen is critical to animals, consequently, soil is an essential part of natural life on this earth. Since soil is so important, it is necessary that the soil is maintained as a permanent, useful resource.

The military is taking part in trying to take care of this important resource. The characterization of the soils at a range was to find any contamination. If contamination is found proper actions will be taken toward solving the problem.

PROCEDURES

Range 22 was mapped out for soil sampling areas. The location from which each soil sample was taken is shown on the map of Range 22 in Figure 1. Each flag represents the location that the soil samples were taken from. Samples were taken randomly from target butt 413 and the concrete target butt next to the Ballistics Experimentation Facility(BEF). The target butts are where metal would first be deposited. Soil samples were also

taken from the wetlands approximately 120 ft north of target butt 413. Since shots are fired into the Choctawhatchee Bay, samples were taken along the shore of Choctawhatchee Bay at the range. Three samples were taken with a dredge from the creek located in the middle of the range. These samples were taken to analyze the migration of metal contaminants due to weather, wind, and other things that might disturb the soil. Two soil samples were taken from an undisturbed area that has similar soil texture to the soil from Range 22. One sample was taken from an undisturbed creek that had similar soil content as the creek located in the middle of Range 22. These controls were used to compare the normal pH level and metal content of this particular type of soil to the samples collected to determine contamination. Using a sterilized spatula for each sample, a 12 inch by 12 inch by 1 inch hole was dug. The soil was sifted with a USA standard testing sieve with an opening of 2 millimeters. All particles 2 millimeters or larger were not collected for sampling. The soil was then poured into plastic bags. We then labeled the soil sample bags by the location from which each soil sample was collected. The samples were then brought to the chemical laboratory for characterization.

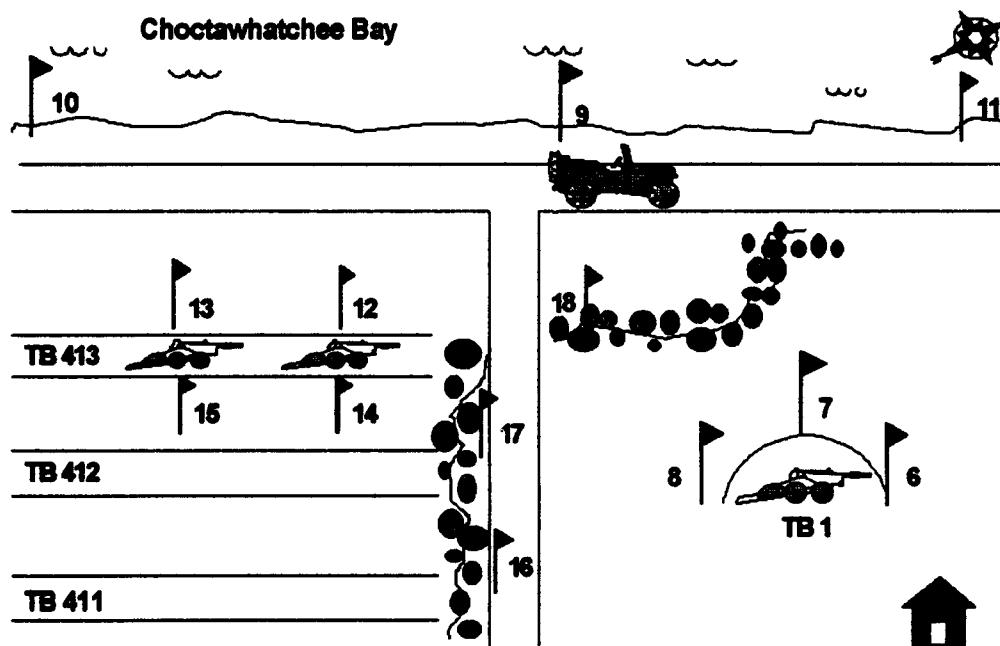


FIGURE 1

The samples collected at the creek and the wetlands northwest of target butt 413 had a large amount of moisture absorbed in the soil. These samples were dried in the sun so they would be ready for processing. All

samples were then evenly homogenized with a ball jar roller mill. Next 5 grams of each soil sample were weighed. The measured soil was poured into small spectra cups.

The first analysis was done using the Portable X-ray Fluorescence Spectrometer. The soil samples, as well as, 10 metal fragments that were randomly collected at Range 22 were analyzed using the Portable X-ray. This instrument uses two radioisotope sources, cadmium 109 and iron 55. These sources excite the electrons causing an electron displacement. The X-ray reads the displacement energy levels of each element peak. The Portable X-ray has the capability to simultaneously measures and analyzes 21 of the common alloying elements in a full range of Fe, Ni, Co, Cu, and Al based alloys in any size or shape material. Depending on the type of surface on the sample, the instrument will read the sample using two different settings: universal, for samples with rough or ridged surface, and special flat, for samples with a flat surface. Then the instrument prints out the percentage of each element present in the sample placed on the probe, with the exception of calcium, silicon, sulfur, potassium, carbon, hydrogen, and oxygen that can not be detected by the Portable X-ray. Although the instrument can not detect the element Aluminum, it will give you the nearest Aluminum alloy.

For the second test conducted, 10 grams of each soil sample was mixed with 10 milliliters of distilled water. Samples 17 and 18 absorbed the added distilled water. An extra 10 milliliters distilled water was added to these two samples. These mixtures were used for pH testing. The Expandable Ionalyzer 940 in its pH mode was used to find the pH level of each soil sample. The pH meter is calibrated with a standard that has a pH level of 7 and a standard with a pH of 10. The pH meter then automatically calculates the pH level of the samples.

To process the samples for analysis with the Inductively Coupled Plasma Spectrophotometer (ICP), 50 grams of each soil sample was weighed. Then 25 milliliters of distilled water and 25 milliliters nitric acid was added to the measured soil. An extra 50 milliliters, half distilled water and half nitric acid, were added to soil sample 16. The soil sample had absorbed most of the first 50 milliliters added to the soil. The samples and the nitric acid solutions digested for 42 days. Then the samples were filtered with number 2 qualitative filter paper. The filtered liquid was used for the ICP analysis.

The ICP works by comparing the wave length of light of a standard or known substance to the wave length of light of your sample. Using a standard or known substance you calibrate the ICP so it reads the

standard's element parts per million (ppm). The ICP uses the calibrated peak for reference to read the ppm of your sample.

RESULTS

The results from the Portable X-ray analysis of the fragments that were randomly collected from Range 22 are shown on Figure 2. As you can see there is a high percentage of copper (Cu) in fragments number 1, 4, 5, 7, and 8. There is almost 50 percent copper in fragment number 9. There is a high percentage of iron (Fe) in samples 2 and 3. There is a high percentage of lead (Pb) in sample 6. These metal fragments are where potential contamination begins. These results are helpful in telling what metals are in the fragments. The results would be more informative if the location from which each fragment was collected had been recorded and more fragments had been collected.

X-ray Analysis Of Fragments from Range 22						
Fragment	Cu (%)	Fe (%)	Mo (%)	Pb (%)	Ti (%)	Zn (%)
1	94.81	0.41			0.2	4.58
2	1.66	96.36	1.08		0.31	
3		97.02	1.36		0.24	
4	92.14					7.86
5	72.02	11.22		1.31		4.67
6	2.05			97.95		
7	74.01	0.34				25.25
8	94.53	0.41			0.22	4.84
9	49.87	0.56		2.68		4.16
10				99.05	0.95	

FIGURE 2

The results from the Portable X-ray analysis of the soil samples are shown on Figure 3. There is a higher percentage of iron in samples 16, 17, and, 18 than in the 3 control samples 19, 20, and 21. Samples 16, 17, and 18 were collected from the creek in the middle of Range 22. The Portable X-ray analysis results show possible iron contamination in the creek.

X-ray Analysis Of Soils from Range 22				
SAMPLE	Fe (%)	Sn (%)	Ti (%)	Zr (%)
6	0.3	0.19		
7			0.11	0.02
8			0.25	
9	1.84		0.73	0.07
10			0.13	
11				
12			0.28	0.03
13			0.26	
14			0.17	
15			0.18	
16	0.57	2.4	0.63	
17	3.07	1.08	0.23	
18	1.63		0.28	
19	0.4		0.13	0.02
20	0.35		0.25	0.02
21	0.33	1.11	0.28	

FIGURE 3

The results from the Inductively Coupled Plasma Spectrophotometer analysis is shown in Figure 4. There is a notably larger amount of aluminum and iron in samples 6, 9, 13, 16, 17, and 18. Samples 16, 17, and 18; which were collected from the creek in the middle of Range 22; and 9; which was collected from shore of Choctawhatchee Bay; have an extremely high aluminum and iron content compared to the controls. These results suggest possible iron contamination as does the Portable X-ray results. Due to the fact that Portable X-ray does not detect the element Aluminum, the ICP results for aluminum content can not be compared to the Portable X-ray results. The ICP results show possible aluminum contamination in some of the soils from Range 22.

ICP Analysis of Soils from Range 22			
SAMPLE	Al (ppm)	Fe (ppm)	
6	1580	140	
7	80	-	
8	600	-	
9	4700	2060	
10	680	-	
11	-	-	
12	840	-	
13	1280	40	
14	-	-	
15	-	-	
16	11760	2660	
17	4480	8720	
18	4620	3540	
19	-	-	
20	380	-	
21	840	-	

FIGURE 4

The results from the pH testing are shown on Figure 5. The controls have an average pH level of 5. Samples 6, 10, and 11 tested to be basic. All the other samples tested to be acetic, like the controls, but are more neutral than the normal average pH of these soils. Some possible reasons for the soils being more alkaline than the controls could be the introduction of new metals and their alkaline salts into the soil. The presence of salts from elements, such as, calcium, magnesium, and sodium carbonates would change the pH level of the soil to an alkaline level. These results are significant due to the fact that the more alkaline the soil is the more contaminants can leach further into the soil.

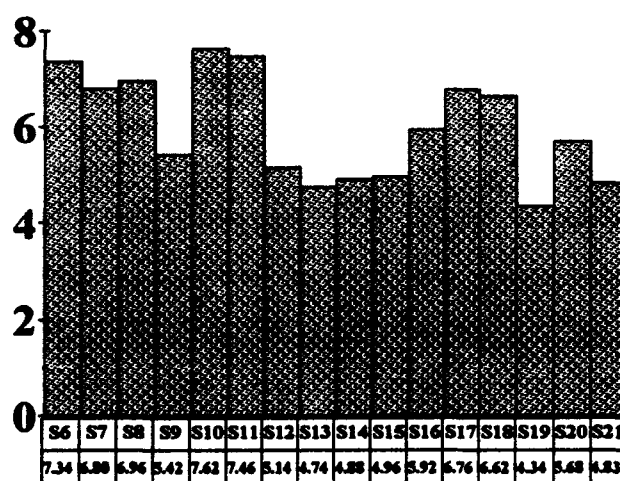


FIGURE 5

CONCLUSION

Further testing is needed before complete conclusions can be drawn on the contamination of the soils on Range 22. The results from the project show possible aluminum and iron contamination in the soils. To decide whether these metals are being introduced into the soils as a result of munitions firing, some other man made disturbance, or a natural disturbance still needs to be investigated further. Some other testing at Range 22 may include contour analysis and core soil testing. Contour analysis will show the boundaries of the contamination. This is done by collecting and analyzing soil samples collected over a large area surrounding the target butts. Core soil testing will show how deep into the earth the contamination has leached. This is done using a core soil sampler to take samples from layers in the earth. Then the samples are analyzed in the laboratory.

MISCELLANEOUS

In addition to conducting my project, I became familiar with the equipment in the chemical laboratory. I was involved in the reorganization of the chemical laboratory. The equipment and mechanical parts were organized into drawers according to similarity for their use. For proper organization of the supplies, I learned how each piece of equipment is used.

I was involved in an inventory of the chemicals in the chemical storage room and the chemistry laboratory. This job revealed the dangers of various chemicals and the proper disposal of hazardous chemicals. It was a great way to become familiar with the large amount of chemicals a chemical laboratory needs for experiments.

ACKNOWLEDGMENTS

Of course, none of this would have been possible without the help of others. I would like to send many thanks to my mentor, Mr. Luis Santana. He was always ready to help me in any way. I thank Mr. Ric Crews for all of his help and time. He was a great substitute mentor for the time Mr. Santana was on vacation. Lt. Noland conducted the ICP analysis and helped with other miscellaneous information. Along with everyone else in the High School Apprenticeship Program, I would like to thank Mr. Don Harrison. I really appreciate all the work and effort he put into this program to make it work. Mr. Michael Deiler was also very valuable in the running of this program. One person not to be forgotten is Mrs. Glenda Apel for all the typing and organizing she did for the program. Another person I would like to show gratitude to is Melissa Griffiths. It was great working with someone willing and ready to work. I was lucky enough to work with two great apprentices. I'd like to thank Mary Pletcher for her help as an fellow apprentice. I thank all of my branch. Everyone in the Envirionics Branch was ready to answer a question or lend a helping hand. I'd like to thank everyone for use of their computer. I would also like to thank the photo lab for their speed in which they developed our veiwwgraphs and for their full cooperation with photographs. I will again thank everyone who helped in anyway. Thanks for all the knowledge and good laughs.

BIBLIOGRAPHY

Thompson, L. M. and F. R. Troeh, "Soils and Soil Fertility," Fourth Edition, McGraw-Hill, Inc., 1978.

Lyon, T. L., H. O. Buckman, and N. C. Brady, "The Nature and Properties of Soils." The Macmillian Company, New York, 1950.

Donahue, R. L., J. C. Shickluna, and L. S. Robertson, "Soils: An Introduction to Soils and Plant Growth," Prentice-Hall, Inc., Englewood Cliffs, New Jersey, 1971, 1965, 1958.

AUTOMATED HISTOGRAM STATISTICS FOR SENSOR FUSION ANALYSIS

**Christie W. Gooden
High School Apprentice
Seeker Technology Evaluation Branch**

**Wright Laboratory Armament Directorate
WL/MNGI
Eglin AFB, FL 32542-5434**

**Final Report for:
High School Apprenticeship Program
Wright Laboratory Armament Directorate**

**Sponsored by:
Air Force Office of Scientific Research
Bolling Air Force Base, Washington D.C.**

August 1993

AUTOMATED HISTOGRAM FUNCTONS FOR SENSOR FUSION ANALYSIS

**Christie W. Gooden
High School Apprentice
Seeker Technology Evaluation Branch
WL/MNGI**

ABSTRACT

Currently, the data fusion work being done by WL/MNGI utilizes LADAR data obtained from the Submunition Guidance program. This display and image processing software provided with the data proved to be inadequate. The goal of this project was to provide histogram statistic capability for use with the data and display software. Initial software adaption produced approximately forty pages of output that then required 1 - 2 hours of manual analysis to extract the desired range of information per image. The output has reduced to 1-2 pages, and requires no perusal. To achieve this reduction of output, Pascal programming was reviewed and then used to modify an existing program. This improvement enables the user to receive the necessary data quickly.

AUTOMATED HISTOGRAM STATISTICS FOR SENSOR FUSION ANALYSIS

Christie W. Gooden

Introduction

To prepare for the future, the United States is taking its "smart" weapons, improving their capabilities and making them into "brilliant" weapons for the next generation of tactical warfare. These brilliant weapons will be completely automated so that the possibility of injury will be reduced for the aircraft operator and maximized for the target. To assist in this directive, research is being done to fuse the data of LADAR channels. Consequently, this process will upgrade existing target detection, and enhance the image processing ability of LADAR sensors.

Background

LADAR, or Laser RADAR, displays multiple channels of data. These channels are known as range, reflectivity (intensity), and doppler. Each one works independently of each other and as a result can be used without each other. This is due to the fact that each channel has its own primary purpose. The data of range is essentially used for the detection of ground targets that are of a considerable size. Intensity's data works to weed out the non-camouflaged, man-made items. Lastly, the data from the doppler channel displays kinetic information. The channels that the LADAR data fusion team are trying to bring together are the former two.

The fusion of range and reflectivity will bring about an enhanced image. Range shows the width, height and length of an object, and reflectivity can reveal the material of which an object is made. This aspect makes targets more discernible. Especially in the case of reflectivity. The intensity of the wave that bounces off an object changes with the composition of the object. For example, an unpainted tank would give off a

completely different wavelength than trees or grass would. The only problem with reflectivity data is that when it is used by itself recognizing and pointing out camouflaged targets is difficult. This is where range comes in. Because the data of range helps to detect the dimensions of an element, a camouflaged target can be flushed out. Consequently, this union would be most suited for ground mobile targets.

Procedure

Ideally, to write computer programs, one must know the language. The same is true for modifying a program. Thus, the first step taken in this venture proved to be research. The Pascal programming language is seen by many to be a stepping stone in learning other languages. It can be used as a learning tool or as an actual programming device. To begin this project research was done on Pascal and C, another programming language. C, which was not used initially, is the programming language used in the display program and the prime directive for the next step in this ongoing project. Due to Pascal's dual use, this language was incorporated first. Linked lists, pointers, and other program necessities were studied to give an overview of programming and finally a basic knowledge of the language.

The program's purpose was to produce numerical data of an image, giving the maximum and minimum range, maximum and minimum intensity and a list of the distribution of pixels. The only problem with this code was that the data was overwhelming in its size and required too much manual analysis to receive useful data. The data given could sometimes equal to forty pages, most of which was useless. The depth of the information warranted a compounding and simplification of the output.

Since the code was written in Pascal, alterations were not needed and perusal of the code began immediately. A week of research was given to learn the program and detail. In Pascal man-made variables and definitions are allowed, thus the language can be slightly altered. This causes difficulties, when one is modifying a program that is not

their own. After the study, remodeling began.

To remodel the code, two windows were run simultaneously, on Turbo Pascal 6.0. One window had the actual program, and the other contained tentative adjustments. The latter window was compiled and tested for errors, thoroughly before tried in the actual program. Running the code with the modifications, was the next step. Copies of the original program and changes made along the way were made for reference sake. The automated program was changed into a manual form in order to monitor the progress of the code. After two weeks of the trial and error process, the program was completely compiled, error-free, and most importantly, achieved the objective.

Result

The display of output shows only the usable data. The modifications of the program have lowered the number of allowable zeroes to three, therefore alleviating the problem of too many pages of unusable data. Instead of approximately forty pages of data per image, the reduced output is one to two pages. Also the man-in-the-loop analysis has been reduced from one hour to approximately two minutes. From an environmental standpoint, hundreds of trees were conserved.

Conclusions

The primary objective has been conquered. The next step will automate the entire process of obtaining and displaying the needed information. The cut on man hours will allow more time for actual research and less time for unnecessary analysis. C programming will need to be reviewed to carry on this process of automation.

ACKNOWLEDGEMENTS

Primarily, I would like to thank Emily Martinez, my mentor and friend. Without her, I would never have gotten through this summer or Pascal programming. Good luck on your thesis, Em. I know that your infinite wisdom will not go unnoticed. I would also like to acknowledge Emily's husband, Otto. Thanks for the laughs (you do a great impression of a fish). I will also like to thank the other apprentices for their companionship, and the good times that we had. I enjoyed everyone one of you. Christina, Jenny, Barry, Kyle, Nancy, Mary, Jon, Melissa, Jack, everyone: THANKS! I learned so much this summer and I am glad to have obtained this experience. I must thank God and my family for keeping me on the straight and narrow all these years. I am also very thankful for William A. Washington, Jr., who has given me strength, love, devotion and a hard time about everything. I can't wait until next year.

FACTORS INFLUENCING THE DEPOSITION OF POLYPYRROLE FILM

**Deanna Harrison
High School Apprentice
Fuzes Branch**

**Wright Laboratory Armament Directorate
WL/MNMF
Eglin AFB, FL 32542-5434**

**Final Report for:
High School Apprenticeship Program
Wright Laboratory Armament Directorate**

**Sponsored by:
Air Force Office of Scientific Research
Bolling Air Force Base, Washington, D.C.**

August 1993

FACTORS INFLUENCING THE DEPOSITION OF POLYPYRROLE FILMS

Deanna Harrison
High School Apprentice
Fuzes Branch
Wright Laboratory Armament Directorate

Abstract

Most polymers are insulators, such as plastics, but a few that have been recently developed are conductive. There has been a great deal of experimentation done with conductive polymers, and in many cases important factors have been ignored or left unreported. Since this is a fairly new field of study, many factors that affect the quality of the films are still unknown. If all of the factors that influence film deposition are not analyzed, data gathered in experimentation can be deceiving. Each factor must be identified and studied in order to attain accurate and consistent results. The purpose of this project was to determine what factors influence the quality of polypyrrole films and how each factor affects them.

FACTORS INFLUENCING THE QUALITY OF POLYPYRROLE FILMS

Deanna Harrison

INTRODUCTION

Most polymers are insulators, such as plastics, but a few that have been recently developed are conductive. In the past few years there has been much research done on conductive polymers because of their many practical applications. They can be used to make rechargeable batteries that do not work by chemical reactions. This process eliminates the problem of corrosion. Smart windows are another recent development in which conductive polymers are used to block out sunlight and heat by turning opaque. This reaction is triggered as light or heat passed through the windows. Double layer capacitors can also be made using conductive polymer films as electrodes [1]. These films can be used with nonaqueous electrolytes and can sustain higher voltages than other materials commonly used in capacitors [2].

There are some significant advantages to using conductive polymers instead of metals. They are very light weight and relatively easy to make. It is also possible to alter their physical and electrical properties by changing the conditions at which the polymer films are deposited [3-5].

DISCUSSION OF PROBLEM

There has been a great deal of experimentation done with conductive polymers, and in many cases important factors have been ignored or left unreported. Since this is a fairly new field of study, many factors that

affect the quality of the films are still unknown. If all of the factors that influence film deposition are not analyzed, data gathered in experimentation can be deceiving. Each factor must be identified and studied in order to attain accurate and consistent results. The purpose of this project was to determine what factors influence the quality of polypyrrole films and how each factor affects them.

METHODOLOGY

By analyzing the results of previous research, eight factors were chosen to be tested for their effects on the quality of polypyrrole. There may be additional factors which have not yet been identified, and future research can be done to search for any other conditions which might affect the deposition of the films. The eight factors that were studied in my project were: dopant, molarity, current density, deposition time, substrate electrode material/quality, anode-to-cathode spacing, temperature, and agitation.

The quality of electrodeposited polypyrrole film material depends greatly on what dopant is used. To analyze this factor, different dopants have been tested. Ammonium chloride was the main dopant that we compared to dodecylbenzenesulfonate (DBS). In the remainder of the experimentation, DBS was used as a controlled dopant.

The molarity of the polymer and the dopant present in the deposition solution also could be a factor, but past research has not shown a noticeable difference in film quality as the molarities of the chemicals are varied. In all previous experiments, 0.05 MPPY and 0.05 M DBS were used. DBS molarities of 0.1, 0.15, and 0.2 were tested and no significant differences in film quality or conductivity resulted.

From experience, as well as from other research, it has been

determined that current density plays a crucial role in determining the quality of polypyrrole films. To find the ideal situation, various current densities were tested. In solutions that contained different dopants, or in solutions that contained different molarities of a dopant, the voltage required to achieve a desired current density would vary.

Another factor that influenced the quality of the films was the time period over which deposition occurred. Film thickness varies directly with the deposition time allowed. The deposition time allowed should depend at least partly upon what the films are to be used for. If a more durable film is desired, a longer deposition time would be beneficial.

The type of electrodes used in the deposition of polypyrrole films can also affect their quality. In some chemicals, certain types of electrodes can corrode, causing the solution to be contaminated. If the electrodes are not polished, abrasions on the surface can cause flaws in the polymer film. Many types of electrodes were tested, including nickel, zirconium, and stainless steel. Different thicknesses of these metals were also tried.

Not only is the type of electrode important, but the distance between electrodes is also a significant factor affecting the quality of polypyrrole films. Various anode-to-cathode spacings were tested, but more experimentation could be done in this area to determine the exact limitation on how small the spacing can be without degrading film quality. Temperature has also been found to affect film quality. There are two different ways of altering film texture and conductivity using temperature. The solution can be exposed to various temperatures during deposition, or the film can be aged at different temperatures to alter physical and electronic characteristics of the film. A temperature chamber was used to perform

both types of tests. The freezing point of the PPY/DBS solution had to be found before any tests were done at low temperatures. Films were deposited slightly above the freezing point at 7° C, and at temperatures of 23°C, 39°C, 60°C, 80°C, and 100°C.

Films that had been previously made were heated to temperatures of 180° C.

The last factor that was determined to influence the quality of polypyrrole films was agitation. Depositions were done using a magnetic stirrer and an ultrasonic cleaner.

RESULTS

It was found that use of ammonium chloride as a dopant in a PPY deposition solution results in poor quality film and is not very useful alone. This process does enhance surface area, however, and can be used to deposit textured PPY material on a smooth PPY/DBS film which has been prepared beforehand. DBS is perhaps the best dopant for optimum film strength and flexibility. As the dopant molarities were altered within the range of 0.05 to 0.2, no significant differences in film quality or conductivity were observed.

A current density of 1 mA/cm² was found to be ideal for creating a film with optimum qualities. Significantly higher current densities cause films to have increased surface area, but increased brittleness as well. There is no increase in conductivity, either, which previous research has shown [6]. Polypyrrole films made at significantly lower current densities are too thin and tear easily. Therefore, in the ideal setting, a current (in mA) used should be equal to the area of the surface being coated on the electrode. The thickness of deposited polypyrrole film material also depends on the time period of the deposition. A time period of one hour generally seems to produce good quality films. Of course, if a thicker

film is desired, the time period must be increased.

In aqueous PPY/DBS deposition solution, nickel and stainless steel electrodes work well. Zirconium electrodes will allow a PPY/DBS film to be formed on them, but what results is of substandard quality. In a polypyrrole solution doped with ammonium chloride, any exposed areas of nickel or stainless steel substrate electrode material may corrode during deposition and contaminate the deposition bath. The only electrochemically stable electrode that we found suitable for this type of electrodeposition treatment is indium tin oxide coated glass. It is also beneficial that such substrate material is highly polished and much smoother than metal sheet material. Resulting film quality is generally better if polished electrodes are used, or if a new electrode is used for each deposition. New stainless steel sheet electrodes were used in all of the other experiments to help control the effects of substrate surface abnormalities.

It was also found that anode-to-cathode spacing of 8 cm and 15 cm promote growth of good quality films. Electrode spacings of less than 4 cm inhibits the deposition of the film, significantly lowering film quality. The limitation on how far apart the electrodes can be is a topic for further research.

It was found that increasing the temperature during deposition increased surface area, and in some cases slightly increased conductivity. The film grown at 40°C was slightly textured in certain areas. The films grown at 60°C and 100°C started to wrinkle as they detach themselves from the substrate. These films were relatively smooth, with the exception of the wrinkles. The film deposited at 80°C had a very fine, even texture. This film was examined using a scanning electron microscope (SEM), which revealed a cauliflower surface structure (see figures 1 & 2). A film was

also made at 7°C, which is slightly higher than the freezing point of the PPY/DBS solution. This produced a good quality smooth film with a slightly higher conductivity than the film deposited at 23°C (room temperature) in the same controlled temperature chamber (see figure 3). The conductivities of these films were good compared to reported conductivities of polypyrrole films (see figure 4). Films were also placed in the temperature chamber after they had been made. This slightly increased conductivity of the films and seemed to make them more flexible. However, the films wrinkled up, especially when they had been removed from the electrodes prior to heating.

Agitation was also found to affect the quality of polypyrrole films. The films subject to the turbulence of a magnetic stirrer had flaws which caused them to tear easily. In the first experiment with ultrasonic agitation, the ultrasonic device overheated after 30 minutes. This film was very textured, and fairly flexible. However, it was postulated that the heat alone could have been responsible for the marked increase in texture. This was proved by repeating the experiment using water to keep the ultrasonic bath from overheating and maintain the solution much closer to room temperature. The film was smooth and flexible. The experiment was repeated once more, using ice water to cool the solution. Although it began to wrinkle and detach itself from the substrate electrode, this film was also quite smooth and confirmed the hypothesis that temperature affects PPY film growth considerably more than ultrasonic vibration does.

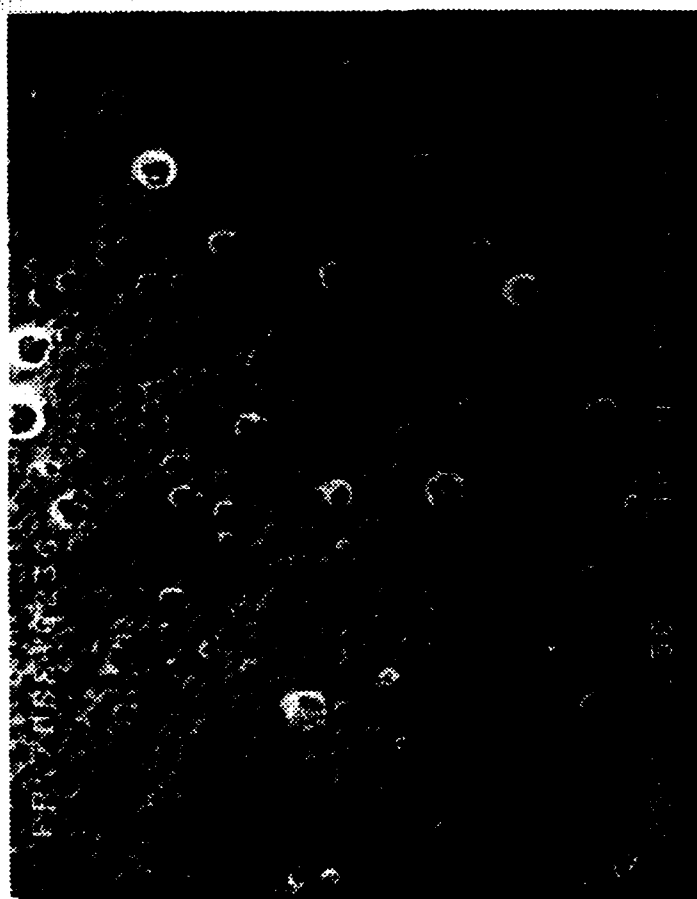
CONCLUSION

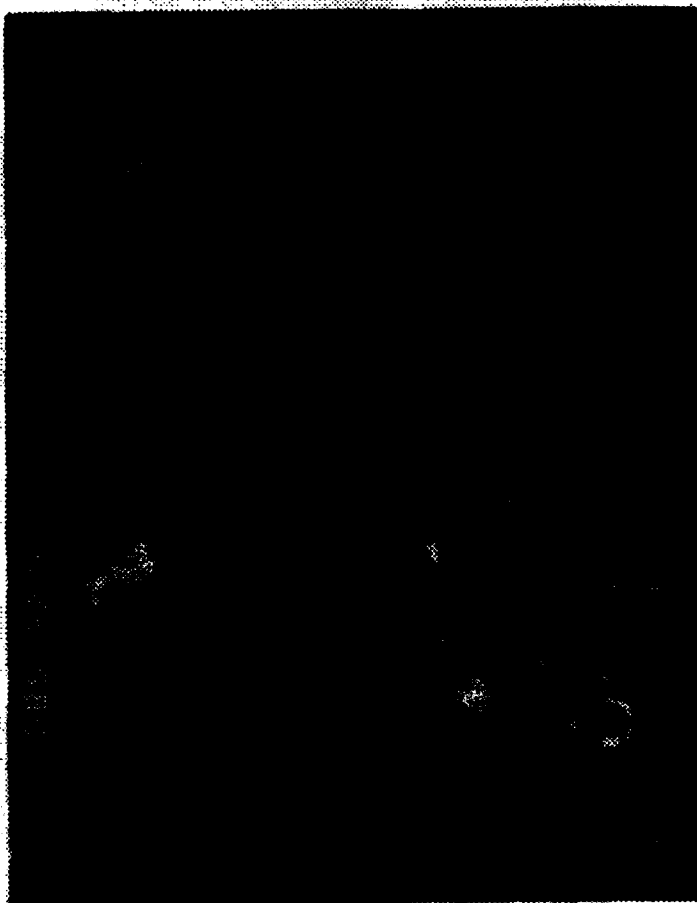
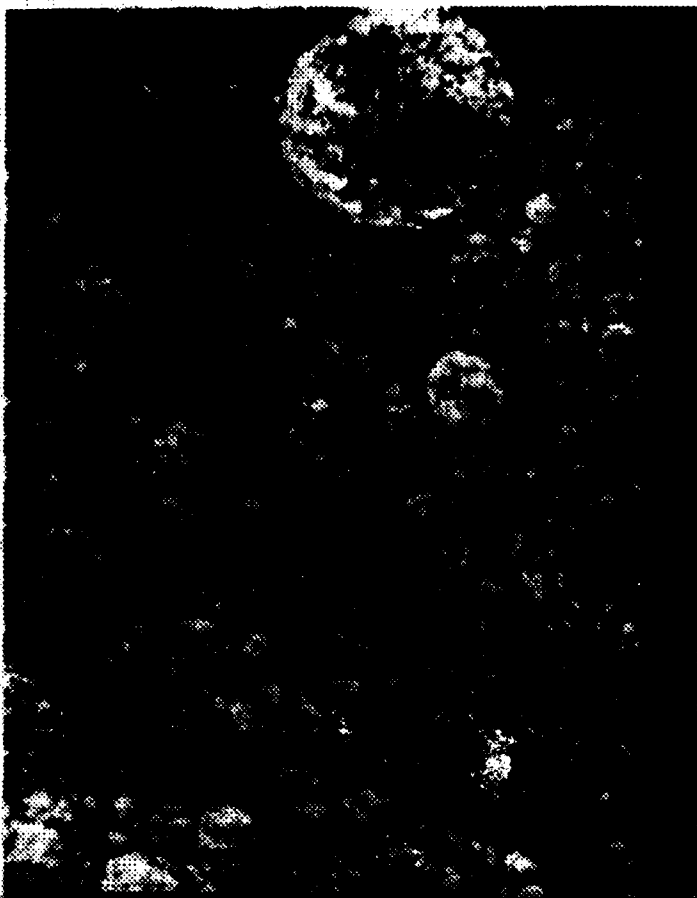
If high surface area films can be made using higher temperatures, coating films with textured material deposited from PPY/ammonium chloride solution may be unnecessary. Since factors such as the temperature of the

room can affect the quality of the films produced, the researcher must be careful to keep a controlled environment. One must remain aware of all the factors that can influence the growth of polypyrrole films in order to keep the experimental environment constant.

REFERENCES

1. M.G. Kanatzidis, "Conductive Polymers," Chemical and Engineering News, Dec. 3, 1990.
2. S. DiStefano, "Conducting Polymers for Thermoplastic Electrodes," JPI Task Plan No. 80-3201, Air Force Armament Laboratory, August 1991.
3. Same as above
4. D. Harrison, "High Surface Area Conductive Polymers," High School Apprenticeship Program Final Report, August 1992 (Wright Laboratory Armament Directorate, Eglin AFB, FL) p.18-1 to 18-6.
5. D. Finello, D. Harrison, R. K. Bunting, "High Surface Area Conductive Polymers." From: Proceedings of the 2nd International Seminar on Double Layer Capacitors and Similar Energy Storage Devices, December 1992.
6. R. C. D. Peres, J.M. Pernaut, and Marco-a. De Paoli, "Polypyrrole/Dodecylsulfonate: Effects of Different Synthesis Conditions," Journal of Polymer Science: Part A: Polymer Chemistry, Vol. 29, 1991.

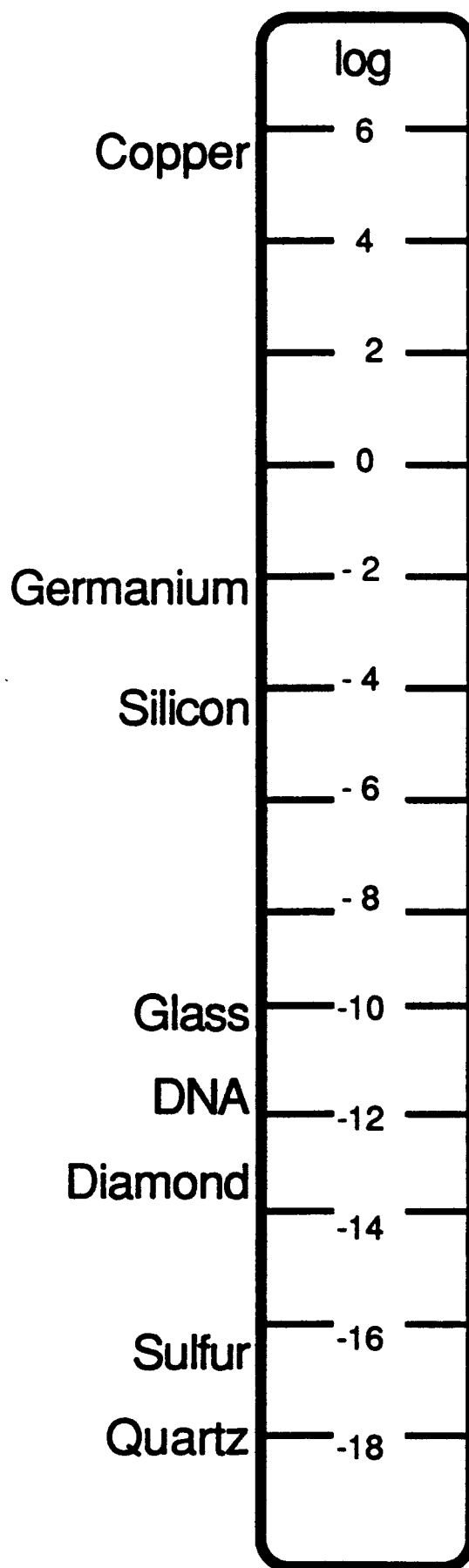
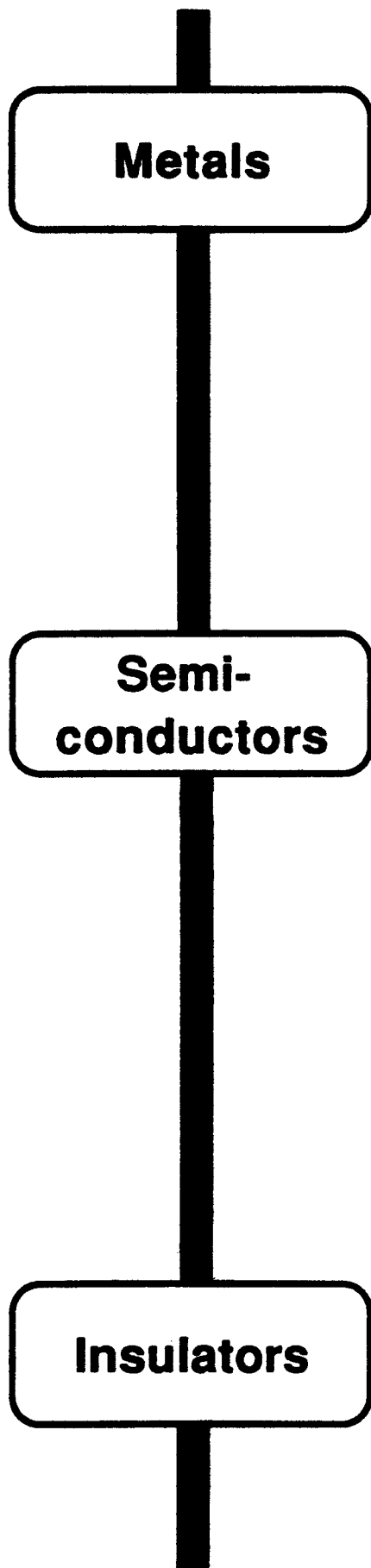




31-12

Characteristics of PPY/DBS Films Deposited On Stainless Steel Electrodes

Temperature	Texture	Conductivity (S)
7 C	smooth	67
23 C	smooth	16
40 C	slightly textured in certain areas	38
60 C	detached from electrode	89
80 C	fine texture	89
100 C	detached from electrode	38



Polypyrrole

HIGH SURFACE AREA CONDUCTIVE POLYMER FILMS
USING AN AMMONIUM CHLORIDE AQUEOUS SOLUTION

Laura Hemmer
High School Apprentice
Fuzes Branch

Wright Laboratory Armament Directorate
WL/MNMF
Eglin AFB, FL 32542-5434

Final Report for:
High School Apprentice Program
Wright Laboratory Armament Directorate

Sponsored by:
Air Force Office of Scientific Research
Bolling Air Force Base, Washington, D.C.

August 1993

HIGH SURFACE AREA CONDUCTIVE POLYMER FILMS
USING AN AMMONIUM CHLORIDE AQUEOUS SOLUTION

Laura Hemmer
High School Apprentice
Fuzes Branch
Wright Laboratory Armament Directorate

Abstract

In recent years, researchers have found numerous applications for conductive polymers. For example, polymer films can serve as electrodes in capacitors [1].

The goal of this project was to increase the surface area of conductive polymer electrodes thereby increasing their capacitance. The method tested was to increase surface area by coating polymer electrodes of dodecylbenzenesulfonate (DBS) doped polypyrrole (PPY) with chlorine doped polypyrrole electrodeposited from an ammonium chloride (NH_4Cl) aqueous solution (Figure 1.)

4

These textured polymer electrodes were then used to make a double layer capacitor [2].

HIGH SURFACE AREA CONDUCTIVE POLYMER FILMS
USING AN AMMONIUM CHLORIDE AQUEOUS SOLUTION

Laura Hemmer

INTRODUCTION

Conductive polymers have become a growing interest for scientists in recent years. Many experiments have been undertaken to determine uses for these "organic metals." Past work has determined that conductive polymers have numerous applications. They can be fabricated into rechargeable batteries or serve as electrodes in capacitors. Conductive polymers are even used in "smart windows," which are light sensitive devices. Their versatile nature has opened up many new possibilities [1].

DISCUSSION OF PROBLEM

One way to increase the capacitance of a double layer capacitor is to increase the surface area of the electrodes. This creates more interaction along the interface between the electrolyte and the electrodes. The objective of this project was to make high surface area conductive polymer electrodes to be used in a double layer capacitor. This was done by coating base polymer films with a textured layer of chlorine doped PPY grown from an aqueous ammonium chloride solution. Other methods of making high surface area films, such as pulsing the deposition current, have been explored but none of the results have been quantified in terms of capacitor performance [3].

METHODOLOGY

The first step in this experiment was to make base polymer films. Two 8x15cm electrodes were placed 15cm apart in a 17x12x8cm container (Figure 2.) Stainless steel electrodes were used for the majority of the experimentation. However nickel, zirconium, and indium tin oxide coated glass were also tested. The indium tin oxide glass electrodes were made using standard microscope slides (7.5 x 2.5 cm.) One liter of a solution of 0.05 M PPY mixed with 0.05 M DBS was used to electrochemically deposit a conductive PPY film onto the anode (Figure 1.) For the deposition a current density of 1 mA/cm² was used for one hour. These conditions were found to produce good quality PPY films.

A solution of 0.05 M PPY and 0.05 M NH₄Cl could then be used to deposit a textured layer of chlorine doped PPY onto the base polymer film (Figure 1.) Again, two 8x15cm electrodes were placed in a 17x12x8cm container 15cm apart (Figure 2.) Nickel, stainless steel, zirconium, and indium tin oxide glass electrodes were all tested with the ammonium chloride solution. Indium tin oxide glass electrodes produced the best quality films and were the only electrodes which showed no evidence of deterioration in the ammonium chloride solution. One liter of the solution was used for the deposition while the length of the deposition was reduced to 45 minutes. The current used in this stage of the experiment was varied to determine the level of current which produced high surface area films with good quality. Agita-

tion was also experimented with to evaluate its effect on textured film growth.

Following the ammonium chloride deposition, the films were then tested on the four point probe to measure resistance. Film sheet resistance was displayed by a Precision LCR Meter in order to calculate the resistivity and the conductivity of the PPY film for each experiment unless precluded by extreme surface roughness.

Two double layer capacitors were then made, one using two textured PPY films as electrodes and the other using base polymer electrodes. The electrolyte in these capacitors was created using strips of Whatman filter paper soaked in a solution of nitromethane and potassium iodide at approximately half the solubility limit [4,5]. Once the capacitors were constructed, they were charged for several minutes and the steady state voltage (V) was measured by an multimeter. A coulometer was then used to measure the charge (Q) stored in the capacitors. Following voltage and charge measurements, the capacitance (C) of the capacitors could be calculated using the equation $C=Q/V$ [6]. Since surface area is directly proportional to capacitance, comparison of the calculations would be indicative of the increase in surface area [7].

RESULTS

Optimum deposition parameters were determined for the depo-

sition of chlorine doped PPY from an ammonium chloride solution. Three main variables were tested: the effects of agitation, current density, and the type of electrode used. After much experimentation it was determined that agitation of the solution decreased the film quality. Agitation also caused uneven coating of the base PPY films.

In order to study the effects of changing the current density, the size of the film was kept constant while the current was changed. The currents tested ranged from 5 - 45mA. However, the most textured films were made at 30 - 35mA (0.87 mA/cm^2). High resolution (1500x) scanning electron micrographs of the most textured film material and the base film material are compared in Figures 3 and 4.

Four different types of electrodes were tested in this project. Both nickel and zirconium electrodes could be used in the PPY/DBS depositions but they proved to be electrochemically unstable during the PPY/NH Cl depositions. Stainless steel electrodes also exhibited deterioration during deposition but to a much lesser extent. The indium tin oxide glass electrodes proved to be the best for this study. The films deposited on these electrodes were better quality and had more texture than the films made on the other electrodes. Also, the indium tin oxide glass showed no evidence of corrosion during PPY deposition in the ammonium chloride solution. These results provide the best known conditions for textured PPY film depositions.

The textured PPY films were then used as electrodes to construct a double layer capacitor. The double layer capacitor with chlorine doped PPY electrodes was successfully charged to 0.5 volt with 2.92×10^{-2} coulomb while the one using base PPY electrodes could only store 1.0×10^{-7} coulomb when given the same source voltage. The capacitance of the double layer capacitor using textured PPY electrodes was 5.84×10^{-2} farad while the capacitor made from base PPY electrodes had only 2.0×10^{-7} farad. Because surface area is directly proportional to capacitance, it can be deduced that the surface area was much greater for the electrodes made of chlorine doped PPY films [7]. The large increase in measured capacitance indicates that the surface area can readily be increased by a factor of almost 3×10^5 through surface texture enhancement.

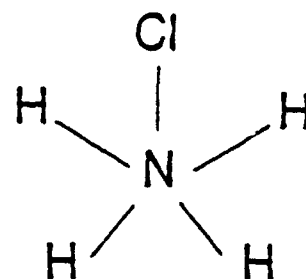
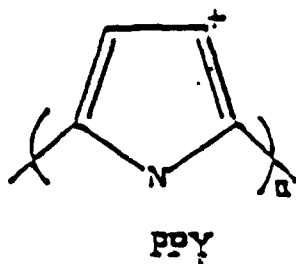
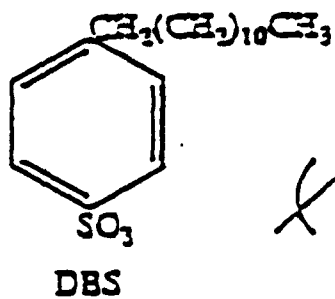
CONCLUSION

The goal of this project was to make high surface area conductive PPY films by coating base films with a layer of textured PPY material from an aqueous mixture of ammonium chloride and PPY. Through experiment, improved conditions for making textured PPY films were determined. These conditions were used to produce high surface area conductive polymer films. After textured PPY films were made, they were used as electrodes to make a double layer capacitor. The measured capacitances were indicative of the surface area of the PPY films. The results

substantiated the hypothesis that coating base PPY films with chlorine doped PPY will increase the surface area thereby increasing the capacitance.

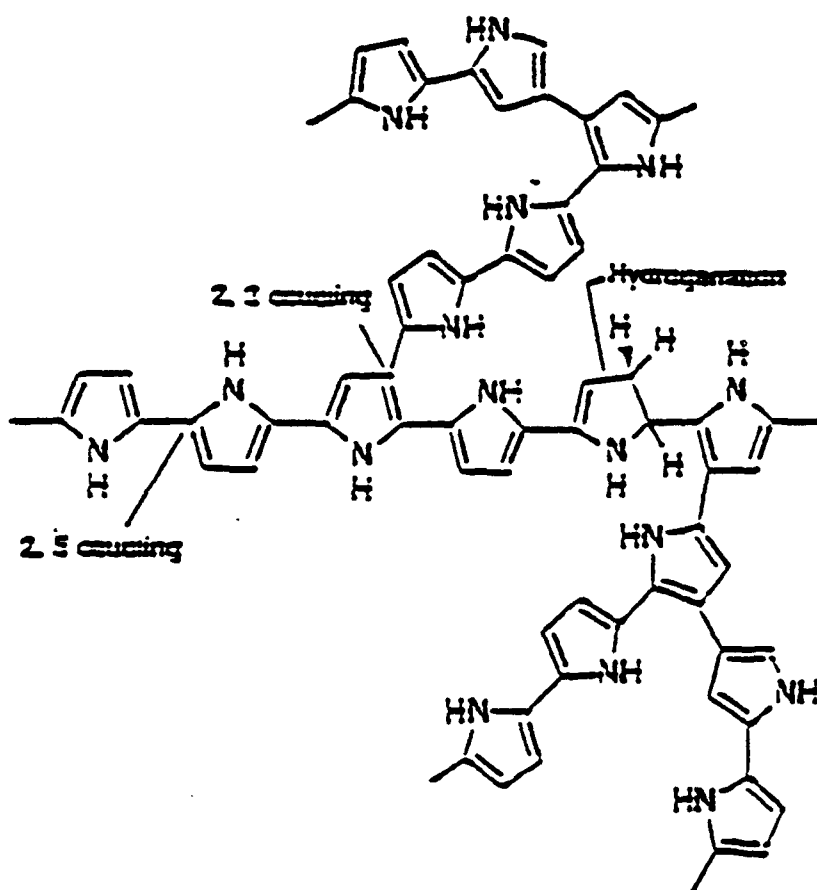
REFERENCES

1. M.G. Kanatzidis, "Conductive Polymers," Chemical and Engineering News, Dec. 3, 1990.
2. D. Finello, "Solid Laminated Double Layer Capacitor," AFATL-TR-90-72, Air Force Armament Laboratory, July 1990.
3. D. Harrison, "High Surface Area Conductive Polymers," High School Apprenticeship Program Final Report, August 1992 (Wright Laboratory Armament Directorate, Eglin AFB, FL).
4. D.J. Anderson, General Review of Electrolytes, J. Electrochemical Society, 1977. 124: pp. 401c-409c.
5. H.B. Oakley and J.C. Philip, Conductivity and Ionization of Solutions of Potassium Iodide in Nitromethane, J. Chemical Society, 1924. 125: pp. 1189-1195.
6. M.E. Van Valkenburg, Network Analysis, Prentice-Hall, Inc., Englewood Cliffs, New Jersey, 1974. pp. 7-19.
7. V. Del Toro, Principles of Electrical Engineering, Prentice-Hall, Inc., Englewood Cliffs, New Jersey, 1972. pp.41.



Chemical structure of polypyrrole PPY with dodecylbenzenesulfonate DBS counterion

Ammonium Chloride



Proposed disordered structural model for polypyrrole

DEPOSITION OF PPY

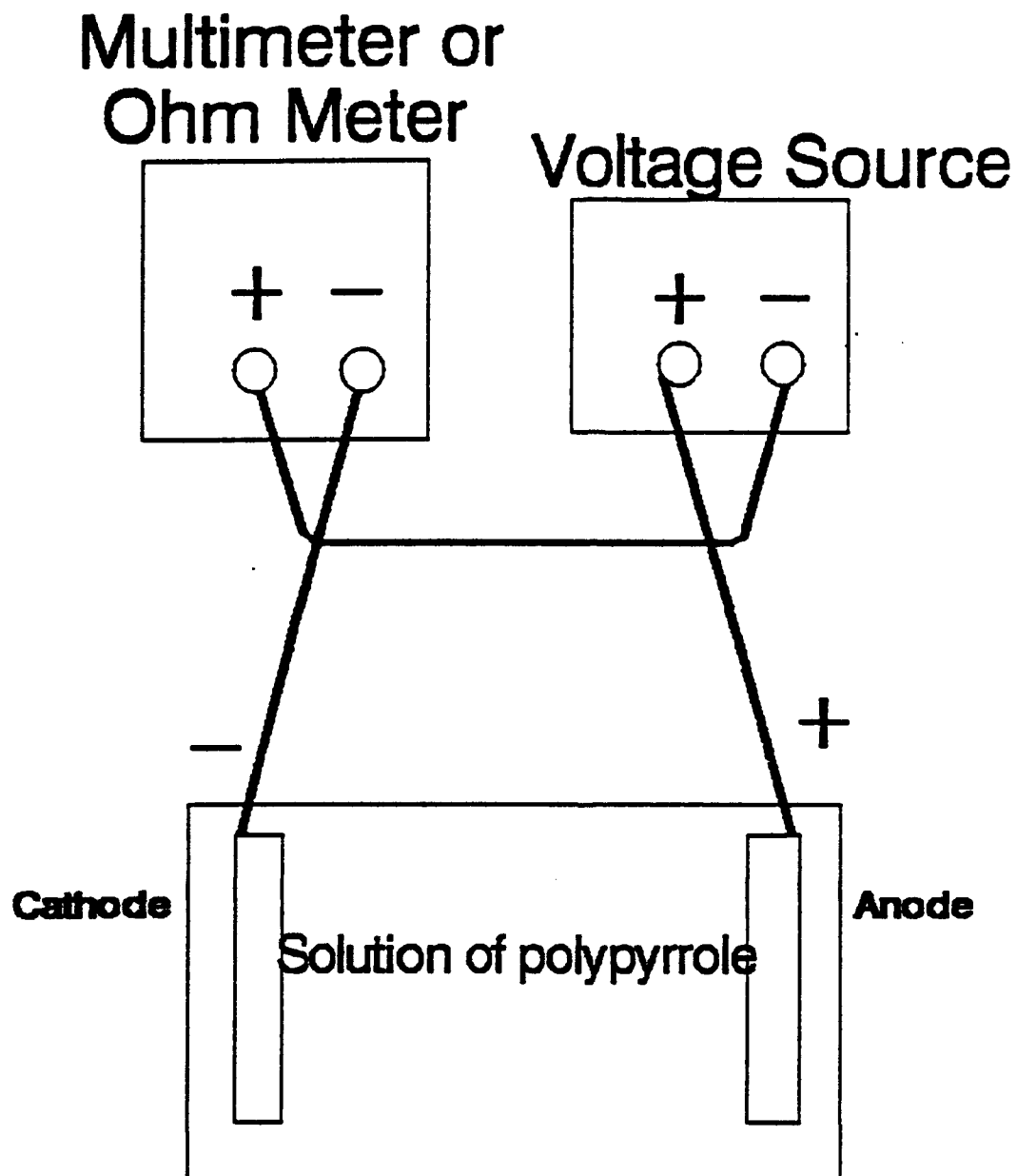
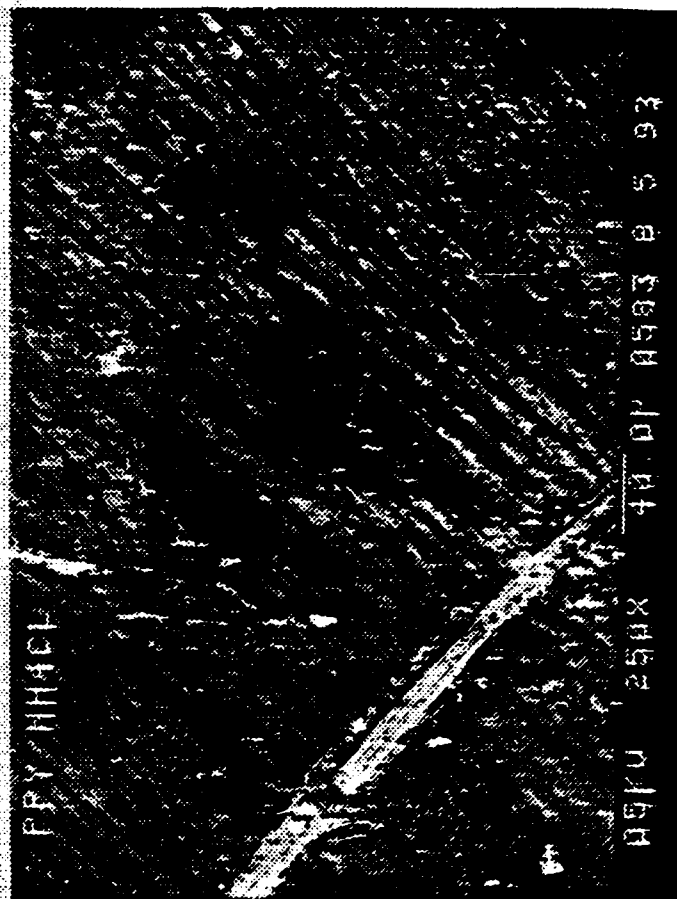
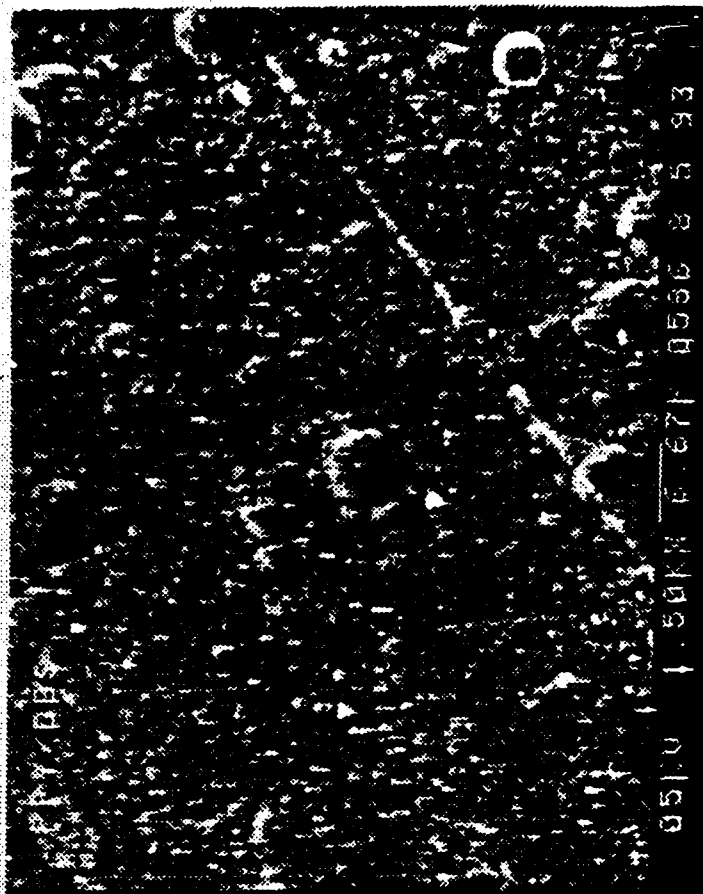
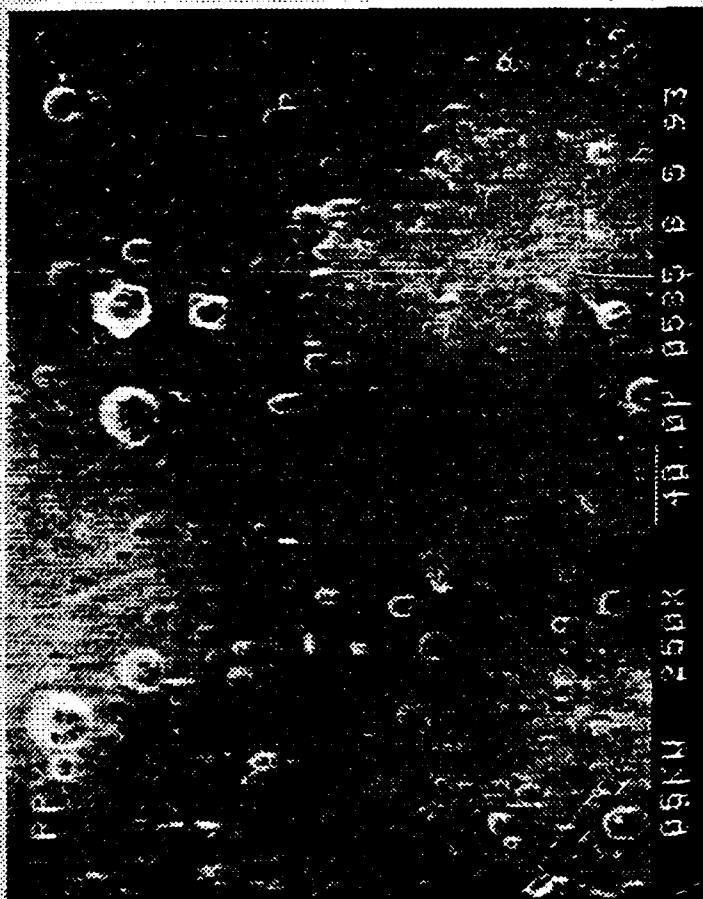


FIGURE 2



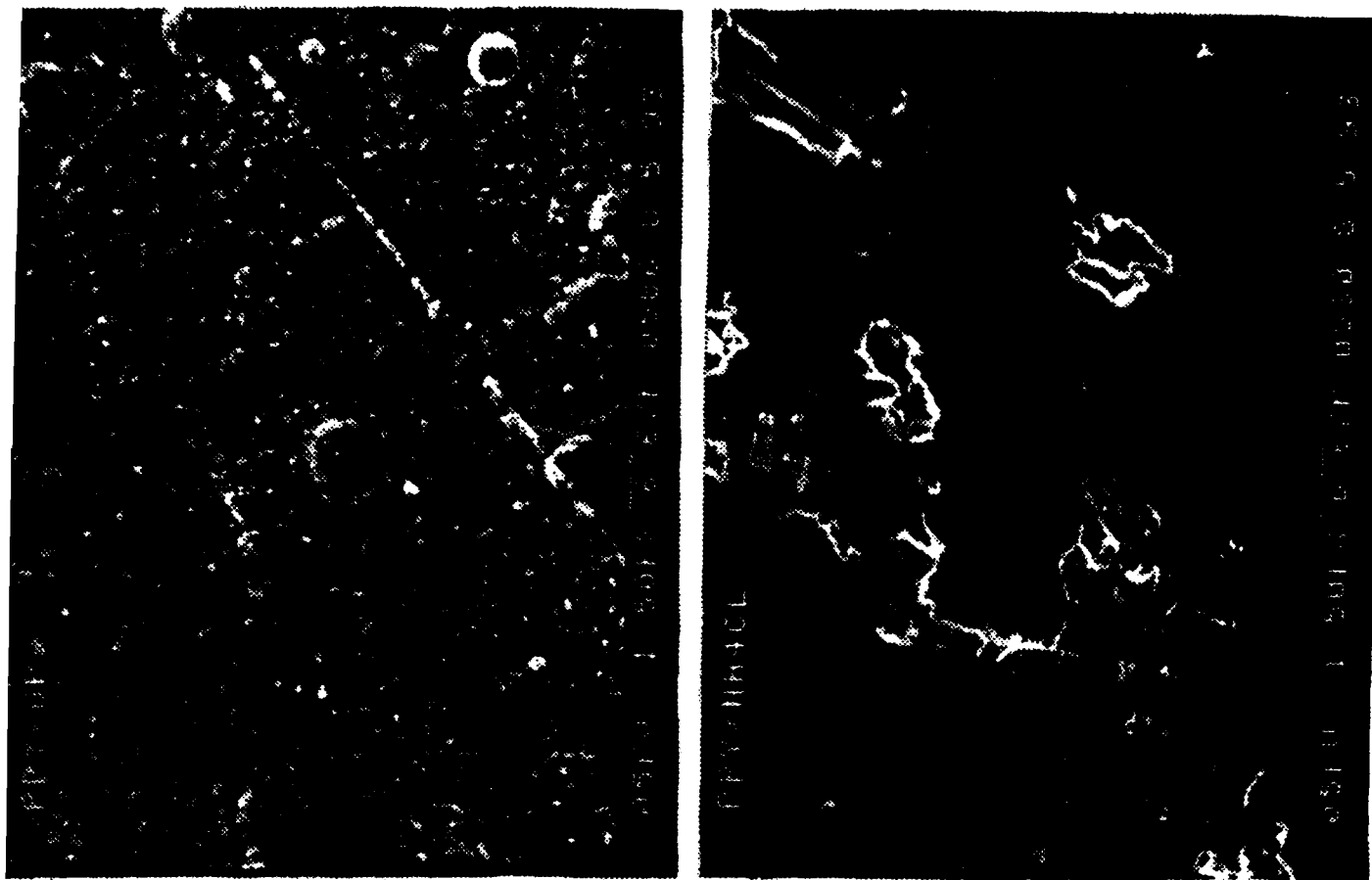


FIGURE 4

**USING NEURAL NETWORKS FOR THE DETECTION OF POTENTIAL
TARGETS IN AN IMAGE SEGMENTED BY FRACTAL DIMENSION**

Mark E. Jeffcoat

High School Apprentice

Advanced Guidance Branch

Wright Laboratory Armament Directorate

WL/MNGA

Eglin AFB, Florida 32542-5434

Final Report for:

High School Apprenticeship Program

Wright Laboratory Armament Directorate

Sponsored by:

Air Force Office of Scientific Research

Bolling Air Force Base, Washington, D. C.

USING NEURAL NETWORKS FOR THE DETECTION OF POTENTIAL TARGETS IN AN IMAGE SEGMENTED BY FRACTAL DIMENSION

Mark E. Jeffcoat

High School Apprentice

Advanced Guidance Branch

Abstract

This paper discusses the use of neural networks to detect potential targets within an image, specifically one from the Advanced Technology LAdar (Laser Detection and Ranging) System (ATLAS) program. The ATLAS sensors include a Ladar beam and an infrared sensor. This research included only the active (range) and passive (infrared) sensor data. A neural net removed defects from the active images, caused by atmospheric interference with the Ladar beam (not present in the passive images). A neural net separated an image into road, building, and natural pixels, given both the original and fractal dimension data, with very few unknowns or errors.

Introduction

A goals of image processing, especially for military applications, is to develop methods to identify points of interest within an image without human assistance. The use of computers to detect targets can result in improvements in speed and accuracy. The first objective of the research was to evaluate the usefulness of fractal dimension data in detecting targets within an image. If the fractal algorithm is successful, then the second objective was to find an automated technique to apply the fractal data toward detecting potential targets.

Apparatus

A Sun SPARCstation 1 workstation, with occasional assistance (over an Ethernet network) from a SPARCServer MP690, provided the processing power necessary to execute the fractal dimension algorithm. Khoros, an image processing package from the University of New Mexico, assisted in routine manipulation of the sample images and provided useful image manipulation routines, which could be easily called from the C programming language.

Background

Fractal geometry deals with shapes difficult to describe in traditional topological terms. Mathematical fractals often exhibit properties such as infinite surface area or perimeter. The normal topological concept of dimension fails to properly describe such a shape. The quantity of fractal dimension gives a more accurate description of a fractal shape, and will generally be a higher number than the topological dimension. Natural shapes, often highly fractal, should have

a higher fractal dimension than a man-made shape. Ideally, this difference would allow the segmentation of images based solely on fractal dimension. Reality is not quite as consistent. {1}

The Hurst Dimensional Estimate finds an approximation of the fractal dimension (D) of an object by examining an image over various areas to find the degree of variation in an area: a fractal shape should vary to a much higher degree than a non-fractal. In equation (1), the function M is defined at each sub-area A. R is the resolution of the image inside the sub-area. K is a constant.

$$M(A,R) = K * R^{D-1} \quad (1)$$

M(A,R) can be found by equation (2). The maximum and minimum pixel values from each sub-area are subtracted and summed.

$$M(A,R) = \sum_i (Max[A_i] - Min[A_i]) \quad (2)$$

Taking the natural log of each side in (1), and then taking the partial derivative of equation (3) with respect to ln R, (D-1) appears; the constant disappears. (4)

$$\ln M(A,R) = (D-1) * \ln R + \ln K \quad (3)$$

$$\frac{\delta \ln M(A,R)}{\delta \ln R} = D - 1 \quad (4)$$

A log-log plot of M versus R is a line. (D-1) is the slope. {2}

A neural network is a method of arriving at a solution of a problem without standard algorithmic procedures. A neural network has at least three layers: input, processing (the "hidden" layer), and output. Each layer consists of nodes in which data is processed. Each internode connection has a numerical weight associated with it, which adjusts to a specific set of problems during the training of the network. There may be multiple hidden layers. The training can be supervised or unsupervised. The output from a supervised network is an evaluation of the conformity of the input to the possible categories of output, defined by the training. In supervised training, the network receives both sample data from each solution category and the correct answer. The network weights are adjusted until its answers match the given solutions and it can predict in which category to place new input. {3}

In both preprocessing and detection, a backward error propagation learning style was used. In training, the comparison of the computed classification to the given classification determines the error. The error is used to calculate the correction for the weights. The error backpropagates through the network, adjusting the weights. {3}

The data used was from the Advanced Technology Ladar (Laser Detection and Ranging) System (ATLAS) program, which combines Ladar and infrared sensors. Ladar is an active sensor that uses short wavelength laser beams to determine range and intensity. This paper deals primarily with the range and infrared data.

When the laser beam leaves the aircraft, it will usually travel down to the ground and reflect back toward the Ladar. Some of the beam's intensity is lost through atmospheric attenuation, but, in most cases, the beam will return to the sensor. If the beam strikes water, it will be reflected off away from the sensor. The only return will be some small

portion that struck something in the air and came back. This results in a random distribution of range values over water, leading to interesting fractal effects. Also, when the laser beam either does not return in time or too little returns, the pixel at that location receives a value of zero; that location is a "dropout." (Note that both of the above phenomena will only occur in the active data.) Preprocessing is necessary. [4]

Methodology

Lt. Matthew Whiteley provided two images from the ATLAS data, each of which contained active and passive data. The first was an image of an Astros mobile missile launcher (foreign), with few surrounding terrain features, and no outstanding natural objects to compare to. The second was an image taken from the local area, containing a building adjacent to water, with a road leading up to it and piers jutting out into the water. Trees cover the rest of the image.

The first image, the missile launcher, contained many dropouts, as described above. There are two problems with these. Of primary importance is their effect on the fractal algorithm: the dropouts create false variations in the image, damaging to a routine whose purpose is to detect variation. Secondly, the dropouts make it difficult to display the image, as the normalization would destroy all variation in the image. Khoros offers a median filter to remove errors such as these, but the filter smooths out variation in the image as well as removing the dropouts, which is unacceptable. Two methods offered a solution to the problem. The simplest method was using linear interpolation to fill in the point based on the surrounding points. As the objectives of the project included neural networks anyway, a neural network also tried to repair the images. Pixels of known values, not dropouts, served as test data. A comparison was made by taking the absolute difference between the actual pixel value and the value computed by the two algorithms. The total error of the neural network was only half the error from the linear interpolation. When the passive data (the passive data does not contain dropouts) supplemented the data used by the neural net, the net error decreased slightly. The finished form of the replacement routine replaces pixels with values greater or less than three standard deviations from the mean (calculated from random sampling of one thousand pixels). The values used by the neural network are differences of the pixels surrounding the pixel (cardinal directions only) from the active data, and differences with the pixel and the surrounding pixels from the passive data. Training the network with differences instead of actual values resulted in a range-independent network.

This works well in an image without a body of water. Because of the random placement of range values, almost all water pixels are more than three deviations from the mean, and replacing them often deadens the randomness that separates water from other pixels. This is no perfect solution to this, unless the routine can be taught to recognize water (perhaps by checking to see how prevalent dropouts are in a region), but, whether using a preprocessed image or not, the detection algorithm is robust enough to recognize water as natural. No attempt was made to distinguish water from other natural terrain.

The previous implementation of the fractal dimension algorithm, by Jason Lindsey, assumed a square image. The modified routine still uses square areas, but checks to ensure that it does not expand beyond the bounds of the image. The current pixel is always placed in the upper-left corner of each sub-area, for the sake of simplicity. A slight improvement in accuracy could be obtained by placing the pixel in the center of the sub-areas. In some cases, accuracy may be improved with non-square areas centered around the pixel.

The final neural network, used to distinguish between artificial and natural features, considered three possible categories of output. The net assigns each pixel a number from zero to one, quantifying how well a pixel fits into the categories of artificial structure, road, or natural. The training data, due to time constraints, came solely from the second image, which had a range too large to see any vehicles that may have been present. With a greater set of training data, vehicles could be included. To classify each pixel, the network used twenty pieces of data, the pixel and surrounding pixels from the active and passive images, plus the output from the fractal routine from the active and passive images. The training data for the building category came solely from the building; the piers were not included in either the road or building data sets.

All of the algorithms were implemented in C, using routines included in Khoros for reading and writing the image files.

Observations and Conclusions

The fractal routine alone, on visual examination, demonstrated the ability to set off the edges of objects. The fractal dimension is higher at the edges, even though a high fractal dimension is usually only associated with natural objects. This is a result of fuzzy edges, which look very fractal. Ladar, when bouncing around the edges of an object will tend to return a fuzzy result. This should be remedied at closer ranges with higher resolution, but such short ranges are useless to a program interested in mounting Ladar devices on aircraft.



Figure 1 - Fractal Image of Astros



Figure 2 - Sobel Image of Astros



Figure 3 - Fractal Image Hurlburt

The fractal image (Figure 1) was compared with a sobel routine (Figure 2), a more common method of edge detection. The results were very similar (again, visual inspection only), but the fractal dimension was much clearer, apparently not detecting extremely fine edges. The fractal routine, when ran on both images (results displayed in Figures 1 and 3), set off the edges of objects in the images successfully.

The neural network was very successful in distinguishing roads (light grey), buildings (white), and trees (dark grey) (Figure 4). Unknowns are in black. The network classified the piers as buildings, which was good. The road category consists primarily of artificial planes, but the net may classify certain naturally low and flat areas as roads; anything in the building classification is definitely artificial. The only building in the image was clearly marked.

No objective method tested the accuracy of the detection, but the results of the neural network agree with human interpretation of the image. General areas are definitely marked correctly, most individual pixels are marked correctly; the ones not marked correctly or marked unknown are not important to visually interpreting the image.

Other tests concluded that the fractal data was very useful in aiding the network in classification. The training process is erratic and undependable when the network's training does not include the fractal data or includes only the fractal data. Using both together produced twice the accuracy of the fractal data alone, and more than three times the accuracy of the Ladar data without the fractal data.

The fractal dimension routine alone is a useful tool for segmenting images and providing information about the image. Except in the case of edge detection, it requires another algorithm or a human to interpret the output into useful form. A neural network can use this data to create a useful image, leading toward greater image understanding. Work is still on-going in testing and developing these methods and their application to the ATLAS program.



Figure 4 - Classification of Hurlburt

References

1. Feder, Jens. *Fractals*. Plenum Press, New York: 1988.
2. Lindsey, Jason. *Image Analysis: A Fractal Application*. Research and Development Laboratories: 1992.
3. M. Kabrisky and S.K. Rogers. *An Introduction to Biological and Artificial Neural Networks for Pattern Recognition*.
The International Society for Optical Engineering, Bellingham, Washington: 1991.
4. Lt. Whiteley. Technical Meeting, Eglin Air Force Base: July 1993.

EFFECTS OF VARYING GAUGE LENGTHS ON
"MINIATURE SPECIMEN" INSTRON AND
SPLIT-HOPKINSON TENSILE RESULTS

Barry W. Kress

Wright Laboratory
101 W Eglin Blvd.
Eglin AFB, Fl. 32542-6810

Final Report for:
High School Apprenticeship Program
Wright Laboratory

Sponsored by:
Air Force Office of Scientific Research
Bolling Air Force Base, Washington, D.C.

August 1993

EFFECTS OF VARYING GAUGE LENGTHS ON "MINIATURE SPECIMEN"
INSTRON AND SPLIT-HOPKINSON TENSILE RESULTS

BARRY W KRESS
HIGH SCHOOL APPRENTICE
WARHEAD BRANCH
WRIGHT LABORATORY ARMAMENT DIRECTORATE

ABSTRACT

A new miniature tensile specimen is proposed for use in the evaluation of explosively formed penetrators (EFP'S) liners. This is necessitated due to the desire to evaluate "real life" liners that are fully processed and too thin for machining current tensile specimens. Tensile testing was performed at both low (Instron) and high (Split-Hopkinson) strain rates and results compared back to the current 0.125" diameter/0.350" gauge length sample. The proposed miniature specimen size requirement was established as 0.090" diameter because of liner thickness. Various gauge lengths were evaluated from 0.214" to 0.304" in 0.030" increments. Since the average results varied no more than 1.11% for all gauge lengths tested, the 0.244" gauge length was chosen as the new length since it preserved the gauge length/diameter ratio of the current tensile specimen. From the tensile tests performed, the average stress for the 0.125" diameter specimens was 266 KSI and the 0.090" specimens was 269 KSI. The difference between the two was 1.12% which is well within experimental error.

INTRODUCTION

The purpose of these tests is to establish a miniature Instron and Split-Hopkinson tensile sample size that is small enough to be cut from Explosively Formed Penetrator (EFP) liners. The major problems encountered are the liner's thickness and curvature. The standard 0.125" diameter tensile size cannot be used because the "sample thread" diameter is too large to be cut from the liner. Therefore a smaller tensile specimen was needed that could be cut from the liner. After careful deliberation a diameter of 0.090" was decided upon. The gauge lengths to be tested were 0.214", 0.244" (the gauge length which utilizes the established gauge length/diameter ratio), 0.274" and 0.304". Once the new miniature sample size is developed, the actual liner can be directly evaluated and actual results fed into a computer hydrocode model for more accurate modeling and performance prediction.

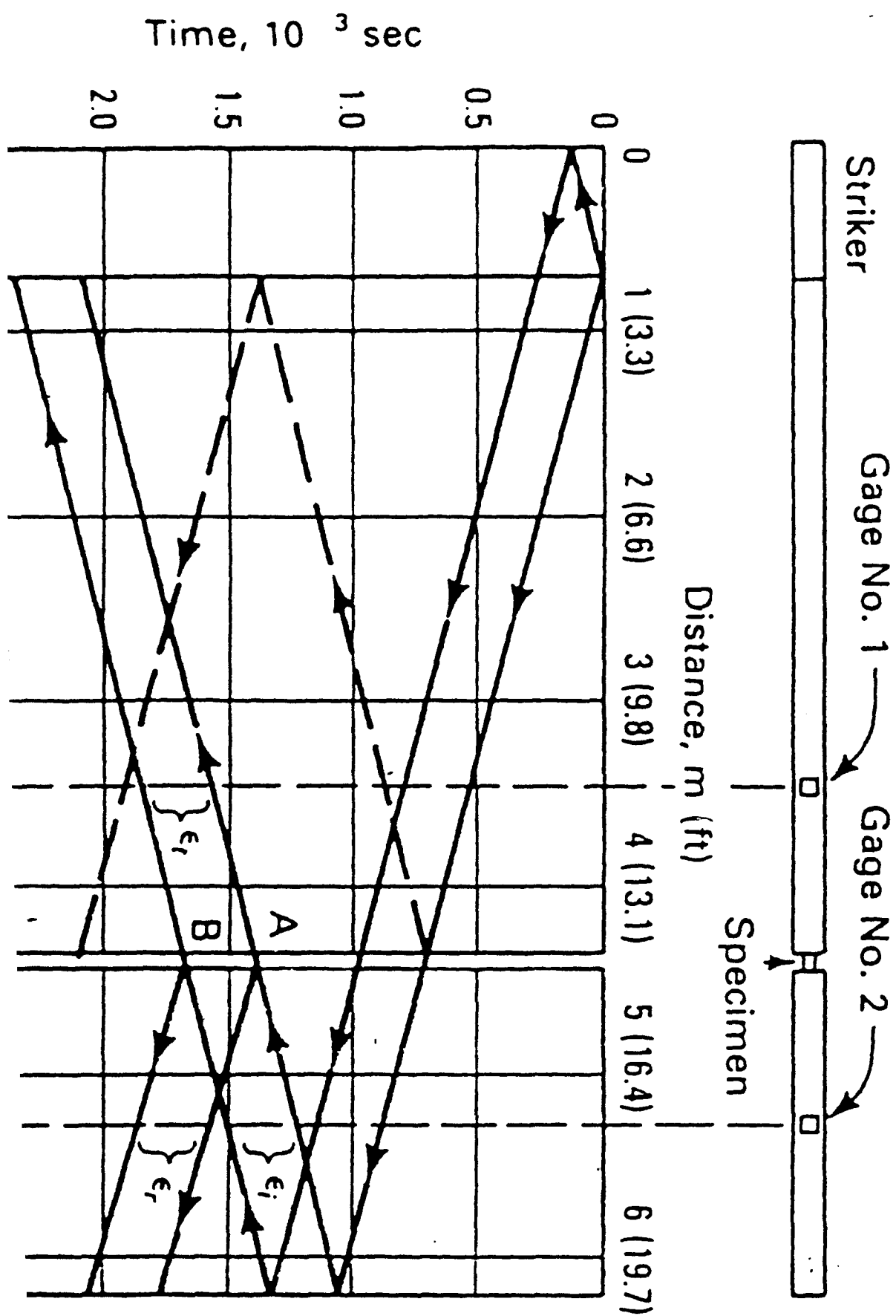
EQUIPMENT AND EXPERIMENTAL CONDITIONS

Two types of tensile testing were utilized in the development and evaluation of "miniature" tensile specimens. The standard .125 inch diameter Hopkinson tensile specimen was chosen as the control specimen for comparison purposes in the development of the new .090 miniature specimen. The slow rate testing was performed on a Instron tensile testing system. The Instron machine is capable of applying uniformed uniaxial loading on metal tensile specimens under various test conditions. The particular machine used in the testing relies on a constant rate of extension that is independent of the applied load. This enables the production of consistent results, even when using rate-sensitive materials. The machine is programmed to move a specified distance in a given amount of time. For our testing of the .0125 inch "Hopkinson" and the new .090 inch miniature samples, the speed was 10^{-1} in/in/sec. The tensile forces are created by a high-torque motor that drives two vertical lead screws that in turn operate a moving crosshead. A closed-loop servodrive system ensures that a constant crosshead speed is achieved. The servomechanism controls the crosshead position and therefore is able to reduce any error and sustain the inputted crosshead speed. The applied force is measured by strain-gauges that in the presence of mechanical deformation result in electrical resistance changes. These changes are measured by a load cell connected to a bridge circuit. A load cell amplifier sends a signal to the circuit that excites the circuit and at the

same time, an applied force causes an unbalancing effect. The resulting signal once again returns to the amplifier, is boosted and converted into an output signal proportional to the applied force. This output is then recorded onto a digital storage oscilloscope. It is then transferred via computer controller interface to a computer that reduces the data and calculates the peak stress, strain rate, engineering stress and true stress. The computer then stores the reduced data and is able to plot the engineering stress vs. strain, true stress vs. strain, and the strain rate vs. strain graphs. The data can then be evaluated and conclusions deduced.

The high rate testing was performed on a tensile Split-Hopkinson Bar system. The unit used in our testing is composed of a striker bar and an incident bar split into two parts, all parts are made of Inconel 718. The two mating ends at the split junction have threaded inserts for mounting of small tensile specimens as noted in figure 1. The tensile specimen is screwed into one end of the incident bar, and then a collar is placed over the specimen which is subsequently screwed into the adjoining end of the bar. It is important to make sure that the bars fit tightly against the collar to avoid erroneous data. The specimen is pulled into by a tensile pulse created by the reflection of a compressive pulse that transmits through the bar. This pulse is achieved by accelerating the striker bar against the incident bar containing the specimen in the split area. This impact generates a compressive wave that travels down the bar and ideally passes through the collar without prestraining

Figure 1



the specimen. The pulse continues to travel until it reaches the free end of the bar and is then reflected back as a tensile pulse. Upon making contact with the specimen, the tensile pulse is partially transmitted and partially reflected back towards the free end of the bar. The collar is not subjected to any tensile loads because it is not connected to the bar. Two strain gages, one on each bar approximately 3 feet each from the test specimen, measure the initial pulse and then the distortion of each future pulse in order to determine the peak stress of the specimen. This data is then collected and recorded by a digital storage oscilloscope. The data is subsequently transferred to a computer via computer uplink where it is condensed and the peak stress of the specimen is calculated. A plotter is also on-line to plot the true stress versus strain curve.

RESULTS AND DISCUSSION

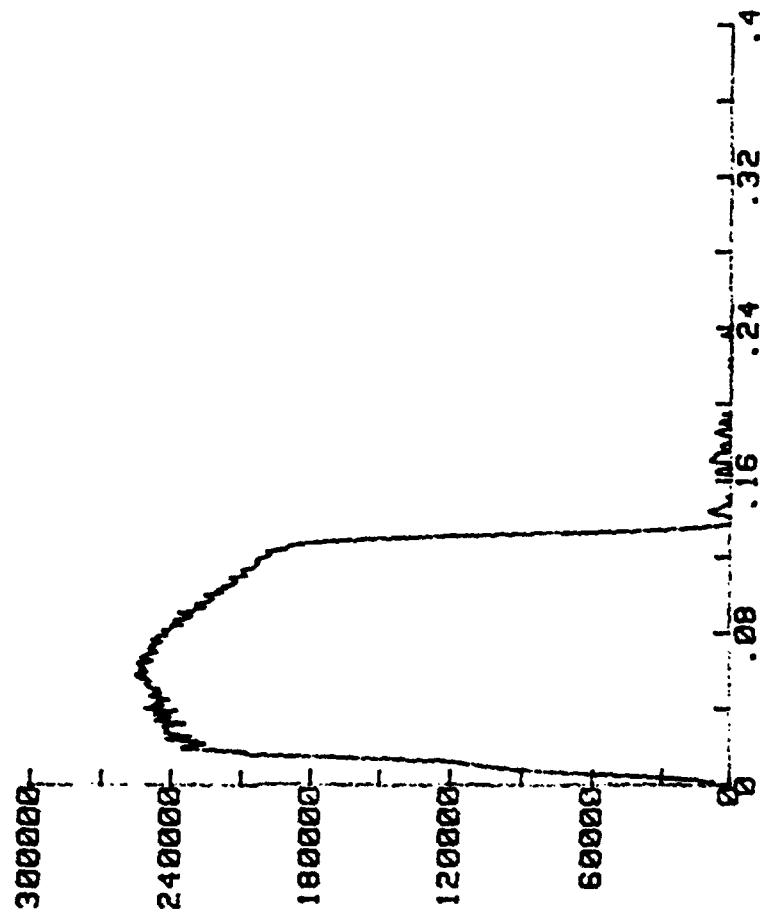
The tensile Instron was used to evaluate two sets of specimens for the 0.0125" diameter/0.350" gauge length. This yielded an average of 266 KSI for set 1 and 254 KSI for set two. The difference being 4.51%. Four gauge lengths were evaluated for the new 0.090" diameter miniature specimens. These gauge lengths were 0.214", 0.244", 0.274", and 0.304" and the resulting average stresses were 268 KSI, 271 KSI, 268 KSI, and 269 KSI respectively. The difference between the high and low is 1.11%. The difference between the 0.125" diameter high average value of 266 KSI and the average 0.090" sample value of 269 KSI is 1.12%.

The tensile Split-Hopkinson Bar was used to evaluate the differences between the 0.125" diameter/0.350" gauge length samples and the 0.090" diameter miniature specimens. The 0.125" diameter samples yielded an average stress of 265 KSI. Testing of the 0.090" samples was limited however to the 0.244" gauge length and yielded an "exaggerated" average peak stress of 289 KSI and an "apparent" actual stress of 255 KSI. The exaggerated peak stress was influenced by a misalignment in the bar. Although this misalignment was also present for the 0.125" diameter sample, it had little effect because of the relative size of the data signal. The raw data signal for the 0.090" diameter sample was much smaller than the 0.125" sample. In fact, the 0.090" peak signal was slightly smaller than the misalignment signal and this therefore caused a peak in the stress curve that is erroneous (see figures 2 & 3). The difference between the 0.125" diameter/0.350" gauge length

figure 2

SPLIT HOPKINSON PRESSURE BAR TEST

MATERIAL DESCRIPTION:4340	TEST DESCRIPTION:4340
GAGE LGTH(IN)=.380	DIA(IN)=.125 TEMP(C)= 23
STRAIN RATE PER/SEC:469.53	VELOCITY IN/SEC:195.58
PEAK STRESS (PSI)=254927.92	PEAK STRAIN (IN/IN).2674
TEST DATE:24 Jun 1993	DRAWBACK DIST (INC):4.50
AREA (psi) UNDER THE CURVE: 27637.12	

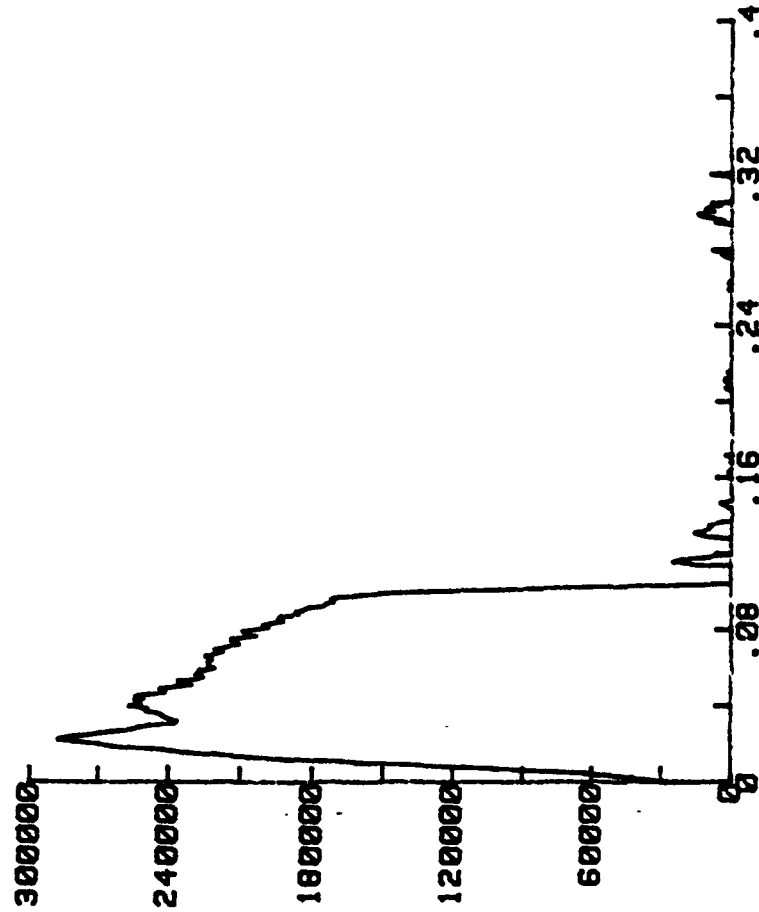


TRUE STRESS (PSI) VS TRUE STRAIN

figure 3

SPLIT HOPKINSON PRESSURE BAR TEST
MATERIAL DESCRIPTION:4340-1
GAGE LGTH(IN)=-.380
STRAIN RATE PER/SEC:597.80
PEAK STRESS (PSI)=287574.96
TEST DATE:22 Jun 1993
AREA (psi) UNDER THE CURVE: 19655.05

TEST DESCRIPTION:244A
DIA(IN)=-.090 TEMP(C)= 23
VELOCITY IN/SEC:195.58
PEAK STRAIN (IN/IN).3197
DRAWBACK DIST (INC):4.50



TRUE STRESS (PSI) VS TRUE STRAIN

average stress of 265 KSI and the 0.090" diameter/0.244" gauge length average "apparent" stress of 255 KSI is 3.77%.

CONCLUSIONS

The 0.090" diameter specimens with gauge lengths ranging from .214" to .304" have very little variation in their stresses. In fact the difference between the 0.090" diameter/0.244" gauge length specimen and the 0.125" diameter/0.350" gauge length specimen tested on the Split-Hopkinson Bar was less than the difference of the two 0.125" diameter/0.350" gauge length specimen sets tested on the Instron machine. Therefore the results achieved by testing miniature samples of diameter 0.090" with gauge lengths ranging from 0.214" to 0.304" are acceptable and within experimental accuracy. The 0.244" gauge length was chosen as the gauge length for a 0.090" diameter sample in order to adhere to the established gauge length/diameter ratio.

Bar stock mechanical properties can still be used on initial hydrocode development and then the actual mechanical properties from manufactured liners can be fed into a finalized hydrocode model. This will ensure that final hydrocode models are realistic and result in the most accurate "warhead performance" evaluation tool possible.

ACKNOWLEDGEMENTS

First of all, I would like to thank my fellow apprentices for all the fun times this summer. Especially Jenny, Christie, Christina, Kyle, Jon, Nancy, Mary, and Melissa.

Secondly, I would like to thank Don Harrison and Glenda Apel for not only sponsoring the program, but also for lending help whenever it was needed.

Thirdly, I would also like to thank all the guys at the lab that made my summer enjoyable and who shared their advice and expertise with me. Thank you: Bob LeBeau, who was always ready with a joke, Homer Garner, who was always there to help me get things done, The Model Shop, who made my testing possible, Tony Weekly, who let me mess up his desk all summer, Thad Wallace, who took the time to teach me how to operate all the machines in the metallurgy lab, Aaron Brinson, for letting me work in his branch, Al Welle, for allowing me to work in his section, and all the other guys in Warheads that treated me as a professional.

Most of all, I would like to extend my gratitude to my mentor, Dr. Morris F. Dilmore. Dr. Dilmore not only taught me about metals and warheads, but about life. In the process he also replaced a four year old dream of becoming a chemical engineer, and in its place left a new dream of becoming a materials engineer. For all of this and so much more that cannot be put into words I thank him.

REFERENCES

Metals Handbook. Vol. 8. Ed. John R. Newby. Ninth Edition.
American Society for Metals: Metals Park, Ohio, 1985.

DEVELOPMENT OF AN ENGINEERING ANALYSIS
TOOL USING FORTRAN

Elliot Moore II
High School Apprentice
Warheads Branch

Wright Laboratory Armament Directorate
WL/MNMW
Eglin AFB, FL 32542-5434

Final Report For:
High School Apprenticeship Program
Wright Laboratory Armament Directorate

Sponsored By:
Air Force Office of Scientific Research
Bolling Air Force Base, Washington D.C.

August 1993

DEVELOPMENT OF AN ENGINEERING ANALYSIS TOOL USING FORTRAN

Elliot Moore II
High School Apprentice
Warheads Branch
Wright Laboratory Armament Directorate

ABSTRACT

For a second summer, I worked as an apprentice to Mr. Michael E. Nixon. in the computational mechanics section of the Warheads Branch. My project involved the development of a FORTRAN program to be used in testing strain values from Taylor Impact Specimens. The main purpose of the program was to find the location of elastic/plastic interface, as a function of time. The location is based on given strain criteria. The elastic/plastic interface data are points written to a separate file for use with the Microsoft EXCEL spreadsheet. The data was then plotted and used for analysis by the engineer.

DEVELOPMENT OF AN ENGINEERING ANALYSIS TOOL USING FORTRAN

Elliot Moore II

INTRODUCTION

The principle behind this entire paper centers around the Taylor Impact Test. The Taylor Impact Test was designed to determine the behavior of material deformation under varying strain rates. To a certain point, every object is elastic. Elasticity refers to a materials ability to return to its natural state, after a certain level of deformation, like a rubber band. A rubber band can be stretched, or deformed, and then snap back into its original position because it is highly elastic. However, there is a point where the strain exceeds an object's elasticity, and it can no longer return to its original position. The deformation is no longer elastic, but instead becomes plastic. For instance, if a rubber band is stretched too much, or too far, the rubber band breaks. Determining the behavior of objects at their elastic/plastic interfaces is an area of interest for Warhead Branch activities. The test observes the deformation of a cylinder as it is impacted against an anvil of hard material.

METHODOLOGY

Before any program can be effective, it must have data to use. The data is obtained from the EPIC hydrocode. Hydrocodes are lengthy and complex computer programs that are used to simulate warhead formations, penetrations, and target responses. The EPIC hydrocode is widely used by the Department of Defense and is sponsored by Wright Laboratory. Fittingly, EPIC stands for Elastic Plastic Impact Computations. Figure 1 shows an example of a partially deformed cylinder. The line across the cylinder represents the points where

the elastic/plastic interface occurs. The enlarged block indicates how EPIC simulates the material in a Taylor Impact Specimen. The nodes represent mass and the elements represent volume of the material in the specimen. The positions of the nodes versus time the cylinder impacts, are simulated by EPIC and this data is written into a file for post processors. The data is eventually written to two files, one containing time vs. x-position data and the other containing time vs. z-position data. X-position represents the position of the nodes radially and z-position represents the position of the nodes axially. These files are used by the program to determine elastic/plastic interface information. Figure 2 is an example of a file containing time vs. x-position.

The data from EPIC determine the position of the nodes at various times. My program determines the time and position of elastic/plastic interface from this data. The point of elastic/plastic interface is found by determining when the exterior node has met a given strain criteria. Data is saved when a given node reaches a critical strain as determined by $\text{scrit} = (R - R_0) / R_0$. R_0 represents the original position of the node radially (along the x axis) and R represents the current position of the node. When the node meets this criteria, it has reached the elastic/plastic interface. A flow chart containing the overall logic of the program is shown in Figure 3, and the final source code is contained in Appendix A. My program, called plastic.f, is the result of trial and error. About five or six different derivatives for the program were written, each one a little better than the last, until the final version was tested and completed.

The first section of the program is responsible for the variable declaration. This simply means that the type of variables to be used in

the program are defined as integers, real numbers, characters, or an array. This lets the program understand how to read or write the variable values. The first section also opens the files that will be used for input and output. The statement "open(unit=3,file='plasticx.in',status='old')" defines the file named 'plasticx.in' as the unit number 3. This is important for the read and write statements in FORTRAN which reads and writes to files by unit number. Each file is designated by a unit number. The "status='old'" phrase, at the end of the first two open statements, signifies that the files 'plasticx.in', which contains data on x-position, and 'plasticz.in', containing data on z-position, already exist and will be used as input files. The same basic logic holds true for the next OPEN statements concerning the files 'plasticz.dat' and 'plastic.out'. The "status='new'" phrase, at the end of the last two open statements, signifies that the files do not exist yet and will be the destination of written output. The final two statements in the section initialize a counter for counting the number of nodes and data points later in the program.

The second section of the program is the internal documentation of the program logic. It defines to the user of the program the people responsible for its design and the purpose of the program overall. Section 3 of the program is also for user reference. It defines what each variable in the program represents. The next section is used by the program to find out how many strain criteria the engineer wants to test, and what the values of the strain criteria will be. When run, the question "HOW MANY STRAIN VALUES?" will appear on the screen. After a number is input, the computer will ask the engineer to "INPUT STRAIN CRITERIA VALUE" for as many times as the engineer requested. These strain criteria's will be stored in the 'scrit(k)' array.

Section 5 sets the program in motion. First, the program finds the number of data points per node, represented by the variable 'count2'. Then it finds the number of nodes, represented by the variable 'count1'.

After finding the number of nodes and the number of data points per node, the command 'rewind 3' tells the program to go back to the beginning of unit file 3 (named 'plasticx.in' by the OPEN statement). The program then begins to read the data values again, this time placing the data into their appropriate array names, such as time values being written to the 'time(j)' array. Data is also placed in the 'xdata(i,j)' array and 'zdata(i,j)' array containing data on x and z-position respectively. The next section of the program is very important because it determines the strain for each data point of the nodes. In the last section of the program, the strain values are tested against the strain criteria values input by the user at the start of the program, to determine the data points at which the elastic/plastic interface first occurs. These data points, one for each node, are written to a written to unit file 10 (named 'plasticz.dat' by the OPEN statement). Once the points of elastic/plastic interface have been determined, they are transferred into a worksheet program for data organization. We used Microsoft EXCEL to chart the data from the program. These charts are used for the engineer's analysis. An example is shown in Figure 4.

RESULTS AND CONCLUSIONS

The program has been used successfully by Warheads branch engineers. It has calculated the elastic/plastic interfaces for seven different strain criteria at once. I was personally responsible for several modifications to the program to make it more efficient, and in the process, I learned a lot of FORTRAN. This was my first real exposure to the FORTRAN language. With my

mentor's help, I was able to learn FORTRAN fairly quickly, and know enough to assist him in designing this program analysis tool. I also learned debugging skills after each program modification. There were several problems with logic and syntax, but the problems were solved and I gained valuable knowledge that I will take with me into my college years and the rest of my life.

ACKNOWLEDGMENTS

Once again, I have enjoyed a totally unbelievable summer here at Wright Laboratory under Mr. Michael E. Nixon. I thank GOD for allowing me the abilities to be in such a wonderful program. My mentor's efforts are greatly appreciated. His patience and trust in my ability has helped me to learn on my own, make my own mistakes, and learn how to correct them. More than once I would come to him with a problem and he would trust me enough to simply say, "Well, fix it!" He is truly the standard by which all mentors should be measured! Also very important to the success I enjoyed are Ms. Pam Cortner, Mr. Randy Anderson, and Mr. Bizhan Aref who are contractors with Sverdrup, assigned to the computational mechanics section. Dr. Bill Cook and Dr. Harbans Sidhu were excellent sources of any technical information when needed. And last of all, but most definitely not the least, is my "partner in crime", Ms. Jennifer R. Bautista, another second year apprentice at the lab. This was our second year working together, and once again, I enjoyed her company and unique insight. The entire office was very cordial and understanding. I only regret that this is my last year to be an apprentice. If I was given the opportunity to do it all again, I would not hesitate.

Figure 1

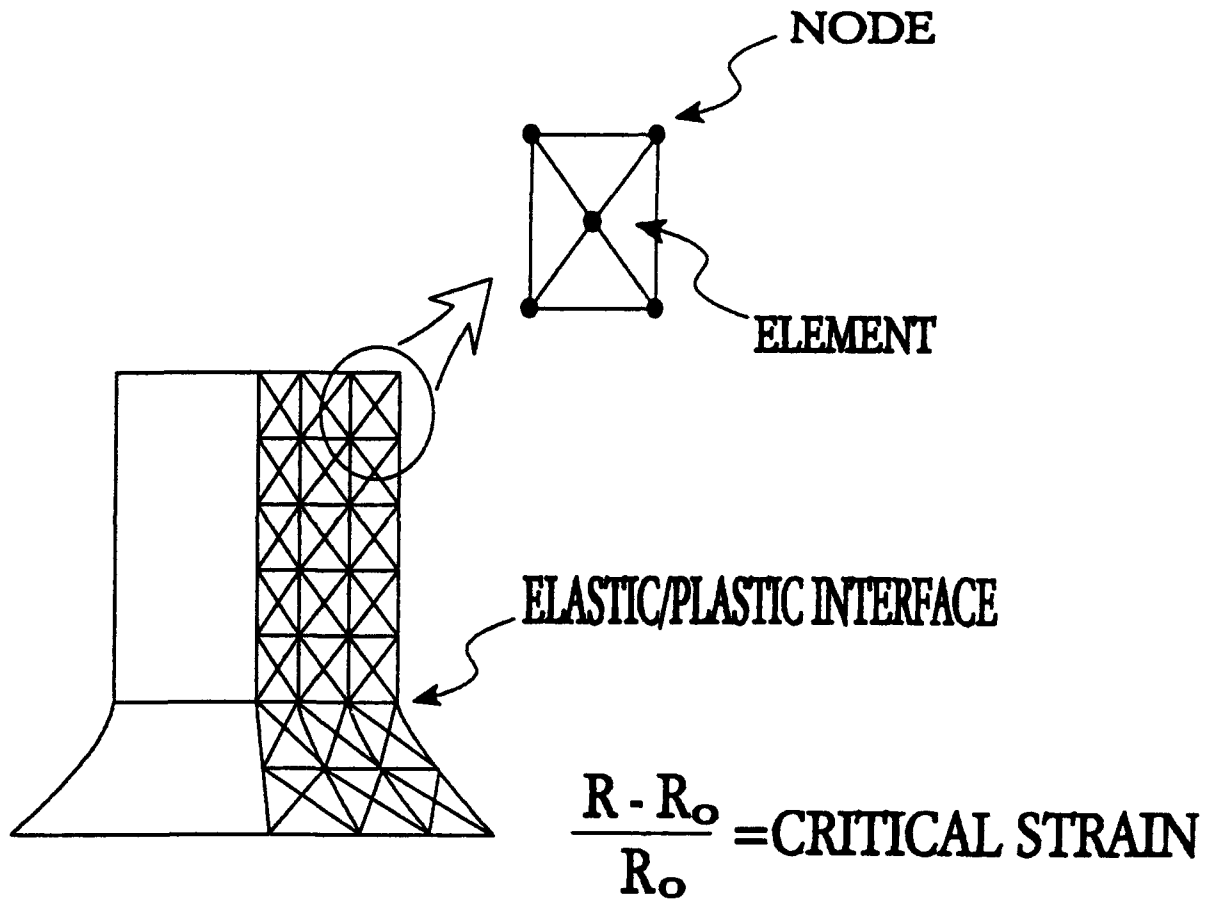


Figure 2

"XYDATA, "	NODE0001
2.26E-06	-9.25E-06
2.90E-06	7.05E-04
4.19E-06	1.41E-03
5.97E-06	2.10E-03
8.16E-06	2.77E-03
1.07E-05	3.42E-03
1.33E-05	4.08E-03
1.55E-05	4.74E-03
1.75E-05	5.41E-03
1.93E-05	6.09E-03
2.10E-05	6.77E-03
2.28E-05	7.45E-03
2.46E-05	8.12E-03
2.67E-05	8.79E-03
"XYDATA, "	NODE0002
2.87E-05	9.46E-03
3.07E-05	1.01E-02
3.27E-05	1.08E-02
3.49E-05	1.15E-02
3.73E-05	1.21E-02
3.98E-05	1.28E-02
4.24E-05	1.35E-02
4.50E-05	1.41E-02
4.77E-05	1.48E-02
5.02E-05	1.55E-02
5.30E-05	1.62E-02
5.60E-05	1.68E-02
5.93E-05	1.75E-02
6.27E-05	1.82E-02
6.65E-05	1.89E-02
7.07E-05	1.96E-02
7.86E-05	2.03E-02
"XYDATA, "	NODE0003
2.87E-05	9.46E-03
3.07E-05	1.01E-02
3.27E-05	1.08E-02
3.49E-05	1.15E-02
3.73E-05	1.21E-02
3.98E-05	1.28E-02
4.24E-05	1.35E-02
4.50E-05	1.41E-02
4.77E-05	1.48E-02
5.02E-05	1.55E-02
5.30E-05	1.62E-02
5.60E-05	1.68E-02
5.93E-05	1.75E-02
6.27E-05	1.82E-02
6.65E-05	1.89E-02
7.07E-05	1.96E-02
7.86E-05	2.03E-02

Figure 3

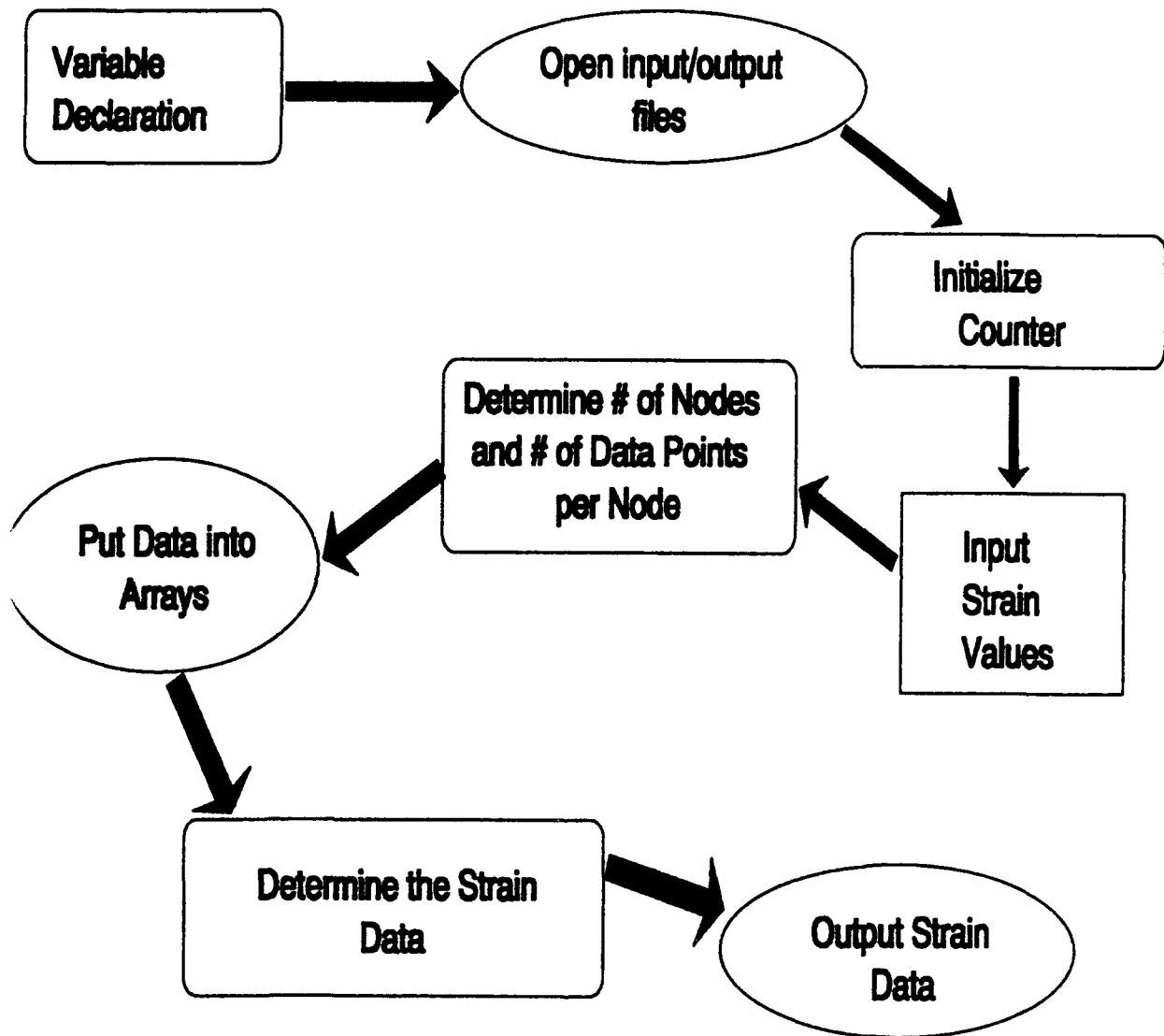
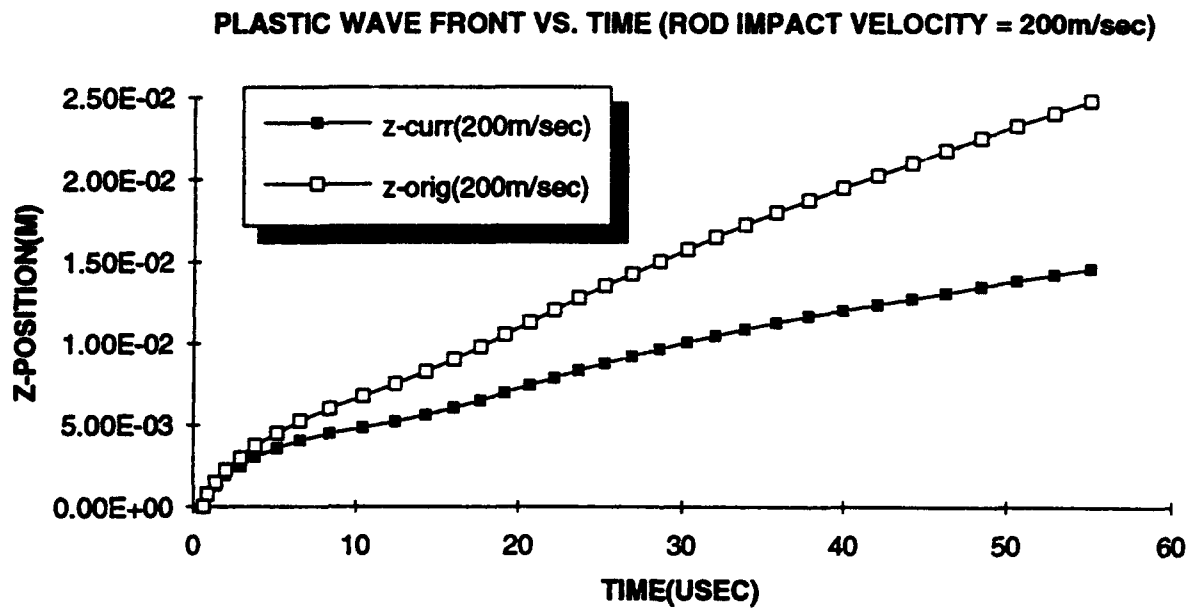


Figure 4



APPENDIX A

PROGRAM PLASTIC

[illegible]

```

C
C
C      VARIABLES:
C
C      count1          - number of nodes or elements
C      count2          - number of data points per node or element
C      num             - number of strain values to be tested
C      scrit(k)        - array of strain criteria values
C      choice          - decision to output full data information or not
C      dummy1          - a dummy variable used for counting
C      dummy2          - a dummy variable used to determine z-data
C      time(i)         - array of time data
C      xdata(i,j)      - array of x-position data
C      zdata(i,j)      - array of z-position data
C      strain(i,j)     - array of strain values
C
C
C
C      OPTION OF HOW MANY STRAIN VALUES TO CALCULATE
C
C      write(6,*)'HOW MANY STRAIN VALUES?'
C      read(5,*)num
C
C      OPTION OF WHAT STRAIN VALUES TO USE
C
C      do k=1,num
C        write(6,*)'INPUT STRAIN CRITERIA VALUE'
C        read(5,*)scrit(k)
C      enddo
C
C      OPTION TO OUTPUT FORT.11 IF THERE IS ONLY 1 STRAIN VALUE
C
C      if(num.gt.1) goto 6
C      write(6,11)
C      read(5,12)choice
C      if(choice.eq.'Y'.or.choice.eq.'y') goto 6
C      if(choice.eq.'N'.or.choice.eq.'n') goto 6
C      write(6,13)
C      goto 5
C
C      FIND count2 FROM plasticx.in
C
C      6 read(3,10)dummy1
C      7 count2=count2+1
C      read(3,10)dummy1
C      if(dummy1.eq.'XYDATA') then
C        count2=count2-1
C        goto 8
C      else
C        goto 7
C      endif

```



```

c      FIND count1 FROM plasticx.in
c
8      count1=count1+1
      do i=1,count2+1
      read(3,10,end=9)dummy1
      enddo
      goto 8
c
c      PUT DATA IN ARRAYS time(j), xdata(i,j), AND zdata(i,j)
c
9      write(95,14)count1,count2
      rewind 3
      do i=1,count1
      read(4,10)dummy1
      read(3,10)dummy1
      do j=1,count2
      read(3,*)time(j),xdata(i,j)
      read(4,*)dummy2,zdata(i,j)
      enddo
      enddo
c
c      ARRAYS ARE SET
c
c      R0 IS SET TO THE ORIGINAL X-POSITION. ALL NODES OR ELEMENTS ARE
c      ASSUMED TO START AT THE SAME X-POSITION.
c
c      STRAIN FOR EACH NODE OR ELEMENT IS CALCULATED FOR EACH TIME
c
      r0=xdata(1,1)
      do i=1,count1
      do j=1,count2
      strain(i,j)=((xdata(i,j) - r0)/r0)
      enddo
      enddo
c
c      UNIT 10 IS CREATED CONTAINING THE TIME AND Z-POSITIONS WHERE EACH
c      NODE OR ELEMENT GOES PLASTIC, AS WELL AS, THE ORIGINAL Z-POSITION.
c
      do k=1,num
      write(10,*)'SCRIT = ',scrit(k)
      write(10,15)
      iflag=0
      do i=1,count1
      do j=1,count2-1
      if(strain(i,j).ge.scrit(k).and.iflag.eq.0) then
      iflag=1
      write(10,*)time(j),zdata(i,j),zdata(i,1)
      else
      continue
      endif
      enddo
      iflag=0
      enddo
      enddo

```

```

c
c      CHECKS TO SEE IF UNIT 11 SHOULD BE CREATED
c
      if(choice.eq.'Y'.or.choice.eq.'y') goto 900
      goto 999

c
c      CREATES UNIT 11, CONTAINING TIME VS. STRAIN, Z-POSITION, AND
c      X-POSITION.
c
900    do i=1,count1
        do j=2,count2
            write(11,*)i,time(j),strain(i,j),zdata(i,j),xdata(i,j)
        enddo
    enddo

c
c      FORMAT STATEMENTS
c
10     format(a6)
11     format('DO YOU WISH TO OUTPUT STRAIN DATA FOR ALL DATA POINTS?'
1 ' <Y or N>')
12     format(a1)
13     format('INVALID ENTRY. RE-ENTER CHOICE.')
14     format('DATA FOR THE X AND Z POSITIONS CONTAIN/'
1 I3,' NODES OR ELEMENTS WITH/'
2 I5,' PER NODE OR ELEMENT.')
15     format(5x,'TIME(SEC)',6x,'Z-CURRENT',6x,'Z-ORIGINAL')

c
999    stop
      end

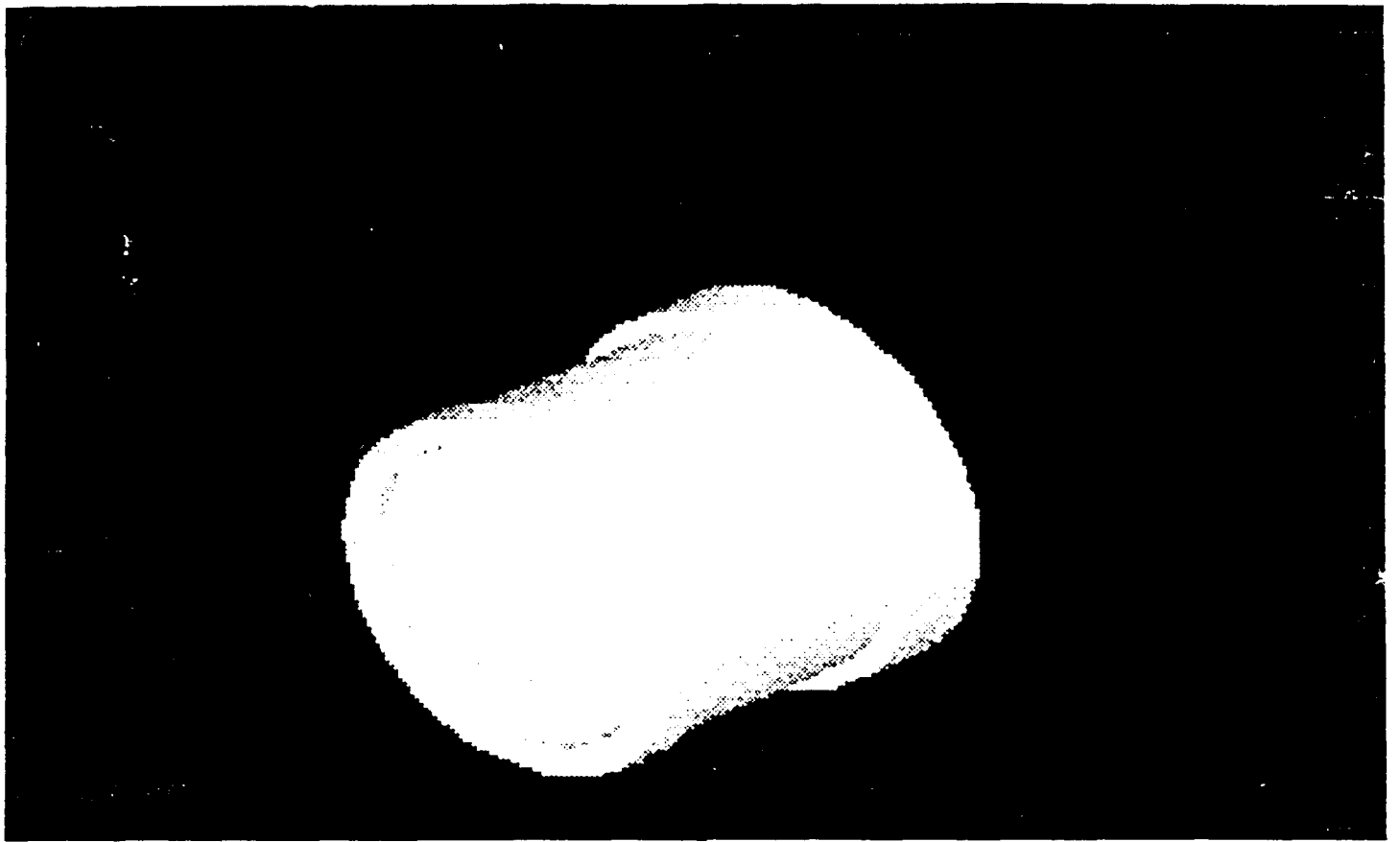
```

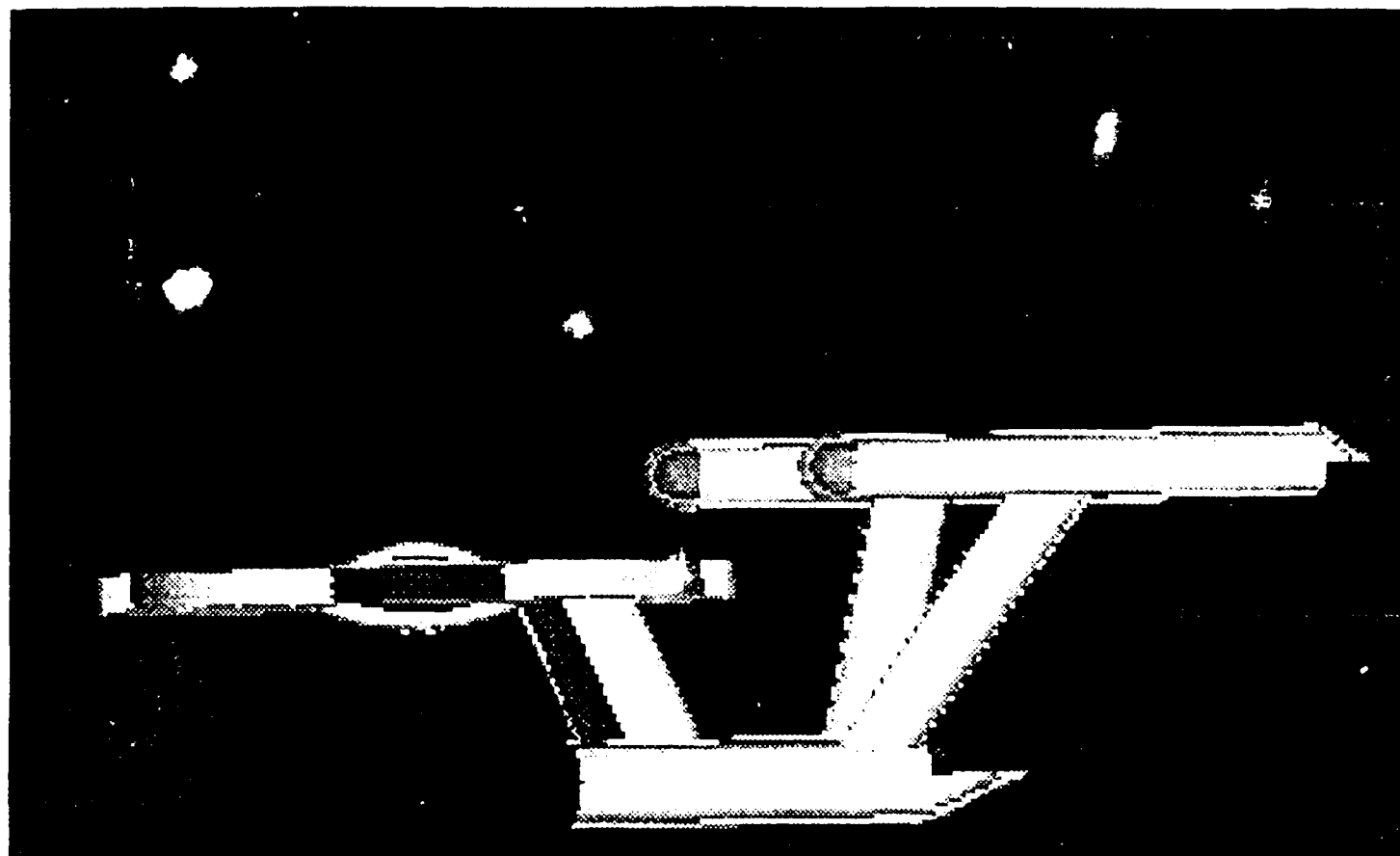
APPENDIX B

AutoCAD

I began my summer working with the AutoCAD program. AutoCAD is a general purpose Computer Aided Design program for preparing 2-D drawings and 3-D models. We installed AutoCAD on a Bernoulli Disk, which acts like a portable hard drive. I spent about a week on the AutoCAD tutorial learning how to use some of the functions. To help hone my skills, my mentor, Mr. Nixon, had me draw a 3-D model of an Explosively Formed Penetrator, or EFP, shown in Figure 1-B. It took about a day because I wasn't yet proficient with the commands. I took it upon myself to create other tasks in AutoCAD modeling. Over the course of one week, I used some of my spare time to create my own version of the U.S.S. Enterprise, shown in Figure 2-B.

AutoCAD has the ability to save its images to an IGES-(Initial Graphics Exchange Specification) file. IGES files contain the geometry of the AutoCAD drawings and models. It is possible to take these images, and using a special device, input them into PATRAN for simulation. PATRAN is a post processor program used partially for graphic representation of EPIC computations. Unfortunately, the device is not yet available locally.





EFFECTS OF THE ATMOSPHERE ON LASER RADAR

**Alexander H. Penn
Assistant Laser Radar Technician**

**Final Report for:
High School Apprenticeship Program
Wright Laboratories
WL/MNGS
Eglin AF Base**

**Sponsored by:
Air Force Office of Scientific Research
Bolling Air Force Base, Washington, DC.**

August 1993

EFFECTS OF THE ATMOSPHERE ON LASER RADAR

Alexander H. Penn
Summer Apprentice

Abstract

A system for measuring the effects of the atmosphere on LADAR was set up and data collection was begun. It consisted of three parts: a LADAR to take images of a fixed stationary object, a weather station to measure existing weather conditions, and a Helium Neon laser to measure the attenuation of the beam due to atmosphere. The initial medium for the LADAR has been Nd: Yag, which lases at 1.06 microns, but it will be replaced by a Ti-Sapphire laser of adjustable wavelength. Data collection to date has consisted of fair weather, rain, fog, and nighttime data. It will later cover other atmospheric conditions including snow, sleet, and high aerosol content (smoke and dust). The data when fully collected will be used to develop filter algorithms and to evaluate the most useful wavelengths under differing conditions.

EFFECTS OF THE ATMOSPHERE ON LASER RADAR

Alexander H. Penn

Introduction

In recent years, LAsER Detection and Ranging (or LADAR) has become of increasing interest to the military and to the scientific community. Whether it will ever completely replace the microwave radar is difficult to say, but LADAR has already proved that it has many advantages over the traditional radar. The much smaller wavelength (over a thousand times) allows for a much higher accuracy and precision resolution. The highly collimated nature of laser beams also gives the LADAR a much smaller angular beam width. This characteristic provides the LADAR with that most important ability, imaging. Small angular beam width also allows aim point assessment, precise target tracking, and autonomous operation. The precision of the LADAR system's range and velocity measurements also give it direct target size determination, segmentation of stationary and moving targets, and improved clutter rejection and target recognition. The downside of LADAR systems is that they are subject to varying weather and atmospheric conditions. This means that they are usually restricted to shorter ranges in the lower atmosphere in other than totally clear weather.

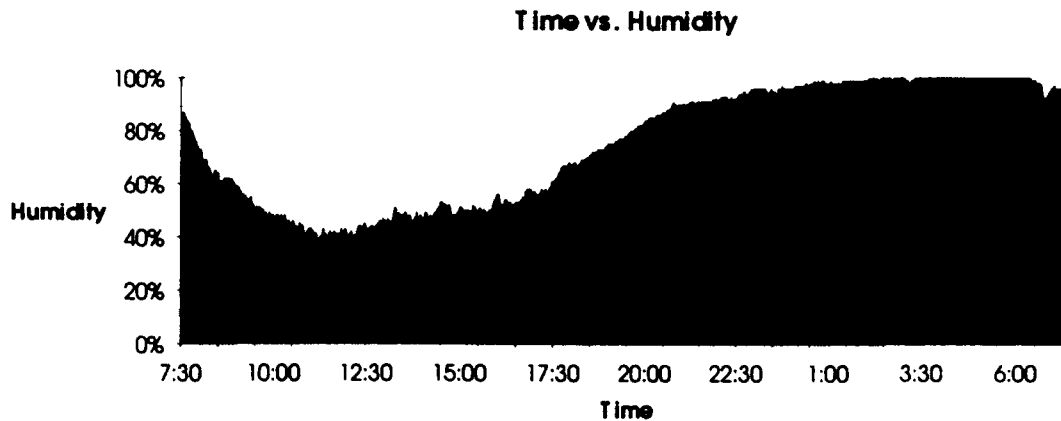
Because of the limitations on tactical LADAR use, it was decided that the exact effect of the atmosphere on a LADAR image needed to be studied. It has become necessary to find a way of actually measuring the effects so that a way of counteracting them may be developed. The immediate task was to set up and then coordinate whatever systems were necessary to characterize atmospheric effects on LADAR. Data was then to be collected in such conditions as fog, heavy rainfall, high temperatures (with heat shimmers), and whatever else that might come along and prove to be interesting. These images would later be compared with that of "normal" conditions.

Apparatus

The first system set up was the LADAR itself. For the initial tests the laser medium being used was Nd: YAG (output at 1.06 microns in the near infra-red). This is the current standard medium for laser radar because of the atmospheric "window" at that wavelength. Except for the case of aerosols in the air, there will be little attenuation of the beam due to atmosphere and little or no scattering. Subsequent tests will be conducted using a Ti-Sapphire medium of adjustable wavelength so as to find the best possible wavelength for each weather condition. The system scans by means of two revolving mirrors. The receptor, located immediately beside the laser, receives the light reflected off the target and calculates the range based on the time of flight between the impulse and its reception. The raw data already shows up as an image often recognizable to the human eye. But for the computer to recognize it as a target, the image must first be run through filters to get rid of background "noise", the objects segmented out of the

terrain, and each object evaluated against a template to see if it matches a target's description. The data collected here will be run through a special algorithm to "score" how easily the computer is able to recognize the "target" (a large truck approximately 85 meters away), from the images taken under differing conditions.

The second system used was the one actually able to measure those conditions. A Texas Weather Instruments weather station was employed to measure such important factors as temperature, humidity, and rate of rainfall at any given time. The information was recorded into computer via a communications port and translated into usable form by KEAterm (a simple communications program). The data is then imported into the Excel Spreadsheet and parsed. At this point the data may be used to match up an image to its weather conditions or graphed to study weather trends. Here is an example of humidity graphed against time:



The last system used was a small Helium Neon laser (.6328 micron wavelength) in tandem with a voltage meter. The purpose of this system is to measure the transmissiveness of the atmosphere via attenuation of the beam. Attenuation is measured using Beer's Law :

which states that attenuation is based on starting intensity, final intensity, and the distance involved. Using a power meter to measure the intensity and a retro-reflector to return the beam, it is possible to get a good idea of the amount of attenuation due to atmosphere that the LADAR beam undergoes in the same distance. This is because the atmosphere has much the same attenuating effect on light at .6328 microns as it does on light at 1.06 microns. Only in the cases when there are large amounts of aerosols present will there be a discrepancy.

Problems Encountered

The sheer number of problems to be faced during this project has been both

phenomenal and daunting. Delays sprang up one after the other. To begin with, no work could even begin until the weather station arrived. When it finally arrived, as it was being set up, it was discovered that one of the sensors was broken. It had to be sent in to be fixed, another delay. The first data collections were not until July 15, leaving less than 3 weeks to work on the rest of the project. Therefore, data collection began immediately, though the power meter for the HeNe laser had not arrived yet. This turned out to be a very wise choice because to date it still has not come in. The rest of the HeNe system is set up, but the power meter is a crucial piece without which the rest is useless. The weather system is also not running perfectly, because around ten and eleven 'o'clock the sun sends waves of heat off the concrete to the outdoor sensor located under the shade of some eaves. So during this portion of the day the sensor reports erroneously high temperatures and, because it is based on temperature, incorrect humidity. It was decided the problem would best be solved by putting the sensor in a sort of birdhouse-like shelter which would be placed away from the building. The shelter has not arrived yet but this does not prevent data collection during other parts of the day or during storms.

As if this weren't enough, the LADAR itself is having problems. To begin with the laser is not a very good one. We have been getting a lot of background "noise". This simply means getting false returns. Normally a little noise is to be expected, but we've been getting a lot more than a little. After reviewing all the data collection to date a few observations and a tentative hypothesis to explain at least some of the noise were reached. First, during the day it seems as if the image gets worse and worse the longer the LADAR is left on. This is exactly opposite from the way it should be. Normally about 15 minutes should be allowed for the LADAR's diode pump to warm up, and at the beginning of the summer this was basically true. Now however, the best images are at around ten minutes and things go downhill from there. Secondly, data taken early in the morning, say before and around dawn, seems unaffected by this rule. It does like it is supposed to do, giving the best images at around fifteen minutes and generally staying good after that. The worst images in the morning at 100% humidity are better than the best images in the afternoon at 50% humidity. Lastly, during the afternoon imaging, the noise becomes more and more concentrated at just one range, a spot between one and two meters from the LADAR. From these three observations, some conclusions were drawn and a guess hazarded as to the cause. First, for the worst of the noise it is safe to assume that the cause of the noise is not directly related to outside conditions because all the noise is occurring at one particular distance, which is still in the shelter of the building! This means that the problem is inherent to the system itself. Second, the problem is not likely in the power source because the exact same thing happened when the LADAR was hooked up to the generator (used during storms so as to prevent loss of power to the LADAR). Third, though by no means is the data dismissed, the fact that better images are gotten in higher humidities (early morning data) goes against common sense and the literary research that was done, thus leading to the believe that the problem does not concern that variable but the other changing variable in the situation

described, temperature. The hypothesis is that the problem is some how tied up with the temperature of the system. This would explain why the images are worse in the afternoon and why the longer the LADAR is left on, the worse the images become.

As serious as that is, it isn't even the only problem with the LADAR. It is also exhibiting periodic line shifts in which a whole or part of a line is shifted to the right (which is directly related to the fact that the LADAR scans from right to left). This seems to be a purely electric problem and is being worked on by a hardware expert. There is also a small, much less serious problem with the scanning system itself. The beginning of the scan (and thus the top of the picture) is not always starting at its default position thus shifting the entire image either up or down.

Conclusions

Despite all these problems which are clouding the images it has become clear that the actual effects of the atmosphere at this range are almost nil. It will require a greater distance than 85 meters for there to be any measurable effect. Therefore the lab is trying to obtain a tank which will be placed much farther down the range in hopes that an increased distance will increase results.

Future Work

The data, once it is all collected will be used for a variety of purposes. First, as it is the experiment being conducted here, the data will be used in the weather vs. wavelength study. Secondly, it will be used for the possible generation of special filters to remove the effects of any given weather condition from a LADAR image. Thirdly, it will be used to test the effectiveness of existing algorithms for target detection and identification. Finally it will be used to compare against synthetic LADAR data to check for accuracy. Though all of this is in the future, hopefully by next year there will be much more to show.

References

Jelalian, Albert V.. Laser Radar Systems. Artech House; Boston; 1992

**AIR POLLUTION DETECTION:
A DUAL USE FOR LADAR**

**Kyle D. Perry
High School Apprentice
Crestview High School**

**Crestview High School
1304 Ferdon Blvd.
Crestview, FL 32536**

**Final Report for:
High School Apprenticeship Program
Wright Laboratory**

Air Pollutant Detection: A Dual Use for LADAR

Kyle D. Perry
High School Apprentice
Crestview High School

Abstract

Research was done to find laser line absorbance data on various airborne pollutants in order to determine if it is possible to detect these airborne pollutants in smokestack plumes using infrared spectrometry in the 0.79 to 2.0 micron region. A computer program containing this data was eventually found and various parameters in the program were manipulated in order to fit the conditions that LADAR would be used to detect polluting emissions contained in the smokestack plume. It was found that a few molecules contained significant absorbance peaks in the 0.79 to 2.0 micron range, namely HCL, OH, HF, and CH₄.

Air Pollution Detection: A Dual Use for LADAR

Kyle D. Perry

Introduction

With the encouragement of finding peace time uses for weapons technology, the Air Force and Wright Laboratories has a growing need to find a use for Laser Imaging Systems not only as a tool in combat but as a tool to directly benefit the public. One way to accomplish this is to utilize the lasers normally used for imaging enemy tanks and weapons to also identify airborne pollutants emitted from factory plumes. Using these laser systems, the government would be able to fly over or around these smoke stack plumes and identify the molecular composition of the emissions just by activating a laser and assessing the atmospheric absorption. The absorption values of the plume emissions could then be taken at certain frequencies and compared to the known absorption values of airborne molecules at the same frequencies and thus determine if the plume contains pollutants. There are some obstacles, however, before this ideal scenario can be enacted. The objectives given deal with some of these obstacles.

One of the major problems in developing a second application is the wavelength of the current lasers being used. The lasers currently used for missile guidance are Neodymium:YAG, Helium- Neon, and semiconductor diode which operate in the 0.79-2.0 micron range. Most of the research in the past was with the use of LADAR to identify airborne pollutants was done with CO₂ lasers which operate in the 9-11 micron range. Another objective given was to find data containing peak absorption rates that coincided with the frequencies in the range of the lasers that the Air Force uses. From this data a spreadsheet was to be composed presenting the information easily and concisely so that the data collected on these pollutant compounds may be compared with the results from laser spectrometry tests conducted on smokestack plume emissions. Hopefully, the progress made in this stage of the project may serve as a foundation for actual experimentation of an atmospheric pollutant detection system in later stages.

Background

The earlier research of this project was done to find any information on design and charts on previous pollutant identification systems. The problem with this research was that most information found on the application of LADAR for pollutant detection was found with a CO₂ laser which operates in the 9-11 micron range. The purpose of this project was to find the absorption peak values for various airborne pollutants in the 0.79 to 2.0 range.

Another problem with conducting this research was the need to manipulate the absorption data found due to the conditions plume would be analyzed. In this application of LADAR, the laser will be activated in a plane or helicopter approximately 500 meters from the smokestack plume with the plume width approximately 20 meters. These conditions yield 3 parts of absorption for the laser path. The first is the absorption the laser beam will encounter while traveling approximately 500 meters to the plume. The second is the absorption the laser beam will encounter while traveling ten meters through and ten meters back through the plume. The third is the absorption encountered while the laser beam is traveling 500 meters back to the detector that is adjacent to the source. All these parts must be taken into account in two separate calculations. The first is the absorption of a laser beam at a certain frequency with a path length of a 1000 meters through normal atmospheric molecular composition. The second is the absorption of the laser beam through 20 meters of the compound with a concentration of .1%. Both of these problems were easily solved through the use of a spectrometry database containing absorption information in the 0.79 to 2.0 micron range. This program also had the ability to modify data to suit the given test conditions.

A chart was composed containing the different types of units used to describe the wavelength/frequency of an electromagnetic wave. The greatest use of this chart was for the conversion between wavelength (which is used by laser catalogs) and wave number (which is used by spectrometrists). The conversion formula used (with y as the wavelength):
$$\text{wave number} = 1/y * 10^{-4}$$

Problem

The main objective of this project was to locate laser coincident absorption bands of pollutant compounds in the 0.79 to 2.0 micron range for identification in smokestack plumes by means of remote sensing. Identification of the pollutant would be done by comparing the intensity of a laser aimed through a smokestack plume and comparing it to the intensity when aimed through clean air. The presence of a pollutant would then be determined by the increase in absorption.

Methodology

Once the HitranPC database was received, a overall sweep of the 0.79-2.0 micron absorption spectrum was done using the TRANS part of the HitranPC program to find any pollutant compounds that could be detected in that wavelength range (graph 1). The following compounds had absorption peaks in the 0.79-2.0 micron range :OH, N₂O, HBR, HCL, CH₄, CO, HI, HF. After these candidates for detection were found the laser path length in the Hitran PC program was reduced from 1000m to 20m to take into account only the stack plume. The concentration of the pollutant to be tested in the plume was increased from its normal atmospheric proportion to .1% and a graph was made (graph 2). Molecule absorption peaks that still contained significant values above non-pollutant molecules for means of identification were narrowed down into separate files in order to be transferred to the spectra program. These files account for the amount of absorption in the 20 meter plume but duplicate graphs containing the same range and normal molecular proportions had to be made to take into account the 1000 meters that the laser beam travels through normal air to get to and back from the plume (graph 3).

These pairs of files were added to form a composite absorption line to give an approximate value of the absorption that the laser beam would encounter from a plane through the plume containing pollutant emissions (graph 4). A percentage was taken of the absorption of the pollutant peak to the composite absorption value at the same frequency. If the pollutant absorption accounts for 10% of the composite absorption then it was

determined that the LADAR system could detect the pollutant (chart 1). Laser wavelengths of Diode, Neodymium:YAG, and Helium-Neon lasers were then found to see if any coincided with the absorption peaks of detectable pollutants (chart 2). The peaks of detection were then divided into two categories. The first category was a list of compound absorption peaks that were detectable by LADAR with its present wavelength capabilities. The second category consisted of the set of compound absorption wavelengths that did not coincide with the current LADAR wavelength capabilities but were still detectable in the 0.79 to 2.0 micron range.

Results

Graphs 5,6,7 and 8 show the absorption values for pollutant compounds that LADAR is capable of detecting with its present wavelength capabilities. The absorption peak data is displayed by a set of two graphs. The first graph displays the absorption of the pollutant and the absorption of the atmosphere in separate lines. The second graph shows the composite graph from the two sets of data. Both graph lines are composed on wavelength versus absorption. The wavelength the peak occurs is shown on the x axis in microns and the absorption value of the peak is shown on the y axis as a percentage. Graphs 5-8 show the absorption lines for the following pollutants, respectively; HF (1.270-1.286 microns), OH (1.450-1.453 microns), OH (1.479-1.483 microns), HF (1.33-1.30 microns).

Another set of graphs was composed to show absorption lines that contained significant absorption peaks in the 0.79-2 micron range but were not detectable by LADAR. Graphs 9-11 shows the absorption lines for the following pollutants, respectively: HF (1.2594-1.3 microns), CH₄ (1.641-1.706 microns), HCL (1.1.863-1.714 microns).

From the absorption data, a chart was composed listing the exact wavelength an absorption peak occurred, its absorption value, the component absorption value at the same frequency as the pollutant absorption peak, and a percentage value of the pollutant absorption to component absorption.

If the pollutant absorption accounted for more than ten percent of the composite

absorption then the compound containing the absorption peak was considered detectable by LADAR (chart 1). From the research and calculation performed, the following pollutant compounds were found detectable by LADAR with its present wavelength capabilities: OH, HF, CH₄ and HCL are also detectable in the 0.79 to 2.0 micron range, but LADAR presently lacks the wavelength capabilities to detect these compounds.

Acknowledgments

I would like to thank the following for their help in making this paper happen. First I'd like to thank my family for their love and support. I'd also like to thank my fellow apprentices Barry, Chris, Christie, Jenny, Mary, Nancy, Melissa, Jon, Laura, Elliot, Alex, Mark, Darcie, and Deanna. I'd like to thank some of my non-apprentice friends. . .

Lila (Beth) Harbour, Harbour Family, Robert Johnson, Aaron Green, Mr. Shraeder, Mike Reavey, Charlene Dubois, Lynda and Andy Hart, Laura Northington, Meade Family, Jenny Jones, and Bryun Souther.

I'd also like to thank Don Harrison for all the work and time that he has put into the HSAP Program. Most of all I would like to thank my mentor, Lynn Deibler, for his guidance, and friendship to make this paper possible.

Bibliography

Air Pollution. Part A: analysis, Ledbetter, Joe O., Marcel Debberdoe, NY 1972

Fundamentals of air pollution, Williamson, Samuel J., Addison Wesley, MA, 1973

IR; Theory and practice of infrared spectroscopy, Alpert, Nelson L., Plenum Press, NY, 1970

Methods of Air Sampling and Analysis by Inter society Committee, American Public Health Association, Washington D.C., 1972

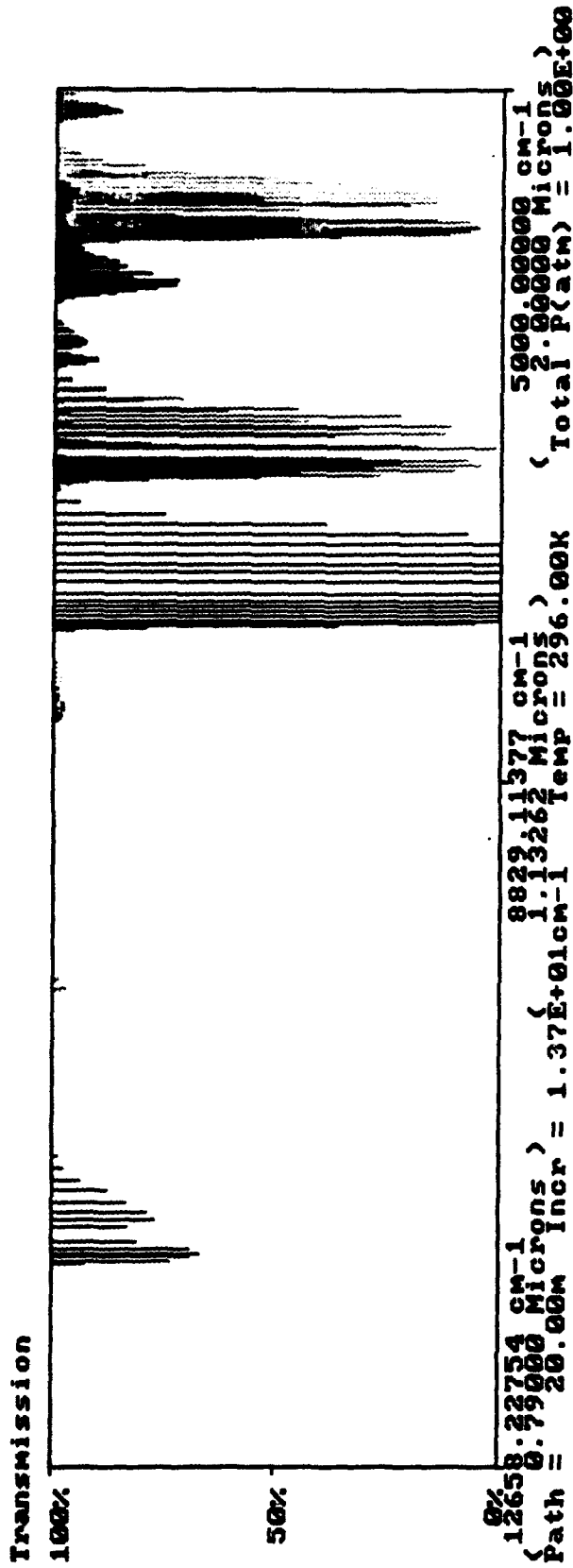
Pollutant Detection by Absorption using MIE scattering and Topographic Targets as Retroreflectors, Byer, Robert L., Garbuny, Max, Applied Optics, Vol 12,7,73

Infrared Remote Sensing and Determination of pollutants in G plumes, Prengle, William H., Morgan, Charles A., Huang, Cheng- Shen, Camani, Paola, Wu, William W., Vol 7,5,73

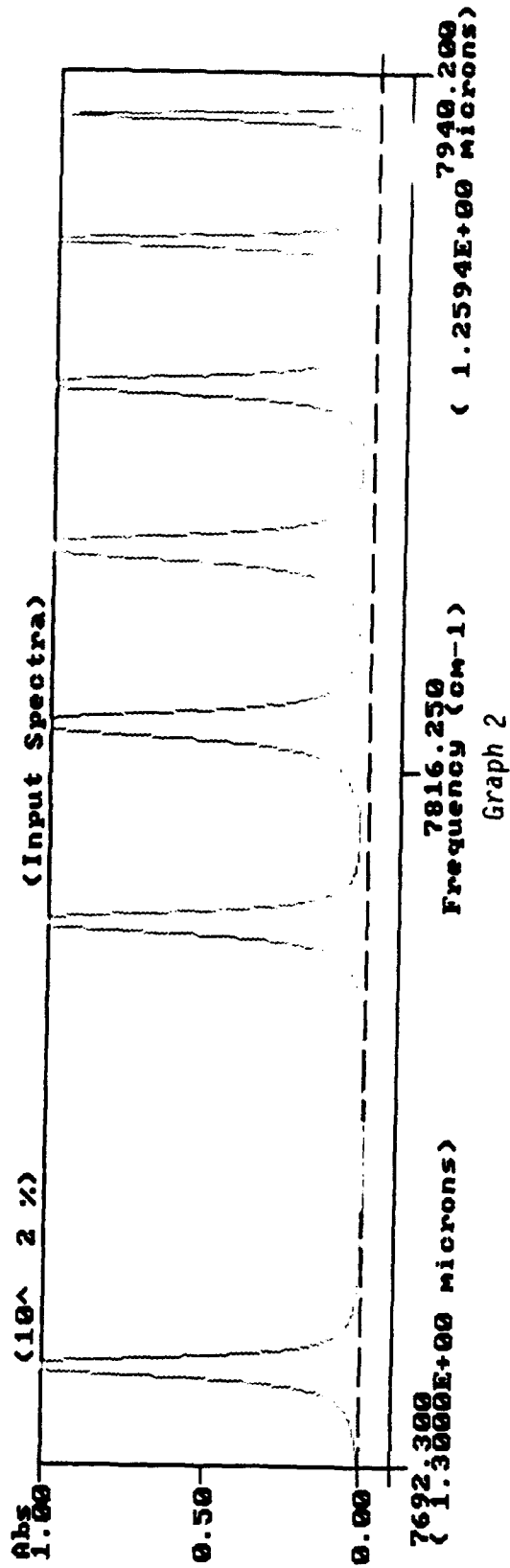
Mobile Remote Sensing System for Atmospheric Monitoring, Edner, Hans, Fredriksson, Kent, Sunesson, Anders, Svanberg, Sune, Applied Optics, 26, 19, 87

Mobile Atmospheric Profiling System, White, Kenneth O., Guttman, William N., Dowling, James A., Applied Optics, 24,21,85

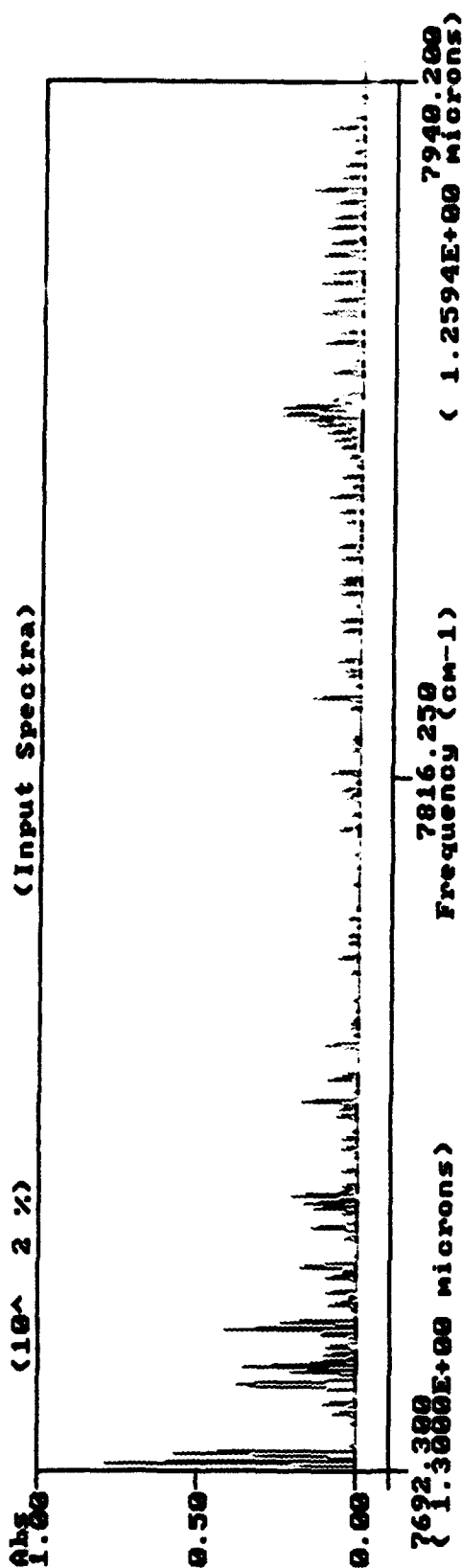
HitranPc Database(2.0) , University of South Florida, 91



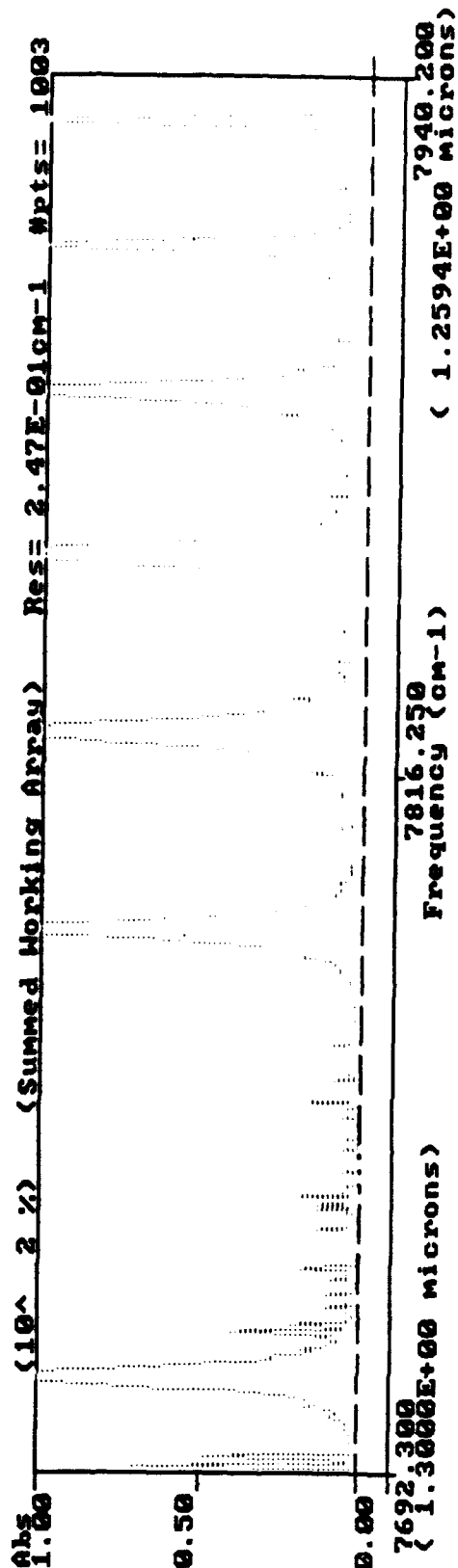
Graph 1



Graph 2



Graph 3



Graph 4

POLLUTANT ABSORPTION OF LADAR

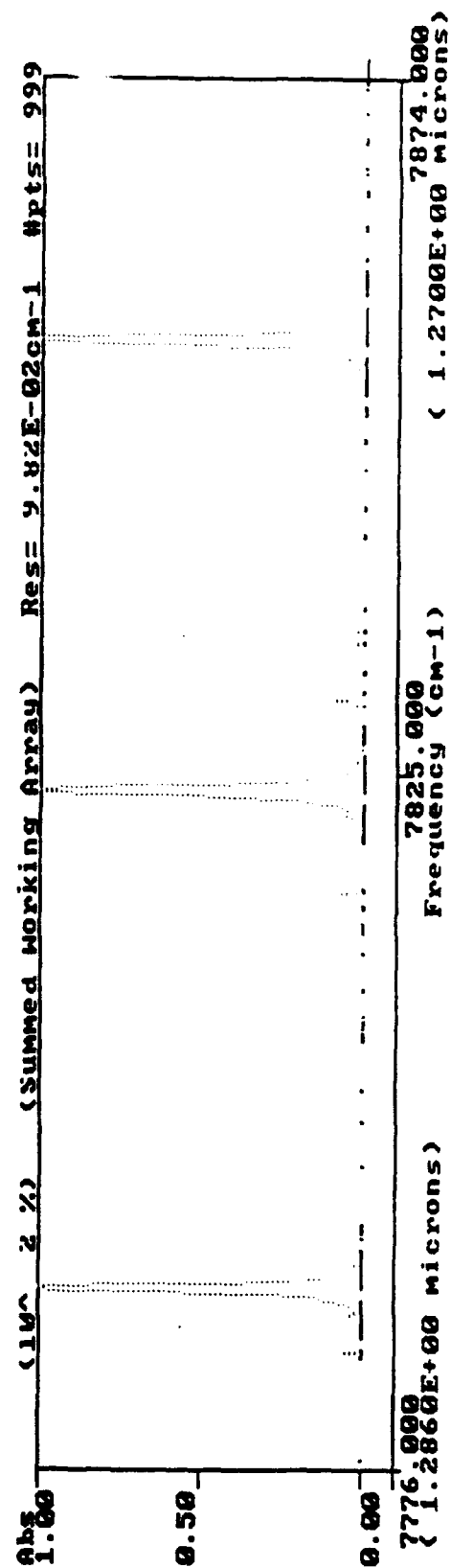
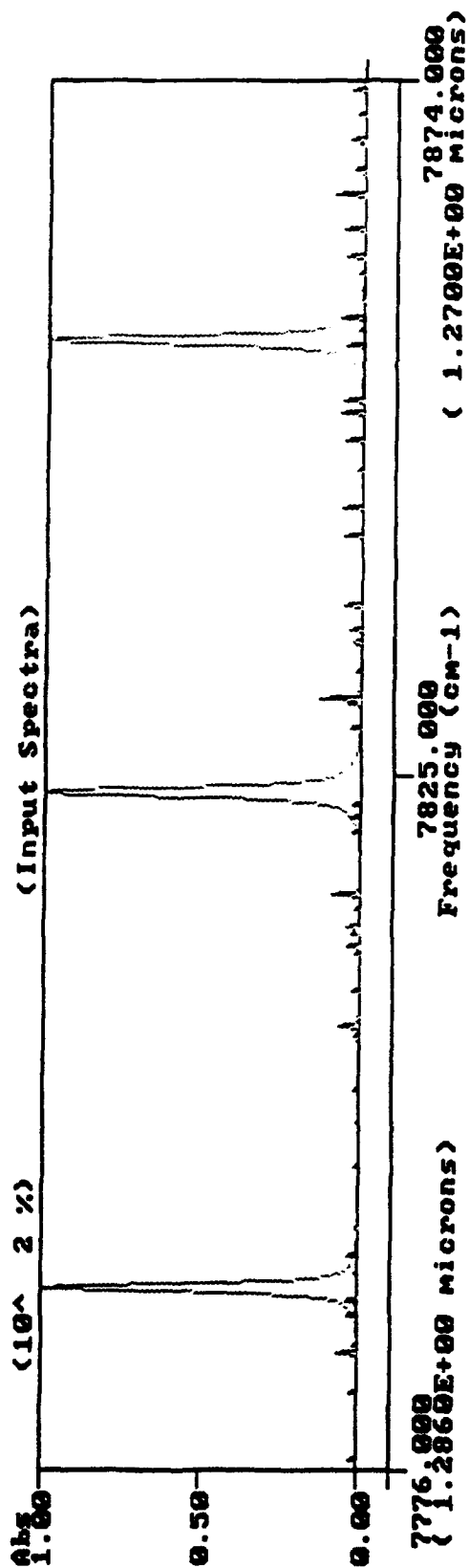
MOLECULE	WAVELENGTH	POLLUTANT	AIR	PERCENT
HF	1.2839	99.9	0.0	100
HF	1.2782	99.4	0.0	100
HF	1.2729	99.9	0.1	99.8
OH	1.4519	89.8	34.8	72.0
OH	1.4800	54.6	20.4	72.8
OH	1.4799	54.7	14.7	78.7
HF	1.2972	100	0.4	99.6
HF	1.2837	100	0.1	99.8
HF	1.2781	100	0.0	99.9
HF	1.2731	100	3.8	96.3
HF	1.2684	100	8.4	92.2
HF	1.2642	100	6.5	93.9
HF	1.2607	100	10.7	90.3
HF	1.3213	99.9	17.4	85.1
HF	1.3125	99.9	2.2	97.7
HF	1.3045	99.9	0.5	99.4

Chart 1

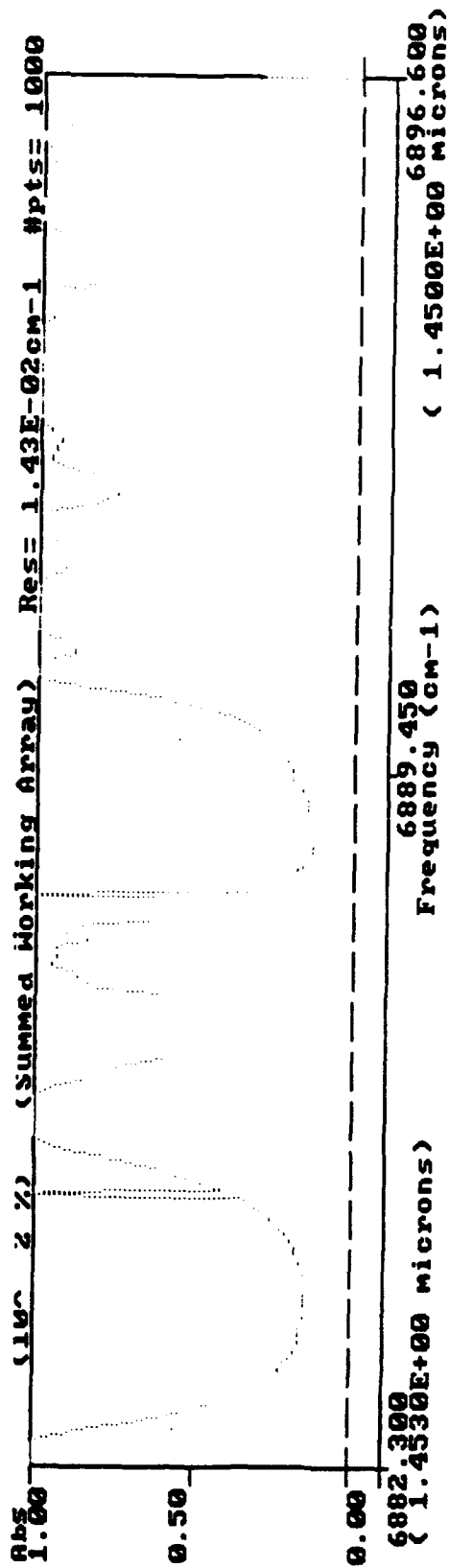
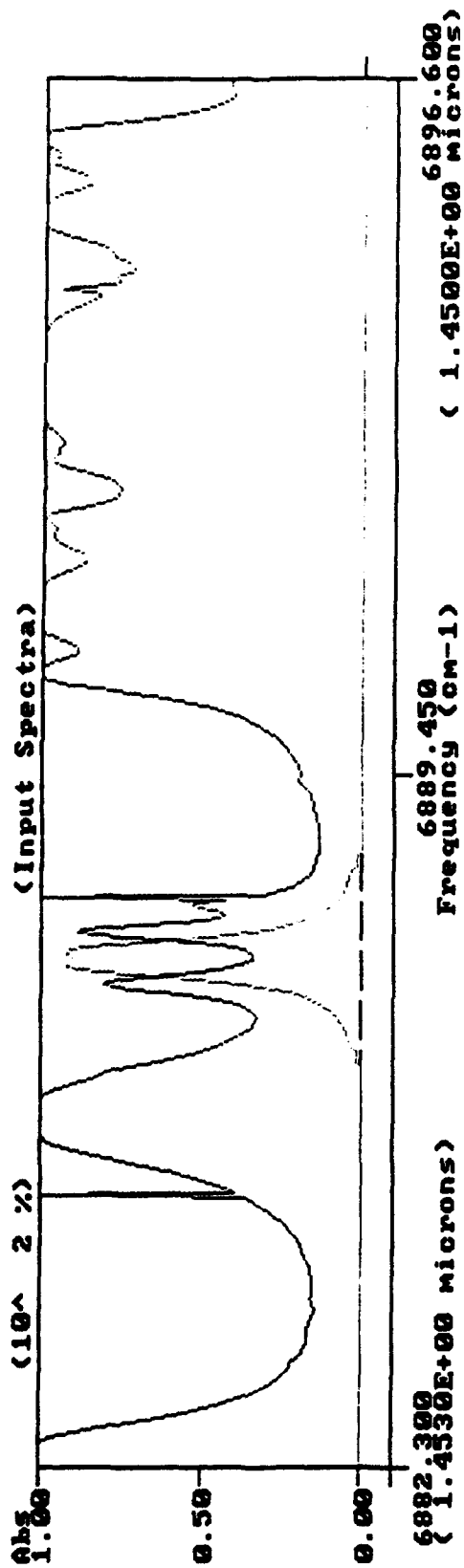
Useful Lasers

frequency	laser	useful for detection?
1.15	he-ne	no
1.152	he-ne	no
1.153	he-ne	no
1.523	he-ne	no
1.532	he-ne	no
.79-.81	diode	no
1.06	diode	no
1.2-1.3	diode	yes
1.27-1.33	diode	yes
1.3	diode	no
1.45	diode	no
1.48	diode	yes
1.5	diode	no
1.51	diode	no
1.52-1.58	diode	no
1.55	diode	no
1.06	neodymium	no
1.061	neodymium	no
1.064	neodymium	no
1.064-1.319	neodymium	yes
1.3	neodymium	no
1.32	neodymium	no

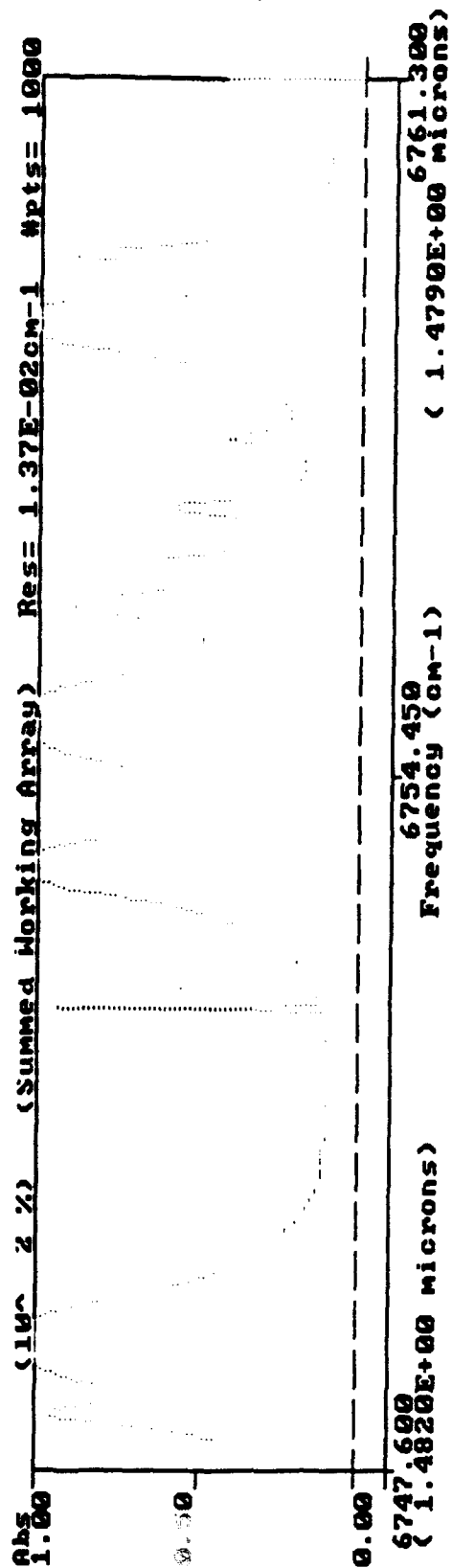
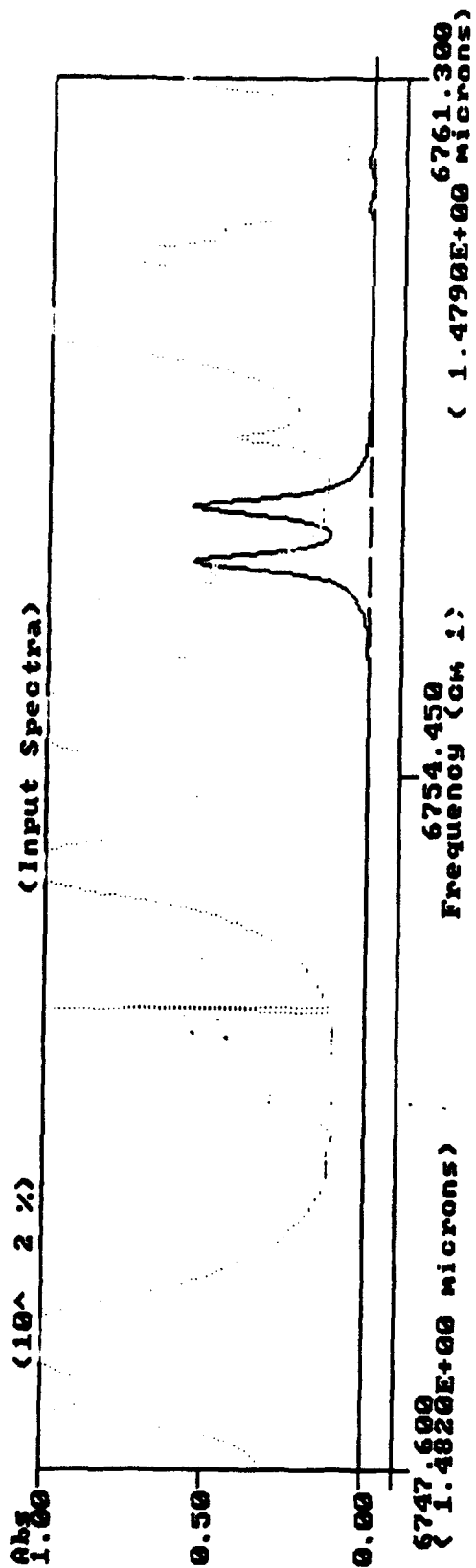
Chart 2

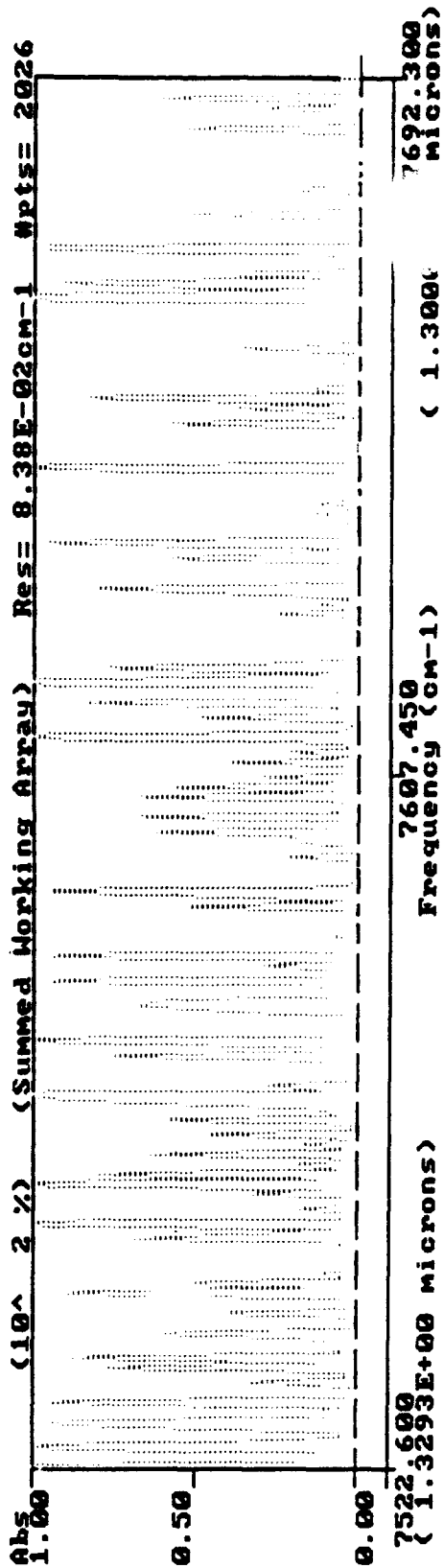
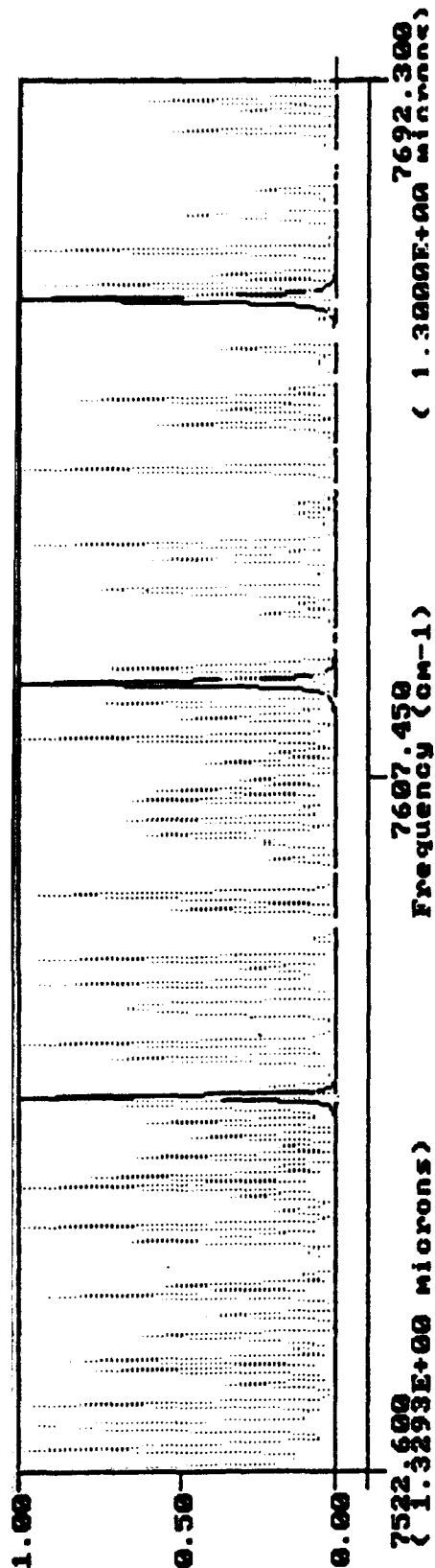


Graph 5

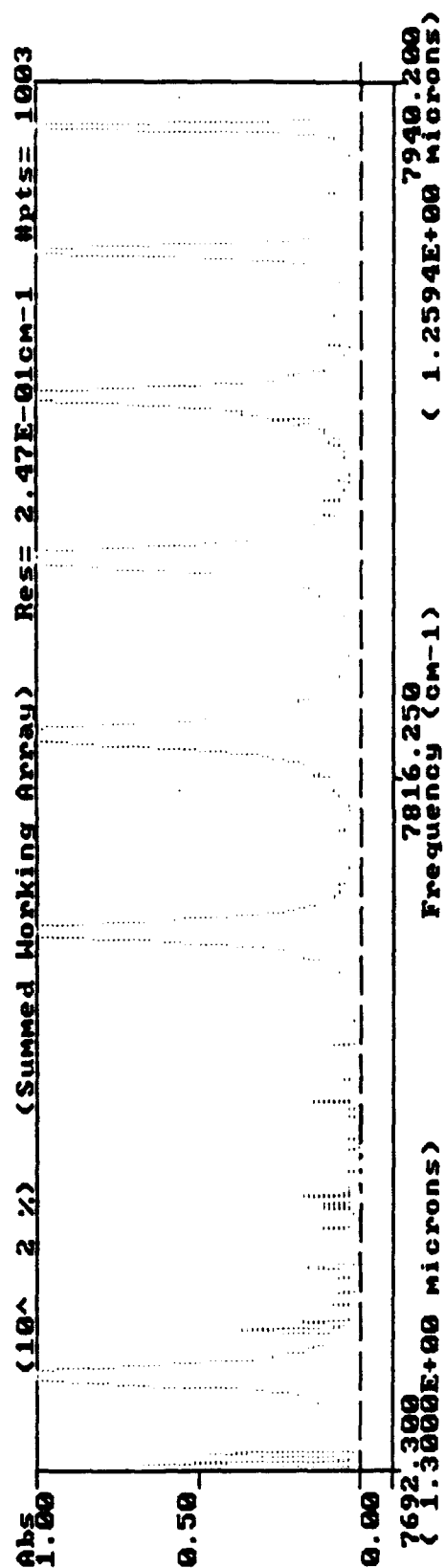
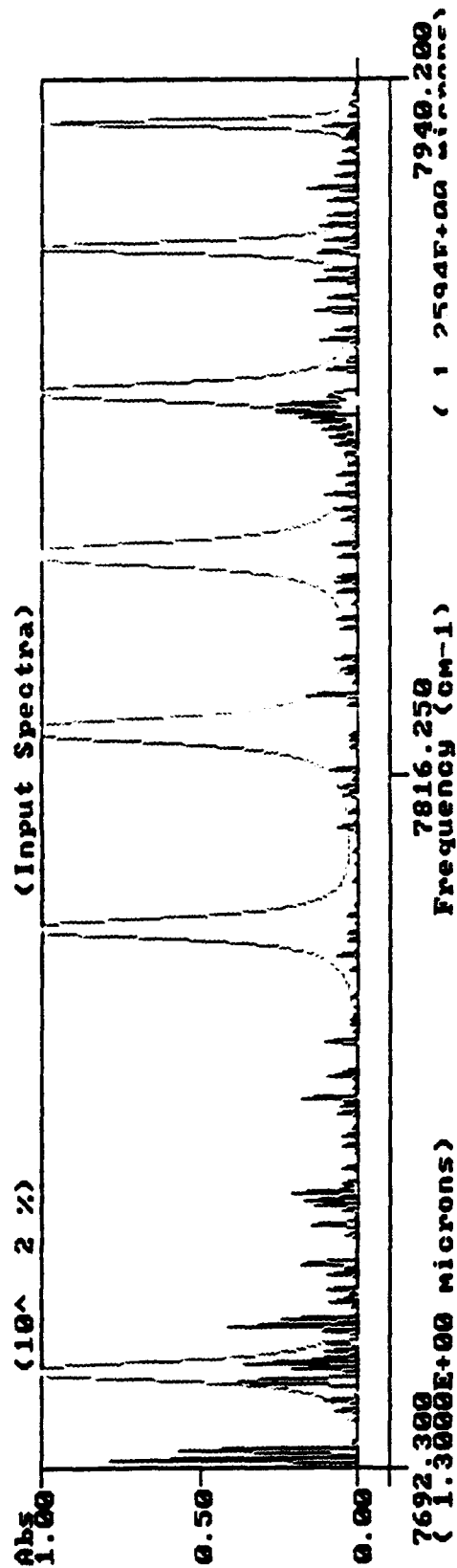


Graph 6

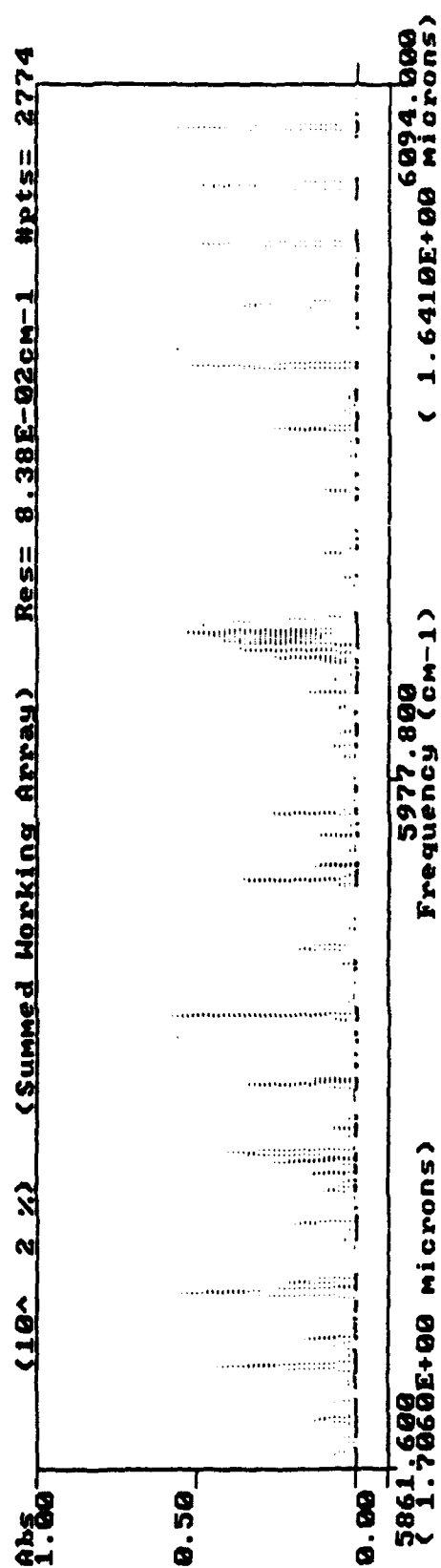
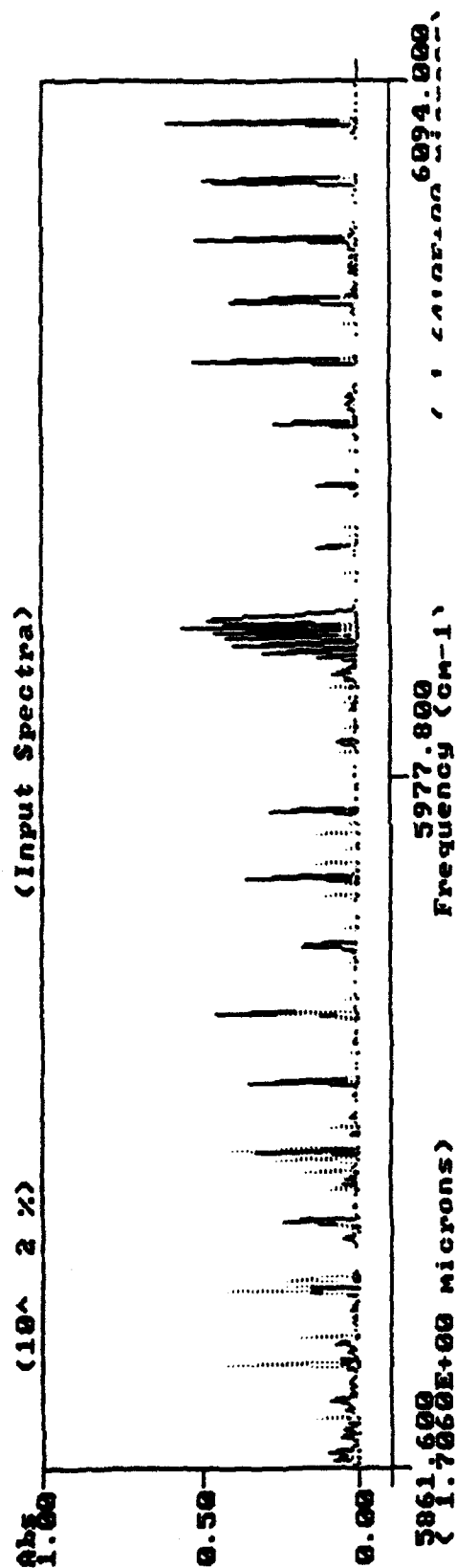




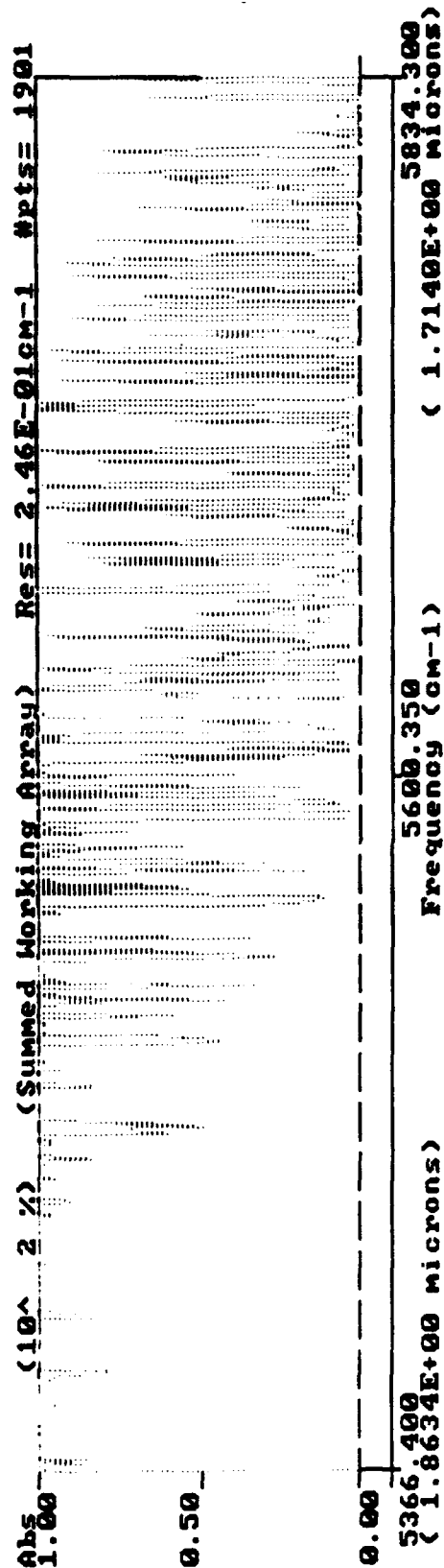
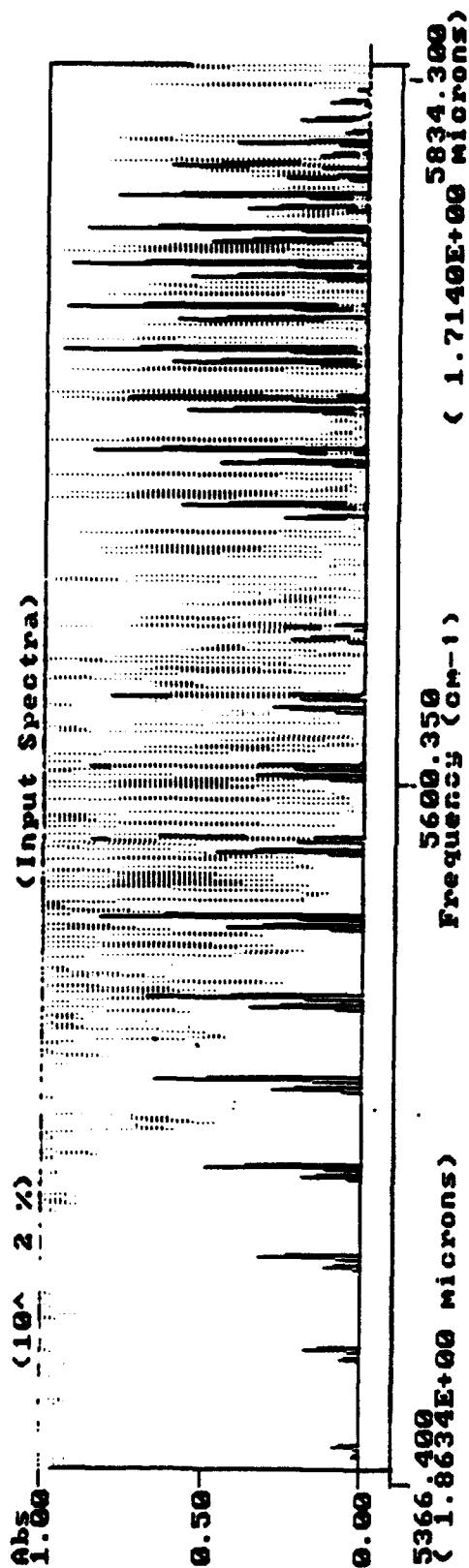
Graph 8



Graph 9



Graph 10



Graph 11

Environmental Movement of Heavy Metals in Soils and Vegetation

**Mary F. Pletcher
High School Apprentice
Environics Branch**

**Wright Laboratory Armament Directorate
WL/MNOE
Eglin AFB, FL 32542-5434**

**Final Report for:
High School Apprenticeship Program
Wright Laboratory Armament Directorate**

**Sponsored by:
Air Force Office of Scientific Research
Bolling Air Force Base, Washington DC.**

August 1993

Environmental Movement of Heavy Metals in Vegetation and Soils

**Mary F. Fletcher
High School Apprentice
Environics Branch
WL/MNOE**

Abstract

Currently tantalum (Ta) and tungsten (W) are used in the construction of penetrators for warheads. While the two elements have not been proven to be toxic to humans and animals, the ability of the elements to enter the food chain is unknown. Thus, this study tested tantalum, tungsten, and a tungsten alloy's abilities to enter the food chain. The project consisted primarily of a plant uptake study, however, a leaching study was also started.

The study consisted of planting two species of plants; *Zea mays* 'Hunters Choice' (corn) and *Phaseolus vulgaris* 'Blue Lake' (bean), into soils containing different exposures of tantalum, tungsten and the alloy. Plants were grown in a growth chamber insuring uniform conditions. Results from this preliminary study suggest that there will be a minimal plant uptake.

Contents

Introduction.....	4
Background.....	4
Procedure and Results.....	6
Miscellaneous.....	13
Acknowledgements.....	13
References.....	14

Environmental Movement of Heavy Metals in Vegetation and Soils

Mary F. Fletcher

Introduction

The uptake of heavy metals used in the construction of various military weapons into the food chain has been the subject of previous studies. However, two heavy metals, tantalum (Ta) and tungsten (W), have not been studied due to the only recent increase of the metals use for military weapons. Currently, tantalum and tungsten are used in the construction of penetrators of warheads as an alternative to depleted uranium, which has some undesirable effects associated with its use. Laboratory studies have shown that the elements are not toxic to humans, however, no studies have been conducted to determine the elements' ability to enter the food chain. A secondary study, leaching ability, was also started though inadequate time did not allow for completion of the study.

Background

Tantalum Tantalum is one of the most inert of all metals, not reacting with chemicals below 150 degrees Centigrade. Tantalum's inertness is caused by a dielectric oxide film. Medically, tantalum gauze is used for surgical repairs such as closing skull defects and tantalum powder is used for the visualization of lung morphology and angiography. The current OSHA (Occupational Safety and Health Administration) permissible exposure limit, also known as PEL, is 5 milligrams per cubic meter (source 1).

Tungsten Tungsten is a gray hard metal with many industrial uses due to its high melting point and strength. For a long time, tungsten was used primarily used as wire for incandescent lamp filaments and for electric vacuum devices (source 2). Early toxicity studies of tungsten and its compounds show a difference between the metal's soluble and insoluble compounds. Soluble compounds have a PEL of 1 mg per cubic meter versus that of the insolubles which have PEL's of 5 milligrams per cubic meter (source 1).

Literature Review Technical reports about the plant uptake of heavy metals excluding tantalum and tungsten have been published. In Trace and Toxic Metal Uptake by Marsh Plants as Affected by Eh, pH and Salinity, a study was conducted to determine whether pH, redox potential, and salinity affected trace and toxic metal availability to marsh plants. The metals studied were mercury, lead, cadmium, copper, iron and manganese. The results of this study showed that the uptake of mercury is enhanced by decreases in salinity and an increase in pH. Lead uptake was increased in more acidic soil. Cadmium uptake was also increased in high oxidation conditions and acidic soils. Zinc uptake was increased under higher oxidation conditions. Copper uptake was unaffected. The study concluded that pH, redox potential, and salinity did affect uptake (source 3).

In A Hydroponic Study of Heavy Metal Uptake by Selected Marsh Plants, eight marsh plants were grown in chemically concentrated hydroponic solutions containing three concentrations of heavy metals (0.0, 0.5, and 1 parts per million) to evaluate the ability of each plant species to uptake and accumulate heavy metals. The heavy metals used in the study were zinc, cadmium, nickel, lead and chromium. The study concluded that specific plant species had higher uptake of heavy metals. However, lead and chromium accumulated in the roots of all the species with little translocation into plant tops. The results also indicated that phosphorous and iron content in the roots appeared to be a major factor in determining the ability of the marsh plants to translocate heavy metals from the roots into other plant parts (source 4).

In Influence of Disposal Environment on Availability and Plant Uptake of Heavy Metals on Dredged Material, the heavy metal uptake by *Cyperus esculentus* from fifteen highly contaminated freshwater water sediments under reduced (flooded) and oxidized (upland) disposal conditions was studied. Heavy metal uptake by *Spartina alterniflora* and *Distichlis spicata* from fourteen highly contaminated saltwater sediments under flooded disposal conditions was also investigated. The plants were analyzed for the heavy metals zinc, cadmium, copper, iron, manganese, arsenic, mercury, nickel, chromium, and lead. Plant uptake of heavy metals, especially zinc and cadmium, was shown to be greater in plants grown in upland sediments compared to with flooded sediments. The study thus concluded that the plant uptake of heavy metals was site specific (source 5).

In Ability of Salt Marshes to Remove Nutrients and Heavy Metals From Dredged Material Disposal Area Effluents, experimental raceways were constructed in a salt marsh adjacent to a dredged material confinement area. The research program was designed to determine the ability of the salt marsh systems to remove nitrogen, phosphorous, iron, manganese, cadmium, copper, nickel and zinc from the effluent. During the study all contaminants were found to decrease in the effluent as it passed through the experimental raceways. Mean metal removal efficiencies ranged between fifteen and thirty-two percent. Inorganic chemical and physical processes probably account for much of the removal (source 6).

Apparatus

Growth Chamber All plants for the study were grown in a growth chamber measuring 3'x2'x2'9," in order to maintain uniform growing conditions. Lighting, temperature, and humidity could be controlled. Lighting, incandescent and full florescent, was on a twelve hour cycle. The temperature was set on 84.5 degrees Fahrenheit/ 29.5 degrees Centigrade. The relative humidity within the chamber was 60%.

ICP In order to detect trace amounts of elements in the ash; the ICP/6500 Inductively Coupled Plasma System for Atomic Spectroscopy by Perkin-Elmer was used. The system consists of a radio-frequency (RF) power supply and plasma torch housing, a Model 5000 Spectrophotometer and a Perkin-Elmer 7000 Professional Computer. The system can identify elements in a sample due to the wavelengths generated (characteristic property). However, standard solutions containing elements of interest are needed. Using the standard, the user calibrates the ICP to read a peak of the standard's wavelengths. The ICP then uses the calibrated peak to determine the quantity of the element of interest in a sample. Results are reported in parts per million (ppm) (source 7).

Procedure and Results

Plant Uptake Study The plant uptake study consisted of planting two species of plants; *Zea mays* 'Hunters Choice' (corn) and *Phaseolous vulgaris* 'Blue Lake' (bean), into soils containing different exposures of tantalum, tungsten and a tungsten alloy. The alloy was 4.04% iron, 4.36% nickel, 2.56% copper, and 89.04% tungsten. The exposure ranged from 25 to 800 parts per million.

The soil used in the study came from Range 52-North located approximately 17 miles northeast of Eglin Main, because this area is known to have had no heavy metal contamination from past test and evaluation programs. The soil was placed into plastic bags and brought back to the chemistry lab where it was then sieved. 350 grams of soil was then measured as was the appropriate amounts of tantalum, tungsten or the alloy.

PPM In Terms of Grams	
ppm	grams per 350 grams of soil
25	0.00875g
50	0.0175g
100	0.035g
200	0.070g
400	0.140g
800	0.280g

Figure 1- Conversion of ppm to grams

The plastic containers containing the soil and metal were then spun on a Ball Jar Roller Mill for ten minutes to insure that the metal and soil was homogenized.

After the soil and metal was mixed, the mixture was placed in a plastic pot. Then two seeds, corn or bean, were planted approximately one inch deep in the pot. There were four pots of each tantalum and tungsten exposure levels of 100, 200, 400, and 800 parts per million. There were two pots of each tungsten exposure level of twenty-five and fifty parts per million and of each exposure level of the tungsten alloy. Initial planting in the tantalum and tungsten soils was on June 10, 1993. Planting in the alloy soil was done a week later on June 17, 1993 due to the delayed arrival of the alloyed material.

The plants were grown for a little over a month in the growth chamber. Watering was done approximately every other day with a nutrient solution which was 5% Nitrate Nitrogen, 5% Ammoniacal Nitrogen, 30% Phosphoric Acid, and 20% Soluble Potash. There were a few problems in the study; by June 22, 1993, eleven of the initial forty four plants had not germinated, thus replanting was necessary. Fortunately, the majority of these did germinate.

plant				date of germination
species	metal	dosage	number	
corn	control	-	1	18-Jun
corn	control	-	2	17-Jun
bean	control	-	1	19-Jun
bean	control	-	2	20-Jun
corn	tantalum	100 ppm	1	14-Jun
corn	tantalum	100 ppm	2	13-Jun
bean	tantalum	100 ppm	1	26-Jun
bean	tantalum	100 ppm	2	26-Jun
corn	tantalum	200 ppm	1	15-Jun
corn	tantalum	200 ppm	2	19-Jun
bean	tantalum	200 ppm	1	25-Jun
bean	tantalum	200 ppm	2	no germination
corn	tantalum	400 ppm	1	no germination
corn	tantalum	400 ppm	2	15-Jun
bean	tantalum	400 ppm	1	25-Jun
bean	tantalum	400 ppm	2	25-Jun
corn	tantalum	800 ppm	1	19-Jun
corn	tantalum	800 ppm	2	no germination
bean	tantalum	800 ppm	1	25-Jun
bean	tantalum	800 ppm	2	25-Jun
bean	tungsten	25 ppm	1	26-Jul
bean	tungsten	25 ppm	2	25-Jul
bean	tungsten	50 ppm	1	26-Jul
bean	tungsten	50 ppm	2	26-Jul
corn	tungsten	100 ppm	1	16-Jun
corn	tungsten	100 ppm	2	19-Jun
bean	tungsten	100 ppm	1	25-Jun
bean	tungsten	100 ppm	2	25-Jun
corn	tungsten	200 ppm	1	15-Jun
corn	tungsten	200 ppm	2	15-Jun
bean	tungsten	200 ppm	1	no germination
bean	tungsten	200 ppm	2	15-Jun
corn	tungsten	400 ppm	1	15-Jun
corn	tungsten	400 ppm	2	14-Jun
bean	tungsten	400 ppm	1	15-Jun
bean	tungsten	400 ppm	2	15-Jun
corn	tungsten	800 ppm	1	6/13/93
corn	tungsten	800 ppm	2	6/13/93

Figure 2- Germination dates of plants

bean	tungsten	800 ppm	1	15-Jun
bean	tungsten	800 ppm	2	15-Jun
corn	alloy	100 ppm	1	20-Jun
bean	alloy	100 ppm	1	23-Jun
corn	alloy	200 ppm	1	20-Jun
bean	alloy	200 ppm	1	22-Jun
corn	alloy	400 ppm	1	20-Jun
bean	alloy	400 ppm	1	22-Jun
corn	alloy	800 ppm	1	20-Jun
bean	alloy	800 ppm	1	no germination

Figure 2- Germination dates of plants (continued)

Additionally, when I returned from a week long trip, I discovered that over half of my plants had died (Figure 3). The majority of these were corn plants, including the controls. Apparently the corn plants were not able to grow the root structures they needed to survive. My mentor and I decided to proceed, analyzing the remaining plants.

Dead plants on 12 July			
plant			
species	metal	dosage	number
corn	control	-	1
corn	control	-	2
bean	control	-	1
corn	tantalum	100 ppm	1
corn	tantalum	100 ppm	2
corn	tantalum	200 ppm	1
corn	tantalum	400 ppm	1
corn	tantalum	400 ppm	2
bean	tantalum	400 ppm	2
corn	tantalum	800 ppm	2
corn	tungsten	100 ppm	2
bean	tungsten	200 ppm	1
bean	tungsten	200 ppm	2
corn	tungsten	400 ppm	1
corn	tungsten	400 ppm	2
bean	tungsten	400 ppm	1
bean	tungsten	400 ppm	2
corn	tungsten	800 ppm	1
corn	tungsten	800 ppm	2
bean	tungsten	800 ppm	1
bean	tungsten	800 ppm	2
corn	alloy	100 ppm	1
corn	alloy	200 ppm	1
corn	alloy	400 ppm	1
corn	alloy	800 ppm	1

Figure 3- Dead plants on July 12, 1993

On July 21, 1993, the plants were removed from the soil so that I could begin processing for ICP analysis. First, I rinsed the roots of the plants in distilled water to wash off the remaining soil. I then dried the plants in the growth chamber. Second, I ashed the samples at 1200 degrees Fahrenheit in a Muffle Furnace to eliminate the organics. After ashing the plants, I placed the remains in a plastic specimen cup. I then poured 25 milliliters of Nitric Acid and 25 ml of distilled water into the cups so that the inorganics could digest for the ICP analysis. The acid, water and ash solution was then filtered. ICP analysis was then performed.

plant			results	
species	metal	dosage	dry weight	ppm
corn	control	-	3.08g	0
bean	tantalum	100	2.86g	0
bean	tantalum	200	5.69g	0
corn	tantalum	400	0.95g	0
bean	tantalum	400	0.34g	0
corn	tantalum	800	0.29g	0
bean	tantalum	800	3.78g	0
corn	tungsten	25	2.50g	0
bean	tungsten	50	2.75g	0
corn	tungsten	100	0.10g	0
bean	tungsten	100	4.39g	0
bean	tungsten	200	0.26g	0
bean	tungsten	400	0.90g	0
bean	tungsten	800	0.20g	0
bean	alloy	100	2.41g	4
bean	alloy	200	1.33g	0
bean	alloy	400	1.57g	0
bean	alloy	800	0.41g	0

Figure 4- ICP analysis results

The results of the test were very good. Based upon this study there was no plant uptake of tantalum or tungsten. In terms of the alloy, only one plant exposed to the alloy, the bean at 100 parts per million, had any uptake and this uptake was only four parts per million. These results suggest that there will be a minimal of uptake of these metals. However, this is only a preliminary study dealing with only two kinds of plants, monochodoleans (*Zea mays 'Hunters Choice'*) and dichodoleans (*Phaseoulous vulgaris 'Blue Lake'*). Other plants could uptake the metals in higher concentrations.

Leaching Study

I was only able to begin the leaching study due to inadequate time however, my mentor will continue it. The leaching study consists of 6 leaching columns filled with the top four layers of soil from random sites of range 52-North. Each layer is six inches deep. The columns have 12.56 grams of various metals across the top. Two columns contain tungsten, two tantalum, one copper, and one nickel. The columns

will be exposed to a simulated yearly rainfall to see how much metal will leach. The runoff will be collected via tubes connected to the columns. The runoff will then be analyzed using the ICP.

Miscellaneous

Besides completing my plant uptake study I also accomplished many other things. I was responsible for the chemical inventory of the MicroAnalysis Laboratory. I participated in the cleanup and organization of the Chemistry Laboratory. I also learned many different computer operations including MicroSoft Word, Excel, Charisma and the VAX and other instruments within the chemistry laboratory. And perhaps most importantly I was able to gain valuable experience to help me to determine future plans such as my college major.

Acknowledgments

Without the support of many individuals this summer would not have been as rewarding as it has been. I would first like to acknowledge my mentor, Lt. Brad Noland. I really could not have asked for a better mentor. Secondly I would like to thank the Eglin HSAP coordinators, Mr. Don Harrison who was also my Branch Chief, Mr. Mike Deiler, and Mrs. Glenda Apel. These individuals truly make the program successful, without their time and energy there would not be a HSAP. I would also like to acknowledge Mr. Ric Crews and Mr. Luis Santana and the rest of the Environics Branch. Everyone was always willing to answer my questions, take me to the photolab and range and make sure I felt at home. Finally I would like to thank Miss Nancy Deibler, Miss Melissa Griffiths and all of my fellow HSAPs. They all made a rewarding educational program into a lot of fun.

References

1. Harvey, Gregory J: Certified Industrial Hygienist, Biochemical Toxicology Branch. "Memo to MNOE on Tantalum/Tungsten Toxicity". 12 May 1992
2. Drobysheva, Ye. K., Pavlov, I.M., Ushakov, Ye. V. Cold Brittleness and Structure of Tungsten. U.S. Army Foreign Science and Technology Center; Charlottesville, Virginia: 19 February 1987. 4.
3. Center for Wetland Resources. Trace and Toxic Metal Uptake By Marsh Plants as Affected By Eh, pH, and Salinity. Waterways Experiment Station-Corps of Engineers: Vicksburg, Mississippi: December 1977.
4. Landin, Mary C., Lee, Charles H., Sturgis, Thomas C.. A Hydroponic Study of Heavy Metal Uptake by Selected Marsh Plant Species. Waterways Experiment Station-Corps of Engineers; Vicksburg, Mississippi: September 1975.
5. Folsom, Bobby L. Jr., Lee, Charles R., Bates, Derrick J. Influence of Disposal Environment on Availability and Plant Uptake of Heavy Metals in Dredged Material. Waterways Experiment Station; Vicksburg, Mississippi: December 1981.
6. Windom, Herbert L. Ability of Salt Marshes to Remove Nutrients and Heavy Metals From Dredged Material Disposal Area Effluents. Waterways Experiment Station-Corps of Engineers: December 1977.
7. "Principles of Operation". Perkin-Elmer ICP/6500 Inductively Coupled Plasma System for Atomic Spectroscopy Handbook.

SOLUBILITY AND RECRYSTALLIZATION OF
1,3,3-TRINITROAZETIDINE (TNAZ)

DAVID A. ROSENBAUM

FINAL REPORT

HIGH SCHOOL APPRENTICESHIP PROGRAM

WRIGHT LABORATORY

HIGH EXPLOSIVES RESEARCH AND DEVELOPMENT(HERD) FACILITY

WL/MNME

SPONSORED BY:

RESEARCH AND DEVELOPMENT LABORATORIES

CULVER CITY, CA

AUGUST 18, 1993

TABLE OF CONTENTS

I. Abstract

II. Background

III. Procedures and Results

IV. Conclusion

V. Miscellaneous

VI. References

SOLUBILITY AND RECRYSTALLIZATION OF
1,3,3-TRINITROAZETIDINE (TNAZ)
DAVID A. ROSENBAUM
HIGH SCHOOL APPRENTICESHIP PROGRAM
ENERGETIC MATERIALS BRANCH
WRIGHT LAB ARMAMENT DIRECTORATE
SECTION 1

1,3,3-trinitroazetidine (TNAZ) is a heterocyclic compound (energetic material) under investigation as a melt cast base for composite high explosive applications. TNAZ's high density, thermal stability, and enhanced performance over other military formulations make it suitable for high energy applications. This ability to melt cast and provide higher energy output combined with less sensitivity, makes TNAZ attractive as a military explosive. Thirty four pounds (15.5 kilograms) of TNAZ was procured by the High Explosives Research and Development (HERD) Facility in a joint action with the Army Research, Development, and Engineering Center (ARDEC) through a commercial best effort contract with Aerojet Ordinance. The TNAZ was contaminated with nitric acid. Explosive charges fabricated under hydraulic pressing at 30,000 psi, exuded nitric acid contaminating the die, ram, and press. This necessitated the removal of the nitric acid. Solvent recrystallization was chosen as the best method of purification. Solubility tests were done to determine the most efficient solvent. The solvents consisted of alcohols, water, and acetone. The TNAZ was recrystallized from ethanol by crash precipitation in distilled ice water. Drophammer was conducted to determine the impact sensitivity. Thermal analysis was completed to determine the melt point and decomposition exotherm. The structure of TNAZ was verified by NMR and FTIR, its morphology studied by Scanning Electron Microscopy, and its particle size determined. The 15.5 kilograms of TNAZ was successfully recrystallized in two batches removing all detectable traces of nitric acid contamination.

BACKGROUND

SECTION II

The military is faced with many problems when developing explosives. They must take into account the explosives performance, insensitivity, cost and many other factors. The HERD and the military are addressing the problem of developing a melt cast base using heterocyclic materials for High Energy Composite Explosive Applications. The present melt cast binder commonly used with Cyclic Nitramines is TNT. TNT when combined with RDX, PETN, and HMX produce the composites Comp B, Pentolite, and Octol. Although TNT has a stable low temperature melt phase and good thermal stability it has a low density and low energy which dilutes the Heterocyclic Nitramine. TNAZ not only has a stable low melt temperature liquid phase but also has high density and high energy. TNAZ when combined with PETN, RDX, and HMX produces a composite explosive which greatly exceeds Pentolite, Comp B, and Octol in energy output. Secondly when TNAZ is combined with insensitive particulate explosives such as NTO, NQ, CL-14, and ADNBF produces a composite explosive equivalent in energy to Octol, yet much less sensitive to initiation. Increased energy content of warheads in air-to-air and surface-to-air missiles can greatly improve the lethality and effectiveness of those warheads. Heterocyclic materials possess high density, high energy, and thus high performance. One goal of the program addressed is to use 1,3,3-trinitroazetidine (TNAZ) as this high energy melt cast base.

Heterocyclic materials are organic ring compounds containing atoms other than carbon in the skeletal ring. These materials are ideal for high energy insensitive applications. TNAZ is a heterocyclic compound consisting of a four-membered ring (Figure 1) containing one nitrogen in the ring. Because of its 101 degree Celsius melt

point, TNAZ is melt castable using existing steam jacketed melt kettles which usually operate at 80-110 degrees Celsius, depending upon the steam pressure. Two alkyl (geminal) nitro functional groups are attached to the number three carbon and one nitramine functional group is located in the number one position. It has the unique structure of containing both aliphatic nitro and nitramine functional groups (Ref. 1). TNAZ is synthesized by the condensation of t-butyl and epichlorohydrin (1) to form the azetidol (2). The azetidol is then reacted with methanesulfonyl chloride to form the mesylate (3). Displacement of the mesylate with sodium nitrate gave t-butyl-3-nitroazetidine (4) which is converted to t-butyl-3,3-dinitroazetidine (5) by oxidative nitrolysis. Nitrolysis of 5 with acetyl nitrate gave TNAZ (Ref. 2).

THE PRESENT SYNTHESIS OF TNAZ

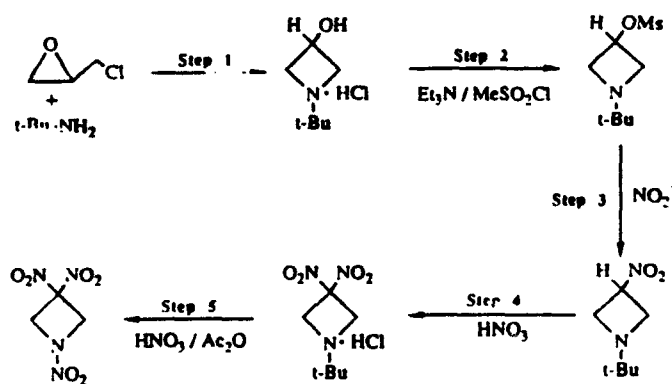


Figure 1

The high levels of interest in utilizing TNAZ as a military high explosive has stimulated extensive research to improve its synthesis (Figure 2) and preparation by alternative, less costly, and higher yielding methods (Ref. 2).

ANOTHER APPROACH

Simultaneous Introduction of Geminal Dinitro Groups and Nitrolysis :

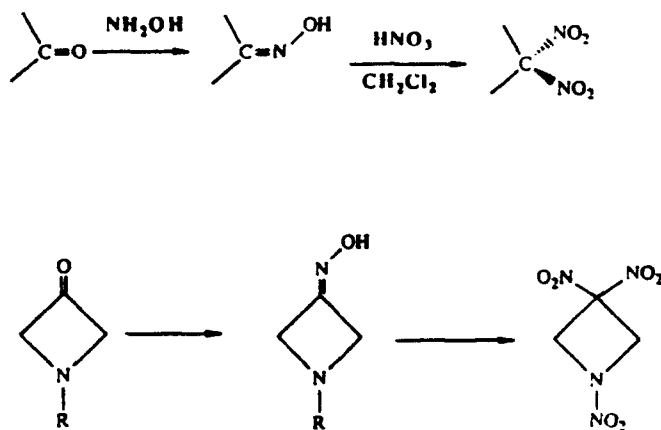


Figure 2

The density of TNAZ is 1.84 g/cm³, greater than all commonly used military high explosives except HMX. TNAZ has a high performance level with a detonation velocity of 9 km/sec and a detonation pressure of 360 kbar which compares favorably to HMX with a detonation velocity of 9.11 km/sec and a detonation pressure of 390 kbar (Ref. 3).

The scientific approach used was divided into four stages. The first phase involved solubility tests to determine the best solvent to use in the recrystallization. The second phase included a small scale (100 g) recrystallization to verify our process procedure and technique. On successful completion of phase two, phase three was initiated. This phase involved recrystallization of 33.94 pounds in two separate batches. Phase four consisted of analyzing the recrystallized TNAZ. This included determination of structure, morphology, thermal properties, and sensitivity.

PROCEDURES AND RESULTS

SECTION III

Solubility of TNAZ in 20 ml of acetone, ethanol, methanol, 2-propanol, and distilled water(200 ml at ambient) was determined at ambient and elevated temperature. Solubility tests were conducted to determine the most efficient solvent to use to recrystallize TNAZ. Solubility is defined to be the maximum amount of solute that will dissolve in a fixed amount of solvent at a defined temperature. When a two component system contains the maximum quantity of solute in a solvent, it is saturated (Ref. 4).

The results of the tests are in the chart below.

SOLVENT (TEMP C)	QUANTITY OF TNAZ DISSOLVED(g) IN 20 ml	SOLVENT (TEMP C)	QUANTITY OF TNAZ DISSOLVED(g) IN 20 ml
ACETONE (34)	11.08	ACETONE (50)	15.17
ETHANOL (29)	1.46	ETHANOL (70)	5.40
METHANOL (25.2)	1.78	METHANOL (60)	3.75
2-PROPANOL (23.5)	0.38	2-PROPANOL (70)	2.0
WATER (23.3)	0.04 in 200 ml	WATER (70)	0.2

Figure 3

The determining factor in choosing a solvent was yield. To maximize the yield ethanol was used because it had a strong temperature versus solubility gradient and could dissolve a large percentage of TNAZ. The TNAZ was crashed out in distilled water because it is minimally soluble in cold water and the ethanol is soluble. Precipitation in water made the TNAZ easily separable from the ethanol and traces of the ethanol easily removed from the TNAZ. A one liter scale recrystallization of 100 g of TNAZ was conducted to test the procedure and techniques. 278 ml of ethanol was added to the one liter glass jacketed reactor. The system was heated to 70 degrees Celsius, under

solution was stirred until all of the TNAZ was dissolved. The hot solution was discharged into a crash tank with 80 ml of distilled ice water. The TNAZ precipitated and while still cool the precipitate was suction filtered. The TNAZ air dried overnight and was then dried in the oven under Atmospheric Pressure at 50 degrees Celsius overnight. 95.30 g was recovered, corresponding to a 95.3% yield. This test validated the process procedures and the techniques. Subsequently preparations for a 50 Liter scale recrystallization were undertaken.

The third phase consisted of the 50 Liter recrystallization. The first step entailed all of the planning. Thirty gallons of distilled ice was made in preparation for the final crash of the hot solution. The 50 L glass reactor was assembled. The cooling and heating unit was connected to the exchange coils located inside the reactor. The suction filtration equipment consisting of Buchner funnels, four liter side flasks, #5 filter paper, and the vacuum connections was assembled. The full set up is shown in the schematic drawing (Figure 4) and picture below (Figure 5).

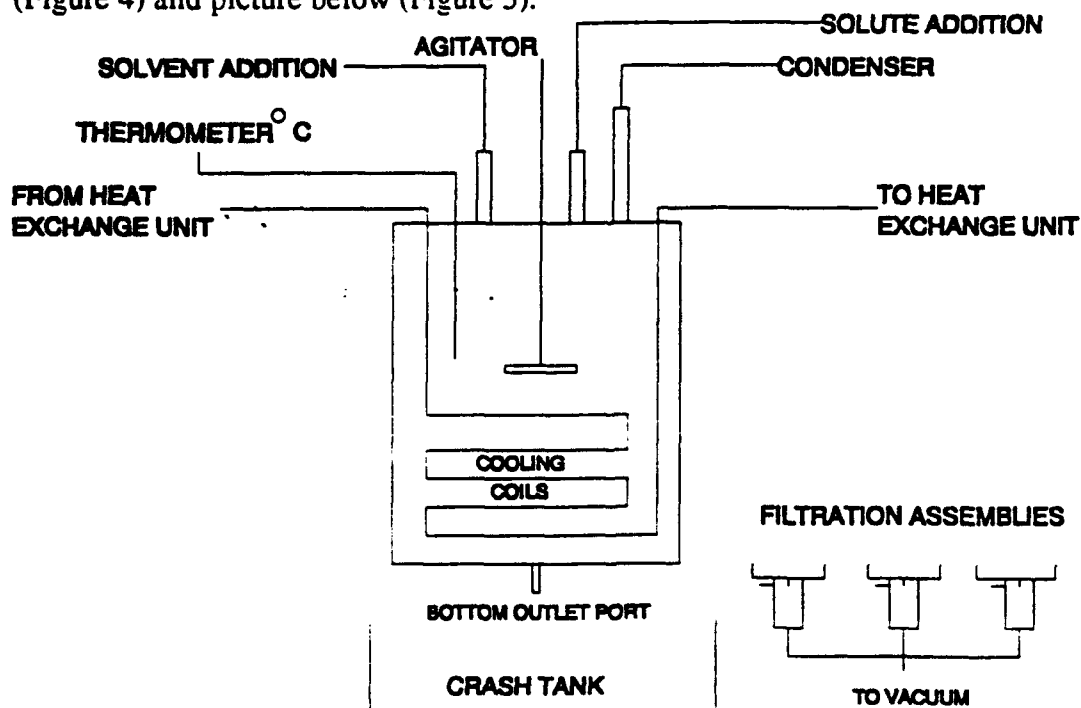


Figure 4



Figure 5

After all the preparations were made, the recrystallization was ready to begin. To avoid exceeding the optimum operating capacity of the reactor the recrystallization was conducted in two batch operations. Batch one consisted of 16.675 pounds of coarse grain and pellet TNAZ. The pellets were crushed to increase the dissolving rate. 5.6 gallons of ethanol was added to the reactor through the inlet port by the liquid addition system. TNAZ was added slowly with agitation and the system was heating to 70 degrees Celsius. Within one and a half hours the TNAZ had dissolved and was ready to precipitate out. Six gallons of distilled ice and two gallons of distilled water was added to each of two crash tanks. The hot solution was discharged out the bottom outlet port into the ice water and the TNAZ precipitated rapidly. The quick precipitation and sub-zero temperatures experienced in the crash tanks was due to the water/alcohol azeotrope. The water/alcohol azeotrope, the point at which the composition of the vapor and liquid compositions are equal, explains the below zero temperatures and rapid precipitation in the crash tanks. The quantity of ice used was excessive to that required hence it was reduced by half in the second batch. The precipitated TNAZ was suction filtered using

the already prepared suction filtration assemblies. The TNAZ was first air-dried and then oven dried for two days at 50 degrees Celsius. The remaining equipment used is shown in the pictures below.



Figure 6

For Batch one, 16.094 pounds of TNAZ was recovered, corresponding to a 96.51% yield. Batch two was conducted using the same procedure with the exception of a reduction in half the amount of ice/water slurry in each tank. 16.976 pounds was recovered in Batch two, corresponding to a 99.04% yield. The next step was to clean the reactor and all the equipment. In the cleaning process 15.66 g of TNAZ was recovered from the reactor. A small scale recrystallization was conducted to purify it using the established procedure. The TNAZ was added to 43.6 ml of ethanol at 70 degrees Celsius with agitation. The solution was crashed into a 50/50 mixture (65 ml each) of distilled ice and water. 14.4 g of TNAZ was recovered, corresponding to a 92% yield.

The recrystallized TNAZ was then analyzed. The first step was a verification of structure. Carbon 13 and proton NMR spectra were obtained by using a Bruker AC-300, 300 MHz Fourier Transform Super conducting NMR Spectrometer. One 20 mg sample

of TNAZ was dissolved in 4 ml of deuterio-acetone. Nuclear magnetic resonance spectrometry measures the applied field strength plotted against the absorption signal. In NMR a super conducting magnet produces a homogenous magnetic field of approximately 7.1 Tesla between poles. The sample is spun about its mainfield (Z) axis by a stream of air to average out any existing homogeneities in the xy plane. The number of signals in the spectrum indicates the number of like atoms there are in the molecule. The position of the signal indicates the electronic environment of each atom. The splitting of a signal into several peaks indicates the environment of carbon with respect to other, nearby carbons. In the proton NMR, the hydrogen nuclei absorb the magnetic radiation and create peaks. The peak shifts (Figure 7 and 8) are observed and represent the different functional groups of the molecule (Ref. 5).

The FTIR was also used to confirm the structure of TNAZ. As the molecule absorbs the infrared light its molecular bonds bend, stretch, and create absorption peaks. These peaks are observed and represent the different functional groups of a molecule (Figure 9). A particular group of atoms gives rise to characteristic absorption bands, that is, a particular group absorbs light of frequencies that are much the same from compound to compound. For example, C-N Amine group absorbs strongly at 1180-1360 reciprocal centimeters (Ref. 5). The three charts below illustrate the plots of the verification process.

INFRARED SPECTRUM (FTIR)

BOND INDICATED	PEAK LOCATION (WAVE NUMBERS)
C-H	2914.62, 1427
C-C	867.50, 842.46
NO ₂	1544.59, 1366.85
C-N	1328.26, 1279.12, 1218.3

Figure 9

The Carbon-13 NMR Spectrum of TNAZ in deuterio-acetone revealed peak shifts of 84.889 ppm and 105.012 ppm. The peak at 84.889 ppm represents the carbon atoms in the number two and four ring positions and the peak at 105.012 ppm represents the geminal carbon group in the number three position. Both peaks representing TNAZ's different functional groups were found. The proton NMR spectrum indicated a peak at 5.482 ppm corresponding to the Alkyl protons in the number two and four position. The FTIR was also successful in recording TNAZ's functional groups. All three techniques yielded spectra consistent with that expected from TNAZ and confirmed its structure.

The particle size of TNAZ was determined using a Brinkman Particle Size Analyzer 2010. The average particle size was 11.72 microns. Scanning Electron Micro graphs revealed that TNAZ's particle shape was somewhat rectangular (Figure 10).



Figure 10

The thermal properties of TNAZ were then determined. Half a milligram samples of TNAZ were thermally analyzed by Differential Scanning Calorimetry. Heat was applied at a rate of 10.00 deg C/min. The scan produces a trace of endothermic and exothermic events which take place as the temperature of the sample rises in an inert Nitrogen environment (Ref. 6). The following plot (Figure 11) is an example of an endothermic and exothermic run on TNAZ.

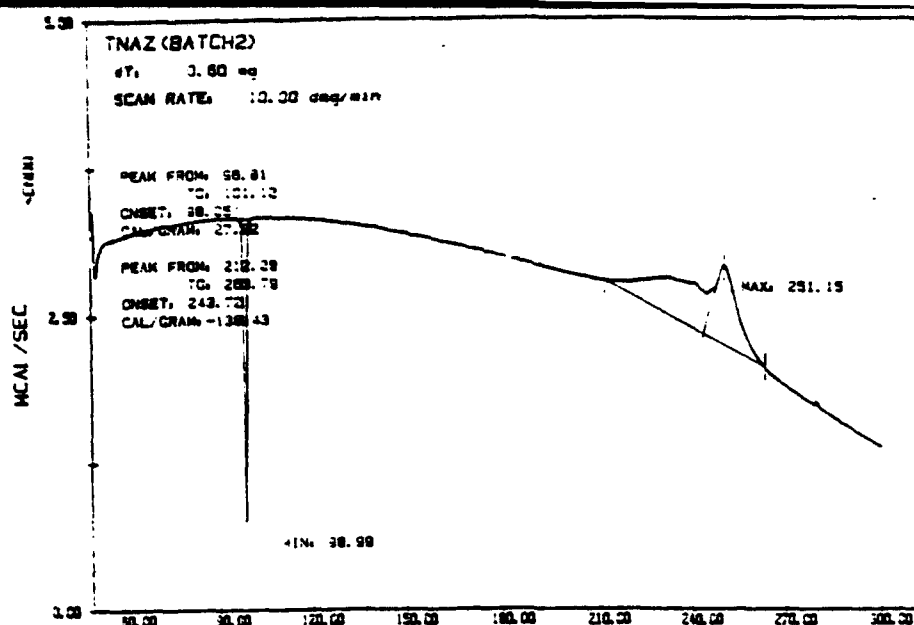


Figure 11

The DSC results indicate that TNAZ's melt onset ranges from 98.05 to 98.17 degrees Celsius and the decomposition onset ranges from 243 to 243.4 degrees Celsius.

Impact sensitivity was determined using the Bureau of Mines Type 12B Drophammer. Twenty five samples weighing 35 milligrams each were placed on pieces of abrasive sandpaper. A 2.5 kg weight was dropped at varying heights registering go's and no go's. The $H_{50\%}$ of TNAZ was 20.1 cm. The chart below (Figure 12) compares TNAZ's impact sensitivity to other sources of TNAZ.

MATERIAL	H50%(cm) 2.5 kg wt.
TNAZ(BATCH ONE)	20.1
TNAZ(ARMY POWDER)	17.1
TNAZ(AEROJET POWDER)	23.8
TNAZ(ARMY POWDER)	25.3

Figure 12

Charge fabrications were initiated. 1.5 g of TNAZ was pressed at 70 degrees Celsius at 30,000 psi in three intensifications. The mean density achieved on the pellets was 1.812 g/cm³ corresponding to a 98.5% Theoretical Maximum Density. The sixteen

pellets were detonated to measure detonation velocity. 10 piezoelectric pins were placed 10 mm apart to record the shock wave arrival time using a Textronix 710A waveform digitizer. Velocity was obtained by differentiation of distance with respect to time

$$v=dx/dt$$

where v is the velocity, x is the distance (10 mm), and t is the time. The average detonation velocity achieved was 8.71 mm/usec.

CONCLUSION

SECTION IV

The solubility and recrystallization of TNAZ was successfully completed. Ethanol was found to be an efficient solvent from which to crash precipitate TNAZ in distilled ice water. The yield average was 98 % in the batch processes. The purity of the recovered material was in excess of 99%. The melt onset of TNAZ was found to be 98 degrees Celsius. The NMR and FTIR verified the structure of TNAZ. The particle size was found to be 11.72 microns and rectangular in shape. Pressing of the TNAZ to fabricate charges to determine its explosive properties has resumed.

MISCELLANEOUS

SECTION V

This summer through HSAP I learned the importance of patience and safety in conducting an explosive scientific operation. I have a more complete understanding of organic chemistry and explosive technology. I gained experience with actual chemical engineering which will be useful when I begin to study chemical engineering. My summer project would not have been such a success without the guidance and support I received from the personnel at the HERD facility. First of all I would like to thank Mr. Stephen Aubert for creating a step-by-step project that involved hands on operation of different types of lab equipment. I would also like to thank everyone at the HERD for helping me to use the equipment in the labs. I appreciate everyone's cooperation and eagerness to assist me at all times. It was most definitely a pleasure to be a part of this program.

REFERENCES

SECTION VI

1. Iyor, Dr. Sury, et. al. Scaled-up Preparation of 1,3,3-trinitroazetidine. Army Armament Research, Development, and Engineering Center. Picatinny Arsenal, NJ.
2. Archibald, T.G., Richard Gilardi, K. Baum, and Clifford George. Synthesis and X-Ray Crystal Structure of 1,3,3-trinitroazetidine. American Chemical Society, 1990.
3. Dobratz, B.M. LLNL Explosives Handbook: Properties of Chemical Explosives and Explosive Simulants. University of California, 16 March 1981.
4. Shugar/Shugar and Bauman/Bauman. Chemical Technician's Ready Reference Handbook, Second Edition. New York: McGraw Hill Book Co., 1981.
5. Morrison, Robert T. and Robert T. Boyd. Organic Chemistry, Third Edition. Boston: Allyn and Bacon, Inc., 1973.
6. Dobratz, B.M. LLNL Explosives Handbook. Lawrence Livermore National Laboratories. March 16, 1981.

Hypervelocity Impact Studies Utilizing Semi-Empirical Codes

Randy Thomson

High School Apprentice

WL/MNSA

Eglin Air Force Base, Florida

Final Report for:

High School Apprenticeship Program

Wright Laboratory/Armament Directorate

Sponsored by: Air Force Office of Scientific Research

Bolling Air Force Base, Washington, D.C.

August 1993

Hypervelocity Impact Studies Utilizing Semi-Empirical Codes

Randy Thomson

High School Apprentice

Abstract

One of the tasks of the Technology Assessment Branch (MNSA) is to assess the lethality of hypervelocity kinetic energy weapons against foreign aerospace threats. MNSA uses several analytical tools to fulfill this task. Chief among these tools are Eulerian codes with fixed grids, excellent for modeling the massive distortions that occur in the initial hypervelocity impact; Lagrangian codes with flexible grids that accurately model late time structural response; and semi-empirical codes, which rely on engineering models based on actual theories that are empirically fit to experimental data using regression techniques. The Eulerian and Lagrangian codes provide accurate results, but require enormous amounts of computer time, even on modern supercomputers. A need was seen for a fast-running code that could provide accurate data on desired lethality criteria. These codes have existed for some time, but due to their nature, require extensive amounts of ongoing analysis to accurately portray hypervelocity impacts as more experimental data becomes available. During the summer of 1993, the accuracy of semi-empirical tools for modeling hypervelocity impact was studied, and the information drawn from this research is the basis for this report.

Hypervelocity Impact Studies Utilizing Semi-Empirical Codes

Randy Thomson

BACKGROUND

One of the main tasks of the Technology Assessment Branch (MNSA) is to assess the lethality of hypervelocity kinetic energy weapons against foreign aerospace targets. To fulfill this task, MNSA utilizes several techniques, including full and sub-scale tests as well as analytical modeling. The Branch uses three main analytical techniques. Lagrangian codes utilize a flexible grid that allows the cells to be appropriately distorted as stress is applied, but permits neither mixed material cells nor loss of material within any one cell. This makes Lagrangian codes excellent for late time analysis of hypervelocity impact. Eulerian codes utilize a fixed grid that allows material to flow through the grid cells, but does not allow deformation of the grid cells themselves. This makes these codes good for measuring early time effects, when massive fluid deformation occurs. Semi-empirical codes do not divide the projectile into many small sections or use cells to measure an integrated response. Rather, semi-empirical models treat the projectile holistically, and directly calculate lethality parameters from explicit equations. The equations start by making an assumption based on theory that a lethality quantity is proportional to an expression in several variables, implying that the quantity is equal to the expression multiplied by some constant of proportionality. If the equation is a differential equation, as many of these equations tend to be, the equation is integrated. Regression analysis is used to fit the resulting curve to an experimental database. The resulting equation, then depends both on physics-based material parameters and interrelationships of those parameters, as well as empirical constants resulting from the curve fitting. The resulting equation is simple to evaluate by a computer code, and lends itself to modular architecture, evaluating each group of parameters in a separate module and linking and outputting the results through the main program shell. If accurate assumptions are made in the development of the model, the semi-empirical algorithm will have the powerful advantages of high accuracy and fast running time. However, even with accurate assumptions, the inherently semi-empirical nature of the algorithms can make it difficult, unwise, or even impossible to extrapolate beyond the extreme values of the calibration

database. Thus, continual calibration with experimental data is necessary. A particular semi-empirical code developed by MNSA is KAPPII (Kinetic Energy Analytic Projectile Effects Program II). The main focus of my work was to test the effectiveness of the current version of KAPPII for accuracy versus theoretical predictions as well as experimental data. If the accuracy was lacking, input parameters would be manipulated to better fit the experimental data and empirical constants would be varied if necessary. Other duties directly and indirectly related to this goal will also be discussed.

KAPPII

KAPPII is a set of fast running modular algorithms in FORTRAN 77 used to calculate damage to complex three-dimensional targets impacted by multiple hypervelocity projectiles including long and short rods, long and short hollow rods, and spheres. It has been calibrated against an extensive experimental database covering a wide range of impact conditions. Targets include Theater Ballistic Missiles (TBMs), Reentry Vehicles (RVs), Post Boost Vehicles (PBVs), and a variety of both simple and complex flat plate targets. Targets can be modeled either with a simple series of flat plates for calibration and querying purposes, or with a computer modeling program such as FASTGEN, GIFT, or BRL-CAD. An extensive and easily customizable materials database contains all material parameters necessary for the code. Due to its modular architecture, various algorithms can be either combined singly or in groups called emulation modes to better model the particular scenario at hand and output the appropriate damage values. The code is also portable and can be implemented on anything from Intel x86-based or Macintosh PCs, to Silicon Graphics or Sun workstations, up to a supercomputer such as the Cray Y-MP. To keep all of this flexibility in check, a configuration management system with a configuration control board oversees all changes, evaluates all errors discovered, and rates various corrections and enhancements for priority of implementation into the next code release. MNSA is working toward incorporating additional models into the code that are based more upon physics than empirical curve fits to experimental data. Even the most purely scientifically based model is no good if it does not reflect reality, however, and the complex nature of these algorithms requires large amounts of

data to gain confidence in their output. MNSA implements this code by entering necessary parameters for a hypervelocity impact scenario into a series of ASCII files containing projectile and target data, as well as control keywords and, optionally, non-standard values for empirical constants. The code is run on a Silicon Graphics workstation and manipulated through one of several X terminals throughout the Branch.

TRAINING

First, a study was conducted to increase proficiency in UNIX in order to simplify access to the code and its associated files. Also during this initial training period, hypervelocity impact theories were studied through a short course in penetration mechanics to allow the evaluation of the code and algorithms from a more theoretical point of view. This along with a study of the KAPPII user's manual, algorithms, code structure, and goals helped avoid the "black box" syndrome when manipulating the code. Now with a firmer understanding of the theories and tools that would be involved, the project proper could begin.

METHODOLOGY

Then it was time to conduct hands-on testing and manipulation of the code. First, the sample input files were executed and the outputs studied. A series of variations on the original flat plate models in the example was tested with reasonable results. A flat plate approximation of an RV-type target was developed, attempting to keep the materials as accurate as possible. The output damage values were inaccurate, however. Damage readouts in the lower semi-infinite layer of the target, made of uranium and intended to model the fissionable section of a nuclear warhead, were grossly exaggerated, resulting in crater volumes far greater than they should have been. It took a thorough search of the code and the input files to finally discover that there was a faulty parameter in the material database resulting in extremely low target strength. Many of the errors in the output could be traced to the materials database. Due to its inherent customizability and the rapid addition of material parameters needed for more accurate models rarely accessed by anyone outside of MNSA and the developers of the algorithms,

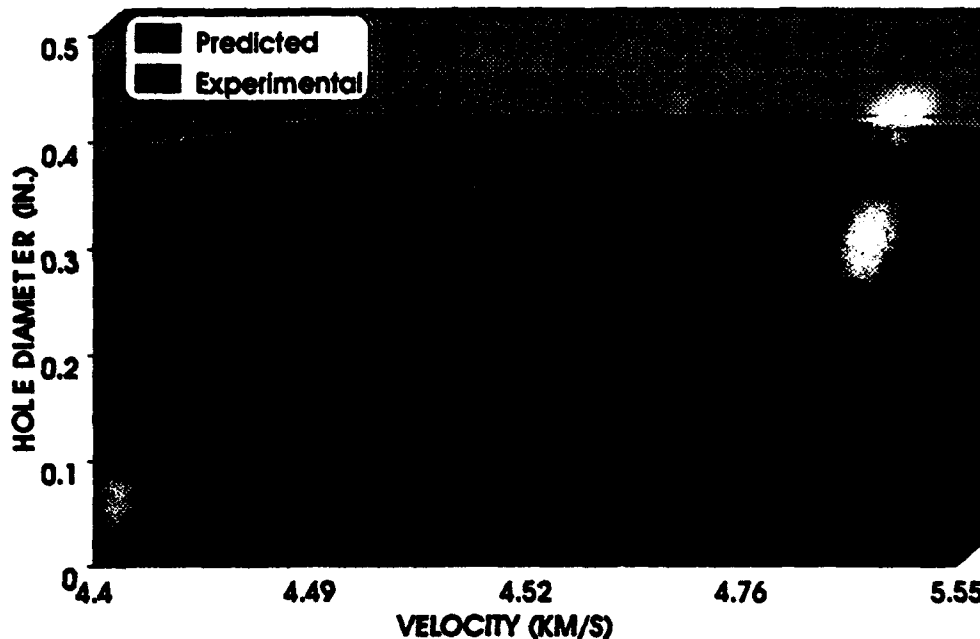
several typographical errors had been made in the database. To fix this problem, as well as the problem of searching a pure ASCII file for the desired material, the database was exported to a PC and manipulated using Microsoft Excel. This made the database easier to read, analyze and use. Utilizing simple search and organization tools, the database could be searched for materials meeting any desired criteria and errors were easily weeded out. Without large numbers of varied trial runs and the subsequent update of the database, many less severe errors could have gone unnoticed, leading to inaccurate data.

PROCEDURES AND RESULTS

With a basic confidence in the output from KAPPIL after gaining familiarity in possible problems and successfully surmounting them, it was time to test KAPPIL against actual experimental data. Obviously, data to which the code had not already been calibrated was necessary. For these purposes, the NASA/Marshall Space Flight Center (MSFC) hypervelocity impact database was selected. This particular database consists of a large series of damage values for hypervelocity impacts on targets at up to 8 km/s. Target configurations included single and multiple bumper specimens constructed from a wide range of engineering materials, including aluminum, Kevlar, graphite epoxy, cadmium, and alumina, of various thicknesses with variable spacing. Tests were performed with and without multi-layer insulation between the bumper plates and pressure wall plates. This resulted in an excellent database for comparison, but not without some drawbacks. NASA developed the database with an eye to assessing vulnerability of space station materials to orbital debris impact. This reflected itself in the database. Large numbers of composite materials were used in the test database. KAPPIL, or even a hydrocode, for that matter, does not adequately treat composite materials because it assumes materials to have equal tensile, compressive, and shear strength in all directions; in other words, it assumes the material to be isotropic, meaning that the material is symmetric in its response to stress. This is a grossly inadequate assumption for composite materials, whose strength factors could vary by orders of magnitude depending on alignment of the force with respect to the fibers within the material due to their

anisotropic nature. Second, KAPPII can not adequately handle multi-layer insulation in its present form. Third, the vast majority of projectiles were spherical, to approximate space debris. This is perfectly fine, but MNSA is more concerned with long rod penetrators than spheres. The projectile materials, Lexan, various aluminums, and steel, were designed to model the various densities of micrometeoroids. Lexan was designed to simulate ice, aluminum was designed to model rocky meteoroids, and steel was designed to simulate iron meteoroids. These were perfectly modelable projectiles, but there was a lacking in the higher strength and density regimes, such as data for tungsten and depleted uranium projectiles. In general, if the proper test series were extracted, the data would be useful, but care was needed in extracting the data. First, the data was converted from the native Lotus 3-D format to an Excel Workbook. The file was then searched for a moderate size test series with enough constant parameters for KAPPII to yield consistent data. After much searching, an adequate test series was extracted. The parameters were converted to input files for use by KAPPII. After setting up parameters to gain the highest amount of accuracy available from KAPPII as it stood, the test series was evaluated by KAPPII. Also, to make it easier to compare KAPPII results to experimental data, a huge input file was set up to give a wide range of projectile velocities, masses, materials, and target configurations. This database could be used by future researchers to quickly compare KAPPII's predictions for an impact regime of interest and evaluate KAPPII's performance when a more extensive database becomes available in the future. Once the damage readouts had been obtained from KAPPII, the predicted damage numbers could be compared to the experimental values in the NASA database. After unit conversion to ensure compatible units, the results were compared. In Figure 40-1, the good correlation between KAPPII and the database can be seen. KAPPII underpredicts the damage values by approximately 9 percent. This is good correlation for an extraction from a database this size, allowing for experimental error. It is good that KAPPII underpredicts rather than overpredicts the damage, for this means that if KAPPII predicts a kill, there is an extremely high probability that a kill will take place due to the conservative damage readouts.

**Figure 40-1
First Bumper Damage**



However, due to improper characterization of the debris cloud, damage readouts for the second layer of the target are 30-40% lower than expected. One of MNSA's major research thrusts is to better characterize the debris cloud. By this time next year, algorithms should be in place to correct this deficiency by modeling impulse loading of targets by debris clouds. In the meantime, simple manipulations of the debris cloud empirical constants result in accuracies approximately on the order of that obtained for the first layer. Otherwise, damage predictions for the target are excellent. Similar results were obtained from extractions of other sections of the database. Figure 40-2 displays the KAPPIL input files for this particular experiment.

Figure 40-2

KAPPIL Projectile Input File

```
.363319818 'AL 1100' 4.4 10. 0. 0. 0./
/
.363319818 'AL 1100' 4.49 10. 0. 0. 0./
/
.363319818 'AL 1100' 4.52 10. 0. 0. 0./
/
.363319818 'AL 1100' 4.76 10. 0. 0. 0./
/
.363319818 'AL 1100' 5.55 10. 0. 0. 0./
```

KAPPII Target Input File

```
0. 10. 90. 'VOID'/
1. 0.08128 90. 'AL 6061-T6'/
0 10.16 90. 'VOID'/
2. 0.08128 90. 'AL 6061-T6'/
0 2.54 90. 'VOID'/
3. 0.3175 90. 'AL 2219-T87'/
```

KAPPII Input File

```
title SB2 NASA Calibration Run
projectile platt51
model platt56.pmd
kapdir /disk6/thomson/kappii/sys/
material kappall.dat
Plot
write title
one ovel 0
one pden 0
one odiam 0
max hatot 1
max hatot 2
max hatot 3
control
emulate sb2
prtpst true
trace hits
idohat 1,2,3,0/
constants
pencrt=0.75
qkgsiz =.25
```

KAPPII Plot Output File

ovel_o00	pdem_o00	odiam_o00	hatot_x01	hatot_x02	hatot_x03
4.40	2.71	0.635	0.615	2.31	0.000E+00
4.49	2.71	0.635	0.620	2.81	0.000E+00
4.52	2.71	0.635	0.622	3.13	0.000E+00
4.76	2.71	0.635	0.636	3.00	0.000E+00
5.55	2.71	0.635	0.685	2.63	0.000E+00

^ SB2 NASA Calibration Run cpu= 88.2 elapse= 94.0

CONCLUSIONS

On the basis of the results of this summer's research, it would seem that if used properly, KAPPII in its present incarnation does fulfill many of its design requirements. It is very fast running compared to the hydrocodes, and with appropriate parameters, gives accurate results. It directly outputs the requested damage readings without searching through a long output file and setting up complicated equations to solve for the desired values. It is an excellent tool for obtaining results for hypervelocity impact scenarios if one stays within its limitations. The biggest problem is the fact that for many combinations of algorithms, those limitations are not well defined. Hopefully, the test series set up during this research period will make it easier to see where KAPPII's difficulties lie as more experimental data becomes available. The verification and validation process of the code continues, and its accuracy grows by leaps and bounds with every revision. To sum up, KAPPII gives relatively reliable results for predicting hypervelocity impact damage in its present configuration and should only improve in the year to come.

ACKNOWLEDGMENTS

The author would like to thank Research & Development Laboratories (RDL) for sponsoring this program and the Wright Laboratory/Armament Directorate for serving as a host site for the 1993 HSAP. Thanks are also in order for Mr. Don Harrison, Mr. Mike Deiler, and Ms. Glenda Apel for running the local aspects of the program smoothly. This project could not have been accomplished without Mr. Bruce Patterson, who served as a mentor for the author and provided guidance. These people also gave assistance from a supervisory perspective: Major Paul Coutee; MNSA Branch Chief, Mr. Ron Hunt and Mr. Dave Jerome; MNSA Section Chiefs, and Mr. Walt Maine, MNS Division Chief. Other people who gave the author assistance included Dr. William Schonberg, an associate professor at the University of Alabama-Huntsville, who attempted to provide technical explanations for the more bizarre results the code provided. Mr. Larry Cohen from Science Applications International Corporation (SAIC) provided

technical support for problems with the code itself. Mr. Brian Peterson, a co-op student from North Carolina State University, helped with too many little things to possibly mention. Mr. Dan Brubaker (MNSA) helped with preparing outbriefings and the final report. Everyone else in MNSA also deserves thanks for assistance rendered and for suffering through the summer with this apprentice. Thank you all for your support, for this project could not have been done alone.

Area Centroid Analysis

**Christina M. Trossbach
High School Apprentice
Advanced Processing Systems Branch**

**Wright Laboratory Armament Directorate
WL/MNGA
Eglin Air Force Base, FL 32542-6810**

**Final Report for:
High School Apprenticeship Program
Wright Laboratory Armament Directorate**

**Sponsored by:
Air Force Office of Scientific Research
Bolling Air Force Base, Washington, D.C.**

August 1993

Area Centroid Analysis

Christina M. Trossbach
High School Apprentice
Advanced Processing Systems Branch
WL/MNGA

Abstract

The project studied was to determine the effects of the Gain & Offset Compensation on the Area Centroid. Gain & Offset and Area Centroid are two of seventeen signal processing algorithms that were used in the testing and evaluation. The Area Centroid is the location of the center of the area of a target. A program in Pascal was created to calculate the output, and the Area Centroid was found in coordinate form.

Area Centroid Analysis

Christina M. Trossbach

Introduction

Reagan's Administration implemented a new mission in the Air Force in 1983. It was called the Strategic Defense Initiative (SDI), but was changed to the Ballistic Missile Defense Organization (BMDO) in 1993. Its goal is to provide new technology for our country's defense. One of Wright Laboratory's tasks for BMDO is to develop components for interceptor missiles. The Advanced Processing Systems Branch (WL/MNGA) works with the development, analysis, and evaluation of signal processing hardware and algorithms. Through the work of different branches at Wright Laboratory and contractors, a component program called the Signal Processor Package Design, or SPPD, was created.

Although I now work for MNGA, the project I completed this summer can be tied into my project done last year, in that it involves incorporating additional calculations with some of the Signal Processing Algorithms of SPPD. Each of the seventeen algorithms completes a specific task, but for the purpose of my studies, I was concerned with only two algorithms—Gain & Offset and Area Centroid. The final objective was to find the location of the Area Centroid in coordinate form.

Background

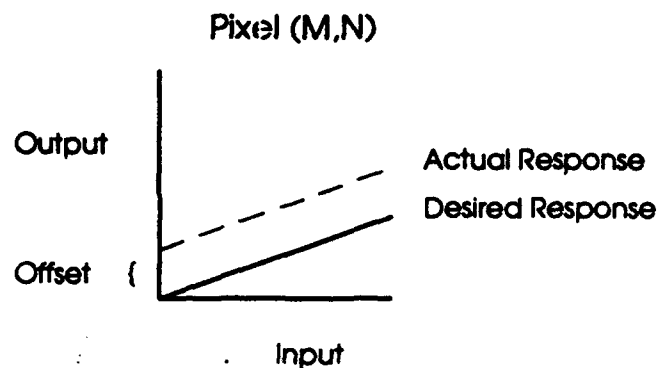
SPPD is one example of a signal processor that the engineers in MNGA have developed. A signal processor, when put with a sensor make up a seeker, which is located at the front of an interceptor missile. The sensor is made up of a matrix of detectors, and is called an FPA, or focal plane array. The sensor absorbs radiation from the target and creates an image, which then is transferred to an A/D (analog to digital) converter. The converter then sends the image to the signal processor which processes the image to find the target. SPPD has a set of algorithms which perform these tasks in order to find the target.

Theoretically, the image that the sensor creates can be either an ideal or a non-ideal image. An ideal image which is given the same intensity on every pixel in turn gives every pixel the same output

value. This case does not happen in reality, so the pixels may have different values, such as the example below.

Ideal				Non-Ideal			
1	1	1	1	1	2	1	2
1	1	1	1	1	1	1	0
1	1	1	1	0	1	2	1
1	1	1	1	1	3	1	1

When the sensor produces a non-ideal image, the Gain & Offset algorithm is needed to compensate for the different values of intensity. Below is an example of the graph of a non-ideal response, or a non-uniformity.



The gain is the slope of the actual response, and the offset is the difference between the desired response and the actual response.

Methodology

My first task was to learn the Pascal programming language, because it was going to be the main tool used for calculating the Area Centroid. I started out with simple programs, and I gradually built up to more complicated programs involving arrays, like what I would be using to find the Gain & Offset. My second task was to acquire more knowledge of the Gain & Offset and Area Centroid functions. It was necessary for me to completely understand what the arrays of Gain & Offset stood for before I could implement them in Pascal.

I started out with the Gain & Offset algorithm, which is the first of the functions that the signal processor Performs. Below is the equation used in the program.

$$PC[M,N] = G[M,N] * PV[M,N] + O[M,N]$$

The array G[M,N] is the gain adjustment, PV[M,N] is the raw pixel value, O[M,N] is the offset adjustment, and PC[M,N] is the corrected pixel value for the array. The value of PC[M,N] was then used in solving the next function, the Area Centroid.

The Area Centroid algorithm solves for the location of the center of area of the target. The output is given in (X,Y) form. The equations below solve for the X coordinate and the Y coordinate of the Area Centroid, respectively,

$$XCA = \text{Sum}(N * PC[M,N] / \text{Sum}(PC[M,N]))$$

$$YCA = \text{Sum}(M * PC[M,N] / \text{Sum}(PC[M,N]))$$

The final output of the program is the location of the Area Centroid, which is the location of the center of area of the target, in coordinate form.

Conclusions

The program I wrote implementing the SPPD Algorithms Gain & Offset and Area Centroid was successful. However, there were delays in the coding because I encountered some memory problems. At the beginning of my program, you have to set the X and Y values to the maximum size array you are using. I used a frame size of 128x128 because that is what SPPD uses in the actual design. After many, many days of unsuccessful rewrites, my mentor suggested decreasing the array size. I tried many combinations, and the largest the PC could accommodate was an array size of 64x64, which is one-fourth the size of the actual SPPD design. As a result, it was impossible to evaluate and analyze any real data, so we tested some simple values in which we were able to calculate the results in another fashion, so we could compare them with the results of the program. Consequently, the program cannot be used in its present form, because of the varying frame size, and there was not any image data in Pascal form to test.

Acknowledgements

I would like to thank all the people that made my apprenticeship this summer an enjoyable and worthwhile experience. Paul McCarley-my mentor and friend. Emily Martinez-my other mentor. Thanks for all the help with Pascal and thanks for adopting me as your second apprentice. I would also like to thank the other apprentices in the HSAP Program for making this an awesome summer, especially Christie Gooden, who I shared knowledge and personal experiences with-Christie, Emily, and I went through a lot together. Jennifer Bautista-thanks for being a special friend, you silly goose! Barry Kress-the Stallion of the Earth. Jon Ward-the Domino Guru. Kyle Perry-the GQ God himself. Elliot Moore-Mr. Apprentice. And all the others in the program. I'll miss you all. I especially want to thank Mr. Harrison, Mr. Deiler, and Mrs. Apel for their support of this wonderful program. I've learned so much in these past two summers, and the experience I've gained is priceless. Thanks again.

Area Centroid Analysis

Christina M. Trossbach

References

Christina Trossbach, "Sensor Computation Analysis." 1992 HSAP Final Report

Paul McCarley, General knowledge on SPPD Algorithms

Emily Martinez, General knowledge on Pascal Programming

Area Centroid Analysis

Program Listings

This program solves for the Gain & Offset correction to find the compensated output pixel value.

```
program Gain & Offset;
const
  X = 64;
  Y = 64;
type
  MyArrayType = ARRAY[1..X,1..Y] of integer;
var
  M: Integer;
  N: Integer;
  Ans: Integer;
  PV: MyArrayType;
  G: MyArrayType;
  O: MyArrayType;
  PC: MyArrayType;
  File_Name: String[30];
  New_File: file of integer;
begin

  Write('Enter the filename to receive the output data: ');
  Readln(File_Name);

  Assign(New_File, File_Name);
  Rewrite(New_File);

  for M:=1 to X do
    for N:=1 to Y do
      begin
        PV[M,N] := 1;
        G[M,N] := 1;
        O[M,N] := 0;
      end;

  for M:= 1 to X do
    for N:= 1 to Y do
      Write(New_File, PV[M,N]);
  for M:= 1 to X do
    for N:= 1 to Y do
      Write(New_File, G[M,N]);
  for M:= 1 to X do
    for N:= 1 to Y do
      Write(New_File, O[M,N]);
  Close(New_File);
end.
```

This program reads the data from the first program to solve for the location of the Area Centroid.

```
program Area Centroid;
const
  X = 64;
  Y = 64;
type
  MyArrayType = ARRAY[1..X,1..Y] of integer;
var
  M: Integer;
  N: Integer;
  Ans: Integer;
  PV: MyArrayType;
  G: MyArrayType;
  O: MyArrayType;
  PC: MyArrayType;
  File_Name: String[30];
  Old_File: file of integer;
  New_File: text;
  Sum1: Longint;
  Sum2: Longint;
  Sum3: Longint;
  XCA: Real;
  YCA: Real;

begin
  Write('Enter the filename containing the input data: ');
  Readln(File_Name);

  Assign(Old_File, File_Name);
  Reset(Old_File);

  Write('Enter the filename to receive the output data: ');
  Readln(File_Name);

  Assign(New_File, File_Name);
  Rewrite(New_File);

  for M := 1 to X do
    for N := 1 to Y do
      read(Old_File, PV[M,N]);
  for M := 1 to X do
    for N := 1 to Y do
      read(Old_File, G[M,N]);
  for M := 1 to X do
    for N := 1 to Y do
      read(Old_File, O[M,N]);
  for M := 1 to X do
    for N := 1 to Y do
      PC[M,N] := G[M,N] * PV[M,N] + O[M,N];
  Sum1 := 0;
  Sum2 := 0;
```

```

Sum3 := 0;
for M := 1 to X do
  for N := 1 to Y do
    begin
      Sum1 := Sum1 + PC[M,N];
      Sum2 := Sum2 + (N * PC[M,N]);
write(NEW_FILE,sum2:6,n:5,pc[m,n]:4);
    if (N mod 5 = 0) then
writeLn(NEW_FILE);
      Sum3 := Sum3 + (M * PC[M,N]);
    end;
    XCA := Sum2/Sum1;
    YCA := Sum3/Sum1;
    WriteLn('XCA,YCA)=','(,XCA,',',YCA,');
    WriteLn(New_File, '(,XCA,',',YCA,');
    WriteLn('Sum1)=','(,Sum1,');
    WriteLn('Sum2)=','(,Sum2,');
    WriteLn('Sum3)=','(,Sum3,');
    Close(New_File);
end.

```

THE DEVELOPMENT AND ANALYSIS OF A SPARKGAP FIRESET

**Darcie Tutin
High School Apprentice
Fuzes Branch**

**Wright Laboratory Armament Directorate
WL/MNMF
Eglin AFB, FL 32542-5434**

**Final Report for:
High School Apprenticeship Program
Wright Armament Laboratory Directorate**

**Sponsored by:
Air Force Office of Scientific Research
Bolling Air Force Base, Washington, D.C.**

August 1993

THE DEVELOPMENT AND ANALYSIS OF A SPARKGAP FIRESSET

Darcie Tutin
High School Apprentice
Fuzes Branch
Wright Armament Laboratory Directorate

Abstract

The purpose of this project was to make a fireset which would be an accurate way to send high currents through test items. The development of a sparkgap fireset was ideal because of its low inductance and resistance. It was possible to analyze waveforms received on an oscilloscope from the current viewing resistor to find total circuit resistance and inductance. These values were then compared to P-spice simulations.

THE DEVELOPMENT AND ANALYSIS OF A SPARKGAP FIRESET

Darcie Tutin

INTRODUCTION

The purpose of this project was to construct a sparkgap fireset which would be an effective way to send high currents through test items. An ideal fireset should have both a low inductance and a low resistance. Total circuit inductance and resistance determine the peak current output as well as waveform frequency and risetime.

DISCUSSION OF THE PROBLEM

Previously, problems with switching high currents using an extended range gap switch have been that the triggering grid places a severe drain on the triggering source. The voltage necessary to trigger the circuit is quite high so repetitiveness and accuracy are very difficult to achieve. This type of switch requires a very fast triggering pulse which is often impossible to apply without increasing overall circuit inductance and resistance.

METHODOLOGY

In order to achieve low inductance a planar stripline circuit was constructed. This stripline minimizes enclosed loop area, maximizes peak pulse current, and significantly reduces pulse rise time.

The setup (See Figure 1), begins with an application of between 2000 and 3500 volts to the fireset from the high voltage source. A resistor of

5 megohms serves as a current limiter. A .01 microfarad capacitor is trickle-charged from the high voltage source to serve as a storage capacitor. The high current then travels through a 300 megohm resistor. This resistor significantly reduces the voltage. Next in line on the low voltage side of the circuit is the zener diode. The diode sets a maximum voltage reference of 280 volts. At this point the second capacitor of .02 microfarad is waiting to be discharged. In order to discharge this capacitor a silicon controlled rectifier (SCR) must be switched. The SCR, recommended for its capabilities [1], acts as an intermediate low current switch and having a normally off state. In order to switch the SCR on, so that the capacitor can be discharged, a pulse generator is used. This pulse generator is set in single shot mode to produce a square wave pulse of 5 volts. Following a voltage divider consisting of two 1k ohm resistors, in series, the pulse opens the SCR switch. As a result of sending the SCR into a state of conduction, the discharge from the second capacitor advances to the high voltage trigger transformer. The transformer is a TR130 and has a 40:1 turns ratio. The high voltage pulse travels through a 4.7k ohm resistor and triggers the CP Clare sparkgap switch.

The sparkgap switch (See Figure 2) is made up of three main components. One side of the switch is the anode electrode with a very high potential. On the other side there is an identically sized electrode. This electrode is known as the cathode or adjacent electrode because directly in its center is the trigger probe. The sparkgap is an excellent

switch because of its ability to change from an insulator to a conductor by straightforward application of the proper voltage to each electrode. This is controlled by the fireset circuit. A high voltage pulse creates the signal the sparkgap needs to arc across the gap between the electrodes. Total gap breakdown and conduction of current successfully completes the circuit. The switch has the ability to conduct effectively in this circuit between the applied voltages of 2000 and 3500 volts. This normal operating range takes into account the resistance of the switch between the cutoff region and the region of self breakdown (See Figure 3).

The relatively small values of resistance and inductance are very difficult to measure. Contributions to the total circuit resistance and inductance are made by each circuit component since the capacitor, switch, current viewing resistor, and stripline are non-ideal devices. Theoretical predictions of circuit inductance were made using derived equations. It is possible to find the total inductance within a circuit by examining the first dampened cycle of the waveform obtained from circuit discharge. Knowing that:

$$V_1 = V_0 e^{-Rt/2L} \sin(\omega t)$$

$$V_2 = V_0 e^{-Rt/2L} \sin(\omega t)$$

when $t_1 = T_d/4$ and $t_2 = 5T_d/4$

$$\text{setting } V_1/V_2 = e^{-RT_d/2L} \sin(\omega t_1) / e^{-RT_d/8L} \sin(\omega t_2)$$

it is possible to see that:

$$L(\text{inductance}) = T_d / C [\ln (V_1/V_2) + 4(3.1415)]$$

Total parasitic resistance , primarily due to the switch, is determined by subtracting known values of resistance (such as the current viewing resistor plus the known resistance of the test item) from the total resistance in the fireset circuit.

Waveforms obtained from the oscilloscope via the current viewing resistor can be simulated using P-spice computer modeling. Iterative substitution of hypothetical values of resistance and inductance was performed in order to best match the data with the theoretical predictions of total circuit resistance and inductance. With this program it is possible to model the total resistance and inductance within the high current portion of the sparkgap fireset.

The sparkgap switch has a high current path controlled by a low current path. The P-spice model developed was primarily concerned with the high current path; this greatly simplified circuit analysis (See Figure 4). The low current path consists of any triggering circuit components which are well isolated from the high current portion of the switch. A simple high voltage switch can be used in computer simulation of the high current path, yet the P-spice simulation requires the user to specify a resistance within the switch [3]. Since it is not possible with ordinary test equipment to simply measure the internal resistance of the switch, the on-state switch resistance must be found via simulation through trial and error.

RESULTS

P-spice modeling validated the measurements from the oscilloscope as

well as serving as an accurate simulation of the circuit as a whole. The simulations do, as will any simulation, exhibit small discrepancies (See Figures 5,6&7). These differences can be tolerated because experimental variations occur due to existing signal-to-noise limitations. Measuring the voltage at node 4 (See Figure 4) is the simulation of the point at which the current viewing resistor takes measurements from the actual stripline. Comparing the voltage at this point leaves a difference of between eight and ten volts. Since typical measurements were scaled to 50 volts, less than 15 percent error existed between the measured and calculated values.

The sparkgap fireset proved to be an effective way to send high currents (up to 10kA) through test items. The inductance of the circuit was very low and remained below 25 nanohenry during all experimentation. The resistance of the entire circuit was also very low. By comparing resistances at different applied high voltage source voltages it is possible to examine variations in switch resistance as a function of applied voltage (See Figure 8). This is in agreement with Figure 3. Internal resistance losses of the switch are expected to decrease as the applied high voltage increases.

CONCLUSION

Sparkgap switches can be used to construct low inductance firesets, offering many kiloamperes of current and capable of high voltage operation. Switches are available with maximum ratings well beyond the 4kV limit used for this experimentation. P-spice modeling

validated measured values of current and voltage determined by a digital storage oscilloscope. In addition, this modeling revealed the values of total circuit inductance and resistance which were virtually impossible to measure by alternative methods.

REFERENCES

1. Boberg, R., "Trigger Circuits" General Purpose 1993
pg.02
2. "Ceramic Metal Triggered Spark Gaps" Electric Components
Data Sheet G600E-3 Salem, Mass. pg.1-7
3. Tuinenga, Paul W., SPICE A Guide to Circuit
Simulation and Analysis Using P-Spice Prentice Hall,
N.J. 1988 pg. 183-184

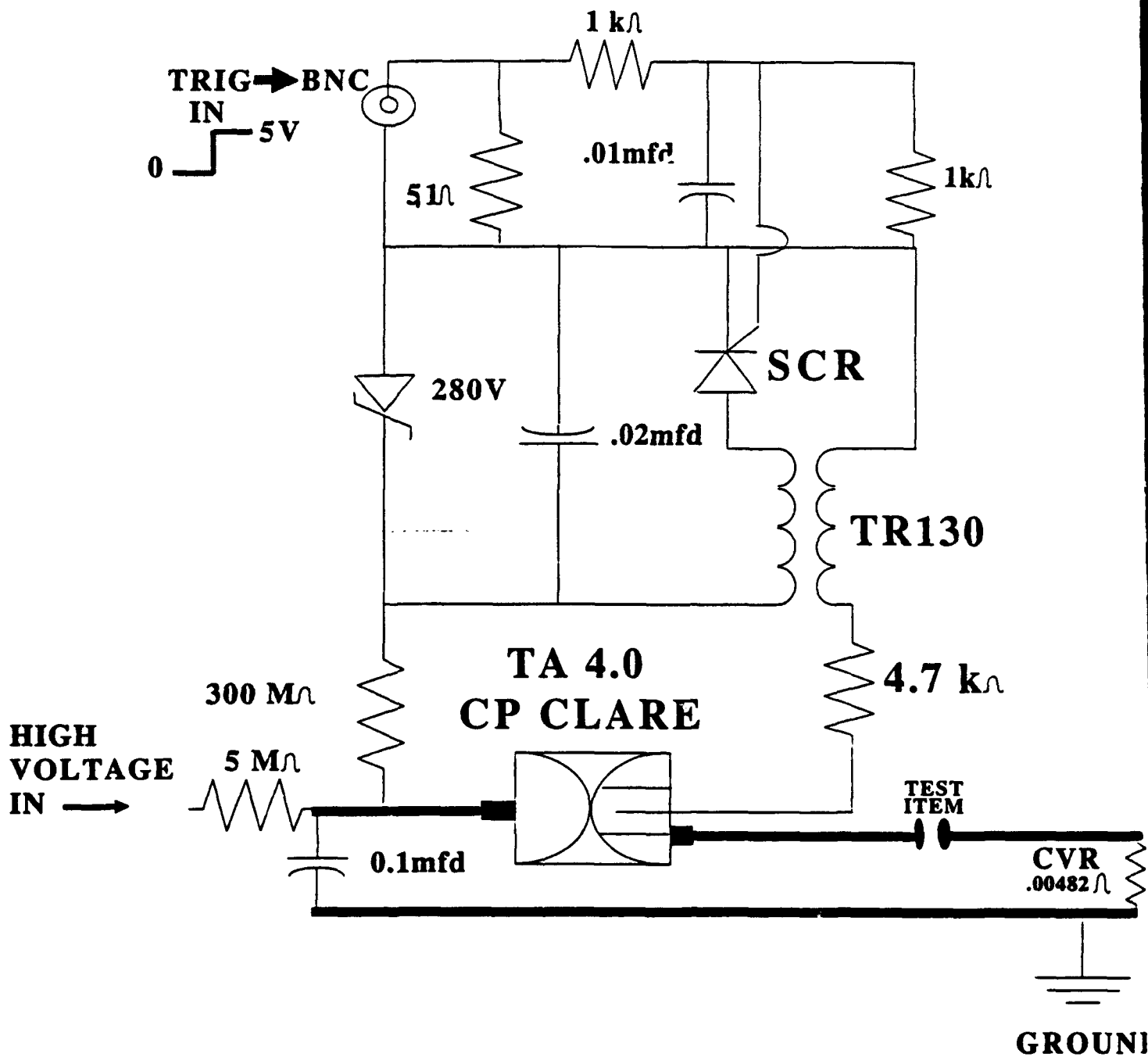


FIGURE 1

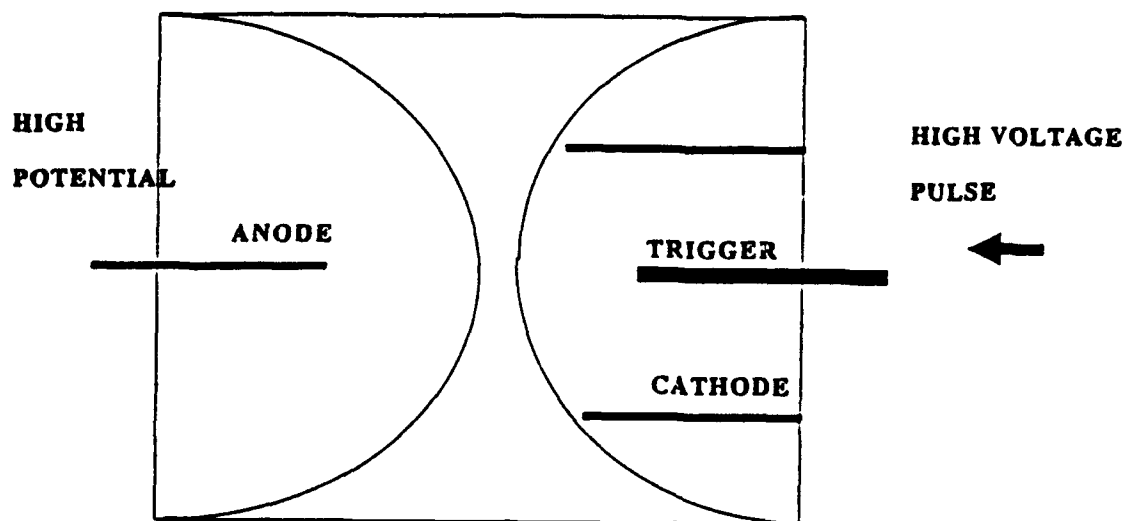
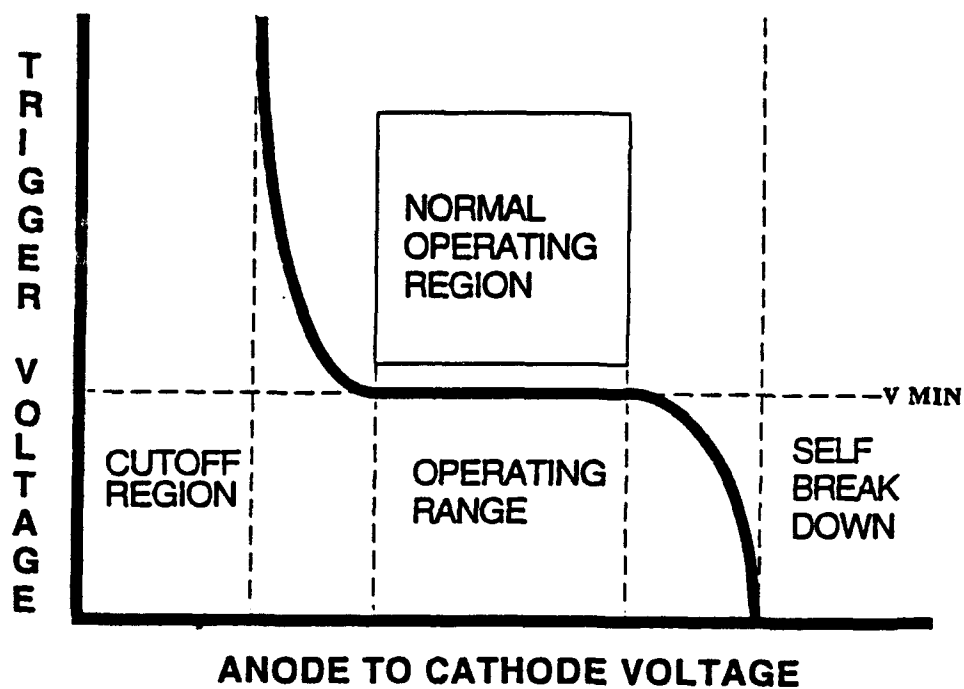
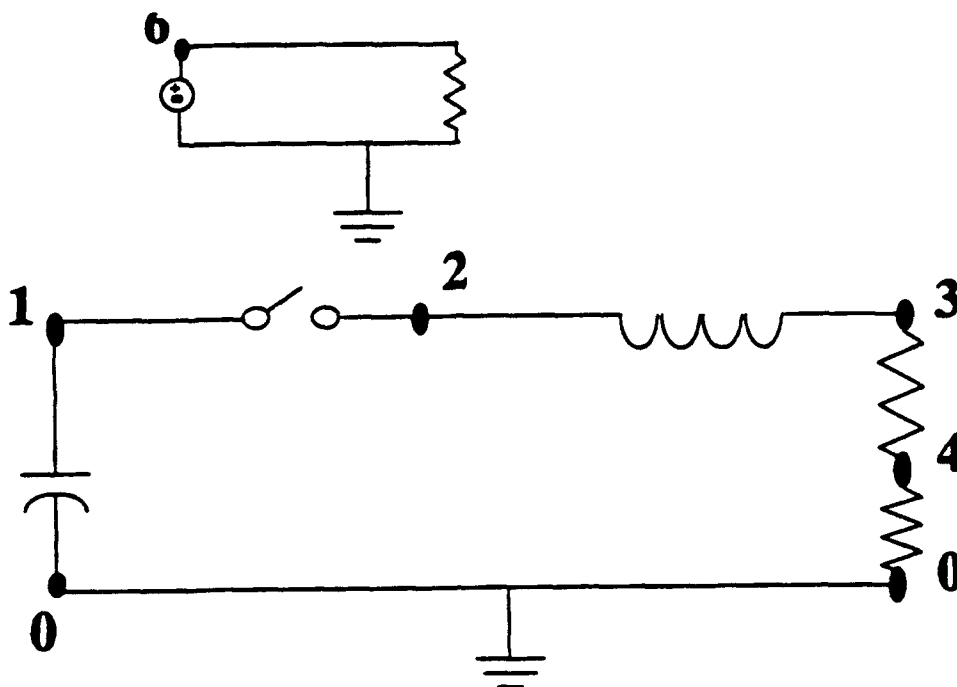


FIGURE 2



CHARACTERISTICS OF A SPARKGAP SWITCH

FIGURE 3



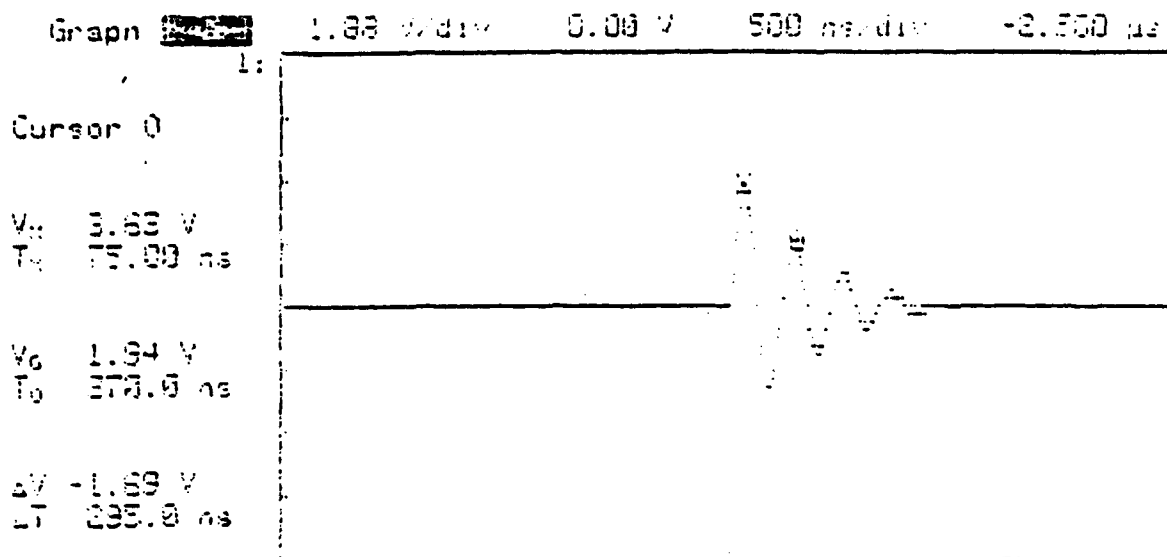
*Spark Gap Trigger
*Darcie

C1 1 0 0.1U IC=3.5K
L1 2 3 12.153N
R1 3 4 60.208M
R2 4 0 4.82M
S1 1 2 6 0 SMODEL

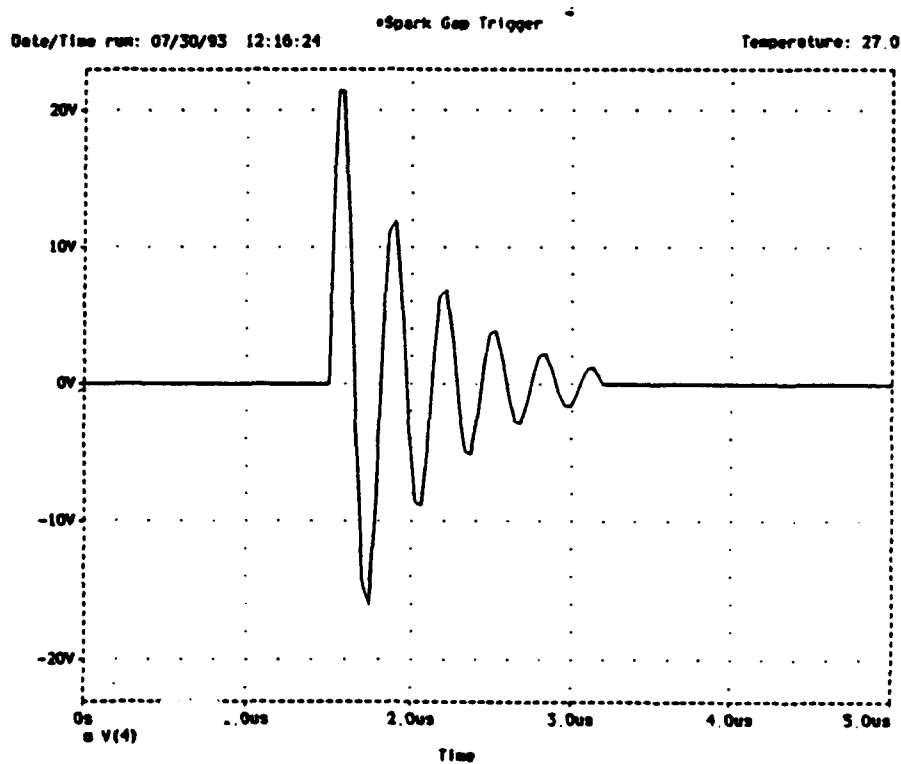
*SWITCH CONTROL CKT
VSW 6 0 PULSE(0 1 1.5U 10N 0.5U 1.5U 10U)
RSW 6 0 1

.OP
.MODEL SMODEL VSWITCH(ROFF=10G)
.TRAN 2M 5U UIC
.PLOT TRAN I(R1)
.PLOT TRAN I(R2)
.PLOT TRAN V(3)
.PLOT TRAN V(4)
.PROBE
.OPTIONS LIMPTS=1000
.END

FIGURE 4



OSCILLOSCOPE READING AT 2.5 KV



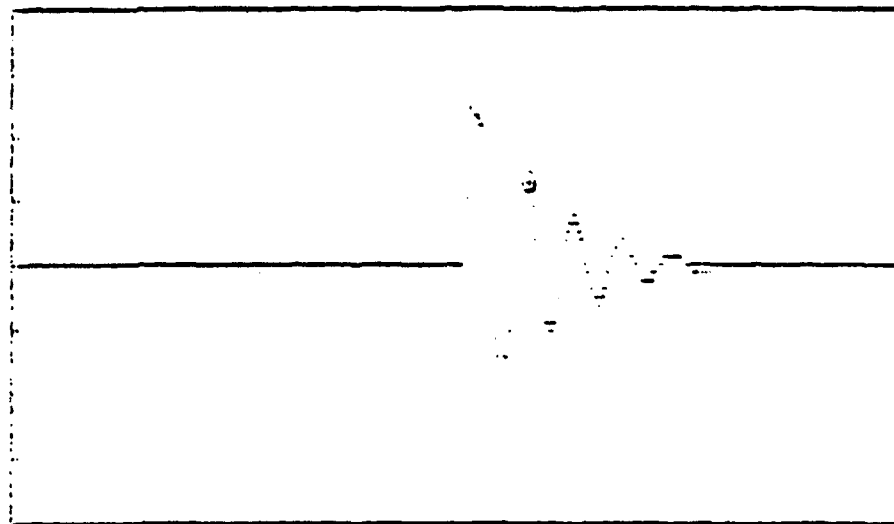
P-SPICE SIMULATION AT 2.5 KV

Cursor 0

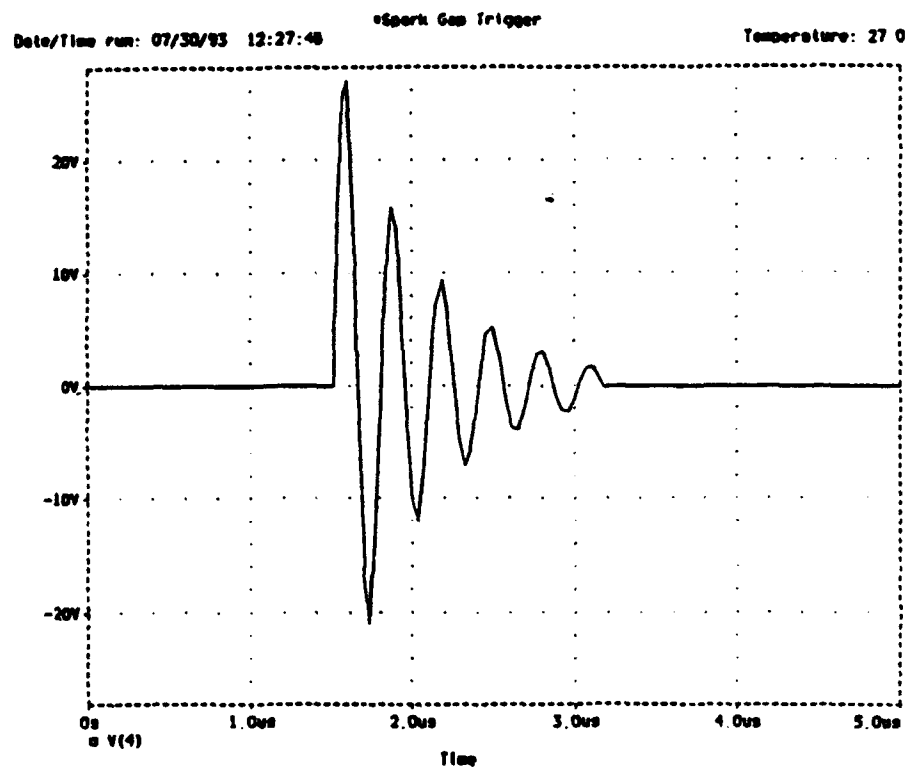
V₁ 4.35 V
T₁ 90.00 ns

V₂ 3.42 V
T₂ 370.0 ns

ΔV -1.04 V
 ΔT 280.0 ns

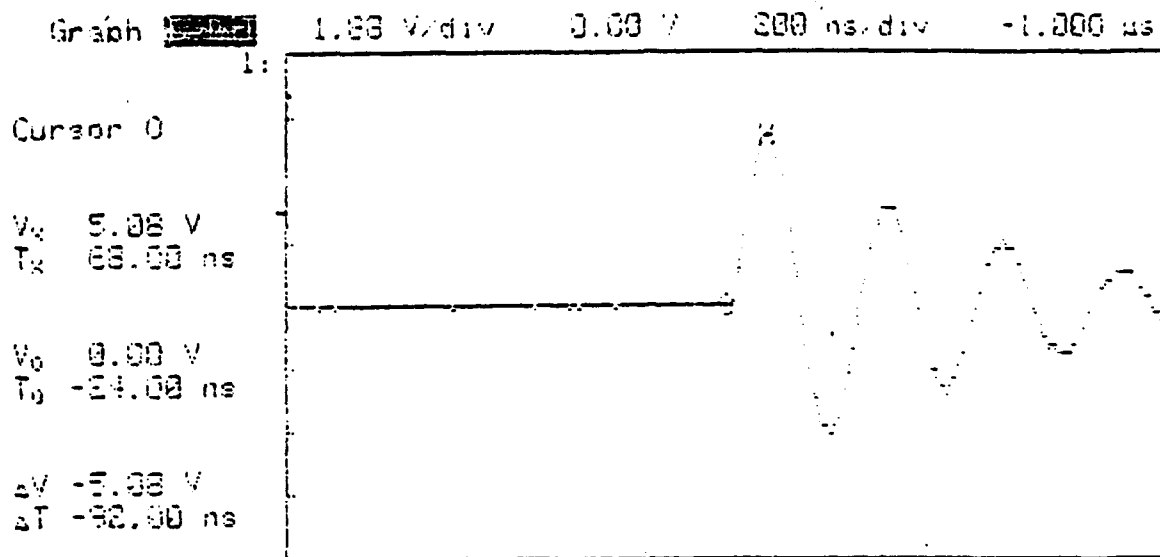


OSCILLOSCOPE READING AT 3 KV

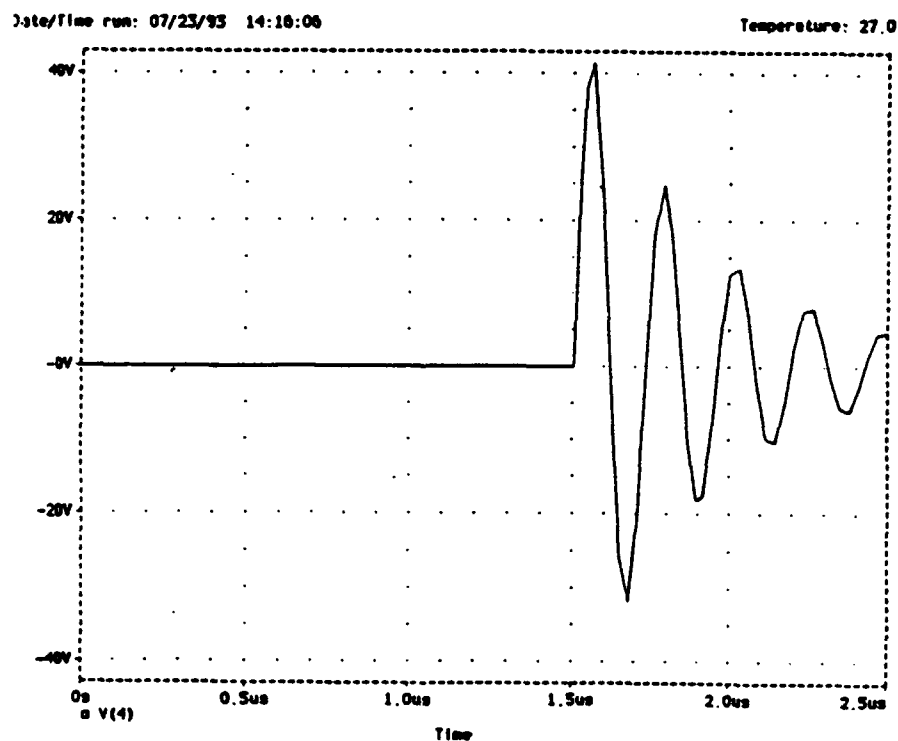


P-SPICE SIMULATION AT 3 KV

FIGURE 6



OSCILLOSCOPE READING AT 3.5 KV



P-SPICE SIMULATION AT 3.5 KV

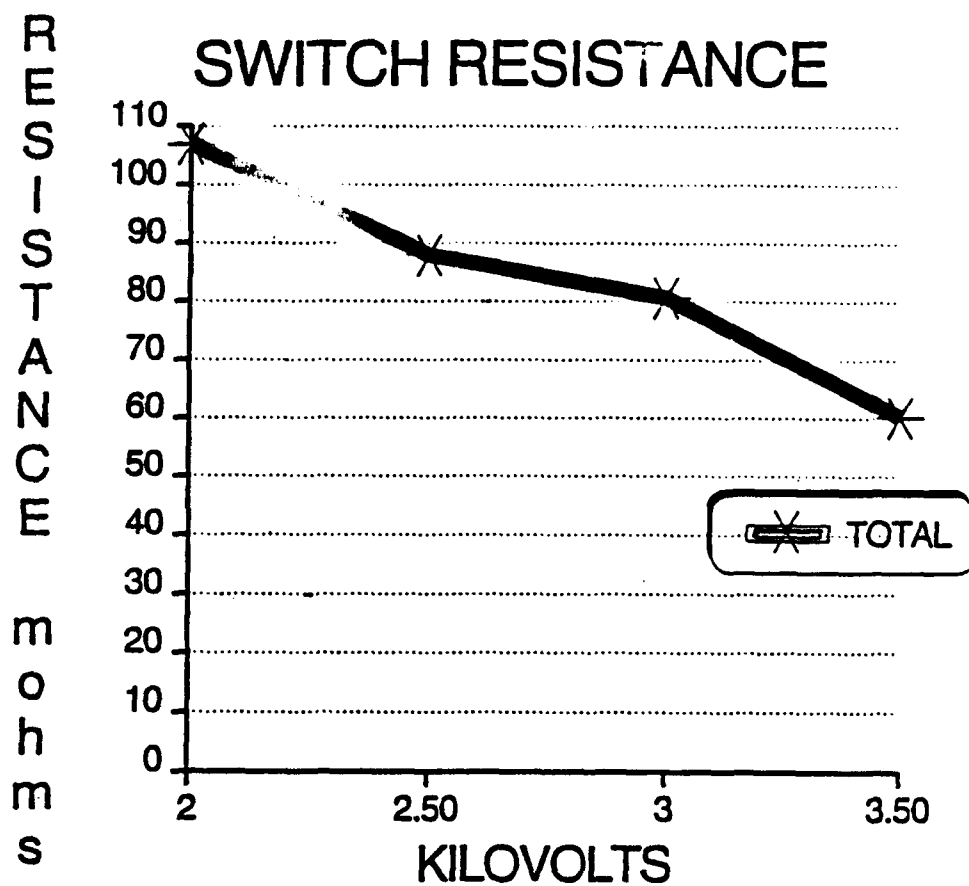


FIGURE 8

BALLISTIC HOLOGRAPHY

**Jon R. Ward
High School Apprentice
Instrumentation Technology Branch
Mentor: Mr. David Watts**

**Wright Laboratory Armament Directorate
WL/MNSI
Eglin AFB, FL 32542-5434**

**Final Report For:
High School Apprenticeship Program
Wright Laboratory Armament Directorate**

**Sponsored By:
Air Force Office of Scientific Research
Bolling Air Force Base, Washington D. C.**

August 1993

BALLISTIC HOLOGRAPHY

**Jon R. Ward
High School Apprentice
Instrumentation Technology Branch
Wright Laboratory Armament Directorate**

ABSTRACT

My summer was spent working as an apprentice in the Instrumentation Technology Branch (WL/MNSI) on Eglin Air Force Base. My mentor was Mr. David Watts and my project focused on ballistic holography in the laboratory run by Advanced Ballistic Holography program manager, Mr. Joseph Gordon. This technology can be used in place of orthoganol flash X-ray to make replicated three-dimensional images of any objects in ballistic testing. A computer program may be developed to turn the image into digital data and analyze the fragmentation. It can be used in three-dimensional modeling, behind panel fragmentation analysis, and lethality/survivability analysis.

BALLISTIC HOLOGRAPHY

INTRODUCTION

Ballistic holography is a new instrumentation technology that allows a person to view the full three-dimensional image of a ballistic event. One holographic picture can show a bullet's path, the fragmentation of the object hit, and the spall pattern, shock wave, and other events of ballistic importance created by the projectile. There are two main types of holograms: reflective and transmission. The reflective holograms are viewable by white light, while the transmission holograms are viewable by laser light. The kind used in ballistic holography is a cylindrical transmission hologram.

METHODOLOGY

The methodology includes the setup of optics and the angle at which the laser beam strikes the holographic film. Before the setup of optics and beam angles are discussed, it is important to understand the materials used in the science of holography. The most important material to making holograms is the laser. I worked with two different types of lasers this summer, the sixty milliwatt Helium-Neon laser and the three joule Ruby laser. The Helium-Neon laser has a firing time of six to eight seconds. The length of time that it fires requires a two minute waiting period for the room to settle and all objects in the hologram must remain static. The Ruby laser has a firing time of twenty nanoseconds. The speed of its firing time allows quickly moving objects to be viewable on a hologram by the use of cylindrical transmission holography. The firing burst can be split into two shots milliseconds apart, allowing two images of the same ballistic event to be exposed in one hologram. This is double-pulse ballistic holography, which creates what is called an interferogram. For any form of ballistic holography the Ruby laser must be used.

Another important instrument is the variable beamsplitter, it may be used to split a single beam into two beams by refracting part of the beam and allowing part to pass through. It is only used in split-beam holography. the variable beamsplitter may be manipulated to increase or decrease reference or object beam strength. For transmission holography, the object beam should be nearly equal the strength of the reference beam, so the beamsplitter would be set at fifty/fifty. At this setting forty-five percent of the beam will be refracted, forty-five percent of the beam will pass through, and ten percent of the beam will be absorbed or lost in the beamsplitter. For a reflective hologram, the object beam should be only thirty percent as strong as the reference beam, but a fifty/fifty setting is still used because only about thirty percent of the original object beam reaches

the film after it reflects off the object, creating the image.

The spatial filter is used in both single beam and split-beam holography. It, along with mirrors and lenses, is the most integral of the optics equipment required. The spatial filter collects the beam through a pinhole, which cleans up the beam, then the beam passes through a series of precision focusing devices that projects the beam onto the film. There are two types of films we have used in the making of the holograms: The holographic plate and the holographic film. Both are special holographic films that have a small layer of emulsion on one side storing the image in three-dimensions. The holographic plate is made of glass with emulsion and isn't practical for ballistic holography. The holographic film is flexible and is wrapped around 180 degrees of the inside of the cylindrical tube.

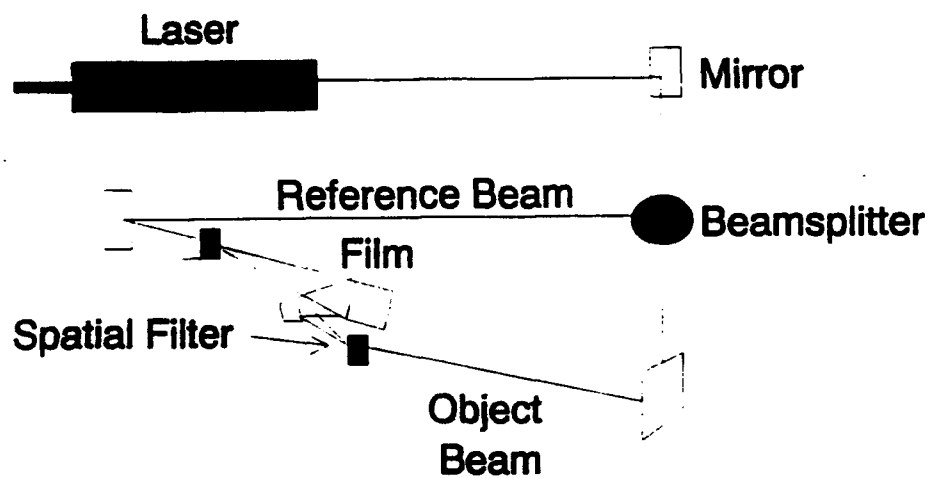
Now that the materials have been clarified, the setup of optics will be discussed for each separate type of hologram; first, the transmission hologram. Transmission holography is usually a split-beam technique with both the reference and object beams striking the emulsion of the film on the same side. The laser beam is directed through a beamsplitter, creating the object and reference beams. The object beam continues through the beamsplitter and reflects off a turning mirror into the spatial filter. The spatial filter focuses the beam onto the object, which then reflects it onto the film. The reference beam was refracted by the beamsplitter onto a turning mirror, which then reflects the beam through a spatial filter onto the film. Both beams strike the film from the same side, creating an interference pattern on the emulsion on the film, thus yielding a three-dimensional image viewable by laser. The diagram on page 43-7 is an example of the setup for creating a transmission hologram.

In order to produce a reflective hologram, it may be single beam or split-beam. The single beam method is rather simple. The single laser beam serves as both the reference

and object beams. The beam is sent through a spatial filter and projected onto the film. The beam which passes through the film and strikes the object is the reference beam. The beam that is reflected off the object and onto the film is the object beam. The object and reference beams strike the emulsion from opposite sides, creating an interference pattern which yields a hologram when viewed in the presence of adequate white light. The diagram on page 43-8 shows the setup of a reflective hologram (both single beam and split-beam). The split beam holography technique is done by using a beamsplitter to divert the object beam around the back of the film where a spatial filter projects it onto the film from behind the object. The reference and object beams leave an interference pattern in the emulsion creating a three-dimensional image viewable by the use of white light.

The technique used in ballistic holography is cylindrical transmission holography. The laser beam is sent through a spatial filter projecting the beam onto the cylinder. This illuminates the cylinder, which is wrapped on the inside with 180 degrees of a reflective material and 180 degrees of film. The reflective material reflects the beam onto the film creating an interference pattern which yields a three-dimensional image of a ballistic event with a clear 180 degree point of view of fragmentation and the projectile. The image is viewable by use of laser light. The diagram on page 43-9 is a good example of this technique.

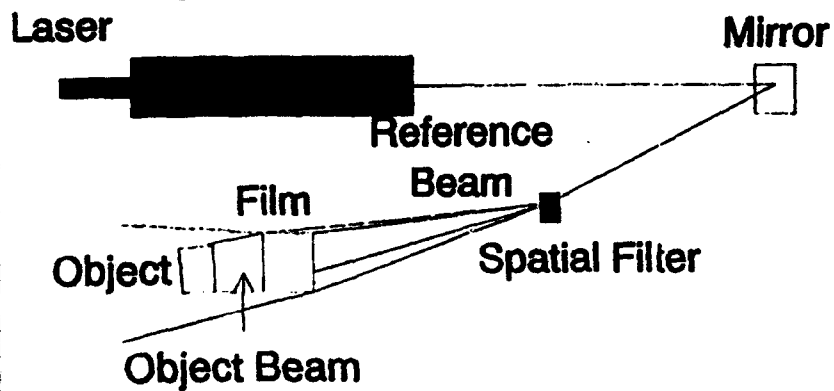
Split Beam Transmission Holography



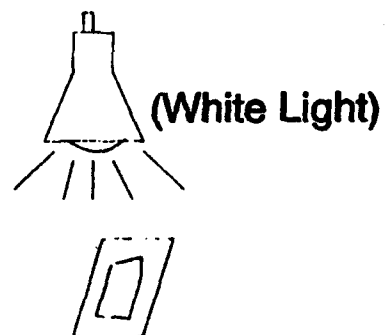
Reconstruction



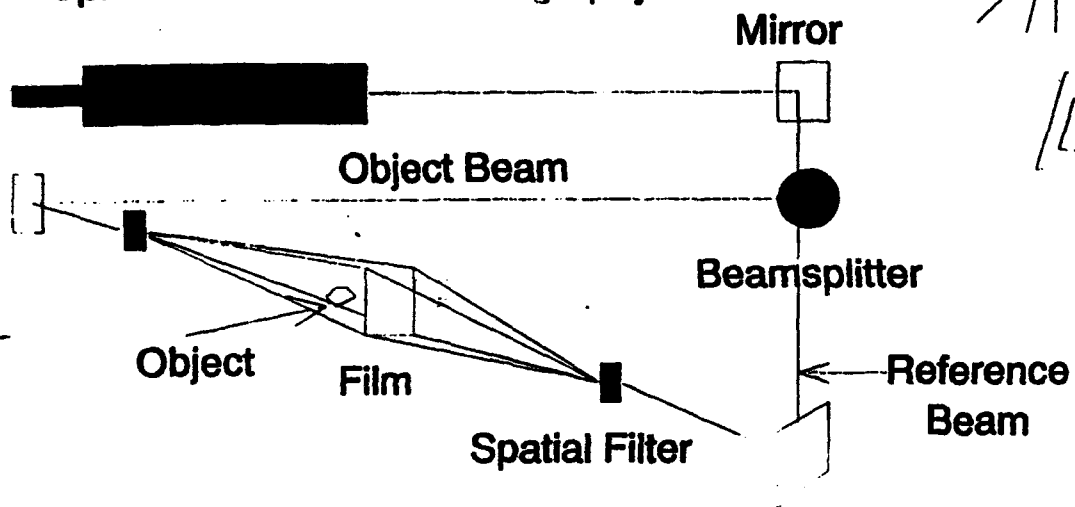
Single Beam Reflective Holography



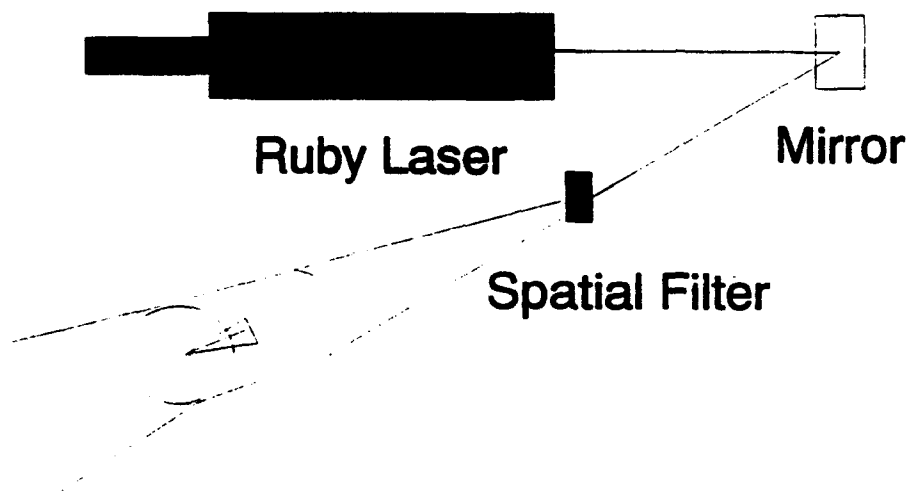
Reconstruction



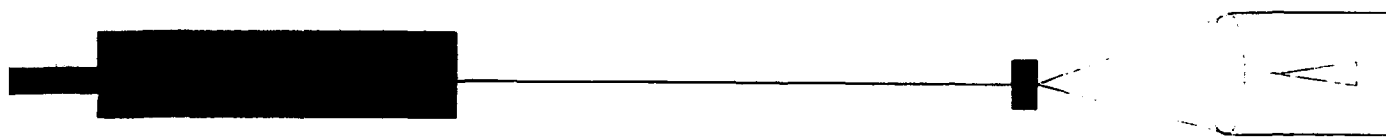
Split Beam Reflective Holography



Cylindrical Transmission Holography



Reconstruction



CONCLUSIONS AND RESULTS

My work this summer has been in the preparation for an actual ballistic hologram. Before it was attempted my summer research was ended, but the goal we had been working for was accomplished after acquisition of precise optics equipment. We were creating high resolution transmission holograms in one month after starting at the holography laboratory in Gun Bay 10. Our most vivid picture was that of a static model F-16 with such high resolution that the shadow it created was visible in the background. Though we didn't make a dynamic cylindrical hologram over the summer, the holography lab in Gun Bay 10 is ahead of schedule and I look forward to next summer working in the proposed mobile holography unit.

ACKNOWLEDGEMENTS

I have enjoyed this summer greatly because of the many people who showered me with help and support. First and foremost, I would like to thank God for getting me through these seventeen years and giving me a natural ability needed to make it this far (into the HSAP). Next, I would like to thank my fellow apprentices; I have made many close friendships that could last for years, especially Christie Gooden, Christina Trossbach, Jennifer Bautista, Barry Kress, and Kyle Perry. I thank them for either throwing great parties or for putting up with my innate sense of charm, corniness, and chauvinism. I would also like to thank the HSAP coordinators, Mr. Mike Deiler and Mr. Don Harrison. I thank Mrs. Glenda Apel for getting my pay vouchers to RDL and making sure they got our pay back to us. I want to thank Mrs.. Kip Cooper for showing me around the MNSI branch. Last but not least, I would like to thank my co-mentors, Mr. David Watts and Mr. Joseph Gordon for introducing me to the civil service as an engineer. I worked on projects from data reduction to developing film. I learned that an engineer either knows everything or will someday.

**THE TRANSPORT OF A FUEL JET
IN SUPERSONIC FLOW**

**Brian J. Banaszak
High School Apprentice
Aero Propulsion and Power Directorate**

**Tecumseh High School
9830 West National Road
New Carlisle, OH 45344**

**Final Report For:
Summer Research Extension Program
Wright Laboratories/POPT**

**Sponsored by:
Air Force Office of Scientific Research
Bolling Air Force Base, Washington, D.C.**

and

**Wright- Patterson Air Force Base
August 1993**

THE TRANSPORT OF A FUEL JET IN SUPERSONIC FLOW

Brian J. Banaszak
High School Apprentice
Aero Propulsion and Power Directorate
Tecumseh High School

Abstract

The Wright-Patterson laboratory is currently studying the effects of fuel injection in supersonic flow. To obtain supersonic air speeds, engineers developed a wind tunnel that provides air at specified Mach numbers ranging from 1.5 to 3.0, depending on the nozzle that is in place. Also, a splitter plate was developed in order to inject helium into the supersonic stream. The splitter plate simulates strut injection, one possible method of fuel injection in a scramjet. The test section of the wind tunnel contains windows on 3 sides and there is a window in the diffuser that allows the flow to be sliced in all 3 directional planes. Having this capability will allow concentration measurements of helium, at various locations to be made using acetone PLIF (Planar Laser-Induced Fluorescence). A YAG laser in conjunction with a Wavelength Extender (WEX) was used to generate a sheet of UV (266nm) laser light to pass through the test section causing the acetone to fluoresce. A CCD camera was positioned to take pictures of the fluoresced acetone, thus capturing the helium flow pattern. An excimer laser was used to measure the velocity of the fuel flow through an OH flow-tagging method. These laser diagnostics provide a good reference for future experiments that will use hydrogen instead of helium. The results of the hydrogen combustion will be applied to design a new scramjet engine capable of travelling at hypersonic speeds.

THE TRANSPORT OF A FUEL JET IN SUPERSONIC FLOW

Brian J. Banaszak

Introduction

The development of a faster airplane has been a topic of conversation since the Wright brothers. In the Experimental Research Branch (WL/POPT), Advanced Propulsion Division, Aero Propulsion and Power Directorate, at Wright-Patterson Air Force Base, engineers are developing the cornerstones to create a hypersonic airplane. Fuel injection in supersonic flow is presently being studied. Gaseous helium is being injected and studied as a reference to the eventual study of hydrogen flow. When hydrogen is injected, the lab will deal with supersonic combustion at different Mach numbers (M 1.5, 2.0, 3.0) and observe the different shock waves. Soon, this will lead to the development of a hydrogen fueled scramjet engine that will be able to power an airplane to move at hypersonic speeds. Estimated speeds will be at 21,000 mph+. The development of this kind of aircraft will put the United States in the driver's seat of technology.

Combustion Facility Design

The combustion facility (Figure 1) is a wind tunnel made up of the air supply system, the inlet section, the settling chamber, the nozzle section, the test section, and the diffuser section. The facility was just completed a couple of months ago and its design is the only type in the world; it may run continuously for long periods of time.

The air supply system (Figure 2) is the source for the necessary amount of flow rates in the facility. The laboratory's air supply system is made up of two air lines, hot and cold, in order to have better control of the flow rates allowed during testing. The facility allows one to have control on how much each air line is open in order to have better control of temperature and pressure of the air that enters the test section. One final note on the air

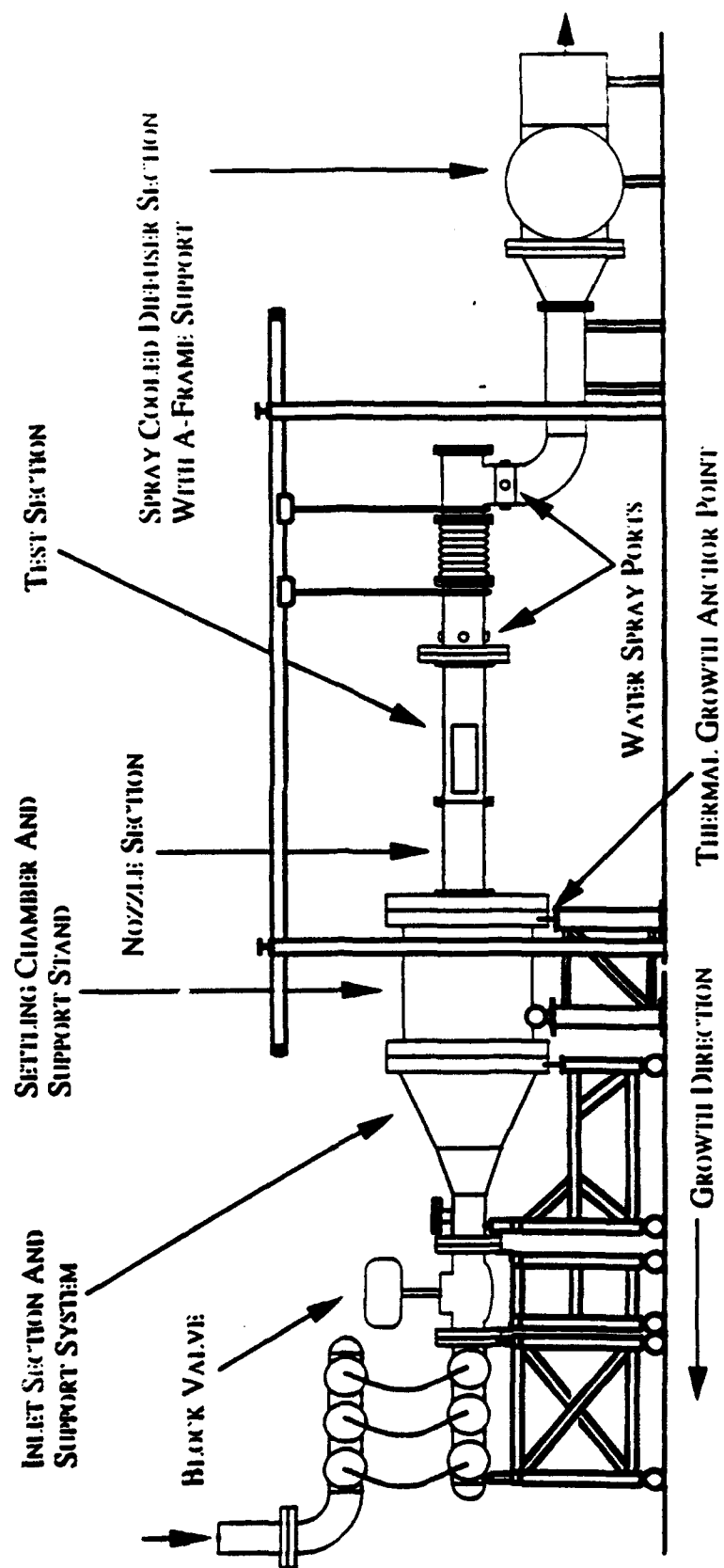


Figure 1 Schematic of Supersonic Combustion Tunnel

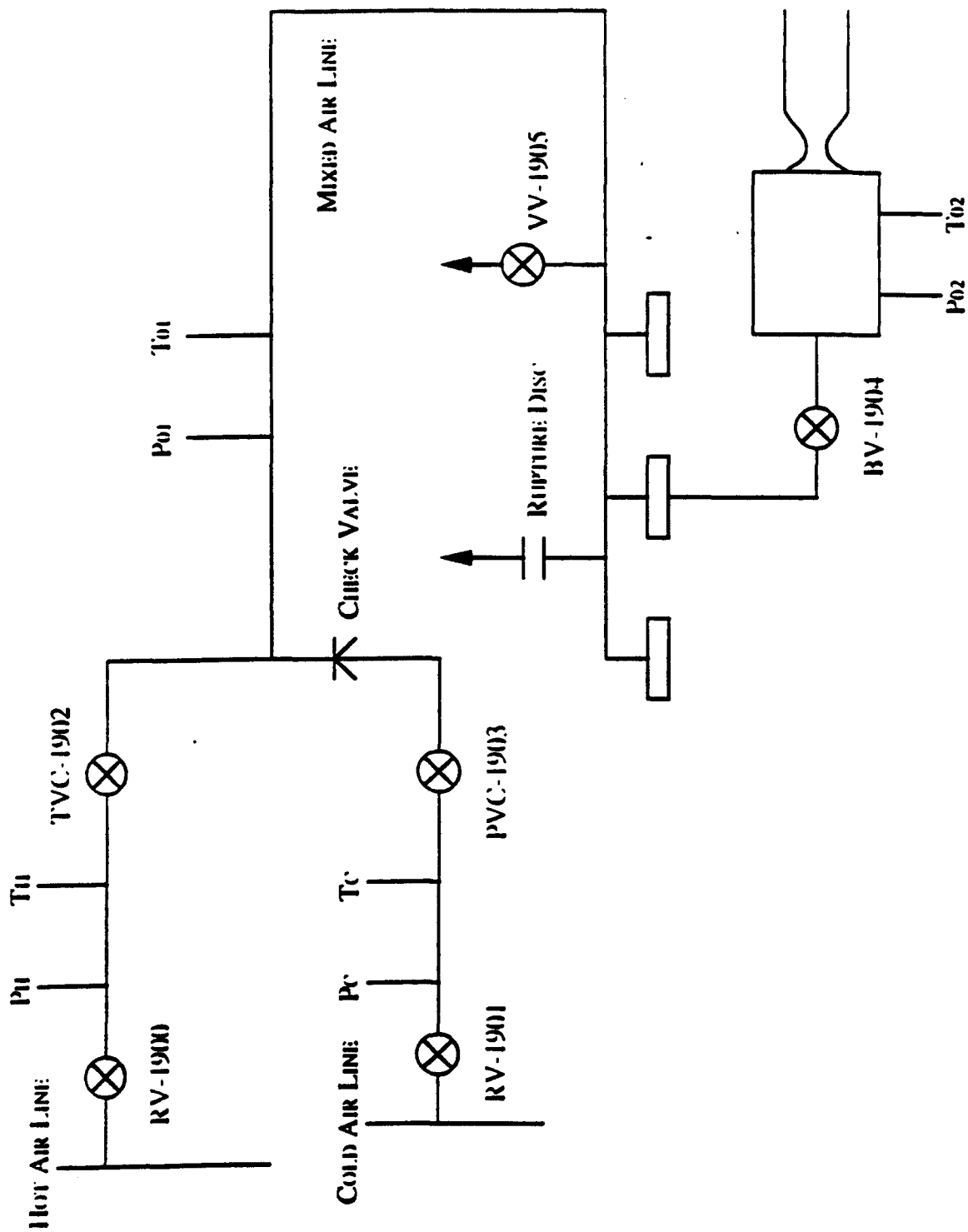


Figure 2 Air Supply System Schematic

supply system is the placement of a rupture disk downstream of the mixing. If an over pressure condition were to occur, the disk would burst and prevent any damage from occurring downstream in the test section.

The inlet section (see Figure 1) was developed to transport the air from the supply manifold to the settling chamber. This section consists of four parts including the upper manifold, the lower manifold, the block valve, and the expansion section. The upper manifold penetrates from the ceiling into the laboratory. The upper manifold consists of six outlet ports made up of flexible stainless steel hose that take the air supply from the upper manifold to the lower manifold. The lower manifold is also connected to the six outlet ports and it serves the purpose of transporting the air supply from the upper manifold to the block valve. The lower manifold looks exactly like the upper manifold. The block valve controls the air supply that goes through the test section. It can be either fully opened, partially opened, or fully closed and it requires two air lines for operation. The expansion section serves as the transition section from a 6 inch line to the 24 inch diameter of the settling chamber. This section allows the air to spread out before it enters the settling chamber.

The settling chamber (Figure 3) straightens the air flow before entering the test section. The chamber contains 3 screens and a honeycomb section to reduce turbulence levels and straighten the air flow. This chamber prepares the air for its entrance into the nozzle section.

The nozzle section (Figures 4 and 5) produces the engineer's desired Mach number. During my stay, the desired nominal Mach number was 2.0. However, by changing nozzle blocks, different Mach numbers can be achieved in this facility. This is a vital section in the wind tunnel because it allows the engineers to control and reach the velocity required for the air flow.

The test section (Figures 5 and 6) is where the engineers acquire most of their data. This section is sealed by silicone O-rings and graphite packing material in order to keep the test section air tight like the rest of

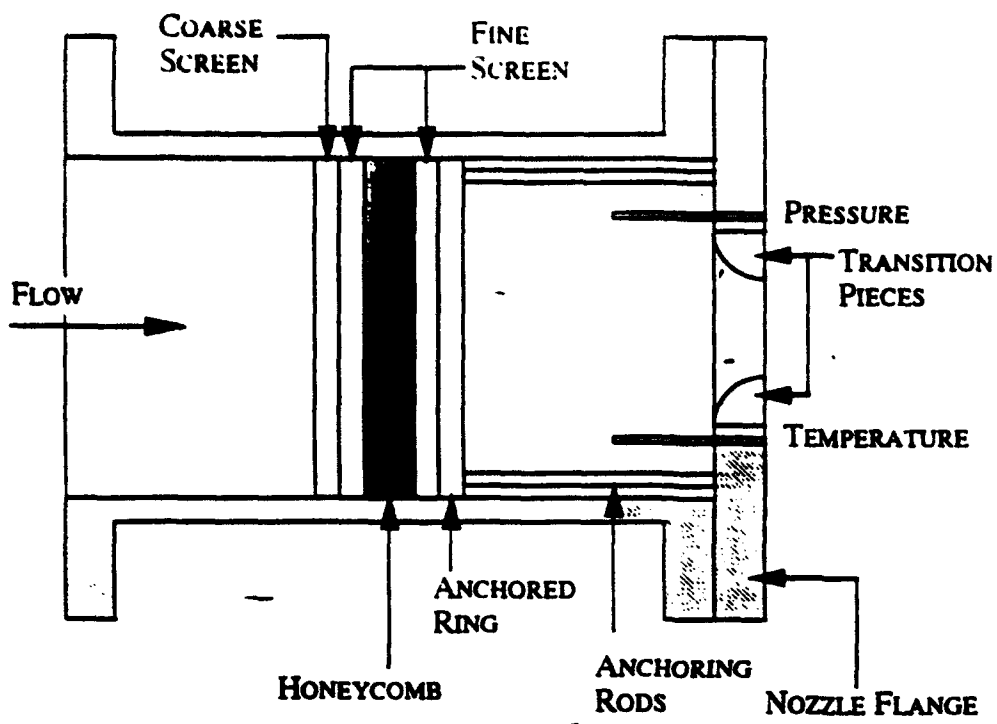


Figure 3 Settling Chamber Schematic

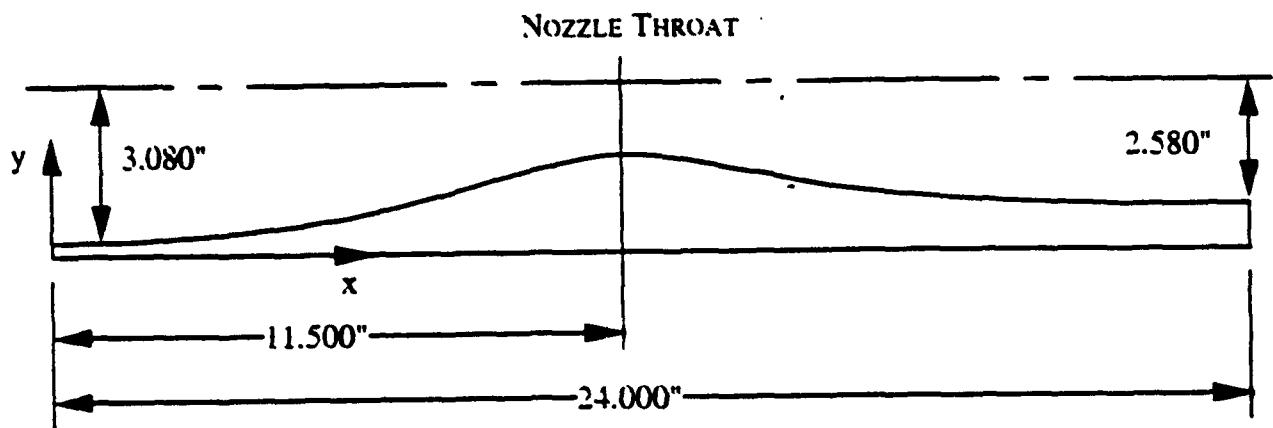


Figure 4 Nozzle Block Geometry

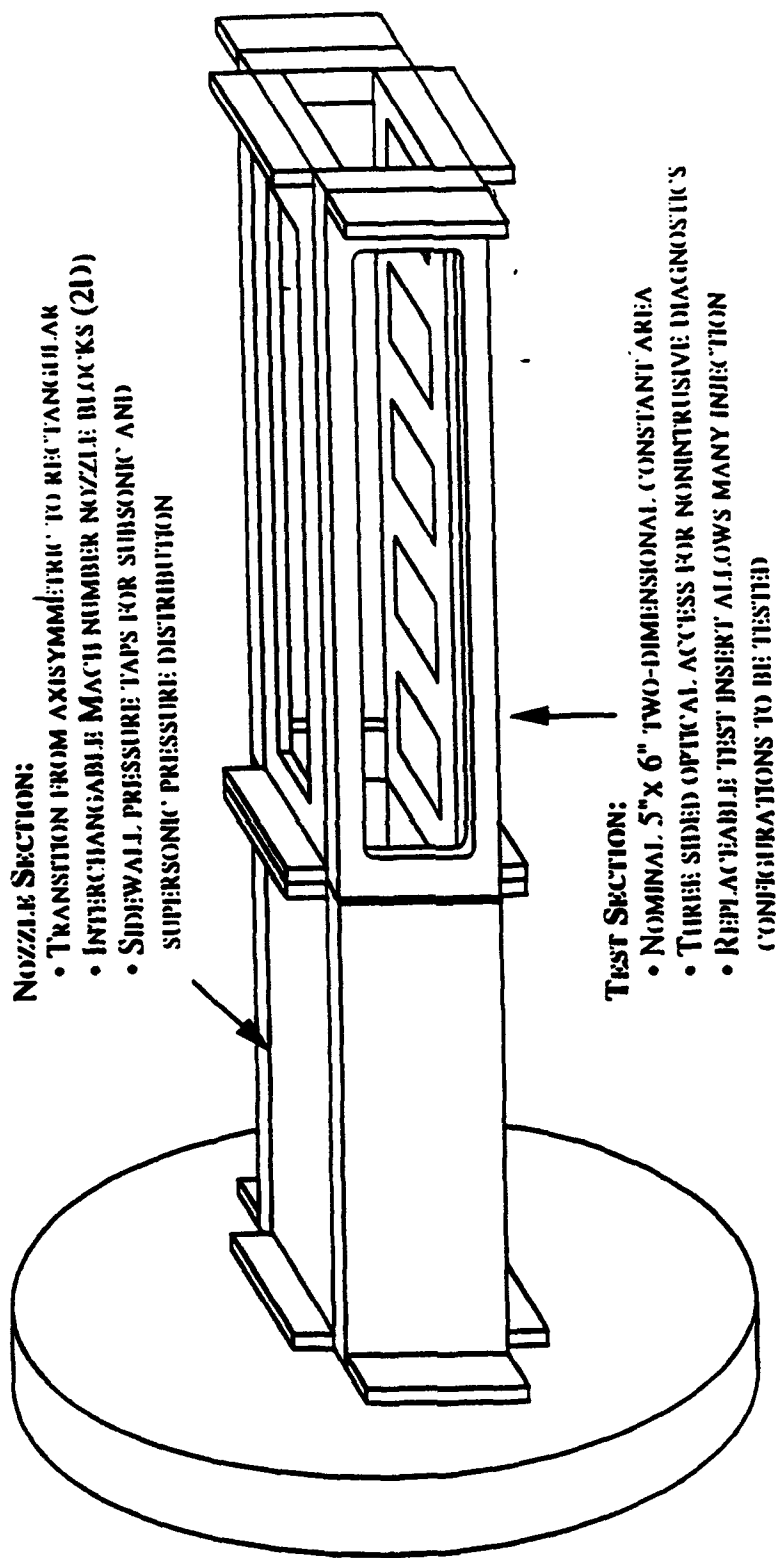


Figure 5 Nozzle Section/Test Section Schematic

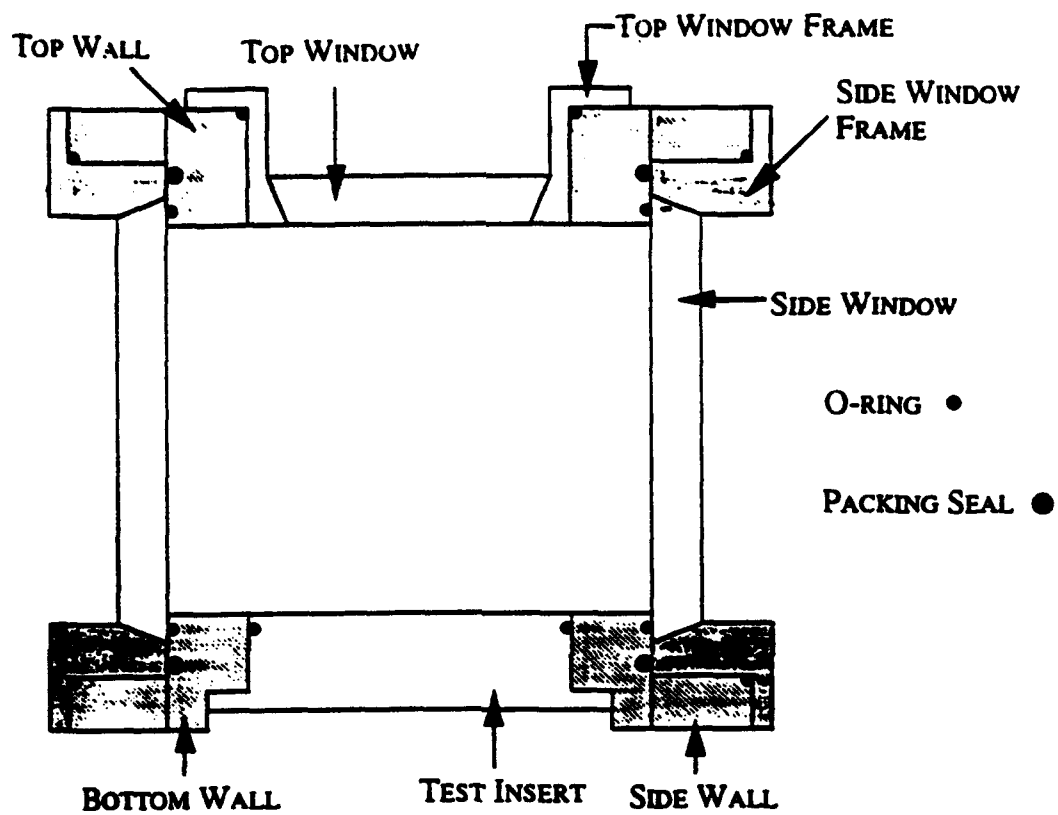


Figure 6 Test Section Cross- Section Schematic

the facility. Also, the connections to the nozzle and diffuser sections are designed so the surfaces stay perfectly flush in order to avoid any kind of disturbance in the air flow. The section is made up of four walls. The bottom wall provide 5 modular ports so different fuel injection experiments can take place in the test section via these ports. The other three sides each have their own window that are 17.5 inches long. These windows provide a great view of the entire test section. The windows are made up of fused silica. Fused silica poses very good light transmission in the UV range, which is necessary when performing acetone PLIF. Also, the fused silica works well at high and low temperatures because of its extremely low thermal expansion rate.

The last feature of the basic supersonic combustion facility design is the diffuser section (see Figure 1). This section is designed to decelerate and cool down the air before it goes into the exhausters of the air facility. The air flows through a series of pipe lines which help decelerate and cool down the air before it enters the exhausters. In addition, a water cooling system has been installed in the diffuser and water is sprayed into the diffuser section causing additional air to deceleration and cooling down. One last feature of the diffuser section is the addition of a window which looks directly into the flow of the test section. This window gives the viewer an additional optical access to another dimension of the jet flow.

Methodology

During my stay in WL/POPT, the transport of a fuel jet in supersonic flow was studied. This specific experiment consisted of a splitter plate, which contained a sonic helium injector on center line. The experiment also involved the use of a YAG laser, an excimer laser, and additional optical lenses in order to project an image and measure the velocity of the fuel jet.

A splitter plate (Figure 7) is installed parallel to the two nozzle blocks of the nozzle section and the plate extends 3 inches into the test section. In the center of the splitter plate, a 3.5mm diameter hole is

Supersonic Wind Tunnel:
(H,W,L) -- 12.70 x 24 x 91.44 cm

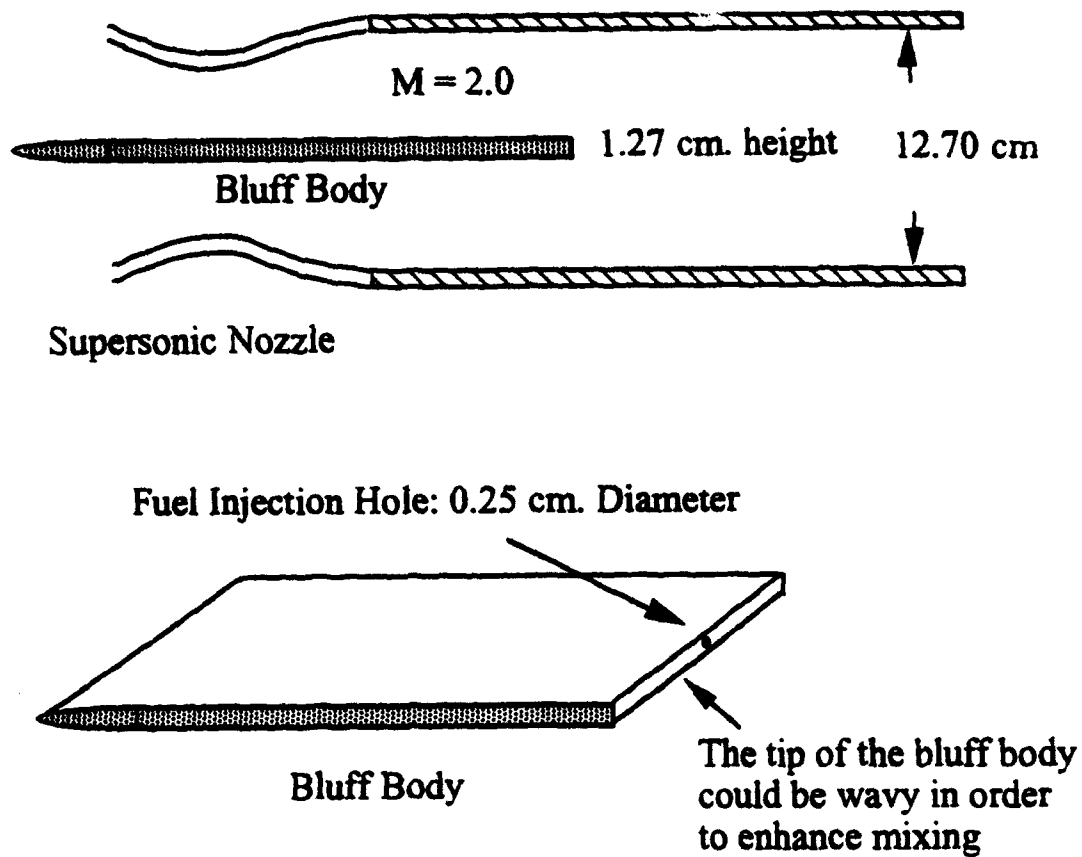


Figure 7 Supersonic Parallel Fuel Injection Tunnel

present in order to provide an injection port for different fuels. In this experiment, helium is the fuel injected. The helium is injected at various pressures in order to observe the helium at sub-sonic and sonic speeds. It is obvious that the helium flow has gone sonic with the presence of the barrel shock wave.

In order to get an image of the fuel flow, we have developed a planar laser- induced fluorescence (PLIF) system. In this procedure, we create a seeder containing acetone. The seeder includes 2 pressure regulators and a heater. The pressure regulators allow the engineers to control and know the acetone and helium flow rates. The heater is heated to approximately 250° F and the liquid acetone is injected into this super heated gas mixture. This vaporizes the acetone so it flows with the helium through the splitter plate and out of the injector. A YAG laser is combined with a Wavelength Extender (WEX) to produce a laser sheet at 266nm. A cylindrical lens, a thin lens, and a prism are used to produce a uniform laser sheet that is approximately 2mm by 50mm. The laser is set to have its best definition when it is covering the injection hole of the splitter plate. The optics are arranged three different ways in order to show three different profiles of the flow jet: a streamwise profile (vertical beam plane), a spanwise profile (horizontal beam plane), and a transverse profile (vertical beam plane perpendicular to flow velocity). In this experiment, the YAG laser causes the acetone to be excited and a well-focused CCD camera is set in accordance with the laser to take a picture of the helium flow as the acetone is fluorescing. The image is then displayed on a computer screen with an option to save the good jet images. In the images, one can observe the barrel shock, other shock waves, and the general flow pattern of helium at different flow pressures. This imaging technique will come into great use when hydrogen combustion takes place in the test section; since helium and hydrogen are closely related, the engineers are able to predict ahead of time what the flow pattern of the hydrogen will be during combustion based of the helium flow tests.

Supplied with krypton, fluorine, and helium, the engineers developed a UV beam to come out of an excimer laser with a wavelength of 248nm. This powerful laser is the facility's source to set up our OH-Flow-Tagging Velocimetry System (Figure 8), which measures the velocity of the helium jet flow. In this procedure, water is the media used to measure the velocity of the jet flow. The radiation of the excimer laser beam splits the water into hydrogen (H) and hydroxide (OH) molecules. The OH radicals are "tagged" in the flow one after another on a known time delay and the displacement can be found. This gives one enough information to decipher the velocity of the fuel flow. The time interval must be very short because the fuel is flowing ~1000 meters per second.

Results

The planar laser-induced fluorescence scheme showed the profiles of the helium flow from three different views. The streamwise profile (Figure 9) shows that the helium is at sonic speed with a pressure of 40 psi. The barrel shock shows that the helium is flowing at a sonic speed and the rest of the flow give the onlooker a good idea of the way hydrogen will flow when it flows at sonic speed. The spanwise profile (Figure 10) also shows that the helium flow is sonic at 40 psi. The barrel shock is evident from the top view as well and the viewer can see how hydrogen will flow on the top of the jet when it reaches sonic speed. Finally, the transverse profile (Figure 11) shows what the fuel flow will look like from a bottom view of the thrust and how the flow will spread out. This profile is not at a good angle to find the barrel shock to indicate a sonic speed but it does show the pattern the fuel will flow downstream. Profiles were down at pressures other than 40 psi, but 40 psi seemed to be the pressure at which the fuel flow was distinctly flowing sonic. Throughout this experiment, the nozzle flow was at a nominal Mach number of 2 and the fuel injector would allow a maximum nominal Mach number of 1.

Conclusion

The Experimental Research Branch is on the verge of a breakthrough. Presently, the laboratory is testing helium to study how its related counterpart, hydrogen, will react under certain air pressures. Later, hydrogen will be injected in our test section at high speeds in order to perform

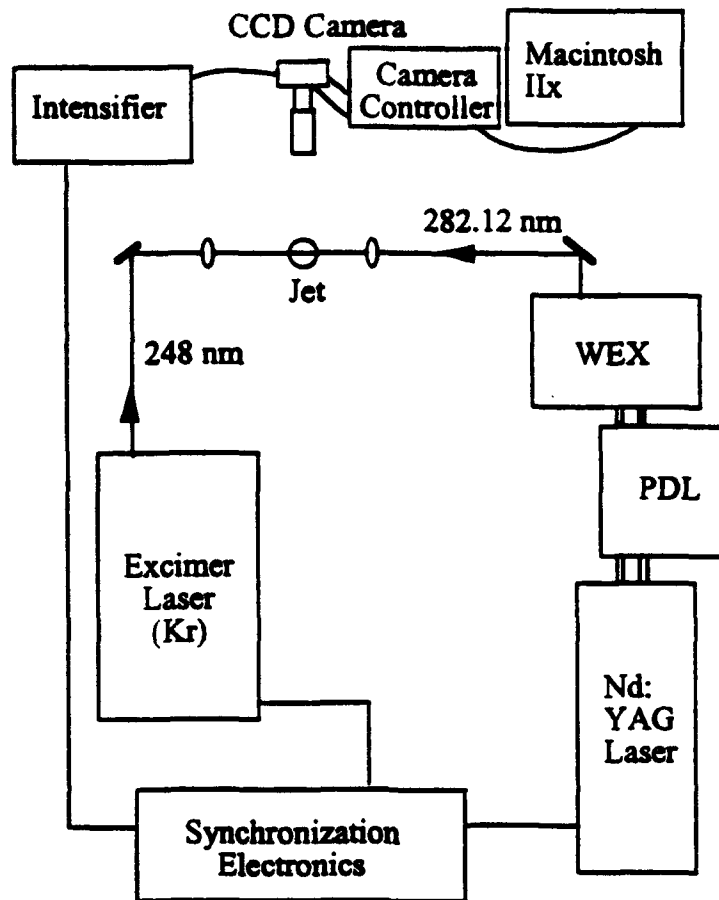


Figure 8 Schematic of OH- Flow- Tagging Velocimetry System



^{streamwise}
Figure 9 ~~side~~ Profile of Helium Flow at 40 psi
(vertical laser beam plane)

transverse
Figure 11 ~~transverse~~ profile of Helium Flow at 40 psi
(vertical laser beam plane at 90° of side profile)

supersonic combustion. After years of further research and development, a scramjet engine will be built based on the data acquired from our engineers to fly an airplane at hypersonic speeds at 21,000mph+.

REFERENCES

1. Anderson, John D Jr. Introduction To Flight. McGraw- Hill Book Company. New York, NY. 1989.
2. Chen, T H; Goss, L P; Trump, D D; Sarka, B; Nejad, A S. "The Effects of Nozzle Geometry Upon Sonic Fuel Injection as Studied by OH- Flow- Tagging Velocimetry." AIAA paper 91- 0575. Reno, Nevada. January 7- 10, 1991.
3. Donbar, J M; Glawe, D D; Nejad, A S; Driscoll, James F; Chen, Tzong H; Goss, Larry P. "Transport of Fuel Jet in Supersonic Flow." AIAA 32nd Aerospace Sciences Meeting. Reno, Nevada. January 10- 13, 1994.
4. Eckbreth, Alan C. "Laser- Induced Fluorescence Spectroscopy (LIFS)." Laser Diagnostics for Combustion Temperature and Species. Abacus Press. Cambridge, MA. 1988.
5. Goss, L P; Chen, T H; Trump, D D; Sarka, B; Nejad, A S. "Flow- Tagging Velocimetry Using UV- Photodissociation of Water Vapor." AIAA paper 91- 0355. Reno, Nevada. January 7- 10, 1991.
6. Gruber, M R; Nejad, A S. "Supersonic Combustion Research Laboratory." Experimental Research Branch. Wright- Patterson AFB, OH. January 1993.
7. John, James E A. Gas Dynamics. Allyn and Bacon, Inc. Boston, MA. 1984.
8. "The Pocket Ramjet Reader." Chemical Systems Division. United Technologies. Sunnyvale, CA.

FREQUENCY CONVERTOR REPAIR

Nick DeBrosse

**Final Report for:
Summer Research Extension Program
Wright Laboratory**

**Sponsored by:
POTX
Wright Patterson Air Force Base**

July 1993

FREQUENCY CONVERTOR REPAIR

Nick DeBrosse

Abstract

The Compressor Research Facility (CRF), located in Wright Patterson Air Force Base, studies and records the behavior of full scale, multistage, single pool, axial flow compressors and small fans. The 44,00 horsepower, 6,900 volt frequency convertor contributes a vital role in CRF's overall operation. If the frequency convertor should malfunction, CRF's compressor testing would be terminated until the frequency convertor would be once again operational. Therefore, proper annual preventive maintenance is mandatory.

FREQUENCY CONVERTOR REPAIR

Nick DeBrosse

During the annual preventive maintenance, a meggar check (a method to check electrical isolation characteristics) was performed on the frequency convertor. When tested, the machine read zero resistance with respect to the ground. This reading was not within previous specifications for this electrical machine. Therefore, the technicians with my help went through a process of trying to isolate the cause of the electrical anomaly. Bearing pedestals #1, #4, #3, #2 [1] were cleaned up in that order. The bearing pedestals were raised by lifting the shaft through the bearing clearance and then lifting the pedestal whatever distance required for shim removal. All shims were in very bad condition. The shims were coated with an oily residue. They also appeared to be corroded and ill-fitted to the pedestals. The embossed serial numbers and rough edges on the shims hampered proper positioning. Although the phenolic sheets meggared o.k., they were in very poor condition and should have been replaced. With the amount of oil and water found in the shims, the phenolic sheets were probably saturated in oil as well.

After all the shims were cleaned and reinstalled, all water lines and temperature probes removed, the machine meggared at approximately 55 Kohm. With the 500V range on the meggar the value in 1968 was 300 Kohm but 3.3 Kohm in 1982.

With all of the water lines hooked up and the temperature probes installed the one minute reading was 47 Kohm, but after five minutes the reading was 53 Kohm. We then started testing all of the motors and pedestals separately. The following results are from those tests.

South motor, east side [1]

South ring to ground: 1 and 5 minute readings - 46 Kohm

North ring to ground: 1 minute reading - 46 Kohm

North ring to shaft: instantaneous reading - 80 Kohm

South ring to shaft: instantaneous reading - 80 Kohm

#2 Bearing Pedestal [1] to ground read about 47 Kohm for a one minute reading.

North motor, east side [1]

North ring to ground: 1 minute reading - 45 Kohm

South ring to ground: 1 minute reading - 45 Kohm

South ring to shaft: instantaneous reading - 80 Kohm

North ring to shaft: instantaneous reading - 80 Kohm

#3 Bearing Pedestal to ground read 50 Kohm for a 1 minute reading.

#4 Bearing Pedestal to ground read 50 Kohm for a 1 minute reading.

North brush holders between frequency convertor and bearing #4 to ground read 12 Mohm for all holders. 1000+ Mohm for slip rings.

Bearing #4 to ground, with water flowing through the pipes, read 17 Kohm.

30 second reading on the brush rings between the frequency convertor and bearing #4 were 650-800 Mohm.

Shaft to brush holders read 5.5 Mohm.

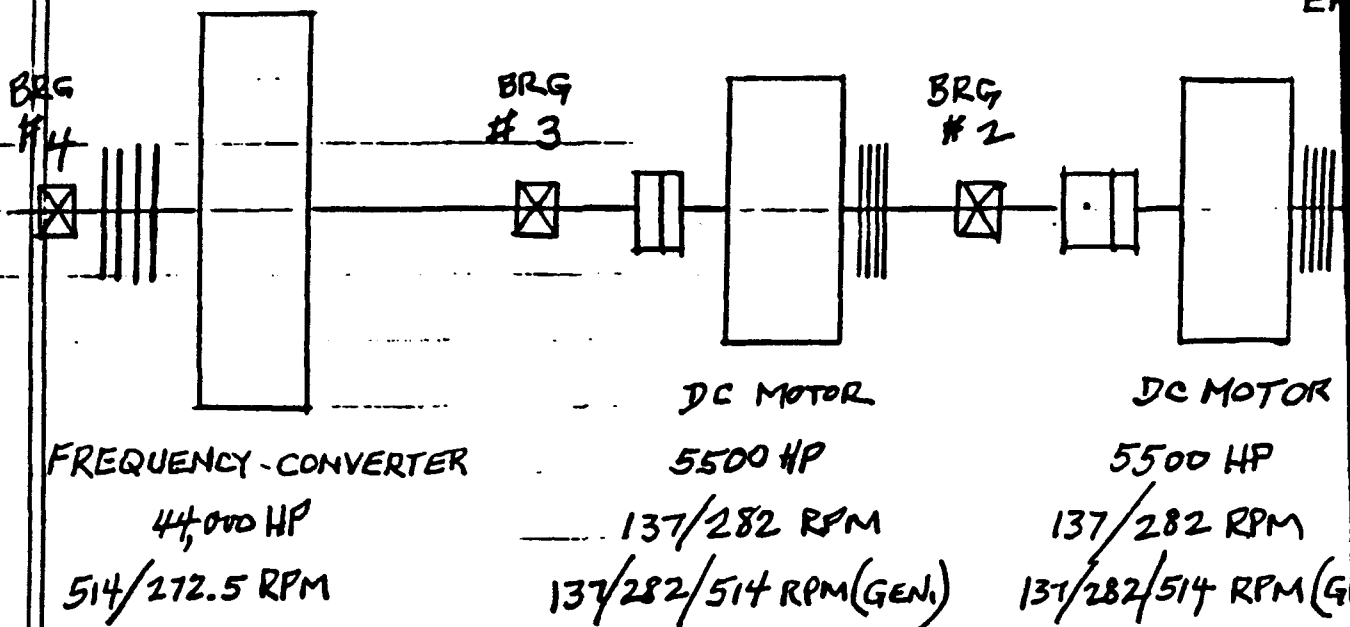
Shaft to slip ring read 1000-2000 Mohm.

At this point everything looked all right and ready to run, so we began the long process of reassembly. A run was made the day after everything was assembled with no apparent problems. Oil tests were taken immediately after the run to see if the oil was a part of the problem, besides an insignificant high lead count nothing seemed to be wrong. A final meggar reading was taken the day after the test and it read about 10 Kohm.

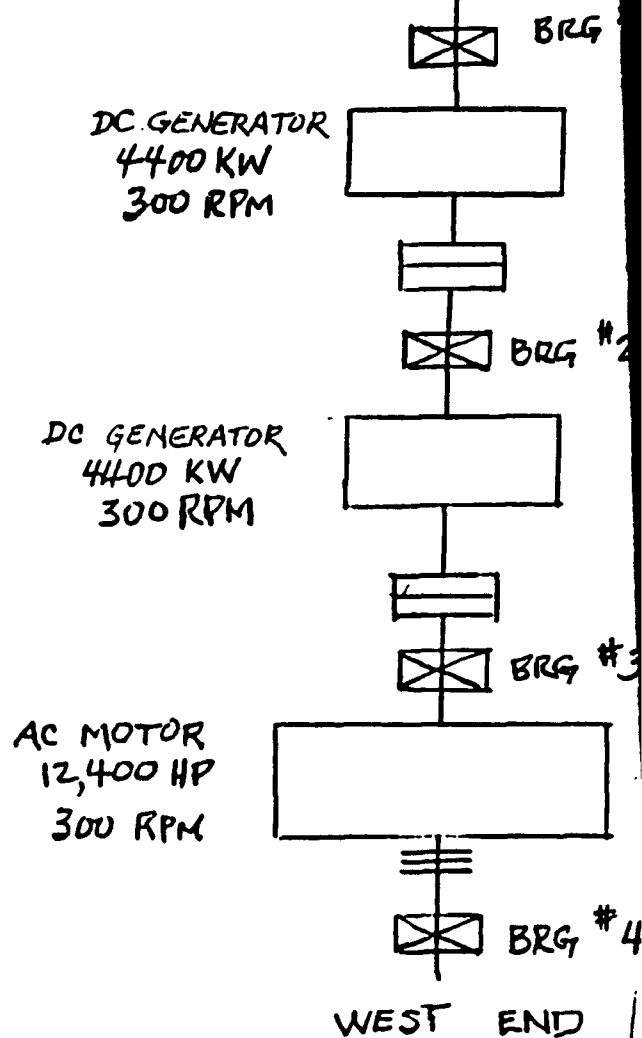
CRF ELECTRICAL DRIVE ROOM (BLDG 20)

NORTH
END

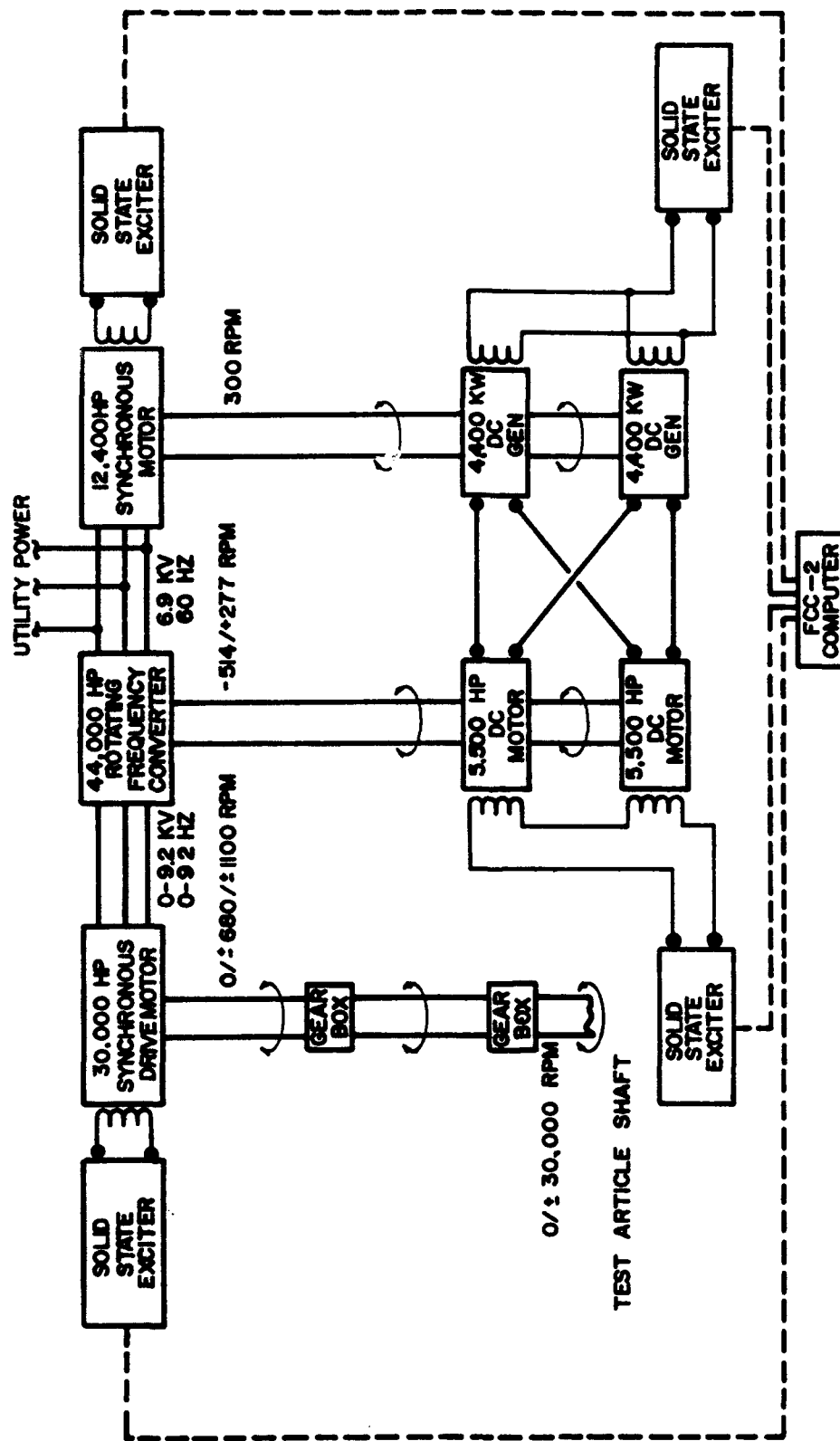
SOUTH
END



EAST END



9/14/90



SCHEMATIC DIAGRAM
CRF VARIABLE SPEED ELECTRIC DRIVE
FIGURE 1.11-b

**A STUDY OF THE MECHANICAL
DRIVE SYSTEM**

**David B. Hartsock
Apprentice
Operations Group**

**Compressor Research Facility
1950 Fifth Street
WPAFB Dayton, OH 45433-7251**

**Final Report for:
RDL's Summer Apprentice Program
Aero-Propulsion Laboratory**

July 1993

During my summer job at the Compressor Research Facility (CRF) I was involved with the Mechanical Drive System. The CRF is presently upgrading their drive system. This allowed me to do an intricate study of the CRF's Mechanical Drive System. The majority of my job I was studying up on the design requirements so I would be properly prepared when we needed to make the new designs for the drive system.

PURPOSE OF SYSTEM

The Mechanical Drive System interconnects the existing 30,000 HP drive motor and the driven equipment of the CRF to transmit power and provide shaft rotation ranges to match those required for test articles.

SYSTEM DESCRIPTION

The Mechanical Drive System consists of the existing drive motors, speed increasing gearboxes, turning gear, support bearings, inter connecting shafts and couplings.

A combination of one low speed gearbox in series with one of three high speed gearboxes containing fixed ratios will be used in order to cover the operating range. For speeds below the minimum drive motor speeds listed above, the horsepower will decrease no more than proportionally to the cube of the speed.

PERFORMANCE CRITERIA

The design of this system assures that the following criteria will be satisfied:

The speed increasing gears will operate over their design speed and power range with minimum objectionable noise and vibration.

The entire test stand including the drive motors, gears bearings, and shafting will be free of serious resonant vibration either lateral, torsional or axial, throughout the entire operating speed range. This requirement applies to all operating test conditions including cycling tests of the compressor for which the loads may be varied from full load to 20% load and back to full load at maximum facility acceleration/deceleration rates. The time between successive cycles may be varied to avoid potential resonance effects.

The entire drive system is designed to withstand, without damage, a minimum of 105% of the maximum operating speed.

All partitions, cover plates and other parts of the machinery will be free from resonant vibration arising from either the drive system or the test compressor.

The drive system gearing is designed to have an expected service life of at least 5,000 hours under the most arduous operating conditions.

The drive system will have a minimum backlash to provide for smooth transition from drive to brake of the test article.

Drive system components will be protected from test article induced failures by the use of a shear section located in the final shafting which drives the compressor. The shear shaft will be supported by bearings located at the shear notched section to restrain fractured components.

The entire drive system will be designed to accommodate a future expansion of the drive capability to a dual drive configuration. The second drive will power the front or fan spool of dual spool compressors. Space is provided at the input side of the high speed gearboxes to accommodate and provide access to the additional drive.

Gearbox sets are designed to provide as much speed overlap at the ratio change points as can reasonably be obtained.

The drive system gearing is designed to operate with both clockwise and counter clockwise input rotation. Output rotation will be in the same direction as the input rotation in either case.

Gear assemblies will be given a full factory speed test, and oil flow, gear losses and temperature rise of bearings from the test will be recorded.

Overspeed tests in both directions at 105 percent speed for five minutes will also be performed at the factory as a minimum.

A variable speed, electric motor powered turning gear will be provided in the drive system for turning the drive train during cool down, inspection, and coupling alignment periods. Rotation in either direction will be possible, and the motor will be normally disengaged from the drive when not in use.

The drive system design includes an electric motor for starting the main synchronous drive motors. The starting motor will be coupled through a clutch and chain drive, and turn the main motor shaft up to 10 rpm in either direction. The time to accelerate the system to 10 rpm will not exceed 20 seconds.

All mechanical parts will be designed for operation over an ambient temperature range of -20 to +110 degree F. The equipment will meet specifications with the relative humidity as high as 100% and as high as 95% without condensation.

All bearings used in the drive system are designed to allow there removal and replacement with minimum disturbance of the associated shafting.

Guards will be installed around all rotating equipment to prevent accidental contact with moving parts by operating and maintenance personnel.

Seals are provided at each shaft location which extends outside of the casing to prevent oil leakage throughout the design speed range of the shaft.

DESIGN APPROACHES

The design approaches available for the drive system involved considerations of the gearboxes, types of couplings, pedestal bearing locations, and drive shafting. The selection of the gearbox arrangement had the greatest overall influence on the configuration of the rest of the drive system. The location of the pedestal bearings, and the lengths of the shafting in particular were affected by the gearbox arrangement. The types of couplings, bearings, and shafting used are dependent on the application; i.e. speed, horsepower, and alignment requirements. The design of the shafting and couplings which connects the test compressor to the Mechanical drive system jackshaft will be designed by the test article vendor.

Three design approaches were available, based on gearbox considerations. One used the reconditioned DTT60 and three additional interchangeable sets of increaser gears. Another approach used a replacement for the existing DTT60 and three additional interchangeable sets of increaser gears. The third approach eliminated the use of the DTT60, and replaces it with a set of interchangeable speed increaser gearboxes.

In each case the remainder of the drive system had to meet the same performance requirements for shafting, couplings, and bearings although the particular arrangement and number of individual components varied for each configuration.

COUPLINGS

The couplings interconnect the drive and driven equipment of the facility and allow for misalignment and axial expansion of shafting and housings. Due to the high power and speed requirements, only two types of couplings are suitable for the application; gear tooth or diaphragm type. The number of sets of couplings required will be in accordance with the shafting requirements for the particular speed and torque ranges. The performance criteria established for the total drive system is applicable to the couplings. In addition, the couplings will also meet the following criteria regardless of their type:

Couplings will operate over the CRF power and speed range without deleterious vibration and axial oscillations.

Couplings will be capable of interchange without disturbing the fixed elements of the drive.

All coupling components will be supplied in match marked sets to ensure dynamic balance.

The couplings will be capable of operation at a misalignment of .002 inches per inch of coupling length and a minimum axial displacement of .050 inches.

Couplings and shafting will be capable of supporting the instrument conduits.

The couplings will be of a commercially available type.

The choice of coupling size will be decided on the specific application and performance required for the coupling location. Flexible diaphragm coupling types will be used due to their more favorable operational characteristics. Final dimensions and coupling selection will reflect critical speed, torsional and axial vibration considerations.

SHAFTING

For the gearbox configuration selected with a low speed section of shafting and a high speed section of shafting will be required to encompass the full operating range of the test facility. Each shafting assembly used will incorporate a shear section rated to fail at 90% of the rated torque of the selected high speed gearbox. The shear section will be a diaphragm coupling assembly, centrally notched.

Individual sets of shafting between the pedestal housing and the test article will be required and will be furnished as part of the test article system.

MAJOR INTERFACE DEFINITION

The following major system interfaces have been considered in the design of this system.

TEST CHAMBER SYSTEM

The location of the final gearbox output shaft centerline defines the location of the test chamber centerline in both a horizontal and vertical direction. The core flow collector will not heat the drive shaft or its supporting structure an excessive amount. There is no requirement for the drive shafting to be supported by test chamber structural members.

FACILITY CONTROL SYSTEM

In the event that an out of tolerance condition of any of the drive system components is detected, the Facility Control System will initiate proper action commensurate with the degree of severity of the condition detected.

FOUNDATIONS AND STRUCTURES

The existing foundation will be used and a new structural base will be mounted on it. The existing gearbox and pedestal shaft cover are redundant to the new facility.

DRIVE LUBE OIL SYSTEM

The existing lubrication system will furnish 1,000 rpm of filtered oil to the entire drive system at a temperature of +100 degree F to +120 F. The supply pressure will be increased from 10 psig to 25 psig for all components of the drive system.

Oil piping connections will be located to minimize piping runs to the existing lube oil system and still permit access to and around the drive system components.

INSTRUMENTATION

Instrumentation interfaces include vibration pickups, RTD's, and speed indication means located on the final output shaft. Provisions are made for mounting slip rings to obtain rotating measurements from the test article.

SERVICE AIR

Service air connections currently used by the DTT-60 will be updated as necessary.

HYDRAULIC SYSTEM

The Mechanical Drive System will interface with the Hydraulic System as required for proper operation.

COOLING WATER SYSTEM

Interface of the Mechanical Drive System directly with the cooling water system will not be required. Cooling of the drive system components will be performed by the lubricant. The lubricant will then be cooled in a water-to-oil heat exchanger in the Drive Lube Oil System.

TEST ARTICLE

Interface of the Mechanical Drive System with the Test Article will be by means of test article peculiar shaft and coupling assemblies, one end of which mates with the facility coupling and the other with the Test Article. Provisions will be made in the design of the test article system to balance the thrust applied to the test article drive shaft in this typical turbine engine operation.

This is what I did and learned over the eight week period that I worked at the Compressor Research Facility. Although the process of what the CRF is doing will not be done until the future, I feel that I have done an ample job of helping the CRF complete their project.

TRANSVERSE INJECTION STUDIES INTO A MACH 2 FREESTREAM

**Melanie L. Hodges
Research Apprentice
Advanced Propulsion Division**

**Wright-Patterson Air Force Base
Area B, Building 18
WL/POPT
Wright-Patterson AFB, OH 45433-6563**

**Final Report for:
Summer Research Program
Wright Laboratory**

**Sponsored by:
Air Force Office of Scientific Research
Bolling Air Force Base, Washington, D.C.**

August 1993

TRANSVERSE INJECTION STUDIES INTO A MACH 2 FREESTREAM

Melanie L. Hodges
Research Apprentice
Advanced Propulsion Division
Wright Laboratory
Wright-Patterson Air Force Base

Abstract

Transverse injection studies were performed in a Mach 2 freestream using schlieren photography and Mie scattering with carbon dioxide as the injectant. The turbulent structure and penetration characteristics of three typical injector geometries were examined. One of these was positioned at a low angle to the freestream while the others were injected perpendicular to the freestream. Results of the schlieren photography revealed typical features of the flow including a bow shock, barrel shock, Mach disk, and recirculation zones. The Mie scattering images showed a variety of flow structures along the boundary between the jet and the freestream. These structures were more evident in the flowfields created by the perpendicular injectors than by the angled injector. This preliminary research merits further analysis and investigation.

Acknowledgments

I would like to thank the following people for their time and patience during my summer research at Wright-Patterson: Capt. Lou Carreiro, Mark Gruber, Jeffrey Donbar, Capt. Dean Petters, Diana Glawe, Charlie Smith, Gary Haines, Tzong Chen, Dave Schommer, Abdi Nejad, Lt. Jeffrey Fillmore, Lt. James Clegern, and others.

TRANSVERSE INJECTION STUDIES INTO A MACH 2 FREESTREAM

Melanie L. Hodges

Introduction

Goals for the National AeroSpace Plane (NASP) include flight velocities in the hypersonic regime. In order to achieve such velocities, a fundamental knowledge of the fuel injection, mixing, and combustion processes carried out in the combustion chamber is necessary. These processes will take place in a supersonic stream and therefore, must occur quickly since the residence time within such combustors will be small. Numerous fuel injection concepts have been proposed for such combustors, including sidewall or transverse injection. This paper focuses on the preliminary investigation comparing the turbulent structures and penetration of two typical injector geometries.

Background

Interest in transverse injection processes began in the mid-sixties and has recently resurfaced with the increased interest in hypersonic flight and the NASP program. Early studies in this area were conducted by Schetz and Billig¹ and Zukoski and Spaid². These investigations produced schlieren photographs and concentration measurements of the jet flowfield. Schlieren photographs revealed a bow shock wave upstream of the injector exit, rapid turning of the injectant gas, a Mach disk, and recirculating flow regions upstream and downstream of the injector exit. These features are represented in Figure 1.

Recently, Papamoschou, et al.³ used schlieren photography to study the penetration characteristics of supersonic transverse jets. Their study examined the effects of changes in the freestream Mach number, static pressure ratio, density ratio, and momentum ratio on the extent of the jet's penetration. Their investigation revealed that penetration of the jet is primarily dependent on the jet-to-freestream momentum ratio (J) given by

$$J = \frac{(\rho u^2)_{jet}}{(\rho u^2)_{freestream}} = \frac{(\gamma p M^2)_{jet}}{(\gamma p M^2)_{freestream}}$$

where ρ is the gas density, u is the gas velocity, γ is the gas's specific heat ratio, p is the static pressure, and M is the Mach number. Other results of their investigation included observations that the jet Mach number and the jet-to-freestream density ratio have no effect on the extent of jet penetration. Based on this observation, the present investigation concentrates on the study of sonic jets.

The effectiveness of a transverse jet for combustion purposes depends not only on the jet penetration, but also on fuel/air mixing. This issue was addressed by Zukoski and Spaid², who used a probe to obtain concentration profiles within the jet flowfield. These studies suggested the presence of two vortices, which played an important role in the jet-to-freestream mixing. More recent investigations have utilized nonintrusive diagnostic techniques to study the concentrations in various flowfields. Planar laser induced fluorescence (PLIF), one of the more commonly used of these techniques, was applied by Hollo, et al.⁴ in their examination of the complex flowfield between two staged transverse injectors.

In an effort to improve the operating characteristics of scramjet fuel injectors, Mays, et al.⁵ experimented with an injector oriented at a low transverse angle to a Mach 3 freestream. Their work showed that this injector geometry operated in an overpressurized mode results in a lower total freestream pressure loss than the same jet injected perpendicular to the freestream. The same injector operated in a pressure matched condition produced slower mixing and reduced penetration compared to the overpressurized case.

Experimental Methods

The new supersonic combustion facility at Wright Laboratory offered a perfect environment for the transverse injection studies reported on in this paper. The combustion tunnel and the fuel injectors used for study, along with the diagnostic techniques employed in these experiments are discussed in the following paragraphs. For further details concerning the combustion tunnel, see Gruber and Nejad⁶.

The state of the art research facility at Wright Laboratory is a result of a collaborative in-house design effort. The preliminary planning began in 1990 and the facility was completed by the end of 1992. It offers a wide range of flow capabilities, including:

- Variable Mach number capability (1.5 to 3.0)
- Continuous flow operation
- Stagnation conditions up to 400 psig at 1660 °R
- 5-inch by 6-inch test section
- Peak air flow rate of 34 lb_m/sec
- Optical access to test section from four sides including the end.

The results of their efforts are shown in a schematic of the facility (Figure 2). The test section allows optical access on three sides and the end for the use of nonintrusive diagnostic techniques. The windows are made of fused silica, which allows exceptional UV laser penetration for diagnostic techniques such as PLIF of acetone or OH-Flow-Tagging Velocimetry as described by Chen, et al.⁷. The test section also contains five access ports on the bottom wall. These ports allow various test articles or injectors to be easily installed for experiments (see Figure 3).

For this investigation, several injector geometries were available, including a circular jet injected perpendicular to the flow (a), a circular jet injected at 15° with the flow (b), and an elliptical jet injected perpendicular to the freestream. (c) All injectors have the same cross sectional area (perpendicular to the jet flow direction) of 0.049 square inches. Therefore, the mass flow rate through each injector is the same at a given pressure, allowing for a proper comparison of each injector's performance. Consequently, injector (a) has an exit diameter of 0.25 inches, and the elliptical exits of injectors (b) and (c), though similar in geometry, are different in exit area. Figure 4 offers an illustration of the three injector configurations.

The diagnostic methods used in this study include schlieren photography and Mie scattering. Schlieren photography served as the preliminary source for flowfield characteristics. This technique relies on density differences within the injector flowfield. Parallel light was passed through the test section and focused on a knife edge. Regions of the flow with different density caused the light to be bent. The knife

edge cut off the light that was bent toward it and these regions of the flow appeared dark on the film. A schematic of the schlieren system used for these experiments is shown in Figure 5.

Mie scattering was used in addition to schlieren photography to identify positioning of injectant in the freestream. Heated carbon dioxide was injected into the test section and allowed to mix with the freestream. A laser beam was passed through cylindrical and spherical lenses to create an ultraviolet laser sheet at a wavelength of 266 nm. An illustration of the laser configuration is shown in Figure 6. This sheet was then passed through the top window of the test section, parallel to the side windows. Naturally occurring water vapor within the test section reflected the laser light and was collected through the side window using a CCD camera. These digital images were then stored on a personal computer for analysis at a later time.

Results and Discussion

The diagnostic techniques used in this investigation allowed a variety of flow characteristics to be examined. Schlieren photography was used to observe the general characteristics of the jet's flow region during continuous operation. The photographs taken of each injector flowfield revealed steady bow shocks ahead of the jet. They also illustrated the barrel shock and Mach disk for each jet-to-freestream momentum ratio. These images were used for insight into the major flowfield characteristics.

Still-framed images of the various injector flowfields were obtained using Mie scattering. Figures 7-9 illustrate the results of the Mie scattering technique. In these images, light regions represent the freestream (and in some areas solidified carbon dioxide), while gaseous carbon dioxide is represented by dark areas. In each image, the freestream flows from right to left. Each image was collected at a jet-to-freestream momentum ratio of 3.

Figure 7 depicts the flowfield created by the circular jet (a) injected perpendicularly to the freestream. This image is characterized by the presence of large scale turbulent structures created at the jet/freestream boundary. The development of these structures indicates that the carbon dioxide has a higher velocity than the freestream air at the boundary. The barrel shock and Mach disk of the overpressurized jet are also evident in the image. The barrel shock region is seen to be a light region in

this image. It is believed that the light region appears due to frozen carbon dioxide rather than freestream air. The gas accelerates as it exits the injector. This acceleration creates a decreasing pressure and temperature in the carbon dioxide resulting in a phase change from gas to solid. As the CO_2 passes through the Mach disk and slows to subsonic velocity, sublimation occurs and the jet appears dark once again. In addition to these features, the bow shock is visible and carbon dioxide is seen to be in the recirculation region upstream of the injector.

Figure 8 illustrates the flowfield of the low angle injector (b). This image also reveals the presence of a bow shock, however the barrel shock is absent. The bow shock is situated at a lower angle than in the previous case; this indicates a weaker shock and thus, lower total pressure loss of the freestream. There is no apparent recirculation of CO_2 upstream of the injector in this case. The turbulent structures at the jet/freestream boundary are comparably smaller and less frequent than those found in Figure 7. However, the penetration of the jet is consistent with that of the circular injector (a). The bright regions in the jet suggest the presence of solid carbon dioxide particles. The low angle of the injector may cause the CO_2 to accelerate faster than the other injector geometries.

The flowfield created by the elliptical injector (c) is shown in Figure 9. The structures found in this image are similar to those displayed in Figure 7 in that they are large in scale, and they also seem to occur more frequently than the small scale eddies of injector (b). The bow shock shown in the figure is steeper than the ones created by both of the previous injectors. As in Figure 8, there is no evidence of carbon dioxide in the upstream recirculation region of this injector. In addition to these characteristics, the barrel shock for this case shows evidence of the same phase change which seems to occur in Figure 7 and is created at a steeper angle to the freestream than the other perpendicular injector (a).

Conclusions

This study represents a preliminary investigation into the behavior of three transverse injector geometries supplied with carbon dioxide. Results of the schlieren photography revealed typical features of the flow including a bow shock, barrel shock, Mach disk, and recirculation zones. The Mie scattering images showed a variety of large and small scale flow structures along the boundary between the jet and

the freestream. These structures were more evident in the flowfields created by the perpendicular injectors than that of the angled injector. Penetration of the three jets appeared to be similar which may suggest that the jet-to-freestream momentum ratio is a useful term for the prediction of the jet's penetration. This research merits further analysis and investigation.

References

1. Schetz, J.A. and F.S. Billig, "Penetration of Gaseous Jets Injected into a Supersonic Flow," AIAA Journal, Vol. 3, No. 11, pp. 1658-1665, 1966.
2. Zukoski, E.E. and F.W. Spaid, "Secondary Injection of Gases into a Supersonic Flow," AIAA Journal, Vol. 2, No. 10, pp. 1689-1696, 1964.
3. Papamoschou, D., et al., "Observations of Supersonic Transverse Jets," AIAA Paper 91-1723, 1991.
4. Hollo, S.D., et al., "Characterization of Supersonic Mixing in a Nonreacting Mach 2 Combustor," AIAA Paper 92-0093, 1992.
5. Mays, R.B., et al., "Low Angle Injection into a Supersonic Flow," AIAA Paper 89-2461, 1989.
6. Gruber, M.R. and A.S. Nejad, "Development of a Large-Scale Supersonic Combustion Research Facility; Volume 1-Design and Fabrication," Wright Laboratory Report No. WL-TR-93-2052, 1993.
7. Chen, T.H., et al., "Multi-Zone Behavior of Transverse Liquid Jet in High-Speed Flow," AIAA Paper 93-0453, 1993.

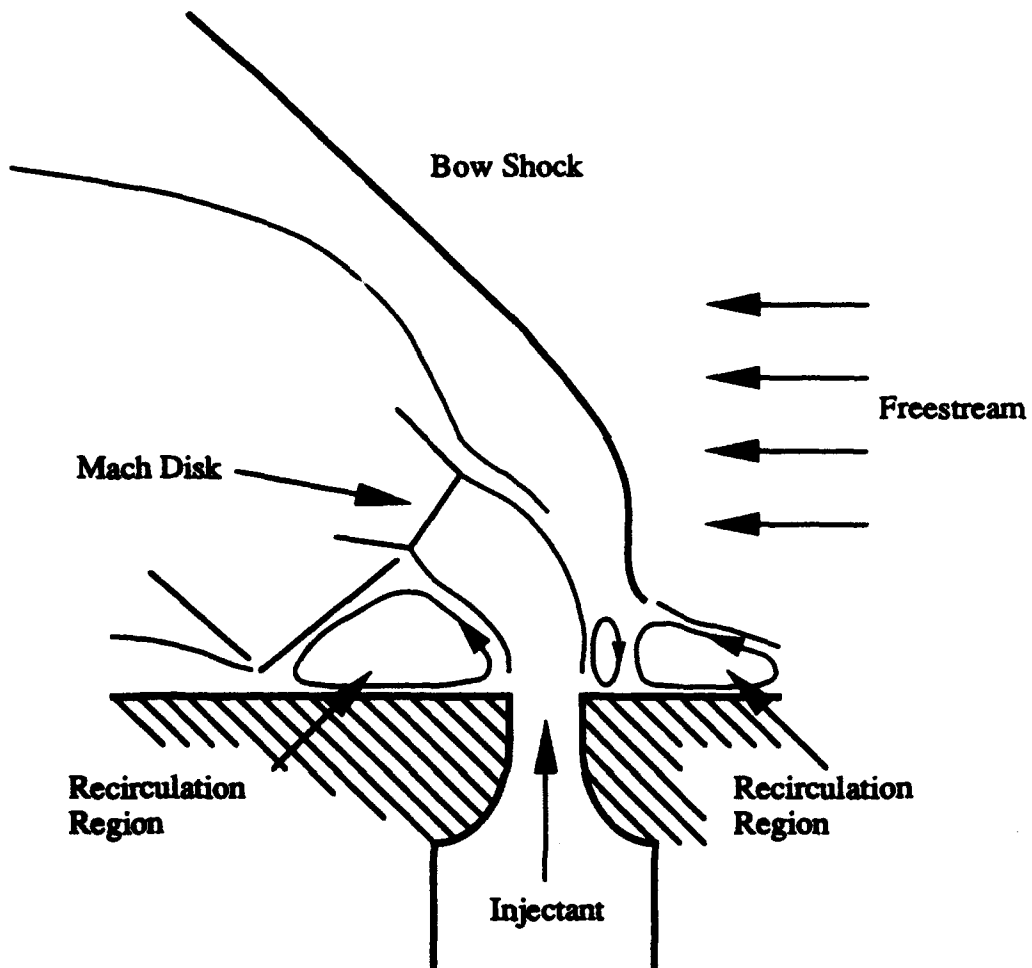


Figure 1 Flow Regions of a Transversely Injected Jet

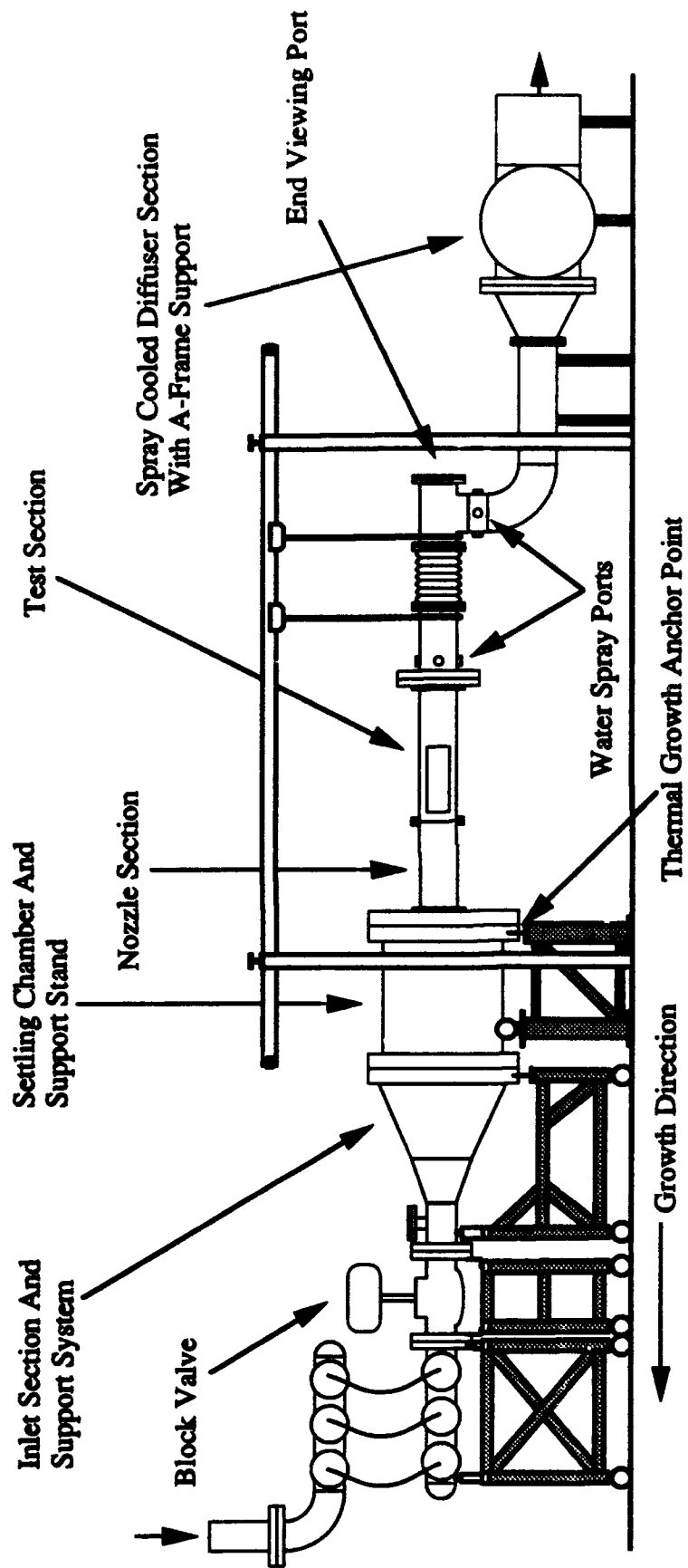


Figure 2 Schematic of Supersonic Combustion Tunnel

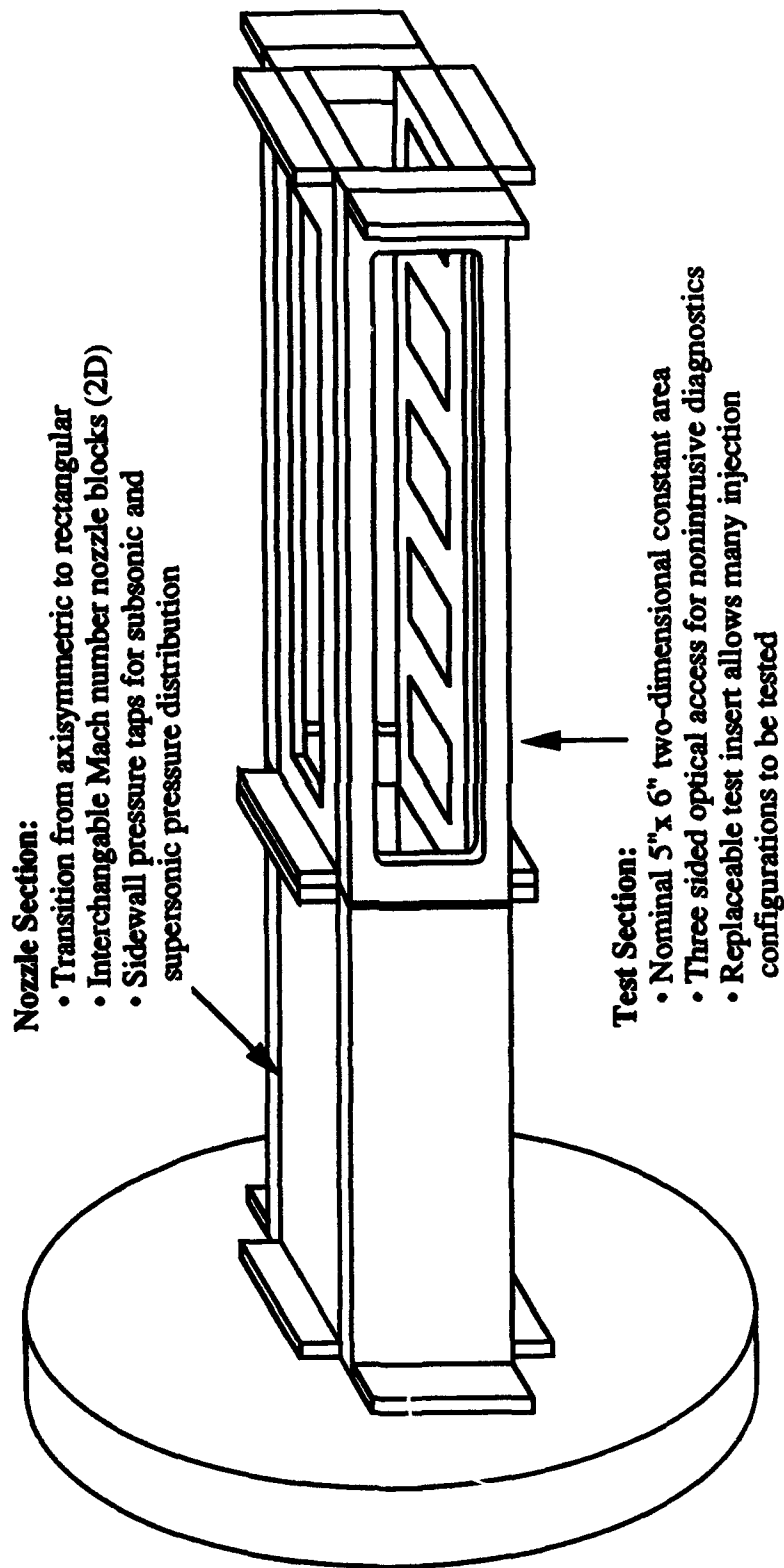
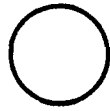
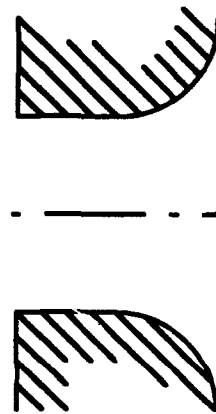
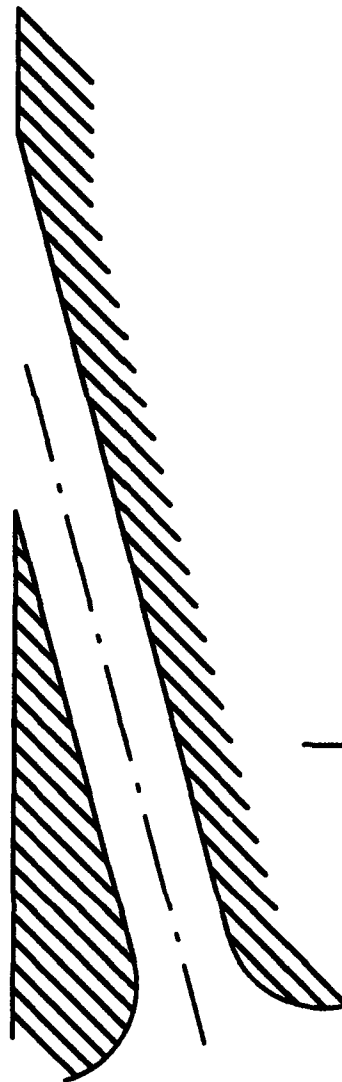
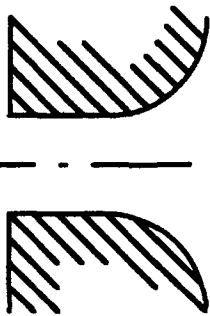


Figure 3 Nozzle Section/Test Section Schematic

Plan View



Cross Section View



(a)

(b)

(c)

Figure 4 Illustration of Injector Configurations

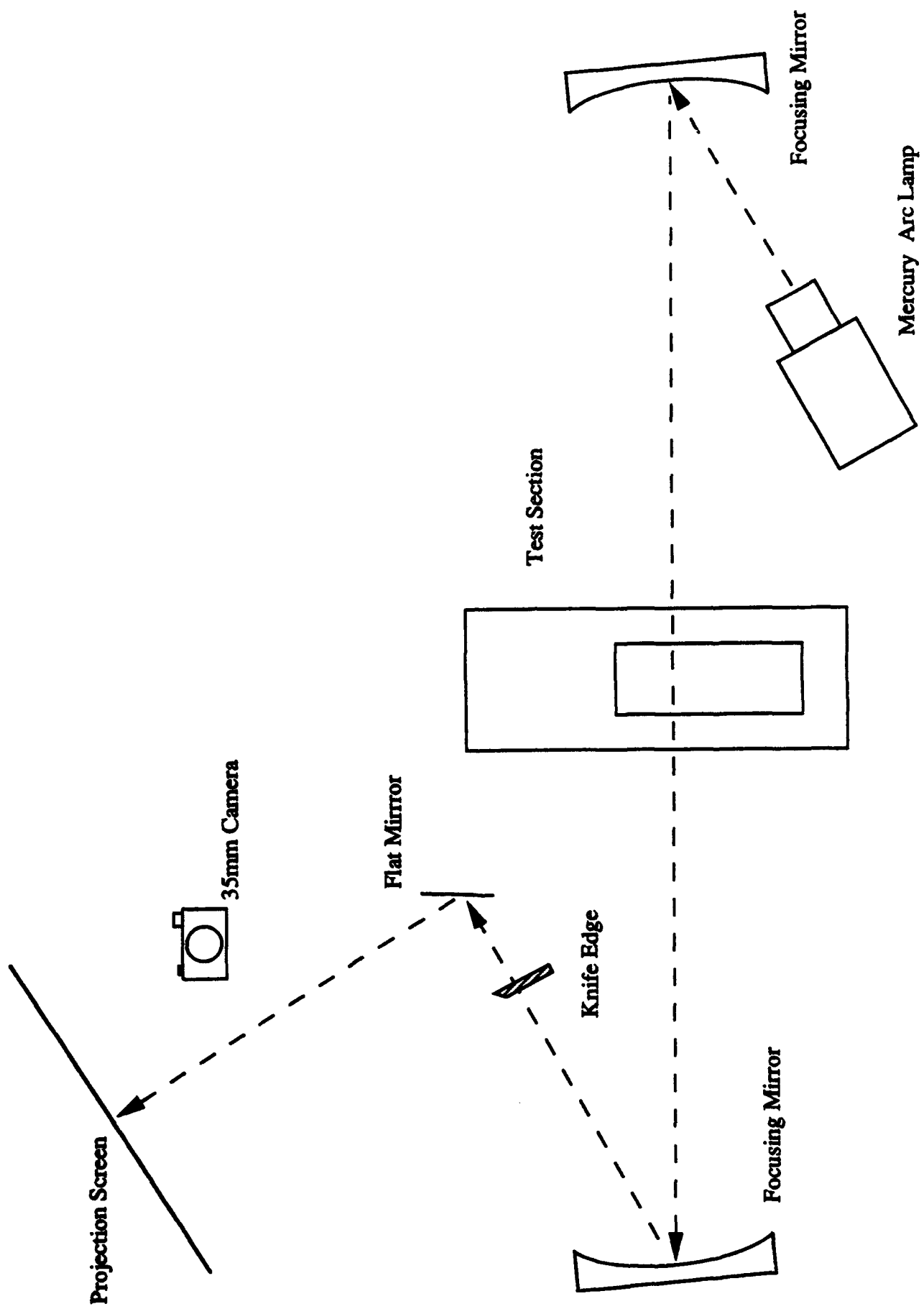


Figure 5 Schlieren Configuration

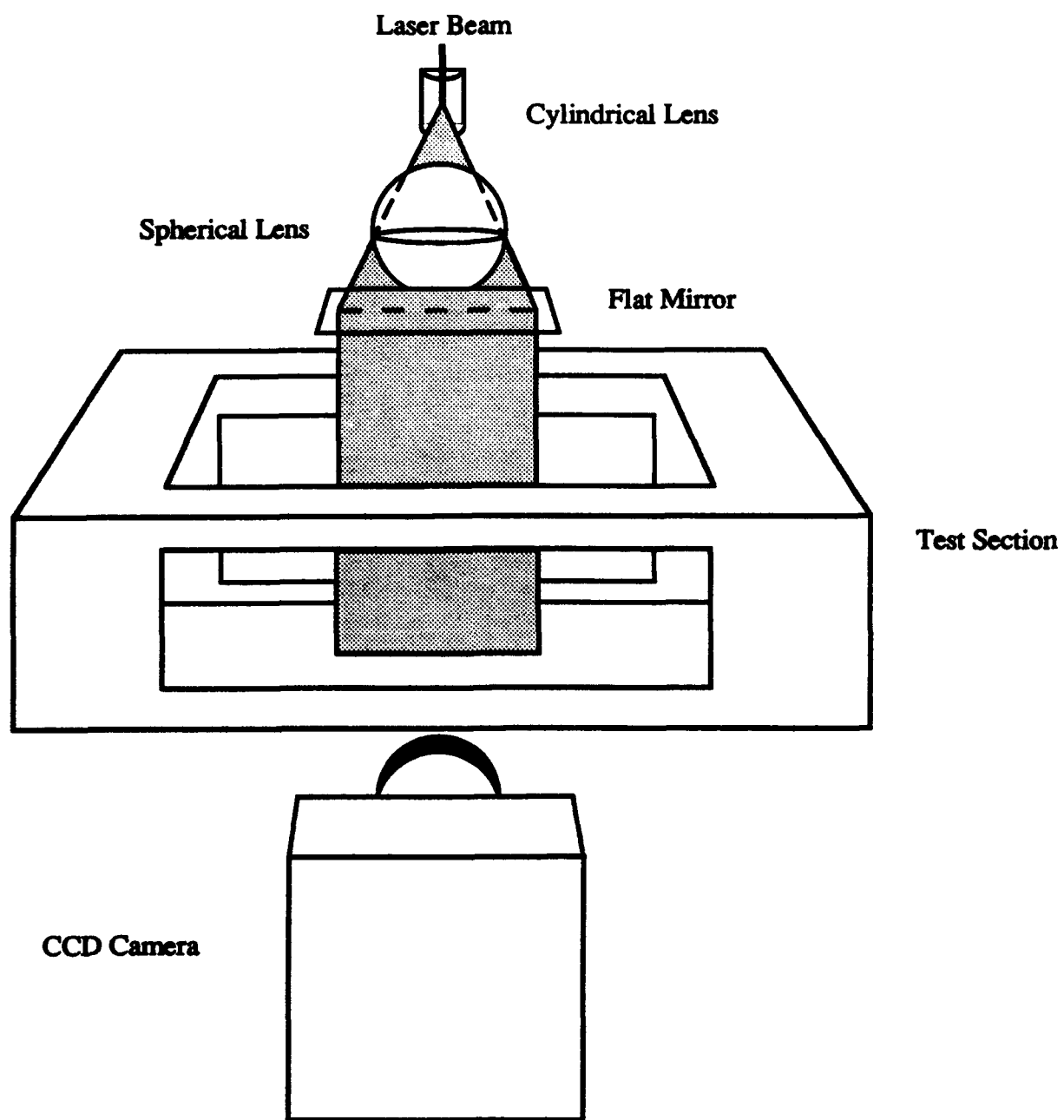


Figure 6 Laser System Schematic



Figure 7 Mie Scattering Image of Injector (a)

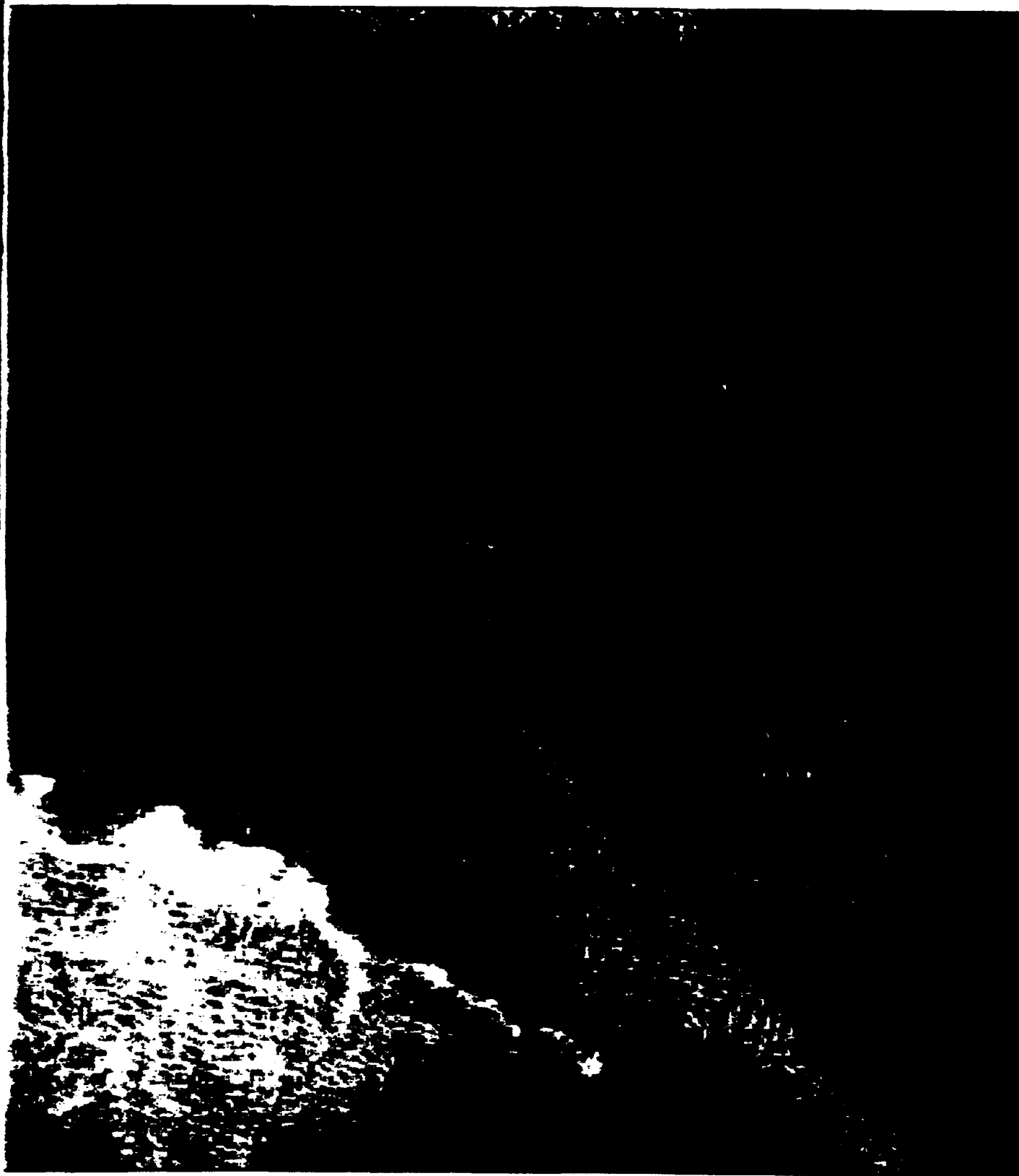


Figure 8 Mie Scattering Image of Injector (b)



Figure 9 Mie Scattering Image of Injector (c)

USAF JET FUEL THERMAL STABILITY TESTING

Daniel L. Prevost

Student

Kettering Fairmont High School

3301 Shroyer Road

Kettering, OH 45429

Final Report for :

AFOSR Summer Research Program

Wright Laboratory

Sponsored by:

Air Force Office of Scientific Research

Wright Patterson Air Force Base, Dayton, OH

August 1993

USAF JET FUEL THERMAL STABILITY TESTING

**Daniel L. Prevost
Student
Kettering Fairmont High School**

Abstract

Fuel thermal stability has always been a problem for the designers of aircraft engines who must balance component life against high temperatures, high heat fluxes and the thermal stability of fuels. Due to newer high performance and fuel efficient engines that stress fuel beyond its thermal stability limits, a large amount of maintenance time and energy is spent removing and cleaning fouled nozzles, afterburner spraybars, and sprayrings. Current investigations show that future engine systems will stress fuels even further. This has lead the Air Force to embark on a program to improve the thermal stability of its fuel. This program would increase the thermal limits of the fuel by 100°F through the use of an additive package. However, before it can be put into use any additive package must be thoroughly tested in a variety of systems in a variety of fuels in order to maximize its performance.

USAF Jet Fuel Thermal Stability Testing

Introduction

For the past 40 years the United States Air Force has operated the majority of its jet planes on a fuel known as JP-4(Jet Propellant-4) while commercial jets have flown on Jet A. During the Southeast Asian Conflict combat experience demonstrated that USAF aircraft using the highly volatile JP-4 fuel had higher combat losses than US Navy aircraft using low volatility JP-5. Also crash data showed that the probability of a postcrash fire was almost 100 percent when using JP-4; much higher than with a kerosene-based fuel such as JP-5 or commercial Jet A. The increased safety of kerosene fuels, as compared to wide distillation range fuels such JP-4, was also evident in the number of ground handling accidents.¹ Therefore, JP-8 was developed to give the USAF a safer fuel that still performed well. To simplify the production of JP-8, the properties selected closely match those of commercial fuels. However, due to the differences in engine temperature and flight altitude, commercial jet fuel proved not to be thermally stable enough to handle the Air Force's differing fuel system. Fuel is used in integrated aircraft thermal management systems to cool aircraft subsystems and the engine lubricating oil prior to being consumed. All current U.S. fighter aircraft circulate fuel on the airframe to match heat loads with available heat sink. These thermal stresses push current fuels to temperatures as high as 163°C at the inlet to the main burner fuel nozzles and 205°C inside the fuel nozzle passages.² At these conditions, engine fuel nozzles, afterburner spray assemblies and manifolds are plugging, causing increased maintenance and cost. In some instances fuel degradation changes the spray pattern in the combustion chamber of afterburners leading to damage to engine components.

A large amount of thermal stability research over the years has focused on fouling and coking of engine components. Current investigations show that damage goes well

beyond the simple plugging of spray nozzles, to actual damage to the hot section components due to improper spray patterns, and on some engines, rumble, a low frequency acoustic condition that can damage engine parts.² Advanced fighters that will be produced in the late 1990's will require even more cooling resources. Fuels will be subjected to higher temperatures, heat fluxes and multiple heating and cooling cycles as fuel is used as the primary cooling medium for aircraft engines (Figure 1). It is anticipated that these aircraft using current fuels, such as JP-8, will require increased fuel system maintenance to replace fouled components. Anticipating these problems the USAF initiated a program in 1989 to improve the thermal stability of JP-8. Two approaches were originally considered; one would be to develop a new refinery specification for a more thermally stable JP-8. This approach was discarded early on since a new fuel would be costly to obtain. Instead the approach chosen by the Air Force was to develop an additive package that would improve the thermal stability by 100°F without costing more than \$.001 per gallon, referred to as "JP-8 + 100". Current research indicates that the additive package will consist of four main additive types: antioxidants, metal deactivators, detergents, and dispersants.² The Air Force contacted major additive manufacturers and oil companies to supply additives for further study.

Each additive received from a manufacturer goes through a complex screening and testing process (Figure 2).² Each additive is put through a series of tests in a variety of different fuels to determine its anticipated effectiveness. This is how most of my time working at Wright Patterson AFB has been spent. I have had the opportunity to become familiar with most of the tests run here.

MCRT

The Micro Carbon Residue Test (MCRT) determines the amount of carbon residue formed after evaporation and pyrolysis of petroleum materials under certain conditions and is intended to provide some indication of the relative coke forming

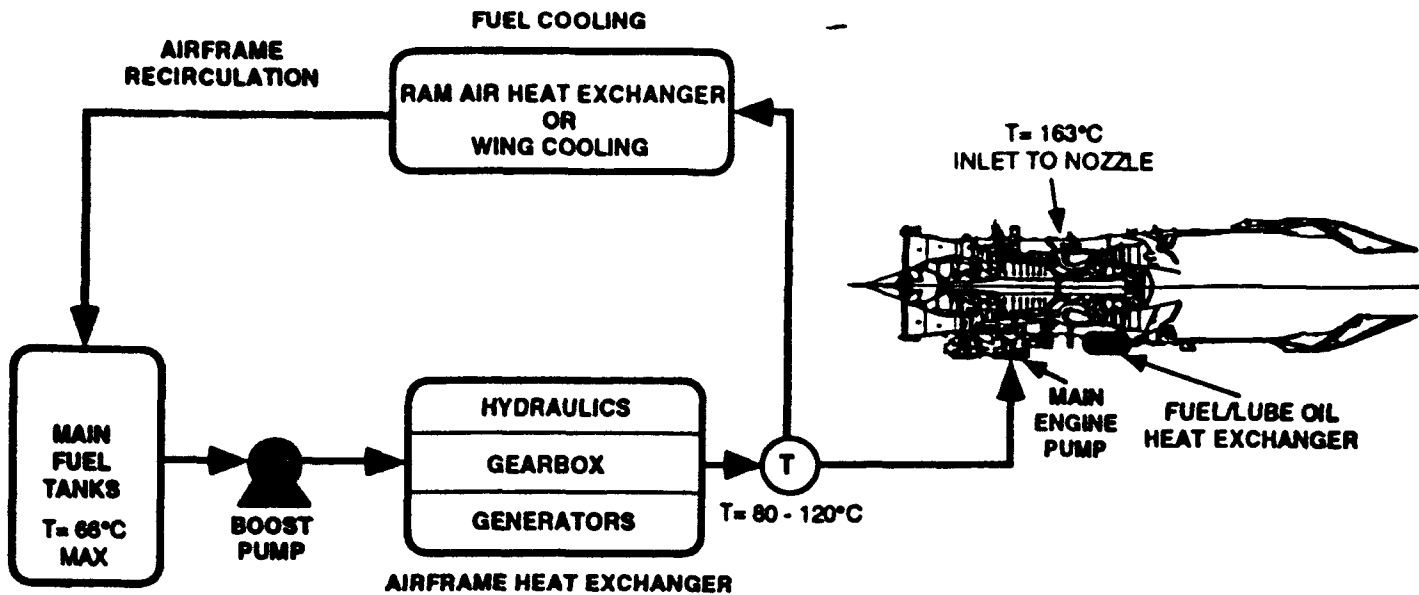


Figure 1. Fuel System, Current Fighter Aircraft

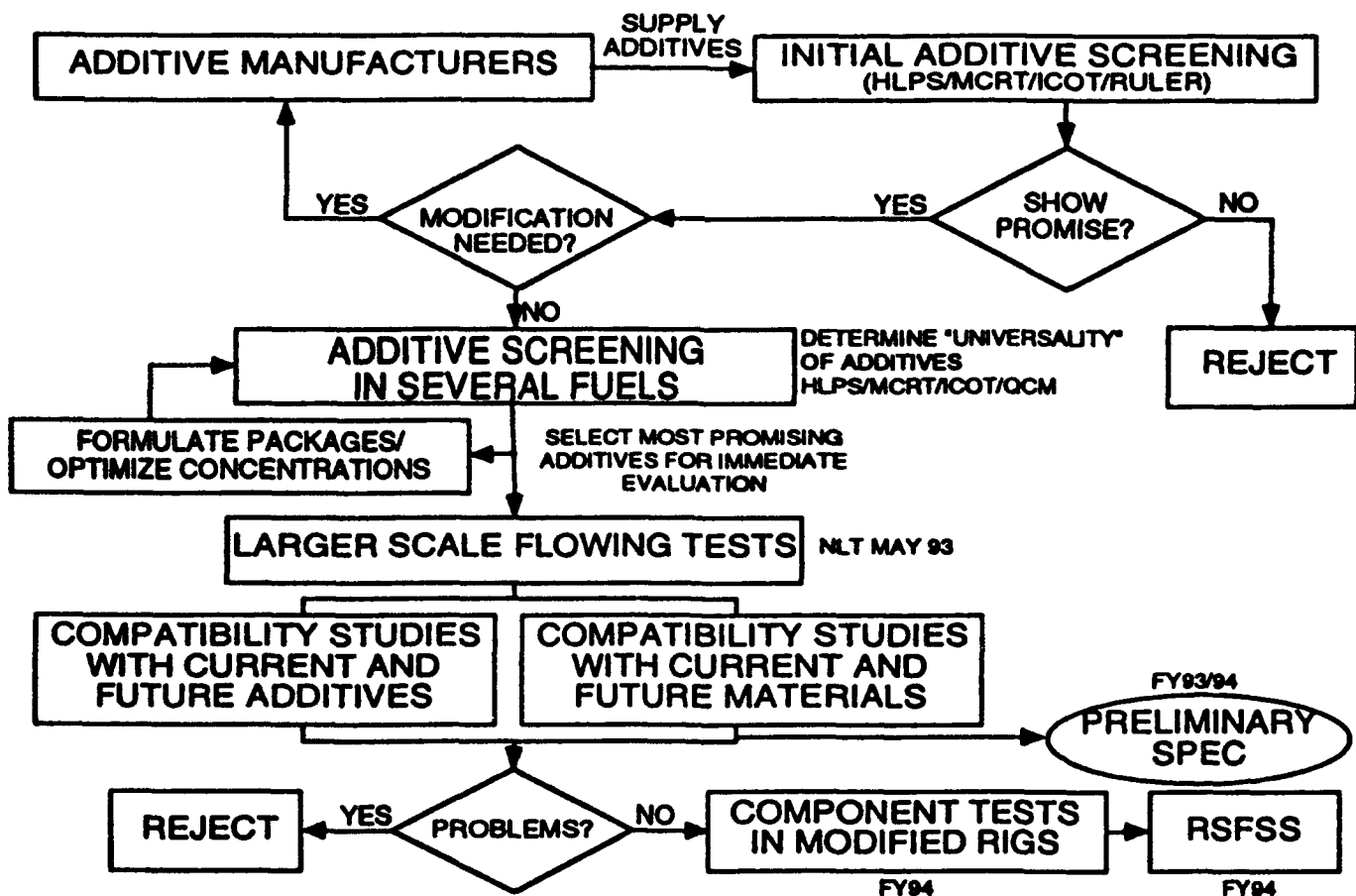


Figure 2. Additive Screening Approach

tendency of such materials. The MCRT oven consists of a test chamber surrounded by a hollow wall containing tubular heaters. Gas flows through this hollow wall into the chamber via 12 small holes at the top of the chamber. A circular sample basket containing six vials is placed into the chamber where it is continuously purged with air at 150 cc/min and heated at a constant rate. The fuel boils, oxidizes, and degrades somewhat simulating the conditions found in fuel nozzles and afterburner assemblies at cancellation or during leakage across the valves. At the conclusion of the test the vials are cooled, weighed and the degraded fuel that has been condensed and trapped is filtered, dried and weighed (Figure 3).² The carbon residue value of the various petroleum materials serves as an approximation of the tendency of the material to form carbonaceous type deposits under similar degradation conditions, and can be useful as a guide in manufacture of certain stocks.³

ICOT

The Isothermal Corrosion Oxidation Test (ICOT) has been proven to be very effective in screening the relative behavior of the thermal stability additives. In this test up to ten samples of fuel are heated in a block heater, usually for five hours. Air is bubbled through a glass blower tube. The stressed samples are first visually inspected for color and visible particulates, then filtered, dried and the deposition measured gravimetrically or by carbon burn-off (Figure 4).²

RULER AND PERFECT

A device that has been developed to study the effectiveness of antioxidants in fuels is the Remaining Useful Life Evaluation Rig (RULER). The RULER technique is a cyclic voltametric test that is performed with a commercially available voltammograph equipped with a glassy carbon disk working electrode, a platinum wire reference electrode, and a platinum wire auxiliary electrode. The oxidatively stressed fuel sample is diluted (1:8) with isopropanol containing an electrolyte. The voltage of the auxiliary

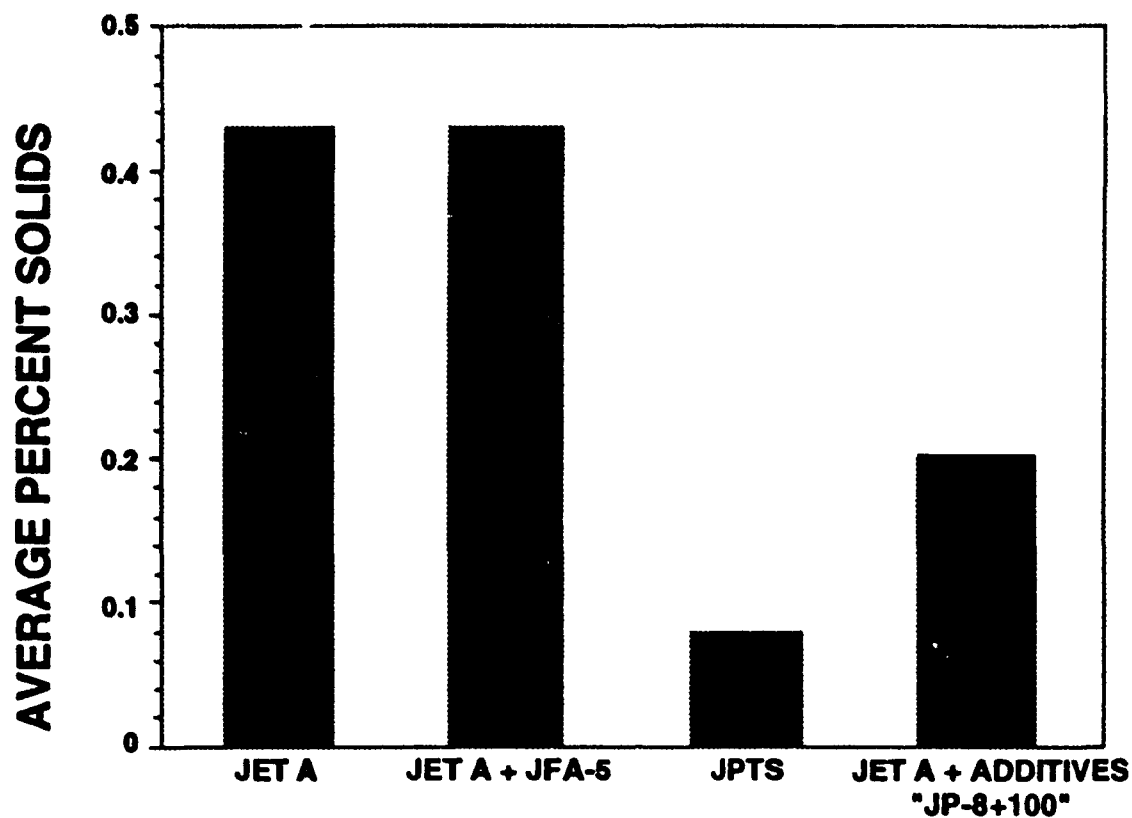


Figure 3. Micro Carbon Residue Test (MCRT) Results

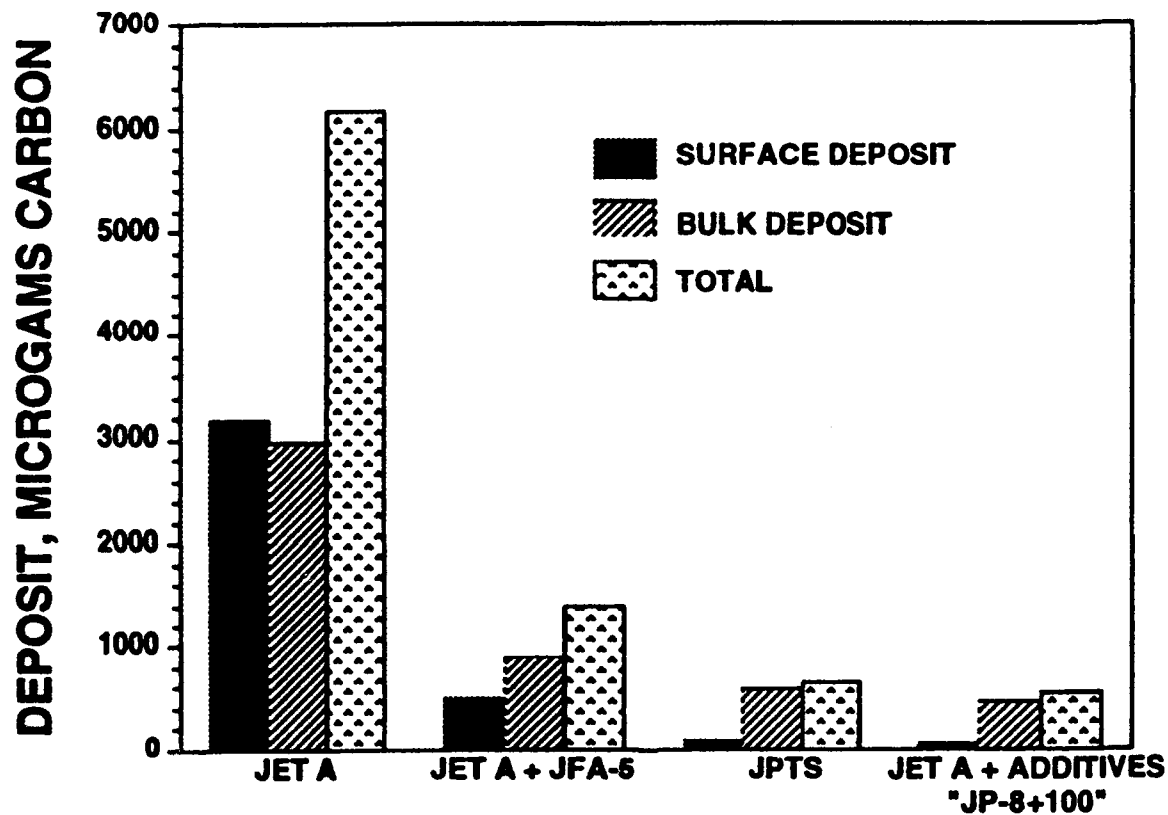


Figure 4. Isothermal Corrosion Oxidation Test (ICOT) Results

electrode is increased for 0.0 to 1.0 Volts at a rate of 0.1V/second. The derivative of the current produced by the glassy carbon working electrode is plotted versus scan voltage by a microcomputer system interfaced to the voltammograph. The peaks produced by the stressed fuel are integrated and normalized to the peaks produced by the fresh fuel to determine the concentrations of the additives remaining in the stressed fuels.

A variation of the RULER is the Peroxide in Fuel Estimation and Concentration Test (PERFECT). In the PERFECT technique, the peroxides are reduced by potassium iodide in an acidic medium. An equivalent amount of iodide is liberated and quantified by voltammetry calibrated with measured amounts of iodine.² The magnitude of the peroxide number is an indication of the quantity of oxidizing constituents present. Deterioration of turbine fuel results in the formation of peroxides and other oxygen-carrying compounds. The peroxide number measures those compounds that will oxidize potassium iodide. The determination of the peroxide number of aviation fuel is significant because of the adverse effect of peroxides upon certain elastomers in the fuel systems.⁴

BOCLE

The Ball-on-Cylinder Lubricity Evaluator assesses the wear aspects of the boundary lubrication properties of aviation turbine fuels on rubbing steel surfaces. The fuel under test is placed in a test reservoir in which atmospheric air is maintained at 10% relative humidity. A non-rotating steel ball is held in a vertically mounted chuck and forced against an axially mounted steel ring with an applied load. The test cylinder is rotated at a fixed speed while being partially immersed in the fluid reservoir. This maintains the cylinder in a wet condition and continually transports the test fluid to the ball/cylinder interface. The wear scar generated on the test ball is a measure of the fluid lubricating properties. Wear due to excessive friction resulting in shortened life of engine

components such as fuel pumps and fuel controls has sometimes been attributed to lack of lubricity in aviation fuels.⁵

Total Acid Number

Some acids may be present in aviation turbine fuels due to either the acid treatment during the refining process or to naturally occurring organic acids. Significant acid contamination is not likely to be present because of the many check tests made during the various stages of refining. However trace amounts of acid may be present and are undesirable because of the consequent tendencies of the fuel to corrode metals that it may contact or to impair the water separation characteristics of the aviation turbine fuel. The sample is dissolved in a mixture of toluene and isopropyl alcohol containing a small amount of water. The resulting single phase solution is blanketed by a stream of nitrogen bubbling through it and is titrated with standard alcoholic potassium hydroxide to the end point indicated by the color change of the added *p*-naphtholbenzein solution. Acid number is the quantity of base, expressed in milligrams of potassium hydroxide per gram of sample that is required to titrate a sample in the solvent to an endpoint using *p*-naphtholbenzein.⁶ Figure 5 shows the TAN results from a fuel with different combinations of additives after having been stressed in the ICOT.⁷ The total acid number (TAN) is calculated by the below calculations:

$$\text{TAN} = [(A-B)N \times 56.1] / W$$

where:

A = milliliters of KOH solution required for titration of the sample

B = milliliters of KOH solution required for titration of the blank

N = normality of the KOH solution

W = grams of sample used

2922 stressed in ICOT for 5hrs @ 180C

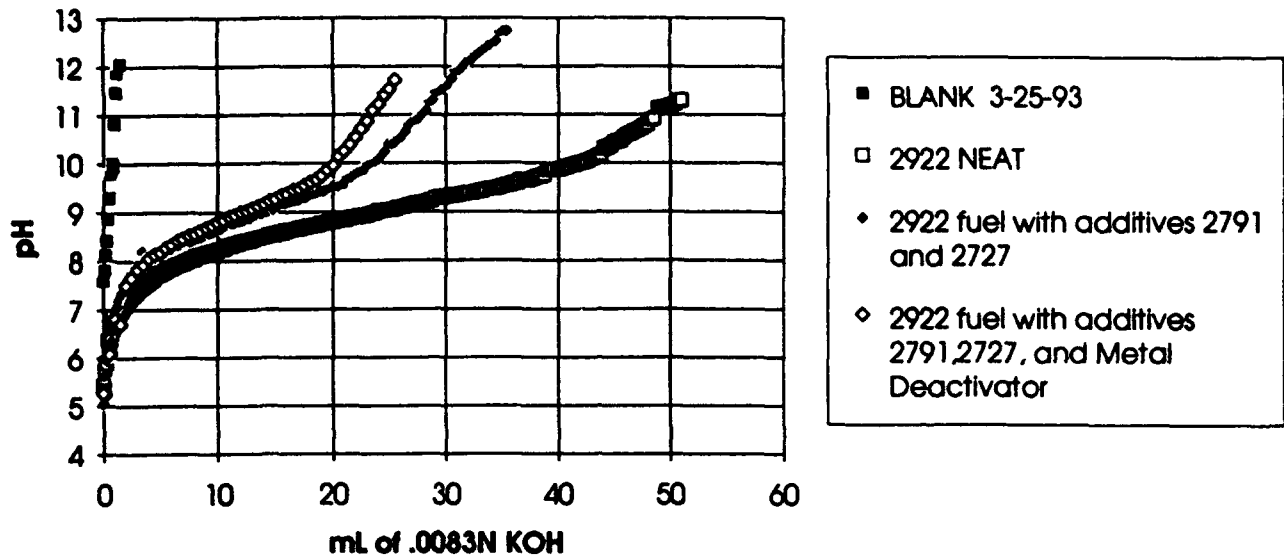


Figure 5. Total Acid Number (TAN) Results

JFTOT

Static tests do not simulate the actual environments found in aircraft subsystems and engines. To accurately simulate these environments, flow tests must be used. Tests have been conducted using the Jet Fuel Thermal Oxidative Tester (JFTOT). This test method subjects the test fuel to conditions that can be related to those occurring in gas turbine engine systems. The fuel is pumped at a fixed volumetric flow rate through a heater after which it enters a precision stainless steel filter where fuel degradation products may become trapped. The test results are indicative of fuel performance during gas turbine operation and can be used to assess the level of deposits that form when liquid fuel contacts a heated surface that is at a specified temperature.⁸

Flash Point Test

Flash point, the lowest temperature at which application of a test flame causes the vapor of a specimen to ignite under specified conditions of test, can indicate the possible presence of highly volatile and flammable materials in a relatively nonvolatile or nonflammable material. For example, an abnormally low flash point on a sample of kerosene can indicate gasoline contamination. The flash point is also used in shipping and safety regulations to define flammable and combustible materials. In this test a 50 ml sample of fuel is placed in to a closed cup and heated at a slow, constant rate (about 1.0°C/minute). A small flame is directed into the cup every 1.0°C until the flash point is reached. The flash point is the lowest temperature at which application of the test flame causes the vapor above the sample to ignite.⁹

Existent Gums

It has been proven that high gum content in a fuel can cause induction-system deposits and sticking of intake valves, and in most instances it can be assumed that low gum will ensure absence of induction-system difficulties. This test determines the amount of existent gum, the evaporation residue of aircraft fuel, in aviation fuel. A

measured quantity of fuel is evaporated under controlled conditions of temperature and flow of air or steam. The resulting residue is weighed and reported as milligrams per 100 ml. Large quantities of gum are indicative of contamination of fuel by higher boiling oils or particulate matter and generally reflect poor handling practices in distribution downstream of the refinery.¹⁰

Kinematic Viscosity

Kinematic viscosity is the measure of the resistive flow of a fluid under gravity. In this test the time is measured for a fixed volume of liquid to flow under gravity through the capillary of a calibrated viscometer under a reproducible driving head and at a closely controlled temperature. The kinematic viscosity is the product of the measured flow time and the calibration constant of the viscometer. Many petroleum products, as well as non-petroleum materials, are used as lubricants for bearings, gears, compressor cylinders, hydraulic equipment, etc. The proper operation of the equipment depends upon the proper kinematic viscosity of the liquid. Therefore, the accurate measurement of kinematic viscosity is essential to many product specifications.¹¹

Conclusion

Due to the number of fuels, additives, and tests that must be run it is impossible at this point in time to make any conclusions about which additives and which fuels are good or bad. The JP-8 + 100 plan does call for engine testing to begin in 1995 and in service use to begin in 1997.

References

1. AFWAL-TR-87-2062, "Military Jet Fuels, 1944-1987, "November 1987, Charles R. Martel.
2. Harrison, W. E. III, T. Edwards, S. D. Anderson, "U.S. Air Force Improved JP-8 Development Program-An Overview," Wright-Patterson AFB, OH.
3. ASTM D 4530, "Standard Test Method for Micro Carbon Residue of Petroleum Products," 1992 Annual Book of ASTM Standards, Volume 5.03, pp 441-445.
4. ASTM D 3703, "Standard Test Method for Peroxide Number of Aviation Turbine Fuels," 1992 Annual Book of ASTM Standards, Volume 5.03, pp 52-54.
5. ASTM D 5001, "Standard Test Method for Measurement of Aviation Turbine Fuels by the Ball-on-Cylinder Lubricity Evaluator (BOCLE)," 1992 Annual Book of ASTM Standards, Volume 5.03, pp 757-762.
6. ASTM D 3242, "Standard Test Method for Acidity in Aviation Turbine Fuel," 1992 Annual Book of ASTM Standards, Volume 5.02, pp 664-667.
7. Grinstead, Becky, UDRI, "Total Acid Number Results." March 25, 1993.
8. ASTM D 3241, "Standard Test Method for Thermal Oxidation Stability of Aviation Turbine Fuels (JFTOT Procedure)," 1992 Annual Book of ASTM Standards, Volume 5.02, pp 644-663.
9. ASTM D 93, "Standard Test Methods for Flash Point by Pensky-Martens Closed Tester," 1992 Annual Book of ASTM Standards, Volume 5.01, pp 28-40.
10. ASTM D 381, "Standard Test Methods for Existent Gum in Fuels by Jet Evaporation," 1992 Annual Book of ASTM Standards, Volume 5.01, pp 142-147.
11. ASTM D 445, "Standard Test Methods for Kinematic Viscosity of Transparent and Opaque Liquids (and the Calculation of Dynamic Viscosity," 1992 Annual Book of ASTM Standards, Volume 5.01, pp 154-159.

MY AVIATION FUEL RENDEZVOUS

**Jonathan D. Servaites, high school apprentice under
2d Lt John M. Garver**

**Centerville High School
500 East Franklin St.
Centerville, OH 45459**

**Final Report for:
High School Apprenticeship Program
Wright Laboratory/Air Propulsion Directorate/Fuels Branch**

**Sponsored by:
Research and Development Laboratories
Livermore City, CA**

August 1993

MY AVIATION FUEL RENDEZVOUS

Jonathan D. Servaites
High School Apprentice
Centerville High School

Abstract

During my summer tour I participated in research with both sections of the Fuels Branch of the Air Propulsion and Power Directorate at Wright Laboratory (WL/POSF), Fuel Development and Fuel Combustion. A primary concern of Fuel Development is based around the rapidly growing heat loads generated by the engine and aircraft subsystems. Fuel Development works with this problem by analyzing aviation fuel's role as a cooling medium for aircraft subsystems. All U.S. aircraft match heat load with available heat sink of the fuel. However, with increasing temperatures, greater thermal stability and heat sink capability are needed to help curb fuel fouling in current systems and to provide further security in the future. Therefore, Fuel Development has established the "JP-8+100" program that offers a JP-8 fuel with 100°F (56°C) improvement in thermal stability. This task is to be accomplished by the means of an additive package. The additive package should cost less than \$0.001 per gallon and would significantly reduce the amount of engine and subsystem maintenance that is currently needed.¹ During the latter part of my summer tour, I also spent time working in Fuel Combustion. The primary objective of this program is to provide the fundamental understanding of gas and liquid fueled combustor flows needed to develop gas turbine combustor design models that result in errors of less than 5% in predicted flow field parameters such as temperature, velocities, and species concentrations. In the program's hope of bettering methods for designing gas turbine combustors, a "vaporline" visualization technique was developed where water droplets, vapor from the droplets, and their interaction with the carrier gas are observed simultaneously.²

MY AVIATION FUEL RENDEZVOUS

Jonathan D. Servaites

Introduction

As in most cases, compromise is necessary in the analysis of fuel thermal stability. Engine designers have been forced to balance the significance of component life with high temperatures, high heat fluxes, and the thermal stability of a fuel (all three of which affect the aircraft's performance). As fuel is circulated throughout the aircraft to cool airframe and engine components, it undergoes dramatic thermal stress which can affect aircraft performance. Figure 1.¹ Thermal stability research programs over recent years have continued to focus on the importance of limiting fuel fouling and coking of engine components. Meanwhile, a number of test devices have been developed to analyze the effect of JP-8+100 additive packages. Figure 2.¹ Many of these tests simulate the environment of the actual aircraft in an effort to determine an additive's ability to reduce the amount of residue left behind after fuel circulation. Test devices employed by Fuel Development include the following: the Micro Carbon Residue Test (MCRT), the Peroxide in Fuel Estimation and Concentration Test (PERFECT), the Isothermal Corrosion Oxidation Test (ICOT), the Total Acid Number Test (TAN), the Leco RC-412 Surface Carbon Analyzer, and the Ball-on-Cylinder Lubricity Evaluator (BOCLE).

In the past, combustor development has been a gradual, evolutionary process with each generation being only slightly different from the preceding one. However, in meeting future Air Force engine performance requirements, the process has become revolutionary rather than evolutionary. Computational Fluid Dynamic and Chemistry (CFDC) models used by the engine companies in developing combustors for Air Force weapon systems offer the potential of exploring revolutionary combustor concepts in an economical and time efficient way.² Fuel Combustion has set out to better understand and to improve CFDC design model capabilities. Several tests have been established to simulate the combustor environment with the intention of fulfilling this goal. This understanding of revolutionary combustor concepts will be needed by future Air Force programs in the 21st century.

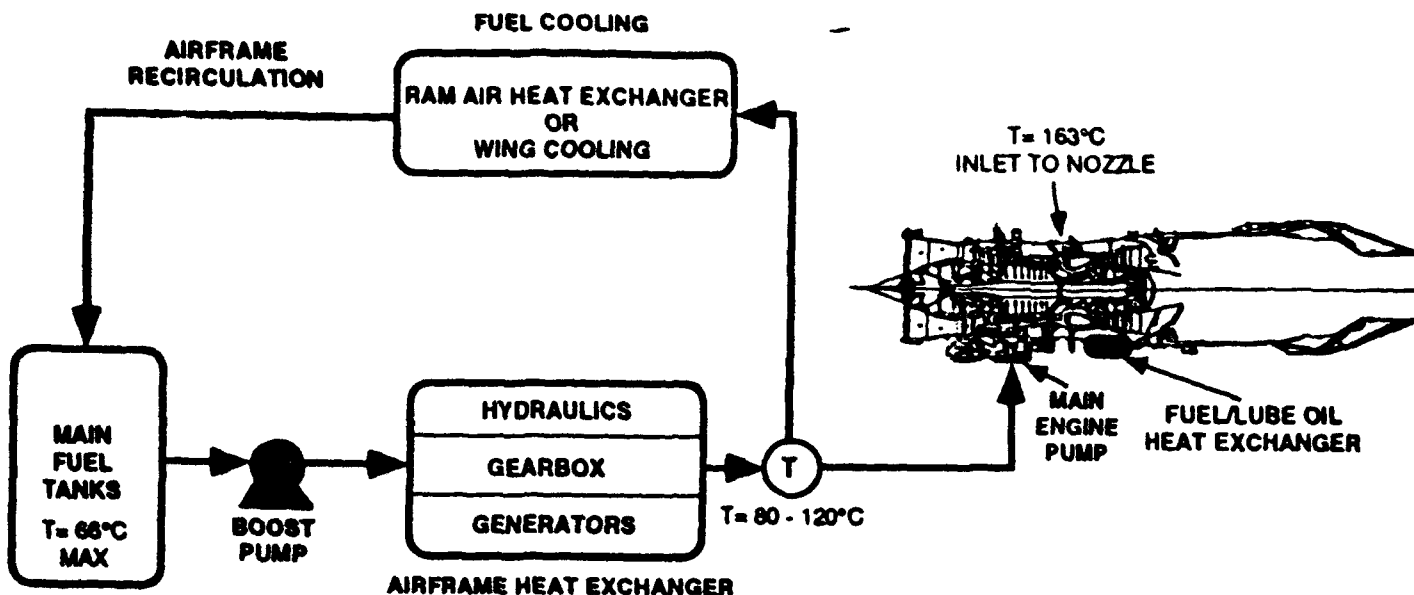


Figure 1: Fuel System, Current Fighter Aircraft

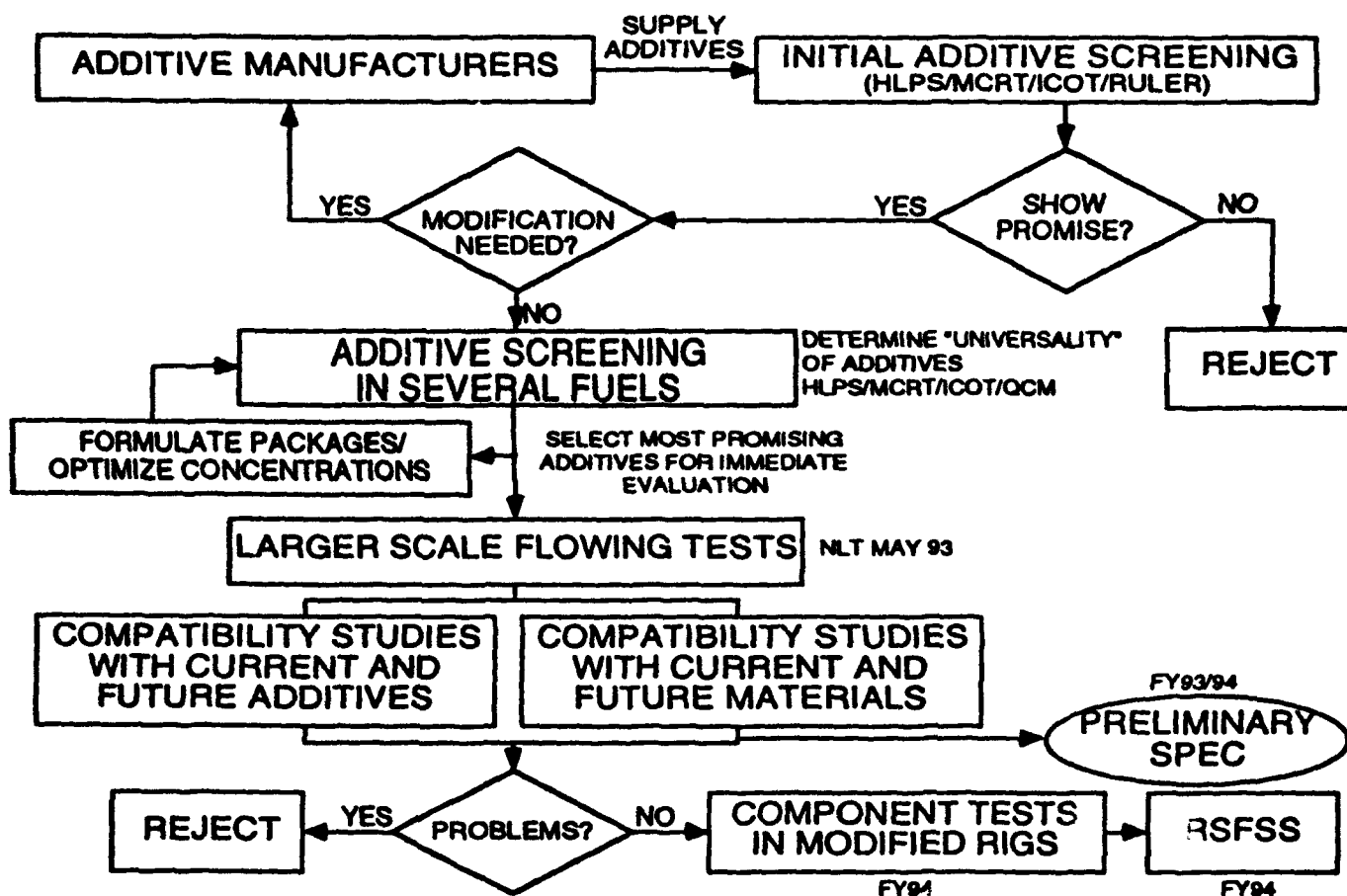


Figure 2: Additive Screening Approach

MICRO CARBON RESIDUE TEST (MCRT)

The MCRT, a static test that is being used to screen additives in the JP-8+100 program, helps determine the amount of carbon residue after the fuel has been thermally stressed. In this procedure six small vials are filled with approximately 50 milliliters of fuel each, placed in a furnace, and heated to 250°C at a constant rate of 8.3°C per minute. Air is purged through the chamber at a rate of 150 milliliters per minute. During the heating process the sample undergoes extreme coking reactions.³ The environment roughly simulates the conditions found in fuel nozzles and afterburner assemblies at cancellation or during leakage across the valves.¹ At the conclusion of the test, the vials are cooled, weighed, and the amount of residue determined by difference. The degraded fuel which has been condensed and separated is filtered, dried, and weighed allows the user to determine the amount of gum left behind. Figure 3.⁴ The MCRT illustrates the tendency of the sample to form carbonaceous type deposits under similar conditions.

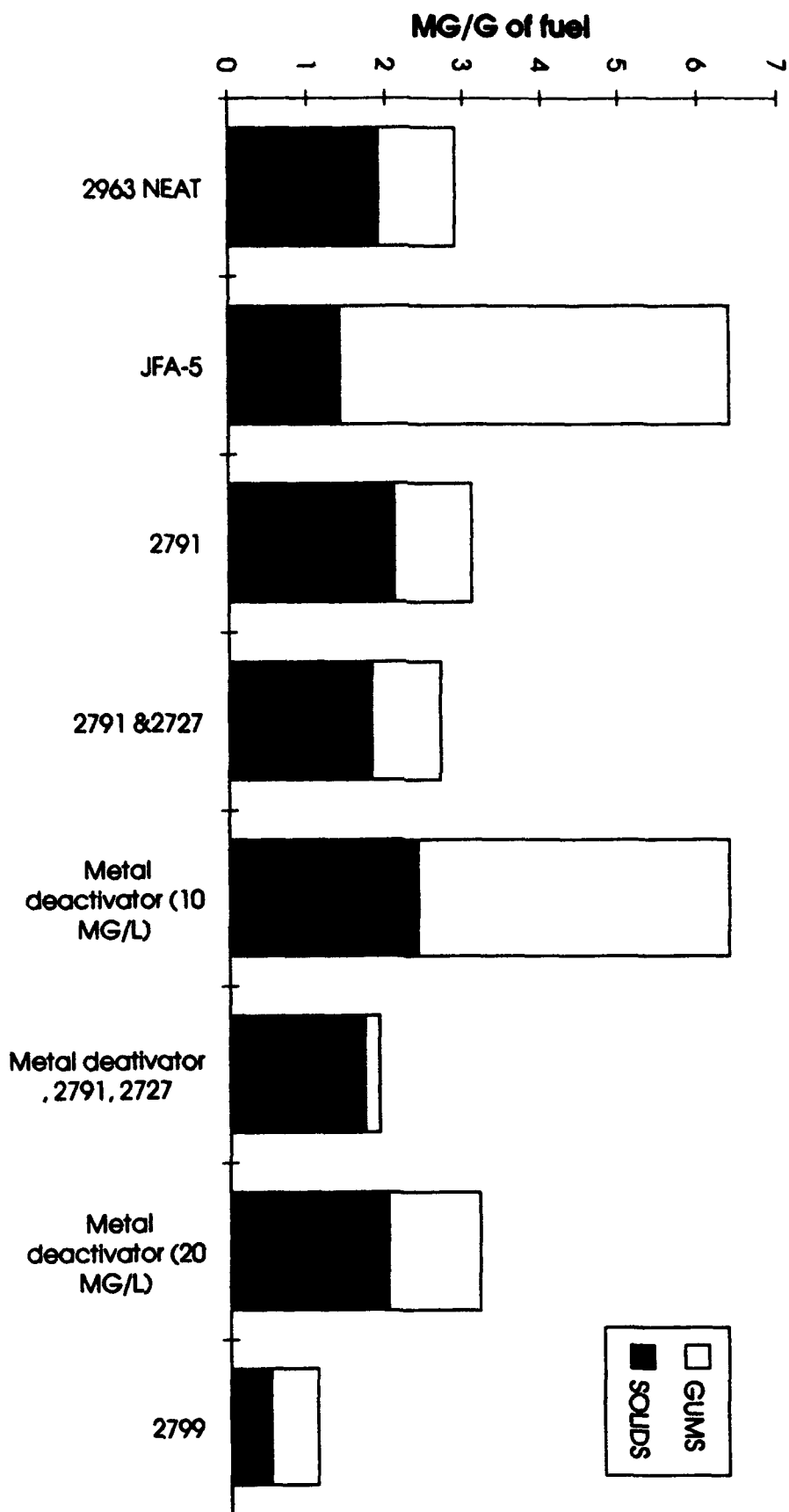
PEROXIDE IN FUEL ESTIMATION AND CONCENTRATION TEST (PERFECT)

The PERFECT covers the determination of the peroxide content of aviation turbine fuels. In the PERFECT technique, the peroxides (especially hydroperoxides) are reduced by potassium iodide in an acidic medium (acetic and hydrochloric acid). An equivalent amount of iodide is released and measured by voltammetry calibrated with known amounts of iodine. The results are reported as milliequivalents of peroxide per liter of fuel¹. Although the PERFECT is not a *perfectly* consistent and flawless test, it does provide helpful information concerning the magnitude of the peroxide number of JP-8+100 test samples which indicates the quantity of oxidizing constituents present. Deterioration of turbine fuel results in the formation of peroxides and other oxygen-carrying compounds. These compounds tend to have adverse effects upon certain elastomers in the fuel system.⁵

ISOTHERMAL CORROSION OXIDATION TEST (ICOT)

The ICOT measures the oxidation or thermal stability of liquids by subjecting them to temperatures in the range from 50°C to 375°C in the presence of air, oxygen, nitrogen, or other gases (for Fuel Development's purposes, air is used) at rates of 1.5 to 13 liters per

Figure 3: Evaluation of the effects that various additive packages have had in the MCRT @ 250°C for 3 hours with 9 L/hour air flow.



hour. The sample is subjected to thermal or oxidative degradation or both. The gas may also be bubbled through the liquid to provide agitation or to promote oxidation. The ICOT provides helpful versatility which is required to conduct oxidation or thermal stability tests on liquids using a wide variety of test conditions. The test is also utilized for the purpose of stressing fuels that will be further tested for acidity (see Total Acid Number Test below).⁶

TOTAL ACID NUMBER TEST (TAN)

After heating, the acidity of fuels increases, thereby producing the threat of corrosion to metals that the fuel comes in contact with. The purpose of the TAN test is consequently to measure the acidity in aviation turbine fuel after it has been thermally stressed in the ICOT. In this test a mixture of toluene and isopropyl alcohol containing a small amount of water (1000 mL, 990 mL, and 10 mL respectively) is blanketed by a stream of nitrogen gas in order to displace surrounding carbon dioxide.⁷ This solution is called "the blank." Using an automatic titrator, the blank is titrated with 0.083 N potassium hydroxide (KOH). Next, the same process is repeated, but this time a fuel sample is added. The purpose of adding the toluene/isopropyl alcohol/water solution is to dissolve the fuel sample (its contribution to the fuel solution acidity is later subtracted). In calculating the acid number one uses the following equation:

$$TAN = (mL \text{ of sample} - mL \text{ of blank}) \times 56.1 \text{ (atomic mass of KOH)} \times 0.083 \text{ (normality of KOH)} / mL \text{ of KOH.}$$

LECO RC-412 SURFACE CARBON ANALYZER (LECO)

The LECO is another test utilized to determine the source of several types of carbon content. By analyzing the sample in an oxidizing atmosphere, all forms of carbon (except for some carbides such as SiC) are converted to carbon dioxide. Organic forms produce water and CO₂. Consequently, organic compounds can be found by determining coincident peaks in H₂O and CO₂. This device employs a furnace control system which allows the temperature of the furnace to be stepped or ramped. From there various sources of carbon can be differentiated by the temperature at which they volatilize or oxidize. The LECO's

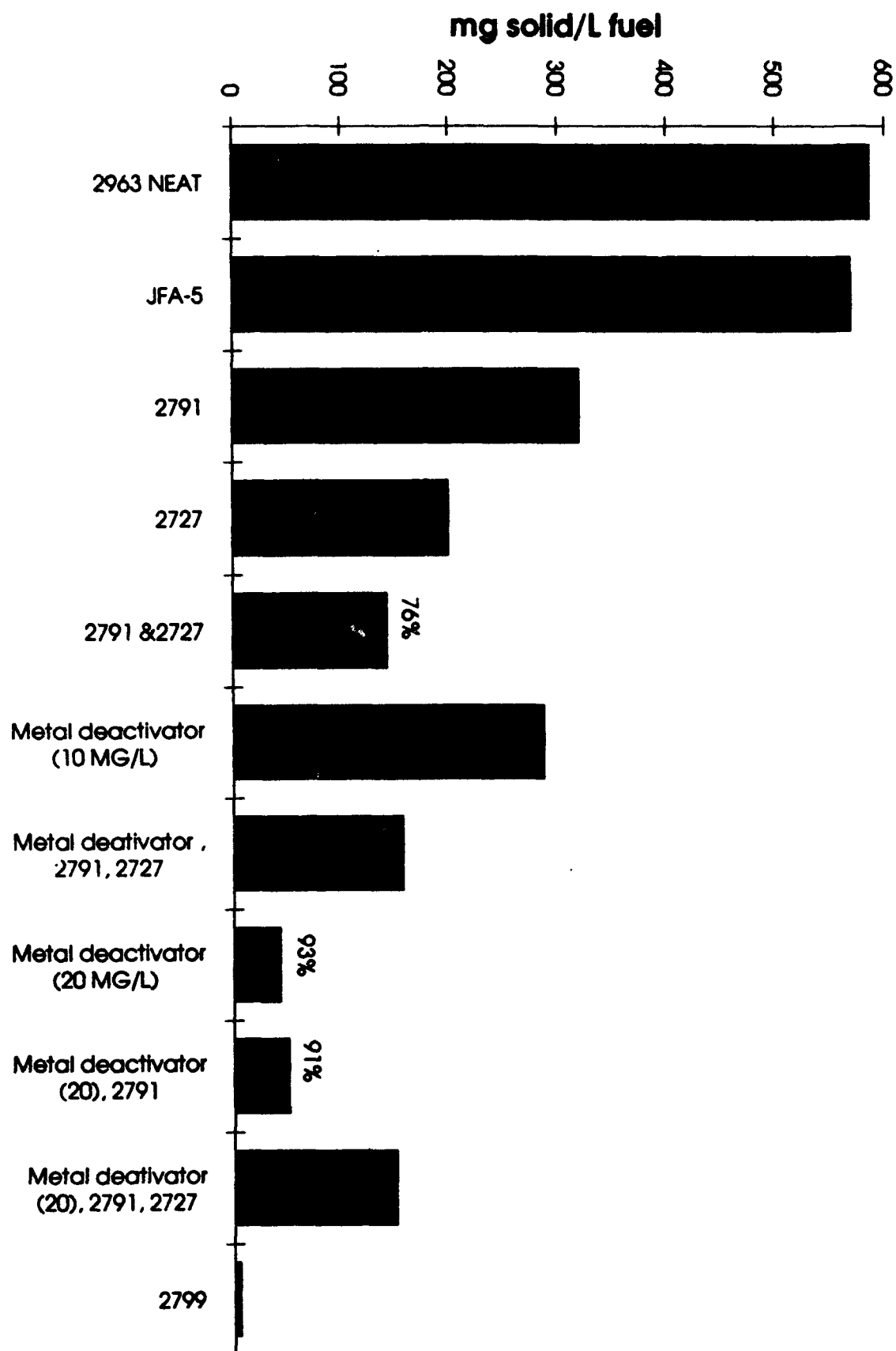
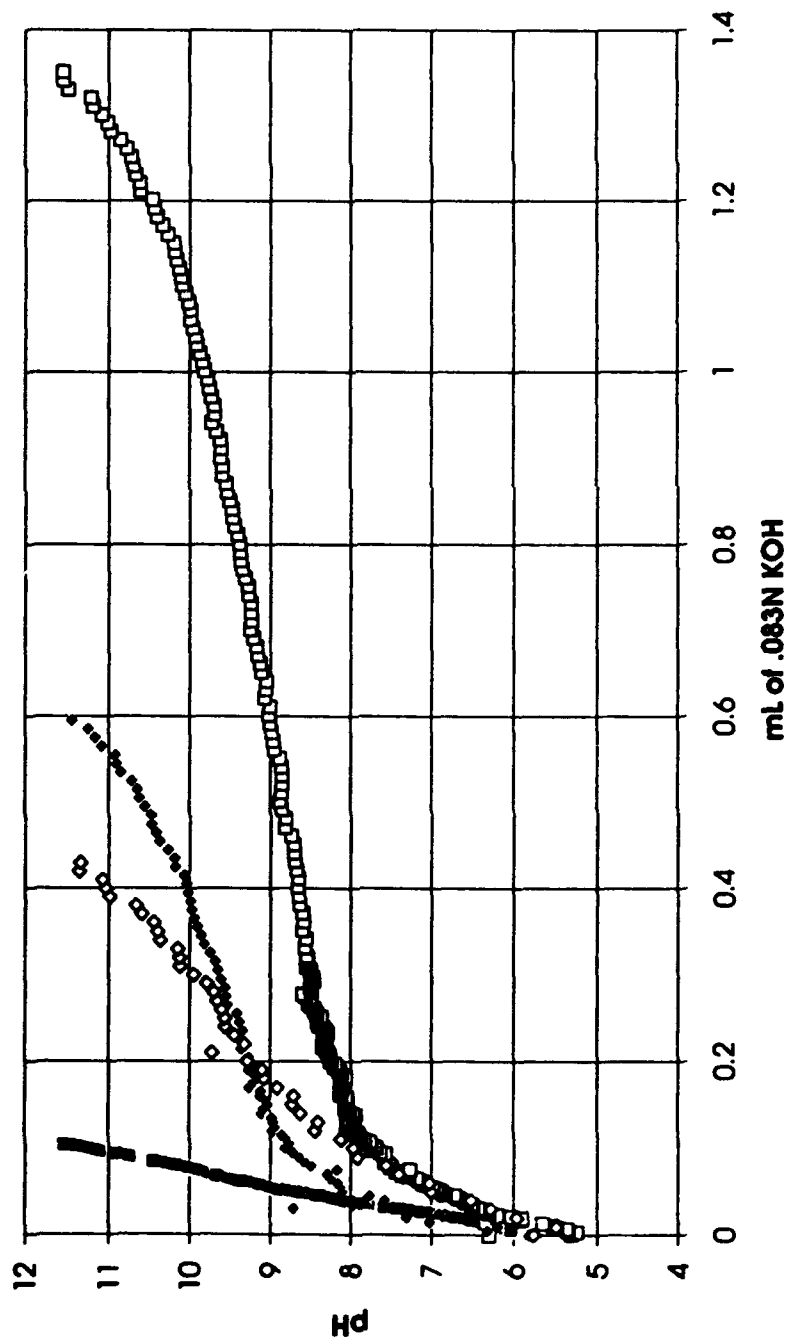


Figure 4: Evaluation of additive packages in the ICOT at 180°C for 5 hours with 1.3 L/hour

Figure 5: Evaluation of the acidity of various additive packages

ADDITIVE POSF-2958



capabilities are very helpful in determining a fuel sample's tendency to leave behind carbon residues. After fuel is circulated through simulated aircraft tubing, the LECO analyzes the fuel residue and provides the necessary data in determining the sample's thermal stability qualifications.⁹

BALL-ON-CYLINDER LUBRICITY EVALUATOR (BOCLE)

The previous tests discussed have dealt with a fuel's effect on the engine and aircraft subsystems due "remains" left behind; however, fuel residue is not the only threat to the aircraft's well-being. With each additive package, a sample possesses a certain level of lubricity. In the case of this test lubricity is defined "in terms of a wear scar, in millimeters, produced on a stationary ball from contact with the fluid wetted rotating cylinder operating under closely defined and controlled conditions."¹⁰ The BOCLE simply assesses the wear aspects of aviation turbine fuels on steel surfaces. The test method calls for the fuel under test to be placed in a test reservoir in which atmospheric air is maintained at 10% relative humidity. A non-rotating ball is held in a vertically mounted steel ring with an applied load. The cylinder is rotated at a certain velocity while being partially immersed in the fuel. Once a section of the cylinder is brought out of the reservoir, it is brought up to the ball/cylinder contact-point. After one thirty minutes of testing, the size of the scar on the ball is measured and is indicative of the fuel lubricity properties. The BOCLE has aided Fuel Development in identifying an JP-8+100 additive package that reduces wear due to excessive friction in turn lengthening the life-span for engine parts such as fuel pumps and fuel controls.¹⁰

FUEL COMBUSTION

After half of my eight week period had been completed, I began working with the other section of the Fuels Branch, Fuel Combustion. Initially, this work involved entering hazardous material (HAZ-MAT) information into a database, but I soon obtained the chance to become involved in several of the tests that were being conducted. One task that I became involved with, "Effects of a Driven Cross Flow Over a Constant Heat Flux Wall," enabled me to engage in hands-on research with engineers working on the project. Before I

arrived, initial tests had been done where piezoelectric actuators (also known as "flappers") were used to manipulate or drive the jet flow. These preliminary tests were performed primarily to determine if the jet flow could be controlled, thereby preparing the engineers for the test that I participated in where the heat transfer to the jet air from a heated wall would be measured.¹¹ Titanium tetrachloride (TiCl_4) is used in the test so that once the wet air from the jet comes in contact with TiCl_4 in the chimney, titanium dioxide (TiO_2) forms. Figure 6.¹² The TiO_2 in turn scatters the light from the laser sheet enabling the jet flow to be seen. Photographs are then taken of the transparent chimney, thereby allowing the engineers to obtain a visual illustration of effects the cross flow has on the jet air. Note that the actuators used in these tests are not used in an actual combustor, however they do provide very useful information as to how the jet air should be controlled in order to most effectively cool the combustor walls. Particularly with recent combustor designs, temperatures have continued to escalate, thermally stressing the combustor walls. By taking thermocouple readings and using heat sensitive paper, the project's goal is to set the jet and cross flow so that the coolest temperatures could develop. ("Cool" is to be taken in relative terms; for this test, a cool temperature is somewhere below the melting point of the combustor walls.)

Another task that I have had the chance to participate in revolved around advanced dual-dome combustor designs from General Electric and Pratt & Whitney (two competing aircraft engine companies). A primary concern of these combustors dealt with reducing the amount of ozone-depleting nitrogen oxygen (NOX) emissions. The environmental advantage of these designs is that the dual-dome allows for a large range of functions depending upon what stage of flight the aircraft is in (ie. idle, take-off, cruise, landing). In contrast to the inflexible combustor design, the dual-dome allows the Air Force to ready the combustor for a certain stage of flight, thereby preventing any unnecessary functions from being performed (a diagram would be included, however for propriety reasons it cannot be included.) This technology's value is very significant when one considers the danger high-altitude aircraft pose to the ozone layer. For instance, the envisioned high-speed civil transport would fly at an altitude of 120,000 feet. At this level in the atmosphere, nitrogen oxide emissions effect ozone depletion at a rate thirty times greater than those emissions

released from ground level."¹¹

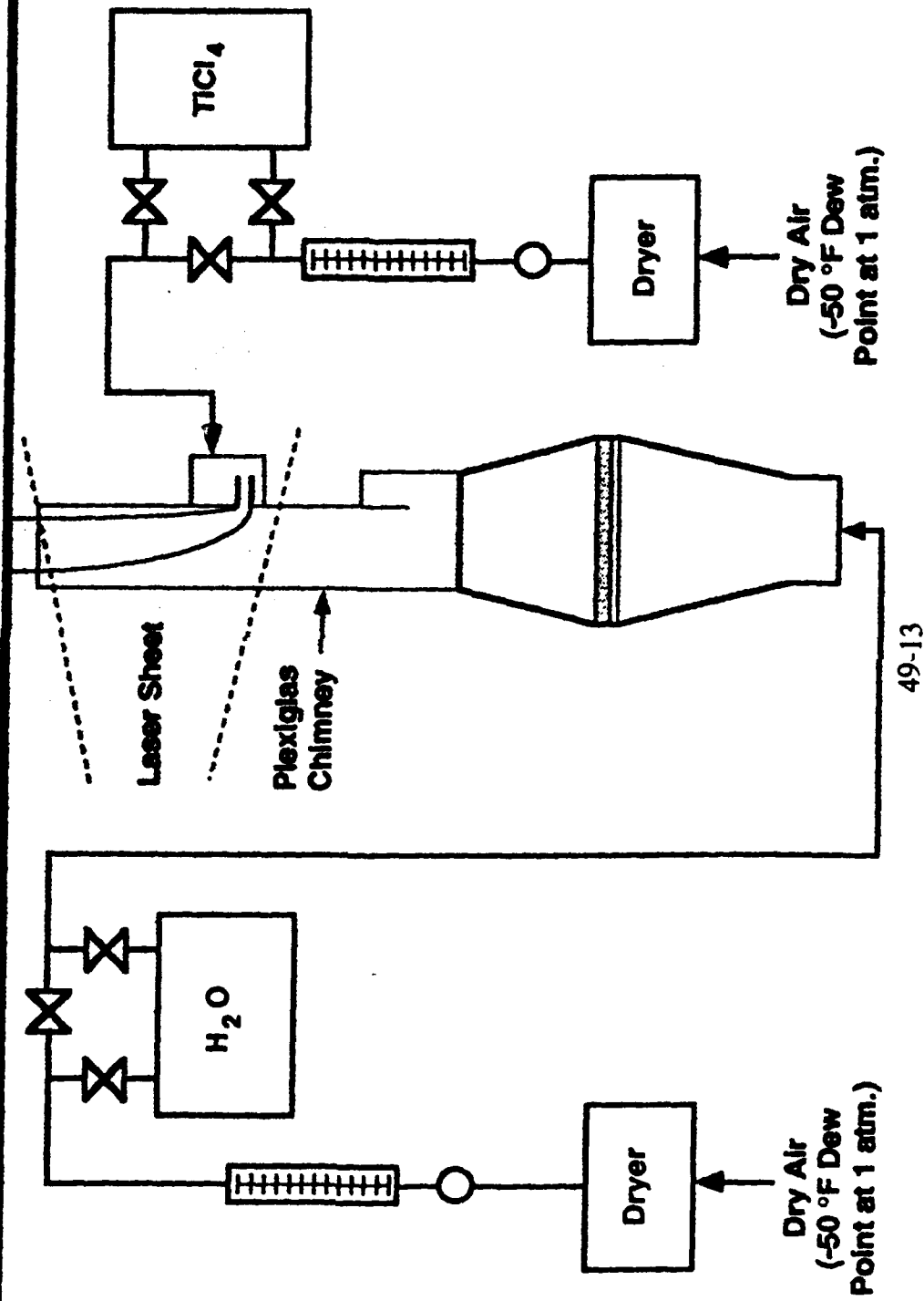
CONCLUSION

This summer's tour provided a variety of opportunities to become familiarized with numerable aspects of fuels research (more specifically, with fuel heat stability and fuel combustion). At the conclusion of my eight week stay, the major tests I had participated in had yet to be completed; therefore, final results are not available. Nevertheless, this experience has been extremely productive in the light that my understanding of the my potential career field has grown and that my future decisions and expectations can now be more knowledgable.



Figure 6: Effects of a Driven Cross Flow Over a Constant Heat Flux Wall

FACILITY SCHEMATIC



REFERENCES

1. Harrison, W.E. III, T. Edwards, S.D. Anderson, "U.S. Air Force Improved JP-8 Development Program: An Overview," Wright-Patterson AFB, OH.
2. Roquemore, Dr. W.M., "Annual Report for Task 2308BW," Wright-Patterson AFB, OH.
3. ASTM D 4530, "Standard Test Method for Micro Carbon Residue Petroleum Products," 1992 Annual Book of ASTM Standards, Volume 5.03, pp. 441-445.
4. Grinstead, Becky, UDRI, "MCRT Results," 14 March 1993.
5. ASTM D 3703, "Standard Test Method for Peroxide Number of Aviation Turbine Fuels," 1992 Annual Book of ASTM Standards, Volume 5.03, pp. 52-54.
6. ASTM D 3241, "Standard Test Method for Thermal Oxidation Stability of Aviation Turbine Fuels (JFTOT Procedure)," 1992 Annual Book of ASTM Standards, Volume 5.02, pp. 644-663.
7. ASTM D 1242, "Standard Test Method for Acidity in Aviation Turbine Fuel," 1992 Annual Book of ASTM Standards, Volume 5.02, pp. 664-667.
8. Grinstead, Becky, UDRI, "Total Acid Number Results," 11 June 1993.
9. Leco Corporaton, Instrumentation for: Metals, Energy, Agriculture, Geology, Mining, St. Joseph MI.
10. ASTM D 5001, "Standard Test Method for Measurement of Aviation Turbine Fuels by the Ball-on-Cylinder Lubricity Evaluator (BOCLE)," 1992 Annual Book of ASTM Standards, Volume 5.03, pp. 757-762.
11. Sutkus, Don, "Conversation on 6 August 1993," Wright-Patterson AFB, OH.
12. Hancock, Robert D., Glezer, Ari, and Rivir, Richard B., "Manipulation of a Jet in a Cross Flow Using Piezoelectric Actuators," Wright-Patterson AFB, OH.

**DIAMOND GROWTH BY LOW-PRESSURE
CHEMICAL VAPOR DEPOSITION
WITH BIAS PRETREATMENT**

David J. Spry
Summer Apprentice
Department of the Air Force

Final Report:
Summer Research Program
Propulsion Laboratories WL/POOC-3
Wright Patterson Air Force Base
Dayton, OH 45433-6563

Sponsored by:
Research and Development Laboratories
5800 Uplander Way, Culver City, CA 90230-6608

August 1993

DIAMOND GROWTH BY LOW-PRESSURE CHEMICAL VAPOR DEPOSITION WITH BIAS PRETREATMENT

David J. Spry
Summer Apprentice
Department of the Air Force
Wright Patterson Air Force Base

Abstract

This report discusses the preliminary results of several microwave plasma assisted chemical vapor deposition (MPCVD) biasing experiments. Substrate biasing was shown to substantially increase nucleation of diamond on silicon. Possible reasons for this effect are also proposed.

DIAMOND GROWTH BY LOW-PRESSURE CHEMICAL VAPOR DEPOSITION WITH BIAS PRETREATMENT

David J. Spry

Introduction

Diamond is relatively rare in nature, and is in a very difficult form to use. For this reason, the only main use for diamond has been in the realm of cutting tools. However, diamond has many outstanding physical characteristics. One example of these qualities is diamond's transparency to infrared light and other wavelenghts of light that could be used in optical applications. If diamond VLSI was possible it would allow computer components to be packed closer together enabling them to be 60 times smaller and operate four times faster¹. This is because diamond is an outstanding thermoconductor and an electrical insulator permitting chips to be stacked on top of each other. There are other interesting properties of diamond that are discussed in other papers^{1,2}, but this report discusses the development of a bias pretreatment to overcome the problem of nucleation of diamond on hetergeneous substrates.

Although production of electronic devices using polycrystalline diamond films, homoepitaxial film grown on single-crystal diamond, and

natural IIB diamond has been accomplished³, it is necessary to produce a homoepitaxial film grown at an affordable cost to take full advantage of the electrical and thermal properties of diamond. Biasing a silicon substrate during the initial stages of microwave plasma CVD has been shown to cause increase in crystalline alignment and an increase in nucleation⁴. The understanding of the enhancement of diamond nucleation by biasing for approximately the first 15 minutes of deposition may be the key to understanding diamond nucleation itself and the possible development of single-crystal diamond.

Previously, the only effective way of causing diamond nucleation on a silicon wafer was to first scratch it with diamond polish. This caused great debate over what caused the nucleation of diamond. Additionally, this method would not be good for VLSI because the physical scratching would damage any previous processing. Biasing allows the diamond to be grown without modifying the silicon substrate. Also biasing may help give a clue to how diamond nucleates and grows.

Bias experiments and study were investigated as follows. First, the bias conditions were duplicated⁵ and observed. Next some hypothesis was made. Finally, tests were set up for this hypothesis and was performed.

Experimental Procedure

All the diamond deposition experiments were performed with an Astex high pressure microwave source (H.P.M.S) as shown in figure 1. For the first run of biasing (BEN005), a square centimeter piece of silicon(100) was placed on a two inch diameter clean graphite disk that was 3.3 mm high which, in turn, sat on a 4 inch diameter graphite stage. The sample was run in an hydrogen atmosphere at 20 torr with a microwave power of 1 KW for five minutes at a flow rate of 360 sccm in

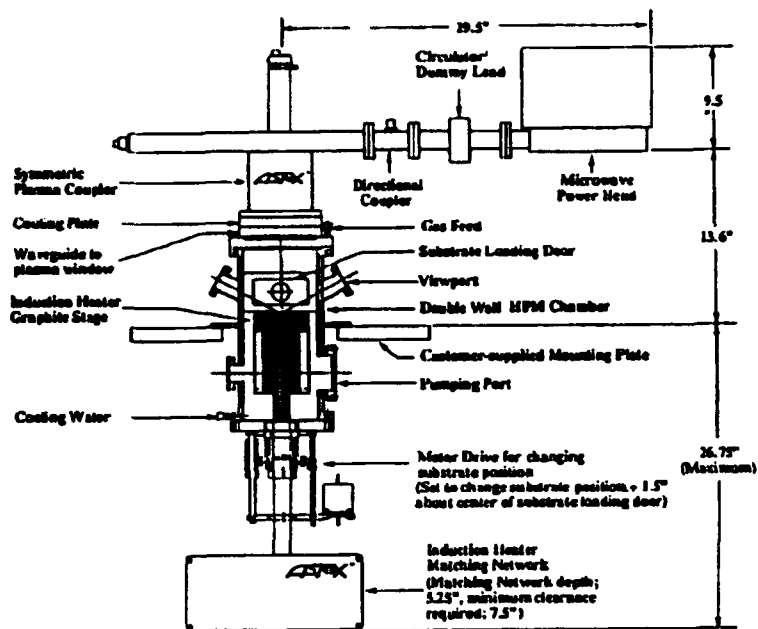


FIG. 1 HPMS SOURCE

order to remove the silicon-oxide layer. The sample was also heated to 850°C as measured by the optical pyrometer. Then 7.2 sccm (2%) methane was added to the system. A bias of -200 VDC which drew 25 mA current

was applied and maintained for 16 minutes. Longer bias time was not used because other researchers observed that after 15 minutes of biasing the nucleation decreases⁵. It was observed that the biasing made a region of faintly blue gas discharge directly over the substrate. There was a gap between this small region and the main plasma ball. When the bias was turned off, the plasma became one ball. Then the methane was changed to 1.8 sccm (0.5%) to produce high quality diamond and was run for 18 hours.

The next run (BEN006) was set up the same as BEN005 except the temperature was 775°C according to the optical pyrometer. When the bias was run for fifteen minutes it had the same -200 VDC, but it drew 150 mA current. The smaller plasma disk that was distinct from the main plasma ball was again observed during the time of biasing. The sample was run under the same growth conditions for 18 hours and 20 minutes.

For the third run (BEN007), the hydrogen plasma was run for ten minutes. Then the bias was run at the same 7.2 sccm of methane and 360 sccm of hydrogen at a temperature of 845°C for fifteen minutes with a DC voltage of -230 drawing a current of 120 mA. The plasma conditions were changed to the same as before for diamond growth and was run for 26 hours.

Results

Using a scanning electron microscope (SEM), the samples were analyzed to see how the biasing affected nucleation and growth. The BEN005 sample had some good quality diamond crystals very intermittently spaced on the silicon with a particle density of $4 \times 10^3/\text{cm}^2$ figure 2. The BEN006 sample was very highly nucleated with a complete covering of the surface figure 3. It was possible to even see steps on the faces of the diamond crystals. Sample BEN007 was almost the same except the crystals appeared to be slightly bigger figure 4. The particle

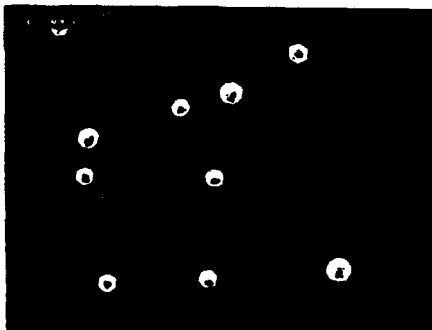


Figure 2 sample BEN005

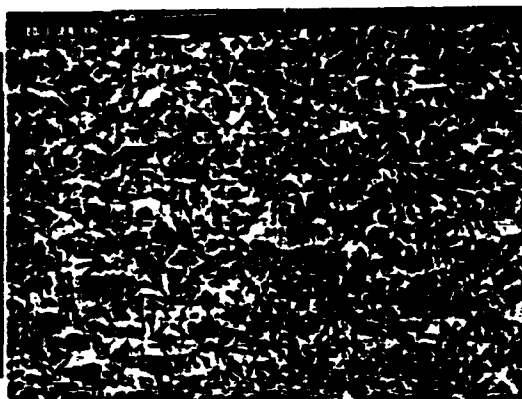


Figure 3 sample BEN006



Figure 4 sample BEN007

density of both BEN006 and BEN007 was between 10^8 and $10^9/\text{cm}^2$ which is slightly higher than diamond scratched silicon that has a particle density of 10^7 - $10^8/\text{cm}^2$ ⁶. This phenomenon of the biasing pretreatment working only after the first run has been noted in other places⁵. This may be due to a film that forms after the first run on the surrounding graphite causing the whole graphite stage to act like a cathode. It is also important to note that the current changed from 25 mA to 150 mA after the first run.

Conclusions

It is evident that biasing will increase nucleation without other pretreatment. The orientation of diamond with bias did not occur, but that is most likely because a carburized layer was not formed as in Wolter's experiments⁵. One reason for this may be an oriented silicon-carbide layer must be formed before an oriented layer of diamond could be formed because the lattice parameter of silicon-carbide is closer to diamond than is silicon. Cleaning the silicon with hydrofluoric acid will clean off the silicon-oxide layer. Also biasing a piece of clean single crystal silicon-carbide should improve orientation. A run where cleaning the silicon with hydrofluoric acid and then carburizing it before biasing and deposition

was done, but was not yet examined.

The biasing process is likely causing a larger flux of positive ions such as CH_3^+ , CH_2^+ , CH^+ , H^+ , and H_3^+ to the surface of the silicon while not effecting the non ionized radicals like CH_3 , CH_2 , CH , H , and H_3 and the stable gasses like CH_4 and H_2 . The increase of CH_3^+ at the surface is possibly responsible for the increase in nucleation thus may be responsible for nucleation itself. CH_3^+ is possibly responsible for nucleation because with its trigonal planer shape it is closer to the same spacing of silicon-carbide than CH_3 which is trigonal pyramidal. However, CH_3 along with CH_4 may be closer to diamond's spacing and may be responsible for diamond growth. A study of the gasses above the substrate during biasing would be helpful, but distinguishing between ionic radicals and neutral radicals is difficult.

Acknowledgements

The author of this report would like to thank Bob Knight, Pat Emmert, Sean McGinnis, the workers at Wright Patterson AFB, and RDL HSAP Program for supporting this project.

References

¹Vic Comello, R&D Magazine. 48, (1992).

²*Aerospace America*. 27, (Feb. 1991).

³Hideo Kiyota, Ken Okano, Tatsuya Iwasaki, Hiroshi Izumiya, Yukio Akiba, Tateki Kurosu, and Masamori Iida, Japanese J. of Appl. Phys. 30, L2015 (1991).

⁴J. J. Chang and T. D. Mantei, J. Appl. Phys. 11, 72 (1992).

⁵S. D. Wolter, B. R. Stoner, and J. T. Glass, Appl. Phys. Lett. 11, 62 (1993).

⁶Yarborough, W., and Messier, R., Science. 247, 688, (1990).